Evaluation of human induced pluripotent stem cell (ipsc)-derived mesenchymal stromal/stem cells (msc) for use in cell-based therapy

Gasparini Devito, Liani

Awarding institution:
King's College London

EVALUATION OF HUMAN INDUCED PLURIPOTENT STEM CELL (iPSC)-DERIVED MESENCHYMAL STROMAL/STEM CELLS (MSC) FOR USE IN CELL-BASED THERAPY

LIANI GASPARINI DEVITO

King's College London
Faculty of Life Sciences and Medicine
Division of Women and Children's Health
Stem Cell and Regenerative Medicine
(2018)

Thesis submitted for the degree of Doctor in Philosophy

DECLARATION

I, *Liani Gasparini Devito*, declare that this PhD thesis contains no material that has been submitted previously, in whole or in part, for the award of any academic degree. Where information has been derived from other sources, I confirm that this has been indicated in the thesis.

The work presented in this thesis is my own except for the following:

- RT-qPCR was performed by Dr. Aleksandra Cvoro
- part of the immunomodulatory assay was performed by Dr. Antonio Galleu
- part of the statistical analysis was performed by GenoSplice Technology

ABSTRACT

Donor procurement makes the logistics of obtaining human bone marrow (BM) as a source of mesenchymal stem/ stromal cells (MSCs) complicated. Although BM MSCs from adult donors still have satisfactory abilities to be used for regenerative medicine purposes, from the manufacturing perspective, the best donors are in the pediatric age range. In addition, the procedure requires planning and it is painful; the derivation and identification of the MSCs according to ISCT are still controversial among scientists, and the isolation and quality of cells also varies among donors. Therefore, the MSCs therapy field is constantly looking for alternative sources.

We hypothesized that human MSC derived from induced pluripotent stem cells (iPSCs) have biological qualities of native MSC and could be scaled up and used for therapeutic purposes. To test the hypothesis, we isolated native MSC (nMSC) from umbilical cord's Wharton's Jelly (WJ) of two donors (#012 and #013) in xeno-free conditions. Next, we reprogrammed them into iPSC (iPSC012 and iPSC013) and subsequently differentiated them back into MSC using two different protocols ARG and TEX (iMSC012ARG, iMSC012TEX, iMSC013ARG, and iMSC013TEX). Using the same protocols, we also differentiated the clinical grade human embryonic stem cell line (ESC) KCL034 into MSC (eMSC034ARG and eMSC034TEX).

To assess which of the two differentiation protocols worked better, we compared differentiation capability, transcriptomics and immunomodulatory potential of the iMSCs (iMSC012ARG, iMSC012TEX, iMSC013ARG and iMSC013TEX) and eMSCs (eMSC034ARG and eMSC034TEX) with nMSCs (nMSC012, nMSC013 and BM MSC). Based on the expression of all expressed genes, the data demonstrated that both iMSCs and eMSCs differentiated following TEX protocol are closer to nMSC with higher differentiation potentials but lower immunomodulatory properties than ARG.

Our data suggest that, following a careful selection and screening of donors, nMSCs from umbilical's cord WJ can be reprogrammed into iPSCs providing an extensive source of material for differentiation into iMSCs of similar therapeutic potential as nMSC. iMSCs could be scaled up under GMP conditions and serve as an alternative to BM and MSCs from other sources for therapeutic purposes.

TABLE OF CONTENTS

LIST OF FIGURES

LIST OF TABLES

ABBREVIATIONS

ACTB	beta actin gene
ALF	acute liver failure
aMSCs	adipose mesenchymal stem/ stromal cells
Ang-1	angiopoietin-1
ARG	Argentina
AT	adipose tissue
bFGF	basic FGF
BLI	bioluminescence imaging
BM	bone marrow
BMP	bone morphogenetic protein
BSA	bovine serum albumin
CD	cluster of differentiation
cDNA	complementary DNA
CFU-F	colony forming units-fibroblasts
CI	confidence interval
CM	conditioned medium
cm	centimetres
COL11A1	collagen 11
CXCL11	chemokine ligand 11
D	days
DAPI	4',6-diamidino-2-phenylindole
DMEM	Dulbecco's modified Eagle medium
DMSO	dimethyl sulfoxide
DNA	deoxyribonucleic acid
DPBS	Dulbecco's phosphate-buffered saline
dXF	defined xeno free
EB	embryoid body
EDTA	ethylenediaminetetraacetic acid
EMP	embryonic stem cell derived mesenchymal progenitors
eMSCs	embryonic mesenchymal stem/stromal cell

ESC	embryonic stem cells
EV	extracellular vesicles
FABP4	fatty acid binding protein 4
FBS	foetal bovine serum
FGF	fibroblast growth factor
Fluc	firefly luciferase
g	gravity/ g-force
GBP4	guanylate binding protein 4
GF	growth factor
GFP	green fluorescent protein
GMP	good manufacturing process
GO	gene ontology
GvHD	graft-versus-host-disease
h	hour
hESC	human embryonic stem cell
HFF	human foreskin fibroblast
hiPSC	human induced pluripotent stem cell
HLA-DR	Human leukocyte antigen D related
HPL	human platelet
HPRT1	hypoxanthine phosphoribosyltransferase 1
ICM	inner cell mass
IDO1	indoleamine 2,3-dioxygenase activity 1
IFNγ	interferon gamma
IL	interleukin
iMSCs	induced mesenchymal stem/ stromal cells
iPSC	induced pluripotent stem cell
ISCT	International Society for Cellular Therapy
ITGB1	integrin β1
KCL	King's College London
KEGG	Kyoto Encyclopedia ofGenes and Genomes
KLF4	Krüppel-like factor 4

LNGR	nerve growth factor receptor
MEM	modified eagle medium
MHC I	major histocompatibility complex
min	minutes
ml	millilitre
MMLV	Moloney Murine Leukaemia virus
mM	millimole
mm	millimetre
MS	multiple sclerosis
MSCA-1	mesenchymal stem cell antigen 1
MSC	mesenchymal stem/ stromal cells
NANOG	homeobox protein NANOG
NCAM1	neural cell adhesion molecule 1
NFκB	nuclear factor kinase
nMSC	native mesenchymal stem/ stromal cells
NAT	Native
NT	nuclear transfer
NuFF	newborn human foreskin fibroblast
nXF	non-defined xeno-free
µg	micro grams
µl	micro litre
µM	micro mole
O_2	oxygen
OCT	octamer
PBS	phosphate-buffered saline
PBMC	peripheral blood mononuclear cells
PCR	polymerase chain reaction
PD	population doublings
PD-L1	programmed death ligand 1
PFA	paraformaldehyde
PHA	phytohaemagglutinin

PRP	platelet rich plasma
PSC	pluripotent stem cells
qPCR	quantitative polymerase chain reaction
RNA	ribonucleic acid
RUNX2	runt related transcription factor 2
SCNT	somatic cellular nuclear transfer
SD	standard deviation
SOX	sex determining region Y (SRY)-box
SeV	sendai virus
STD	standard
TEX	Texas
TGFβ	transforming growth factor beta
THY1	Thy-1 cell surface antigen
TNSALP	tissue non-specific alkaline phosphatase
UC	umbilical cord
VEGF	vascular endothelial growth factor
VPA	valproic acid
WJ	Wharton's jelly
XF	xeno free

ACKNOWLEDGEMENTS

First, I would like to say a special thanks to my supervisor Dr. Dusko Ilic, who accepted me as his part-time Ph.D. student and has always been there for all my questions and doubts.

My sincere ‘thank you’ to everyone in the Assisted Conception Unit (ACU) on the 11th floor of Guy’s Hospital Tower wing, including my Stem Cell team colleagues and the PGD team.

I would like to say a massive ‘thank you’ to my collaborators Dr. Alekssandra Cvoro, Carl Hobbs, Dr. Antonio Galleu and Dr. Francesco Dazzi.

I would also like to say ‘thank you’ to my family in Brazil, my mother Vanderci Gasparini, my father Liberato Devito and my step-mother Miriam Devito, who believed and will always believe in my courage and capacity to conquer the world even when this is far from the truth.

Finally, I would like to say a huge ‘thank you’ to my husband Toby Benjamin Davis, who encouraged and supported me throughout the six years of Ph.D. I do not have words to express my gratitude for you. I would not have finished this doctorate without you. Thank you so much, and I love you dearly.

CHAPTER 1

1. INTRODUCTION

1.1 Stem Cells

Stem cells (SCs) are defined as unspecialized cells characterized by both the ability to self-renew and the ability to differentiate into functional adult cell types. Stem cells are responsible for the constant renewal of our skin and blood and are also responsible for wound healing. Stem cells enable us to exist and function. Furthermore, 'dormant' reserves of stem cells in our bodies await the opportunity either to replicate and produce more stem cells or to differentiate into more-specialized cells. Typically, when a stem cell divides, either both daughter cells remain stem cells, or one daughter cell remains a stem cell while the other daughter cell undergoes differentiation into a more-specialized cell type. This characteristic is restricted to stem cells, although some fully adult stem cells such as liver cells can divide to give rise to more cells like themselves only. Stem cells are not exclusively human cells; they can be found in all multicellular organisms, from plants to animals, including humans (Thomson *et al.*, 1998; Weissman, 2000; Reubinoff, 2007).

Stem cells are classified according to their capacity for differentiation or plasticity. *Totipotent* cells can form all lineages of an organism and extra-embryonic layers; only zygotes and first-cleavage blastomeres are totipotent. After a certain number of cell divisions, the cells of the zygote lose totipotency and become pluripotent. Embryonic stem cells (ESCs) and induced pluripotent stem cells (iPSCs) are examples of *pluripotent* stem cells, with the ability to self-renew infinitely and the capability of generating all cell types belonging to the three embryonic germ layers (endoderm, ectoderm and mesoderm) *in vivo* and *in vitro*. *Multipotent* stem cells (also called somatic or adult stem cells) are derived from pluripotent cells through cell division and differentiation. Mesenchymal stem/stromal cells (MSCs) and haematopoietic stem cells (HSCs) are classified as *multipotent* stem cells, and they can only give rise to cells

of a particular lineage. They have been recognized in different tissues, such as bone, central nervous system, muscles and intestines. The most important function of these cells is to preserve the tissue through cell proliferation when needed. *Unipotent* stem cells are able to generate only one cell type, for example, spermatogonial stem cells, which give rise to sperm, and skin stem cells, which are one of the most abundant types of unipotent stem cell (Jaenisch and Young, 2008).

From the time when Gurdon transplanted intestinal epithelium-cell nuclei from *Xenopus* tadpoles into enucleated frog eggs and managed to produce 10 normal tadpoles: Molly and her fellow clones (Gurdon, 1962), and Dolly the sheep was generated (Wilmut *et al.*, 1997), the use of somatic cell nuclear transfer (SCNT) or nuclear cloning demonstrated that the epigenetic state of somatic cells, including the totally differentiated ones, is not irreversibly fixed but can be reprogrammed to an embryonic state that is able of developing a new organism. Nuclear transfer (NT), cell fusion and genetic manipulation can induce reprogramming.

Thomson *et al.* (1998) were the first scientists to generate ESCs *in vitro.* To isolate and culture those cells, the inner cell mass (ICM), a cluster of pluripotent stem cells within an embryo in the blastocyst stage, is extracted following appropriate culture techniques. Because human ESCs arise from human embryos, there are significant ethical concerns surrounding this technology. Therefore, since then, biomedical research has focused on overcoming the ethical and immune rejection issues associated with human ESCs. In 2006, Takahashi and Yamanaka discovered that somatic or adult cells could be reprogrammed into a pluripotent state. Those cells, called iPSCs, were first generated by reprogramming adult cells via ectopic expression of transcription factors normally expressed in embryos. iPSCs exhibit the same characteristics as ESCs and have opened a new and exciting area in regenerative medicine.

Regardless of their potency, stem cells can also be divided into four groups based on their origin: ESCs and foetal, perinatal and somatic (resident or tissue-specific) stem cells

(O'Donoghue and Fisk, 2004; Toma *et al.*, 2001; Jaenisch and Young, 2008). Perinatal stem cells are harvested from extra-embryonic tissues, such as the placenta, foetal membranes and umbilical cord, and even though the cells isolated from these tissues are considered multipotent stem cells, some have proven to be more potent than was first thought. The focus of my thesis is the isolation of stem cells from umbilical cord tissue, iPSCs and, most importantly, MSCs derived from iPSCs.

1.2 Mesenchymal stem/stromal cells

MSCs were first isolated from animal bone marrow (BM) by Friedenstein *et al.* (1970), and they represent a rare population of nucleated cells (0.0001 – 0.01%) within adult BM. MSCs can also be found in muscles, periosteum, adipose tissue and other connective tissues (Castro-Malaspina *et al.*, 1980; Pittenger *et al.*, 1999).

Human MSCs are broadly characterized as a population of non-haematopoietic multipotent stem cells. Similarly to other stem cells, MSCs hold the potential for self-renewal and differentiation into further specialized cells of a particular lineage (Pittenger *et al.*, 1999). MSCs were first described as plastic, adherent, clonogenic, colony-forming, fibroblast-like cells (Friedenstein *et al.*, 1987). The lineage potential of these multipotent cells includes almost all derivatives of the mesoderm, such as the skeletal tissues bone, cartilage, fat and tendon and the non-skeletal tissues smooth muscle, skeletal muscle and possibly myocardium and endothelial cells. MSCs are found in BM, liver, synovium, adipose tissue, heart and other postnatal connective tissues, such as umbilical cord (UC) (Bianco *et al.,* 2008).

MSCs from neonatal tissues, including the placenta, amniotic membranes and UC, can provide a source of stem cells that is ethically non-controversial and easily accessible, since perinatal tissues are normally discarded after birth (Wolbank *et al.,* 2010). They are ideal

candidates for regenerative medicine because they can be effortlessly isolated and expanded from adult and foetal tissues, they possess multilineage capacities, they hold immunomodulatory properties, they release growth factors, and they are capable of migration to damaged sites (Frausin *et al.,* 2015). MSCs may exert a beneficial trophic effect on injured tissues, even without replacing dying cells (Crigler *et al.,* 2006; Shen *et al.,* 2013), establishing these cells as a good choice for cell therapies.

Although criteria defining MSCs are still not available (Wagner and Ho, 2007; Wagner *et al*., 2006), MSCs can be identified by a combination of different markers and by phenotypic and functional characteristics. The ISCT (International Society of cell Therapy) proposes a set of criteria to identify MSCs intended for research and pre-clinical studies (Table 1.1). However, according to Dominici *et al.* (2006), future research will conduct to a revision of the criteria as new findings emerge. In addition, they have low levels of HLA class I and II and do not express CD14, CD34 or CD45 (haematopoietic surface markers) or CD31 (endothelial marker) and show no expression of costimulatory molecules (CD80, CD86). MSCs should demonstrate multipotency by *in vitro* differentiation into the three mesenchymal lineages: adipocytes, chondrocytes and osteocytes (Bobis *et al.*, 2006; Conget and Minguell, 1999; Djouad *et al.*, 2005; Fibbe and Noort, 2003; Gronthos *et al.*, 2003; Pittenger *et al.*, 1999). Additionally, MSC antigen-1 (*MSCA-1*) was present in cells that showed a >100-fold increased yield of colony-forming units. Therefore, *MSCA-1*, which has been associated with cells of the osteoblast lineage, might also be a marker of BM MSCs (Gronthos *et al*, 2007; Battula *et al.*, 2009; Bühring *et al.*, 2009; Sobiesiak *et al.*, 2010; Jones *et al.*, 2006).

Table 1.1 Summary of ISCT criteria to identify MSCs (Dominici *et al.*, 2006)

1. Adherence to plastic culture vessel		
2. Phenotype	Positive (≥ 95%)	Negative (≤ 2%)
	CD105	CD34
	CD73	CD45
	CD90	CD14
		CD19
		HLA-DR
3. *In vitro* differentiation: osteoblasts, chondroblasts, adipocytes (demonstrating by staining)		

MSCs exhibit low immunogenicity and do not stimulate T-cell proliferation *in vitro* and can also suppress lymphocyte proliferation induced by phytohaemagglutinin (PHA). In addition, they do not express major histocompatibility complex class II (*MHC-II*) and only express low levels of *MHC-I* (Le Blanc *et al.*, 2003), which are both proteins responsible for presenting peptides on the cell surface for recognition by T-cells, a feature that is essential for adaptive immunity (Wieczorek *et al.*, 2017). However, the mechanisms of the immunomodulatory effects are still controversial among scientists. Some believe that contact between cells activates the immune regulatory activity, while others believe that it is linked to other factors, such as hepatocyte growth factor, interleukin (IL)-10, Interferon-γ (IFNγ) and transforming growth factor (TGF)-β1 (Nasef *et al.*, 2007).

Human MSCs hold great potential in today's biomedical research and new approaches in the treatment of human diseases. The plasticity and *in vitro* proliferation of these cells make them an important instrument for cell transplantation (Mark *et al.*, 2013). MSCs have been successfully used in treatments for various diseases, such as *osteogenesis imperfecta* (OI) and to reduce graft-versus-host disease (GvHD) via immunosuppression (Horwitz *et al.*, 2002). In addition, MSCs have contributed to the regeneration process after myocardial infarction in mice (Kawada *et al.*, 2004) and are also able to increase the results of allogeneic transplantation because those cells have immunomodulatory effects (Nesselmann *et al.*, 2011).

1.3 Wharton's Jelly mesenchymal stem/stromal cells

The umbilical cord (UC) is an elastic structure that connects the placenta to the foetus during pregnancy. The UC consists of two umbilical arteries and one umbilical vein, both surrounded by a mucous proteoglycan-rich matrix known as Wharton's Jelly (WJ), which is covered by amniotic epithelium (Figure 1) (Kim *et al.*, 2013). The UC provides bidirectional flow, providing oxygen and nutrients that contribute to the adequate development of the foetus and eliminating waste and carbon dioxide (Taghizadeh *et al.*, 2011).

The UC is derived on day 26 of gestation from extra-embryonic mesoderm and/or embryonic mesoderm. At birth, the UC weighs approximately 40 g, is approximately 30–65 cm long, and has a diameter of 1.5 cm. WJ is composed of water (90%), sulphated glycosaminoglycans (GAGs) and a collagen-rich 3D extracellular matrix (ECM). The most abundant GAG is hyaluronic acid (~70%), and collagens of types I and III are more prevalent than IV, VI and VII (Sobolewski *et al.*, 1997). The composition of the 3D matrix can be divided into three distinct zones—the sub-amnion, WJ per se, and peri-vascular zone—and even though different types of stromal cells are dispersed in different zones, the term WJ MSCs is often extended to all UC stromal cells (Corrao *et al.*, 2013). They share common features with MSCs from adult tissues, for example from the bone marrow (BM), such as being positive for CD44, CD73, CD90, CD105, α-smooth muscle actin and vimentin (Huang *et al.*, 2012; De Kock *et al.* 2012).

Thomas Wharton was the first to describe WJ (1656) as a gelatinous substance composed of various isoforms of collagen and proteoglycans. The main function of the WJ is to protect the arteries and veins from the compression and torsion that they can be exposed to during gestation. It has been demonstrated that human WJ MSCs present an elevated capacity for autoregeneration, and they have been compared with those obtained from BM (Kern *et al.*, 2006).

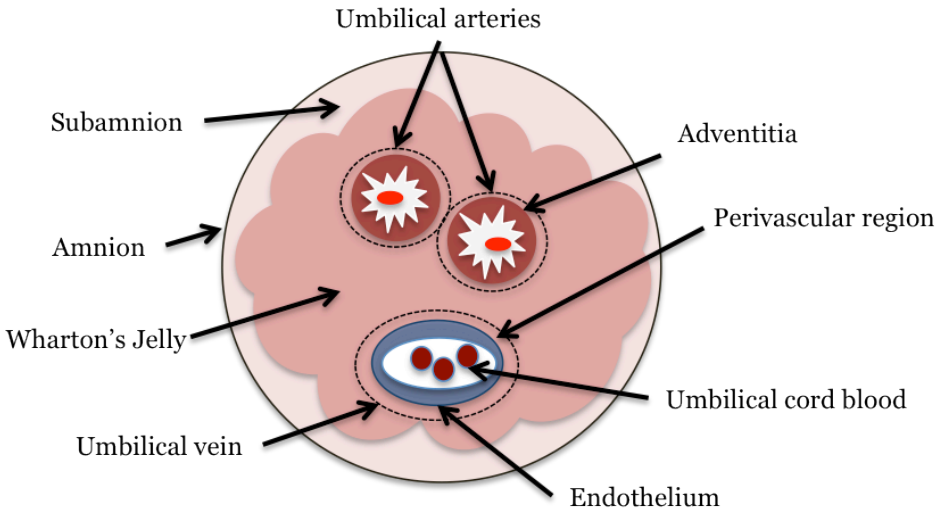

Figure 1.1 Diagram of a cross section of human umbilical cord illustrating the anatomical compartments, including Wharton's jelly (Figure adapted from Kim *et al.*, 2013).

There are a few hypotheses on how stem cells arrive in the WJ and their possible function during gestation. First, the cells within the WJ are primitive mesenchymal stromal cells (myofibroblasts) originating from the mesenchyme within the UC matrix or WJ. The function of these cells might be to secrete various glycoproteins, mucopolysaccharides, glycosaminoglycans (GAGs) and extracellular matrix (ECM) proteins to compose a gelatinous material whose main purpose is to prevent strangulation of the UC vessels during gestation. WJ stem/stromal cells release a secretion containing bioactive molecules such as interferons, growth factors, interleukins, GAGs and cell adhesion molecules, which are involved in immunomodulatory mechanisms and tissue repair and thus can be used for the repair of bone, cartilage and bone defects (Angelucci *et al.*, 2010; Fong *et al.*, 2012; Gauthaman *et al.*, 2012). Second, there may be two waves of migration of foetal MSCs in early human expansion. The first wave consists of MSCs migrating from the yolk sac and aorta-gonadal mesonephros (AGM) to the placenta. In the second wave, the migration of MSCs is reversed, i.e., from the

placenta via the UC to the foetal liver and bone marrow. During these waves, MSCs are trapped in the gelatinous WJ. The stemness of these cells appears to be modified in their new environment, and they can differ from bone marrow MSCs (Wang *et al.*, 2008; Taghizadeh *et al.*, 2011).

The hypothesis is that MSCs of foetal origin show potential between those of embryonic and adult stem cells. Stem cells harvested directly from the WJ have been shown to have low immunogenic properties (Weiss and Troyer, 2006). Weiss *et al.* (2008) demonstrated that WJ MSCs did not stimulate T-cell proliferation in a mixed lymphocyte reaction (MLR) assay but inhibit the proliferation of stimulated T-cells in a two-way MLR assay. They further showed that WJ MSCs do not express the co-stimulatory surface antigens CD40, CD80 and CD86. These researchers concluded that there is no evidence of immune rejection of undifferentiated WJ MSCs, and this cell type might be a good candidate for allogeneic transplantations.

The definition and characterization of WJ MSCs remains unclear, and the general definition is not entirely accepted. However, the most significant *in vitro* characteristics of MSCs are the abilities of self-renewal and of differentiation into cells of adipogenic, osteogenic and chondrogenic lineages, proving their multipotent potential. Furthermore, there are a large number of stemness markers used to characterize these cells, including embryonic stem cell markers, such as *OCT3/4*, *SSEA4*, nucleostemin, *SOX2*, and *NANOG* (Ma *et al.,* 2005; Tong *et al.*, 2011; Prasanna *et al.*, 2010; Khadan and Bhonde, 2010; Struys *et al.*, 2011). In addition, WJ MSCs can express specific cell surface markers, including CD90, CD105, CD44, CD29, and CD73, and are negative for the haematopoietic markers CD34 and CD45 (Friedman *et al.*, 2007; Martin-Rendon *et al.*, 2008; Majore *et al.*, 2009; Moodley *et al.*, 2009; Tsai *et al.*, 2009).

1.4 Potential therapeutic use of MSCs

Among all stem cells currently available for clinical applications (Table 1.1), MSCs have been reported to be the most appealing source in regenerative medicine due to their therapeutic potential in various diseases, including heart attack, asthma, osteoarthritis, cartilage repair, critical limb ischaemia and stroke, to mention a few, resulting from their immunomodulatory, secretory and neoangiogenic properties. Currently, several clinical trials are investigating autologous and allogeneic hMSC therapy and show great promise (Cuomo *et al.,* 2018).

For a long time, MSCs have been the focus of cell-based therapies to promote cartilage repair, not only in humans but also in working animals such as horses (Branly *et al.*, 2017). MSCs derived from adult tissues have fewer safety concerns and ethical issues regarding their applications, and they are the dominant source of MSCs for cell therapy for osteoarthritis (OA). Numerous studies have attempted to overcome the poor healing ability of articular cartilage. However, despite progressive advancements in MSC *in vitro* culture and the introduction of bioactive scaffolds, the feasibility and efficacy of these treatments are still uncertain. MSCs derived from adult tissues are the dominant source of MSCs for clinical trials involving osteoarthritis (OA) (Lee *et al.*, 2017).

BM MSC isolation involves uncertain safety and painful aspiration of BM, making it a challenge to recruit donors. However, clinicaltrials.gov showed 46 registered clinical trials displaying clinical status as: active, completed and/or recruiting, using BM MSCs, as of April 2018, indicating the popularity and benefits of those cells in the regenerative medicine field. Out of the 46 studies, 12 are being performed in the Middle East, ranging from treating knee osteoarthritis and liver failure to emphysema. In Europe, there are 11 studies in total, of which 4 are occurring in Italy, 4 in Spain, 3 in France and 3 in Germany. The studies vary between bone fractures, liver transplantation rejection, chronic renal failure, and osteonecrosis of the jaw to critical limb ischaemia. There are no such studies underway in the U.K.

UC MSCs are straightforwardly isolated and expanded *in vitro,* and they hold anti-inflammatory and immunomodulatory activity and are also able to migrate to the injury site, making them an attractive tool for cellular therapy. At present (as of April 2018), 43 registered clinical trials displaying clinical status as active, or completed and/or recruiting using UC MSCs can be found on clinicaltrials.gov, indicating the popularity of those cells in the field of regenerative medicine, similar to BM MSCs. The majority of clinical studies are happening in China (28 studies found) and only 1 in Europe, specifically in Italy, which is recruiting 47 patients to treat severe cases of GvHD using UC MSCs. In Chile, one study is using UC MSCs to treat knee osteoarthritis, the only such study in South America. More than 195 conditions are being treated and/or will be treated by those cells in those studies, including heart failure (in China), Alzheimer's disease (Neurostem® in Seoul, South Korea), GVHD (Kansas Medical Center, U.S.A.) and erectile dysfunction (Cell Therapy Center, Jordan).

Can *et al.* (2017) performed a systematic analysis of 93 peer-reviewed published results, limitations and obstacles of clinical trials using UC MSCs. The first problems that they noted were the name and origin of those cells. MSCs can be isolated from different sources, and UC-derived "multipotent stromal cells" have several stem cell-like properties; thus, they should be classified differently than MSCs isolated from the amnion, placenta and cord blood. However, several published reports are not clear about the origin of the cells used in the studies they describe. The subsequent concerns were the route of application, followed by the biodistribution of UC MSCs in a living human body, which is one of the most controversial topics in the cell therapy field. The majority of *in vivo* data are on rodents, and UC MSCs can be detectable at low frequencies in tissues after transplantation; moreover, when they are injected intravenously, signals were found in the lungs, as well as in the liver and spleen (Leibacher and Henschler, 2016). Moreover, the dose of cells administered (i.e., the number of cells per transplantation, the number of cell deliveries, and the intervals between deliveries)

varied immensely between the studies. The maximum number of cell deliveries was reported as seven by Zheng *et al.* (2015) in patients with acute GvHD (article in Chinese) and by Patel and Riordan (2015) in one patient with Duchenne muscular dystrophy (DMD), who, after each treatment, had an improved quality of life lasting 5-6 months and no side effects. However, repeated local or systemic delivery of UC MSCs may generate reactive antibodies that would block the beneficial effect, even though those cells lack HLA class II antigens and T-cell costimulatory molecules (Cho *et al.*, 2008).

Cells intended for cell therapy should be produced under internationally recognized current GMP conditions and acquire clinical-grade status. In spite of this, only 26 (28%) of the 93 trials reviewed by Can *et al.* (2017) described GMP when isolating and preparing their clinical-grade UC MSCs for cell therapy. In addition, only 18 of those trials reported cell viability assessment and characterization of those cells. Furthermore, there are cells going into clinical applications outside clinical trials.gov, for instance by Hospital Exemption for Advanced Therapy for Medicinal Products, which only local hospital's R&D have access to the data. Unfortunately, in the stem cell field, positive findings are more likely to be published, and there are a variety of biases in some of the publications, with all the reviewed trials reporting no serious acute or chronic reactions (Fung *et al.*, 2017).

Table 1.2 Comparison of advantages and limitations of different types of SCs for clinical applications (adapted from Sun *et al.*, 2014)

Stem Cell Type	***Advantages***	***Limitations***
Embryonic Stem Cells	Pluripotent; differentiate into any type of cells from the three germ layers (endo-, ecto- and mesoderm)	Ethical issues; possible high immunogenicity; may lead to teratocarcinomas; genetic instability
Induced Pluripotent Stem Cells	Pluripotent; differentiate into any type of cells from the three germ layers (endo-, ecto- and mesoderm); possible autologous treatment; low immunogenicity; avoids ethical concerns; few clinical trials in progress	High costs; genetic instability; ethical issues (genetic material); more research is needed
Adult Stem Cells	Avoids ethical concerns; lower risk of immune rejection; available for some clinical treatments	Acquisition and isolation difficulties; more research is needed
Mesenchymal Stem/Stromal cells	Allow for allogeneic grafting without the use of immunosuppressive agents; can self-renew, proliferate and differentiate into specific lineages (multipotent); promote growth of adjacent cells; less susceptible to mutations; easy to collect and isolate	More research needed; do not have specific characterization; signalling pathways still not fully characterized
Haematopoietic Stem Cells	Capable of myogenesis and angiogenesis; proliferate and migrate to injury site in response of physiological/ pathological stimuli	High maintenance; unknown signalling pathways; low frequencies

MSCs are known to have the ability to differentiate into different types of cell progenitors, including bone, cartilage, skeletal muscle and neural precursors. For that reason, the regenerative field, at first, studied those cells to regenerate defective cartilage and bone.

Because MSCs can be effortlessly isolated from different sources, such as BM, synovium and adipose tissue, autologous MSCs could represent an alternative source for cell therapy, avoiding the immunological adverse effects of allogeneic treatment. MSCs from UC are known to have lower immunogenicity and increased self-renewal, proliferation and expansion capacities, as well as trilineage differentiation capacities. The selection of the most suitable MSC population for cartilage and bone repair depends on their availability and ease of isolation and on their potential for chondrogenic and osteogenic differentiation (Orth *et al.*, 2014; Pittenger *et al.*, 1999; Sudo *et al.*, 2007; Campagnoli *et al.*, 2001; Yang *et al.*, 2008; Hu *et al.*, 2003; Romanov *et al.*, 2003; Heng *et al.*, 2004).

The therapeutic effects of MSCs in different cardiovascular and neurodegenerative disorders have also been investigated in clinical trials. In addition to their multilineage differentiation potential, MSCs might have regenerative properties via the secretion and stimulation of different paracrine factors, such as IL-6, vascular endothelial growth (VEGF), hepatocyte growth factor (HGF), brain-derived neurotrophic factor (BDNF), neurotrophin-3 (NT3), thrombospondin, glial-derived neurotrophic factor (GDNF) and fibroblast growth factor (FGF) (Kalladka and Muir, 2014; Mastri *et al.*, 2014; Hsuan *et al.*, 2016). Furthermore, secretory product of MSCs, such as exosomes, can have a similar regenerative effect as the parental MSCs. It is believed that MSCs-exosomes release biologically active molecules that affect migration, proliferation and survival of neighbouring cells without the risks associated with cells transplantation making them a more safe and efficient therapy (*Wu et al.*, 2017).

1.5 Immunomodulatory effects of MSCs

The major advantages of MSCs are their anti-inflammatory and immunosuppressive effects, which make them suitable and desirable cells for clinical applications. They secrete an array of biological mediators, such as cytokines, chemokines and growth factors, that are involved in tissue regeneration and other functions, including anti-fibrotic, mitogenic, anti-apoptotic, wound-healing and angiogenic functions (Koelling and Miosge, 2009; Caplan, 2007; Goldberg, 2012; Gupta *et al.*, 2012).

The immunosuppressive function of MSCs is activated by pro-inflammatory cytokines. It has been reported that, *in vitro,* IFN-γ can interact with TNF-α, IL-1α, and IL-1β to induce the ability of MSCs to inhibit T-cell proliferation (Zhang *et al.*, 2008). Cytokines are small glycoproteins that regulate immunity, inflammation and haematopoiesis and are produced by a number of cells, such as leukocytes. They regulate physiological and pathological immune and inflammatory functions, and their secretion is a self-limited event (Khan, 2008).

T helper type 1 (Th1) cells are a lineage of CD4 T-cells responsible for cell-mediated immune responses and are activated during host defence against intracellular viral and bacterial pathogens. Th1 cells secrete IFNγ, IL-2, IL-10, and TNFα/β. As an effector cytokine of Th1 immunity, IFNγ is a regulator, and its production by natural killer (NK) cells, CD4 T-cells and CD8 T-cells targets antigen recognition in antigen-presenting cells (APCs), such as macrophages and dendritic cells. IFNγ activates macrophages stimulating them to express high levels of pro-inflammatory cytokines, such as TNFα, IL-12, IL-23 and IL-1β, and also by promoting Th1 T-cell responses and robust inflammation. APCs express major histocompatibility complex (MHC) I and II proteins, providing signals to stimulate proliferation and differentiation of lymphocytes by cross-presentation of antigenic pathways. Concomitantly, IFNγ signalling releases other cytokines and factors that sustain inflammation for longer maintenance of Th1 responses and to inhibit differentiation of regulatory T (Treg)

cells (Sica and Mantovani 2012, Shachar and Karin, 2013). Treg cells suppress the activation, proliferation and cytokine production of CD4 T-cells and CD8 T-cells, suppressing the immune response, and they may also suppress B-cells and dendritic cells by producing soluble messengers such as TGFβ, IL-10 and adenosine. Tregs are formed by the differentiation of naïve T-cells outside the thymus (Moncrieffe, 2018). Therefore, IFNγ expression is an important parameter for which exposure levels, target organ and cellular environment define the outcome of the immune response and impact the balance between physiological protection and pathological autoimmune responses. Thus, independent of the signalling pathway, IFNγ will directly or indirectly define the intensity of the inflammatory response (Green *et al.*, 2017).

MSCs from certain tissues have a unique tumour-homing capacity that enables them to serve as vehicles for gene therapy of advanced cancers. The tumour tropism of these MSCs is mediated by multiple chemokine receptors such as *CXCR4* and *CXCR6*, CD44, and *VEGFR1* and by integrins such as *ITGA6* and *ITGB1* (Zhao *et al.*, 2015).

Chemokines are dependent on IFN-γ and can be secreted by endothelial cells, fibroblasts, keratinocytes, MSCs, thyrocytes and more. High levels of CXC chemokines in peripheral fluids are therefore a marker of the host immune response (Antonelli *et al.*, 2014; Khan 2008). Chemokines are a large family of small heparin-binding chemotactic cytokines released by many cells and consist of four groups based on cysteine number and amino acids: CXC, CC, C and CX3C. Neutrophils and lymphocytes are the targets of CXC chemokines, including *CXCL1* to *CXCL17*. CXC chemokines contribute to the pathogenesis of many autoimmune diseases from type 1 diabetes to rheumatoid arthritis and systemic lupus erythaematosus (SLE).

BM MSCs constantly supply new stem cells to support natural cell turnover and repair in various tissues, including the kidneys (Cornacchia *et al.*, 2001; Poulsom *et al.*, 2001). Of the two major marrow-derived stem cell lineages, haematopoietic and mesenchymal, MSCs

possess unique promises for renal repair because nephrons are largely of mesenchymal origin. In a model of cisplatin-induced acute kidney injury (AKI), MSCs were more efficacious than haematopoietic stem cells in repairing damage (Morigi *et al.*, 2004). Li *et al.* (2006) successfully infused BM MSCs to prevent death by renal failure in a rodent model.

1.6 Issues with using MSCs in cellular therapy

The production of MSCs faces limitations, including the variability among donors, scarcity of MSCs in adult tissues, dependence upon donors (younger donors have advantages over older ones), and a low proliferative rate compared to other pluripotent stem cells (Siegel *et al*, 2013).

BM MSCs are the most common and generally used MSCs for human stem cell research and clinical applications. In the BM, MSCs contribute to the formation of the haematopoietic stem cell niche, making them the first choice of treatment for haematological malignancy (Uccelli *et al.*, 2008). However, the procedure to obtain BM is painful and carries the risk of infection, and it is difficult to recruit donors. For this reason, the cell therapy field is continually searching for new, non-invasive sources of MSCs. Among the various options are peripheral blood, placental tissue, amniotic tissue, dental pulp, nasal mucosa and adipose tissue-derived (AD) MSCs isolated from extra fat tissue obtained from cosmetic surgery. AD MSCs have proven suitable for clinical applications, although there are hypotheses that these cells bear abnormal metabolic features related to excessive body weight (Devito *et al,* 2014; Pikula *et al.*, 2013).

BM MSCs appear to be clearly different and have disadvantages over UC MSCs in regard to *in vitro* culture and clinical applications (Huang *et al.,* 2012). UC MSCs have higher proliferation rates and show increased colony-forming units (CFUs) and stemness characteristics that last longer after serial cell passaging (Fong *et al.,* 2010). Additionally, UC MSCs express some of the ESC markers at different levels, such as *OCT4*, embryonic surface marker antigens (*SSEA-4, TRA-1-60* and *TRA-1-80*), alkaline phosphatase (*ALP*), *DNMT3B* and

GABRB3 and genomic markers (*SOX2, NANOG, REX2*) (Conconi *et al.,* 2011; Carlin *et al.*, 2006; Hoynowski *et al.,* 2007).

MSCs from different sources have proven to suppress immunological responses in different diseases in animal models and *in vitro*, but the mixed results in clinical trials for the treatment of autoimmune and inflammatory diseases make them an unpredictable source. The major challenge is to develop a consistent and effective MSC-based immunosuppressive therapy using MSCs from different tissues of origin, different manufacturing processes and different donors (Griffin *et al*, 2013; Sharma *et al.*, 2014; English, 2013; Klinker and Wei, 2015; Ho *et al.*, 2008; Phinney *et al.*, 2012).

Based on their capacity to migrate to injuries sites, MSCs promise an improved treatment for cancer patients. They are able to repair tissues damaged by cancer and/or by radical therapies, and they are also capable of delivering different anticancer agents. Donnenberg *et al.* (2010) reported promising regeneration capacities of MSCs after radical cancer treatment in animal models and after soft tissue reconstruction after damaging surgery of the neck, breasts or head. Moreover, the osteogenic differentiation properties of MSCs combined with their injury-homing capacities make them the best candidate for tumour-induced osteolysis (Fritz *et al.,* 2008; Li *et al.*, 2011). However, tissue-derived MSCs, including those from the UC, BM and AD, have also shown a predisposition to promote cancer rather than inhibit it, and endogenous MSCs can promote cancer growth (Droujinine *et al*., 2013; Zimmerlin *et al.*, 2013; Chaturvedi *et al.*, 2013; Quante *et al.*, 2011; Song *et al.*, 2011; Jung *et al.*, 2013).

As mentioned before, UC MSCs hold great advantages over adult MSCs, first because they can be isolated in a non-invasive, low-cost and pain-free manner; second, because of their high proliferation rate and their low immunogenicity because of their naive cell character; and last, because of their potential allogeneic and autologous application in congenital disorders

and, when cryopreserved, in adulthood (Erices *et al.*, 2000; Joerger-Messerli *et al.*, 2016). However, these progenitor cells isolated from post-natal or adult tissues are susceptible to differences between lines, i.e., between donors, and to senescence during *in vitro* expansion. Human PSC MSCs, including those derived from ESC MSCs and those derived from iPSC MSCs, could avoid this issue and represent a cell source with consistent qualities and an expanded source of MSCs but without the tumorigenicity issues associated with the pluripotent cells (Yen *et al.*, 2009). PSC-derived MSCs are able to differentiate into mesodermal lineages and show immunomodulatory effects similar to those of adult BM MSCs (Peng *et al.*, 2016).

1.7 Reprogramming and Induced Pluripotent Stem Cells

Resetting the epigenome of a somatic cell to a pluripotent state, i.e., reprogramming, is a technology developed from various advances in the field of developmental biology. First, somatic cell nuclear transfer (SCNT), or nuclear cloning, the procedure used to generate Dolly the cloned sheep, demonstrated that a somatic cell nucleus could change its epigenetic state and reset to an early developmental state, inducing reprogramming (Wilmut *et al.*, 1997). Second, ESC isolation and culture conditions were developed and improved, allowing the successful *in vitro* culture of pluripotent stem cells (Martin, 1981; Evans & Kaufman, 1981; Thomson *et al.*, 1998). Last, various studies of early embryonic development identified a set of transcription factors able to contribute to the maintenance of the ESC phenotype and proliferation in culture, including *OCT3/4* (Nichols *et al.*, 1998; Niwas *et al.*, 2000), *SOX2* (Avilion *et al.*, 2003), and *NANOG* (Chambers *et al.*, 2003; Mitsui *et al.*, 2003), which could be used alongside transcription factors associated with genes that are upregulated in tumours, such as *c-MYC* and *KLF4* (Cartwright *et al.*, 2005; Li *et al.*, 2005).

Weintraub *et al.* (1989) were the pioneers in cellular reprogramming, reporting successful reprogramming of human fibroblasts into muscle cells via overexpression of the

transcription factor *MYOD1*, the first report showing that cell development could be modified and that transcription factors are crucial for determining cell fate (Ronquista *et al*., 2017).

In 2006, Takahashi and Yamanaka investigated the properties of 24 transcription factors involved in the conventional biology of ESCs. Using retroviruses as vectors to introduce and overexpress all 24 of those transcription factors, four factors in particular were able to convert mouse somatic cells (fibroblasts) into cells showing characteristics similar to those of ESCs. The four factors were SRY-related HMG-box 2 (*SOX2*), Octamer binding protein 4 (*OCT4*), also known as *POU5F1*, Kruppel-like factor 4 (*KLF4*) and *MYC.*

In 2007, James Thomson (Yiu *et al.*, 2007) and colleagues derived iPSCs using a different combination of reprogramming factors that included *NANOG* and *LIN28* instead of *MYC* and *KLF4*. More than 10 years later, the same transcription factors (*OCT4, SOX2, KLF4, MYC, NANOG* and *LIN28*) remain the foundation of the iPSC field (Li and Belmonte, 2016).

Transcription factors (TFs) are proteins that bind specific sites or elements in regulatory regions of DNA sequences (silencers and enhancers). Those factors may increase or decrease gene transcription and protein synthesis and consequently change cellular behaviour. Their activation is complex and consists of multiple intracellular signalling pathways, which are stimulated by cell-surface receptors and by ligands such as glucocorticoids and vitamins A and D. Transcription factor activation can be temporary and can produce effects ranging from transient changes at the cell surface to long-term changes in gene transcription. Therefore, transcription factors can be activated within the nucleus, binding directly to the DNA, or within the cytoplasm, sending specific nuclear signals to target the nucleus, acting as a "nuclear messenger". Many transcription factors have been identified, and a large amount of the human genome appears to code for these proteins (Adcock and Gaetano, 2009).

Reprogramming somatic cells comprises various steps that result in the expression of markers associated with pluripotency such as *NANOG*. Although morphological changes can

be identified in the early stages of the reprogramming process, the gene expression of those markers occurs during the late stage and indicates complete reprogramming. The main reprogramming factors used for reprogramming are *OCT4*, *SOX2* and *KLF4* (O, S and K - OSK), but additional factors, such as *c-MYC*, which was used to convert mouse fibroblast into iPSCs in the original reprogramming experiment by Takahashi and Yamanaka (2006) but later shown to be dispensable, are used to enhance the efficiency of iPSC generation (Okita *et al.*, 2007; Maherali *et al*., 2007; Nakagawa *et al.*, 2008; Wernig *et al.*, 2008; Wernig *et al.*, 2007). Furthermore, two- or three-factor reprogramming using exogenous *OCT4* with either *SOX2* or *KLF4* were able to establish transient states of pluripotency of mouse embryonic fibroblasts (MEF) (Nemajerova *et al.*, 2012). In another study by Kim *et al.* (2008), *OCT4* together with either *KLF4* or *c-MYC* were sufficient to generate iPS cells from adult mouse neural stem cells, showing the possibility of reprogramming cells with less transcription factors.

In humans, there is limited natural regeneration of cells and tissues, and it can be produced through activation of somatic stem cells located in a niche (for example, blood cells) or by inducing differentiated cells to proliferate (for example, the liver). Transdifferentiation, a natural mechanism in which manipulation of chromatin dynamics occurs to the point at which cells can switch lineages, and reprogramming studies have documented that reprogramming somatic cells directly to a cell of another somatic fate involved dedifferentiation and passage through a less differentiated progenitor state. Dedifferentiation is another mechanism that occurs before the transdifferentiation associated with natural regeneration of cells and tissues, and it involves the reversion of a fully differentiated somatic cell back to a less differentiated state. This stage allows the cell to proliferate again before re-differentiating, allowing the regeneration of cells that have been lost (Xie *et al.*, 2004; Jopling *et al*., 2011).

The reprogramming efficiency at which somatic cells transform into iPSCs is typically below 1%, suggesting not only that are the reprogramming factors essential in initiating the

changes but also that the subsequent events are required to maintain the reprogramming process. Changes in epigenetic status, such as DNA methylation and histone modification, are critical events for reprogramming, but their mechanisms and driving force are still unclear (Takahashi, 2014). It is known that TFs are responsible for restructuring the chromatin landscape in the regions where they bind, either by allowing the binding of other TFs or by inducing locus-specific DNA demethylation. However, the success of the reprogramming process requires complete erasure of the existing somatic epigenetic memory followed by the formation of a new epigenetic signature. Therefore, although ectopic expression of TFs such as OSK can change cell fate, chromatin modifications are still a well-described barrier to the reprogramming process (Mikkelsen *et al.*, 2008; Pasque *et al.*, 2012; Chen *et al.*, 2013; Gaspar-Maia *et al.*, 2013; Sridharan *et al.*, 2013).

The low reprogramming efficiency of some cell types, including melanocytes, neural stem cells, adipose stem cells, meningiocytes, keratinocytes and fibroblasts (Aasen *et al.*, 2008; Kin *et al.*, 2008; Sun *et al.*, 2009; Utikal *et al.*, 2009; Qin *et al.*, 2008), has prompted scientists to look for not only better reprogramming methods but also highly reprogrammable and better accessible tissues. The advantages and disadvantages of reprogramming different human cell types are still uncertain, but a specific cell type might result in a better reprogramming efficiency. The umbilical cord and vessels of the placenta originate from the hypoblast, while the amniotic membrane of the placenta and the foetus originate from the epiblast. The amniotic membrane contains a layer of epithelial cells surrounding the amniotic cavity, and the internal layer is formed of mesenchymal-like cells. The trophectoderm, the outer layer of the blastocyst (embryo), is responsible for implantation of the embryo in the mother's uterus and also gives rise to extra-embryonic tissues, and its cells may retain an immature phenotype while the embryo itself develops. Thus, the placenta and umbilical cord, normally discarded after birth, contain a valuable source of cells with stem-cell-like properties (Red-Horse *et al.*, 2004; Can

& Karahuseyinoglu, 2007; Yen *et al.,* 2005; Fukuchi *et al.,* 2004; Miki & Strom, 2006), and they may represent a better choice of cells for reprogramming and a useful tool for cross-comparisons with iPSCs generated from other tissues. Moreover, it is interesting to think that extra-embryonic tissues are less differentiated and carry fewer mutations than adult somatic cells; thus, iPSCs from these sources can be more faithfully reprogrammed. Likewise, neonatal tissues, such as umbilical cord, are commercially stored, and they could perhaps be used for future personalized stem cell-based therapies (Cai *et al.*, 2010).

Another important factor in the successful generation of iPSCs is the reprogramming method used (Table 1.1). The method should be chosen according to the goals of the research project and whether the presence of integrated sequences will hold back the applications of the iPSC line. If the iPSC line is generated for research purposes, with no translational aim, a viral infection with the STEMCCA (stem cell cassette expressing OSKM) will be adequate, as this method works well for multiple cell types. On the other hand, if the research goal has translational purposes, the reprogramming method chosen should cause no genome-sequence modifications (Malik and Rao, 2013). A variety of methods for delivering transcription factors to somatic cells have been reported. Some are classified as integrating methods, which involve the integration of genetic material; others are classified as non-integrating and involve no genetic modifications of the target cells. The original method of reprogramming murine fibroblasts by Takahashi and Yamanaka used a retrovirus as a vector, an integrating method, to transduce the four transcription factors OSKM into mouse fibroblasts (MEFs). Other integrating methods of reprogramming are excisable lentiviral and adenovirus vectors. Non-integrating methods include direct protein transduction (Kim *et al.,* 2009), episomal vectors (Yu *et al.,* 2009), RNA-based Sendai virus (Fusaki *et al.,* 2009), micro-RNA transfection (Anokye-Danso *et al.,* 2011; Miyoshi *et al.,* 2011) and mRNA-based methods (Warren *et al.,* 2010).

Table 1.3 Summary of reprogramming methods for derivation of iPSCs

Delivery Method	*Advantages*	*Disadvantages*
MMLV-derived retrovirus	Very efficient	Genome integration; infects dividing cells; random viral integration with risk of mutagenesis
Adenovirus	Infects dividing and non-dividing cells; transgene-free and vector-free; no genomic integration	Slow and inefficient
Lentivirus	Infects dividing and non-dividing cells; very efficient	Genome integration with risk of mutagenesis
Protein	Non-integrating	Low efficiency; slower reprogramming kinetics; short protein half-life; requires multiple transfections
Sendai virus	Non-integrating RNA virus; high efficiency	Multiple passages are required to eliminate viral transgenes; virus biosafety concerns
mRNA	Non-integrating; non-virus; high efficiency; fast kinetics	Requires multiple transfections; requires use of B18R to suppress interferon response
miRNA	Non-integrating; non-virus; no overexpression of transcription factors	Low efficiency; requires multiple transfections
Minicircle vectors	Non-integrating; non-virus	Works for a few cells; super-low efficiency
PiggyBac transposon	Non-virus; non-integrating; good efficiency	Works for a few cells; low efficiency
Episomal plasmid	Non-integrating; non-virus	Super-low efficiency; requires transfections daily for long period of time

The rapid advances in iPSC technology in regenerative medicine have motivated many exciting research advances, and the major two applications of iPSCs are as follows: (1) to develop human disease models that can be used to better understand the disease and also to provide more accurate toxicity assessment of new drugs, leading to new treatments, and (2) to treat diseases or injuries, i.e., cell-based therapy; however, the iPSCs must be fully differentiated into a tissue-specific cell type before use in cell therapy. In 2014, in a Japanese clinical trial, the first patient received a transplant of iPSC-derived retinal pigmented epithelial cells for age-related macular degeneration, which was the first of its kind using iPSC-based therapy and without any report of adverse effects (Bahmad *et al.*, 2017; Li and Belmonte, 2016).

1.8 Differentiation of iPSCs into MSCs

To address the limitations of the *in vitro* expandability and uniformity of MSCs, Zhao *et al.* (2015) and Luzzani *et al.* (2015) derived MSCs from iPSCs that can be expanded consistently and provide cell banks from a single cell clone. We have chosen these two protocols because the modifications from previous reports of ESCs and iPSCs differentiated MSCs (de Peppo *et al.*, 2013; Sanchez *et al.*, 2011) lead to better results.

Zhao *et al.* (2015) reported a protocol capable of producing highly enriched MSC-like cells with high efficiency, without the invasion and stemness of cancer cells as is seen with BM MSCs. Moreover, their iPSC MSCs expressed lower levels of pro-tumour factors, including IL-6, prostaglandin E2 (PGE2) and hyaluronan, than BM MSCs, revealing an alternative and valuable source of MSCs. They adapted the protocol from Sanchez *et al.* (2011), who reported that inhibition of *SMAD-2/3* signalling promoted derivation of MSCs from ESCs. They used a chemically defined medium supplemented with *SMAD-2/3* inhibitor. *SMAD* is a transcription factor involved in TGFβ signalling, and it plays an important role in directing fate decisions for MSCs. TGFβ is considered a potent inhibitor of haematopoiesis, a mesodermal tissue and Sanchez *et al.* (2011) hypothesized that inhibition of *SMAD-2/3* would have an effect similar to that in the hematopoietic system, generating MSCs from PSCs. However, their protocol was not xeno-free, and their medium and coating matrix, for cellular attachment and growth, contained animal-derived products. Because the aim of our experiment was to derive MSCs for clinical purposes, we adapted their protocol to xeno-free conditions.

Luzzani *et al.* (2015) developed a simple protocol of derivation of pluripotent-derived (PD) MSCs using only human platelets and B27 (Thermo Fisher) as supplements, a xeno-free derivation. Human platelets (HPLs) are known to produce significant levels of growth factors (Rauch *et al.*, 2011; Iudicone *et al.*, 2014). B27 is a supplement made with 21 ingredients, including hormones such as corticosterone, fatty acids such as linoleic acid and L-carnitine, as

well as insulin and glutathione, and it supports neuronal cultures (Chen *et al.*, 2008). This protocol generated significant numbers of cells in a consistent and robust way in only 3 – 4 weeks at low cost. The group also performed parallel tests using the same protocol but with foetal bovine serum (FBS) as a supplement; however, the growth rate of those cells was much lower than with HPL. Because MSC autologous therapies often require large and repeated doses, a limitless source of MSCs generated from an individual could offer an economical and valid alternative. We used this second protocol to differentiate iPSCs into MSCs and subsequently compared them to iPSC MSCs derived using the protocol adapted from Zhao *et al.* (2015).

Currently, Australian company Cynata is testing their technology of producing mesenchymoangioblasts (MCAs) from a single-donor iPSC at a commercial scale. The clinical trials for GvHD using these cells are already underway, with promising results, in the U.K., U.S.A., Japan and Australia, showing that these technologies are valuable for the future of cell therapy.

Aims and objectives

The overall goal of the project is to investigate the potential of WJ MSCs in cellular therapy.

We hypothesized that WJ MSCs

- Have the potential to replace BM MSCs for clinical applications and
- Can be reprogrammed into iPS cells suitable for clinical applications.

The first aim of the project is to critically assess WJ MSCs as a potential replacement for BM MSCs in cellular therapy.

Objectives:

1) To develop chemically defined, animal-product-free culture conditions for derivation and expansion of WJ MSCs.
2) To compare the expression profile of putative MSC "markers" in clinical-grade BM MSCs with that of WJ MSCs grown under animal-product-free conditions.
3) To determine the proliferative potential of WJ MSCs cultured under chemically defined, animal-product-free culture conditions.
4) To test the adipogenic, osteogenic and chondrogenic differentiation potential of WJ MSCs grown under chemically defined, animal-product-free culture conditions.
5) To assess the immunomodulatory potential of WJ MSCs grown under chemically defined, animal-product-free culture conditions.

The second aim of the project is to critically assess WJ MSCs as a potential tissue source for clinical-grade iPSCs.

Objectives:

1) To develop a reprogramming protocol in chemically defined, animal-product-free culture conditions using a genome non-integrating delivery system.
2) To determine the reprogramming efficiency of various WJ MSC fractions.
3) To compare the transcriptome profile and differentiation potential of WJ MSC-iPSCs with clinical-grade hESCs derived under GMP conditions in our laboratory.

CHAPTER 2

2. EXPERIMENTAL PROCEDURES

2.1 HUMAN TISSUE PROCESSING AND CELL CULTURE

2.1.1 Umbilical cord (UC) collection

The National Health Service Research Ethics Committee protocol 12/NE/0371 was used for isolation and derivation of WJ MSC and 14/SW/0042 was GMP compliance of the protocol. The protocols include reprogramming and characterization of iPSCs. Informed consent was obtained in the morning before the scheduled Caesarean sections (C-section) of Caucasian healthy women at gestational age ≥ 37 weeks. We collected the UCs from C-sections only to minimize bacterial contamination.

After C-section delivery, whole placenta with the attached UC was inspected by the nurse in charge for any possible anomalies. After inspection, she consented to proceed with collection. Subsequently, a 10 -20-cm piece of the UC was cut and placed immediately inside a sterile 500-ml bottle containing PBS (ThermoFisher, cat. no. 10010023). The cord was then rinsed twice, in the same bottle, with PBS to eliminate any remaining blood. The bottle containing the UC in PBS supplemented with gentamicin/amphotericin solution (ThermoFisher, cat. no. R01510) was transported inside a Bio Carrier Bag at room temperature (RT) to the laboratory.

2.1.2 Material and Medium preparation for MSC derivation

We cultured UC explants under three different conditions.

1) Chemically defined, xeno-free conditions (dXF): We used the xeno-free (XF) defined culture medium StemGro (Corning, cat. no. 40-410-KIT) and CTS CELLstart substrate (ThermoFisher, cat. no. A1014201)-coated 100-mm tissue culture dishes (Corning, cat. no.

430167). The CELLstart was diluted according to manufacturer's instruction. Briefly, 133.4 µl of CELLstart was diluted in 10 ml of Dulbecco's Phosphate Buffered Saline with calcium and magnesium (DPBS $^{+Ca\ +Mg}$) (Thermo Fisher, cat. no. 14040133). Subsequently, the plate was incubated for a minimum of 1 h 45 min and a maximum of 2 h at 37°C with 5% O_2.

2) Non-defined, XF conditions (nXF): we used Alpha Minimum Essential Medium Eagle (α MEM) (ThermoFisher, cat. no. 32561029) supplemented with 5% GMP graded Human Platelet Lysate (hPL) (Stemulate; Cook Regentec, cat. no. G35220).

3) Standard (STD) conditions: we used Dulbecco's Modified Eagle Medium (DMEM) (ThermoFisher, cat. no. 41965039) supplemented with 10% foetal bovine serum (FBS) (HyClone; GE Healthcare, cat. no. SH3007).

2.1.3 Plating UC explants

The bottle containing the UC was placed inside a biosafety cabinet, and the UC was transferred into a 140-mm dish (Nunc, cat. no. Z717231). We cut the cord into three equal pieces and washed each piece thoroughly with PBS until any remains of blood were eliminated. Each piece of the cord was cut open longitudinally with a sterile scalpel to expose the Wharton's jelly (WJ) and then sliced into 0.5 - 1 cm^3 pieces. Ten to fifteen pieces (explants) were transferred into a pre-labelled 100-mm dish that had been previously coated with CTS CELLstart for dXF conditions and/or into a pre-labelled 100-mm tissue culture dish without any coating for nXF and/ or STD conditions. To facilitate the attachment of the UC to the plastic surface, the plated explants were exposed to air inside the biosafety cabinet for 5 - 10 min before slowly adding 15 - 25 ml of cell culture medium (Reinisch and Strunk, 2009).

Three conditions, dXF, nXF and STD, as described before, were tested. After covering the plated explants with the appropriate medium, the plates were transferred to an incubator (Heraus) and cultured at 37 ˚C with 5% or 20% O_2.

2.1.4 WJ MSC derivation, passaging, counting of cells, cryopreservation and thawing

We replaced the explant medium freshly every 3 days until cell outgrowth was observed under a phase contrast microscope. The WJ MSCs were expanded for 7 - 14 days before the first passaging.

For cell passaging, we first washed the cell monolayer with pre-warmed DMEM and then incubated it in Tryple Select (ThermoFisher, cat. no. 12604-021) for 3 min at 37°C. The Tryple Select was then diluted in an equal amount of pre-warmed DMEM. Cells were collected, counted and centrifuged at 160 *g* for 5 min. The cell pellet was resuspended according to the number of cells in complete medium and seeded into a new cell culture flask or resuspended in freezing solution for cryopreservation. For freezing, we froze 0.8 - 1 x 10^6 cells/ vial. For passaging, 1:3 ratios were used, i.e., one confluent T75-cm^2 flask (between 1 - 3 x 10^6 cells) (Corning, cat. no. 3276) was seeded into three T75-cm^2 flasks (between 0.33 - 1.0 x 10^6 cells/ flask).

For cell counting, the cells were resuspended in growth medium and counted using a haemocytometer (Hausser). Population doublings (PDs) were calculated according to the formula: PD = [log (A/B)] / 0.301, where A is the number of cells harvested and B is the number of cells seeded into the plate.

The cells grown under STD conditions were frozen in 10% DMSO (Merck, cat. no. D4540) in FBS, whereas the cells grown under nXF or dXF conditions were frozen in Cryostor CS10 (Merck, cat. no. C2874) and stored in liquid nitrogen (LN_2). For freezing, we resuspended

1 x 10^6 cells/ ml in freezing solution and aliquoted them into Nalgene freezing vials (ThermoFisher, cat. no. 5000-1012). Subsequently, the vials were stored in a freezing container, Mr. Frosty™ (ThermoFisher), for the first hour at -20°C and then transferred to -80°C freezer for at least 4 h, prior to being transferred into LN_2 for extended storage at -196°C.

For thawing, the cryovial was thawed inside the incubator at 37°C for 5 min. Subsequently, the thawed contents of the vial were transferred to a 15-ml conical tube (Thermo Scientific) containing 5 ml of pre-warmed DMEM and centrifuged at 160 *g* for 5 min. The cell pellet was resuspended in complete medium and seeded into a new cell culture flask or plate.

2.1.5 Maintenance of WJ MSCs

Cells were ready for passaging when they reached 60 - 80% confluence levels, and the subculture was performed based on the general methods described above. Before plating, the cells were counted, and the concentration was readjusted to 0.5 - 1.0 x 10^6 cells/ ml. Next, typically 1 ml of resuspended cells was seeded in a new flask, and the remaining cells were frozen. WJ MSCs used for the reprogramming protocol in this study were no older than passage number 6 (PD = 16).

2.1.6 Culture of Bone Marrow MSCs

The human bone marrow (BM) MSCs used in this study were derived and donated by the Department of Haematology, Imperial College London. The BM MSCs were used as part of a collaboration agreement with Prof. Dr. Francesco Dazzi and Dr. Antonio Galleu.

Human BM MSCs were cultured in DMEM supplemented with 10% hPL. The medium was exchanged every 4 - 5 days, and the cells were ready for subculture when the monolayer

reached 60 - 80% confluence. To passage BM MSCs, the same procedure for WJ MSC as described above (section 2.1.4) was followed.

2.1.7 Culture of the Kasumi Cell line

During this study, we also used the commercially available cell line Kasumi (ATCC-CRL-2724), which was generated from the peripheral blood of an acute myeloid leukaemia patient. Cells were maintained in RPMI-1640 medium (ThermoFisher, cat. no. 11875093) supplemented with 20% FBS. Fresh medium was added every 2 days, and the cells were passaged after 5 to 7 days in culture. These cells were used as a positive control for CD34 and CD45 markers to establish the correct populations of cells by flow cytometry.

2.1.8 Culture of Dermal Fibroblasts

During this study, we used commercially available fibroblast primary cells: the BJ cell line (ATCC, cat. no. CRL-2522). Cells were recovered for culture by transferring the purchased cryovials from liquid nitrogen to the incubator at 37°C until most of the cells were thawed. The cells were then transferred into a 15-ml conical tube containing 5 ml of pre-warmed fibroblast medium and then centrifuged at 160 *g* for 5 min to wash away the DMSO, followed by aspiration of the supernatant and cell pellet resuspension in 10 ml of fibroblast medium. The resuspended cells were then transferred to a T75-cm^2 flask for further expansion. The medium was changed every other day.

The fibroblasts were ready for subculture when the monolayer reached 80 to 90% confluence based on the above-described WJ MSC protocol. The passage number used for generation of iPSC lines was no more than passage number 6.

To passage dermal fibroblasts, the same procedure for WJ MSCs as described above (section 2.1.4) was followed.

2.1.9 Human Embryonic Stem Cells (hESCs)

The human embryonic stem cell line (hESC) used in this study was KCL034, a hESC line derived in the Stem Cell Laboratory at King's College London with Guy's Hospital ethical approval (06/Q0702/90) under Human Fertilisation and Embryology Authority (HFEA) research license R0133 (Devito *et al.*, 2014; 2016).

The KCL034 cell line was grown on Vitronectin XF™ (STEMCELL Technologies, cat. no. #07180 kit), a defined XF cell culture coating matrix For Vitronectin XF coating, the matrix was diluted in CellAdhere buffer provided with the kit to a final concentration of 10 µg/ ml (i.e., 40 µl of matrix in 1 ml of buffer). We coated each well of a non-tissue culture-treated 6-well plate with 1 ml and incubated the plate at RT for at least 1 h at 37˚C, 5% O_2. The excess coating was then removed from each well, and the well was gently washed once with 1 ml of CellAdhere buffer before plating the cells. The culture medium used for expansion and maintenance of hESCs was TeSR2™ (STEMCELL Technologies, cat. no. #05860). To improve the recovery of cryopreserved hESCs, we added the ROCK inhibitor Y-27632 dihydrochloride (Santa Cruz, cat. no. CAS129830-38-2) to a final concentration of 10 µM in the culture medium in the first 24 h of culture.

When the hESC colonies were large and beginning to merge, normally at 4 to 6 days after initial seeding, we performed enzymatic passaging using dispase (STEMCELL Technologies, cat. no. #07923) at a concentration of 1 U/ml. The culture medium was aspirated, and the cell monolayer was rinsed twice with pre-warmed DMEM. Dispase was added to the well (1 ml per well in a 6-well plate), followed by incubation at RT for 1 min. Subsequently,

the dispase was aspirated, and the cell monolayer was rinsed twice with pre-warmed DMEM to wash away any residue. In the last step, TESR2 was added to the well, and the cells were removed with the assistance of a cell lifter (Corning, cat. no. 3008). The colonies were detached and disaggregated into a smaller cluster of cells by gently pipetting up and down. Finally, we plated the cells and distributed them evenly into a new Vitronectin XF-coated 6-well plate. Between 1 – 1.5 x 10^5 cells were plated into each new well of a 6-well plate. The colonies were expanded for further procedures such as immunocytochemistry and cell differentiation.

2.2 CHARACTERIZATION OF NATIVE WJ MSCs (nMSCs)

2.2.1 Flow Cytometry

Using flow cytometry, we analysed cell surface epitope profiles to compare nMSCs isolated under different conditions.

To determine the correct antibody concentration and avoid wasting antibodies, we titrated each antibody used in this experiment. The concentration of all antibodies was not given, and the manufacturers' recommended dilution was 1:11 for up to 1 x 10^7 cells/100 µl. Using the recommended dilution as the starting point, three more concentrations were tested (1:25; 1:50 and 1:100). The dilution of 1:25 (4 µl of the antibody into 100 µl of PBS) was found to be the best dilution for all antibodies.

Using a FACS CANTO II and FACSDIVA software (BD Biosciences), the expression of cell surface molecules was evaluated on WJ MSCs (STD, nXF and dXF conditions) in different passages, and BM MSCs and dermal fibroblasts were used for comparison. For this purpose, 1 x 10^6 cells were resuspended in 100 µl of ice-cold PBS supplemented with 10% FBS and then mixed with the appropriate primary antibody (Table 2.2.1). Subsequently, they were incubated in the dark for 15 min at RT. After washing with PBS, the cells were resuspended in

500 µl of ice-cold PBS with 10% FBS. All antibodies used in the flow cytometry experiment were purchased from Miltenyi Biotech.

The data were analysed using FACSDIVA software. Briefly, using the most common parameters to estimate cell size, forward scatter (FSC) and side scatter (SSC), we selected only viable, single cells events and eliminated dead cells and cell debris from the analyses. Moreover, gating controls were established with positive and negative controls to determine the correct signal.

Four different fluorophores were used for this experiment: allophycocyanin (APC); fluorescein isothiocyanate (FITC), phycoerythrin (PE or R-PE) and Violet or Pacific Blue (e-Fluor) (Figure 2.2.1).

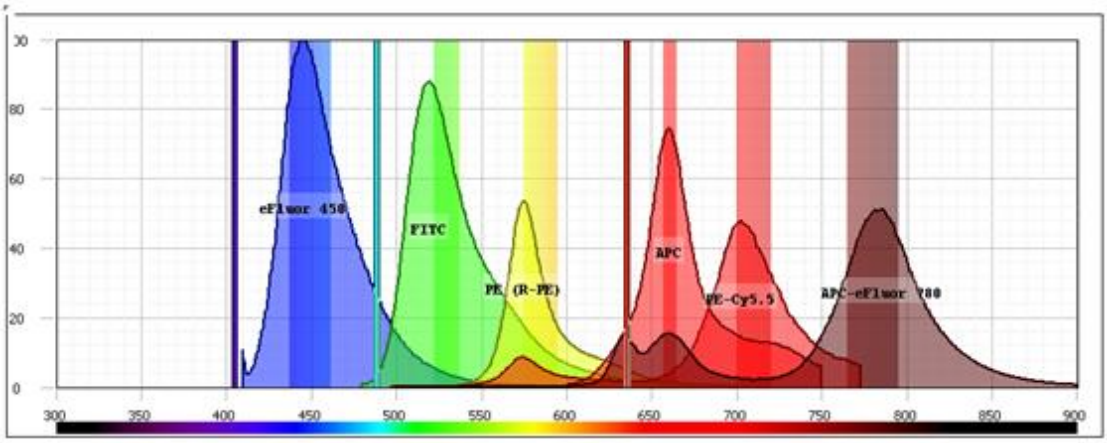

Figure 2.2.1 Map of the multicolour spectral overlap of the fluorophores. Map showing absorption/ emission (wavelengths) spectra of the fluorophores used for flow cytometry (Parenteau, 2011). APC, allophycocyanin; FITC, fluorescein isothiocyanate, PE, phycoerythrin; e-Fluor, Violet or Pacific Blue.

Table 2.1 Antibodies used for Flow cytometry. The antibodies were diluted in PBS with 10% FBS. All antibodies used in the flow cytometry experiments were purchased from Miltenyi Biotech. APC, allophycocyanin; FITC, fluorescein isothiocyanate, PE, phycoerythrin

Antigen Cat.no.	fluorophore conjugate
CD90 130-095-403	*FITC*
CD105 130-094-926	*APC*
CD73 130-095-182	*PE*
CD44 130-095-195	*FITC*
CD29 130-101-280	*APC*
CD56 130-100-698	*APC*
MSCA-1 130-093-587	*PE*
CD45 130-080-202	*FITC*
CD34 130-081-002	*PE*

Table 2.2 Markers for characterization of MSCs (adapted from Feng-Juan *et al.*, 2014)

Marker	***What?***	***Where?***	***Comment***
CD90	Cell surface glycoprotein	Subset of fetal liver cells and fetal thymocytes, fibroblasts, MSCs, activated endothelial cells, and some leukemia cell lines. $CD34^{+}CD90^{+}$ cells are primitive hematopoietic stem cells	Promotes T cell activation and is involved in cellular adhesion, neurite outgrowth, migration, cell death, and tumor growth.
CD105	Cell membrane glycoprotein (also known as endoglin)	Endothelial cells, some bone marrow cells, MSCs and activated macrophages	A receptor for transforming growth factor (TGF) beta
CD73	Membrane-bound enzyme	Present on subsets of T and B lymphozytes, follicular dendritic cells, endothelial cells and MSCs	The encoded protein is used as a determinant of lymphocyte differentiation.
CD44	Cell-surface glycoprotein involved in cell–cell interactions, cell adhesion and migration	Found in stem cells (including MSCs); normal adult and fetal tissue; cancer cells	A receptor for hyaluronic acid (HA)
CD29	Integrin beta-1 is a protein that in humans is encoded by the ITGB1 gene	Involved in cell adhesion and recognition in a variety of processes including embryogenesis, hemostasis, tissue repair, immune response and metastatic diffusion of tumor cells	ITGB1: Integrins are ubiquitously expressed adhesion molecules
CD56	Neural cell-adhesion molecule (NCAM)	Marker for natural killer, muscle cells and neural cells. Expressed in BM MSCs.	MSCA-$1^{+}CD56^{+}$ MSC were able to differentiate into adipocytes. MSCA-$1^{+}CD56^{+}$ MSC may be used as the starting population of choice for the treatment of several diseases, in particular for rheumatoid arthritis, trauma, acute osteochondral fractures, and spinal disk injuries.
MSCA1	Mesenchymal stroma cell antigen 1	MSCs and ESCs	MSCA-1 is identical to tissue non-specific alkaline phosphatase (TNAP), an ectoenzyme known to be expressed at high levels in liver, bone, and kidney as well as in ESCs

2.2.2 Mitogen-induced proliferation assay

To evaluate the nMSC immunosuppressive potential *in vitro*, human peripheral blood mononuclear cells (PBMCs) were isolated from leukocyte cones purchased from the National Blood Service, UK. Leukocyte cones were diluted 1:1 with PBS and layered on Histopaque (Merck, cat. no. 10831) for density gradient separation.

We performed the PBMC proliferation assays in 0.2 ml of medium (RPMI supplemented with 10% HPL) per well of a 96-well flat-bottom plates (Corning Costar, cat. no. CLS3596). The vial of PBMCs was thawed at 37°C, and the cells were washed in PBS and then resuspended at a concentration of 1 x 10^6 cells/ ml. Native MSCs from four donors derived under dXF conditions and three clinical grade BM MSCs were serially diluted and plated overnight. A total of 5 x 10^5 PBMCs per well were added to nMSCs to obtain co-cultures with increasing PBMC/nMSC ratios from 10:1 to 80:1. PBMCs were then stimulated with 5 μg/ml phytohaemagglutinin (PHA; Sigma, cat. n. L8754), and after 72 h, proliferation was measured by the incorporation of radiolabelled [^{3}H]-thymidine (TdR; Amersham Bioscience, no cat. no.) during the final 18 h of incubation. Briefly, cell cultures were pulsed with 0.5 μCi/well of [3H]-TdR for 18 h before the cultures were harvested onto a glass fibre Wallac filter mat A (Perkin-Elmer, cat. no. 1450-421) using a Skatron 96-well plate automated cell washer (Molecular Devices). Scintillation fluid was added, and [3H]-TdR incorporation was measured by liquid scintillation spectroscopy on a counter (Wallac Quantulus). The results are expressed as the percentage of control proliferation for triplicate cultures. Cultures of stimulated PBMCs without nMSCs were used as a positive control.

The relative proliferation of each PBMC/nMSC ratio was calculated using the following formula: A/B x 100, where A is the proliferation at one specific PBMS/nMSC ratio and B is the proliferation of the positive control. The percentage of inhibition was then calculated by subtracting the percentage of proliferation from 100 (maximum of inhibition).

2.3 GENERATION OF INDUCED PLURIPOTENT STEM CELL (iPSC) LINES

2.3.1 Preparation of NuFF as a feeder-layer and for medium conditioning

Mitotically inactivated new-born foreskin fibroblast (NuFF) vials with 4 - 5 x 10^6 cells (Global Stem, cat. no. GSC-3001G) were recovered per the manufacturer's instructions. Briefly, the vial was thawed inside the incubator at 37°C for 5 to 6 min. Subsequently, we transferred the thawed contents of the vial to a 15-ml conical tube containing pre-warmed DMEM, followed by centrifugation at 160 *g* for 5 min. We aspirated the supernatant, and the cells were resuspended at a concentration of 1 x 10^6 cells/ ml (4 – 5 ml) in DMEM supplemented with 10% FBS.

NuFFs were used either to condition the Pluriton™ Reprogramming Medium (Stemgent, cat. no. 00-00070), a chemically defined serum-free medium, and/or used as feeder-layer to support newly transduced WJ MSCs on day 7 of Sendai virus reprogramming.

For medium conditioning, 4.0 - 4.5 x 10^6 of NuFF were plated in a T75 flask in 12 ml of DMEM supplemented with 10% FBS, and they were incubated for 24 h at 37°C with 5% CO_2. Next, the attached NuFFs were rinsed twice with PBS to remove any residual FBS before supplementation with 30 ml of Pluriton with 4 ng/ml of recombinant human fibroblast growth factor basic protein (rhFGF) (Bio-techne, cat. no. 233-FB-025). After every 24 h of incubation, we collected the medium, and fresh Pluriton medium with rhFGF was added. After 7 to 10 days, we pooled all the daily aliquots, which were then filtered by a bottle-top vacuum 0.22 μm filter (Corning, cat. n. CLS430624), aliquoted into 30-ml aliquots and frozen at -20°C.

2.3.2 Reprogramming by Sendai Virus (SeV)

SeV carrying four transcription factors, OCT3/4, SOX2, KLF-4 and c-MYC, was used to promote the reprogramming of primary donor nMSCs. The entire system is commercially available as a kit CytoTune™ - iPS Reprogramming Kit (ThermoFisher, cat. no. A16517) that contains all the synthesized transcription factors listed above.

The protocol was followed per the manufacturer's instruction with a few modifications. Briefly, the reprogramming timeline (Table 2.3 and Figure 2.3.1) describes the steps required to produce iPSCs using the reprogramming kit.

The CytoTune kit recommends the use of iPSC medium from day 7 after transduction onwards. However, according to our own experience with previous reprogramming protocols, we decided to switch to Pluriton Reprogramming medium (Stemgent), which is normally used in the mRNA reprogramming Factors Set™ (Stemgent). Pluriton supports the emerging colonies very well (day 8 to 21) and is conditioned in NuFF as described previously.

The protocol recommends 'Fibroblast' medium (see Appendix) for the first 7 days after transduction. However, this medium contains FBS and could not be used for our XF conditions. Therefore, FBS was replaced with the CTS KnockOut™ SR XF (ThermoFisher, cat. no. 12618013), a supplement that maintains the pluripotency, normal morphology, and karyotype of human pluripotent stem cells.

Inactivated human foreskin fibroblast (HFF) feeder layers (described further on 2.3.3) were used to allow the expansion and propagation of iPSC lines. The primary iPSC colonies showing defined colony edges, uniform and compact cells were manually picked using a hypodermic needle and re-plated onto 4-well plates containing the HFF feeder layer. We used hESC defined medium or KOSR medium (see Appendix) for the culture and expansion of the cells in this step.

Table 2.3 Reprogramming timeline of modified CytoTune - iPSC Reprogramming kit		
Description	***Day***	***Activity***
Prepare cells for transduction	**- 2**	Plate 2 or 3 wells (6-well plates) of target cells at different densities (1.5 to 2 x 10^5 cells/ well) in XF Fibroblast medium. The cell number on the day of transduction should be less than 5 x 10^5 cells/ well
Transduction of cells	**0**	Choose the best well among the 2 or 3 (70% confluence). The additional wells can be collected, counted and snap frozen for use as a negative control in RT-PCR. Add the indicated volumes (according to the manufacturer's manual, the titre of each vector is lot-dependant) of each of the four CytoTune Sendai tubes to 2 ml of XF medium
Replace medium	**1**	Replace the medium (XF Fibroblast media) with fresh medium 24 h after transduction and daily until day 7
Prepare NuFF feeders	**5**	Plate NuFF feeders in P60 culture dishes at a density of 3 x 10^5 cells/ dish. Prepare two P60 NuFF dishes per transduced well
Plating transduced cells onto feeders	**7**	The transduced cells (one well) are plated onto two P60 NuFF feeder dishes Transduced cells from the additional wells can be collected and snap frozen for use as a positive control in RT-PCR Pluriton NuFF conditioned medium is used from now on until day 21 to 28. Replace medium daily
Emerging colonies	**8 - 28**	iPSC colonies were allowed to grow and expand in culture with daily exchange of the medium

Picking and passaging iPSC colonies	**22 to 28**	Primary iPSC colonies with the best morphology (uniform and compact cells) were manually picked and passaged onto HFF feeder-layer plates (2 x 10^5 cells/well).

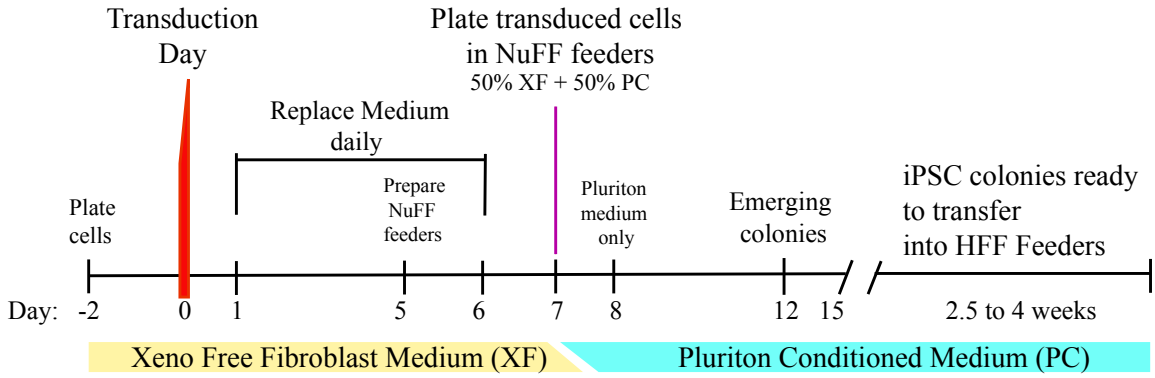

Figure 2.3.2 Reprogramming timeline of the production of iPSCs. Figure adapted from Life technologies website CytoTune™ - iPS Reprogramming Kit (thermofisher.com, 2017).

2.3.3 Preparation of HFF as a feeder layer

Mitotically inactivated human Foreskin fibroblasts (HFFs) were used as feeder layer to support the expansion and growth of iPSC colonies after their generation. Those cells were expanded and frozen in the Stem Cell Laboratory at King's College London.

The frozen vial containing 1 x 10^6 HFF cells with PD 7.3 was thawed in the incubator at 37 ˚C for 5 min. Subsequently, we transferred the cells from the vial into a 15-ml conical tube containing 5 ml of pre-warmed DMEM. A 20-µl aliquot was acquired for subsequent cell counting. After centrifugation at 160 *g* for 5 min, the supernatant was aspirated, and the cells were resuspended in sufficient HFF medium (DMEM with 10% FBS) to achieve a concentration of 1 x 10^5 cells/ml.

For plating, we coated 4-well plates with CELLstart as described in section 2.1.2. The cells were seeded in a number of 2 x 10^5 cells per well (200 µl of resuspended cells/ well) and then transferred to the incubator (Heraus) for culture at 37 ˚C with 5% O_2. The feeder layer was ready to use after 48 h. The HFF feeder medium was replaced every 3 days, and the feeder-layer plates were used within a maximum of 2 weeks from generation.

2.3.4 iPSC expansion, maintenance and cryopreservation

Before picking the iPSC colonies, the HFF feeder-layer plates were rinsed twice with pre-warmed DMEM to eliminate any trace of FBS in the culture, and Pluriton and KOSR complete media were added at a 50:50 ratio. The plate was equilibrated for a minimum of 1 h at 37 ˚C with 5% O_2 before the procedure.

Using a hypodermic needle or a pipette tip, we manually picked the iPSC colonies and replated them onto the 4-well plates of the HFF feeder layer. They were then cultured for the first 2 days in a mixture of Pluriton and KOSR complete media at a 50:50 ratio for gradual

adaptation in the new medium. Following the first 2 days, the iPSCs were cultured in pure KOSR medium.

The iPSC colonies were ready for passaging onto new feeders or to be adapted feeder-free either when there were an excessive number of colonies per well or when the colonies in each well reached an average size of 300-400 cells per colony as estimated visually, showing delimited borders, a dense centre with bright phase compared with their edges.

For feeder-free adaptation, we manually picked up the colonies and subcultured them in Vitronectin XF-coated dishes. For the first 2 days after plating, the cells were cultured in KOSR complete medium and TESR2 at a 50:50 ratio before replacing it with pure TESR2. Any differentiation parts were scraped mechanically using a pipette tip and discarded.

When iPSCs in feeder-free conditions reached higher densities, which normally occurred at 4 to 6 days after initial seeding, they were passaged and/or frozen. The same procedure of enzymatic passaging for hESCs with dispase as described in section 2.1.9 was used for iPSCs.

For cryopreservation, cells were frozen in Cryostor CS10 (Merck, cat. no. C2874) and stored in LN_2. A total of 1 x 10^6 cells was resuspended in 1 ml of freezing solution and transferred into Nunc 1-ml freezing vials (Thermo Fisher, cat. no. 374081). Next, the vials were stored in a freezing container, Mr. Frosty™ (Thermo Fisher, cat. no. 5100-0001), for the first hour at -20°C and then transferred to a -80°C freezer for at least 4 h before being transferred into liquid nitrogen for storage.

2.4 VITRIFICATION OF FEEDER-DEPENDANT iPSC COLONIES

The iPSC colonies (on the HFF feeder layer) were vitrified at passage 2 and/or 3 to preserve earlier passages of the line and to avoid loss of the line due any possible drawback. We vitrified at least 10 - 15 straws for each iPSC line.

The colonies to be vitrified were cut into smaller pieces using a pipette tip or a hypodermic needle and placed inside a well (4-well plate) containing ES-HEPES solution (see Appendix).

Before starting the process of vitrification, we prepared two lines of 30 µl microdrops each, one with 10% and another with 20% vitrification solution (see Appendix) using a 4-well plate lid. Subsequently, a timer was set to start for 1 min and 25 sec. Immediately, 4 to 8 iPSC colony pieces were transferred to the first microdrop containing 10% vitrification solution for 1 min. When the timer reached the last 25 sec, all iPSC pieces were then transferred to the adjacent microdrop with 20% vitrification solution. When the timer ended, the pieces were aspirated into a labelled vitrification straw using capillary action, followed by plunging into LN_2 (using a portable Dewar or a Styrofoam box). Once all the colonies were vitrified, the straws were then placed inside labelled 4,5-ml Nunc Cryogenic tubes (Thermo Scientific, cat. no. 337516) and transferred to the appropriate Dewar for extended storage.

2.5 ANALYSIS OF SeV GENE EXPRESSION IN iPSC LINES

To confirm that the generated iPSC lines were vector-free, we investigated the expression of SeV by initially isolating RNA from all iPSC lines followed by reverse transcription polymerase chain reaction (RT-PCR) using the Precision nanoScript2 Reverse Transcription kit (Primerdesign, no cat. no.) and GoTaq Green Master Mix (Promega, cat. no. M712).

2.5.1 Isolation of Total Cellular RNA

Prior to starting the RNA extraction, the bench and all equipment (i.e., pipettes) were wiped with RNA-Zap (Thermo Fisher, cat. no. AM9780) to remove any RNase enzymes present on the workstation. All samples containing RNA were stored at -80°C, and the number of times the samples were freeze-thawed was maintained at a minimum. Total RNA was isolated from cells using the QIAgen RNeasy Mini kit (Qiagen, cat. no. 74104) according to the manufacturer's instructions. This protocol uses a silica-based membrane and a series of high salt buffers that enable binding of up to 100 µg of RNA (over 200 bases in length). Briefly, 1 ml of lysis buffer (RLT) containing 10 µl/ml β-mercaptoethanol was added to the cell pellet. The cell lysate was then homogenized by pipetting the lysate through a QIAshredder spin column (QIAgen) and centrifugation at RT for 2 min at high speed. One volume of 70% ethanol was added to the homogenized lysate and the sample were transferred to an RNeasy spin column, which was centrifuged for 15 sec at 8,000 *g*. The flow-through was discarded, and the column was washed with 700 µl of RW1 buffer by spinning for 15 sec at 8,000 *g*. Subsequently, 500 µl of RPE buffer was added to the column, and the tube was centrifuged one more time for 2 min at 8,000 *g* to wash the membrane. The spin column containing RNA bound to the silica-based membrane was then placed in a new 1.5-ml microfuge tube, and the RNA was eluted using 40 µl nuclease-free water (Thermo Fisher, cat. no. AM9937), which was added to the membrane of the spin column. The samples were then centrifuged for the last time for 1 min at

8,000 *g*. The resultant total RNA was either used immediately for cDNA preparation or stored at -80°C.

2.5.2 RNA quantification and quality control

Using a NanoDrop ND-100 Spectrophotometer (Labtech International), we assessed the concentration of total RNA and the optical density at 260 and 280 nm. The ratio of the light absorbance indicated the purity of the RNA. The ideal ratio ranges were between 1.8 and 2.1, and RNA of sufficient purity was used for RT-PCR.

2.5.3 cDNA synthesis

The Precision nanoScript2 Reverse Transcription kit (Primer Design, no cat. no.) was used according to manufacturer's instruction to convert RNA into cDNA. Briefly, we chose to convert 150 ng of RNA, and the RNA was diluted in nuclease-free water (Thermo Fisher, cat. no. AM9937) to a total volume of 10 µl and incubated with 1 µl of oligo-dT primers (0.5 µg/ml final concentration) for 5 min at 65°C and then cooled to 4°C. For the master mix, in a total of 10 µl for RT reaction, 1 µl dNTPs (10 mM final concentration), 1 µl nanoScript enzyme, 5 µl NanoScript buffer, and 3 µl RNase-free water were added to each sample and incubated at 42°C for 20 min, followed by heating to 75°C for 10 min. cDNA samples were either used immediately for RT-PCR or stored at -20°C.

2.5.4 RT-Polymerase chain reaction (PCR)

SeV expression was assessed by RT-PCR using GoTaq Green Master Mix (Promega, cat. no. M712) according to manufacturer's protocol. Briefly, the reaction contained 12.5 µl GoTaq Green Master Mix, nuclease-free water, the respective template (2 µl) and primers (10 µM) (see Appendix) in a total volume of 25 µl.

We placed the reaction tube in a thermal cycler G-star (Thermo Fisher) and performed 35 cycles of PCR amplification (3 steps) as follows:

Denaturation: 95°C for 30 sec

Annealing: 55°C for 30 sec

Elongation: 72°C for 30 sec

The PCR products were analysed by agarose gel electrophoresis (see Appendix). The products were visualized using a PhotoDoc-IT UVP Imaging system transilluminator (Cole-Parmer, cat. no. 97-0274-05).

2.6 CHARACTERIZATION OF iPSC LINES

2.6.1 Embryoid Body Formation

iPSC lines were evaluated for spontaneous differentiation *in vitro*. The lines were cultured until they formed a round cluster of cells resembling an embryo: the embryoid body (EB).

After enzymatic passaging of 70-80% confluent iPSCs as described before (section 2.1.9), the cells were gently harvested into small clumps and then transferred into a new 6-well plate with an ultra-low attachment surface (Corning, cat. no. CLS3471) for spontaneous formation of 3-dimensional aggregates. EB formation was completed following culture in DMEM with 20% FBS for 7 days at 37^0C with 5% O_2, exchanging the 50% of the medium every 3 days.

2.6.2 Immunocytochemistry

To examine the expression of markers associated with pluripotency in undifferentiated iPSCs and germ layer markers for spontaneous differentiated iPSCs, all lines were fixed and processed for immunocytochemistry.

The iPSC lines were cultured on top of a Vitronectin XF-coated coverslip previously placed inside a 4-well plate (Thermo Scientific, cat. no. 144444).

For undifferentiated iPSCs, the cells were processed after 24 – 48 h of plating. For spontaneous differentiation, cells were cultured for an extra 7 days in DMEM supplemented with 20% FBS before processing.

When cells were ready for immunocytochemistry, the medium was aspirated, and the cell monolayer was washed twice with $DPBS^{+Ca\ +Mg}$ (Thermo Fisher, cat. no. 14040133). Fixation was carried out with 3.7% paraformaldehyde (PFA) (Merck, cat. no. 252549) at RT for 20 min. After removing the fixative, the cells were rinsed two to three times with $DPBS^{+Ca}$

$^{+Mg}$. Permeabilization was performed by adding 0.5% Triton X100 (Thermo Fisher, cat. no. 85111) / DPBS$^{+Ca\ +Mg}$ to the cells for 5 min at RT. After permeabilization, the cells were rinsed at least three times with DPBS $^{+Ca\ +Mg}$ to eliminate any residual Triton X100.

Subsequently, we incubated the cells overnight with the primary antibody at 4°C. After the incubation period, the cell monolayer was thoroughly rinsed with DPBS$^{+Ca\ +Mg}$, and the cells were incubated for 30 min at RT with the conjugated secondary antibody. The primary antibodies are described in Table 2.6.1 (undifferentiated iPSCs) and Table 2.6.2 (spontaneously differentiated iPSCs), whereas the secondary antibodies are shown in Table 2.6.3.

After secondary antibody incubation, the cells were washed with DPBS$^{+Ca\ +Mg}$, and all remaining liquid was removed. Subsequently, without allowing the samples to dry, a drop of Vectashield mounting medium (Vector Lab, cat. no. H-1200) was added on top of the cells, and the cover slip, with the cells attached, was flipped over on a microscope slide. The mounted cells were ready to be processed for data analysis on a Nikon Eclipse 50i epifluorescence microscope (Nikon). Images were captured and analysed using Infinity Capture software (Lumenera) and processed using Adobe Photoshop CC (Adobe system).

Table 2.6.1 Primary antibodies used for immunostaining of undifferentiated iPSCs.

Antibody	Supplier/ Cat. no.	Host	Species reactivity	Isotype	Concentration	Antigen localization
Anti-OCT3/4	Santa Cruz SC-9081	Rabbit	Human, rat, mouse	IgG	2µg/ml	Intracellular
Anti-TRA 1-60	Millipore MAB4360	Mouse	Human	IgM	8µg/ml	Extracellular
Anti-NANOG	R&D AF1997	Goat	Human	IgG	1 µg/ml	Intracellular
Anti-TRA-1-81	Millipore MAB4381	Mouse	Human	IgM	10 µg/ml	Extracellular

Table 2.6.2 Primary antibodies used for immunostaining of differentiated iPSCs.

Germ layer/ Antibody	Supplier/ Cat. no.	Host	Species reactivity	Isotype	Concentration
Endoderm Anti-α-fetoprotein	Merck, A8452	Mouse	Human	IgG	50 µg/ml
Ectoderm Anti-βIII-tubulin	Merck, T5076	Mouse	Human	IgG	20 µg/ml
Mesoderm Anti-α-smooth muscle actin	Merck, A5228	Mouse	Human	IgG	20 µg/ml

Table 2.6.3 Secondary antibodies used for immunostaining of undifferentiated and spontaneous iPSCs.

Secondary antibody	Supplier/ Cat. no.	Conjugation	Light colour produced
Donkey anti-rabbit IgG	Jackson ImmunoResearch 711-025-152	Rhodamine (TRITC)	Orange-red
Donkey anti-mouse IgM	Jackson ImmunoResearch 715-545-140	Alexa Fluor 488	Green
Donkey anti-goat IgG	Jackson ImmunoResearch 705-025-147	Rhodamine (TRITC)	Orange-red
Donkey anti-mouse IgM	Jackson ImmunoResearch 715-545-140	Alexa Fluor 488	Green

2.6.3 Teratoma Assay

iPSC lines were evaluated for their ability to differentiate into the three germ layers (endoderm, mesoderm and ectoderm) *in vivo.*

iPSCs were expanded in 6-well plates until the cells reached a total of 6 x 10^6, usually when all 6 wells reached approximately 80 - 90% confluency. When the number of cells was achieved, we performed cell detachment using Accutase (STEMCELL technologies, cat. no. #07920), a non-enzymatic cell detachment solution containing EDTA, at a concentration of 1 U/ml to obtain a single cell suspension. The culture medium was aspirated, and Accutase was added to the wells (1 ml/ well) followed by incubation at RT for 1 to 2 min. Subsequently, 1 ml of DMEM was added to the well, and the single cell suspension was collected into a 15-ml conical tube containing an extra 5 ml of pre-warmed DMEM. The cells were then washed by centrifugation at 160 *g* for 5 min. After washing, the supernatant was discarded, and the cell pellet was resuspended into 300 µl of BD-Matrigel: DMEM F-12 at a 1:2 ratio.

In the final step, the cells were transferred into a 1-ml syringe (Terumo, cat. no. PMC0593) fitted with a 30-gauge intradermic needle (BD Microlance, cat. no. 305771) and then transported to the animal facility inside a cooler box.

The animal experiment was performed at James Black Centre Biological Sciences Unit at King's College London by Dr Yanhua Hu. All procedures were performed according to protocols approved by the Institutional Committee for Use and Care of Laboratory Animals.

After inspection of the mice (for any signs of distress and/or injuries), the cells were injected subcutaneously into the right or left flank of female immunodeficient mice (NOD.CB17-Prkdc<scid>/NcrCrl) (Charles River, cat. no. NDSSIFE35D). A total of 2 mice were used per iPSC line (4 in total).

Characteristically, the tumour can be palpated between 6 to 12 weeks post-injection, and the mice were inspected for tumour growth on a weekly basis. When the tumour was palpated and its diameter reached 1 cm or more, the mice were sacrificed in accordance with Schedule 1 of Animal (Scientific Procedures) Act 1986 of the Home Office license guidelines.

The dead mouse was secured with tape around its paws on top of a clean stainless steel working table, exposing its belly with easy access to the tumour. The tumour was removed using surgical scissors and tweezers. After removal, the tumour was placed inside a 50-ml conical tube containing PBS and transported to the laboratory.

In the laboratory, the tumour was washed, sliced into ~0.3-mm^3 pieces and placed in 4% PFA for 48 h in 4°C for fixation of the tissue.

The histological staining, immunohistochemistry staining and sample analysis of all teratomas were performed at the Wolfson CARD Histology laboratory at King's College London by Carl Hobbs.

Each teratoma was processed in paraffin wax (VWR) using a Leica 2010 processing machine. Following processing, the teratoma was embedded into heated moulds containing molten wax. The moulds were then cooled at 4°C until the wax had solidified. Subsequently, the wax-embedded teratoma was sectioned into 6-mm serial slices using a rotary microtome and allowed to float on the surface of water heated to 45°C to soften the wax and allow the tissues to flatten out. Sections were then mounted onto Superfrost Plus microscope slide (Fisher Scientific). These slides are specially pre-treated to allow the tissue sections to electrostatically adhere to the glass. Sections mounted o slides were then placed in a 60°C oven for 1 h to ensure maximum adhesion. The slides were then stored at RT until the next step.

The samples were dewaxed to allow staining of the samples. Briefly, the samples were washed twice in xylene (SLS) under agitation for 10 min per wash at RT to soften the wax, followed by rehydration in four quick baths using absolute alcohol and a final plunge in water. Next, the samples were stained using Mayer's haematoxylin for nuclei (VWR, cat. no. 1.09249.0500) and eosin for cytoplasm and extracellular structures (Merck, cat. no. 230251). Immunohistochemistry was performed using germ layer-specific markers (see Table 2.6.4).

Table 2.6.4 Primary antibodies or dyes used for visualization of germ layers in teratoma histological sections. AFP, α-fetoprotein; DES, desmin; GATA4, GATA binding protein 4; GFAP, glial fibrillary acidic protein; MTCO2, mitochondrially encoded cytochrome c oxidase II; TUBB3, tubulin β 3 class III.

Tissue/antibody or dye	Supplier, Cat. no.	Concentration
Human / Anti-MTCO2	Abcam, AB110258	4 µg/ml
Endoderm / Anti-AFP	Sigma-Aldrich, A8452	1:400
Endoderm / Anti-GATA4	R&D, AF2606	1.3 µg/ml
Mesoderm / Anti-DES	Sigma-Aldrich, D1033	1:1500*
Mesoderm / Alcian Blue	Sigma-Aldrich, B8438	1% Alcian blue in 3% Alcian blue pH 2.5
Ectoderm / Anti-TUBB3	Abcam, ab7751	2 µg/mL
Ectoderm / Anti-GFAP	Abcam, ab7260	1:2500**

*Anti-desmin is an ascites fluid, and the final antibody concentration was estimated.
**Anti-GFAP is a whole anti-serum, and the final antibody concentration was estimated.

2.7 DERIVATION OF MSC-LIKE CELLS FROM iPSCs and hESCs

The iPSC lines derived in this study were differentiated into iMSCs (iMSC, iPSC-derived MSC). As a control, we used the hESC line KCL034. hESC-derived MSCs were termed eMSCs. Two protocols were used to achieve differentiation (Luzzani *et al.*, 2015; Zhao *et al.*, 2015).

The first protocol used was called **TEXAS (TEX)** and was based on the experiment by Zhao *et al.* (2015), who used SMAD 2/3 inhibitor to promote differentiation. On the first day of differentiation, when iPSCs reached 60 – 80% confluency, the cells were harvested using dispase (as described in section 2.1.9), seeded at a concentration of 2 x 10^5 cells/ well in new Vitronectin XF-coated wells (6-well plates) and cultured with TESR2 supplemented with 10 µM SB-431542 (SMAD 2/3 inhibitor) (Sigma) in an atmosphere of 5% CO_2. The cells were further expanded for 25 days with continuous passaging (every 3 to 4 days) under the same culture conditions.

According to the protocol, after 25 days, most of the cells change their morphology and become spindle-shaped cells. At this point, cells were passaged using Tryple Express (Thermo Fisher, cat. no. 12604021) as a dissociation reagent. Briefly, we washed the cell monolayer with pre-warmed DMEM and then incubated it in Tryple Express for 3 min at 37°C. Tryple was then diluted with an equal amount of pre-warmed DMEM. Cells were then collected, counted and centrifuged at 800 *g* for 5 min. Subsequently, the cell pellet was resuspended to a concentration of 1.5 x 10^5 cells/ ml in ESC-MSC medium (see Appendix) supplemented with 10 µM SB-431542 and transferred into a standard tissue culture well without any coating. The cells were incubated under the same conditions for an additional 20 days, with continuous passaging of the cells, at 80 – 90% confluency (Zhao *et al.*, 2015; Sanchez *et al.*, 2011). After 20 days, the cells were treated as fully differentiated MSCs in a standard tissue vessel with αMEM (Thermo

Fisher, cat. no. 32561029) supplemented only with 10% hPL (Stemulate, Cook Regentec, cat. no. G35220).

The second differentiation protocol used was called **ARGENTINA (ARG)** based on the protocol described by Luzzani *et al.* (2015), which consists of several cell passages using αMEM supplemented with hPL at 37°C with 5% O_2. On the first day of differentiation, when iPSCs reached 70 - 80% confluency, the cells were passaged using the dissociation reagent Accutase, as described in section 2.6.3, to obtain a single cell suspension and seeded at a concentration of 2 x 10^5 cells/ well in Vitronectin XF-coated wells (6-well plates). αMEM supplemented with 10% hPL and 2% B27 Supplement (Thermo Fisher, cat. no. A1486701), a supplement used to support induction of human neural stem cells (thermofisher.com, December 2017), was used for the first 14 days of culture and differentiation. In addition, 10 µM of Rock inhibitor Y27632 was added every time the cells were harvested and seeded until day 14 of differentiation. The cells were then passaged using Tryple Express without coating. Subsequently, the cells were continually expanded in αMEM supplemented only with 10% hPL. Characterization experiments were performed after 30 days of differentiation (Luzzani *et al.*, 2015).

The iMSCs and eMSCs transitioning morphologically towards MSC's morphology, from both TEX and ARG protocols, were further expanded followed by cell sorting. When the cells reached 70 - 80% confluency, they were collected as described previously using Tryple Express, and the cell pellet was resuspended to 1 x 10^6 cells/ ml in MSC medium (αMEM supplemented only with 10% hPL) supplemented with the antibiotics penicillin-streptomycin (Gibco). Using a FACSAria II cell sorter (BD) and FACSDIVA software (BD) for acquisition and analysis, only cells that were triple positive for the MSC markers CD73, CD90 and CD105 were sorted. The instrument was operated at the BRC Flow Cytometry Core at King's College London. After sorting, the cells were washed with 5 ml of pre-warmed DMEM by

centrifugation at 160 *g* for 5 min. Subsequently, the cells were plated in a standard tissue vessel with MSC medium supplemented with penicillin/ streptomycin for further expansion.

Subsequently, the iMSC and eMSC lines were subjected to immunomodulatory assays and further differentiation into osteogenic, adipogenic and chondrogenic lineages.

2.8 CHARACTERIZATION OF iMSCs AND eMSCs

2.8.1 Differentiation of nMSCs, iMSCs and eMSCs into -osteo, -adipo and chondrogenic lineages

A) ADIPOGENIC

To assess the adipogenic potential of nMSCs and iMSCs, cells were seeded at a density of 1 x 10^4 cells/cm^2 on a coverslip placed inside a 4-well plate and cultured for 14 days using the StemPro Adipogenesis Differentiation kit (Thermo Fisher, cat. no. A1007001). Thermo Fisher does not supply the compound information, but the most common reagents used for adipogenic induction include insulin, dexamethasone and Isobutylmethylxanthine (IBMX) (Scott *et al.*, 2011).

The medium was exchanged every 3 – 4 days for 14 days in total. After two weeks, the cells were fixed with 3.7% PFA for 20 min. After removing the fixative, we rinsed the cells two times with $DPBS^{+Ca\ +Mg}$. Next, we incubated the cells for 20 min at RT with (1:100) Lipid-TOX™ Green Neutral Lipid Stain (Thermo Fisher, cat. no. H34475) to evaluate the deposition of lipids on the cell membrane. Subsequently, the cells were rinsed two more times with $DPBS^{+Ca\ +Mg}$, and a drop of Vectashield was added to the cells followed by flipping the coverslip on top of a microscope slide. The cells were examined under a Nikon Eclipse 50i epifluorescence microscope. Images were captured and analysed using Infinity Capture software and processed using Adobe Photoshop CS5.

B) CHONDROGENIC

To assess the chondrogenic potential of nMSCs and iMSCs, cells were seeded at a density of 2 × 10^4 cells/cm^2 and cultured for 21 days in αMEM supplemented with 2 mM L-glutamine

(Merck, cat. no. G3126), 347 µM L-proline (Merck, cat. no. P0380), 100 nM dexamethasone (Merck, cat. no. 265005), 1% insulin–transferrin–selenium solution (ITG-S, Thermo Fisher cat. no. 41400045), 137 µM ascorbate-2-phosphate (Merck, cat. no. A8960) and 0.38 µM (10 ng/ml) recombinant human TGF-β1/3 (PeproTech, cat. no. 100-21) (Solchaga *et al.,* 2011).

The medium was refreshed every 3 – 4 days. After 21 days, the cells were fixed in 3.7% PFA for 30 min, washed twice with DPBS$^{+Ca\ +Mg}$, stained with 1% Alcian Blue 8GX (Merck, A5268) for 30 min at RT, washed again twice with DPBS $^{+Ca\ +Mg}$ and examined with an Olympus CK40 inverted phase contrast microscope to detect the formation of glycosaminoglycans. Images were captured and analysed using Infinity Capture software and processed in Adobe Photoshop CS5.

C) OSTEOGENIC

To assess the osteogenic potential of nMSCs and iMSCs, the cells were seeded at a density of 2×10^4 cells/cm^2 and cultured for 21 days in αMEM supplemented with 2 mM L-glutamine (Merck, cat. no. G3126), 100 nM dexamethasone (Merck, cat. no. 265005), 50 µM ascorbate-2-phosphate (Merck, cat. no. A8960) and 2.5 mM β-glycerophosphate (Merck, cat. no. G9422) (Wang *et al.*, 2009).

The medium was changed every 3 – 4 days. After 21 days, the cells were washed twice with DPBS$^{+Ca\ +Mg}$, fixed with ice-cold 70% ethanol for 1 h, rinsed again with DBPS$^{+Ca\ +Mg}$, and stained with 20 mg/ml of Alizarin Red S (Merck, cat. no. A5533) for 30 min at RT. They were then washed again with DBPS$^{+Ca\ +Mg}$. The calcium deposits were visualized under an Olympus CK40 inverted phase contrast microscope. Images were captured and analysed using Infinity Capture software and processed in Adobe Photoshop CS5.

2.8.2 Immunomodulatory assay

To test the immunosuppressive potential of the iMSCs and eMSCs, both TEX and ARG, *in vitro*, the CellTrace™ Violet kit (Thermo Scientific) was used according to the manufacturer's instructions. This method monitors distinct generations of proliferating cells by dye dilution. We performed PBMC proliferation assays in 200 µl of medium (RPMI 1640, Thermo Fisher, cat. no. 11875093, supplemented with 10% HPL) per well of 96-well flat-bottom plates (Costar, cat. no. CLS3595). In summary, at Day 1, cells were collected, and the concentration of each cell line was adjusted to 1 x 10^6 cells/ml. Subsequently, 96-well flat-bottom plates were prepared by adding 100 µl of fresh medium in 18 wells (Figure 2.8.1). The assay was performed in triplicate. The first 3 wells in the same row, the control wells, contained only an extra 100 µl of medium. The second to fifth rows had 1/5 to 1/80 dilutions of cells. Briefly, 200 µl (2 x 10^5 cells) was added to each of the 1/5 dilution wells, and using a multichannel pipette, 100 µl was then collected from each 1/5 well and transferred into the 1/10 wells below. The contents were mixed well, avoiding bubble formation, and without emptying the pipette, another 100 µl was collected from each 1/10 well then transferred to the 1/20 wells below. The same procedure was used in rows with 1/20, 1/40 and 1/80 until all dilutions were completed. The plate was incubated overnight at 37^0C with 5% CO_2.

At Day 2, PBMCs (described in section 2.3.1) were thawed, washed with PBS by centrifugation at 800 *g* for 5 min, counted and resuspended in PBS to a concentration of 1 x 10^6 cells/ ml. Subsequently, Violet tracer was added to a concentration of 1 µM in 2 ml of resuspended cells and incubated at 37°C for 10 min. The cells were then washed twice by centrifugation, first with PBS and then with RPMI 1640 supplemented with 10% HPL. They were then counted and resuspended to a concentration of 1 x 10^6 cells/ ml. Next, 50 µl of the resuspended cells (5 x 10^5 cells) was added to each well containing the different dilutions (1/5

to 1/80), followed by the addition of phytohaemagglutinin (PHA, Merck, cat. no. L1668) at a concentration of 5 μM. For controls, PBMCs without PHA were added to 3 additional wells (with 50 μl of fresh medium), and another 3 wells contained PBMCs without Violet (non-stained PBMCs). The cells were then incubated at 37°C with 5% CO_2 for 72 h and subjected to flow cytometry.

Figure 2.8.1 Preparation scheme of 96-well flat bottom plates for Immunoassay by Violet tracer staining. PBMCs, peripheral blood mononuclear cells; PHA, phytohaemagglutinin.

	No MSCs	No MSCs	No MSCs				
	1/5	1/5	1/5				
	1/10	1/10	1/10				
	1/20	1/20	1/20				
	1/40	1/40	1/40				
	1/80	1/80	1/80				
	PBMCs No PHA	PBMCs No PHA	PBMCs No PHA				
	PBMC No dye	PBMC No dye	PBMC No dye				

Empty wells

2.8.3 GENE EXPRESSION ARRAY RT-qPCR

We investigated the gene expression of osteogenic (*RUNX2*), chondrogenic (*COL11A1*), adipogenic (*FABP4*) and markers associated with pluripotent cells (*NANOG* and *ZFP42*) from all iMSC lines by real-time quantitative PCR (RT-qPCR) using the iScript cDNA Synthesis Kit (Bio-Rad, cat. no. 1708891SP) and SYBR Green Mastermix (Roche, cat. no. 04707516001).

2.8.3.1 Isolation and quantification of Total Cellular RNA

The procedure described previously in section 2.5.1 was used for RNA extraction.

Using the Qubit RNA BR assay kit (ThermoFisher, cat. no. Q10210), we determined the RNA concentrations of the samples. The kit was used per the manufacturer's instructions. Briefly, the master mix volume was calculated by the total number of samples to be quantified, which were individually prepared by diluting the provided kit reagent in kit' buffer to 1:200. Two Standard tubes were individually prepared by mixing 190 µl of the master mix with 10 µl of Standard 1 solution in tube 1 and 10 µl of Standard 2 solution in tube 2. Next, sample tubes were prepared by combining 199 µl of the master mix with 1 µl of sample. The tubes containing the diluted RNA samples were then vortexed for 2-3 sec and incubated at room temperature for 2 min. Using the Qubit 2.0 Fluorometer (Thermo Fisher), the standard curve for the assay was determined by obtaining a reading first from Standard 1 and then from Standard 2; subsequently, the RNA was quantified for each sample.

2.8.3.2 RNA quality control

Using the Agilent RNA 6000 Nano Kit (Agilent, no cat. no. 5067-1511), we assessed the RNA quality, integrity and sample quantification using the 2100 Bioanalyser.

The kit contains chips and reagents designed for analysis of RNA fragments. Each RNA chip contains an interconnected set of micro-channels, which is used for the separation of nucleic acid sections based on their size as they are pushed through it electrophoretically.

The kit was used according to the manufacturer's instructions. Briefly, the bench and all equipment, including pipettes, were wiped with RNA-Zap to remove any residual of RNase enzymes, and the Bioanalyser was cleaned using an electrotrode cleaning cartridge with nuclease-free water. Before starting, the RNA samples and RNA ladder were thawed on ice, heat-denatured for 2 min at 70°C and placed back on ice. The other reagents were thawed for 30 min at RT. Before loading the samples in the chip, the gel-dye mix was prepared by adding 1 µl of dye to 65 µl of filtered gel. After setting up the chip priming station by adjusting the base plate to position C and changing the syringe clip to the lowest position, a new RNA chip was loaded with 9 µl of the gel-dye mix in the first well marked with a 'G'. The syringe was then plunged, and after waiting 30 sec, released back to the start position. The other two wells marked with 'G' were each then loaded with 9 µl of gel-dye mix, followed by the addition of 5 µl of RNA 6000 Nano marker and 1 µl of RNA ladder to the ladder well. Finally, 1 µl of each sample was added to each of the 12 wells of the chip. Subsequently, the chip was vortexed for 60 sec and assessed in the 2100 Bioanalyser instrument within 5 min after preparation.

The 2100 Bioanalyser software uses the RNA integrity number (RIN) tool, allowing us to predict the integrity of the RNA. The RIN is independent of the concentration, instrument and analyst and therefore provides reliable data for RNA integrity. The Bioanalyser provides gel and electrophoretogram traces, and high-quality samples are identified by one marker peak, two ribosomal peaks (18S and 28S) and a high RIN.

2.8.3.3 cDNA synthesis

Using the iScript cDNA Synthesis Kit, we synthesized cDNA from the RNA isolated previously. This kit provides a sensitive and reliable solution for two-step RT-qPCR. The kit was used according to manufacturer's instruction. In brief, the Master mix was calculated according to the total number of samples for each experiment by adding 4 µl of 5x iScript Reaction mix to 1 µl of iScript Reverse transcriptase. Subsequently, 90 ng of RNA was converted, and therefore the RNA was diluted in RNase-free water to a total volume of 15 µl according to the RNA quantity of each sample. In a total volume of 20 µl, the complete reaction mixture was incubated in a thermal cycler using the following protocol:

Priming: 5 min at 25°C

Reverse transcription: 20 min at 46°C

RT inactivation: 1 min 95°C

Hold for 4°C

cDNA sample storage at 4°C.

2.8.3.4 RT-qPCR

To assess the gene expression of target genes, RT-qPCR was performed with the LightCycler 480 RT PCR Instrument using SYBR Green Mastermix according to the manufacturer's protocol. Briefly, the reaction contained 5 µl SYBR Green Master Mix (2X), nuclease-free water (2 µl), the respective template (2 µl) and 10 µM primers (0.5 µl/ each) in a total volume of 10 µl.

We placed the reaction tube in a LightCycler 480 II Instrument (Roche) and performed 45 cycles of PCR amplification as follows:

Pre-incubation : 95°C for 5 min

Amplification (45 cycles): 95°C for 10 sec

60°C for 10 sec

72°C for 10 sec

Melting curve: 95°C for 5 sec

65°C for 1 min

65-97°C for 0.11°C/sec

Primer pairs for target genes are listed in the Appendix. Data were collected and analysed using the comparative threshold cycle method with TBP and GUSB as reference genes. The mean ± SD was calculated, and statistical analysis was performed using the Prism curve-fitting programme (GraphPad Prism, version 6.01).

2.9 ARRAY BASED GENE EXPRESSION ANALYSES

The Illumina HumanHT-12 v4 Expression BeadChip (Illumina, cat no. BD-103-0204) supplies genome-wide transcriptional coverage of well-known genes, delivering high-throughput processing of 12 samples per chip. Each array targets more than 47,000 probes derived from the National Center for Biotechnology Information Reference Sequence (NCBI) and other sources (illumina.com, January 2018). We used the array to compare gene expression in nMSCs, iMSC TX and ARG with and without 18 h of IFNγ treatment.

iMSC TX, iMSC ARG and nMSCs were cultured in HPL media (αMEM supplemented with 5% Stemulate) and expanded until they reached 70 - 80% confluency. Subsequently, recombinant human IFNγ (Peprotech, cat no. 300-02) was added to the media at 10 ng/ml and cells were cultured for 18 h prior to collection for RNA extraction.

2.9.1 Isolation and quantification of total cellular RNA

The procedure described previously in section 2.8.3.1 was used to extract and quantify RNA.

2.9.2 RNA quality control

The RNA quality control using the Agilent RNA 6000 Nano Kit, described previously in section 2.8.3.2, was used to assess the RNA quality, integrity and sample quantification.

2.9.3 cDNA synthesis and labelling kit

RNA samples were converted to cDNA and labelled using the TargetAmp Nano Labelling Kit for the Illumina Expression BeadChip (Epicentre, cat no. TAN07924).

For first-strand cDNA synthesis, SuperScript III Reverse Transcriptase (RTr) (ThermoFisher, cat no. 18080-093) was used to convert RNA into cDNA. Briefly, we chose to convert 500 ng of RNA; therefore, the RNA samples were topped up with Nuclease-free water (Thermo Fisher, cat no. AM9937) to a total volume of 2 µl and incubated with 1 µl of oligo-dT primers (50 µM) for 5 min at 65°C, then cooled on ice for 1 min. For the master mix, in a total of 2 µl for the RTr reaction, 1.5 µl First-strand buffer, 0.25 µl of 0.1 M DTT, and 0.25 µl of SuperScript III were added to each sample prior to incubation at 50°C for 30 min.

For second-strand cDNA synthesis, the TargetAmp Nano Labeling kit 2nd strand cDNA regents were used. For the master mix, in a total of 5 µl per reaction, 4.5 µl of the 2nd-strand cDNA PreMix with 0.5 µl of the 2nd-strand DNA polymerase was added to each 5 µl of the 1st strand cDNA made previously. The 10 µl reaction was then incubated at 65°C for 10 min, followed by a further incubation at 80°C for 3 min, then cooled on ice and stored at -20°C or used immediately.

The next step was the *in vitro* transcription of Biotin cRNA. The reaction produces Biotin cRNA by incorporating Biotin-UTP into RNA transcripts. For each reaction, the reagents were combined in a total of 20 µl per reaction, as follows: 2 µl of T7 transcription buffer, 3 µl of Biotin-UTP, 10 µl of NTP premix, 3 µl of DTT, and 2 µl of T7 RNA polymerase. The reaction was then added to the cDNA made previously (total of 30 µl/ sample) and incubated at 42°C for 4 h. Then, 2 µl of RNAse-free DNase I was added to each reaction, and the samples were incubated at 37°C for 15 min.

The last step was the Biotin cRNA purification. This step uses a silica-based membrane and a series of high salt buffers that enable the binding of cRNA to the membrane. Briefly, 350 µl of lysis buffer (RLT) containing 3.5 µl of β-mercaptoethanol, 250 µl of 100% Ethanol and 48 µl of RNase free-water was added to each sample. The cell lysate was homogenized and then transferred to a spin column and centrifuged at > 8,000 *g* for 15 sec. The flow through was discarded and the column was washed with 650 µl of RPE buffer by spinning for 15 sec at 8,000 *g*. Subsequently, the flow through was discarded again and 650 µl of 80% Ethanol was added to the column and the tube was centrifuged once more for 15 sec at 8,000 *g*. The spin column was then transferred to a new collection tube and centrifuged at full speed for 5 min. In the last step, cRNA was eluted by placing the spin column inside a 1.5 ml collection tube and adding 20 µl of RNase free-water directly to the centre of the silica membrane and centrifuging at high speed for 1 min. The procedure was repeated using the same silica membrane and 1.5 ml collection tube; 20 µl of RNase free-water was added to the centre of the membrane and centrifuged at high speed for 1 min. The total of 40 µl cRNA was stored at -80°C.

2.9.4 Illumina HumanHT-12 v4 Expression BeadChip

The Expression BeadChip step was executed by a Senior Technician at the BRC Genomic Facility at Guy's Hospital.

The BeadChip was used according to the manufacturer's instructions. The process comprises of a series of steps to allow the labelled RNA strand to hybridize to the bead on the BeadChip containing the complementary gene-specific sequence (Assay Guide, illumina.com, January 2018).

Briefly, the steps were as follows: (1) cRNA was prepared for hybridization by preheating cRNA at 65°C for 5 min; (2) the Hyb Chamber was assembled; (3) the BeadChips were placed one by one inside the Hyb chamber; care was taken to ensure that the bar code in the BeadChips is aligned with the symbol in the chamber; (4) the samples were loaded using a single-channel high precision pipette; (5) the BeadChips were hybridized by closing and locking the Hyb Chamber lid and then placing the chamber in the Illumina Hybridization Oven and incubating for 14 - 20 h at 58°C; and (6) the BeadChip was washed in four distinctive steps. The first wash was a high-temperature wash, followed by two RT washes, one with E1BC1 buffer and another with 100% ethanol. The last step, the blocking step, was performed by washing the BeadChip in block E1 buffer. The next steps in the process were as follows: (8) The signal was detected. Cy3-SA was introduced to bind to the probes that have been hybridized to the BeadChip, facilitating the detection of the signal. The BeadChip was bathed in block E1 Buffer containing Streptavidin-Cy3 in a rocker mixer for 10 min at RT. (9) The BeadChip was washed with E1BC buffer 5 times and then bathed in the buffer for 5 min at RT. (10) After the chip was dyed by centrifuging at 8,000 *g* for 4 min, the BeadChip was ready to be scanned using the iScan Reader. The scanner uses a laser to excite the fluorophores of the single-base extension products on the beads of the BeadChip sections. They are then recorded in high-resolution images (Assay Guide, illumina.com, January 2018).

2.9.5 Bioinformatics

The data were analysed by GenoSplice Technology.

2.9.6 RT-qPCR

Using the same RNA isolated from cells with and without 18 h IFNγ treatment that were used in the Illumina Expression BeadChip, we assessed the gene expression of the target genes IDO1, GPB2 and CXCL11.

RT-qPCR was performed using the StepOne System Instrument (ThermoFisher, cat no. 4376357) using a TaqMan® RNA-to-C_T™ *1-Step* Kit (ThermoFisher, cat no. 4392938), according to the manufacturer's instructions.

Briefly, for the master mix, the reaction contained 10 µl of TaqMan RT-PCR Master Mix (2X), 0.5 µl of TaqMan probe, 0.5 µl of TaqMan RT Enzyme Mix, 20 ng of the appropriate RNA template, 1 µl of each primer (900 nM), and up to 20 µl of nuclease-free water.

We placed the reaction tube in a StepOne System and performed 40 cycles as follows:

Holding: 48°C for 15 min

Holding: 95°C for 10 min

Cycling (40 cycles): 95°C for 15 sec

60°C for 1 min

Primers pairs for target genes are listed in the Appendix. Data were collected and analysed using the comparative threshold cycle method with HPRT1 as the reference gene.

CHAPTER 3

3. RESULTS

3.1 WJ MSC ISOLATION AND CULTURE UNDER STANDARD AND XENO-FREE CONDITIONS

The standard medium commonly used by research groups around the world for the isolation and expansion of MSCs is DMEM supplemented with 10% FBS. To avoid high lot-to-lot variability of FBS and risk of contamination with xenopathogens, chemically defined medium would be an ideal replacement in terms of compliance with good manufacturing practice (GMP). However, such chemically defined media are lacking a number of factors that are present in FBS and are required for optimal MSC proliferation.

To validate the performance of the chemically defined medium Stemgro, which has components that are either chemically synthesized or recombinantly produced and purified, we cultured explants from the same UCs (n=7) under STD (DMEM supplemented with 10% FBS) and dXF (Stemgro) conditions. Commonly, chemically defined media do not contain extracellular matrix proteins; therefore, we used CELLstart to coat the surface of the culture dishes. CELLstart is a defined substrate containing only components of human origin, the main one being fibronectin (Hughes *et al.*, 2011).

WJ MSC initial outgrowth from the attached UC explants was typically observed within 8 to 11 days. The mean (± standard deviation, SD) time to the first observation of outgrowth was 9.13 (± 0.3; n=7) under STD and 12.1 (± 0.5; n=8) under dXF conditions (Figure 3.1.1). Based on the Wilcoxon signed-rank test, the difference in observation of the first outgrowth between donor matched STD and dXF conditions was statistically significant (p=0.021).

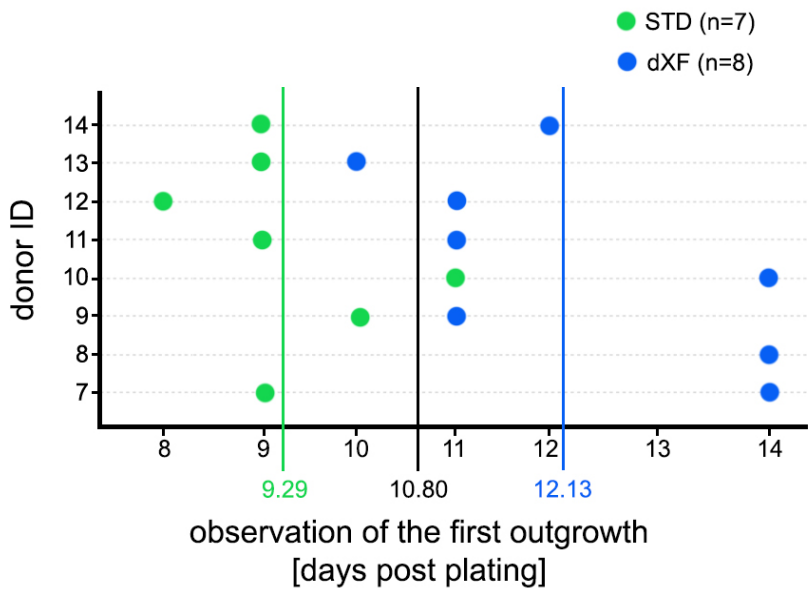

Figure 3.1.1 First outgrowth from UC explants was earlier under STD (medium containing FBS) **than under chemically defined (dXF conditions).** The first outgrowth was observed sooner under STD (9.29 ± 0.3 days post plating, n=7) than under dXF conditions (12.13 ± 0.5 days post plating, n=8). The difference was statistically significant ($p<0.05$). The difference between the groups was tested by Wilcoxon signed-rank test. The value of test statistics V = 28, and p = 0.021. Based on this test, we concluded that STD and dXF groups are non-identical populations. The pseudomedian of the differences between samples from these two groups was 2.5, with 90% confidence interval (1.5, 4.0). The nonparametric confidence interval is calculated here as a continuity-corrected normal approximation.

Apparently, FBS-containing medium supports WJ MSC proliferation better than the xeno-free chemically-defined medium Stemgro. In an attempt to mimic the effects of FBS and retain xeno-free conditions, we then tested hPL, one of the most commonly used FBS alternatives that relies on human blood-derived components (Bieback, 2015).

Non-defined, xeno-free culture (nXF) had a similar effect on appearance of the first outgrowth as STD conditions, with both of them performing significantly better (*$p\leq0.05$) than chemically defined xeno-free culture (dXF) conditions (Figure 3.1.2).

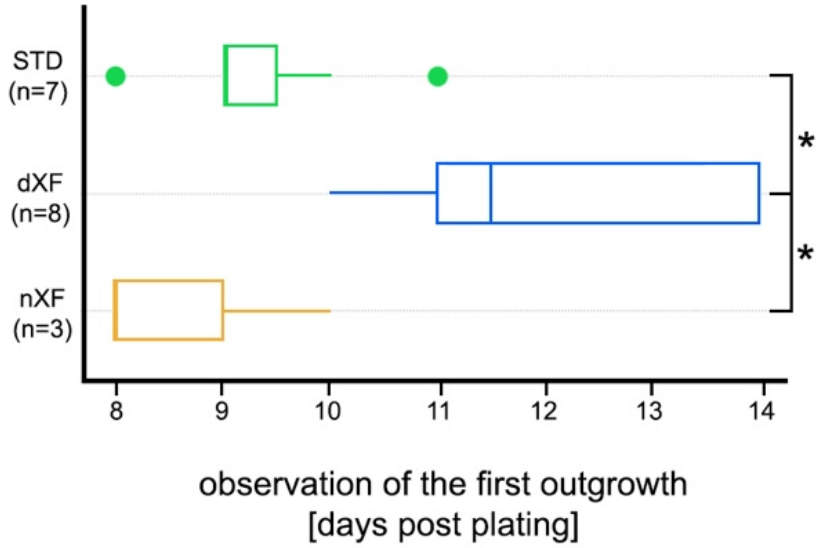

Figure 3.1.2 Both FBS (STD conditions) and HPL (nXF conditions) support better MSC proliferation measured by time of the first outgrowth from UC explants than chemically defined (dXF) conditions. The first outgrowth was observed sooner under STD (9.29 ± 0.3 days post plating, n=7) and XF (8.70 ± 0.8 days post plating, n=3) than under dXF conditions (12.13 ± 0.5 days post plating, n=8). The difference between dXF and the other two conditions is statistically significant (*$p<0.05$), whereas the difference between STD and nXF conditions was not significant by the Wilcoxon rank-sum test. For the significant difference dXF/ nXF test statistic is W=23.5, and p=0.022. The shift in location of the difference between samples from these two groups was 3.0, with 95% confidence interval (1.0, 6.0). For non-significant difference STD/ nXF test statistics is W=14.5, and p=0.403. The shift in location between samples from these two groups was 1.0, with 95% confidence interval (-1.0, 3.0). The nonparametric confidence intervals are calculated here again as continuity-corrected normal approximations.

Appearance of the first outgrowth might be a consequence of higher proliferation rate, faster cellular migration or both. To determine what is causing this effect, we calculated population doublings (PD) between the two first passages (P1 and P2) to establish the

proliferation rate under the conditions used (Figure 3.1.3). The median (range) PD for STD conditions was 105.40 h (85.92 - 115.20) for nXF conditions and 119.00 h (88.08 - 146.90) and for dXF conditions 121.90 h (77.52 – 162.70). Analysis using the Kruskal-Wallis Rank Sum Test showed no significant difference between all groups (p=0.228), and there was also no significant difference between pairs of groups using the Wilcoxon rank-sum and Wilcoxon signed-rank tests.

The Wilcoxon rank-sum test was used to compare nXF to other two groups, whereas the Wilcoxon signed-rank test to compare dXF and STD. The results were:

- nXF/ dXF: W=10; p=1; difference in location = -0.12, 95% CI= (-1.82, 1.73)
- nXF/ STD: W=15; p=0.3605; difference in location = 0.57, 95% CI= (-1.13, 1.95)
- dXF/ STD: V=1; p=0.0625; pseudomedian = -0.795; 95% CI= (-2.61, 0.22).

Taken together, these data suggest that the earlier observation of the initial outgrowth from UCs explants under STD and nXF conditions is due to an increase in cellular migration rather than to faster cell migration. A plausible explanation is that both FBS under STD and hPL under nXF conditions are richer in growth factors and different molecules such as chemokynes and cytokines from the platelet rich plasma that facilitate cellular migration than dXF conditions, which the specific contents of the media is not revealed by the manufacturer.

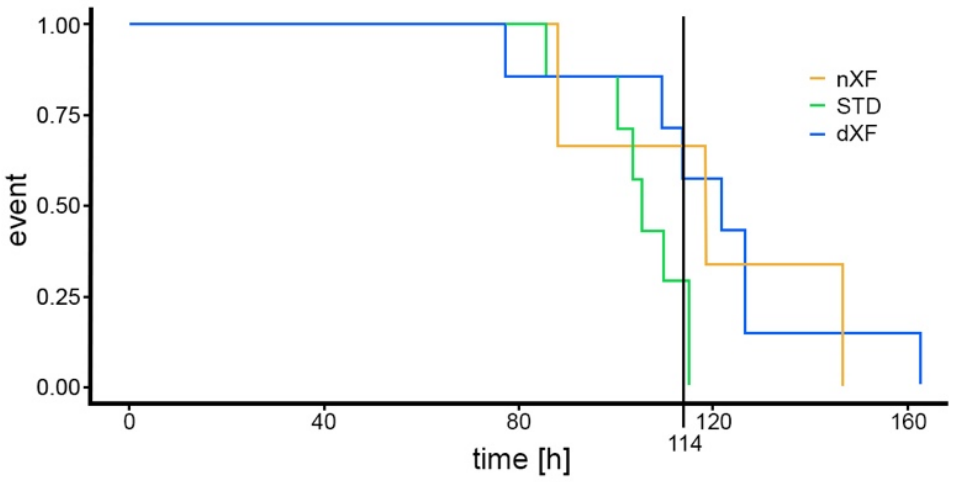

Figure 3.1.3 The Kaplan-Meier curve using an overall median of 114 h indicates that there was no significant difference in the median time to doubling (p=0.086). dXF, chemically defined, xeno-free condition; nXF, non-defined, xeno-free condition (medium containing hPL); STD, standard condition (medium containing FBS). Two-sided 95% confidence intervals were calculated as log(-log(hazard)). For Kruskal-Wallis Rank Sum Test that compared all groups, statistics were as follows: Kruskal-Wallis chi-squared=2.9567, df=2, p=0.228.

In general, cells under all three conditions exhibited a similar spindle shape with a flat polygonal morphology characteristic of mesenchymal stem cells (Figure 3.1.4).

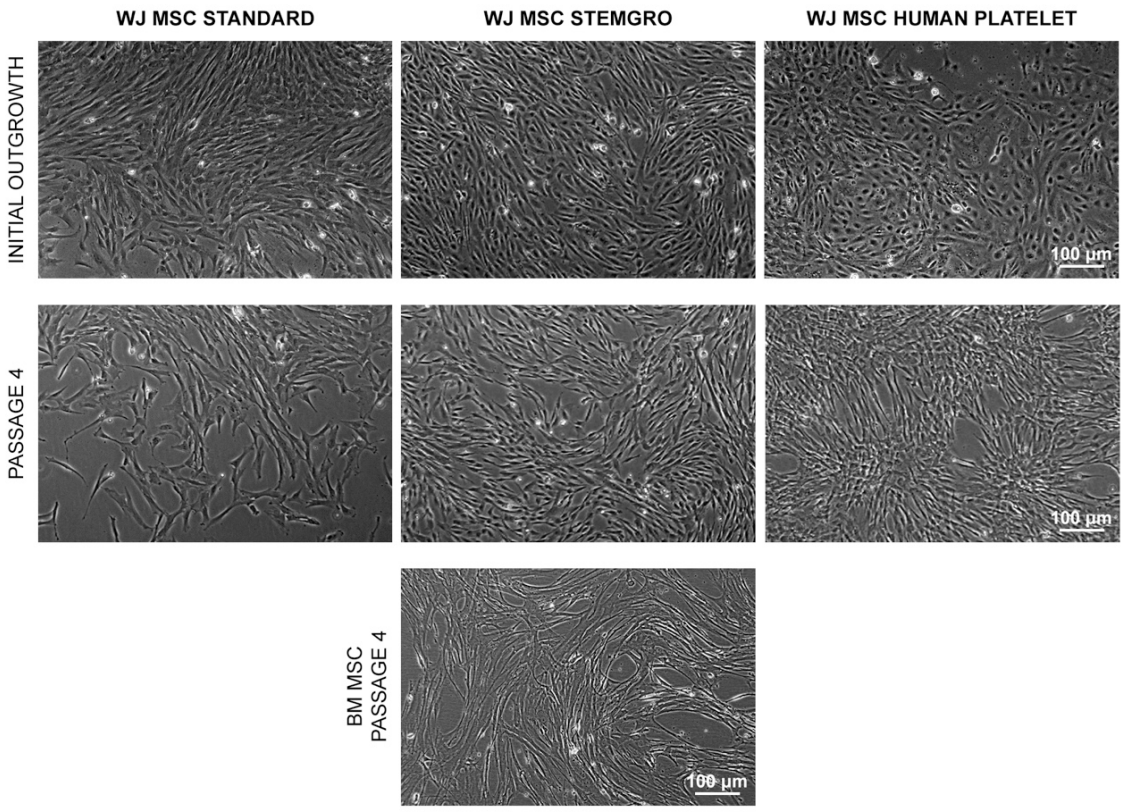

Figure 3.1.4 WJ MSCs in culture. The cells in initial outgrowth from attached UC explants grown under STD and nXF conditions looked more like typical fibroblasts, whereas the cells grown under dXF conditions were less elongated and never as tightly packed as the cells in standard culture. After 4 passages, WJ MSCs under dXF still looked more elongated than the cells under STD and dXF conditions but were still similar to the BM MSCs. Scale bar: 100 µm.

3.2 WJ MSC PROFILING SURFACE MARKERS WITH FLOW CYTOMETRY

3.2.1 WJ MSCs express all markers seen in BM MSC

We assessed the effect of STD (n=3; donors ID: 8, 12 and 13), nXF (n=3; donors ID: 3, 4, and 5) and dXF (n=10; donors ID: 8, 9, 10, 11, 12, 13, 14, GMP 03, GMP 04 and GMP 05) on the isolation and propagation of WJ MSCs by determining the profile of nine surface markers: CD29, CD34, CD44, CD45, CD56, CD73, CD90, CD105 and MSCA-1. Clinical grade BM MSCs (from 3 different donors) cultured under nXF conditions were used for comparison of the expression of cell surface markers with WJ MSCs derived and expanded under STD, nXF and dXF conditions (Figure 3.2.1).

BM MSCs and WJ MSCs cultured under all conditions were negative for CD34 and CD45 hematopoietic markers (Appendix: Figure 5). As positive control for the hematopoietic markers CD34 and CD45, we used the Kasumi cell line.

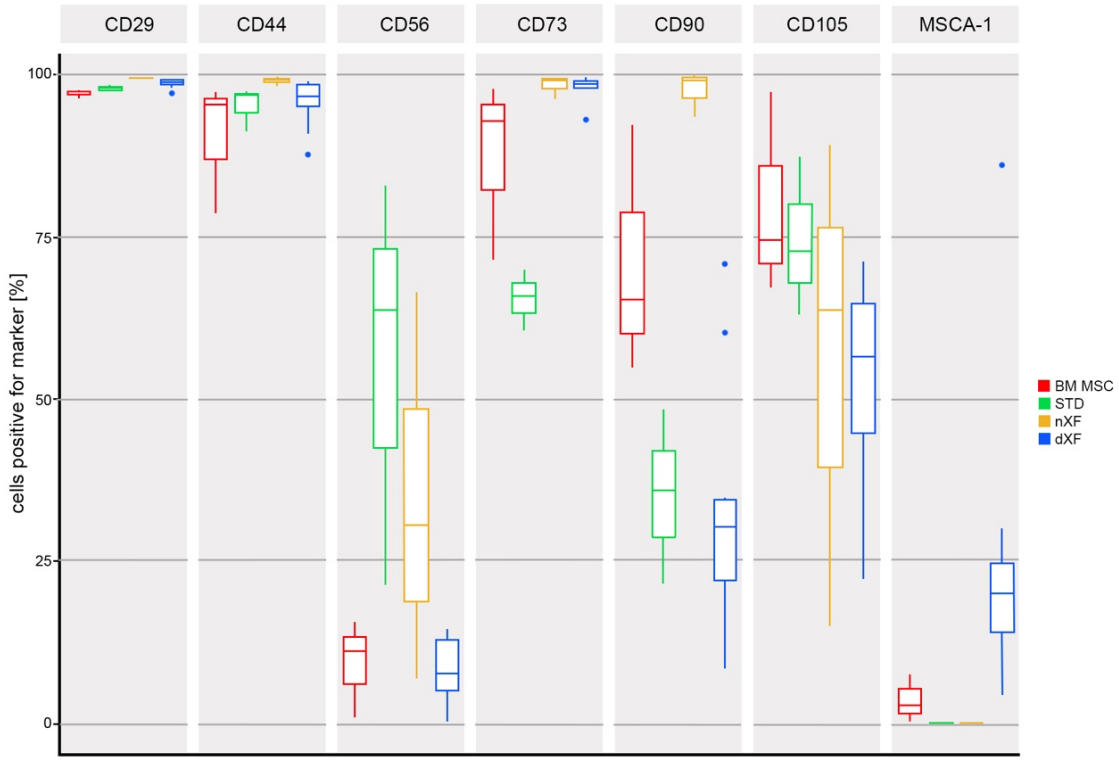

Figure 3.2.1 Surface marker expression of BM MSCs, clinical grade, and WJ MSCs cultured under three conditions: STD, nXF and dXF. Groups were compared with the Kruskal-Wallis test, and in cases in which the differences were statistically significant, pairs of mediums were checked by Wilcoxon (Man Whitney) test. The overall differences between groups were significant for markers CD73, CD56, CD90, CD105 and MSCA-1. Confidence interval (CI) is 90%.

For CD29 (ITGB1 (integrin β1)), clinical grade BM MSCs and all WJ MSCs from all donors, regardless of culture conditions, expressed the marker at higher levels.

CD44, the receptor for hyaluronic acid, was also expressed in almost the entire population of cells isolated from all donors regardless of culture condition, as well as BM MSCs.

The expression of CD56, the neural cell adhesion molecule 1 (NCAM1), varied from donor to donor, with the dXF group having the lowest levels (8 ± 1.7%), followed by BM MSCs (9.2 ± 4.3%), whereas the nXF and STD groups had higher levels (34.6 ±17.3% and 56 ± 18.1%) (*P<0.05).

CD73, ecto-5'-nucleotidase, was expressed in almost the entire population of BM MSCs (87.4 ± 8.1%) and WJ MSCs cultured under dXF (98 ± 0.9%) and nXF (98.3 ± 0.9%), whereas WJ MSCs cultured under STD were approximately 30% less positive for CD73 (65.4 ± 2.7%). Significant differences were observed between BM MSCs and dXF (*p<0.05) and between STD and dXF (***p<0.0001).

The expression of CD90, also known as thymocyte differentiation antigen (Thy-1) was generally lower in the WJ MSC dXF (33.4 ± 5.9%) and STD (35.2 ± 7.7%) groups than in the BM MSCs (70.8 ± 11.1%) and nXF (97.5 ± 2%) groups, varying among donors under dXF conditions (8.4% in donor 13 to 70.8% in donor 05). A significant difference was observed between BM MSCs and dXF (*p<0.05).

Endoglin (CD105) is expressed on endothelial cells and MSCs, particularly proliferating cells (Saad *et al.*, 2004). More BM MSCs (79.7 ± 9%) and STD (74.4 ± 7%) than WJ MSC dXF and nXF were positive for CD105. Although the population of CD105+ cells varied from donor to donor, in general, the results were similar between the WJ MSCs cultured under dXF conditions (54 ± 4.8%) and those cultured under nXF conditions (55.9 ± 21). WJ MSC nXF had an enormous variation among all 3 donors (89.1%, 63.7% and 15.1%). A significant difference was observed between BM MSCs and dXF (*p<0.05).

MSCA-1, however, displayed a curious pattern. Whereas it was barely detectable in nXF (0.03 ± 0.03%) and STD conditions (0.13 ± 0.1%) and was lowly expressed in BM MSCs

(3.5 ± 2%), in WJ MSCs cultured under dXF conditions, 13.5 – 86.1% of cells were positive. Donor 9 and 05 were an exception, with 4.4% and 7.3% MSCA-1^+ cells under dXF.

The profiling of cell surface markers from a total of 10 independent donors cultured under all conditions confirmed that WJ MSCs isolated in this study expressed all MSC markers seen in BM MSCs, although at a variety of levels. Interestingly, it seems that the dXF group favours expression of the MSCA-1 marker, which was barely detectable in STD and nXF or in clinical grade BM MSCs.

3.2.2 Different levels of O_2 did not affect expression of the MSC surface markers examined

Increasing evidence has demonstrated that oxygen (O_2) levels play an important role in cell proliferation and plasticity (Ma *et al*., 2009). An atmospheric oxygen tension of 20% is a non-physiological condition, representing a hyperoxic environment. Culturing the cells at 5%, which is closer to their physiological microenvironment in vivo, increased their proliferation and, in the case of MSC, also affected their differentiation potential (Ma *et al.*, 2009; Ivanovic *et al.*, 2000; Katahira and Mizoguchi, 1987; Bradley *et al.*, 1978). It has been shown that WJ MSCs also proliferate faster at lower O_2 tensions without affecting the profile of their surface markers (Widowati *et al.*, 2014). Therefore, we opted to work at 5% O_2.

To determine whether different levels of O_2 affect the expression of WJ MSC cell surface markers in XF media in our system, we ran a comparison between 20% and 5% O_2 on WJ MSC (n=3) isolation and expansion using nXF and dXF media. We assessed the differences between groups by determining the profile of nine surface markers: CD29, CD34, CD44, CD45, CD56, CD73, CD90, CD105 and MSCA-1.

The WJ MSC isolation and culture conditions were grouped as follows: nXF and dXF in 5% O_2 (5nXF and 5dXF) and in 20% O_2 (20nXF and 20dXF).

WJ MSC lines cultured under all conditions were negative for CD34 and CD45 hematopoietic markers (Appendix: Figure 6.3.1 and 6.3.2).

In general, the expression levels of all surface markers were not significantly different between 5 and 20% O_2 (Figure 3.2.2). However, the levels were different depending on the culture media used (nXF or dXF). Comparison between media in 20% found that the difference is marginally significant for all markers but CD90, and in 5% the difference is seen as marginally significant for markers CD29, CD90, and MSCA1. Bt the Wicoxon (Mann-Whitney) test, CD44 and MSCA1 were the only surface markers with significant differences in expression levels between 5% and 20% (dXF group).

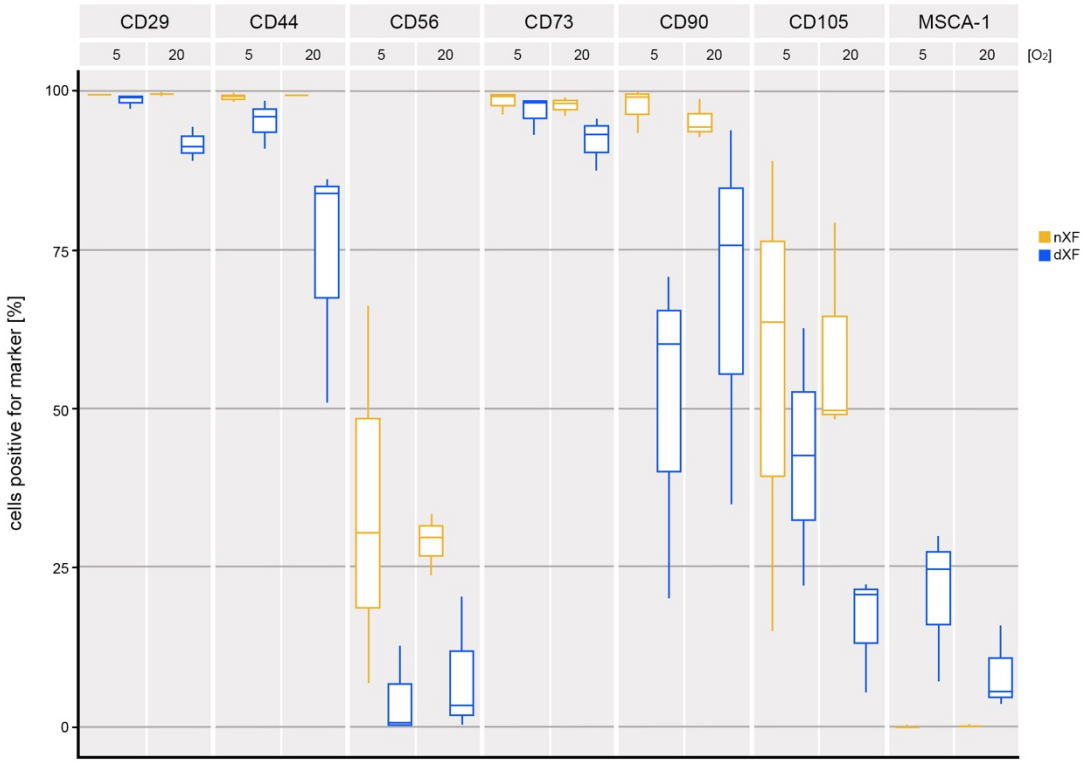

Figure 3.2.2 Expression levels of MSC surface markers were dependent on the culture media used (nXF or dXF), not on the level of O_2. Confidence interval (CI) is 90%.

All 4 groups were positive for CD29 (20nXF: 99.6%; 5nXF: 99.5%; 20dXF: 91.7%; 5dXF: 98.6%) and CD73 (20nXF: 97.8%; 5nXF: 98.3; 20dXF: 92.2%; 5dXF: 96.8%) without significant differences between all groups.

CD44 was lower in the 20dXF group (73.7%) than 5dXF, 20nXF and 5nXF (95.3%, 99.5% and 99.2%, respectively).

CD90 was lower in the 20dXF (68.2%) and 5dXF (50.4%) groups than the 20nXF (95.4%) and 5nXF (97.5%) groups.

CD105 showed higher expression levels in the 5nXF groups independent of the O_2 levels, with 59.2% under 20nXF and 56% under 5nXF conditions versus 16.2% under 20dXF and 42.6% under 5dXF conditions.

MSCA1 was only expressed in the dXF groups, with 8.5% under 20dXF and 20.8% under 5dXF conditions.

Taken together, our data were in agreement with the findings of Widowati *et al.* (2014), who showed that O_2 level does not affect the expression level of surface MSC markers.

3.2.3 MSCA-1 expression is induced by exposing WJ MSCs to dXF conditions.

In spite of large variations in the size of the MSCA-1^+ subpopulation amongst donors (4.4% - 86.1%), MSCA-1^+ subpopulations were detected in MSCs from all donors (Table 3.2.1). However, only under dXF conditions, regardless of the O_2 level.

Table 3.2.1 Population size of MSCA+ cells in the MSC of each of 7 donors when cells were cultured under dXF conditions at 5% O_2.

Donor #	**8**	**9**	**10**	**11**	**12**	**13**	**14**
MSCA-1+ cells [%]	15.8	4.4	23.5	13.5	38.8	86.1	29.5

To confirm that the chemically defined XF culture conditions described here selectively privileged the expansion of MSCA-1+ cells, we transferred WJ MSC derived and expanded under STD conditions (n = 2 donors; donor 12 and donor 14) into dXF medium for 14 days and assessed the proportion of MSCA-1+ cells. For both donors, the numbers of MSCA-1+ cells

increased, from 0.1% to 0.9% in donor 12 and from undetectable (0%) to 9.9% in donor 14 (Figure 3.2.3). Since the population doubling time of WJ MSCs derived under dXF conditions is slightly over two days (55.2 ± 2.6 h) and the cells were cultured for only 14 days, this increase is likely due to the stimulation of MSCA-1 expression, not increased cell proliferation of already present MSCA-1+ cells.

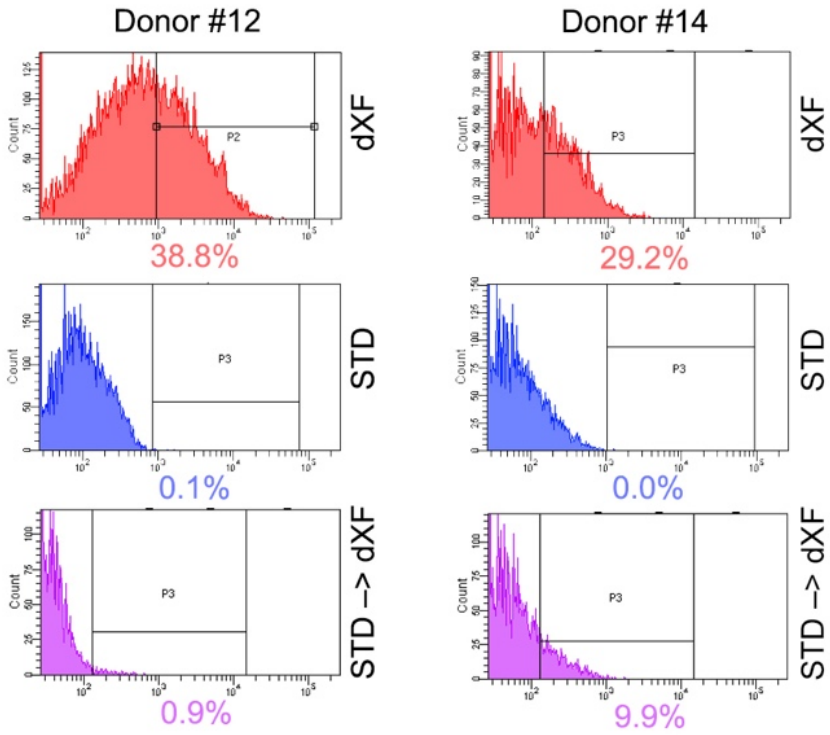

Figure 3.2.3 MSCA-1 expression is induced by exposing WJ MSCs to XF conditions. WJ MSCs derived and expanded under STD condition (n = 2 donors) were exposed to XF conditions for 14 days (STD->XF). That was sufficient to significantly induce an increase in the MSCA-1+ subpopulation from 0.1 to 0.9% in donor #12 and from 0 to 9.9% in donor #14.

3.3 DIFFERENTIATION POTENTIAL

Next, we wanted to determine whether the isolated WJ MSCs (PD 5) have a differentiation potential into the three mesenchymal lineages by testing their response to adipogenic, chondrogenic and osteogenic induction media. To do that, we used the cells isolated from three randomly chosen donors for each of media conditions tested. After 14 days of culture, in adipogenic medium, we could detect fat droplets (Figure 3.3.1). It took 21 days to induce Alcian Blue-positive glycosaminoglycan depositions (cartilage; Figure 3.3.2) or mineralized nodules (bone), as shown by Alizarin Red staining (Figure 3.3.3).

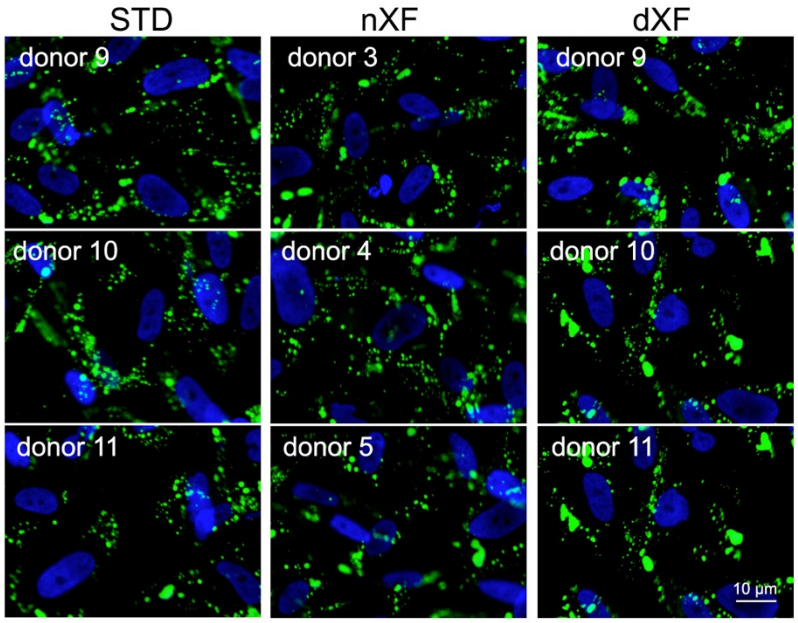

Figure 3.3.1 WJ MSCs derived under one of three conditions (STD, nXF or dXF) displayed adipogenic potential.

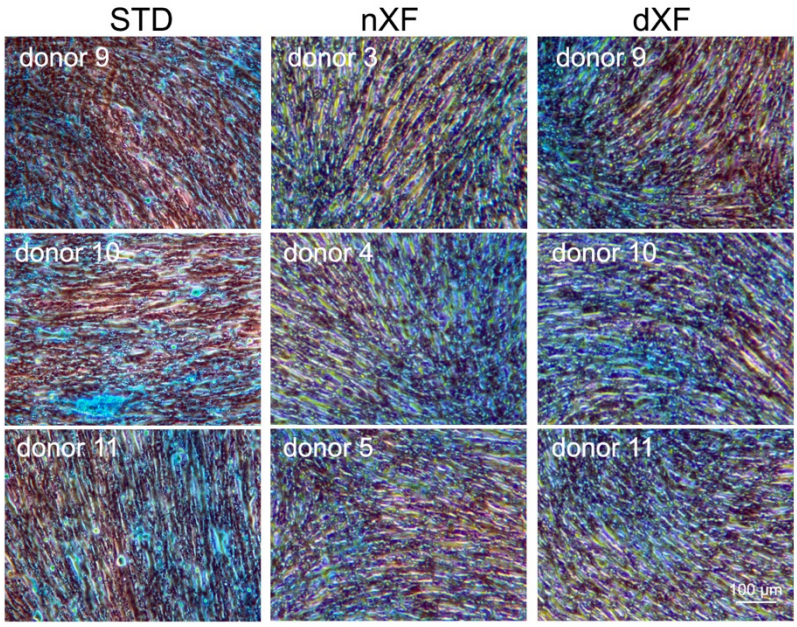

Figure 3.3.2 WJ MSCs derived under one of three conditions (STD, nXF or dXF) displayed chondrogenic potential.

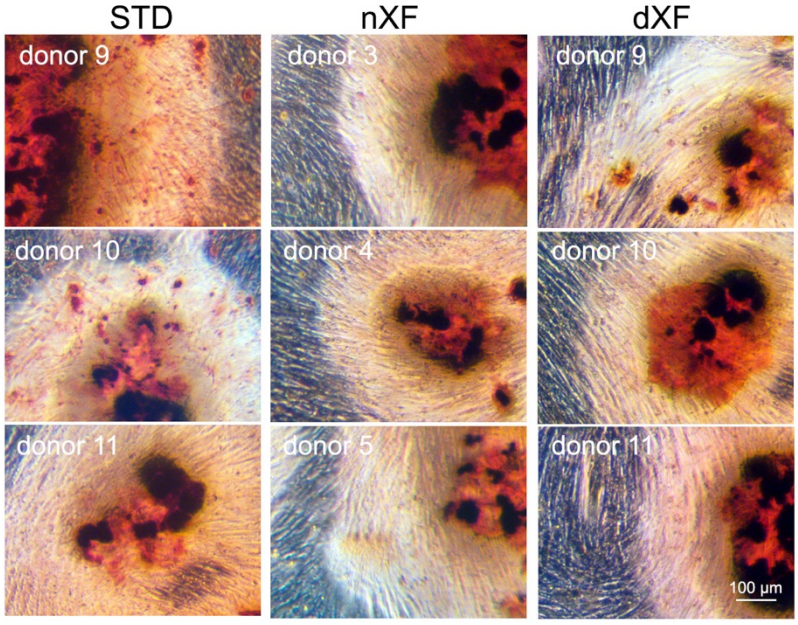

Figure 3.3.3 WJ MSCs derived under one of three conditions (STD, nXF or dXF) displayed osteogenic potential.

We assessed the differentiation potential into three lineages qualitatively. To address whether any of the three media render the cells more prone to adipo-, chondro- or osteogenic lineages, we would need to carry out quantitative analyses with either a much larger number of samples or using the cells from the same donor derived under the three given conditions. Regardless, the qualitative analyses suggested that none of the three different conditions impaired markedly the differentiation potential of WJ MSCs or depleted stem cell subpopulations from the isolated cells.

3.4 IMMUNOMODULATORY ACTIVITY OF WJ MSC

MSCs are known for their ability to exert potent immunosuppressive and immuneregulatory effects on a variety of cell types mediating both adaptive and innate immunities (Marigo and Dazzi, 2011). Next, we compared the immunomodulatory effect of clinical grade BM MSCs (n=3) and WJ MSCs isolated and grown under dXF (n=4).

WJ MSCs inhibited PHA-stimulated PBMC proliferation in a dose-dependent manner in a similar fashion as BM MSCs, although there was a significantly higher antiproliferative activity at the 1/20 ratio (Figure 3.4.1). These data suggest that WJ MSCs retain similar immunosuppressive activities to the ones originally described in BM MSCs.

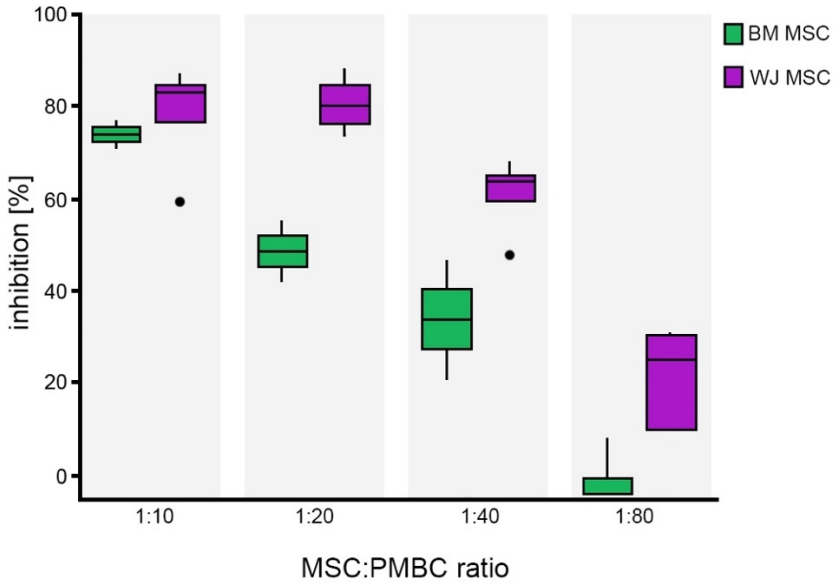

Figure 3.4.1 Immunomodulatory activity of MSCs under XF conditions. The magnitude of the immune response of WJ MSC in dXF and clinical grade BM MSC in nXF were similar between the ratios (PBMCs/MSCs), with the exception of the ratio 20/1, where WJ MSC dXF appears to be slightly superior, but without significant differences between them ($p<0.05$). Confidence interval (CI) is 95%.

3.5 REPROGRAMMING OF WJ MSCs INTO iPSCs

The experiments described in chapters 3.1 – 3.4 demonstrated that WJ MSCs could be isolated successfully from the umbilical cord under dXF conditions. The cells derived in such a way retain all the characteristics of MSCs: the expression of typical MSC surface "markers", differentiation potential into adipocytes, chondrocytes and osteocytes, and immunomodulatory activity. Therefore, to test our hypothesis that clinical grade iPSC-derived WJ MSCs can be derived from the beginning to the end under xeno-free conditions, we chose WJ MSCs derived and propagated under dXF conditions from three of seven donors for reprogramming into iPSC lines. The criterion for the selection of the donors was the size of the MSCA-1^+ subpopulation (Table 3.2.1). MSCA-1^+ cells are mesenchymal precursor cells and its expression is linked with an increased capacity of colony forming units >100-fold in comparison with the MSCA-1^- subpopulation (Sobiesiak *et al.*, 2010; Bühring *et al.*, 2009; Gronthos *et al.*, 2007). WJ MSCs derived under dXF that had the highest number of MSCA-1^+ cells were from donor 13 (86.1%), 12 (38.8%) and 14 (29.5%). To distinguish them from iPSC-derived MSC lines, we dubbed the primary native WJ MSCs as native MSCs (nMSCs). Therefore, from donor 12, we have nMSC12; from donor 13, we have nMSC13; and from donor 14, we have nMSC14.

We reprogrammed WJ MSCs into iPSCs using a commercially available SeV reprogramming kit (CytoTune-iPS Sendai Reprogramming Kit, Life Technologies) following the manufacturer's protocol, with a few modifications (Figure 3.5.1). This method uses incompetent SeV to safely deliver the four transcription factors (OCT4, SOX2, c-Myc and KLF4) responsible for reprogramming somatic cells into iPSCs (Takahashi and Yamanaka, 2006). The kit is simple to use with a few steps involved, and generates iPSCs with an efficiency of 1%, a 100-fold improvement in efficiency compared with other methods such as lentivirus and episomal (efficiency between 0.0001% to 0.01%). In parallel with the three WJ MSC lines

(nMSC12, nMSC13 and nMSC14) no older than passage number 6 (PD 16), we used for reprogramming: primary dermal fibroblast BJ as a control.

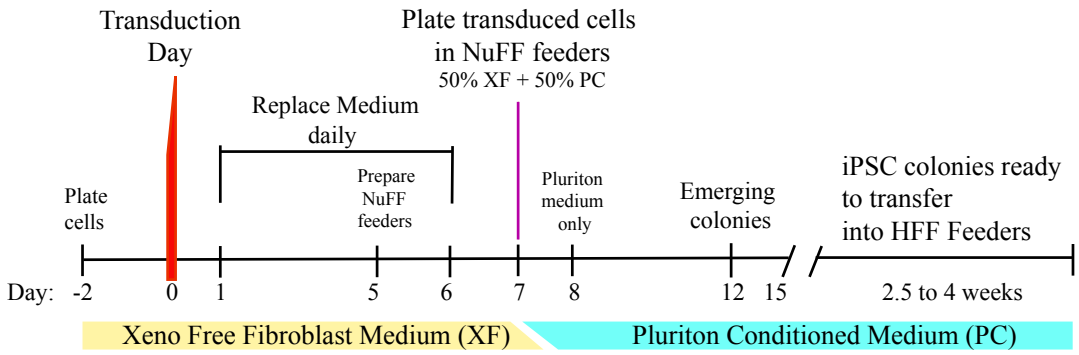

Figure 3.5.1 Reprogramming timeline of production of iPSC. Figure adapted from Life technologies website CytoTune kit (lifetechnologies.com, 2017).

Mitotically inactivated gamma-irradiated newborn human foreskin fibroblasts (NuFFs) were used as the feeder layer for the newly reprogrammed cells. They are commonly used as a foundation for the cells and are capable of secreting growth factors that positively influence the health of the culture, the success of reprogramming and the maintenance of primary iPSC colonies. This particular batch of NuFFs has been previously used in our laboratory to sustain fibroblasts undergoing mRNA reprogramming (Petrova *et al*., 2014).

To increase cell viability following SeV transduction and provide optimal cell culture conditions, we used NuFF-conditioned Pluriton medium from day 7 after reprogramming until the primary iPSC colonies were re-plated onto NuFF feeder plates (normally at Day 22).

After transduction with SeV, the cells were monitored daily for morphological changes. Cell death could be observed in the first 24 h post-transduction. The changes in morphology that occurred during reprogramming were similar among all three lines (nMSC12, nMSC13 and nMSC14) and are illustrated in Figures 3.5.2 – 3.5.4. From day 5, cells started showing visible signs of transition from mesenchymal to epithelial morphology. From day 10, we could identify cell compaction and colony formation. Primary iPSC colonies could be observed from day 14 after SeV transduction.

Compact colonies of cells with distinct borders were easily distinguishable approximately three weeks from the start of reprogramming. A large number of such colonies were present in all 3 lines (Figure 3.5.5 and Table 3.5.1). Ten colonies chosen by their similar morphology as ESC colonies with distinct borders and compact cells were manually picked and transferred onto the HFF feeder layer on day 22 - 25 for each of the three cell lines. Reprogrammed nMSC12 we called iMSC12 (abbreviated from iPSC-MSC12). Reprogrammed nMSC13 we called iMSC13 and reprogrammed nMSC14 we called iMSC14.

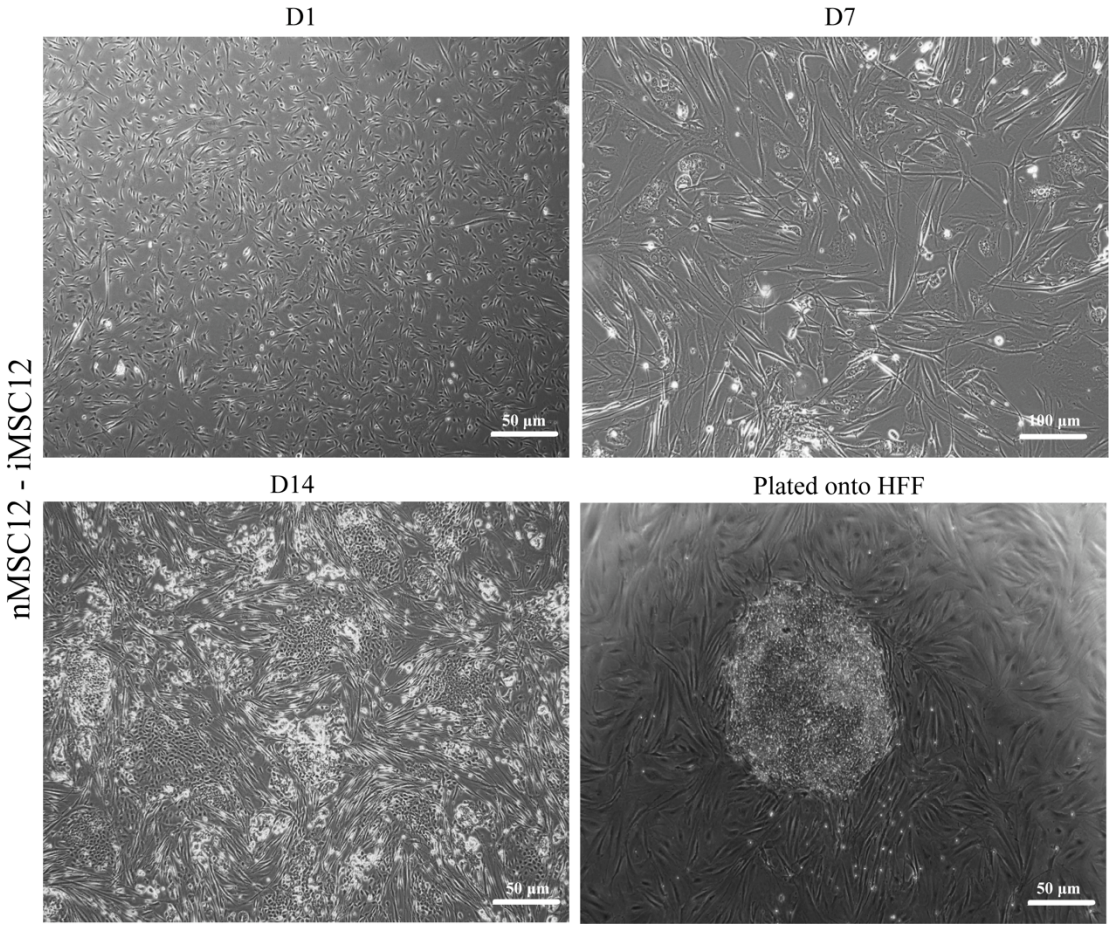

Figure 3.5.2 Changes in morphology of nMSC12 during SeV-mediated reprogramming. D1, donor 12 nMSCs first day of transduction with SeV. **D7,** cell death could barely be observed and the cells showed the first signs of transition. **D14,** cells already plated onto NuFF feeders showing signs of cell compaction and colony formation. **Plated onto HFF,** primary iMSC colony plated and attached onto the HFF feeder layer (day 23 after transduction with SeV and day 4 after plating onto HFF) for further expansion. Scale bar: 50 and 100 µm.

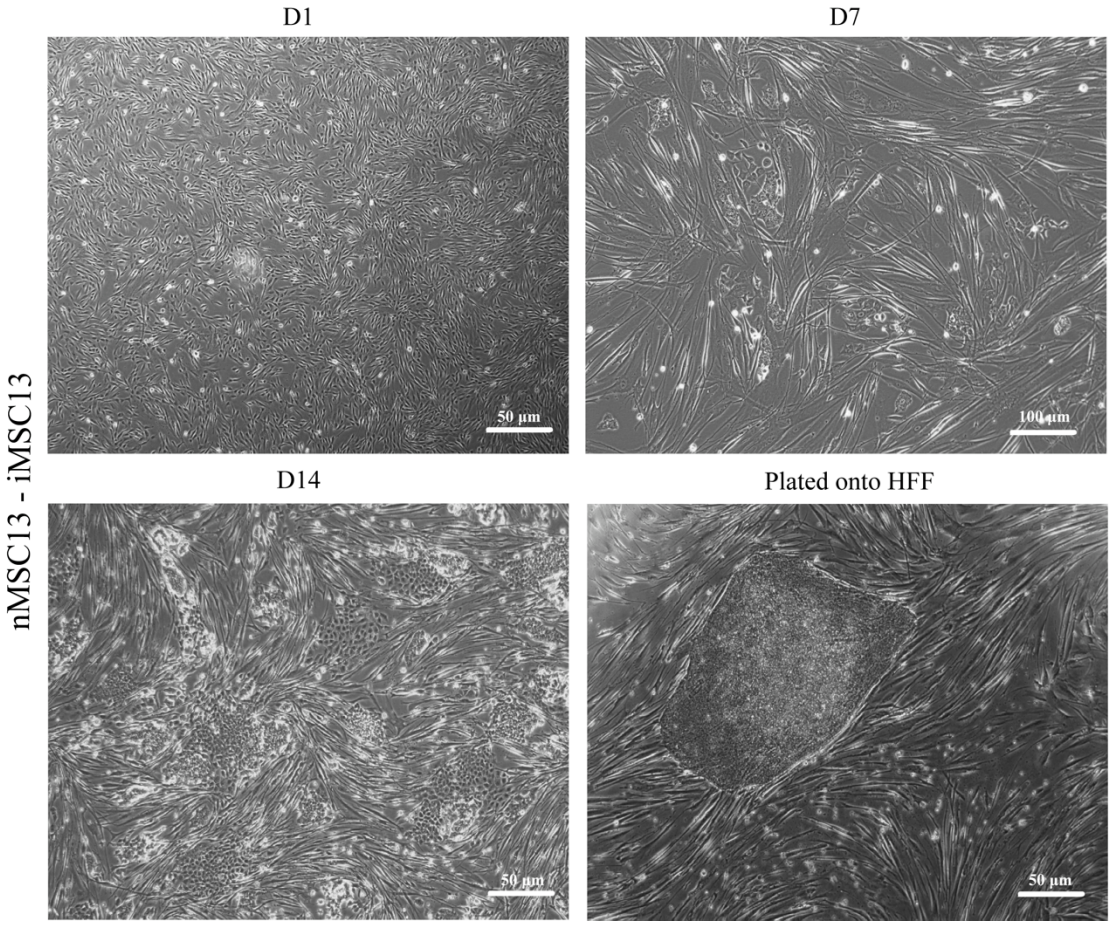

Figure 3.5.3 Changes in morphology of nMSC13 during SeV-mediated reprogramming timeline in pictures. D1, donor 13 nMSCs first day of transduction with SeV. **D7,** cell death could be observed. **D14,** cells were plated onto NuFF feeders and the attachment occurred successfully. **Plated onto HFF,** primary iMSC colony plated and attached onto HFF feeder layer (day 25 after transduction with SeV and day 3 after plating onto HFF) for further expansion. Scale bar: 50 and 100 µm.

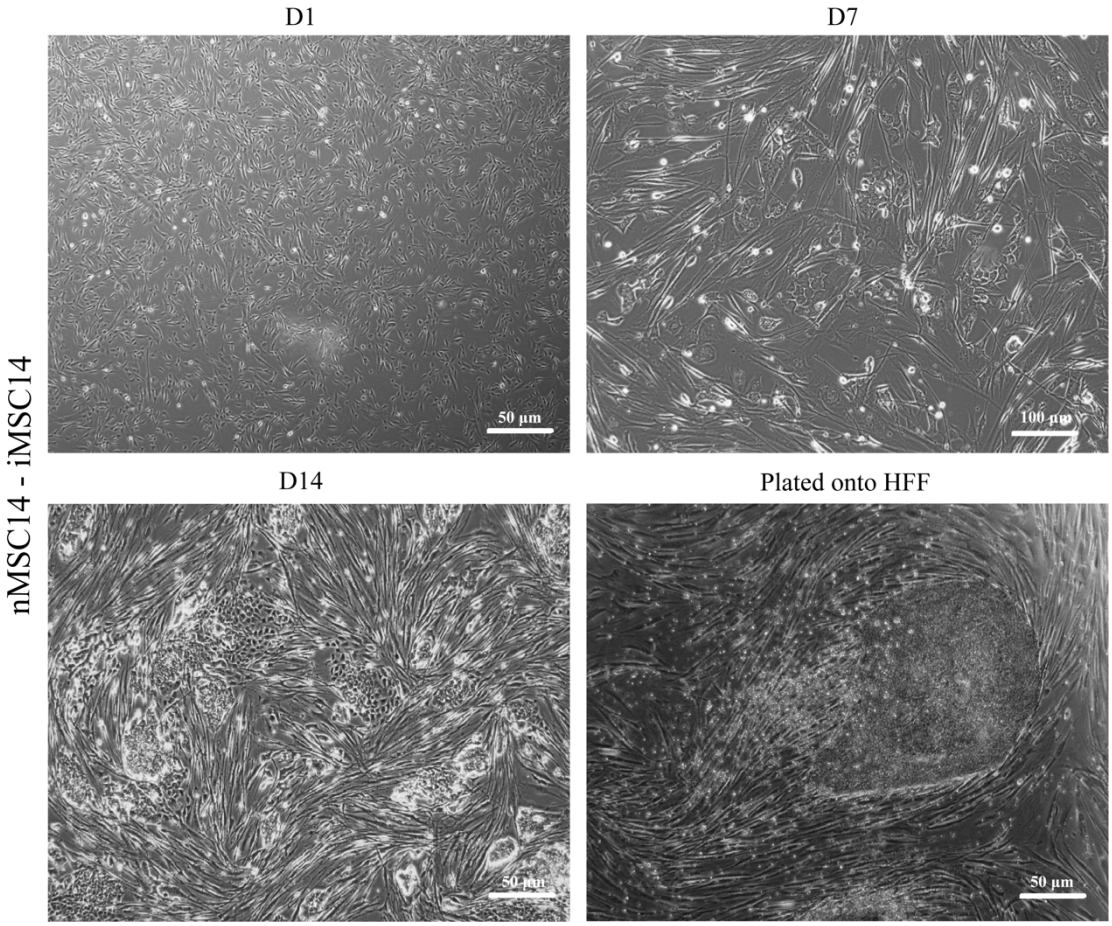

Figure 3.5.4 Changes in morphology of nMSC14 during SeV-mediated reprogramming. D1, donor 14 nMSCs first day of transduction with SeV. **D7,** cell death could be observed and also signs of changes in cell morphology. **D14,** cells were plated onto NuFF feeders and signs of cell compaction and colony formation were identified. **Plated onto HFF,** primary iMSC14 colonies plated and attached onto the HFF feeder layer (day 25 after transduction with SeV and day 3 after plating onto HFF) for further expansion. Scale bar: 50 and 100 µm.

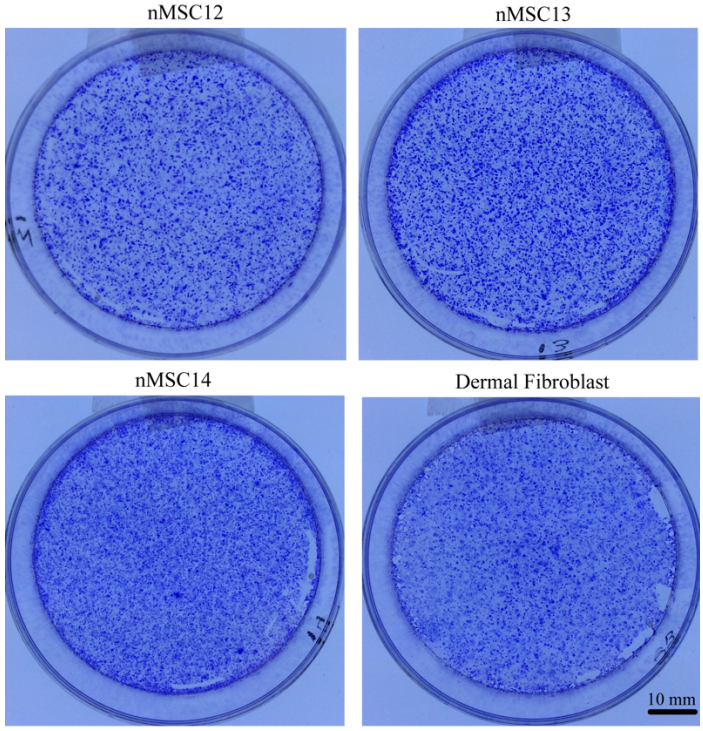

Figure 3.5.5 Trypan blue staining of colonies in one P60 culture dish (60-mm diameter) at Day 21 post SeV transduction.

Table 3.5.1 Colony counting using ImageJ Software.

Donor	Colony count
nMSC12 – iMSC12	1413
nMSC13 – iMSC13	2586
nMSC14 – iMSC14	1789
Dermal Fibroblast - iDF	1989

We continued expanding only four colonies out of the ten chosen previously from each of the three iMSC lines. The four colonies were chosen by their morphology (as similar as possible with ESC colonies, with distinct border and compact cells showing no signs of cell differentiation). After three passages onto HFF feeders, we vitrified the majority of the colonies. However, iMSC14 colonies in general grew slower and were more difficult to maintain than iMSC12 and iMSC13 colonies. Therefore, for further work, we focussed on iMSC12 and iMSC13 only. One colony from each background was expanded further and adapted to feeder-free conditions (Stephenson *et al.*, 2012) (Figure 3.5.6).

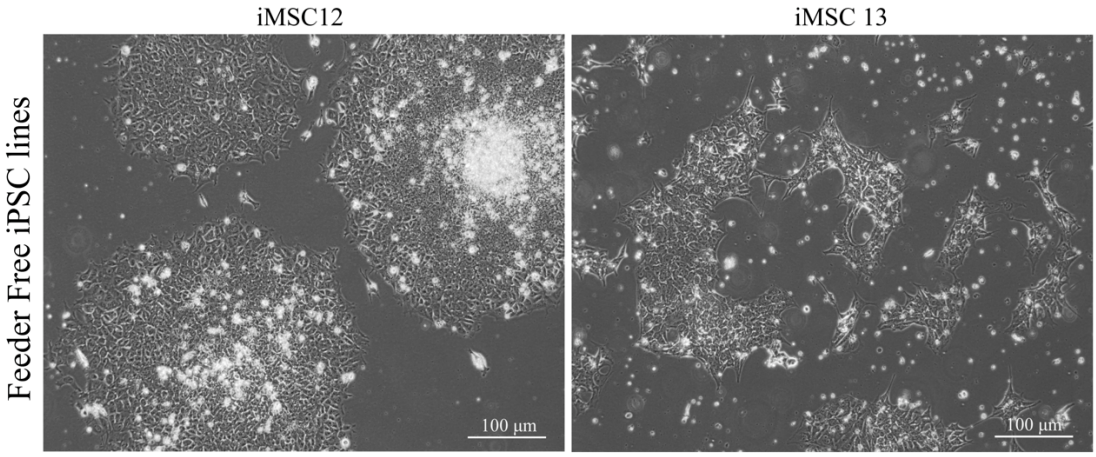

Figure 3.5.6 iMSC12 and iMSC13 adapted to feeder-free conditions showed typical morphology of undifferentiated iPSC. Scale bar: 100 µm.

3.6 ANALYSIS OF SeV GENE EXPRESSION IN iPSC LINES

SeV is a non-integrating RNA virus that remains in the cytoplasm of cells and therefore can be diluted out of the cells after 10 or more passages. Following feeder-free adaptation and 60 days in culture with constant passages, the SeV gene was undetectable in the genome of iMSC12 and iMSC13 (Figure 3.6.7). This means that no exogenously expressed genes were present and the lines from this point were fully reprogrammed. Further characterization and differentiation followed to prove the lines were indeed iPSCs.

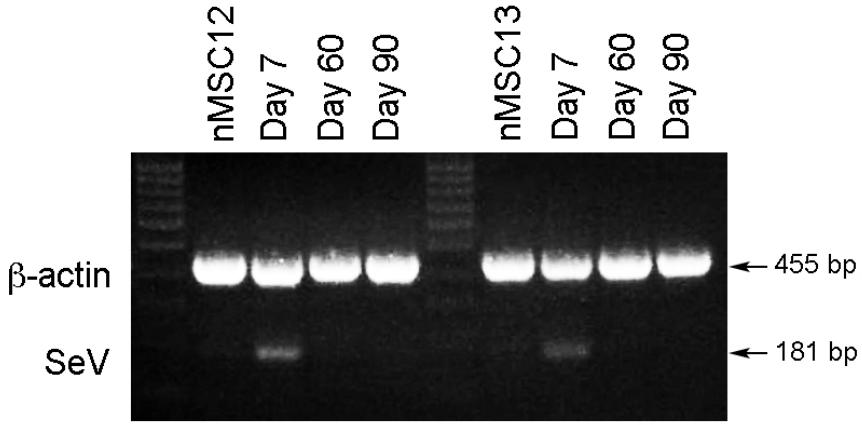

Figure 3.6.7 SeV DNA was undetectable in iMSC12 and iMSC13 two months after transduction. Original non-transduced native MSC lines (nMSC12 and nMSC13) were used as negative controls; 7 days post-SeV transduction cells were used as positive controls (Day 7). Two points were analysed, Day 60 and Day 90 in culture, and both points were negative for SeV expression. B-Actin *(ACTB)* PCR product is 455 bp, whereas SeV is 188 bp. MW: 100 bp ladder.

3.7 CHARACTERIZATION OF iPSC LINES

Characterization was performed following our standard procedures with hESC lines (Stephenson *et al.*, 2012) and included detection of markers associated with pluripotency, spontaneous differentiation into three germ layers *in vitro* and *in vivo*, DNA fingerprinting and array CGH.

3.7.1 Expression of markers associated with pluripotency

Pluripotency was confirmed by immunostaining for four markers associated with pluripotency: transcription factors NANOG and POU5F1 (*OCT4*) and surface antigens TRA-1-60 and TRA-1-81 expressed on a podocalyxin-like sialoglycoprotein (PODXL) (Figure 3.7.1).

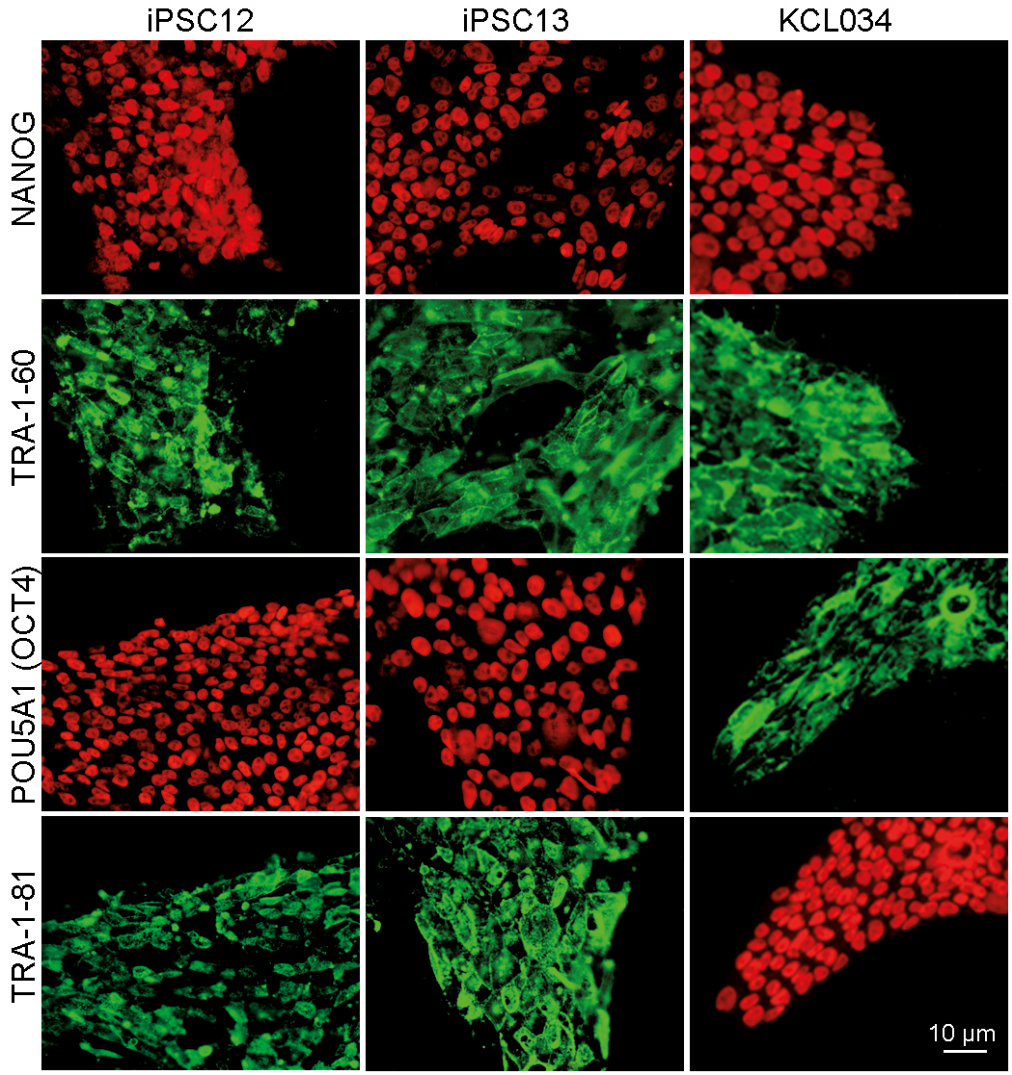

Figure 3.7.1 iMSC12 and iMSC13 showing markers associated with pluripotency by immunostaining (OCT4, NANOG, TRA-1-60, TRA-1-81). hESC line KCL034 was used as a positive control. Scale bar: 10 µm.

3.7.2 Spontaneous differentiation into three germ layers in vitro

Differentiation of three germ layers *in vitro* is confirmed by the detection of the following markers: smooth muscle actin (red) for mesoderm, β-III tubulin (red) for ectoderm and α-fetoprotein (red) for endoderm.

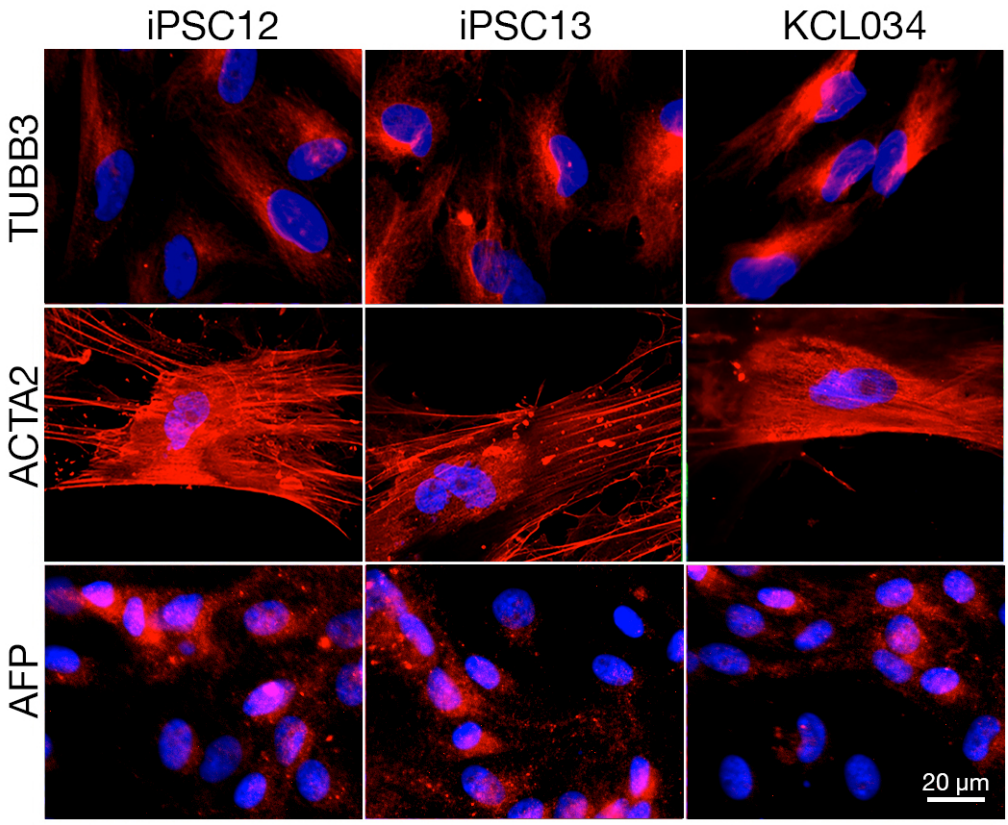

Figure 3.7.2 Both iMSC12 and iMSC13 can differentiate into all three germ layers in vitro. Spontaneous differentiation is confirmed by the detection of germ-layer markers: β-tubulin for ectoderm, α-fetoprotein for endoderm and smooth muscle actin for mesoderm. hESC line KCL034 was used as a positive control. Scale bar: 20 µm.

3.7.3 Spontaneous differentiation into three germ layers in vivo

The standard *in vivo* assay for demonstrating the pluripotency of hESCs and iPSCs is their ability to form teratomas, non-malignant tumours, when implanted into a host animal, commonly an immunocompromised mouse (Prokhorova *et al.*, 2009; Przyborski, 2005). Solid parts of teratomas generated from iMSC12 and iMSC13 contained tissue derived from all three germ layers, confirming their pluripotent nature (Figure 3.7.3).

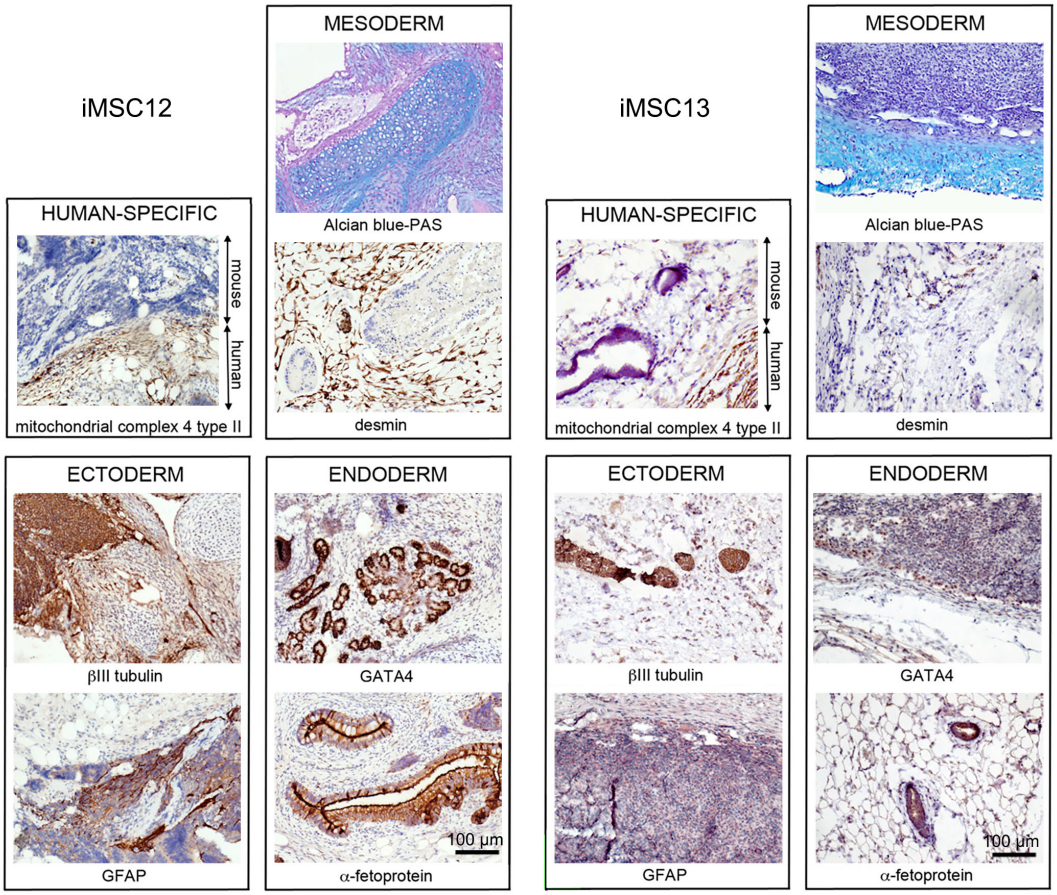

Figure 3.7.3 Both iMSC12 and iMSC13 can differentiate into all three germ layers in vivo. Spontaneous differentiation is confirmed by the detection of germ-layer markers: β tubulin (TUBB3) and glial fibrillary acidic protein (GFAP) for ectoderm, α-fetoprotein (AFP) and GATA binding protein 4 (GATA4) for endoderm and desmin (DES) and Alcian blue – Periodic Acid Schiff (PAS) for mesoderm. Scale bar: 100 µm.

3.7.4 Genotyping – DNA fingerprint

To identify cell lines to the individual level in case of possible cross contamination in the future, we performed DNA fingerprinting on parental nMSC12 and nMSC13 lines (Figure 3.7.4). Although this method is highly specific to the level of an individual and can better discriminate any cross-contamination with cell lines of human origin, it is not designed to detect inter-species contamination. Since the whole laboratory is working under xeno-free conditions and we do not carry any animal cell lines, inter-species contamination was not of concern.

nMSC 12

Marker	Allele 1	Allele 2
D13S252	299	299
D13S305	477	486
D13S325	289	293
D13S628	453	457
D13S634	412	416
D18S386	363	386
D18S390	372	376
D18S391	213	213
D18S535	482	486
D18S819	412	416
D18S976	480	483
D18S978	219	219
D21S11	241	251
D21S1409	224	228
D21S1411	308	312
D21S1435	185	189
D21S1446	311	326

nMSC 13

Marker	Allele 1	Allele 2
D13S252	303	303
D13S305	473	485
D13S325	285	301
D13S628	429	457
D13S634	401	401
D18S386	381	382
D18S390	372	372
D18S391	217	217
D18S535	482	482
D18S819	400	412
D18S976	479	479
D18S978	211	215
D21S11	245	245
D21S1409	212	224
D21S1411	304	308
D21S1435	180	184
D21S1446	311	319

Figure 3.7.4 DNA fingerprinting. Microsatellite markers specific for chromosomes 13, 18, 21, X and Y were amplified. The sex chromosome markers were consistent with a female complement in both lines. The allele sizes in base pairs for markers on chromosomes 13, 18 and 21 are listed.

3.8 DIFFERENTIATION OF iPSCs AND hESCs INTO MSC-LIKE CELLS

To determine how close MSCs differentiated from pluripotent stem cells are to nMSC, we followed two different protocols: ARGENTINA (ARG; Luzzani *et al*. 2015) and TEXAS (TEX; Zhao *et al.*, 2015). The pluripotent lines were iPSC12, iPSC13 and the hESC line KCL034, which was used as a control (Figure 3.8.1).

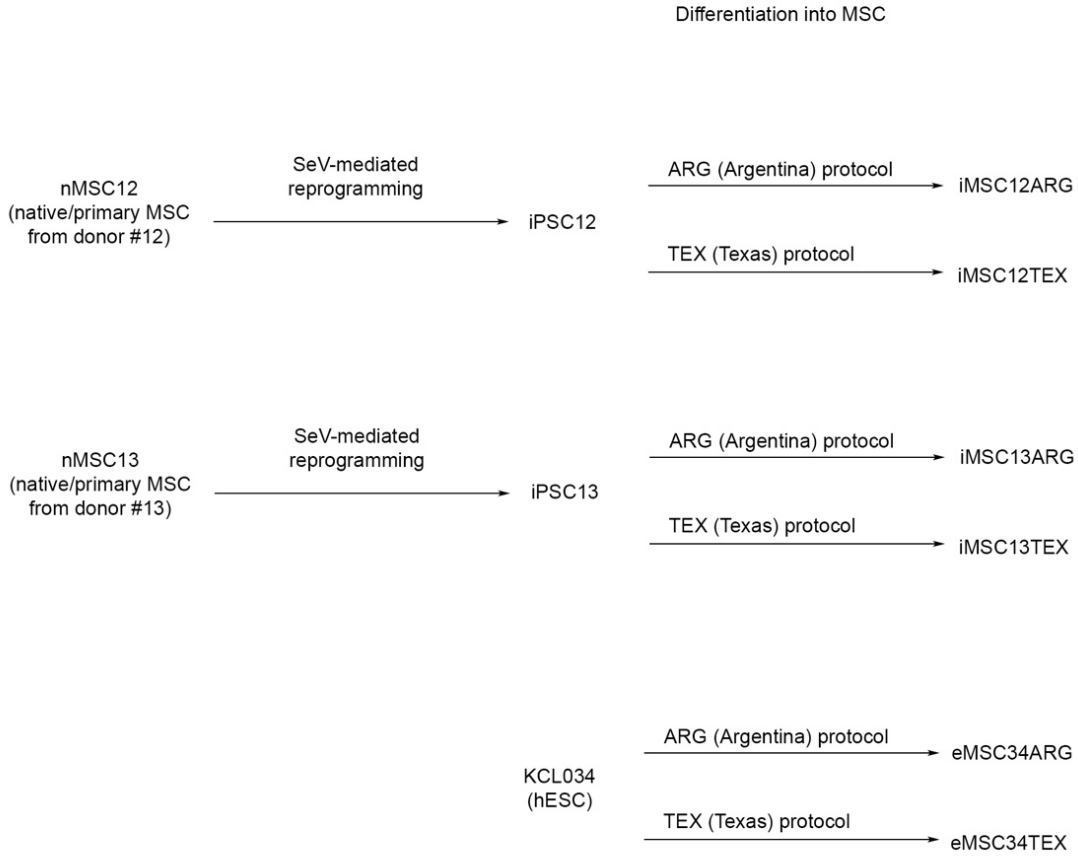

Figure 3.8.1 Schematic diagram of the experimental strategy.

A difference between the two protocols was obvious in cell morphology after 4 days (Figure 3.8.2 and 3.8.3) and it persisted among $CD73^{+}CD90^{+}CD105^{+}$ sorted cells cultured in dXF on tissue culture-treated plastic.

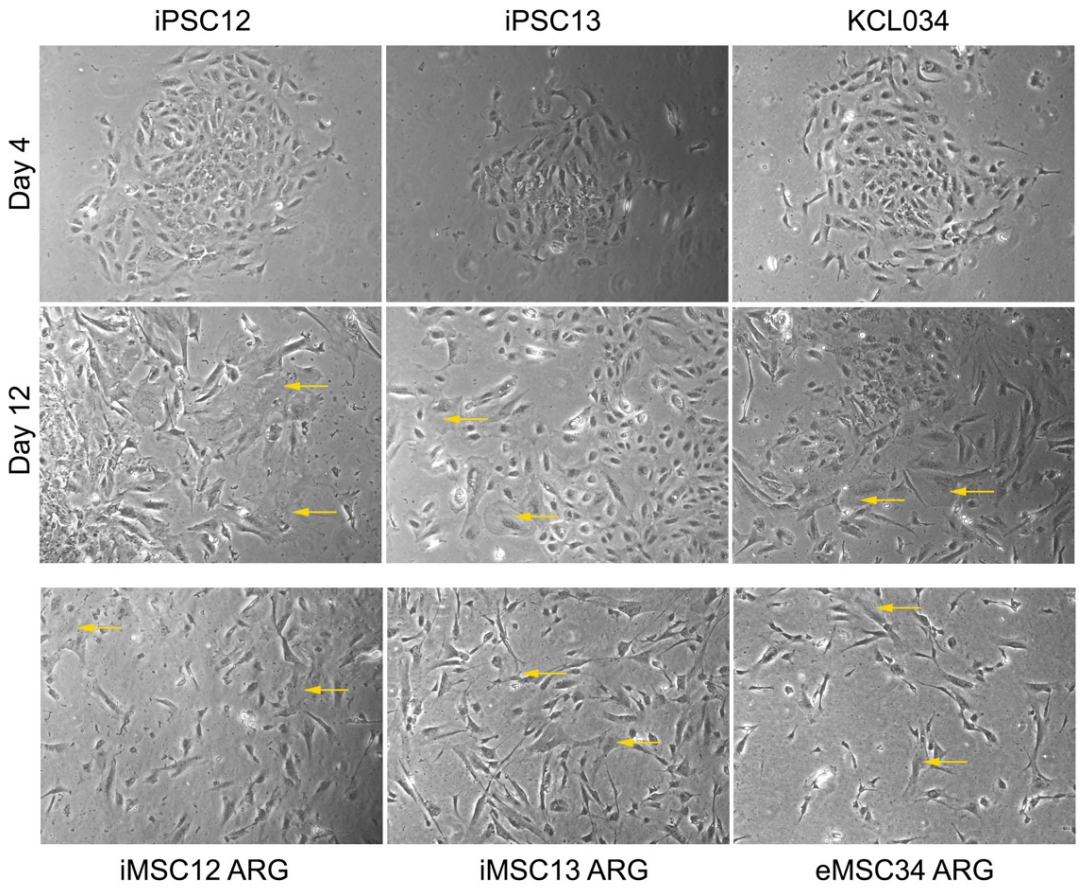

Figure 3.8.2 Change in cell morphology during differentiation of iPSCs into iMSC ARG. Top row (Day 4): Tight cell-cell contacts, typical for densely packed pluripotent stem cell colonies, are completely lost. Middle row (Day 12): Appearance of large flattened cells indicated cellular senescence (yellow arrows). Bottom row: iMSCs and eMSCs growing on tissue culture-treated plastic in dXF.

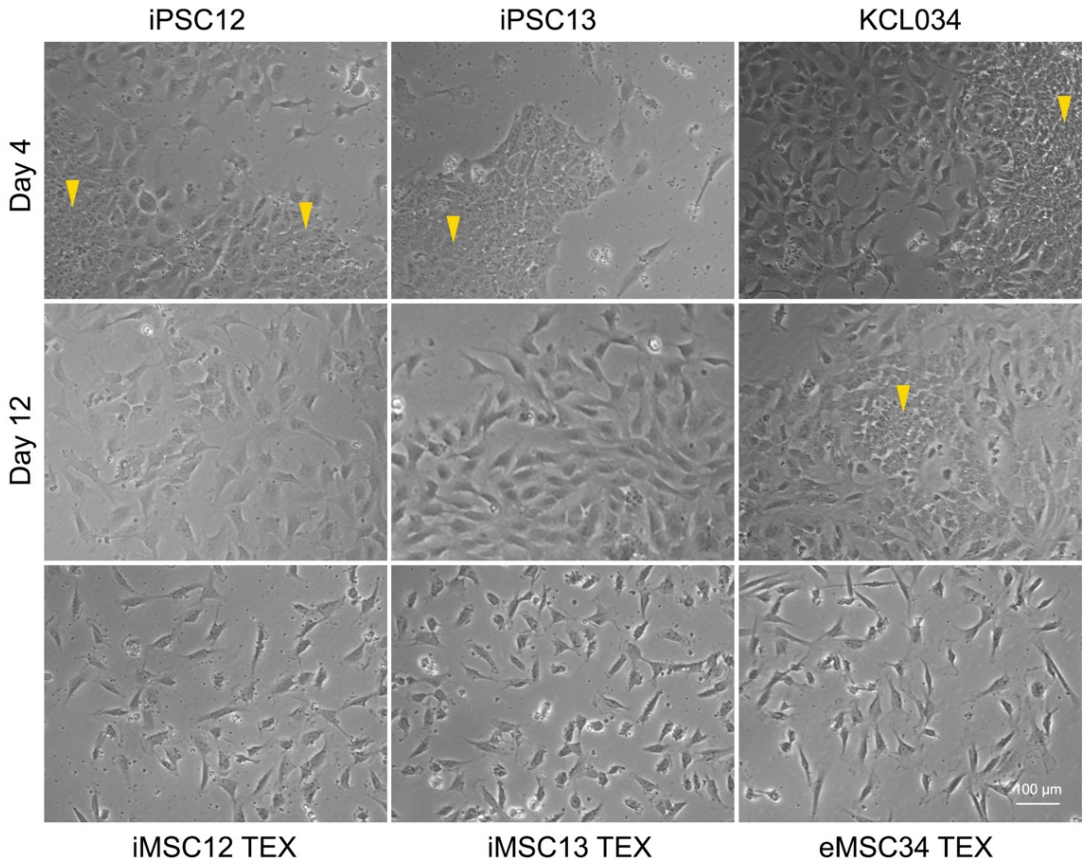

Figure 3.8.3 Change in cell morphology during differentiation of iPSCs into iMSC TEX. Top row (Day 4): The fibroblast-like cells undergoing differentiation are mixed with seemingly intact pluripotent stem cell colonies (yellow arrowheads). Middle row (Day 12): All differentiating iPSC12 and iPSC13 have uniform fibroblast-like morphology, whereas some of the differentiating hESC KCL034 still form colonies resembling pluripotent stem cells (yellow arrowheads). Bottom row: iMSCs and eMSCs growing on tissue culture-treated plastic in dXF.

Senescent cells were observed in both iPSC12 and 13 and hESC KCL034 lines undergoing the ARG differentiation protocol as early as Day 12. They were never observed in any of three lines undergoing the TEX differentiation protocol. This suggested that the iMSC12 TEX, iMSC13 TEX and eMSC34 TEX might maintain some of their stem cell-like characteristics and represent a type of MSC progenitor, whereas iMSC12 ARG, iMSC13 ARG and eMSC34 ARG might be closer to primary MSC, which are a mixture of progenitors and the cells that lost stem cell-like characteristics and have more limited proliferation capacity.

3.9 CHARACTERIZATION OF iMSCs AND eMSCs

3.9.1 iMSCs and eMSC originating from the TEX protocol have significantly higher differentiation potential to adipo- and chondrogenic than those originating from the ARG protocol

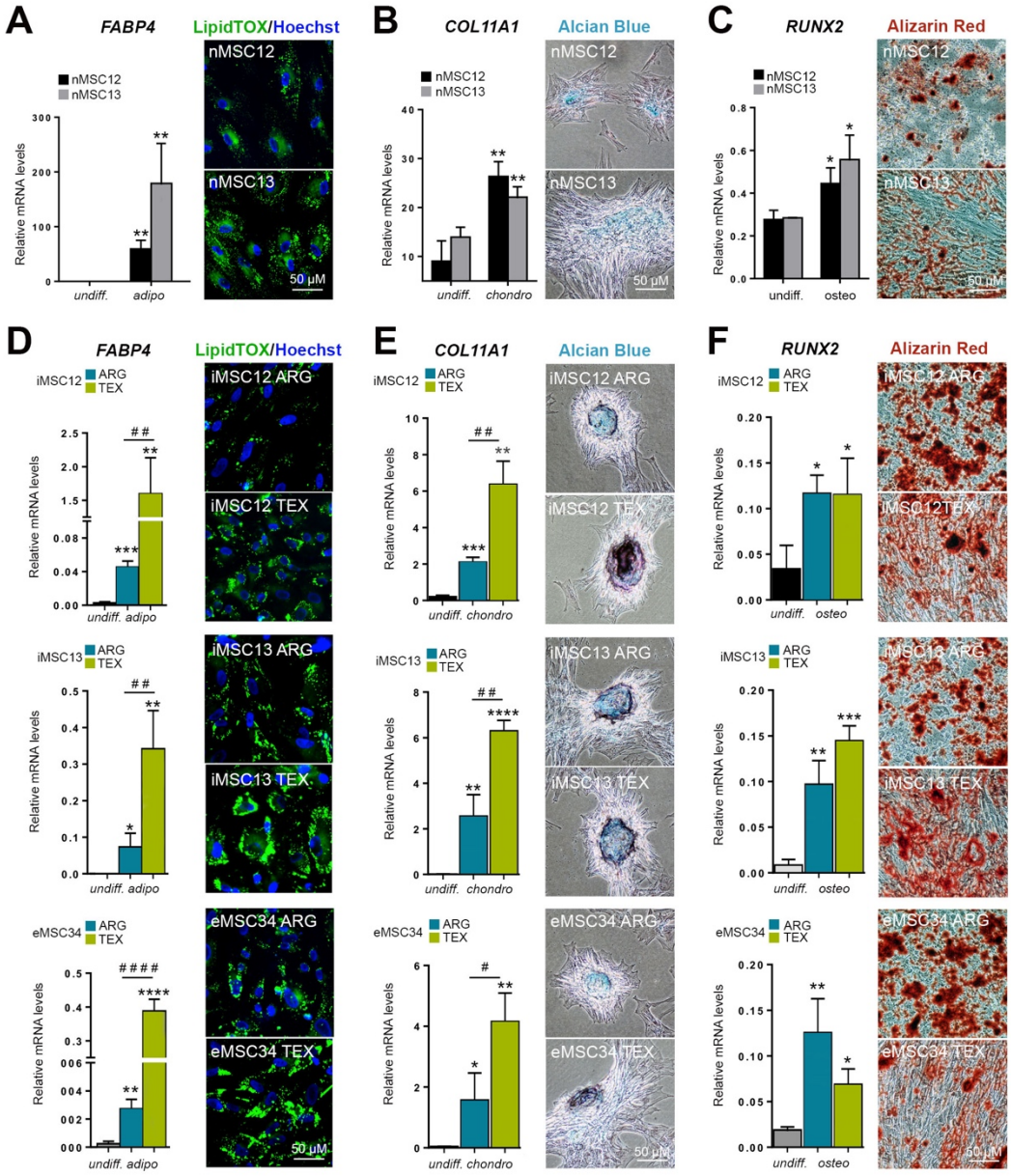

Figure 3.9.1 Differentiation potential. (A) nMSCs that were exposed to adipogenic differentiation medium showed accumulation lipid droplets as detected with LipidTOX stain and had a significantly

higher (**p≤0.01) expression of fatty acid binding protein 4 (*FABP4*). No significant difference in *FABP4* levels was detected between nMSC12 and nMSC13. (B) nMSCs that were exposed to chondrogenic differentiation medium were positive for cartilage glycosaminoglycans as detected by Alcian Blue staining and had a significantly higher (**p≤0.01) expression of collagen 11 (*COL11A1*). No significant difference in *COL11A1* levels was detected between nMSC12 and nMSC13. (C) nMSCs that were exposed to osteogenic differentiation medium were full of mineral accumulations as detected by Alizarin Red staining and had a significantly higher (*p≤0.05) expression of runt related transcription factor 2 (*RUNX2*). No significant difference in *RUNX2* levels was detected between nMSC12 and nMSC13. (D) Following adipogenic differentiation, all i/eMSC lines showed accumulation of lipid droplets and significantly higher (***p≤0.001, **p≤0.01, *p≤0.05) expression of *FABP4*. All lines generated using the TEX protocol (iMSC12 TEX, iMSC13 TEX and eMSC34 TEX) had a significantly higher ($^{\#\#\#\#}$p≤0.0001, $^{\#\#}$p≤0.01) expression of FAPB4 than the lines generated using the ARG protocol (iMSC12 ARG, iMSC13 ARG and eMSC34 ARG). (E) Following chondrogenic differentiation, all i/eMSC lines were positive for cartilage glycosaminoglycans as detected by Alcian Blue staining and had a significantly higher (****p≤0.0001, ***p≤0.001, **p≤0.01, *p≤0.05) expression of *COL11A1*. All lines generated using the TEX protocol (iMSC12 TEX, iMSC13 TEX and eMSC34 TEX) had a significantly higher ($^{\#\#}$p≤0.01, $^{\#}$p≤0.05) expression of *COL11A1* than the lines generated using the ARG protocol (iMSC12 ARG, iMSC13 ARG and eMSC34 ARG). (F) Following osteogenic differentiation, all i/eMSC lines were full of mineral accumulation and had a significantly higher (***p≤0.001, **p≤0.01, *p≤0.05) expression of *RUNX2*. There were no significant differences in *RUNX2* expression between the lines generated using the TEX protocol (iMSC12 TEX, iMSC13 TEX and eMSC34 TEX) and the lines generated using the ARG protocol (iMSC12 ARG, iMSC13 ARG and eMSC34 ARG) after culture under osteogenic conditions.

To determine whether iMSCs and eMSCs possess MSC differentiation ability, we cultured them in adipo-, chondro- and osteogenic differentiation medium. All MSC, regardless of their origin, were positive for markers of adipose tissue, cartilage or bone (Figure 3.9.1). However, when we compared the lines generated from pluripotent stem cells, all that were generated using the TEX protocol had significantly higher expression of adipogenic and chondrogenic markers than those of ARG origin (Figure 3.9.1 D, E). Such a difference was not found after osteogenic differentiation (Figure 3.9.1 F). These data are in agreement with the previous observation of cellular morphology, which suggested that lines of TEX origin are closer to the progenitor level.

3.9.2 iMSCs and eMSC originating from the TEX protocol have significantly lower immunomodulatory potential than those originating from the ARG protocol

Since MSCs can exert potent immunosuppressive and immunoregulatory effects (Wang *et al.*, 2014; Ma *et al.*, 2014; Marigo and Dazzi, 2011), we assessed the immunomodulatory properties of triple positive ($CD73^+CD90^+CD105^+$) iMSCs and eMSCs (Figure 3.9.2). The cells were compared for their ability to inhibit phytohemagglutinin A (PHA)-induced proliferation of peripheral blood mononuclear cells (PBMC). nMSCs had similar immunomodulatory properties with the clinical grade BM MSCs used as a reference. nMSCs performed slightly better, whereas at an MSC:PBMC ratio of 1:80, no immunomodulatory effect was observed with BM MSCs, but nMSCs were still able to inhibit the proliferation of PBMCs. The weakest immunosuppressive effect was observed in the presence of e/iPSCs originating through the TEX protocol (undetectable at 1:20), whereas e/iPSCs originating with the ARG protocol were somewhere between (undetectable at 1:40).

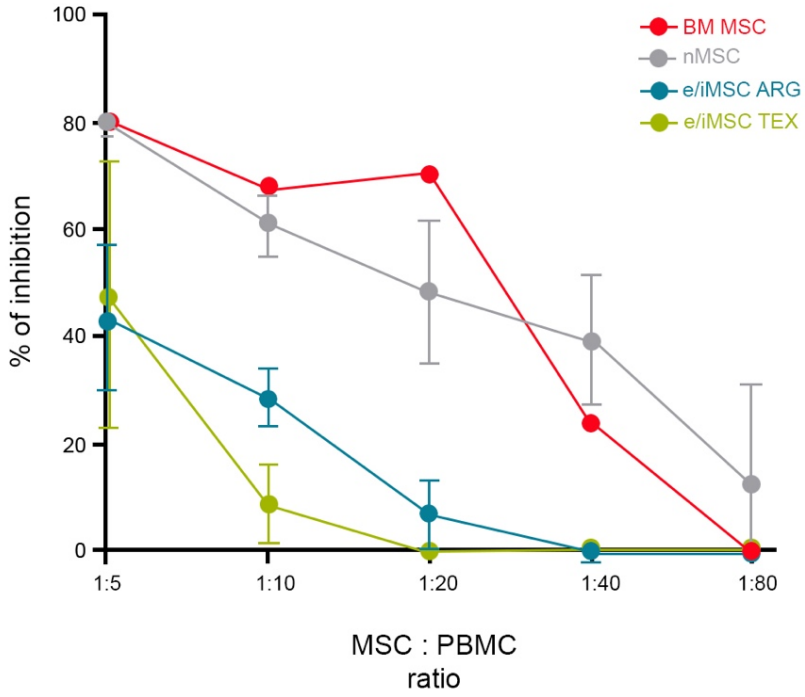

Figure 3.9.2 Immunomodulatory properties are less effective in MSCs derived from pluripotent stem cells. nMSCs inhibited phytohemagglutinin-stimulated human PBMC proliferation in a dose-dependent manner in a similar fashion as BM MSCs (MSC:PSC ratio 1:80), whereas an immunosuppressive effect could not be detected at an MSC:PBMC ratio of 1:20 in e/iMSCs of the TEX protocol origin and at an MSC:PBMC ratio of 1:40 20 in e/iMSCs of the ARG protocol origin.

3.10 TRANSCRIPTOME ANALYSES

To determine which of two differentiation protocols, ARG or TEX, yields MSCs phenotypically and functionally closer to parental nMSCs, we ran multiple comparative analyses of a whole transcriptome array of unstimulated and interferon gamma (IFNγ) stimulated MSC lines of different origin using the Illumina HumanHT-12 v4 Expression BeadChip. To normalise the data, the housekeeping genes used were GAPDH, ACTB and HPRT1 (see Appendix).

3.10.1 Comparison of iMSC12 ARG and iMSC12 TEX with nMSC12

To determine the differentially expressed genes and their associated pathways between iMSC12 TEX and nMSC12 and between iMSC12 ARG and nMSC12, we used the R/Bioconductor software package limma that provides an integrated solution for differential expression analyses of data from gene expression experiments.

We found that iMSC12 from both protocols (TEX and ARG) have a high number of differentially expressed genes (Table 3.10.1). The number of differentially expressed genes is higher using TEX than ARG (2401 vs. 2029). However, there were no significant differences between protocols in terms of fold-change median values (2.85 in iMSC12 ARG vs. nMSC12 and 2.78 in iMSC12 TEX and nMSC12).

Table 3.10.1 Differentially expressed genes in iMSC12.

Comparison	# regulated genes (up/down)	Median FC	Significant pathways
iMSC12 ARG **vs.** nMSC12	2029 (975/1054)	2.85	• Cell adhesion • Immune system
iMSC12 TEX **vs.** nMSC12	2401 (1124/1277)	2.78	• Cell cycle • Cell adhesion • Immune system

Approximately half of the genes with different regulation in iMSC12 ARG (1054 out of 2029 genes or 51.9%) are also differently regulated in iMSC12 TEX (1054 out of 2401 genes or 43.9%). Most of the common genes have the same up/down regulation (Figure 3.10.1).

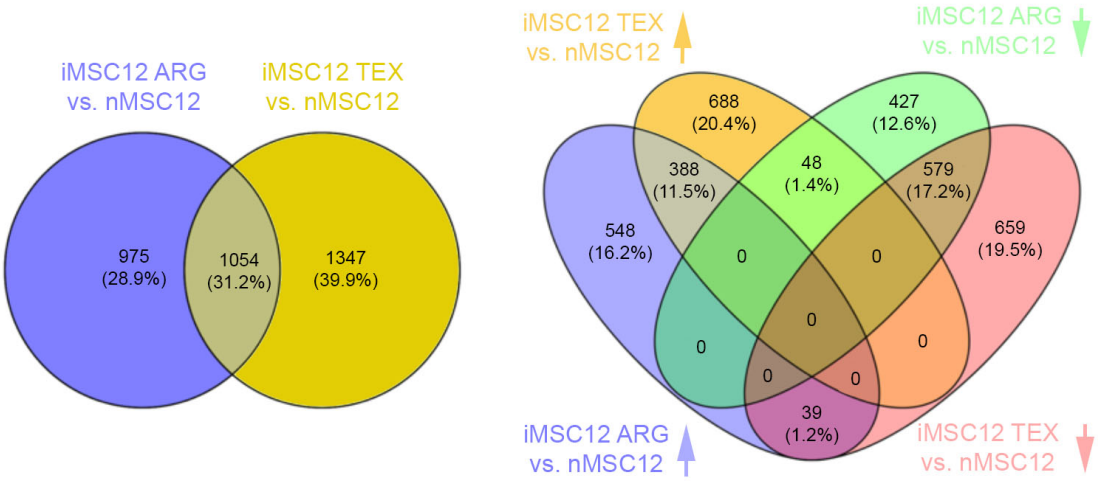

Figure 3.10.1 Overlap between two comparisons (iMSC12 ARG vs. nMSC12 and iMSC12 TEX vs. nMSC12) shown as Venn diagrams.

To determine whether iMSC12 ARG or iMSC12 TEX is closer to paternal nMSC12, we used the R/Bioconductor software packages limma and hclust for Euclidean distance. Even if there were more regulated genes with TEX than ARG (2401 vs. 2029), based on the expression of all expressed genes, samples from the TEX protocol (iMSC12 TEX) were clearly closer to nMSC12 than samples from the ARG protocol (iMSC12 ARG) (Figure 3.10.2).

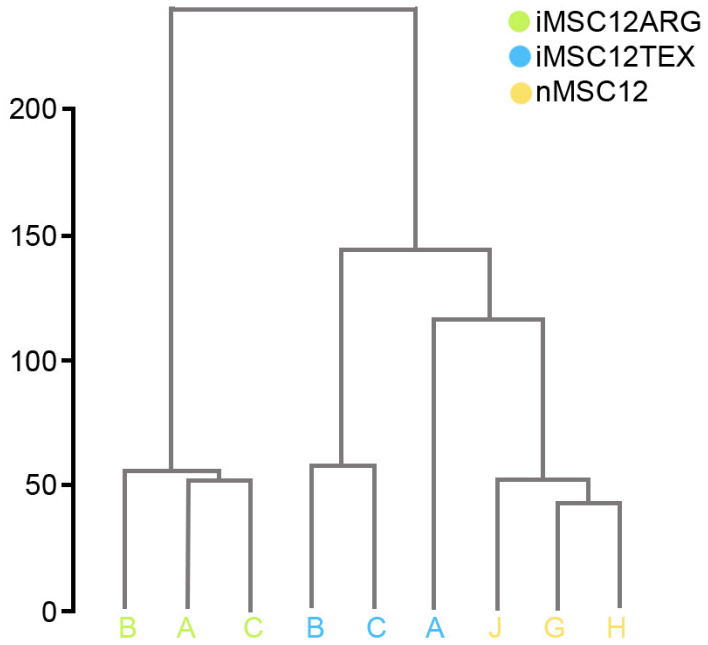

Figure 3.10.2 Unsupervised clustering (Euclidian distance) of samples from donor 12 (nMSC12, iMSC12 ARG and iMSC12 TEX).

To explain this difference, we checked the variance distribution between iMSC12 ARG/nMSC12 and iMSC12 TEX/nMSC12 (Figure 3.10.3). The variances were higher between gene expression from the iMSC12 ARG/nMSC12 groups than between gene expression from the iMSC12 TEX/nMSC12 groups.

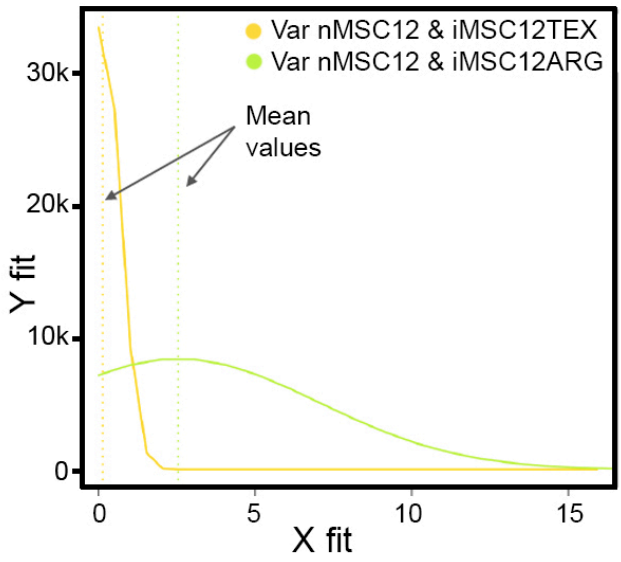

Figure 3.10.3 Distribution variance and mean values.

Taking these data together, even though the number of differentially expressed genes is slightly higher using the TEX protocol, unsupervised clustering and variance analysis show that iMSC12 TEX cells are closer to nMSC12 than iMSC12 ARG.

3.10.2 Comparison of iMSC13 ARG and iMSC13 TEX with nMSC13

Using the same approach, we then determined the differentially expressed genes and their associated pathways between iMSC13 TEX and nMSC13 and between iMSC13 ARG and nMSC13 on the other side.

We found that iMSC13 from both protocols (TEX and ARG) have a high number of differentially expressed genes (Table 3.10.2). However, in this case, the number of differentially expressed genes was higher using ARG than TEX (3065 vs. 2724). Similarly, there were no significant differences between protocols in terms of fold-change median values (2.83 in iMSC13 ARG vs. nMSC13 and 2.87 in iMSC13 TEX and nMSC13).

Table 3.10.2 Differentially expressed genes in iMSC13.

Comparison	# regulated genes (up/down)	Median FC	Significant pathways
iMSC13 ARG **vs.** nMSC13	3065 (1612/1453)	2.83	• Cell cycle • DNA repair • Cell adhesion • Immune system
iMSC13 TEX **vs.** nMSC13	2401 (1371/1353)	2.87	• Cell cycle • DNA repair • Cell adhesion • Immune system

The majority of genes with different regulation in iMSC13 TEX (2312 out of 2724 genes or 84.9%) are also differently regulated in iMSC13 ARG (2312 out of 3065 genes or 75.4%). Most of the common genes have the same up/down regulation (Figure 3.10.4).

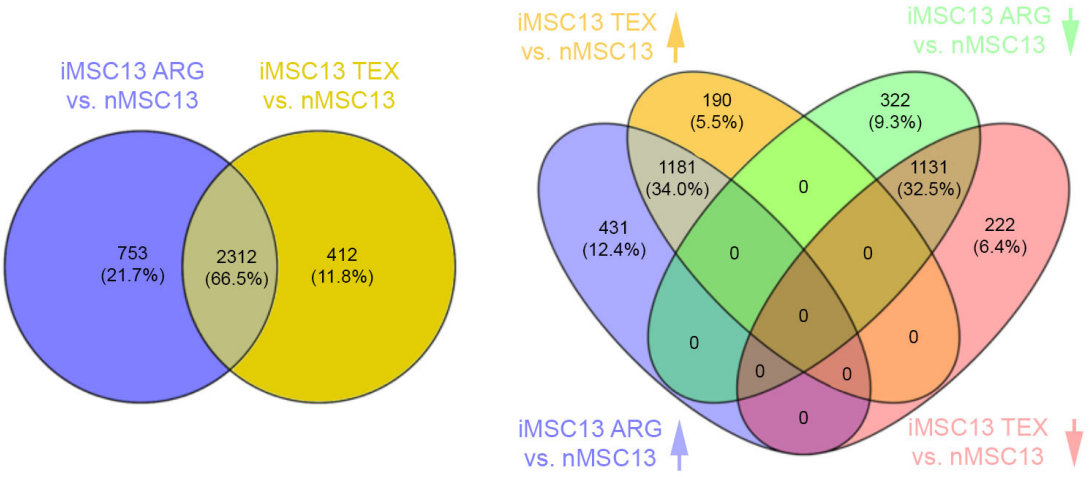

Figure 3.10.4 Overlap between two comparisons (iMSC13 ARG vs. nMSC13 and iMSC13 TEX vs. nMSC13) shown as Venn diagrams.

Based on the expression of all expressed genes, samples from the TEX protocol (iMSC13 TEX) were clearly closer to nMSC13 than samples from the ARG protocol (iMSC13 ARG) (Figure 3.10 5).

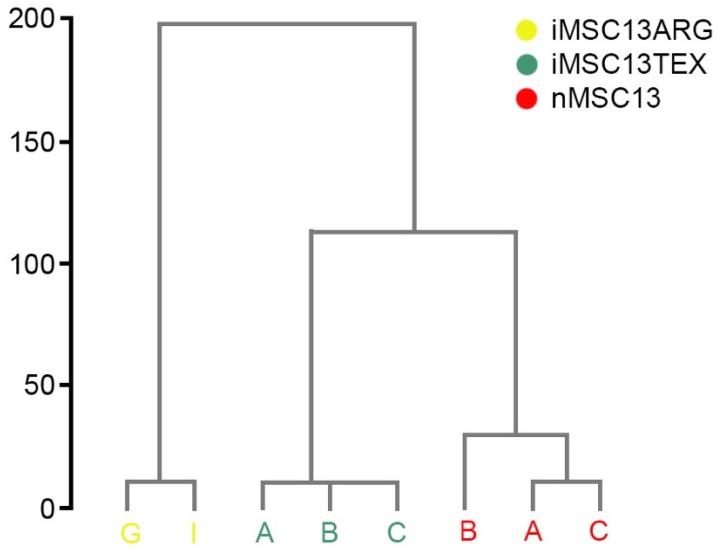

Figure 3.10.5 Unsupervised clustering (Euclidian distance) of samples from donor 13 (nMSC13, iMSC13 ARG and iMSC13 TEX).

Variance distribution between iMSC13 ARG/nMSC13 and iMSC13 TEX/nMSC13 (Figure 3.10.6). The variances were higher between gene expression from the iMSC13 ARG/nMSC13 groups than between gene expression from the iMSC13 TEX/nMSC13 groups.

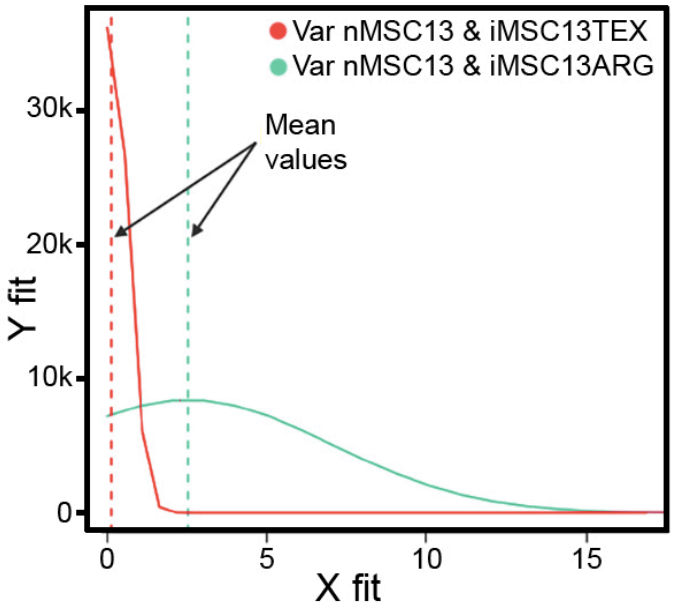

Figure 3.10.6 Distribution variance and mean values.

Unsupervised clustering and variance analysis together show that iMSC13 TEX cells are closer to nMSC13 than iMSC13 ARG.

3.10.3 Comparison of iMSCs and eMSCs obtained with ARG and TEX protocols

iPSC clones might carry epigenetic memory of their parental cell origin and such epigenetic footprints could affect their differentiation propensity (Kim *et al*., 2011; Ohi *et al*., 2011, Lister *et al*., 2011; Polo *et al*., 2011). Therefore, we compared iMSC ARG and iMSC TEX with MSCs differentiated from the hESC line KCL034 (eMSC34 ARG and eMSC34 TEX), which has a naïve/intact epigenome.

We found that eMSC from the TEX protocol have a high number of differentially expressed genes compared to the corresponding iMSCs from the ARG protocol (Table 3.10.3). Compared to the corresponding iMSCs, eMSC from the ARG protocol have a high number of differentially expressed genes for donor 13 and are close to iMSCs for donor 12 (2214 vs 136), whereas eMSC from the TEX protocol have a higher number of differentially expressed genes compared to the corresponding iMSCs for donor 12 than for donor 13 (5489 vs 4761). There were no significant differences between protocols in terms of fold-change median values (2.34 – 2.88).

Table 3.10.3 Differentially expressed genes between iMSCs and eMSC.

Comparison	# regulated genes (up/down)	Median FC	Significant pathways
iMSC12 ARG **vs.** eMSC34 ARG	136 (54/82)	2.34	• Cell adhesion
iMSC13 ARG **vs.** eMSC34 ARG	2214 (1214/1000)	2.80	• Cell cycle • DNA repair • Cell adhesion • Immune system
iMSC12 TEX **vs.** eMSC34 TEX	5489 (2771/2718)	2.87	
iMSC13 TEX **vs.** eMSC13 TEX	4761 (2413/2348)	2.88	

In the ARG protocol, nearly one half of the genes regulated in cells originating from donor 12 (iMSC12 ARG) are also regulated in cells originating from donor 13 (iMSC13 ARG) when compared with eMSC34 ARG (71 out 136 or 52.2%) from which only 19 (26.8%) have the same up/down regulation (Figure 3.10.7).

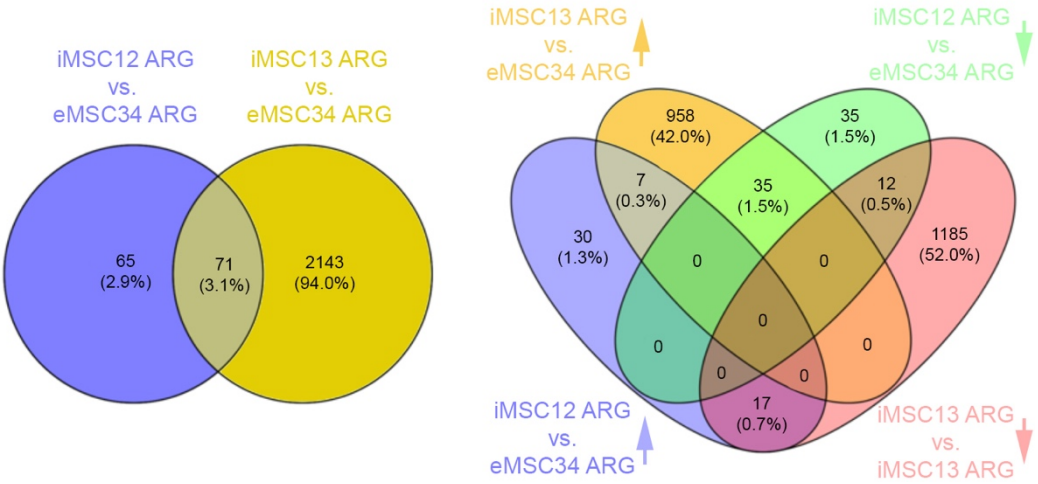

Figure 3.10.7 Overlap between two comparisons (iMSC12 ARG and nMSC12 vs. eMSC13 ARG and iMSC13 ARG and nMSC13 vs. eMSC13 ARG) shown as Venn diagrams.

In the TEX protocol, most of the genes regulated using one of the protocols are also regulated using the other protocol (4065 out of 4761 or 85.4% in cells originating from donor 13 and 4065 out of 5489 or 74.1% in cells originating from donor 12). Almost all the common genes have the same up/down regulation (Figure 3.10.8).

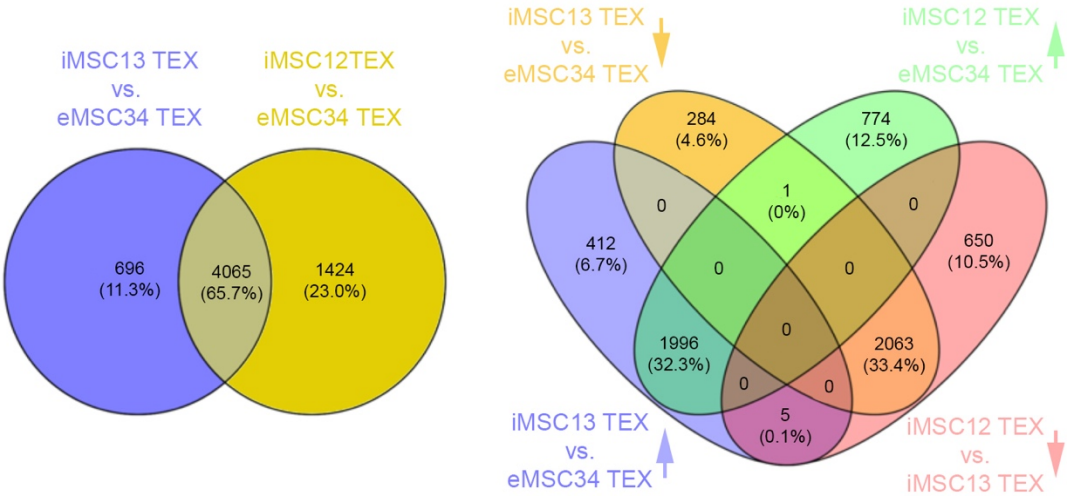

Figure 3.10.8 Overlap between two comparisons (iMSC12 TEX and nMSC12 vs. eMSC13 TEX and iMSC13 TEX and nMSC13 vs. eMSC13 TEX) shown as Venn diagrams.

Unsupervised clustering showed that iMSC12 TEX and iMSC13 TEX are closer to each other than to eMSC34 TEX, whereas iMSC12 ARG are closer to iMSC34 ARG than to iMSC13 ARG (Figure 3.10.9).

Taking these data together, the answer to the question whether hESC-derived MSCs (eMSCs) are similar to iPSC-derived MSCs (iMSCs) is quite disappointing, as it might depend on the donor as well as the protocol. The differential analysis and the unsupervised clustering show that when using the ARG protocol, eMSC (eMSC34 ARG) are close to iMSCs from donor 12 (iMSC12 ARG). When using the TEX protocol, eMSC (eMSC34 TEX) are very different from eMSC34 ARG and all iMSCs regardless of the protocol.

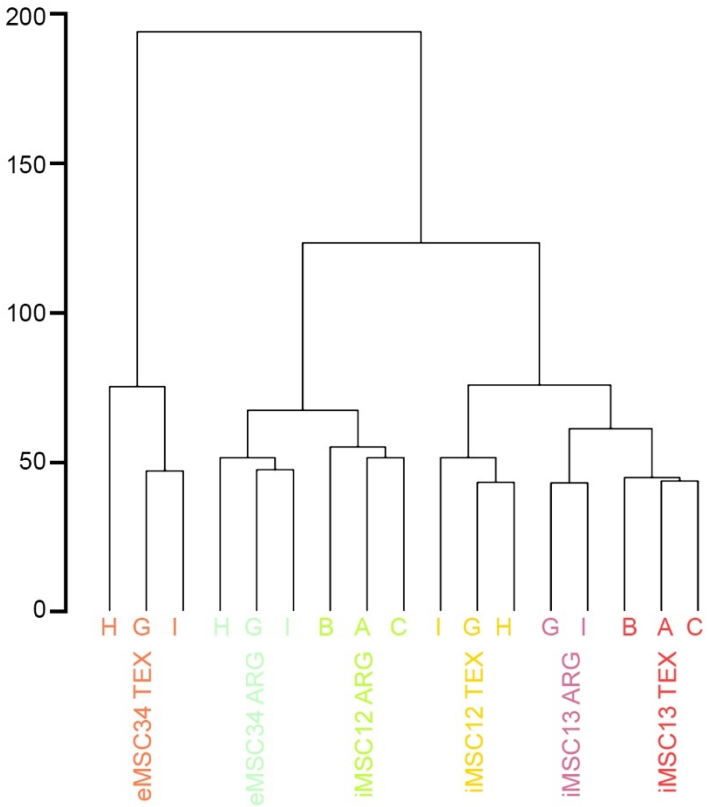

Figure 3.10.9 Unsupervised clustering (Euclidian distance) of nMSC, iMSC and eMSC samples from two donors (donor 12 and 13).

3.10.4 Comparison of native nMSCs with iMSCs and eMSCs obtained with the ARG and TEX protocols

In the final step of transcriptome analysis, to answer the question as to which differentiation protocol is better, ARG or TEX, we compared all MSCs derived from pluripotent lines with the ARG protocol (iMSC12 ARG, iMSC13 ARG, and eMSC34 ARG) with primary native MSCs (nMSC12 and nMSC13) and all MSCs derived from pluripotent lines with the TEX protocol (iMSC12 TEX, iMSC13 TEX, and eMSC34 TEX) with primary native MSCs (nMSC12 and nMSC13).

Table 3.10.4 Differentially expressed genes between nMSCs and MSCs obtained from pluripotent stem cells using ARG and TEX protocols.

Comparison	# regulated genes (up/down)	Median FC	Significant pathways
iMSC12 ARG & iMSC13 ARG & eMSC34 ARG **vs.** nMSC12 & nMSC13	1539 (687/852)	2.84	• Cell adhesion • Immune system
iMSC12 TEX & iMSC13 TEX & eMSC34 TEX **vs.** nMSC12 & nMSC13	2833 (1403/1430)	2.77	• Cell cycle • Cell adhesion • Immune system

We found that MSCs from both protocols, TEX and ARG, have a high number of differentially expressed genes (Table 3.10.4). The number of differentially expressed genes is higher using TEX than ARG (2833 vs. 1539). However, there are no significant differences between protocols in terms of fold-change median values (2.84 in the ARG protocol vs. 2.77 in the TEX protocol).

The majority of differently regulated genes in the ARG protocol (1130 out of 1539 or 73.4% genes) are also differently regulated in the TEX protocol (1130 out of 2833 genes or 39.9%). Most of the common genes have the same up/down regulation (Figure 3.10.10).

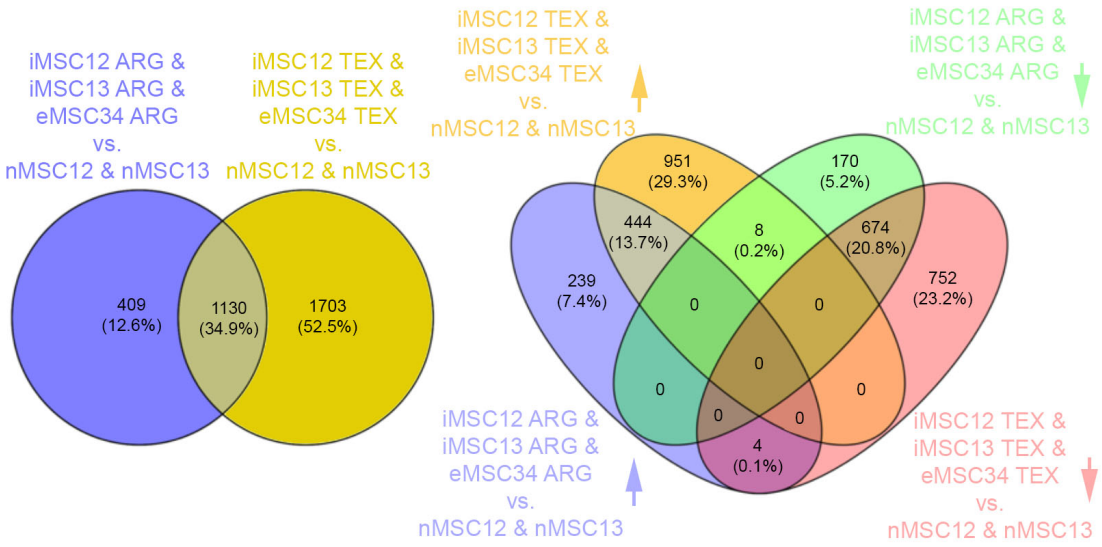

Figure 3.10.10 Overlap between two comparisons (nMSCs vs. all MSCs derived from pluripotent stem cells following the ARG protocol and nMSCs vs. all MSCs derived from pluripotent stem cells following the TEX protocol) shown as Venn diagrams.

Based on expression levels of all expressed genes, iMSCs from the TEX protocol (iMSC12 TEX and iMSC13 TEX) and iMSCs and eMSC from the ARG protocol (iMSC12 ARG, iMSC 13 ARG, eMSC34 ARG) are closer to each other than to native samples (nMSC12 and nMSC13) (Figure 3.10.11).

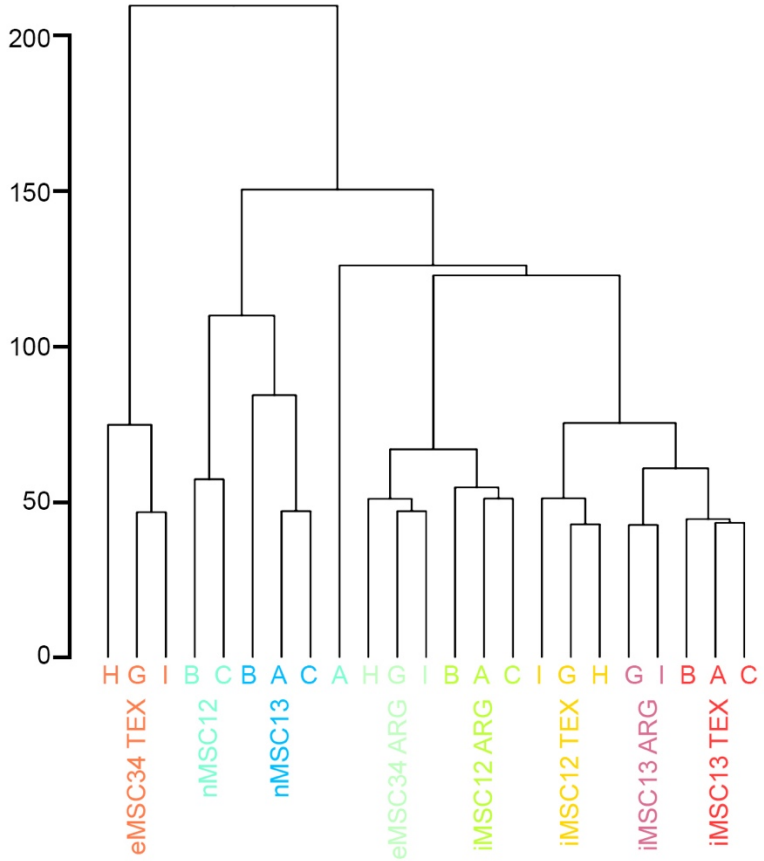

Figure 3.10.11 Unsupervised clustering (Euclidian distance) of nMSCs (nMSC12 and nMSC13) and all MSCs differentiated from pluripotent stem cells (hESCs and iPSCs) following either ARG (iMSC12 ARG, iMSC 13 ARG, eMSC34 ARG) or TEX (iMSC12 TEX, iMSC 13 TEX, eMSC34 TEX) protocols.

The mean variance between primary nMSCs (nMSC12 and nMSC13) and all MSCs differentiated from pluripotent stem cells (hESCs and iPSCs) following the ARG (iMSC12 ARG, iMSC 13 ARG, eMSC34 ARG) protocol is slightly lower than between primary nMSCs (nMSC12 and nMSC13) and all MSCs differentiated from pluripotent stem cells (hESCs and iPSCs) following the TEX (iMSC12 TEX, iMSC 13 TEX, eMSC34 TEX) protocol (Figure 3.10.12).

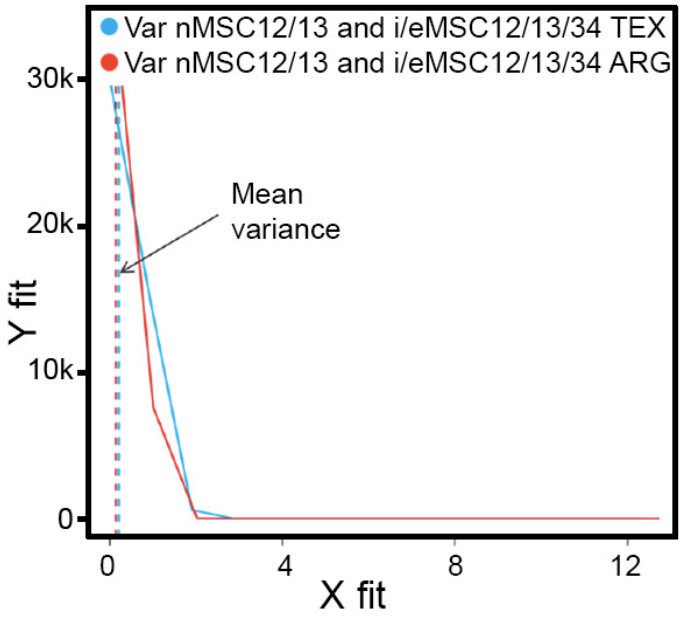

Figure 3.10.12 Distribution variance and mean values.

Taking all data together, we can conclude the following:

- MSCs differentiated from pluripotent stem cells (hESCs and iPSCs) with either the ARG or TEX protocol have a high number of differentially expressed genes compared to the parental primary nMSC line.
- The number of differentially expressed genes is lower using the ARG protocol.
- Unsupervised clustering shows that the MSCs differentiated from pluripotent stem cells with either the TEX or ARG protocols are closer to each other than to primary nMSC.
- Based on differentially expressed genes, in general, the ARG protocol is better than TEX. However, if the parental source of the iPSCs is MSCs, then the TEX protocol is better.

3.10.5 Analysis of signalling pathways related to the immune system

To exercise their immunoregulatory role, which is the basis of their clinical application, MSCs secrete soluble mediators that regulate the proliferation and function of multiple types of immune cells, including induction of regulatory T cells (Treg) either directly or indirectly (Sharma *et al.*, 2014; Le Blanc *et al.*, 2004, 2008).

To determine whether the MSCs differentiated from pluripotent stem cells with either the TEX or ARG protocols react in a similar way as the primary nMSCs, we analysed their response to IFNγ treatment. IFNγ stimulates the production of indoleamine 2,3-dioxygenase activity 1 (*IDO1*), which is the main modulator of the MSC immunosuppressive role (Krampera *et al.*, 2006).

To verify that IFNγ treatment induced the expected signalling response in all lines treated, we compared mRNA levels of *IDO1*, guanylate binding protein 4 (*GBP4*) and CXC

motif chemokine ligand 11 (*CXCL11*) between untreated and treated cells (Figure 3.10.13-15). These three genes have been used extensively as markers of IFNγ responsiveness (Krampera *et al.*, 2006; Vestal *et al.*, 2005; Tensen *et al.*, 1999).

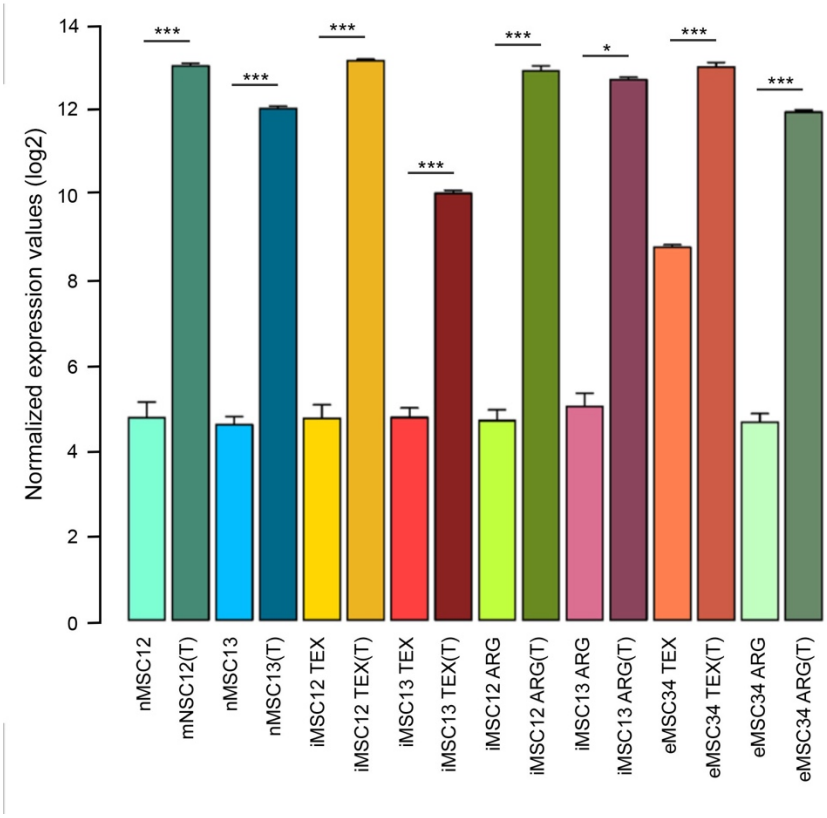

Figure 3.10.13 IFNγ treatment induced *IDO1* mRNA levels across all MSC samples regardless of their origin (probe ILMN_3239965). ***,p≤0.001, *,p≤0.05

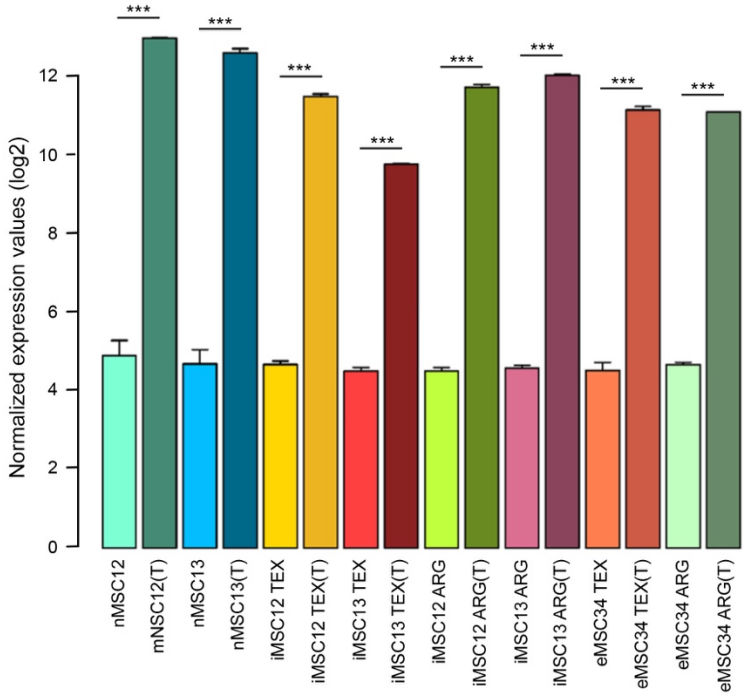

Figure 3.10.14 IFNγ treatment induced *GBP4* mRNA levels across all MSC samples regardless of their origin (probe ILMN_1771385). ***,p≤0.001.

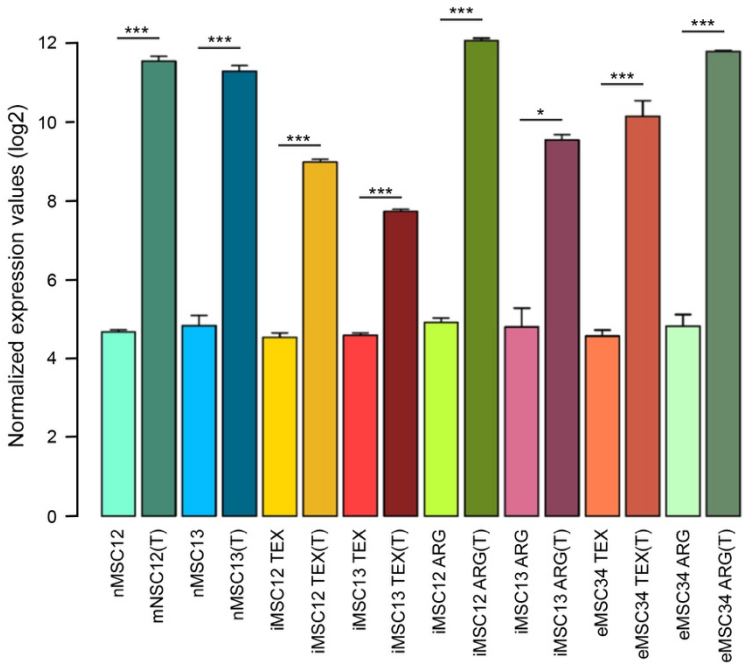

Figure 3.10.15 IFNγ treatment induced *CXCL11* mRNA levels across all MSC samples regardless of their origin (probe ILMN_2067890). ***,p≤0.001, *,p≤0.05

We confirmed the transcriptome array data with *IDO1*-, *GBP4*- and *CXCL11*-specific qPCR (Figure 3.10.16-18).

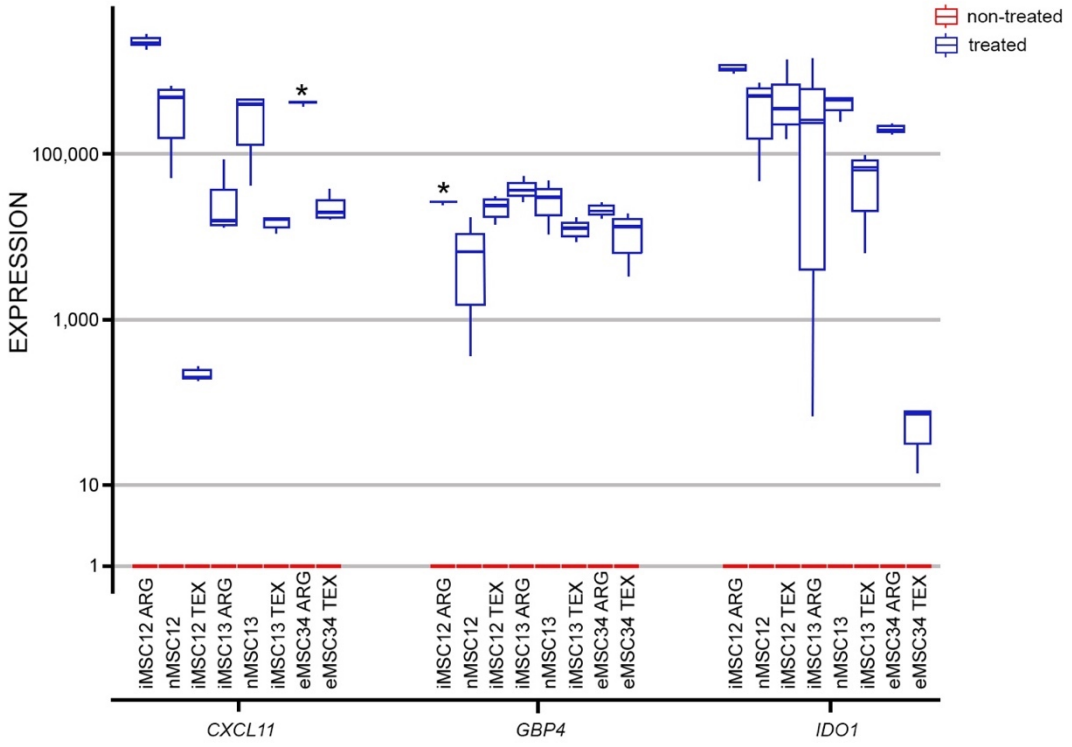

Figure 3.10.16 qPCR analysis confirmed that IFNγ treatment induces expression of *CXCL11*, *GBP4* and *IDO1* in all our eight MSC lines (n=3 for each non-treated and IFNγ-treated sample). Red lines represent values in non-treated cells. Only two treated individual lines significantly differed in one gene expression. p values were determined with t-test and adjusted using Bonferroni correction. *, $p \leq 0.05$.

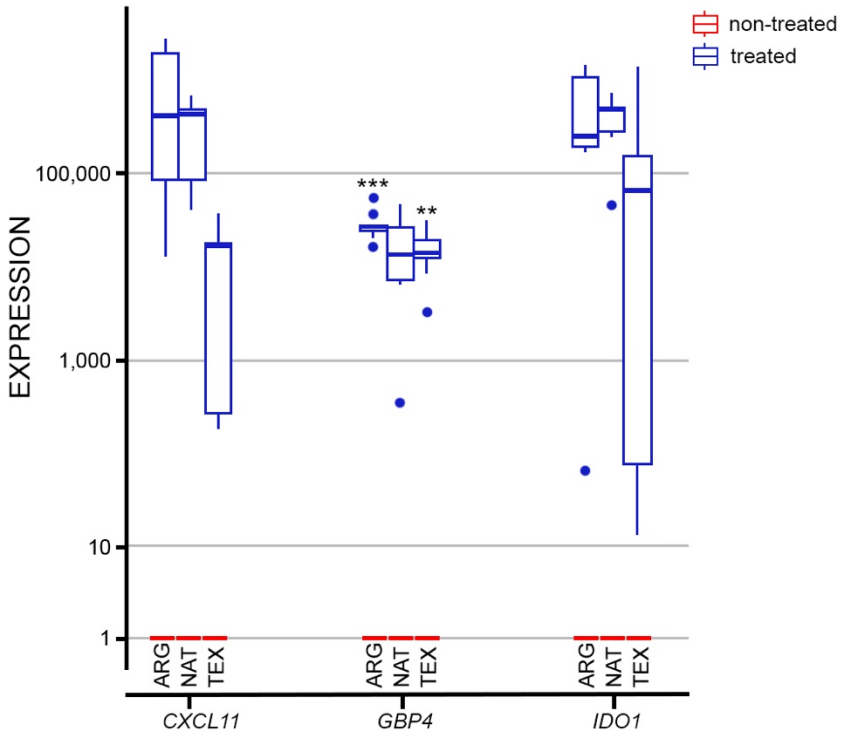

Figure 3.10.17 Upon IFNγ treatment, nMSC (n=6) and the MSC differentiated from pluripotent stem cells with either TEX (n=9) or ARG (n=9) protocols display a similar increase in expression of *CXCL11* and *IDO1*, whereas significant differences were found in expression of *GBP4*. Red lines represent values in non-treated cells. p values were determined with t-test and adjusted using Bonferroni correction. ***p≤0.001; **, p≤0.01

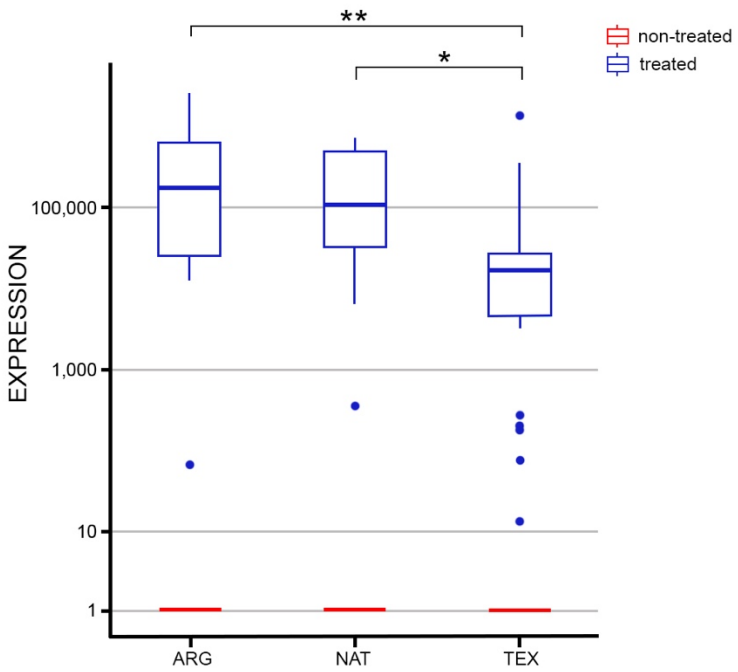

Figure 3.10.18 IFNγ treatment induced significantly higher expression of all three genes (*CXCL11, GBP4, IDO1*) assessed by qPCR in nMSC (n=18) and the MSC differentiated from pluripotent stem cells with ARG (n=27) protocols than in those differentiated with TEX (n=27) protocol. Red lines represent values in non-treated cells. p values were determined with a non-parametric one-way ANOVA on ranks or Kruskal-Wallis H test as well as Tukey's honest significant difference (HSD) post-hoc analysis. **, $p \leq 0.01$; *, $p \leq 0.05$

Having confirmed that the all MSC lines responded in a predictable way to IFNγ treatment, we could analyse their whole transcriptome with confidence.

Treated MSCs differentiated from pluripotent stem cells with either the TEX or the ARG protocol have fewer differentially expressed genes than nMSCs differentiated from untreated cells (Table 3.10.5). Interestingly, whereas a similar number of genes were upregulated (830 out of 1685 genes or 49.3%) and downregulated (855 out of 1685 genes or 50.7%) in nMSCs, MSCs differentiated from pluripotent stem cells with either the ARG or

TEX protocols had many more upregulated genes than downregulated genes. After IFNγ treatment, e/iMSCs differentiated following the ARG protocol had upregulated 642 out 954 differentially expressed genes (67.3%), whereas e/iMSCs differentiated following the TEX protocol had upregulated 716 out of 909 differentially expressed genes (78.8%). There were no significant differences in terms of fold-change median values (2.59 – 2.61).

Table 3.10.5 Differentially expressed genes after IFNγ treatment.

Comparison	# regulated genes (up/down)	Median FC	Significant pathways
nMSC12 & nMSC13 **vs.** nMSC12(T) & nMSC13(T)	1685 (830/855)	2.59	• Cell cycle • Immune system • DNA replication
iMSC12 ARG & iMSC13 ARG & eMSC34 ARG **vs.** iMSC12 ARG(T) & iMSC13 ARG(T) & eMSC34 ARG(T)	954 (642/312)	2.61	• Cell cycle • Immune system • DNA replication
iMSC12 TEX & iMSC13 TEX & eMSC34 TEX **vs.** iMSC12 TEX(T) & iMSC13 TEX(T) & eMSC34 TEX(T)	909 (716/193)	2.60	• Immune system

Whereas most of the downregulated genes were specific to each comparison and only 12 were common for all cell types, almost half of the upregulated genes were common to at least 2 comparisons and 329 upregulated genes were common for all cells (Figure 3.10.19).

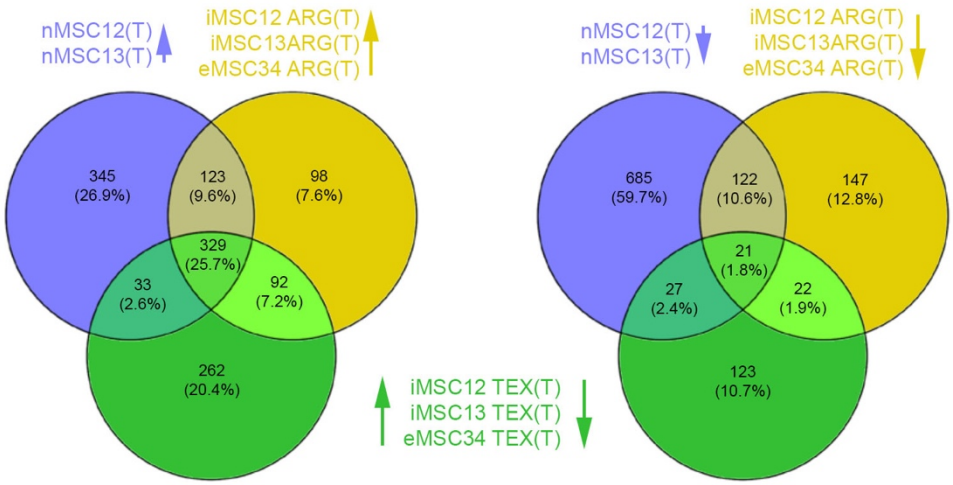

Figure 3.10.19 Overlap between comparisons shown as Venn diagrams.

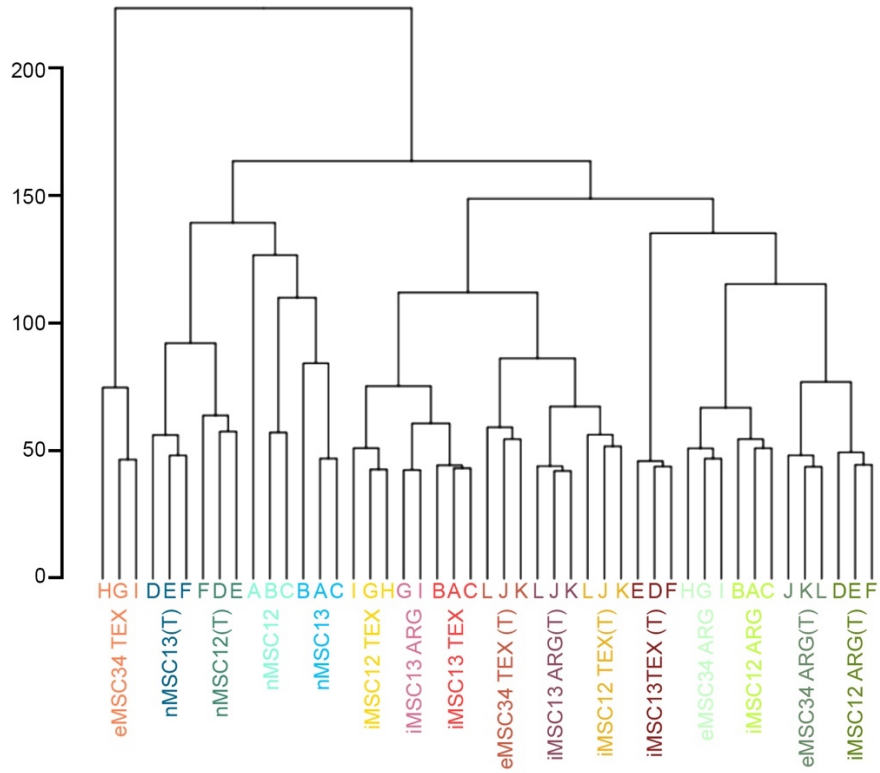

Figure 3.10.20 Unsupervised clustering (Euclidian distance) of IFNγ-treated and untreated cells.

Further analyses have shown that treated cells cluster with their corresponding untreated counterparts (Figure 3.10.20). There were higher differences between each group (e/iMSCs differentiated from pluripotent stem cells with either TEX or ARG protocols and nMSC) than between treated and untreated cells.

This IFNγ experiment demonstrated that:

- All MSC lines, regardless of their background, responded to pro-inflammatory cytokine IFNγ treatment.
- IFNγ treatment had less impact on iMSCs and eMSCs than on nMSCs.
- iMSCs and eMSC differentiated using the ARG protocol have more common regulated genes with nMSCs than iMSCs and eMSC differentiated using the TEX protocol.

Finally, we compared the significantly upregulated pathways in each of the three groups: nMSCs, e/iMSCs differentiated from pluripotent stem cells using the ARG protocol and e/iMSCs differentiated from pluripotent stem cells using the TEX protocol. We used the following three different databases for comparison:

- Kyoto Encyclopedia of Genes and Genomes (KEGG) database (www.genome.jp/kegg/)
- REACTOME database (www.reactome.org)
- Gene Ontology (GO) analysis (www.geneontology.org)

According to the KEGG, IFNγ treatment activated 29 pathways in nMSCs (Table 3.10.6), 26 in e/iMSCs differentiated from pluripotent stem cells using the ARG protocol (Table 3.10.7), and 20 in e/iMSCs differentiated from pluripotent stem cells using the TEX protocol (Table 3.10.8). Interestingly, 19 out of 20 pathways activated in e/iMSCs from the TEX protocol are shared with nMSCs and e/iMSCs from the ARG protocol (highlighted yellow in

Tables 3.10.6 - 3.10.8). nMSCs and e/iMSCs from the ARG protocol share an additional two pathways (highlighted blue in Tables 3.10.6 and 3.10.7).

Table 3.10.6 KEGG pathway analysis of regulated genes highlighted 29 pathways in untreated vs. IFNγ-treated nMSCs. Pathways shared with e/iMSCs from both the ARG and TEX protocols are highlighted yellow, whereas pathways shared only with e/iMSCs from the ARG protocol are highlighted blue.

Link to KEGG Pathway	Pathway Description (KEGG)	Nb Genes in Pathway	Nb Regulated Genes (Up / Down)	P-Value (All)	P-Value (Up)	P-Value (Down)	Min P-Value
hsa04621	NOD-like receptor signaling pathway	62	17 (16/1)	1.39E-05	6.36E-08	NA	6.36E-08
hsa04060	Cytokine-cytokine receptor interaction	262	42 (32/10)	9.82E-06	5.78E-07	NA	5.78E-07
hsa04612	Antigen processing and presentation	83	19 (17/2)	5.31E-05	6.66E-07	NA	6.66E-07
hsa04940	Type I diabetes mellitus	42	12 (12/0)	2.72E-04	1.64E-06	NA	1.64E-06
hsa05330	Allograft rejection	36	10 (10/0)	1.40E-03	2.26E-05	NA	2.26E-05
hsa04640	Hematopoietic cell lineage	86	17 (15/2)	8.61E-04	2.62E-05	NA	2.62E-05
hsa04623	Cytosolic DNA-sensing pathway	55	12 (12/0)	3.01E-03	2.72E-05	NA	2.72E-05
hsa04062	Chemokine signaling pathway	187	25 (23/2)	1.02E-02	3.12E-05	NA	3.12E-05
hsa05332	Graft-versus-host disease	39	10 (10/0)	2.57E-03	4.52E-05	NA	4.52E-05
hsa04350	TGF-beta signaling pathway	87	14 (2/12)	1.68E-02	NA	1.04E-04	1.04E-04
hsa04620	Toll-like receptor signaling pathway	101	15 (15/0)	2.46E-02	1.61E-04	NA	1.61E-04
hsa04622	RIG-I-like receptor signaling pathway	71	12 (12/0)	2.09E-02	3.06E-04	NA	3.06E-04
hsa03030	DNA replication	36	8 (8/0)	1.95E-02	9.83E-04	NA	9.83E-04
hsa04610	Complement and coagulation cascades	69	14 (11/3)	2.29E-03	9.86E-04	NA	9.86E-04
hsa04514	Cell adhesion molecules (CAMs)	132	22 (14/8)	1.24E-03	6.55E-03	NA	1.24E-03
hsa04672	Intestinal immune network for IgA production	49	9 (9/0)	3.45E-02	1.43E-03	NA	1.43E-03
hsa04630	Jak-STAT signaling pathway	155	17 (17/0)	NA	1.63E-03	NA	1.63E-03
hsa00100	Steroid biosynthesis	17	5 (0/5)	3.88E-02	NA	1.86E-03	1.86E-03
hsa05320	Autoimmune thyroid disease	51	9 (9/0)	4.26E-02	1.87E-03	NA	1.87E-03
hsa05416	Viral myocarditis	71	13 (10/3)	8.28E-03	4.47E-03	NA	4.47E-03
hsa05200	Pathways in cancer	328	21 (0/21)	NA	NA	4.65E-03	4.65E-03
hsa05322	Systemic lupus erythematosus	99	13 (13/0)	NA	4.92E-03	NA	4.92E-03
hsa04512	ECM-receptor interaction	84	9 (0/9)	NA	NA	5.75E-03	5.75E-03
hsa05410	Hypertrophic cardiomyopathy (HCM)	85	9 (0/9)	NA	NA	6.18E-03	6.18E-03
hsa05310	Asthma	29	6 (6/0)	NA	8.99E-03	NA	8.99E-03
hsa00512	O-Glycan biosynthesis	30	5 (0/5)	NA	NA	1.54E-02	1.54E-02
hsa04110	Cell cycle	125	12 (12/0)	NA	2.58E-02	NA	2.58E-02
hsa05217	Basal cell carcinoma	55	6 (0/6)	NA	NA	3.26E-02	3.26E-02
hsa05219	Bladder cancer	42	8 (6/2)	4.22E-02	4.00E-02	NA	4.00E-02

Table 3.10.7 KEGG pathway analysis of regulated genes highlighted 26 pathways in untreated vs. IFNγ-treated e/iMSCs differentiated using the ARG protocol. Pathways shared with nMSCs and e/iMSCs from the TEX protocol are highlighted yellow, whereas pathways shared only with nMSCs are highlighted blue.

Link to KEGG Pathway	Pathway Description (KEGG)	Nb Genes in Pathway	Nb Regulated Genes (Up / Down)	P-Value (All)	P-Value (Up)	P-Value (Down)	Min P-Value
hsa04612	Antigen processing and presentation	83	23 (22/1)	4.50E-10	8.91E-12	NA	8.91E-12
hsa04060	Cytokine-cytokine receptor interaction	262	41 (33/8)	1.49E-10	1.03E-09	NA	1.49E-10
hsa04940	Type I diabetes mellitus	42	15 (15/0)	7.79E-08	1.58E-09	NA	1.58E-09
hsa05332	Graft-versus-host disease	39	14 (14/0)	2.69E-07	7.50E-09	NA	7.50E-09
hsa04621	NOD-like receptor signaling pathway	62	14 (14/0)	1.01E-05	2.69E-07	NA	2.69E-07
hsa05330	Allograft rejection	36	12 (12/0)	7.74E-06	4.13E-07	NA	4.13E-07
hsa04630	Jak-STAT signaling pathway	155	23 (18/5)	9.37E-06	4.79E-05	NA	9.37E-06
hsa04514	Cell adhesion molecules (CAMs)	132	21 (15/6)	3.18E-05	1.07E-03	3.44E-02	3.18E-05
hsa04062	Chemokine signaling pathway	187	21 (20/1)	1.18E-03	4.97E-05	NA	4.97E-05
hsa05320	Autoimmune thyroid disease	51	11 (11/0)	9.27E-04	8.44E-05	NA	8.44E-05
hsa04623	Cytosolic DNA-sensing pathway	55	10 (10/0)	1.62E-03	1.55E-04	NA	1.55E-04
hsa05416	Viral myocarditis	71	12 (12/0)	2.90E-03	2.43E-04	NA	2.43E-04
hsa04640	Hematopoietic cell lineage	86	12 (12/0)	3.94E-03	2.85E-04	NA	2.85E-04
hsa04672	Intestinal immune network for IgA production	49	9 (9/0)	2.96E-03	3.68E-04	NA	3.68E-04
hsa04620	Toll-like receptor signaling pathway	101	12 (12/0)	1.30E-02	1.14E-03	NA	1.14E-03
hsa04350	TGF-beta signaling pathway	87	7 (0/7)	NA	NA	1.15E-03	1.15E-03
hsa00980	Metabolism of xenobiotics by cytochrome P450	60	6 (0/6)	NA	NA	1.29E-03	1.29E-03
hsa05322	Systemic lupus erythematosus	99	12 (12/0)	2.82E-02	3.34E-03	NA	3.34E-03
hsa04610	Complement and coagulation cascades	69	10 (9/1)	7.76E-03	3.63E-03	NA	3.63E-03
hsa04622	RIG-I-like receptor signaling pathway	71	9 (9/0)	2.67E-02	4.34E-03	NA	4.34E-03
hsa05020	Prion diseases	35	7 (5/2)	7.68E-03	3.87E-02	NA	7.68E-03
hsa05310	Asthma	29	5 (5/0)	NA	2.08E-02	NA	2.08E-02
hsa00140	Steroid hormone biosynthesis	46	4 (0/4)	NA	NA	2.48E-02	2.48E-02
hsa04512	ECM-receptor interaction	84	5 (0/5)	NA	NA	2.78E-02	2.78E-02
hsa00760	Nicotinate and nicotinamide metabolism	24	5 (4/1)	3.12E-02	NA	NA	3.12E-02
hsa03030	DNA replication	36	5 (5/0)	NA	4.23E-02	NA	4.23E-02

Table 3.10.8 KEGG pathway analysis of regulated genes highlighted 20 pathways in untreated vs. IFNγ-treated e/iMSCs differentiated using the TEX protocol. Pathways shared with nMSCs and e/iMSCs from ARG protocols are highlighted yellow.

Link to KEGG Pathway	Pathway Description (KEGG)	Nb Genes in Pathway	Nb Regulated Genes (Up / Down)	P-Value (All)	P-Value (Up)	P-Value (Down)	Min P-Value
hsa04612	Antigen processing and presentation	83	23 (23/0)	1.84E-10	5.10E-12	NA	5.10E-12
hsa05330	Allograft rejection	36	12 (12/0)	5.06E-06	9.24E-07	NA	9.24E-07
hsa05332	Graft-versus-host disease	39	12 (12/0)	1.11E-05	2.07E-06	NA	2.07E-06
hsa04940	Type I diabetes mellitus	42	12 (12/0)	2.26E-05	4.32E-06	NA	4.32E-06
hsa04610	Complement and coagulation cascades	69	14 (13/1)	2.06E-05	1.55E-05	NA	1.55E-05
hsa04060	Cytokine-cytokine receptor interaction	262	27 (26/1)	3.40E-04	4.14E-05	NA	4.14E-05
hsa04620	Toll-like receptor signaling pathway	101	15 (15/0)	3.25E-04	4.41E-05	NA	4.41E-05
hsa04514	Cell adhesion molecules (CAMs)	132	19 (18/1)	1.89E-04	6.77E-05	NA	6.77E-05
hsa05416	Viral myocarditis	71	13 (13/0)	5.44E-04	1.06E-04	NA	1.06E-04
hsa04621	NOD-like receptor signaling pathway	62	11 (11/0)	7.00E-04	1.56E-04	NA	1.56E-04
hsa05320	Autoimmune thyroid disease	51	11 (11/0)	6.58E-04	1.64E-04	NA	1.64E-04
hsa04622	RIG-I-like receptor signaling pathway	71	11 (11/0)	2.04E-03	4.88E-04	NA	4.88E-04
hsa04672	Intestinal immune network for IgA production	49	9 (9/0)	2.20E-03	6.59E-04	NA	6.59E-04
hsa04630	Jak-STAT signaling pathway	155	18 (15/3)	1.25E-03	3.63E-03	NA	1.25E-03
hsa04062	Chemokine signaling pathway	187	19 (18/1)	3.93E-03	1.28E-03	NA	1.28E-03
hsa04623	Cytosolic DNA-sensing pathway	55	9 (9/0)	4.63E-03	1.44E-03	NA	1.44E-03
hsa05322	Systemic lupus erythematosus	99	12 (12/0)	2.11E-02	6.18E-03	NA	6.18E-03
hsa00590	Arachidonic acid metabolism	56	8 (6/2)	1.77E-02	NA	NA	1.77E-02
hsa04640	Hematopoietic cell lineage	86	10 (9/1)	2.27E-02	2.17E-02	NA	2.17E-02
hsa05310	Asthma	29	5 (5/0)	4.96E-02	2.76E-02	NA	2.76E-02

The REACTOME database (www.reactome.org) suggested involvement of 8 significant pathways in nMSCs (Table 3.10.9), 5 in MSCs differentiated from pluripotent stem cells using the ARG protocol (Table 3.10.10) and 4 in MSCs differentiated from pluripotent stem cells using the TEX protocol (Table 3.10.11). Only one pathway, *Signalling in Immune System*, was shared among all three groups of cells (highlighted yellow in Tables 3.10.9 – 3.10.11). Among the pathways involved, *Signalling in Immune System* was at the first place with 33 genes upregulated in MSCs originated through the TEX protocol, at the second place with 25 genes upregulated in MSCs originated through the ARG protocol and at sixth place with 24 genes upregulated and 6 downregulated in nMSCs.

Table 3.10.9 REACTOME pathway analysis of regulated genes highlighted 8 pathways in untreated vs. IFNγ-treated nMSCs. The pathway shared with e/iMSCs from ARG and TEX protocols is highlighted yellow.

Link to REACTOME Pathway	Pathway Description (REACTOME)	Nb Genes in Pathway	Nb Regulated Genes (Up / Down)	P-Value (All)	P-Value (Up)	P-Value (Down)	Min P-Value
REACT_383	DNA Replication	97	19 (19/0)	3.82E-05	1.10E-07	NA	1.10E-07
REACT_152	Cell Cycle, Mitotic	304	32 (32/0)	7.03E-03	4.25E-06	NA	4.25E-06
REACT_604	Hemostasis	235	32 (18/14)	8.67E-05	2.62E-02	1.06E-03	8.67E-05
REACT_1538	Cell Cycle Checkpoints	112	15 (15/0)	1.31E-02	3.05E-04	NA	3.05E-04
REACT_7970	Telomere Maintenance	56	10 (10/0)	2.72E-02	2.68E-03	NA	2.68E-03
REACT_6900	Signaling in Immune system	286	30 (24/6)	9.83E-03	2.73E-03	NA	2.73E-03
REACT_602	Metabolism of lipids and lipoproteins	150	9 (0/9)	NA	NA	1.29E-02	1.29E-02
REACT_6850	Cdc20	66	8 (8/0)	NA	2.40E-02	NA	2.40E-02

Table 3.10.10 KEGG pathway analysis of regulated genes highlighted 5 pathways in untreated vs. IFNγ-treated e/iMSCs differentiated using the ARG protocol. The pathways shared with nMSCs and e/iMSCs from TEX protocols are highlighted yellow.

Link to REACTOME Pathway	Pathway Description (REACTOME)	Nb Genes in Pathway	Nb Regulated Genes (Up / Down)	P-Value (All)	P-Value (Up)	P-Value (Down)	Min P-Value
REACT_383	DNA Replication	97	14 (14/0)	6.69E-05	7.35E-06	NA	7.35E-06
REACT_6900	Signaling in Immune system	286	25 (25/0)	4.45E-04	1.68E-05	NA	1.68E-05
REACT_1538	Cell Cycle Checkpoints	112	12 (12/0)	3.45E-03	6.57E-04	NA	6.57E-04
REACT_152	Cell Cycle, Mitotic	304	17 (17/0)	NA	2.66E-02	NA	2.66E-02
REACT_13433	Biological oxidations	116	4 (0/4)	NA	NA	4.17E-02	4.17E-02

Table 3.10.11 KEGG pathway analysis of regulated genes highlighted 20 pathways in untreated vs. IFNγ--treated e/iMSCs differentiated using the TEX protocol. The pathway shared with nMSCs and MSCs from ARG protocol is highlighted yellow.

Link to REACTOME Pathway	Pathway Description (REACTOME)	Nb Genes in Pathway	Nb Regulated Genes (Up / Down)	P-Value (All)	P-Value (Up)	P-Value (Down)	Min P-Value
REACT_6900	Signaling in Immune system	286	33 (33/0)	2.32E-08	1.06E-09	NA	1.06E-09
REACT_604	Hemostasis	235	22 (20/2)	1.21E-04	2.06E-04	NA	1.21E-04
REACT_578	Apoptosis	129	10 (10/0)	NA	2.62E-02	NA	2.62E-02
REACT_13552	Integrin cell surface interactions	81	8 (7/1)	3.02E-02	NA	NA	3.02E-02

Gene Ontology (GO) analysis (www.geneontology.org) found that *Immune Response* and *Immune System Process* were the top two biological processes in all three groups analysed (Table 3.10.12).

Table 3.10.12 Top two biological processes highlighted by GO analysis of regulated genes.

nMSC

Term Type	GO ID with Link	Go Term	Nb Genes in Term	Nb Regulated Genes (Up / Down)	P-Value
biological_process	GO:0002376	immune system process	998	145 (121/24)	2.76E-21
biological_process	GO:0006955	immune response	690	113 (97/16)	1.47E-20

e/iMSC differentiated using ARG protocol

Term Type	GO ID with Link	Go Term	Nb Genes in Term	Nb Regulated Genes (Up / Down)	P-Value
biological_process	GO:0006955	immune response	690	109 (106/3)	1.72E-36
biological_process	GO:0002376	immune system process	998	128 (121/7)	7.76E-34

e/iMSC differentiated using TEX protocol

Term Type	GO ID with Link	Go Term	Nb Genes in Term	Nb Regulated Genes (Up / Down)	P-Value
biological_process	GO:0006955	immune response	690	99 (97/2)	1.32E-29
biological_process	GO:0002376	immune system process	998	120 (117/3)	4.62E-29

Taken together, signalling pathway data analyses using three databases demonstrated that MSCs differentiated from iPSCs or hESCs using either the ARG or TEX differentiation protocol share a response to stimulation with pro-inflammatory cytokine IFNγ.

CHAPTER 4

4. DISCUSSION

4.1 WJ MSCs isolation

The isolation of MSCs from WJ has a widely varied procedure, and this variation generates unreliable results between studies (Jeschke *et al.*, 2011). The enzymatic treatment with collagenase is widely used; however, this treatment fluctuates in the literature. Trypsin and other proteases, such as hyaluronidase, are frequently added in different concentrations, and the incubation time also changes from 4 to 24 h at room temperature or at 37°C (Tsagias *et al.*, 2011; Pereira *et al.*, 2008; Kadam *et al.*, 2009; Weiss *et al.*, 2008). We opted to use the explant technique because, aside from being less harsh on cells and less cumbersome for researchers, it was much cheaper, and the results could be standardized.

We successfully isolated fibroblast-like cells from full-term gestational UCs and demonstrated some of their characteristics by analysing their morphology and immunophenotype profile using flow cytometry. The UC explant isolation method used in this study appeared to be efficient, simple and consistent. In all conditions, dXF, nXF and STD yielded good population numbers of stem/ stromal cells (median of 5 x 10^3 cells/ explant).

The UC explant method of WJ MSC isolation possesses advantages over the enzymatic method since cell damage by enzymes is avoided and WJ contains growth factors that support the proliferation of MSCs. However, primary cultures obtained by UC explants appear to be heterogeneous (Conconi *et al.*, 2011). Mark *et al.* (2013) also isolated and expanded a population of fibroblast-like cells with a different cell shape and size. In our experimental setting, MSCs isolated in each condition were morphologically similar but different between conditions (Figure 3.1.4).

The use of animal-derived supplements in clinical grade cells, such as FBS, should be eliminated to avoid the risks in transmitting animal pathogens and the risks of immunogenic reactions after clinical transplantation. The optimization of an XF culture represents a positive step for the future production of these cells in a clinical grade scale. In addition, the content and concentration of cytokines, growth and other soluble factors greatly varies from batch to batch of FBS and even for the purpose of basic research, the trend is to culture cells in a serum-free medium (Amit *et al.*, 2004; Javazon *et al.*, 2004; Li *et al.*, 2005; Shahdadfar *et al.*, 2005; Berger *et al.*, 2006; Moore, 2006; Thirumala *et al.*, 2009). Different research groups have established a range of protocols for the isolation and characterization of stromal cells from Wharton's Jelly (Batsali *et al.*, 2013; Kim *et al.*, 2013; Trivanović *et al.*, 2013; Devito *et al.*, 2014; Hendijani *et al.*, 2014; Swamynathan *et al.*, 2014; Frausin *et la.*, 2015; Watson *et al.*, 2015; Joerger-Messerli *et al.*, 2016; Batsali *et al.*, 2017). However, the effects of the XF culture upon the isolation and expansion of MSCs, on the gene, protein and functional profiles of WJ MSCs have not been completely explored. Defined (XF) culture systems allow for better multipotent differentiation and expansion rates of adipose tissue and BM MSCs, which serve as a preferred alternative to FBS containing media for the production of large scale, functionally competent, clinical grade MSCs (Gottipamula *et al.*, 2013; Patrikoski *et al.,* 2013; Chase *et al.*, 2012). Human platelet lysate (HPL) possesses a variety of growth factors (GFs), which are secreted by alpha granules from platelets (50-80 per platelet). Proteomic studies exposed the complexity of the platelet secretome and found that not only GFs but also different molecules are involved, including cytokines, chemokines, adhesive proteins, enzymes, fibrinolytic and antifibrinolytic proteins (Avanzini *et al.*, 2009). Reinisch *et al.* (2007) showed a successful isolation of MSCs from a full-term UC using HPL, generating cell numbers suitable for clinical applications.

Although our dXF condition showed slower initial outgrowth and population doublings, the end results exhibited a robust and reliable way to isolate MSCs in a clinical grade condition,

completely xeno free. Adding 5% HPL to our cell culture medium improved the efficiency of isolation, expansion and maintenance of the MSC culture, stimulating the proliferation rate of the cells. According to Rubio-Azpeotia and Andia (2014), who performed a meticulous review on platelet rich plasma (PRP), or HPL, and its effects on human MSC proliferation, migration, differentiation and immune response, out of 32 articles using BM MSCs, all articles found a positive correlation between PRP and proliferation and migration, accelerating the time necessary for the population to duplicate (PD). Jenhani *et al.* (2011) also found that HPL enhances the proliferation of UC MSCs. Those findings explain why in our study, the nXF and STD groups had faster population doubling and first outgrowth observations compared to the dXF group.

4.2 Profiling surface markers and trilineage differentiation

The International Society for Cellular Therapy (ISCT) encourages investigators to use as many markers to characterize MSCs as seem relevant to their research, although their established minimal criteria are the expression of CD105, CD73 and CD90 and the lack of expression of CD34, CD45, CD11a, CD19 and HLA-DR (Horwitz *et al.*, 2005; Dominici *et al.*, 2006). However, CD105, CD73 and CD90 are not specific markers for MSCs, as some of them are also expressed by smooth muscle (Kisselbach *et al.*, 2009), vascular populations (Jurisic *et al.*, 2010), and fibroblasts (Halfon *et al.*, 2011; Ishii *et al.*, 2005).

Until now, there is no unique cell marker able to characterize MSCs and there is not yet an absolute agreement on the markers that could characterize MSCs from either fresh BM or other tissues (Samsonraj *et al.*, 2017).

The expanded MSCs in this experiment, from BM and WJ, similar to other experiments in the literature, expressed the marker CD105, CD73, CD29, CD44, MSCA-1, CD56 and CD90, and they lack the expression of CD45 and CD34 (Bianco *et al.*, 2001; Caplan, 1991; Huss, 2000; Jones *et al.*, 2002). We also investigated the expression of the same markers in primary dermal fibroblasts from three different donors (data in Appendix) and found that majority of the cells were positive for all markers and negative for CD34, CD45 and MSCA-1. MSCs have to fulfil consensus criteria regarding their phenotype and biological behaviour (Horwitz *et al.*, 2005), but the criteria are highly debatable and therefore our findings support the previous idea that MSCs lack specific cell markers.

Lim *et al.* (2016) successfully isolated WJ MSCs from three separated segments of an UC. They found differences in the cell viability and expression of pluripotent embryonic markers of WJ MSCs from different segments collected from the same donor. They also found differences between the groups in CD44 and CD73 markers, both markers related to cell migration and proliferation. They concluded that maternal and foetal segments are better than the middle segment of the UC. In contrast, Dinesh *et al.* (2017) did not find any differences between WJ MSCs isolated from different segments of the same UC. Even though we did not compare WJ MSCs from different segments of the UC, we isolated WJ MSCs from the whole UC, and we found differences in CD44 and CD73 expression levels and differences in population doublings between donors.

The WJ MSCs isolated in this study expressed higher levels of CD44 with no differences between conditions. However, CD44 expression was lower in the dXF group isolated and expanded at 20% O_2 than in the other conditions (dXF at 5% O_2 and nXF at both 20 and 5% O_2) (Figure 3.2.2). The difference in expression under one particular condition is unlikely to be of any functional significance for WJ MSCs. CD44, also known as CDW44, CSPG8, ECMR-III, HCELL, HUTCH-I, IN, LHR, MC56, MDU2, MDU3, MIC4, and Pgp1

(https://www.ncbi.nlm.nih.gov/gene/960), is a cell surface glycoprotein and receptor for hyaluronic acid. It can also interact with collagens, osteopontin and matrix metalloproteinases. There are multiple functionally distinct isoforms due to the complex alternative splicing of the transcripts. CD44 is expressed by different cell types, including MSCs and differentiated osteogenic lineages, and is often used in conjunction with other markers to identify MSCs (Bianco *et al.*, 2001; Liu *et al.*, 2008). In addition, CD44 is related to migration and cell adhesion (Lesley *et al.*, 2000; Zhu *et al.*, 2005), but it has also been identified as a marker for some types of cancer stem cells and is connected to metastatic spread. The reduction of CD44 in cancerous stem cells can cause them to differentiate into non-cancerous stem cells (Puré and Cuff, 2001; Sapaeth *et al.*, 2013).

Significant differences in the time to the observation of the first outgrowth among the conditions tested suggested condition-dependent rates of cellular migration and/or proliferation (Figure 3.1.1). Since the population doubling of WJ MSC was relatively similar, it was likely that the difference observed is due to cellular migration. However, there were no differences in the levels of ITGB1 (integrin β1) or CD29, also known as FNRB, GPIIA, MDF2, MSK12, VLA-BETA, and VLAB (https://www.ncbi.nlm.nih.gov/gene/3688), which is involved in MSC migration *in vivo* and *in vivo* (Ip *et al.*, 2007).

The other MSC marker implicated in the cellular migration of MSCs is NT5E or CD73, also known as CALJA, E5NT, NT, NT5, NTE, eN, and eNT (https://www.ncbi.nlm.nih.gov/gene/4907;Ode *et al.*, 2011). CD73 is encoded by the 5'-nucleotidase ecto *NT5E* gene, which is a classic hypoxia-inducible factor (HIF) target gene and its expression and function is stimulated by hypoxic conditions (Antonioli *et al.*, 2016). Moreover, overexpression of CD73 is also involved in the proliferation and migration of cervical cancer cells (Gao *et al.*, 2017). However, there were no marked differences in CD73 expression levels regardless of oxygen tension, indicating further that the expression levels of

MSC surface markers were dependent on the culture media used (nXF or dXF), not on the level of O2 (Figure 3.2.1 and 3.2.2).

THY1 (Thy-1 cell surface antigen) or CD90 was surprisingly lower in cells grown under the dXF and STD groups, and higher in the BM MSCs and nXF groups (Figure 3.2.1). CD90 is a glycoprotein and considered to be one of the T lymphocyte markers, although it is also expressed in different cell types, such as neural cells, fibroblasts, endothelial cells, cancer stem cells, haematopoietic cells and MSCs (Maleki *et al.*, 2014). Campione *et al.* (2009) demonstrated that BM MSCs derived from hMSCs from haematological malignancies showed down-regulation of CD90, suggesting that this molecule might be considered a predictive marker for the inhibitory ability of MSCs, decreasing its inhibitory immunological function. However, our results showed that the dXF group immunogenicity was as high as in the BM MSC group. Moraes *et al.* (2016) showed that a reduction in CD90 expression enhances the osteogenic and adipogenic differentiation in dental pulp, adipose tissue and amniotic fluid MSCs *in vitro*. We did not see any obvious qualitative differences in the adipogenic (Figure 3.3.1) and osteogenic (Figure 3.3.3) potential of our MSCs cultured under different conditions regardless of the CD90 expression level (Figure 3.2.1).

Expression of ENG or CD105, also known as endoglin, END, HHT1, and ORW1 (https://www.ncbi.nlm.nih.gov/gene/2022), had large variations within each of the culture conditions tested (Figure 3.2.1). The smallest variations, though the lowest expression levels, were detected in the dXF medium with 5% O_2 (Figure 3.2.2). CD105 has been shown to be expressed on endothelial cells and is classified as a receptor for transforming growth factor beta (TGF-β). It is also known as a marker for tumour-related angiogenesis and neovascularization, playing an important part in the prognosis, diagnosis and even treatment of neoplasm. The endothelial cells of neoplasms proliferate at a higher rate than the endothelial cells of healthy tissues and, as a result, they expressed higher rates of CD105 (Wong *et al.*, 2000; Miller *et al.*,

1999; Wikstrom *et al.*, 2002). Another study sorted CD105+ WJ MSCs through enzymatic digestion and cultured those cells in suspension. This CD105+ population were positive for CD73 and CD90 and were able to differentiate into adipocytes, chondrocytes and osteocytes lineages, confirming their MSC status. Interestingly, they also expressed markers associated with pluripotency OCT3/4, NANOG and SOX2 suggesting that WJ MSCs are more than multipotent cells (Amiri *et al.*, 2015). In contrast, WJ contains heterogeneous populations of cells which might have different sub-populations of more naive cells. WJ-MSCs do not express markers associated with pluripotency, but they may express them at a very low level and momentarily for a short period in their existence (Mitchell *et al.*, 2003; Sarugaser *et al.*, 2005). All of our isolated WJ MSCs and BM MSCs expressed CD105, although a larger variation was found between the donors in the nXF group than in the other groups, confirming the heterogenicity of cells isolated from WJ.

WJ MSC had relatively low expression of NCAM1 or CD56 across all conditions, especially with dXF (Figure 3.2.1). Bühring *et al.* (2007) have shown that CD56, a marker for natural killer, neural and muscle cells, is expressed in a small population within BM MSC CD271+ cells. In addition, MSCA1 (W8B2 antigen) is also expressed on the same CD271+ sub-population, and they hypothesized that the MSCA1 antibody reacts with CFU-F (colony forming units-fibroblast), as these clonogenic cells are known to be present in the CD271+ population. CD271, a nerve growth factor receptor (LNGR), has been described as one of the most specific markers for human BM MSCs (Bühring *et al.*, 2007; Quirici *et al.*, 2002). However, CD271 was not detected in any of the cells grown in our laboratory including BM MSCs (data in Appendix). Data published by Alvarez-Viejo *et al.* (2013) and Margossian *et al.* (2012) show that CD271 is an undetectable marker for WJ MSCs. In contrast, CD56 expression was lower in the WJ MSCs dXF group but also in the BM MSCs, whereas it was higher in the WJ MSCs STD and nXF groups. Battula *et al.* (2009) introduced MSCA-1 as a marker for

MSCs, showing that only cells MSCA-1+ and CD56- were able to differentiate into adipocytes, whereas MSCA-1+ and CD56+ were phenotypically heterogenous clones able to differentiate into chondrocytes. He claimed that this particular sub-population should be isolated and chosen for the treatment of several diseases, such as rheumatoid arthritis, trauma, acute osteochondral fractures and even spinal disk injuries. Although the differentiation potential tested in this experiment was only qualitative, all of our groups were able to differentiate into adipocytes, chondrocytes and even osteocytes independently of CD56 and MSCA-1 expression.

An exceptionally large population of WJ MSC grown with dXF conditions expressed MSCA-1. MSCA-1, also known as a tissue non-specific alkaline phosphatase (TNSALP) ectoenzyme, was expressed at high levels in the liver, bone and kidney, as well as in ESCs (Jones *et al.*, 2006). MSCA-1/ TNAP is a repressor of NFκB-inducing kinase (nuclear factor kinase, NIK) activity and regulates both classical and alternative NIK-mediated signalling (Hu *et al.*, 2004; Pike *et al.*, 2013). According to an extended review by Li and Verma (2002), the activation of NFκB signalling pathways is crucial for the function of different immune cell interactions leading to an immune response. Overall, alkaline phosphatases dephosphorylate several substrates engaged specifically in the stimulation of inflammation and in such a way possess potent anti-inflammatory effects (Pike *et al.*, 2013). Whether the presence of large MSCA-1/TNAP^{+} subpopulations in WJ MSCs might provide an additional benefit in MSC-based cellular therapy of inflammatory diseases such as graft-vs-host disease, or for the development of novel cellular therapies for regeneration medicine, remains to be explored (Capelli *et al.*, 2011; Fonta *et al.*, 2005; Tisato *et al.*, 2007). In our experiment, the dXF group expressed a higher immunogenic response at a 1:20 ratio (WJ MSC: PBMC) than the BM MSC group, although there were no significant differences, and a broader number of donors should be considered because MSCA-1 positive cells seem to have higher immunogenic properties.

Other criteria for established human MSCs is their capacity for trilineage mesenchymal differentiation. Accordingly, cells must be capable of differentiating into osteoblasts, adipocytes and chondroblasts using traditional *in vitro* culture conditions (Dominici *et al.,* 2006). All of our isolated WJ MSCs were capable of trilineage differentiation.

4.3 Immunomodulatory activity

Perinatal tissues have numerous advantages, including easy accessibility, painless collection from donors, and they can be a possible source for autologous and allogeneic cell therapy. In cord blood, the amount of MSCs isolated is relatively limited and usually the MSCs have low proliferative activity (Musina *et al.*, 2007). WJ can be a better source of MSCs for allogeneic cell therapy since these cells have a low immunogenicity capacity and a higher proliferative rate.

Recent publications demonstrated that WJ MSCs are potential transplantable cells for the treatment of different diseases, such as GvHD cancer and diabetes. They exhibit excellent qualities to be considered for cell therapy, such as a low doubling time, a high proliferate rate, and the capacity to function with non-immune-supressed laboratory animals (Usha *et al.*, 2010; Nagamura-Inoue and He, 2014). Our dXF WJ MSCs and BM MSCs have shown similar immunomodulatory responses; however, at a 1:20 ratio, the dXF group had a stronger immune response than the BM MSCs, agreeing with results from Chang *et al.* (2006), who reported a stronger immunosuppression from placenta-derived MSCs than from BM MSCs.

MSCs are able to pass almost undetected through the immune system, because of the low expression of HLA molecules making them suitable for allogenic cell therapy, and, depending on the cell delivery route and the preparation of these cells, they can survive in recipients and exert their action for weeks (Kurtz, 2008).

Jin *et al.* (2013) compared human MSCs isolated from BM, adipose tissue (AT), and UC for surface antigen expression, differentiation ability, proliferation capacity, tolerance for ageing, clonality, and paracrine activity. All MSCs isolated from different tissues had similar surface antigen expression, immunosuppressive features, and related differentiation capacities. However, UC MSCs had the highest rate of cell proliferation and clonality, and lower expression of p53, p21 and p16, well known markers for senescence. The anti-inflammatory capacity of UC MSCs showed a reduced expression of inflammatory cytokines, including interleukin-1α (IL-1α), IL-6, and IL-8 via angiopoietin-1 (Ang-1). Thus, UC MSCs have biological advantages in comparison to adult sources, making the UC a useful source of cells for clinical applications.

Phenotypically, adult MSCs are very similar to WJ MSCs; however, the WJ MSC gene expression profile is different. Gene ontology analysis showed that WJ MSCs have a higher expression of genes associated with proliferation, cell adhesion and the immune system. Moreover, WJ MSCs overexpress genes associated with neurotrophic support, and their secretome stimulates neuronal maturation to a greater extent than BM MSCs. *In vivo* experiments with WJ MSCs confirmed their immunomodulatory effect on T cells. WJ MSC is an attractive candidate for neurodegenerative and immune-mediated disorders, such as Parkinson's, amyotrophic lateral sclerosis and MS (Donders *et al.*, 2018).

4.4 Reprogramming of WJ MSCs and differentiation into MSCs

MSCs have a great potential for cell-based therapies, and lately, have been the focus of several research groups and clinical trials. On the other hand, these cells require constant isolation from donors to avoid senescence and genomic instability. One way of minimizing the inconsistent manufacturing of clinical-grade cellular products is to derive adult stem cells from PSCs such as iPSCs (Temple and Studer, 2017). Therefore, we first generated iPSCs from WJ MSCs and later differentiated them into MSCs.

Different somatic cells demonstrate a variable vulnerability to reprogramming methods. We assumed that WJ MSCs, which were isolated from 'young' tissue, might have a better reprogramming rate than fully adult cells, such as dermal fibroblasts. Although no significant differences were calculated, donor #13, which had a higher percentage of the MSCA-1 marker, showed a higher colony counting than the other lines (Table 3.5.1). However, the dermal fibroblast line that was used as control showed similar colony counting rates.

One of the most promising applications for iPSC technology is the prospect of investigating key molecules involved in diseases and providing an excellent tool for toxicologic studies (Unternaehrer and Daley, 2011). The reprogramming method chosen is fundamental in the translational use of these cells. We have successfully established a completely xeno-free methodology using a non-integrating method, Sendai virus, for derivation of iPSCs from WJ MSCs.

To use iPSCs in cell-based therapies, differentiation into a more specialized cell type is necessary to avoid the risk of tumourigenicity when cells are transferred *in vivo*. However, differentiation is a complex process and the efficiency is variable. In theory, PSCs (ESC and iPSC), can differentiate into all cell types in the human body; but, in practice, differentiation processes are mostly inconsistent among published scientific papers. In this experiment, we tested two published iPSC MSC differentiation protocols: one based on HPL (ARG protocol;

Luzzani *et al*. 2015) and the other based on the SMAD 2/3 inhibitor to promote differentiation (Zhao *et al.*, 2015). Both differentiation protocols used in this experiment demonstrated that all 6 lines (iMSC #12 TEX, iMSC #13 TEX and eMSC 034; iMSC #12 ARG, iMSC #13 ARG and eMSC 034 ARG) fulfilled the minimal criteria established by ISCT (Dominici *et al.*, 2006) for characterization of MSCs.

Zhao *et al.* (2015) achieved a highly efficient rate of iPSC MSCs positive for CD73 and CD105 (>99.6%) and eliminated the need for flow cytometric sorting. Additionally, their iPSC MSCs expanded faster than BM MSCs. Using the same protocol, our TEX protocol and the ARG protocol, we were unable to get such an efficient positive rate and we chose to sort cells that were triple positive for CD73, CD105 and CD90.

Human ESCs have been differentiated into mesenchymal precursor cells by different research groups, using murine OP9 stromal cells as the feeder layer and an alpha MEM medium containing 20% FBS and supplemented with 2 mM L-glutamine. After 40 days of coculture, CD73 positive cells were sorted, and only approximately 5% of them were positive. Subsequently, the cells were expanded for 7 to 14 days until they were fully characterized for MSCs (Barberi *et al.,* 2005; Peng *et al.*, 2016; Olivier *et al*., 2006). Although we were capable of differentiating PSCs into MSCs in xeno-free conditions using both protocols (ARG and TEX), we also sorted the cells for MSCs markers (data not shown), indicating that it is very difficult to obtain a high differentiation efficiency.

Prockop and Keating (2012) reported that the early introduction of tissue culture plastic dishes was responsible for the selection of MSC progenitors, probably because pre-treated tissue culture dishes increase oxygenated derivatives on their surface, thereby making them more hydrophilic and increasing the adherence of cells. Moreover, the selection by adherence in tissue culture vessels are one of the minimal criteria for human MSCs as defined by the International Society of Cellular Therapy (Dominici *et al.*, 2006). In both differentiation

methods used in this experiment, the capacity of plastic adherence was used as MSC selection. Coating was no longer used from day 25 in TEX differentiation, and from day 14 in the ARG protocol, where cells continued to grow and expand.

Barberi *et al.* (2006) differentiated different lines of hESCs into multipotent mesenchymal precursors and found no obvious differences in the marker and gene-expression profile or in adipo-, chondro- and osteogenic differentiation. However, some of the lines (ECS MSCs) showed a tendency of osteogenic differentiation after prolonged expansion. On the other hand, in our experiments, all of our TEX lines showed enhanced trilineage differentiation: adipogenic, osteogenic, and chondrogenic lineages. TEX lines showed a higher expression rate of genes related to each lineage than the ARG counterparts, possibly because TEX groups exhibited a higher resemblance to PSCs, keeping their stemness instead of fully differentiating into mesenchymal progenitors. Those findings were confirmed by transcriptome array, where the TEX group (iMSC and eMSC) exhibited more differentiated genes than the ARG group when comparing to native groups.

Three recent studies have compared the genomic features of iPSCs from hundreds of individuals (between 100 – 300 individuals), and the iPSC lines have shown to be heterogeneous, raising questions about the suitability of these lines for genetic studies. These studies were able to show that the genetic background of each individual has a superior influence on variation in the iPSC lines compared to other non-genetic factors, including copy number status, culture conditions (cell recovery and processing), passage, and gender. Therefore, even though cell recovery and processing can result in variation among the lines, it seems that the majority of iPSC heterogeneity is driven by inherent genetic variation between individuals, rather than by any variation in culture conditions and duration, or in the reprogramming method used. All three reports showed that a great amount of genomic variations between the iPSC lines affected the genes involved in stem cell maintenance and the

differentiation efficiency of the iPSCs (Lund *et al.,* 2012; Carcamo-Orive *et al.,* 2017; Kilpnen *et al.,* 2017; DeBoever *et al.,* 2017). Our iPSC MSC lines from both groups, TEX and ARG, showed individual differences in gene expression that could be attributed to the genetic background to each parental cell. Comparing both differentiation protocols of eMSCs and iMSCs, we believe that TEX is a better protocol if the parental cells are MSCs; otherwise, if parental cells are from other adult origins, ARG is a better protocol choice to differentiate iPSCs into MSCs based on the comparison of differentiated genes between these cells and native WJ MSCs.

4.5 Analysis of signalling pathways related to the immune system

One of the most important feature of MSCs is their role in the immune system, which makes them the best choice for cell therapy when immunomodulatory activity is desirable.

Wang *et al.* (2018) reported an experiment similar to ours generating and differentiating four lines of human iPSCs into MSCs using different protocols (Yen *et al*., 2009; Yen *et al.,* 2011), and using transcriptome analyses and immunomodulatory activities, compared them to ESC MSCs and BM MSCs. They found iPSC MSC lines significantly supressed *in vitro*-activated human peripheral blood mononuclear cell (PBMC) proliferation to a similar degree as ESC MSCS and BM MSCs, and also modulated the CD4 T-lymphocyte fate and IL-17A-expressing (Th7) cell fate to a regulatory T cell (Treg) phenotype. Additionally, iPSC MSCs significantly supressed cytotoxic CD8 T proliferation and activation. The iPSC MSC immunomodulatory activity results in an overall shift of secreted cytokines from a pro-inflammatory climate to a more immunotolerant environment, which was validated by an *in vivo* mouse model of inflammation. Therefore, their findings support the idea that iPSC MSCs hold low oncogenicity and strong immunomodulatory capacities regardless of cell of origin or

the reprogramming method. However, in our experiment, all lines of iPSC MSCs showed a much lower immunomodulatory activity in supressing PBMC than nMSCs and BM MSCs.

MSCs are surrounded by surface receptors for a large number of factors such as interleukins, inflammatory factors, prostaglandins and a number of vitamins. Treatment of MSCs by such factors, for example, the inflammatory factor interferon gamma (IFNγ), or the cytokine tumour necrosis factor alpha (TNFα) and/or interleukin 17 (IL-17), induces MSCs to react and adapt a more immunomodulatory phenotype modifying their immunogenicity (Prasanna *et al.*, 2010; Sivanatham *et al.*, 2015; de Witte *et al.*, 2015). TEX lines demonstrated a lower ability to inhibit phytohemagglutinin A (PHA)-induced PBMC proliferation than ARG lines, with both groups exhibiting a lower immune response compared to WJ MSCs and BM MSCs. However, both groups, TEX and ARG, responded positively to IFNγ treatment, increasing gene expression of *IDO1*, *GBP4* and *CXCL11*, which are all markers of IFNγ responsiveness (Krampera *et al.*, 2006; Vestal *et al.*, 2005; Tensen *et al.*, 1999).

The therapeutic benefit of MSCs is unpredictable, and despite being immunosuppressive, they are undetectable following *in vivo* injection. Thus, understanding their fate could predict clinical responses. Using a murine model of Graft-versus-Host Disease (GvHD), Galleu *et al.* (2017) demonstrated that MSCs are actively induced to undergo extensive apoptosis after infusion in the presence of cytotoxic granules contained in the recipient cytotoxic cells, which also mediate GvHD. This process is essential to initiate MSC immunosuppressive activity. They found that only cells with high cytotoxic activity responded to MSC infusion, whereas cells with low activity did not. Therefore, the cytotoxic activity against MSCs can be detected in the PBMC of GvHD patients, predicting the therapy response, and it might be used as a potential biomarker to scan patients undergoing MSC treatment. Their study highlights that although MSCs remain the starting point for immunomodulatory activity, patient-derived cells play an important role in delivering immunosuppression, and the next

generation of clinical trials should take this matter into consideration and not only choose the best MSCs but choose patients most likely to respond to the treatment.

Wang *et al.* (2017) investigated the interaction of cells from autoimmune disease systemic lupus erythaematosus (SLE) patients on UC MSCs. Using a co-culture system with PBMCs from SLE patients, they noticed changes in MSCs, mainly a higher proliferation and a greater production of modulatory factors, such as vascular endothelial growth factor (VEGF) and CXCL-12. Moreover, baseline levels of IFNγ predict the clinical efficacy of allogeneic MSC transplantation in SLE patients; i.e., high serum levels of IFNγ indicated a better response to the transplantation when followed-up for 1 year. Of all the cytokines, IFNγ is still the most essential, because it is responsible for inducing high levels of IDO1 and IDO2, indicating that IFNγ mediates the induction expression of IDO family genes (Wang *et al.*, 2014; de Witte *et al.*, 2015).

The CXC family of chemokines are chemoattractants for mononuclear leukocytes and are angiostatic. CXCL4, CXCL9, CXCL10, and CXCL11 chemokine production by these cells can be stimulated by multiple factors, including viruses, bacterial products, TNF, IL-1, C5, LTB4, IL-17, and IFN. CXCL9, CXCL10, and CXCL11 are all ligands for the receptor CXCR3, which is preferentially expressed on Th1 cells (Good et al., 2017).

Immunomodulatory findings for iPSC-MSCs are inconsistent among the published research. Some reports described better immune regulatory effects with *in vivo* disease model studies, which demonstrate that MSCs modulate CD4 T-cells towards a Treg phenotype; however, effects on IFNγ, a cytokine representing effector Th1, were inconsistent and dependent on the disease model used (Cheng et al., 2015; Ng et al., 2016; Frobel et al., 2014; Fu et al., 2012). IFNγ modulates cell mediated immunity and immune rejection, which can be reduced by MSCs. Although these cells do not directly secrete IFNγ, they can reduce its

secretion by human peripheral blood and decreasing the risks of immune rejection (Zhou et al., 2011).

Chung et al. (2006) reported that pre-treatment of placenta-derived MSCs with the cytokine IFNγ enhanced the immunosuppressive effects of these cells by increasing the secretion of TGFβ and upregulating the inhibitory cell surface PD-L1. PD-L1 is a novel class of inhibitors that works as a tumour suppressing factor via the modulation of the immune cell-tumour cell interaction. When activated, PD-L1 leads to the inhibition of T-cell receptor-mediated lymphocyte proliferation and cytokine secretion. These findings agree with our results, where all groups (ARG and TEX, iMSCs and eMSCs) treated with IFNγ showed a positive response in genes related to immunosuppressive effects. Increased levels of IFNγ are found in acute GvHD patients and the infusion with MSCs may lower the incidence of this disease (Alsaab *et al.*, 2017).

Klinker *et al.* (2017) confirmed previous reports that IFNγ pretreatment of MSCs significantly enhanced their immunosuppressive capacity (Krampera *et al.,* 2006; Meisel *et al.*, 2004). Moreover, they also reported the importance of measuring other immunosuppressive factors to prove the capacity of MSCs, such as cytokine secretion and growth factor upregulation, and not only the measurement of T-cell proliferation. The magnitude of the suppression differs between activation measurements, and a combination of assays should be used to indicate the immunosuppressive features of MSC lines.

Luk et al. (2017) pretreated adipose tissue-derived MSCs (aMSCs) for 18 h with IFNγ to simulate inflammatory conditions. Subsequently, to analyse immunogenic function, they co-cultured the aMSCs with B cells from spleens and found a significant reduction of B cell proliferation in the IFNγ-treated group, while the control group (non-stimulated) did not inhibit B cell proliferation. In addition, IDO1 was highly induced in the MSC IFNγ group. The next

step in our experiments would be to determine the immunomodulatory ability in supressing PBMC for the IFNγ-treated, TEX and ARG groups.

In 2009, Yen et al. reported the derivation of mesenchymal progenitors from human ESCs, called hESC-derived mesenchymal progenitors (EMPs). EMPs expressed a number of BM MSCs markers, such as CD73 and CD105, and expressed the ESC marker SSEA-4. They did not express HLA-DR or the costimulatory molecules CD80 and CD86. In contrast, EMPs express HLA-G, a non-classic MHC I protein involved in maternal-foetal immunological tolerance, and its expression was increased by IFNγ stimulation. EMPs might be suitable for cell therapy.

Oh et al. (2018) monitored the migration of MSCs to burn injury sites *in vivo* using MSCs expressing the firefly luciferase (Fluc) gene and green fluorescent protein (GFP) in a mouse model. Cutaneous burn injury was induced in the dorsal skin of the mice and MSC/ Fluc was introduced intravenously. The monitoring of MSC/ Fluc was performed using a bioluminescence imaging (BLI) system at specific timepoints. MSC/ Fluc signals appeared in the injury site after 4 days of injections and decreased consistently afterwards. Furthermore, they carried out an immunoblotting protein analysis to determine the expression of neovascularization genes in the burn injuries. TGF-β1 and VEGF showed higher levels in the MSC/ Fluc-treated group compared to the control group. MSCs might aid burn wound healing and MSCs expressing Fluc are a useful tool to track their migration to injury sites.

4.6 Clinical perspective of MSC therapy

Tissue-derived MSCs have shown to be efficient for a variety of therapeutic applications such as through specific migration to injury site, immunomodulatory and paracrine activity, and also for releasing exosomes. Currently, there are 562 studies with the status of recruiting, active, not recruiting, completed, enrolling by invitation and unknown status published at clinicaltrials.gov (accessed April 2018) and happening all over the world, using autologous and allogeneic MSCs.

Lately, the benefits of MSC conditioned medium (CM) in cell-based therapy have been investigated. It is common knowledge that CM enhances cell growth and stimulates the differentiation of *in vitro* cultured cells through the secretion of different cytokines, chemokines and growth factors. MSCs secrete pro-regenerative mediators that might promote repair. Currently, MSC CM has been investigated for its therapeutic promise, including the regeneration of neurons by secreting neuroprotective factors. Moreover, MSCs are able to secrete immunomodulatory proteins that affect innate and adaptive cells. Recent reports showed that MSC CM from multiple sclerosis (MS) patients reduced the secretion of inflammatory cytokines in a microglia and oligodendrocyte model cell line, and the intravenous injection of MSC CM in an animal model of MS showed significant improvements. In another *in vivo* experiment, MSC CM reduced neural degeneration in a spinocerebellar ataxia mice model (Ballerini *et al.*, 2017; Bai *et al.*, 2012; Suto *et al.*, 2016; Ivanova-Todorova *et al.,* 2012; Zappi *et al.*, 2005; Ucceli *et al.*, 2011; Kyurkchiev *et al.*, 2014).

Furthermore, other mechanisms have been investigated regarding the therapeutic potential of MSCs such as their release of exosomes. Exosomes are a class of extracellular vesicles (EV) belonging to a family of nanoparticles that are produced by multivesicular endosomes and secreted by different cell types, including T cells, B cells, dendritic cells, platelets, mast cells, epithelial cells, endothelial cells, neuronal cells, cancerous cells,

oligodendrocytes, embryonic cells, and MSCs. They are released in extracellular fluids, such as urine, blood, ascites, saliva, breast milk, and seminal, amniotic and cerebrospinal fluid. Their content depends on the cellular origin but, for example, B lymphocytes exosomes can stimulate T cell proliferation (Spees *et al.*, 2016; Tkach and Thery, 2016; Raposo and Stoorvogel, 2013). MSCs EV, especially exosomes, have raised the interest of scientists regarding their use in regenerative therapy. They can be isolated from MSCs of different origin and could be as effective as the parental MSCs in supressing inflammatory response. In addition, MSCs EV are safer and cheaper, and it might become a cell-free alternative treatment. However, their isolation characterization, administration and functional mechanism is not fully understood and still needs further investigation (Keshtkar *et al.,* 2018; Liu *et al.*, 2018).

Loftnia *et al.* (2016) were the first to provide experimental evidence of the potential of human ESC MSC-derived molecules. Differentiating ESCs into MSCs, they reported that these cells showed a similar morphology and cell surface markers compared with BM MSCs. In addition, ESC MSCs had a higher growth rate during early *in vitro* culture, along with osteogenic and adipogenic potential. However, the interesting finding was that treatment of acute liver failure (ALF) with CM ESC MSC improved primary hepatocyte viability and increased immunomodulatory interleukin-10 secretion. Further, using a secretome array, they found a link between higher amounts of secretory proteins, such as VEGF, and cell proliferation, cell migration, immune system processes, and apoptosis. ESC MSC-derived molecules provide trophic support to hepatocytes, which might offer a new treatment for ALF.

Kunter *et al.* (2007) investigated the long-term effects of infused MSCs for renal failure and observed maldifferentiation of glomerular MSCs into adipocytes causing a fibrotic reaction encircling them, although the renal function was better in infused rats than in control ones. Another unwanted reaction of infused MSCs includes trapped cells in the lungs of an animal model that caused the deposition of collagen ‘cysts’ resulting in severe lung damage (Anjos-

Afonso *et al.*, 2004). Moreover, MSC transplantation into infarcted hearts in rodents caused bone formation in the myocardium (Breitbach *et al.*, 2007), exposing the unwanted reactions of MSC treatment. For this reason, CM seems to be a better and valid option for therapy.

Dahbour *et al.* (2018) reported positive results of a prospective phase I/IIa clinical study to treat MS using autologous BM MSCs in combination with CM MSC. They concluded that the combination was safe and efficient in stabilizing the disease and reversed the symptoms. Larger clinical trials are planned after such positive outcomes with both the combination therapy, BM MSC with CM MSC, and with CM MSC therapy by itself.

Zhang *et al.* (2018) reported that hUC MSC injection was effective for the treatment of Crohn's Disease with only mild side effects in a randomized, controlled clinical trial. However, the number of hUC-MSCs to reach the target tissue is limited and could not repair the damaged tissue. It is generally accepted that stem cells may repair damaged tissues by alternative or paracrine mechanisms, and CM is the most common treatment strategy (Liu *et al.*, 2016). Fong *et al.* (2014) reported that CM UC MSC promoted haematopoietic stem cell proliferation and improved diabetic wound recovery. Duan *et al.* (2018) explored the therapeutics effects of CM from UC MSCs on nasal mucosa radiation damage *in vivo* and *in vitro* and concluded that UC MSC secreted a variety of soluble factors responsible for increasing cell proliferation and the migration of nasal epithelial cells. Furthermore, intranasal administration of CM UC MSC repaired nasal mucosa radiation damage, showing the benefits of CM MSC in cell regeneration and injury healing.

5. SUMMARY AND FUTURE WORK

Donor procurement makes the logistics of obtaining human BM as a source of MSCs complicated. Although BM MSCs from adult donors still have satisfactory abilities to be used for regenerative medicine purposes, from a manufacturing perspective, the best donors are in the paediatric age range. In addition, the procedure requires planning, is painful and the quality of cells varies among donors. Therefore, the MSC therapy field is constantly looking for alternative sources.

We hypothesized that human MSCs derived from iPSCs would have the biological qualities of native MSCs and could be scaled up and used for therapeutic purposes. To test this hypothesis, we isolated native MSCs (nMSC) from UC WJ of two donors (#012 and #013) in xeno-free conditions. Next, we reprogrammed them into iPSCs (iPSC012 and iPSC013) and subsequently differentiated them back into MSCs using two different protocols, ARG and TEX (iMSC012ARG, iMSC012TEX, iMSC013ARG, and iMSC013TEX). Using the same protocols, we also differentiated the clinical grade human embryonic stem cell line (ESC), KCL034, into MSCs (eMSC034ARG and eMSC034TEX).

To assess which of the two differentiation protocols worked better, we compared the differentiation capability, transcriptomics, metabolomics and immunomodulatory potential of the iMSCs (iMSC012ARG, iMSC012TEX, iMSC013ARG and iMSC013TEX) and eMSCs (eMSC034ARG and eMSC034TEX) with the nMSCs (nMSC012, nMSC013 and BM MSC). Based on the expression of all expressed genes, the data demonstrated that both iMSCs and eMSCs differentiated following the TEX protocol are closer to nMSC with higher differentiation potentials but lower immunomodulatory properties than when using the ARG protocol.

Our data suggest that, following a careful selection and screening of donors, nMSCs from umbilical cord WJ can be reprogrammed into iPSCs, providing a suitable source of material for the differentiation into iMSCs resulting in a more consistent cell culture and scalability, and with similar therapeutic potential as nMSCs. iMSCs could be scaled up under GMP conditions and serve as an alternative of BM and MSCs from other sources for therapeutic purposes.

In our experiments, as described above, we were able to successfully derive iPSCs from WJ MSCs and differentiate them into MSCs. The next step would be to demonstrate that iPSC-derived MSCs might possess *in vivo* clinical benefits in animal models of specific diseases, such as liver disease models. Furthermore, a larger number of donors should be considered to further investigate donor variability and other individual characteristics should be taken to account depending on the therapeutic target. The use of an iPSC haplobank should be taken to consideration since donors could be selected on the basis of transplant antigen systems to match recipients diminishing the risks if immunological rejection and the degree of immune suppression required (Barry *et al.*, 2015).

Recently, there are ongoing human clinical trials using patented iPSC-derived MSCs for GvHD in the U.K. with successful results thus far. According to the company, its technology addresses the limitations that are inherent to the current adult stem cell technologies, such as donor dependence and variability, inconsistency in cell culture and limited scalability, which are the same limitations driving our experiments. Even though they are using a different protocol to generate and differentiate iPSC-derived MSCs, the outcome MSCs are quite similar to those from our experiments.

6. APPENDIX

6.1 REAGENTS

Fibroblast medium		
Reagent	**Catalog number**	**Company**
DMEM	10566-016	Thermo Fisher
CTS Knockout Serum Replacement	A1099201	Thermo Fisher
Non-essential Amino Acids Solution	11140035	Thermo Fisher

Defined media for hESC (KOSR media)		
Reagent	**Catalog number**	**Company**
Knockout DMEM F12	12660012	Thermo Fisher
CTS Knockout Serum Replacement	A1099201	Thermo Fisher
Non-essential Amino Acids Solution	11140035	Thermo Fisher
L-Glutamine 200 mM	25030081	Thermo Fisher
2β-Mercaptoethanol	21985023	Thermo Fisher
Recombinant Human FGF-basic	100-18B	Peprotech

ESC-MSC medium		
Reagent	**Catalog number**	**Company**
Knockout DMEM	10829018	Thermo Fisher
CTS Knockout Serum Replacement	A1099201	Thermo Fisher
Non-essential Amino Acids Solution	11140035	Thermo Fisher
L-Glutamine 200 mM	25030081	Thermo Fisher
2β-Mercaptoethanol	21985023	Thermo Fisher
Recombinant Human FGF-basic	100-18B	Peprotech

Cryopreservation Solution: Vitrification media			
Base Supplements (List all supplements with appropriate concentrations)	**Concentration**	**Current Supplier**	**Catalogue Num**
1. ES-HEPES solution (for 20mL): DMEM/F12 KSR XF 1M HEPES	 15.6mL 4.0 mL 0.4 mL	 Invitrogen Invitrogen Invitrogen	 10829-018 A1099202 15630-049
2. 1M Sucrose solution: Sucrose ES-HEPES Solution	 3.42g 8.0mL	 Sigma N/A	 s7903 N/A
3. 10% Vitrification Solution ES-HEPES Solution Ethylene Glycol DMSO	 2.0mL 0.25mL 0.25mL	 N/A Sigma VWR	 N/A 10246-6 235000.26
4. 20% Vitrification Solution ES-HEPES Solution 1M Sucrose Solution Ethylene Glycol DMSO	 0.75mL 0.75mL 0.5mL 0.5mL	 N/A N/A Sigma VWR	 N/A N/A 10246-6 235000.26

Agarose gel electrophoresis 1%

40 ml 1x TAE (Tris acetate EDTA)
0.4 g Agarose
2µl ethidium bromide (10mg/ ml)

6.2 PRIMERS USED IN THIS STUDY

Gene	Primer sequence
Sendai virus (SeV)	Forward: 5'- GGATCACTAGGTGATATCGAGC-3' Reverse: 5'-ACCAGACAAGAGTTTAAGAGATATGTATC-3'
β-Actin	Forward: 5'-CAA CCG CGA GAA GAT GAC-3' Reverse: 5'-AGG AAG GCT GGA AGA GTG – 3'
FABP4	Forward: 5'-AGCACCATAACCTTAGATGGG-3' Reverse: 5'-CGTGGAAGTGACGCCTTTCA-3'
COL11A1	Forward: 5'-CCAGCGTCTGTTGGTTCAGT-3' Reverse: 5'-CAGCTTCCCCTTTCTCTCCT-3'
RUNX2	Forward: 5'-TTACTTACACCCCGCCAGTC-3' Reverse: 5'-TATGGAGTGCTGCTGGTCTG-3'
ZFP42	Forward: 5'-GCCTTATGTGATGGCTATGTG-3' Reverse: 5'-ACCCCTTATGACGCATTCTAT-3'
NANOG	Forward: 5'-ATGTCTTCTGCTGAGATGCC-3' Reverse: 5'-GTTGTTTGCCTTTGGGACTG-3'
TBP	Forward: 5'-CAGCGTGACTGTGAGTTGCT-3' Reverse: 5'-TGGTTCATGGGGAAAAACAT-3'
GUSB	Forward: 5'-AAACGATTGCAGGGTTTCAC-3' Reverse: 5'-CTCTCGTCGGTGACTGTTCA-3'
GAPDH	Forward: 5'- CCCACTCCTCCACCTTTGAC-3' Reverse: 5'-TTCCTCTTGTGCTCTTGCTG-3'
ACTB	Forward: 5'-ACCTTCTACAATGAGCTGCG-3' Reverse: 5'-CCTGGATAGCAACGTACATGG-3'
HPRT1	Forward: 5'-TGCTGAGGATTTGGAAAGGG-3' Reverse: 5'-ACAGAGGGCTACAATGTGATG-3'

PRIMERS USED IN THIS STUDY

HPRT1	Hs02800695_m1 (Thermo Fisher)
IDO1	Hs00984148_m1 (Thermo Fisher)
CXCL11	Hs04187682_g1 (Thermo Fisher)
GBP4	Hs00925073_m1 (Thermo Fisher)

6.3 SUPLEMENTARY DATA

FIRST OUTGROWTH AND POPULATION DOUBLINGS OF WJ MSC

Table 6.3.1 WJ MSCs First outgrowth table. First outgrowth observed in the edges of the attached umbilical cord (UC) explants and population doublings of each condition (STG, HPL, STD). STG condition showed a higher proliferative capacity over a period of 7 to 10 days in culture. ND, non-determined.

Donor ID	STG		HPL		STD	
	First outgrowth observed [day]	Population Doubling (PD)	First outgrowth observed [day]	PD	First outgrowth observed [day]	PD
7	D14	ND	ND	ND	D9	0.8
8	D14	2.2	ND	ND	ND	ND
9	D11	2.3	ND	ND	D10	1.3
10	D14	2.4	ND	ND	D11	1.6
11	D11	1.8	ND	ND	D9	1.5
12	D11	2.7	ND	ND	D8	2.2
13	D10	2.7	ND	ND	D9	2.3
14	D12	2.2	ND	ND	D9	1.9
GMP_03	ND	ND	D8	1.6	ND	ND
GMP_04	ND	ND	D8	1.4	ND	ND
GMP_05	ND	ND	D10	1.9	ND	ND

Table 6.3.2 Calculation of Population doublings of Native WJ MSCs from Initial outgrowth

nMSC STD			
DONOR ID	**SEEDED (X 10^6) (B)**	**HARVESTED (X 10^6) (A) P1 FROM T75 FLASK**	**PD [log (A/B)] / 0.301**
7	0.1	2	4.32
8	ND	ND	ND
9	0.1	2	4.17
10	0.1	1	3.58
11	0.1	3	4.8
12	0.1	3	4.8
13	0.1	2	4.39
14	0.1	2	4.58

nMSC XF (HPL)			
DONOR ID	**SEEDED (X 10^6) (B)**	**HARVESTED (X 10^6) (A) P1**	**PD [log (A/B)] / 0.301**
GMP_03	0.1	7	6.12
GMP_04	0.1	3	4.96
GMP_05	0.1	1	3.67

nMSC dXF			
DONOR ID	**SEEDED (X 10^6) (B)**	**HARVESTED (X 10^6) (A) P1 FROM T75 FLASK**	**PD [log (A/B)] / 0.301**
7	ND	ND	ND
8	0.1	1	3.23
9	0.1	1	6.78
10	0.1	3	4.75
11	0.1	3	5.08
12	0.1	2	4.58
13	0.1	4	5.28
14	0.1	4	5.28

Table 6.3.3 Calculation of Population doublings of Native WJ MSCs 12 and 13

nMSC12 XF				
PASSAGE	HARVESTED (A) X10^6	SEEDED (B) X10^6	PD [log (A/B)] / 0.301	PD
P3	1.7	1	1.765	1.76
P10	0.3	0	1	2.76
P11	1.4	1	1.485	4.245
P12	2.5	1	2.322	6.567
P14	0.8	1	0.678	7.245
P15	0.45	0	0.585	7.83
P16	0.4	0	1	8.83

nMSC13 XF				
PASSAGE	HARVESTED (A) X10^6	SEEDED (B) X10^6	PD [log (A/B)] / 0.301	PD
P5	2.4	1	1.585	1.585
P6	3.1	1	2.632	4.217
P7	1.4	1	1.485	5.702
P8	2.8	1	2.222	7.924
P9	6.2	1	3.632	11.556
P10	3.2	0	3.415	14.971
P11	1.25	0	2.059	17.03
P12	0.72	0	1.848	18.878

Table 6.3.4 Calculation of Population doublings of ARGENTINA group ESC and iPSC MSC-differentiated

eMSC034_ARG				
PASSAGE	HARVESTED (A) X10^6	SEEDED (B) X10^6	PD [log (A/B)] / 0.301	PD
P1	0.3	0.072 (after cell sorting)	2.059	2.059
P2	0.96	0	1.678	3.737
P3	2.9	1	1.595	5.332

iMSC12_ARG				
PASSAGE	HARVESTED (A) X10^6	SEEDED (B) X10^6	PD [log (A/B)] / 0.301	PD
P1	0.6	0.15 (after cell sorting)	2	2
P2	1.9	1	1.663	3.663
P3	2.5	1	1.608	5.271

iMSC13_ARG				
PASSAGE	HARVESTED (A) X10^6	SEEDED (B) X10^6	PD [log (A/B)] / 0.301	PD
P1	0.46	0.12 (after cell sorting)	1.938	1.938
P2	0.78	0	0.761	2.699
P3	2.1	1	1.428	4.127

Table 6.3.5 Calculation of Population doublings of TEXAS group ESC and iPSC MSC-differentiated

eMSC034_TEX				
PASSAGE	HARVESTED (A) X10^6	SEEDED (B) X10^6	PD [log (A/B)] / 0.301	PD
P1	2.5	0.47 (after cell sorting)	2.411	2.411
P2	3	1	1.819	4.23
P3	3.2	1	2.415	6.645

iMSC12_TEX				
PASSAGE	HARVESTED (A) X10^6	SEEDED (B) X10^6	PD [log (A/B)] / 0.301	PD
P1	2.4	0.72 (after cell sorting)	1.737	1.737
P2	1.4	1	0.807	2.544
P3	1.6	1	1	3.544

iMSC13_TEX				
PASSAGE	HARVESTED (A) X10^6	SEEDED (B) X10^6	PD [log (A/B)] / 0.301	PD
P1	2.1	0.62 (after cell sorting)	1.76	1.76
P2	1.9	1	1.44	3.2
P3	2	1	1.322	4.522

Table 6.3.6 Percentage of sub-populations for MSC surface markers in Fibroblasts (%)

Fibroblasts	CD29	CD44	CD73	CD90	CD105	CD56	MSCA1
DONOR/ PASSAGE							
BJ P4	99.7	99.1	97.2	99.1	90.1	3.3	0
BRCA1 P6	99.5	98.1	96.1	91.1	56.7	11.9	0
EB P7	99.1	98.8	98.4	89.8	87	1.7	0

WJ MSC FLOW CYTOMETRY MARKERS

Table 6.3.7 Percentage of sub-populations for MSCs surface markers with mean, SD and SEM (%) (Prism Graphpad 6)**.** BM MSC was used as comparison with WJ MSC. ND, non-determined.

BM MSC	CD29	CD44	CD73	CD90	CD105	CD56	MSCA1
BM MSC 01	97.7	97.4	97.9	65.3	97.4	15.53	2.73
BM MSC 02	97.5	95.4	92.9	92.3	67.3	11	7.5
BM MSC 03	96.4	78.7	71.5	54.9	74.5	1	0.4
MEAN	97.2	90.5	87.4	70.8	79.7	9.2	3.5
SD	0.7	10.27	14	19.3	15.72	7.435	3.619
SEM	0.4041	5.928	8.1	11.15	9.075	4.292	2.09
STD (FBS)	CD29	CD44	CD73	CD90	CD105	CD56	MSCA1
8	97.6	91.4	65.9	35.9	72.8	63.6	0
12	98.4	97.3	69.9	48.3	87.3	82.9	0.1
13	98	96.9	60.5	21.4	63.1	21.3	0
MEAN	98	95.2	65.4	35.2	74.4	55.9	0.0333
SD	0.1	3.297	4.7	13.46	12.18	31.51	0.05774
SEM	0.05774	1.904	2.7	7.773	7.032	18.19	0.03333
dXF (STG)	CD29	CD44	CD73	CD90	CD105	CD56	MSCA1
8	99	98.5	99.2	34.6	71.1	5	15.8
9	98.7	96.5	98	31	51.5	8.1	4.4
10	98.1	98.8	98.7	33.9	70.1	5	23.5
11	98.7	98.9	99.5	21.2	65.4	7.1	13.5
12	99.3	95.1	97.8	29.5	61.5	14.3	20.4
13	98.8	97.1	99.2	8.4	49.8	14.5	86.1
14	99.2	87.8	97.9	24.4	43	12.6	19.4
GMP 03 STG	97.3	96	93.2	60.2	22.3	0.6	25
GMP 04 STG	99.2	91.1	98.6	20.3	62.7	12.8	30
GMP 05 STG	99.2	98.6	98.5	70.8	42.7	0.2	7.3
MEAN	98.75	95.84	98.06	33.43	54.01	8.02	24.54
SD	0.4	3.69	1.6	18.76	15.24	5.381	23.01
SEM	0.2309	1.167	0.95	5.931	4.82	1.701	7.277
nXF (HPL)	CD29	CD44	CD73	CD90	CD105	CD56	MSCA1
GMP 03 HPL	99.6	99.7	99.3	99.9	89.1	66.4	0.1
GMP 04 HPL	99.5	99.3	99.2	99.2	63.7	30.5	0
GMP 05 HPL	99.4	98.4	96.4	93.5	15.1	6.9	0
MEAN	99.5	99.1	98.3	97.5	55.9	34.6	0.0333
SD	0.6241	0.6658	1.6	3.51	37.6	29.96	0.05774
SEM	0.1973	0.3844	0.95	2.027	21.71	17.3	0.03333

PERCENTAGE OF SUB-POPULATIONS FOR MSCS SURFACE MARKERS

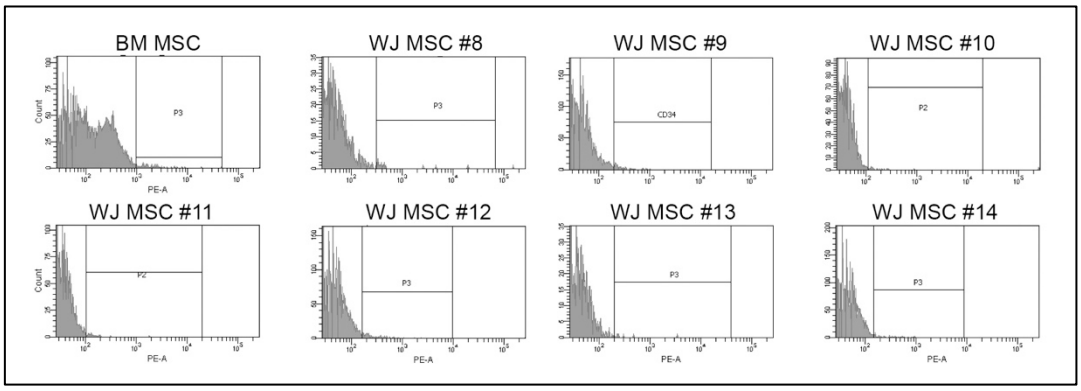

Figure 6.3.1 CD34 expression in WJ MSCs cultured under standard (STD, n=4) and chemically defined xeno-free (XF, n=5) conditions. Clinical grade BM MSCs and Kasumi cell line are used as a control.

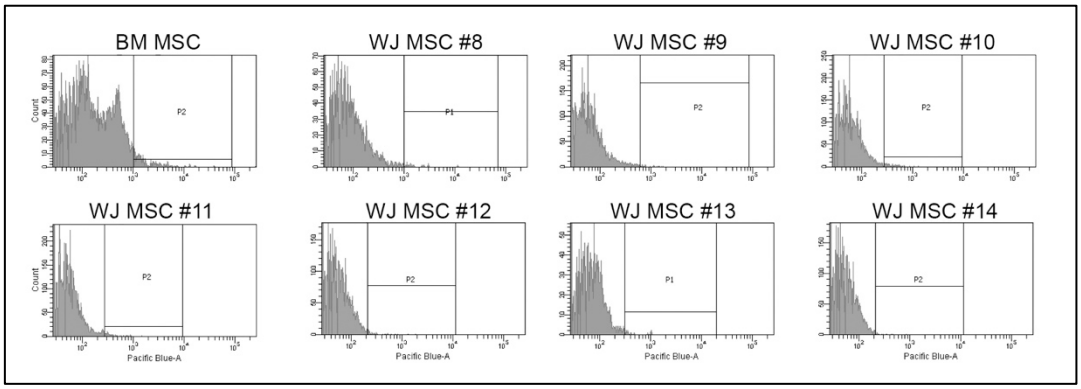

Figure 6.3.2 CD45 expression in WJ MSCs cultured under standard (STD, n=4) and chemically defined xeno-free (XF, n=5) conditions. Clinical grade BM MSC and Kasumi cell line are used as a control.

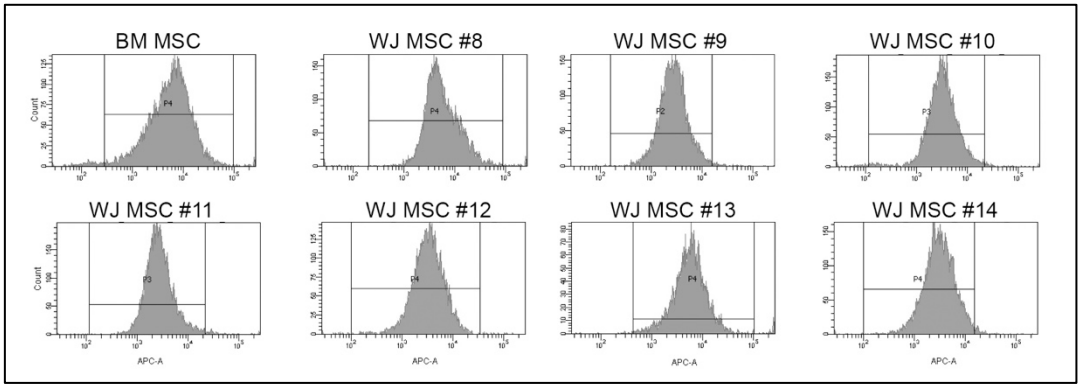

Figure 6.3.3 CD29 expression in WJ MSCs cultured under standard (STD, n=4) and chemically defined xeno-free (XF, n=5) conditions. Clinical grade BM MSCs are used as a control.

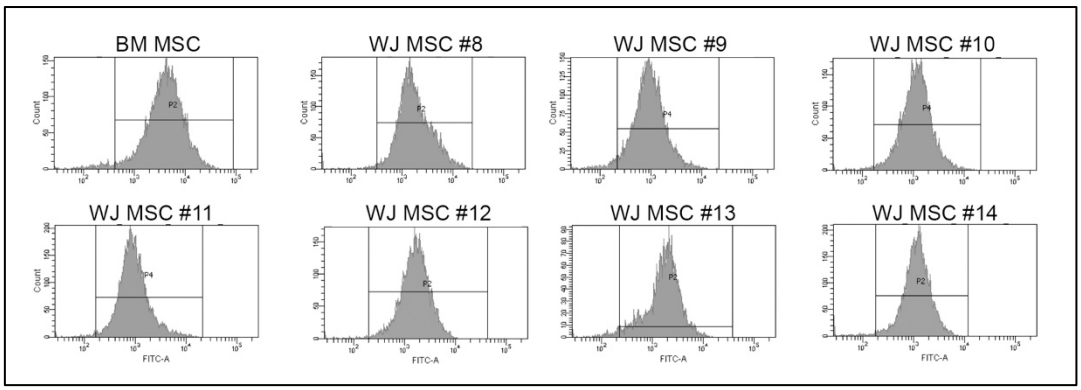

Figure 6.3.4 CD44 expression in WJ MSCs cultured under standard (STD, n=4) and chemically defined xeno-free (XF, n=5) conditions. Clinical grade BM MSCs are used as a control.

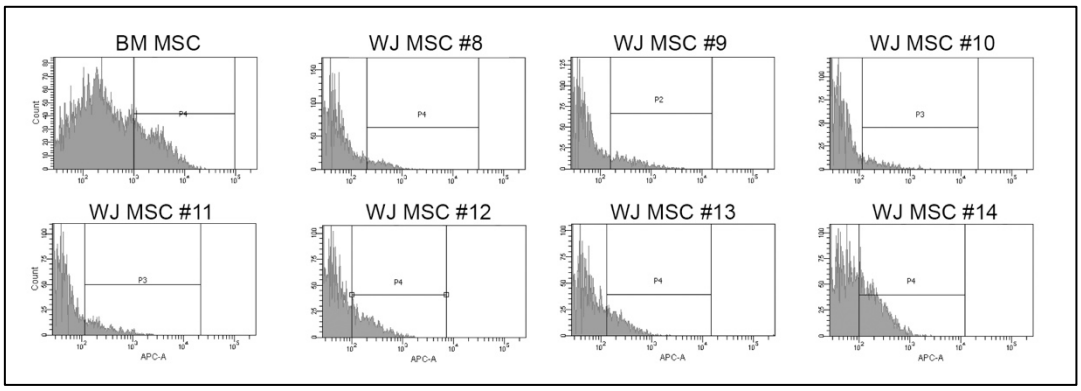

Figure 6.3.5 CD56 expression in WJ MSCs cultured under standard (STD, n=4) and chemically defined xeno-free (XF, n=5) conditions. Clinical grade BM MSCs are used as a control.

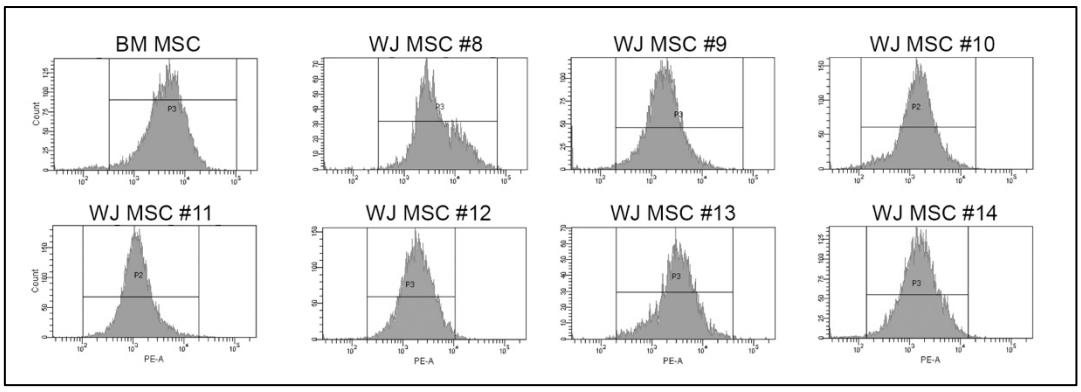

Figure 6.3.6 CD73 expression in WJ MSCs cultured under standard (STD, n=4) and chemically defined xeno-free (XF, n=5) conditions. Clinical grade BM MSCs are used as a control.

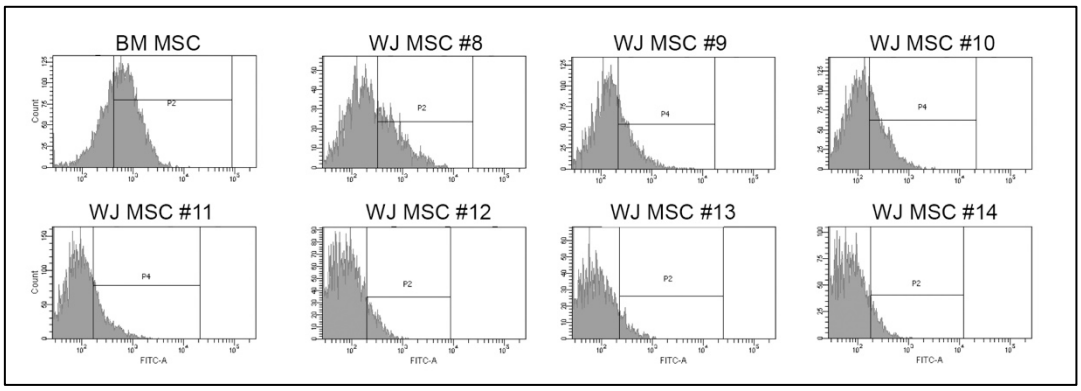

Figure 6.6.6 CD90 expression in WJ MSCs cultured under standard (STD, n=4) and chemically defined xeno-free (XF, n=5) conditions. Clinical grade BM MSCs are used as a control.

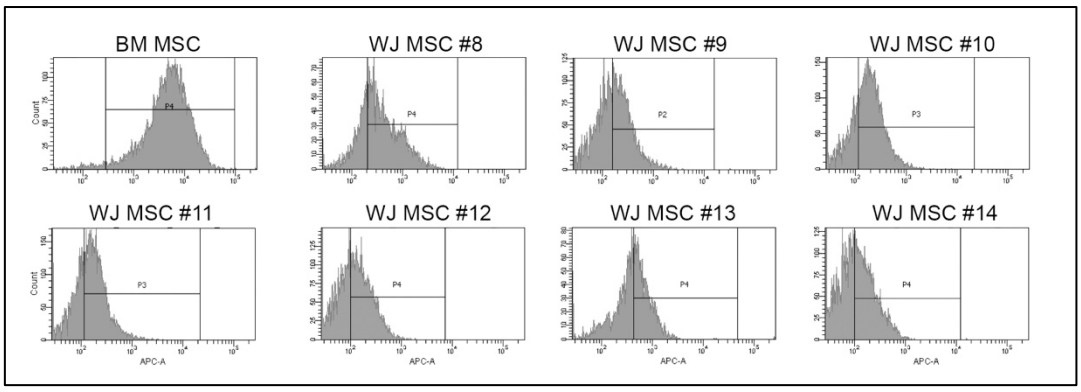

Figure 6.6.7 CD105 expression in WJ MSCs cultured under standard (STD, n=4) and chemically defined xeno-free (XF, n=5) conditions. Clinical grade BM MSCs are used as a control.

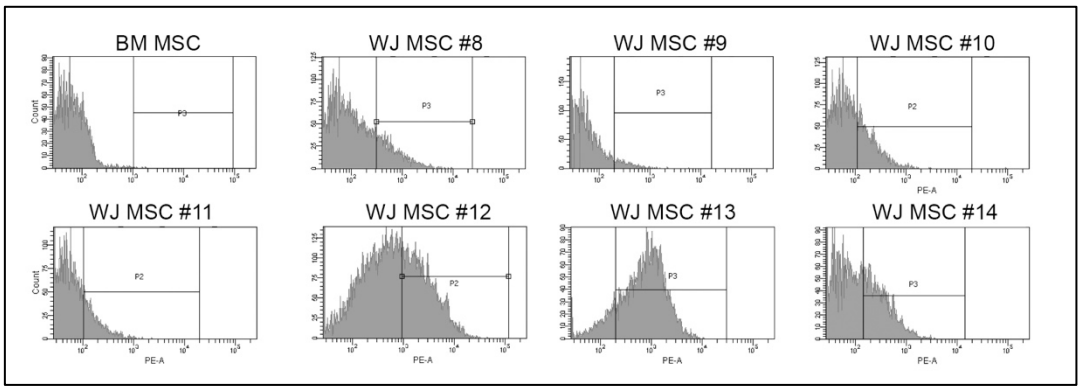

Figure 6.6.9 MSCA-1 expression in WJ MSCs cultured under standard (STD, n=4) and chemically defined xeno-free (XF, n=5) conditions. Clinical grade BM MSCs are used as a control.

Table 6.3.8 Percentage of sub-populations for MSCs surface markers in different passages of iPSC MSC lines (%)

DONOR	P	CD44	CD29	CD90	CD73	CD105	MSCA1	CD56	CD34	CD45
12 ARG	P1	52.9	98.4	46.9	60.4	12.9	31.2	6.9	2.7	0.4
	P9	96.9	99.6	12.8	99.5	18.2	0.3	0.4	1.2	0.1
13 ARG	P1	97.8	98.4	23.7	95.6	46.4	3.1	0.6	0.1	0.2
	P8	77.6	97.6	18.3	85.7	13.3	16.6	0.3	0.1	0.1
34 ARG	P1	98.4	99.8	71.6	96.6	57.6	0.3	10	0.9	0.1
	P9	94.8	98.7	13.5	99.2	6.6	0.2	1.2	0.3	0.1
12 TEX	P1	96.7	99.8	51.2	97.9	73.1	1	22.1	2.2	0.1
	P6	98.1	97.1	39.5	92.4	25.9	0.4	9.8	1.1	0.1
	P11	94.7	96.1	86.7	96	7.1	44	5.1	1.0	0.4
13 TEX	P1	95.9	99.6	16.4	94.5	62	5.9	32.3	0.5	0.4
	P9	95.7	97	75.7	96.3	72.5	54.6	0.3	0.3	0.1
	P11	95.7	97.2	59.8	96.6	45.4	61.7	0.3	0.1	0.1
34 TEX	P2	99	99.9	78.1	99	69.8	0.2	10.4	0.2	0.3
	P6	90.1	99.8	23.4	94.8	35.4	0.2	9.6	0.1	0.2
	P8	81.3	93.5	22	85.8	28.9	12.6	5.1	0.1	0.3

7. REFERENCES

Aasen T, Raya A, Barrero MJ, Garreta E, Consiglio A, Gonzalez F, Vassena R, Bilic J, Pekarik V, Tiscornia G, Edel M, Boue S, Izpisua Belmonte JC. Efficient and rapid generation of induced pluripotent stem cells from human keratinocytes. Nature Biotechnology, 26:1276-1284, 2008.

Alsaab H O, Sau S, Alzhrani R, Tatiparti K, Bhise K, Kashaw S K, Iyer A K. PD-1 and PD-L1 Checkpoint Signaling Inhibition for Cancer Immunotherapy: Mechanism, Combinations, and Clinical Outcome. Frontiers of Pharmacology, 8:561, 2017.

Amiri F, Halabian R, Harati M D, Bahadori M, Mehdipour A, Roushandeh A M, Roudkenar M H. Positive selection of Wharton's jelly-derived CD105+ cells by MACS technique and their subsequent cultivation under suspension culture condition: A simple, versatile culturing method to enhance the multipotentiality of mesenchymal stem cells. Hematology, 20:208-216, 2015.

Amit M, Shariki C, Margulets V, Itskovitz-Eldor J. Feeder layer- and serum-free culture of human embryonic stem cells. Biolology of Reproduction, 70:837-845, 2004.

Andersen DC, Kortesidis A, Zannettino AC, Kratchmarova I, Chen L, Jensen ON, Teisner B, Gronthos S. Jensen C H, Kassem M. Development of novel monoclonal antibodies that define differentiation stages of human stromal (mesenchymal) stem cells. Molecular Cells, 32:133-142, 2011.

Angelucci S, Marchisio M, Giuseppe, FD, Pierdomenico L, Sulpizio M, Eleuterio E. Proteome analysis of human Wharton's jelly cells during in vitro expansion. Proteome Science, 8:18-25, 2010.

Anjos-Afonso F, Siapati EK, Bonnet D. In vivo contribution of murine mesenchymal stem cells into multiple cell-types under minimal damage conditions. Journal of Cell Sciences, 117:5655-5664, 2004.

Antonelli A, Ferrari S M, Giuggioli D, Ferrannini E, Ferri C, Fallahi P. Chemokine (C-X-C motif) ligand (CXCL)10 in autoimmune diseases. Autoimmunity Reviews, 13:272-80, 2014.

Bahmad H, Hadadeh O, Chamaa F, Cheaito K, Darwish B, Makkawi A K, Abou-Kheir W. Modeling Human Neurological and Neurodegenerative Diseases: From Induced Pluripotent Stem Cells to Neuronal Differentiation and Its Applications in Neurotrauma. Frontier in Molecular Neurosciences, 10:50, 2017.

Bai L, Lennon DP, Caplan AI, DeChant A, Hecker J, Kranso J, Zaremba A, Miller RH. Hepatocyte growth factor mediates mesenchymal stem cell-induced recovery in multiple sclerosis models. Nature Neurosciences, 15:862-870, 2012.

Ballerini P, Diomede F, Petragnani N, Cicchitti S, Merciaro I, Cavalcanti MFXB, Trubiani O. Conditioned medium from relapsing-remitting multiple sclerosis patients reduces the expression and release of

inflammatory cytokines induced by LPS-gingivalis in THP-1 and MO3.13 cell lines. Cytokine, 96:261-272, 2017.

Barberi T, Willis LM, Socci ND, Studer L. Derivation of multipotent mesenchymal precursors from human embryonic stem cells. PLoS Medicine, 2:e161, 2005.

Barry J, Hyllner J, Stacey G, Taylor CJ. Setting Up a Haplobank: Issues and Solutions. Current Stem Cell Reports, 1(2):110–117, 2015.

Batsali AK, Kastrinaki MC, Papadaki HA, Pontikoglou C. Mesenchymal stem cells derived from Wharton's Jelly of the umbilical cord: biological properties and emerging clinical applications. Current Stem Cell Research and Therapy, 8:144-155, 2013.

Batsali AK, Pontikoglou C, Koutroulakis D, Pavlaki K I, Damianaki A, Mavroudi I, Alpantaki K, Kouvidi E, Kontakis G, Papadaki H A. Differential expression of cell cycle and WNT pathway-related genes accounts for differences in the growth and differentiation potential of Wharton's jelly and bone marrow-derived mesenchymal stem cells. Stem Cell Research and Therapy, 8:102, 2017.

Battula VL, Treml S, Bareiss P M, Gieseke F, Roelofs H, de Zwart P, Müller I, Schewe B, Skutella T, Fibbe WE, Kanz L, Bühring HJ. Isolation of functionally distinct mesenchymal stem cell subsets using antibodies against CD56, CD271, and mesenchymal stem cell antigen-1. Haematologica, 94:173-184, 2009.

Bianco P, Riminucci M, Gronthos S, Robey PG. Bone marrow stromal stem cells: nature, biology, and potential applications. Stem Cells, 19:180-192, 2011.

Bianco P, Robey PG, Simmons PJ. Mesenchymal Stem Cells: Revisiting History, Concepts, and Assays. Cell Stem Cell, 2:313-19, 2008.

Bharti D, Shivakumar SB, Park JK, Ullah I, Subbarao RB, Park JS, Lee SL, Park BW, Rho GJ. Comparative analysis of human Wharton’s jelly mesenchymal stem cells derived from different parts of the same umbilical cord. Cell Tissue Research, 372:51-65, 2018.

Branly T, Bertoni L, Contentin R, Rakic R, Gomez-Leduc T, Desancé M, Hervieu M, Legendre F, Jacquet S, Audigié F, Denoix JM, Demoor M, Galéra P. Characterization and use of Equine Bone Marrow Mesenchymal Stem Cells in Equine Cartilage Engineering. Study of their Hyaline Cartilage Forming Potential when Cultured under Hypoxia within a Biomaterial in the Presence of BMP-2 and TGF-ß1. Stem Cell Reviews, 13:611-630, 2017.

Breitbach M, Bostani T, Roell W, Xia Y, Dewald O, Nygren J M, Fries J W, Tiemann K, Bohlen H, Hescheler J, Welz A, Bloch W, Jacobsen SE, Fleischmann BK. Potential risks of bone marrow cell transplantation into infarcted hearts. Blood, 110:1362-1369, 2007.

Bühring HJ, Battula VL, Treml S, Schewe B, Kanz L, Vogel W. Novel markers for the prospective isolation of human MSC. Annals of New York Academic Sciences,1106:262-271, 2007.

Bühring HJ, Treml S, Cerabona F, de Zwart P, Kanz L, Sobiesiak M. Phenotypic characterization of distinct human bone marrow-derived MSC subsets. Annals of the New York Academy of Sciences, 1176:124-134, 2009.

Bobis S, Jarocha D, Majka M. Mesenchymal stem cells: characteristics and clinical applications. Folia Histochemistry Cytobiology, 44:215-230, 2006.

Campagnoli C, Roberts IA, Kumar S, Bennett PR, Bellantuono I, Fisk NM. Identication of mesenchymal stem/progenitor cells in human first-trimester fetal blood, liver, and bone marrow. Blood, 98:2396-2402, 2001.

Campione D, Rizzo R, Stignani M, Melchiorri L, Ferrari L, Moretti S, Russo A, Bagnara GP, Bonsi L, Alviano F, Lanzoni G, Cuneo A, Baricordi OR, Lanza F, A decreased positivity for CD90 on human mesenchymal stromal cells (MSCs) is associated with a loss of immunosuppressive activity by MSCs. Cytometry Part B (Clinical Cytometry), 76B:225-230, 2009.

Can A, Celikkan FT, Cinar O. Umbilical cord mesenchymal stromal cell transplantations: A systemic analysis of clinical trials. Cytotherapy, 19:1351-1382, 2017.

Can A, Karahuseyinoglu S. Concise review: human umbilical cord stroma with regard to the source of fetus-derived stem cells. Stem Cells, 25, 2886-2895, 2007.

Can A, Yigman Z. Mesenchymal stem/stromal cells from neonatal tissues. In: Bolontrade MF, Garcia MG, editors. Mesenchymal Stromal Cells as Tumor Stromal Modulators. Academic Press, p.65-101, 2016.

Capelli C, Gotti E, Morigi M, Rota C, Weng L, Dazzi F, Soinelli O, Cazzaniga G, Trezzi R, Gianatti A, Rambaldi A, Golay J, Introna M. Minimally manipulated whole human umbilical cord is a rich source of clinical-grade human mesenchymal stromal cells expanded in human platelet lysate. Cytotherapy, 13:786-801, 2011.

Caplan AI. Adult mesenchymal stem cells for tissue engineering versus regenerative medicine. Journal of Cell Physiology, 213:341-347, 2007.

Caplan A I. Mesenchymal stem cells. Journal of Orthopedic Research, 9:641-50, 1991.

Carcamo-Orive I, Hoffman GE, Cundiff P, Beckmann ND, D'Souza SL, Knowles JW, Patel A, Papatsenko D, Abbasi F, Reaven GM, Whalen S, Lee P, Shahbazi M, Henrion MYR, Zhu K, Wang S, Roussos P, Schadt EE, Pandey G, Chang R, Quertemous T, Lemischka I. Analysis of transcriptional variability in a large human iPSC library reveals genetic and non-genetic determinants of heterogeneity. Cell Stem Cell, 20:518-532, 2017.

Carlin R, Davis D, Weiss M, Schultz B, Troyer D. Expression of early transcription factors Oct-4, Sox-2 and nanog by porcine umbilical cord (PUC) matrix cells. Reproductive Biology and Endocrinology, 4:1–13, 2006.

Castro-Malaspina H, Gay R, Resnick G, Kapoor N, Meyers P, Chiarieri D, McKenzie S, Broxmeyer H, Moore, M. Characterization of human bone marrow fibroblast colony-forming cells (CFU-F) and their progeny. Blood, 56:289-301, 1980.

Chang CJ, Yen ML, Chen YC, Chien CC, Huang H, Bai CH, Yen BL. Placenta-Derived Multipotent Cells Exhibit Immunosuppressive Properties That Are Enhanced in the Presence of Interferon-γ. Stem Cells, 24:2466-2477, 2006.

Chase LG, Yang S, Zachar V, Yang Z, Lakshmipathy U, Bradford J, Boucher SE, Vemuri MC. Development and characterization of a clinically compliant xeno-free culture medium in good manufacturing practice for human multipotent mesenchymal stem cells. Stem Cells Translational Medicine, 1:750-758, 2012.

Chen J, Liu H, Liu J, Qi J, Wei B, Yang J, Liang H, Chen Y, Chen J, Wu Y, Guo L, Zhu J, Zhao X, Peng T, Zhang Y, Chen S, Li X, Li D, Wang T, Pei D. H3K9 methylation is a barrier during somatic cell reprogramming into iPSCs. Nature Genetics, 45:34-42, 2013.

Chen Y, Stevens B, Chang J, Milbrandt J, Barres B A, Hell J W. NS21: Re-defined and Modified Supplement B27 for Neuronal Cultures. Journal of Neurosciences Methods, 171:239-247, 2008.

Cheng PP, Liu XC, Ma PF, Gao C, Li JL, Lin Y Y, Shao W, Han S, Zhao B, Wang LM, Fu JZ, Meng LX, Li Q, Lian QZ, Xia JJ, Qi ZQ. iPSC-MSCs Combined with Low-Dose Rapamycin Induced Islet Allograft Tolerance Through Suppressing Th1 and Enhancing Regulatory T-Cell Differentiation. Stem Cells Development, 24:1793-1804, 2015.

Cheng X, Ying L, Lu L, Galvão AM, Mills JA, Lin HC, Kotton DN, Shen SS, Nostro MC, Choi JK, Weiss MJ, French DL, Gadue P. Self-renewing endodermal progenitor lines generated from human pluripotent stem cells. Cell Stem Cell. 10:371-384, 2012.

Cho PS, Messina D J, Hirsh E L, Chi N, Goldman SN, Lo DP, Harris IR, Popma SH, Sachs DH, Huang CA. Immunogenicity of umbilical cord tissue derived cells. Blood, 111:430-438, 2008.

Chaturvedi P, Gilkes D M, Wong C C L, Kshitiz, Luo W, Zhang H, Wei H, Taklano N, Schito L, Levchenko A, Semenza G L. Hypoxia-inducible factor-dependent breast cancer mesenchymal stem cell bidirectional signaling promotes metastasis. Journal of Clinical Investigation, 123:189-205, 2013.

Christodoulou I, Kolisis FN, Papaevangeliou D, Zoumpourlis V. Comparative Evaluation of Human Mesenchymal Stem Cells of Fetal (Wharton's Jelly) and Adult (Adipose Tissue) Origin during Prolonged In Vitro Expansion: Considerations for Cytotherapy. Stem Cells International, 2013:246134, 2013.

Conconi MT, Di Liddo R, Tommasini M, Calore C, Parnigotto PP. Phenotype and differentiation potential of stromal populations obtained from various zones of human umbilical cord: an overview. Open Tissue Engineering and Regenerative Medicine Journal, 4:6-20, 2011.

Conget PA, Minguell JJ. Phenotypical and functional properties of human bone marrow mesenchymal progenitor cells. Journal of Cellular Physiology,181:67-73, 1999.

Cornacchia F, Fornoni A, Plati A R, Thomas A, Wang Y, Inverardi L, Striker L J, Striker G. Glomerulosclerosis is transmitted by bone marrow-derived mesangial cell progenitors. Journal of Clinical Investigation, 108:1649-1656, 2001.

Cuomo F, Coppola A, Botti C, Maione C, Forte A, Scisciola L, Liguori G, Caiafa I, Ursini M V, Galderisi U, Cipollaro M, Altucci L, Cobellis G. Pro-inflammatory cytokines activate hypoxia-inducible factor 3α via epigenetic changes in mesenchymal stromal/stem cells. Scientific Reports, 8:5842, 2018.

Dahbour S, Jamali F, Alhattab D, Al-Radaideh A, Ababneh O, Al-Ryalat N, Al-Bdour M, Hourani B, Msallam M, Rasheed M, Huneiti A, Bahou Y, Tarawneh E, Awidi A. Mesenchymal stem cells and conditioned media in the treatment of multiple sclerosis patients: Clinical, ophthalmological and radiological assessments of safety and efficacy. CNS Neurosciences and Therapy, 23:866-874, 2017.

de Peppo GM, Marcos-Campos I, Kahler D J, Alsalman D, Shang L,Vunjak-Novakovic G, Marolta D. Engineering bone tissue substitutes from human induced pluripotent stem cells. Proceedings of the National Academy of Sciences of the United States of America, 110:8680-8685, 2013.

de Witte SFH, Franquesa M, Baan CC, Hoogduijn MJ. Toward development of mesenchymal stem cells for immunomodulatory therapy. Frontiers in Immunology, 6:648, 2015.

DeBoever C, Li H, Jakubosky D, Benaglio P, Reyna J, Olson K M, Huang H, Biggs W, Sandoval E, D'Antonio M, Jepsen K, Matsui H, Arias A, Ren B, Narial N, Smith E N, A'Antonio-Chronowska A, Farley E K,

Frazer K A. Large-scale profiling reveals the influence of genetic variation on gene expression in human induced pluripotent stem cells. Cell Stem Cell, 20:533-546, 2017.

Devito L, Badraiq H, Galleu A, Taheem D K, Codognotto S, Siow R, Khalaf Y, Briley A, Shennan A, Poston L, McGrath J, Gentleman E, Dazzi F, Ilic D. Wharton's jelly mesenchymal stromal/stem cells derived under chemically defined animal product-free low oxygen conditions are rich in MSCA-1(+) subpopulation. Regenerative Medicine, 9:723-732, 2014.

Djouad F, Bony C, Haupl T, Uzé G, Lahlou N, Louis-Plence P, Apparailly F, Canovas F, Rème T, Sany J, Jorgensen C, Noël D. Transcriptional profiles discriminate bone marrow-derived and synovium-derived mesenchymal stem cells. Arthritis Research and Therapy, 7:R1304-1315, 2005.

Dominici M, Le Blanc K, Mueller I, Slaper-Cortenbach I, Marini F, Krause D, Deans R, Keating A, Prockop Dj, Horwitz E. Minimal criteria for defining multipotent mesenchymal stromal cells. The International Society for Cellular Therapy position statement. Cytotherapy, 8:315-317, 2006.

Donders R, Bogie JFJ, Ravanidis S, Gervois P, Vanheusden M, Marée R, Schrynemackers M, Smeets HJM, Pinxteren J, Gijbels K, Walbers S, Mays R W, Deans R, Van Den Bosch L, Stinissen P, Lambrichts I, Gyselaers W, Hellings N. Human Wharton's Jelly-Derived Stem Cells Display a Distinct Immunomodulatory and Proregenerative Transcriptional Signature Compared to Bone Marrow-Derived Stem Cells. Stem Cells and Development, 27:65-84, 2018.

Donnenberg VS, Zimmerlin L, Rubin JP, Donnenberg AD. Regenerative therapy after cancer: What are the risks? Tissue Engineering Part B Reviews, 16:567-575, 2010.

Droujinine IA, Eckert M A, Zhao W. To grab the stroma by the horns: From biology to cancer therapy with mesenchymal stem cells. Oncotarget, 4:651-664, 2013.

Duan HG, Ji F, Zheng C Q, Li J, Wang J. Conditioned medium from umbilical cord mesenchymal stem cells improves nasal mucosa damage by radiation. Biotechnology Letters, 40:999-1007, 2018.

English K. Mechanisms of mesenchymal stromal cell immunomodulation. Immunology and Cell Biology, 91:19-26, 2013.

Erices A, Conget P, Minguell JJ. Mesenchymal progenitor cells in human umbilical cord blood. British Journal of Haematology, 109:235-242, 2000.

Evans M J, Kaufman M H. Establishment in culture of pluripotential cells from mouse embryos. Nature, 292:154-156, 1981.

Feng-Juan LV, Rocky ST, Kenneth MCC, Victor YLL. Concise Review: The Surface Markers and identity of Human Mesenchymal Stem Cells. Stem Cells Report, 32:1408-1419, 2014.

Fibbe WE, Noort WA. Mesenchymal stem cells hematopoietic stem cell transplantation. Annals of the New York Academy of Sciences, 996:235-244, 2003.

Fong CY, Gauthaman K, Cheyyatraivendran S, Lin HD, Biswas A, Bongso A. Human umbilical cord Wharton's jelly stem cells and its conditioned medium support hematopoietic stem cell expansion ex vivo. Journal of Cellular Biochemistry, 113:658-668, 2012.

Fong CY, Richards M, Manasi N, Biswas A, Bongso A. Comparative growth behaviour and characterization of stem cells from human Wharton's jelly. Reproductive Biomedicine Online, 15:708-718, 2007.

Fong CY, Subramanian A, Biswas A, Gauthaman K, Srikanth P, Hande MP, Bongso A. Derivation efficiency, cell proliferation, frozen-thaw survival, stem-cell properties, and differentiation of human Wharton's jelly stem cells. Reproductive Biomedicine Online, 2:391-401, 2010.

Fong CY, Tam K, Cheyyatraivendran S, Gan SU, Gauthaman K, Armugam A, Jeyaseelan K, Choolani M, Biswas A, Bongso A. Human Wharton's jelly stem cells and its conditioned medium enhance healing of excisional and diabetic wounds. Journal of Cell Biochemistry, 115:290-302, 2014.

Fonta C, Negyessy L, Renaud L, Barone P. Postnatal development of alkaline phosphatase activity correlates with the maturation of neurotransmission in the cerebral cortex. Journal of Comparative Neurology, 486:179-196, 2005.

Frausin S, Viventi S, Verga Falzacappa L, Quattromani M J, Leanza G, Tommasini A, Valencic E. Wharton's jelly derived mesenchymal stromal cells: Biological properties, induction of neuronal phenotype and current applications in neurodegeneration research. Acta Histochemistry, 117:329-338, 2015.

Friedenstein AJ, Chailakhyan RK, Gerasimov UV. Bone marrow osteogenic stem cells: in vitro cultivation and transplantation in diffusion chambers. Cell and Tissue Kinetics, 20:263-272, 1987.

Friedenstein AJ, Chailakhjan RK, Lalykina KS. The development of fibroblast colonies in monolayer cultures of guinea-pig bone marrow and spleen cells. Cell Tissue Kinetics, 3:393-403, 1970.

Friedman R, Betancur M, Boissel L, Tuncer H, Cetrulo C, Klingemann H. Umbilical cord mesenchymal stem cells: adjuvants for human cell transplantation. Biology of Blood Marrow Transplant, 13:1477-1486, 2007.

Fritz V, Noel D, Bouquet C, Opolon P, Voide R, Apparailly F, Louis-Plence P, Bouffi C, Drissi H, Xie C, Perricaudet M, Muller R, Schwarz E, Jorgensen C. Antitumoral activity and osteogenic potential of

mesenchymal stem cells expressing the urokinase-type plasminogen antagonist amino-terminal fragment in a murine model of osteolytic tumor. Stem Cells, 26:2981-2990, 2008.

Frobel J, Hemeda H, Lenz M, Abagnale. Epigenetic rejuvenation of mesenchymal stromal cells derived from induced pluripotent stem cells. Stem Cell Reports, 3:414-422, 2014.

Fu Q L, Chow Y Y, Sun S J, Zeng Q X, Li H B, Shi J B, Sun Y Q, Wen W, Tse H F, Lian Q, Xu G. Mesenchymal stem cells derived from human induced pluripotent stem cells modulate T cell phenotypes in allergic rhinitis. Allergy, 67:1215-1222, 2012.

Fukuchi Y, Nakajima H, Sugiyama D, Hirose I, Kitamura T, Tsuji K. Human placenta-derived cells have mesenchymal stem/progenitor cell potential. Stem Cells, 22:649-658, 2004.

Fung M, Yuan Y, Atkins H, Qian Shi Q, Bubela T. Responsible translation of stem cell research: an assessment of clinical trial registration and publications. Stem Cell Reports, 8:1–12, 2017.

Galleu A, Riffo-Vasquez Y, Trento C, Lomas C, Dolcetti L, Cheung TS, von Bonin M, Barbieri L, Halai K, Ward S, Weng L, Chakraverty R, Lombardi G, Watt FM, Orchard K, Marks DI, Apperley J, Bornhauser M, Walczak H, Bennett C, Dazzi F. Apoptosis in mesenchymal stromal cells induces in vivo recipient-mediated immunomodulation. Science Translational Medicine 9:416, 2017

Gao Z, Wang H, Lin F, Wang X, Long M, Zhang H, Dong K. CD73 promotes proliferation and migration of human cervical cancer cells independent of its enzyme activity. BMC Cancer, 17:135, 2017.

Gauthaman K, Fong CY, Cheyyatraivendran S, Biswas A, Choolani M, Bongso A. Human umbilical cord Wharton's jelly stem cell (hWJSC) extracts inhibit cancer cell growth in vitro. Journal of Cellular Biochemistry, 113:2027-2039, 2012.

Gaspar-Maia A, Qadeer ZA, Hasson D, Ratnakumar K, Leu NA, Leroy G, Liu S, Costanzi C, Valle-Garcia D, Schaniel C, Lemischka I, Garcia B, Pehrson JR, Bernstein E. MacroH2A histone variants act as a barrier upon reprogramming towards pluripotency. Nature Communication, 4:1565, 2013.

Goldberg VM. Stem cells in osteoarthritis. HSS Journal, 8:59-61, 2012.

Gottipamula S, Muttigi MS, Chaansa S, Ashwin KM, Priya N, Kolkundkar U, Sundar Raj S: Majumdar AS. Seetharam RN. Large-scale expansion of pre-isolated bone marrow mesenchymal stromal cells in serum-free conditions. Journal Tissue Engineering and Regenerative Medicine, 10:108-119, 2016.

Green DS, Young HA, Valencia JC. Current Prospects of Type II Interferon Gamma Signaling and Autoimmunity. Journal of Biological Chemistry, 292:13925-13933, 2017.

Griffin MD, Elliman SJ, Cahill E, English K, Ceredig R, Ritter T. Concise review: Adult mesenchymal stromal cell therapy for inflammatory diseases: How well are we joining the dots? Stem Cells, 31:2033-2041, 2013.

Gronthos S, Fitter S, Diamond P, Simmons PJ, Itescu S, Zannettino AC. A novel monoclonal antibody (*STRO-3*) identifies an isoform of tissue nonspecific alkaline phosphatase expressed by multipotent bone marrow stromal stem cells. Stem Cells and Development, 16:953-963, 2007.

Gronthos S, Zannettino AC, Hay SJ, Shi S, Graves SE, Kortesidis A, Simmons PJ. Molecular and cellular characterisation of highly purified stromal stem cells derived from human bone marrow. Journal of Cell Science, 116:1827-1835, 2003.

Gupta PK, Das AK, Chullikana A, Majumdar AS. Mesenchymal stem cells for cartilage repair in osteoarthritis. Stem Cell Research and Therapy, 3:25, 2012.

Gurdon, J. B. The developmental capacity of nuclei taken from intestinal epithelium cells of feeding tadpoles. Journal of Embryology and Experimental Morphology, 34:93–112, 1962.

Halfon S, Abramov N, Grinblat B, Ginis I. Markers distinguishing mesenchymal stem cells from fibroblasts are downregulated with passaging. Stem Cells and Development, 20:53-66, 2011.

Hendijani F, Sadeghi-Aliabadi H, Haghjooy Javanmard S. Comparison of human mesenchymal stem cells isolated by explant culture method from entire umbilical cord and Wharton's jelly matrix. Cell Tissue Bank, 15:555-565, 2014.

Heng B C, Cao T, Lee E H. Directing stem cell differentiation into the chondrogenic lineage in vitro. Stem Cells, 22:1152-1167, 2004.

Ho A D, Wagner W, Franke W. Heterogeneity of mesenchymal stromal cell preparations. Cytotherapy 10:320-330, 2008.

Horwitz EM, Gordon PL, Koo WK, Marx JC, Neel MD, McNall RY, Muul L, Hofmann T. Isolated allogeneic bone marrow-derived mesenchymal cells engraft and stimulate growth in children with osteogenesis imperfecta: implications for cell therapy of bone. Proceedings of the National Academy of Sciences of the United States of America, 99:8932-8937, 2002.

Horwitz EM, Le Blanc K, Dominici M, Mueller I, Slaper-Cortenbach I, Marini FC, Deans RJ, Krause DS, Keating A. Clarification of the nomenclature for MSC: The International Society for Cellular Therapy position statement. Cytotherapy, 7:393-395, 2005.

Hoynowski SM, Fry MM, Gardner BM, Leming MT, Tucker JR, Black L, Sand T, Mitchell KE. Characterization and differentiation of equine umbilical cord derived matrix cells. Biochemical and Biophysical Research Communications, 362:347-353, 2007.

Hsuan Y CY, Lin CH, Chang C P, Lin MT. Mesenchymal stem cell-based treatments for stroke, neural trauma, and heat stroke. Brain and Behavior, 6:e00526, 2016.

Hu WH, Mo XM, Walters WM, Brambilla R, Bethea JR. TNAP, a novel repressor of NF-kappaB-inducing kinase, suppresses NF-kappaB activation. Journal of Biological Chemistry. 279(34), 35975–35983, 2004.

Hu Y, Liao L, Wang Q, Ma L, Ma G, Jiang X, Zhao R C. Isolation and identification of mesenchymal stem cells from human fetal pancreas. Journal of Laboratory and Clinical Medicine, 141:342-349, 2003.

Huang Y C, Parolini O, La Rocca G, Deng L. Umbilical cord versus bone marrow derived mesenchymal stromal cells. Stem Cells and Development, 21:2900-2903, 2012.

Hughes CS, Radan L, Betts D, Postovit L M, Lajoie GA. Proteomic analysis of extracellular matrices used in stem cell culture. Proteomics, 11:3983-3991, 2011.

Huss R. Perspectives on the morphology and biology of CD34-negative stem cells. Journal of Hematotherapy & Stem Cell Research, 9:783-93, 2000.

Hwang NS, Varghese S, Lee HJ, Zhang Z, Ye Z, Bae J, Cheng L, Elisseeff J. In vivo commitment and functional tissue regeneration using human embryonic stem cell-derived mesenchymal cells. Proceedings of National Academy of Sciences the United States of America, 105:20641-20646, 2008.

Ishii M, Koike C, Igarashi A, Yamanaka K, Pan H, Higashi Y, Kawaguchi H, Sugiyama M, Kamata N, Iwata T, Matsubara T, Nakamura K, Kurihara H, Tsuji K, Kato Y. Molecular markers distinguish bone marrow mesenchymal stem cells from fibroblasts. Biochemical and Biophysical Research Communications, 332:297–303, 2005.

Iudicone P, Fioravanti D, Bonanno G, Miceli M, Lavorino C, Totta P, Frati L, Nuti M, Pierelli L. Pathogen-free, plasma-poor platelet lysate and expansion of human mesenchymal stem cells. Journal of Translational Medicine, 12:28, 2014.

Ivanova-Todorova E, Bochev I, Dimitrov R, Belemezova K, Mourdjeva M, Kyurkchiev S, Kinov P, Altankova I, Kyurkchiev D. Conditioned medium from adipose tissue-derived mesenchymal stem cells induces CD4+FOXP3+ cells and increases IL-10 secretion. Journal of Biomedicine and Biotechnology, 2012.

Javazon EH, Beggs KJ, Flake AW. Mesenchymal stem cells: Paradoxes of passaging. Experimental Hematology, 32:414-425, 2004.

Jenhani F, Durand V, Ben Azouna N, Thallet S, Ben Othmen T, Bejaoui M, Domenech J. Human cytokine expression profile in various conditioned media for in vitro expansion bone marrow and umbilical cord blood immunophenotyped mesenchymal stem cells. Transplantation Proceedings, 43:639-643, 2011.

Jin Jin H, Bae Y K, Kim M, Kwon S J, Jeon H B, Choi S J, Kim S W, Yang Y S, Oh W, Chang J W. Comparative Analysis of Human Mesenchymal Stem Cells from Bone Marrow, Adipose Tissue, and Umbilical Cord Blood as Sources of Cell Therapy. International Journal of Molecular Sciences, 14:17986-18001, 2013.

Jinglei C, Wen L, Huanxing S, Dajiang Q, Jiayin Y, Zhu F, Xu J, He W, Guo X, Labuda K, Peterbauer A, Wolbank S, Zhong M, Li Z, Wu W, So K F, Redl H, Zeng L, Esteban M A, Pei D. Generation of Human Induced Pluripotent Stem Cells from Umbilical Cord Matrix and Amniotic Membrane Mesenchymal Cells. The Journal of Biological Chemistry, 285:11227-11234, 2010.

Joerger-Messerli MS, Marx C, Oppliger B, Mueller M, Surbek DV, Schoeberlein A. Mesenchymal Stem Cells from Wharton's Jelly and Amniotic Fluid. Best Practical Research: Clinical and Obstetrics Gynaecology, 31:30-44, 2016.

Jones EA, English A, Kinsey SE, Straszynski L, Emery P, Ponchel F, McGonagle D. Optimization of a flow cytometry-based protocol for detection and phenotypic characterization of multipotent mesenchymal stromal cells from human bone marrow. Cytometry B Clinical Cytometry, 70:391-399, 2006.

Jones EA, Kinsey SE, English A, Jones RA, Straszynski L, Meredith DM, Markham AF, Jack A, Emery P, McGonagle D. Isolation and characterization of bone marrow multipotential mesenchymal progenitor cells. Arthritis Rheumatology, 46:3349-33460, 2002.

Jones EA, English A, Kinsey S E, Straszynski L, Emery P, Ponchel F, McGonagle D. Optimization of a flow cytometry-based protocol for detection and phenotypic characterization of multipotent mesenchymal stromal cells from human bone marrow. Cytometry Part B: Clinical Cytometry, 70:391-399, 2006.

Jopling C, Boue S, Izpisua Belmonte JC. Dedifferentiation, transdifferentiation and reprogramming: three routes to regeneration. Nature Reviews in Molecular Cell Biology, 12:79-89, 2011.

Jung Y, Kim J K, Shiozawa Y, Wang J, Mishra A, Joseph J, Berry J E, McGee S, Lee E, Sun H, Wang J, Jin T, Zhang H, Dai J, Krebsbach P H, Keller E T, Pienta K J, Taichman R S. Recruitment of mesenchymal stem cells into prostate tumours promotes metastasis. Nature Communication, 4:1795, 2013.

Jurisic G, Iolyeva M, Proulx S T Halin C, Detmar M. Thymus cell antigen 1 (Thy1, CD90) is expressed by lymphatic vessels and mediates cell adhesion to lymphatic endothelium. Experimental Cell Research. 316:2982-2992, 2010.

Kadam SS, Bhonde RR. Islet neogenesis from the constitutively nestin expressing human umbilical cord matrix derived mesenchymal stem cells. Islets, 2:112-120, 2010.

Kadam SS, Tiwari S, Bhonde RR. Simultaneous isolation of vascular endothelial cells and mesenchymal stem cells from the human umbilical cord. In Vitro Cellular Developmental Biololy Animal, 45:23-27, 2009.

Kalladka D, Muir KW. Brain repair: Cell therapy in stroke. Stem Cells and Cloning, 7:31-44, 2014.

Karahuseyinoglu S, Cinar O, Kilic E, Kara F, Akay GG, Demiralp DO, Tukun A, Uckan D, Can A. Biology of stem cells in human umbilical cord stroma: *in situ* and *in vitro* surveys. Stem Cells, 25:319-331, 2007.

Karlsson C, Emanuelsson K, Wessberg F, Kajic K, Axel M Z, Eriksson P S, Lindahl A, Hyliner J, Strehl R. Human embryonic stem cell-derived mesenchymal progenitors--potential in regenerative medicine. Stem Cell Research, 3:39-50, 2009.

Kawada H, Fujita J, Kinjo K, Matsuzaki Y, Tsuma M, Miyatake H, Muguruma Y, Tsuboi K, Itabashi Y, Ikeda Y, Ogawa S, Okano H, Hotta T, Ando K, Fukuda K. Nonhematopoietic mesenchymal stem cells can be mobilized and differentiate into cardiomyocytes after myocardial infarction. Blood, 104:3581-3587, 2004.

Kern S, Eichler H, Stoeve J, Klüter H, Bieback K. Comparative analysis of mesenchymal stem cells from bone marrow, umbilical cord blood, or adipose tissue. Stem Cells, 24:1294-1301, 2006.

Keshtkar S, Azarpira N, Ghahremani M H. Mesenchymal stem cell-derived extracellular vesicles: novel frontiers in regenerative medicine. Stem Cell Research and Therapy, 9:63, 2018.

Khan MM. Role of Cytokines. Immunopharmacology, Springer International Publishing, Switzerland, 2016

Kilpinen H, Goncalves A, Leha A, Afzal V, Alasoo K, Ashford S, Bala S, Bensaddek D, Casale F P, Culley O J, Danecek P, Faulconbridge A, Harrison P W, Kathuria A, McCarthy D, McCarthy S A, Meleckyte R, Memari Y, Moens N, Soares F, Mann A, Streeter I, Agu C A, Alderton A, Nelson R, Harper S, Patel M, White A, Patel S R, Clarke L, Halai R, Kirton C M, Kolb-Kokocinski A, Beales P, Birney E, Danovi D, Lamond A I, Ouwehand W H, Vallier L, Watt F M, Durbin R, Stegle O, Gaffney D J. Common genetic variation drives molecular heterogeneity in human iPSCs. Nature, 546:370-375, 2017.

Kim DW, Staples M, Shinozuka K, Pantcheva P, Kang SD, Borlongan CV. Wharton's jelly-derived mesenchymal stem cells: phenotypic characterization and optimizing their therapeutic potential for clinical applications. International Journal of Molecular Sciences, 14:11692-11712, 2013.

Kim JB, Zaehres H, Wu G, Gentile L, Ko K, Sebastiano V, Arauzo-Bravo MJ, Ruau D, Han DW, Zenke M, Scholer HR. Pluripotent stem cells induced from adult neural stem cells by reprogramming with two factors. Nature, 454:646-650, 2008.

Kisselbach L, Merges M, Bossie A, Boyd A. CD90 Expression on human primary cells and elimination of contaminating fibroblasts from cell cultures. Cytotechnology, 59:31-44, 2009.

Klinker MW, Wei C-H. Mesenchymal stem cells in the treatment of inflammatory and autoimmune diseases in experimental animal models. World Journal of Stem Cells 7:556-567, 2015.

Koelling S, Miosge N. Stem cell therapy for cartilage regeneration in osteoarthritis. Expert Opinion on Biological Therapy, 9:1399-1405, 2009.

Krampera M, Cosmi L, Angeli R, Pasini A, Liotta F, Andreini A, Santarlasci V, Mazzinghi B, Pizzolo G, Vinante F, Romagnani P, Maggi E, Romagnani S, Annunziato F. Role for interferon-gamma in the immunomodulatory activity of human bone marrow mesenchymal stem cells. Stem Cells, 24:386-398, 2006.

Kunter U, Rong S, Boor P, Eitner F, Muller-Newen G, Djuric Z, van Roeyen C R, Konieczny A, Ostendorf T, Villa L, Milovanceva-Popovska M, Kerjaschki D, Floege J. Mesenchymal stem cells prevent progressive experimental renal failure but maldifferentiate into glomerular adipocytes. Journal of American Society of Nephrology, 18:1754-1764, 2007.

Kurtz A. Mesenchymal stem cell delivery routes fate. International Journal of Stem Cells, 1:1–7, 2008.

Kyurkchiev D, Bochev I, Ivanova-Todorova E, Mourdjeva M, Oreshkova T, Belemezova K, Kyurkchiev S. Secretion of immunoregulatory cytokines by mesenchymal stem cells. World Journal of Stem Cell, 6:552-570, 2014.

Le Blanc K, Tammik L, Sundberg B, Haynesworth SE, Ringden O. Mesenchymal stem cells inhibit and stimulate mixed lymphocyte cultures and mitogenic responses independently of the major histocompatibility complex. Scandinavian Journal of Immunology, 57:11-20, 2003.

Leibacher J, Henschler R. Biodistribution, migration and homing of systemically applied mesenchymal stem/stromal cells. Stem Cell Research and Therapy, 7:7, 2016.

Lesley J, Hascall VC, Tammi M, Hyman R. Hyaluronan binding by cell surface CD44. Journal of Biological Chemistry, 35:26967-26975, 2000.

Lian Q, Lye E, Yeo KS, Tan EK W, Salto-Tellez M, Liu TM, Palanisamy N, Oakley RME, Lee EH, Lim B, Lia SK. Derivation of clinically compliant MSCs from CD105+, CD24- differentiated human ESCs. Stem Cells, 25:425-436, 2007.

Li B, Morioka T, Uchiyama M, Oite T. Bone marrow cell infusion ameliorates progressive glomerulosclerosis in an experimental rat model. Kidney International, 69:323-330, 2006.

Li Q, Verma IM. NF-κB regulation in the immune system. Nature Reviews Immunology, 2:725-734, 2002.

Li X, Ling W, Pennisi A, Wang Y, Khan S, Heidaran M, Pal A, Zhang X, He S, Zeitlin A, Abbot S, Faleck H, Hariri R, Shaughnessy JD Jr, van Rhee F, Nair B, Barlogie B, Epstein J, Yaccoby S. Human placenta-derived adherent cells prevent bone loss, stimulate bone formation, and suppress growth of multiple myeloma in bone. Stem Cells, 29:263-273, 2011.

Li Y, Powell S, Brunette E, Lebkowski J, Mandalam R. Expansion of human embryonic stem cells in defined serum-free medium devoid of animal-derived products. Biotechnology Bioengineering, 91:688-698, 2005.

Lim J, Razi Z R, Law J, Nawi A M, Idrus R B, Ng M H. MSCs can be differentially isolated from maternal, middle and fetal segments of the human umbilical cord. Cytotherapy, 18:1493-1502, 2016.

Liu J, Han Z, Han Z, He Z. Mesenchymal stem cell-conditioned media suppresses inflammation-associated overproliferation of pulmonary artery smooth muscle cells in a rat model of pulmonary hypertension. Experimental and Therapeutic Medicine, 11:467-475, 2016.

Liu P, Chen S, Li X, Qin L, Huang K, Wang L, Huang W, Li S, Jia B, Zhong M, Pan G, Cai J, Pei D. Low Immunogenicity of Neural Progenitor Cells Differentiated from Induced Pluripotent Stem Cells Derived from Less Immunogenic Somatic Cells. Public Library of Science One, 26:8, 2013.

Liu Y, Cheng Q, Hu G, Deng T, Wang Q, Zhou J, Su X. Extracellular vesicles in mesenchymal stromal cells: A novel therapeutic strategy for stroke. Experimental and Therapeutic Medicine, 15(5): 4067–4079, 2018.

Lotfinia M, Kadivar M, Piryaei A, Pournasr B, Sardari S, Sodeifi N, Sayahpour F A, Baharvand H. Effect of Secreted Molecules of Human Embryonic Stem Cell-Derived Mesenchymal Stem Cells on Acute Hepatic Failure Model. Stem Cells and Development, 25:1898-1908, 2016.

Luk F, Carreras-Planella L, Korevaar SS, de Witte SFH, Borràs FE, Betjes MGH, Baan CC, Hoogduijn MJ, Franquesa M. Inflammatory conditions Dictate the effect of Mesenchymal stem or stromal cells on B-cell Function. Frontiers in Immunology, 8:e1042, 2017.

Lund R J, Narva E, Lahesmaa R. Genetic and epigenetic stability of human pluripotent stem cells. Nature Review Genetics, 13:732-744, 2012.

Luzzani C, Neiman G, Garate X, Questa M, Solari C, Espinosa DF, García M, Errecalde AL, Guberman A, Scassa ME, Sevlever GM, Romorini L, Miriuka SG. A therapy-grade protocol for differentiation of pluripotent stem cells into mesenchymal stem cells using platelet lysate as supplement. Stem Cell Research and Therapy, 6:6, 2015.

Ma L, Feng XY, Cui BL, Law F, Jiang XW, Yang LY, Xie QD, Huang TH. Human umbilical cord Wharton's Jelly-derived mesenchymal stem cells differentiation into nerve- like cells. Chinese Medical Journal, 118:1987-1993, 2005.

Ma, S, Xie, N, Li, W, Yuan, B, Shi, Y, Wang, Y. Immunobiology of mesenchymal stem cells. Cell Death Differentiation, 21:216-225, 2014.

Maherali N, Sridharan R, Xie W, Utikal J, Eminli S, Arnold K, Stadtfeld M, Yachechko R, Tchieu J, Jaenisch R, Plath K, Hochedlinger K. Directly reprogrammed fibroblasts show global epigenetic remodeling and widespread tissue contribution. Cell Stem Cell, 1:55-70, 2007.

Majore I, Moretti P, Hass R, Kasper C. Identification of subpopulations in mesenchymal stem cell-like cultures from human umbilical cord. Cell Communication and Signaling, 7:6, 2009.

Malik N, Rao M S. A Review of the Methods for Human iPSC Derivation. Methods in Molecular Biology, 997:23-33, 2013.

Margossian T, Reppel L, Makdissy N, Stoltz JF, Bensoussan D, Huselstein C. Mesenchymal stem cells derived from Wharton's jelly: comparative phenotype analysis between tissue and in vitro expansion. Biomedical Materials and Engineering, 22:243-254, 2012.

Marigo, I, Dazzi, F. The immunomodulatory properties of mesenchymal stem cells. Seminars Immunopathology, 33, 593-602, 2011.

Mark P, Kleinsorge M, Gaebel R, Lux CA, Toelk A, Pittermann E, David R, Steinhoff G, Ma N. Human Mesenchymal Stem Cells Display Reduced Expression of CD105 after Culture in Serum-Free Medium. Stem Cells International 2013:698076, 2013.

Martin G R. Isolation of a pluripotent cell line from early mouse embryos cultured in medium conditioned by teratocarcinoma stem cells. Proceedings of the National Academy of Sciences, 78(12):7634-7638, 1981.

Martin-Rendon E, Sweeney D, Lu F, Girdlestone J, Navarrete C, Watt SM. 5-Azacytidine-treated human mesenchymal stem/progenitor cells derived from umbilical cord, cord blood and bone marrow do not

generate cardiomyocytes *in vitro* at high frequencies. Vox Sang, 95:137-48, 2008.

Mastri M, Lin H, Lee T. Enhancing the efficacy of mesenchymal stem cell therapy. World Journal of Stem Cells, 6:82-93, 2014.

Meisel R, Zibert A, Laryea M, Göbel U, Däubener W, Dilloo D. Human bone marrow stromal cells inhibit allogeneic T-cell responses by indoleamine 2,3-dioxygenase-mediated tryptophan degradation. Blood, 103:4619-4621, 2004.

Miki T, Strom, SC. Amnion-derived pluripotent/multipotent stem cells. Stem Cell Reviews, 2:133-142, 2006.

Mikkelsen TS, Hanna J, Zhang X, Ku M, Wernig M, Schorderet P, Bernstein BE, Jaenisch R, Lander ES, Meissner A. Dissecting direct reprogramming through integrative genomic analysis. Nature, 454:49-55, 2008.

Miller DW, Graulich W, Karges B, Stahl S, Ernst M, Ramaswamy A, Sedlacek HH, Muller R, Adamkiewicz J. Elevated expression of endoglin, a component of the TGF-betareceptor complex, correlates with proliferation of tumor endothelial cells. International Journal of Cancer, 81:568-572, 1999.

Mitchell KE, Weiss ML, Mitchell BM, Martin P, Davis D, Morales L, Helwig B, Beerenstrauch M, Abou-Easa K, Hildreth T, Troyer D, Medicetty S. Matrix cells from Wharton's jelly form neurons and glia. Stem Cells, 21:50-60, 2003.

Moodley Y, Atienza D, Manuelpillai U, Samuel CD, Tchongue J, Ilancheran S, Boyd R, Trounson A. Human umbilical cord mesenchymal stem cells reduce fibrosis of bleomycin-induced lung injury. American Journal of Pathology, 175:303-313, 2009.

Moore H. The medium is the message. Nature Biotechnology, 24:160-161, 2006.

Morigi M, Imberti B, Zoja C, Corna D, Tomasoni S, Abbate M, Rottoli D, Angioletti S, Benigni A, Perico N, Alison M, Remuzzi G. Mesenchymal stem cells are renotropic, helping to repair the kidney and improve function in acute renal failure. Journal of American Society of Nephrology, 15:1794-1804, 2004.

Musina RA, Bekchanova ES, Belyavskii AV, Grinenko TS, Sukhikh GT. Umbilical cord blood mesenchymal stem cells. Bulletin of Experimental Biology and Medicine, 143:127-131, 2007.

Nagamura-Inoue T, He H. Umbilical cord-derived mesenchymal stem cells: Their advantages and potential clinical utility. World Journal of Stem Cells, 6:195-202, 2014.

Nakagawa M, Koyanagi M, Tanabe K, Takahashi K, Ichisaka T, Aoi T, Okita K, Mochiduki Y, Takizawa N, Yamanaka S. Generation of induced pluripotent stem cells without Myc from mouse and human fibroblasts. Nature Biotechnology, 26:101-106, 2008.

Nasef A, Chapel A, Mazurier C, Bouchet S, Lopez M, Mathieu N, Sensebe L, Zhang Y, Gorin N C, Thierry D, Fouillard L. Identification of IL-10 and TGF-beta transcripts involved in the inhibition of T-lymphocyte proliferation during cell contact with human mesenchymal stem cells, Gene Expression, 13:217-226, 2007.

Nekanti U, Dastidar S, Venugopal P, Totey S, Ta M. Increased Proliferation and Analysis of Differential Gene Expression in Human Wharton's Jelly-derived Mesenchymal Stromal Cells under Hypoxia. International Journal of Biology Sciences, 6:499-512, 2010.

Nemajerova A, Kim SW, Petrenko O, Moll UM. Two-factor reprogramming of somatic cells to pluripotent stem cells reveals partial functional redundancy of Sox2 and Klf4. Cell Death and Differentiation, 19:1268–1276, 2012.

Nesselmann C, Kaminski A, Steinhoff G. Cardiac stem cell therapy. Registered trials and a pilot study in patients with dilated cardiomyopathy. Herz, 36,2:121-134, 2011.

Ng J, Hynes K, White G, Sivanathan KN, Vandyke K, Bartold PM, Gronthos S. Immunomodulatory Properties of Induced Pluripotent Stem Cell-Derived Mesenchymal Cells. Journal of Cell Biochemistry, 117:2844-2853, 2016.

Ode A, Kurtz A, Schmidt-Bleek K, Schrade P, Kolar P, Buttgereit F, Lehmann K, Hutmacher DW, Duda, GN, Kasper G. CD73 and CD29 concurrently mediate the mechanically induced decrease of migratory capacity of mesenchymal stromal cells. European Cells and Materials, 22:26-42, 2011.

O'Donoghue K, Fisk NM. Fetal Stem Cells. Best Practical Research Clinical Obstetric Gynaecology, 18:853-875, 2004.

Oh EJ, Lee H W, Kalimuthu S, Kim T J, Baek S H, Zhu L, Oh J M, Son S H, Chung H Y, Ahn B C. In vivo migration of mesenchymal stem cells to burn injury sites and their therapeutic effects in a living mouse model. Journal of Controlled Release: Official Journal of the Controlled Release Society, 279:79-88, 2018.

Okita K, Ichisaka T, Yamanaka S. Generation of germline-competent induced pluripotent stem cells. Nature, 448:313-317, 2007.

Okita K, Matsumura Y, Sato Y, Okada A, Morizane A, Okamoto S, Hong H, Nakagawa M, Tanabe K, Tezuka K, Shibata T, Kunisada T, Takahashi M, Takahashi J, Saji H, Yamanaka S. A more efficient method to generate integration-free human iPS cells. Nat Methods 8:409-412, 2011.

Olivier EN, Rybicki AC, Bouhassira EE. Differentiation of Human Embryonic Stem Cells into Bipotent Mesenchymal Stem Cells. Stem Cells, 24:1914-1922, 2006.

Orth P, Rey-Rico A, Venkatesan JK, Madry H, Cucchiarini M. Current perspectives in stem cell research for knee cartilage repair. Stem Cells and Cloning, 7:1-17, 2014.

Pasque V, Radzisheuskaya A, Gillich A, Halley-Stott R P, Panamarova M, Zernicka-Goetz M, Surani M A, Silva J C. Histone variant macroH2A marks embryonic differentiation in vivo and acts as an epigenetic barrier to induced pluripotency. Journal of Cell Science, 125:6094-6104, 2012.

Patel A, Riordan N. Allogeneic transplantation of human umbilical cord mesenchymal stem cells (UC-MSC) for a single male patient with duchenne muscular dystrophy (DMD). Cytotherapy, 17:S46, 2015.

Patrikoski M, Juntunen M, Boucher S, Campbell A, Vemuri MC, Mannerstrom B, Miettinen S. Development of fully defined xeno-free culture system for the preparation and propagation of cell therapy-compliant human adipose stem cells. Stem Cell Research & Therapy, 4:27, 2013.

Peng K Y, Lee Y W, Hsu P J, Wang H H, Wang Y, Liou J Y, Hsu S H, Wu K K, Yen B L. Human pluripotent stem cell (PSC)-derived mesenchymal stem cells (MSCs) show potent neurogenic capacity which is enhanced with cytoskeletal rearrangement. Oncotarget, 7:43949-43959, 2016.

Pereira WC, Khushnooma I, Madkaikar M, Ghosh K. Reproducible methodology for the isolation of mesenchymal stem cells from human umbilical cord and its potential for cardiomyocyte generation. Journl Tissue Engineering Regenerative Medicine, 2:394-399, 2008.Petrova A, Celli A, Jacquet L, Dafou D, Crumrine D, Hupe M, Arno M, Hobbs C, Cvoro A, Karagiannis P, Devito L, Sun R, Adame LC, Vaughan R, McGrath JA, Mauro TM, Ilic D. 3D In Vitro Model of a Functional Epidermal Permeability Barrier from Human Embryonic Stem Cells and Induced Pluripotent Stem Cells. Stem Cells Report, 2:675-689, 2014.

Phinney DG. Functional heterogeneity of mesenchymal stem cells: Implications for cell therapy. Journal of Cellular Biochemistry, 113:2806-2812, 2012.

Pike AF, Kramer NI, Blaauboer BJ, Seinen W, Brands R. A novel hypothesis for an alkaline phosphatase 'rescue' mechanism in the hepatic acute phase immune response. Biochimica et Biophysica Acta, 1832: 2044–2056, 2013.

Pikuła M, Marek-Trzonkowska N, Wardowska A, Renkielska A, Trzonkowski P. Adipose tissue-derived stem cells in clinical applications. Expert Opinion on Biological Therapy, 13(10):1357–1370, 2013.

Pittenger MF, Mackay AM, Beck SC, Jaiswal RK, Douglas R, Mosca JD, Moorman MA, Simonetti DW, Craig S, Marshak DR. Multilineage potential of adult human mesenchymal stem cells. *Science*, 284:143-147, 1999.

Poulsom R, Forbes SJ, Hodivala-Dilke K, Ryan E, Wyles S, Navaratnarasah S, Jeffery R, Hunt T, Alison M, Cook T, Pusey C, Wright NA. Bone marrow contributes to renal parenchymal turnover and regeneration. Journal of Pathology, 195:229-235, 2001.

Prasanna SJ, Gopalakrishnan D, Shankar S R, Vasandan AB. Pro-inflammatory cytokines, IFNgamma and TNFalpha, influence immune properties of human bone marrow and Wharton jelly mesenchymal stem cells differentially. Public Library of Science One, 5: e9016, 2010.

Prockop D J, Keating A. Relearning the lessons of genomic stability of human cells during expansion in culture: Implications for clinical research. Stem Cells, 30:1051-1052, 2012.

Prokhorova T A, Harkness L M, Frandsen U, Ditzel N, Burns J S, Schroeder H D, Kassem M. Teratoma formation by human embryonic stem cells is site-dependent and enhanced by the presence of Matrigel. Stem Cells and Development 18:47-54, 2009.

Przyborski, S A. Differentiation of human embryonic stem cells after transplantation in immune-deficient mice. Stem Cells, 23:1242-1250, 2005.

Puré E, Cuff CA. A crucial role for CD44 in inflammation. Trends in Molecular Medicine, 7:213-221, 2001.

Qin D, Gan Y, Shao K, Wang H, Li W, Wang T, He W, Xu J, Zhang Y, Kou Z, Zeng L, Sheng G, Esteban M A, Gao S, Pei, D. Mouse Meningiocytes Express Sox2 and Yield High Efficiency of Chimeras after Nuclear Reprogramming with Exogenous Factors. Journal of Biological Chemistry, 283:33730-33735, 2008.

Quante M, Tu S P, Tomita H, Gonda T, Wang S S, Takashi S, Baik G H, Shibata W, Diprete B, Betz K S, Friedman R, Varro A, Tycko B, Wang T C. Bone marrow-derived myofibroblasts contribute to the mesenchymal stem cell niche and promote tumor growth. Cancer Cell, 19:257-272, 2011.

Quirici N, Soligo D, Bossolasco P, Servida F, Lumini C, Deliliers GL. Isolation of bone marrow mesenchymal stem cells by anti-nerve growth factor receptor antibodies. Experimental Hematolology, 30:783-791, 2002.

Raposo G, Stoorvogel W. Extracellular vesicles: exosomes, microvesicles, and friends. Journal Cell Biology, 200:373–383, 2013.

Rauch C, Feifel E, Amann E-M, Spötl HP, Schennach H, Pfaller W, Gstraunthaler G. Alternatives to the use of fetal bovine serum: human platelet lysates as a serum substitute in cell culture media. ALTEX, 28:305-316, 2011.

Red-Horse K, Zhou Y, Genbacev O, Prakobphol A, Foulk R, Mc-Master M, Fisher S J. Trophoblast differentiation during embryo implantation and formation of the maternal-fetal interface. Journal of Clinical Investigation, 114:744-754, 2004.

Reinisch A, Bartmann C, Rohde E, Schallmoser KM, Bjelic-Radisic V, Lanzer G, Linkesch W, Strunk D. Humanized system to propagate cord blood-derived multipotent mesenchymal stromal cells for clinical application. Regenerative Medicine, 2:371-382, 2007.

Ren G, Zhang L, Zhao X, Xu G, Zhang Y, Roberts AI, Zhao R C, Shi Y. Mesenchymal stem cell-mediated immunosuppression occurs via concerted action of chemokines and nitric oxide. Cell Stem Cell, 2:141-150, 2008.

Reubinoff, B. Current status of human embryonic stem cell research. Ethics, Law and Moral Philosophy of Reproductive Biomedicine, 2:121-124, 2007.

Romanov YA, Svintsitskaya VA, Smirnov VN. Searching for alternative sources of postnatal human mesenchymal stem cells: candidate MSC- like cells from umbilical cord. Stem Cells, 21:105-110, 2003.

Ronquist S, Patterson G, Muir LA, Lindsly S, Chen H, Brown M, Wicha MS, Bloch A, Brockett R, Rajapakse I. Algorithm for cellular reprogramming. Proceedings of National Academy of Sciences of the United States of America, 114: 45, 2017.

Saad RS, Liu YL, Nathan G, Celebrezze J, Medich D, Silverman JF. Endoglin (CD105) and vascular endothelial growth factor as prognostic markers in colorectal cancer. Modern Pathology 17:197-203, 2004.

Sánchez L, Gutierrez-Aranda I, Ligero G, Rubio R, Munoz-Lopez M, Garcia-Perez J L, Ramos V, Real P J, Bueno C, Rodriguez R, Delgado M, Menendez P. Enrichment of human ESC-derived multipotent mesenchymal stem cells with immunosuppressive and anti-inflammatory properties capable to protect against experimental inflammatory bowel disease. Stem Cells, 29:251-262, 2011.

Sapaeth E L, Labaff A M, Toole B P, Klopp A, Andreeff M, Marini F C. Mesenchymal CD44 expression contributes to the acquisition of an activated fibroblast phenotype via TWIST activation in the tumor microenvironment. Cancer Research, 73:5345-5359, 2013.

Sarugaser R, Lickorish D, Baksh D, Hosseini M M, Davies J E. Human umbilical cord perivascular (HUCPV)

cells: a source of mesenchymal progenitors. Stem Cells, 23:220-229, 2005.

Shachar I, Karin N. The dual roles of inflammatory cytokines and chemokines in the regulation of autoimmune diseases and their clinical implications. Journal of Leukocyte Biology, 93:51-61, 2013.

Shahdadfar A, Tronsdal K, Haug T, Reinholt F P, Brinchmann JE. In vitro expansion of human mesenchymal stem cells: Choice of serum is a determinant of cell proliferation, differentiation, gene expression, and transcriptome stability. Stem Cells, 23:1357-1366, 2005.

Sharma R R, Pollock K, Hubel A, McKenna D. Mesenchymal stem or stromal cells: A review of clinical applications and manufacturing practices. Transfusion, 54:1418-1437, 2014.

Sica A, Mantovani A. Macrophage plasticity and polarization: in vivo veritas. Journal of Clinical Investigation, 122:787-795, 2012.

Siegel G, Kluba T, Hermanutz-Klein U, Bieback K, Northoff H, Schäfer R. Phenotype, donor age and gender affect function of human bone marrow-derived mesenchymal stromal cells. BMC Medicine, 11:146, 2013.

Sivanathan KN, Rojas-Canales DM, Hope CM, Krishnan R, Carroll RP, Gronthos S, Grey ST, Coates PT. Interleukin-17A-induced human mesenchymal stem cells are superior modulators of immunological function. Stem Cells, 33:2850-2863, 2015.

Sobiesiak M, Sivasubramaniyan K, Hermann C, Tan C, Orgel M, Tremi S, Cerabona F, de Zwart P, Ochs U, Muller CA, Gargett C E, Kallbacher H, Buhring HJ. The mesenchymal stem cell antigen MSCA-1 is identical to tissue non-specific alkaline phosphatase. Stem Cells and Development, 19: 669-677, 2010.

Solchaga LA, Penick KJ, Welter JF. Chondrogenic Differentiation of Bone Marrow-Derived Mesenchymal Stem Cells: Tips and Tricks. Methods of Molecular Biology, 698:253–278, 2011.

Song C, Li G. CXCR4 and matrix metalloproteinase-2 are involved in mesenchymal stromal cell homing and engraftment to tumors. Cytotherapy, 13:549-561, 2011.

Sotiropoulo PA, Perez SA, Salagianni M, Baxevanis CN, Papamichail M. Cell culture medium composition and translational adult bone marrow-derived stem cell research. Stem Cells, 24:2888-2890, 2006.

Spees JL, Lee RH, Gregory CA. Mechanisms of mesenchymal stem/stromal cell function. Stem Cell Research & Therapy. 7:(1)125, 2016.

Sridharan R, Gonzales-Cope M, Chronis C, Bonora G, McKee R, Huang C, Patel S, Lopez D, Mishra N, Pellegrini M, Carey M, Garcia BA, Plath K. Proteomic and genomic approaches reveal critical functions of H3K9

methylation and heterochromatin protein-1gamma in reprogramming to pluripotency. Nature Cell Biology, 15:872-882, 2013.

Struys T, Moreels M, Martens W, Donders R, Wolfs E, Lambrichts I. Ultrastructural and immunocytochemical analysis of multilineage differentiated human dental pulp and umbilical cord-derived mesenchymal stem cells. Cells Tissues Organs,193: 366-378, 2011.

Sudo K, Kanno M, Miharada K, Ogawa S, Hiroyama T, Saijo K, Nakamura Y. Mesenchymal progenitors able to differentiate into osteogenic, chondrogenic, and/or adipogenic cells in vitro are present in most primary fibroblast-like cell populations. Stem Cells, 25:1610-1617, 2007.

Sun N, Panetta NJ, Gupta DM, Wilson KD, Lee A, Jia F, Hu S, Cherry AM, Robbins RC, Longaker MT, Wu JC. Feeder-free derivation of induced pluripotent stem cells from adult human adipose stem cells. Proceedings of National Academy of Sciences of the United States of America, 106, 15720–15725, 2009.

Sun Q, Zhang Z, Sun Z. The potential and challenges of using stem cells for cardiovascular repair and regeneration. Genes & Diseases. 1:113-119, 2014.

Suto N, Mieda T, Iizuka A, Nakamura K, Hirai H. Morphological and functional attenuation of degeneration of peripheral neurons by mesenchymal stem cell-conditioned medium in spinocerebellar ataxia type 1-knock-in mice. CNS Neurosciences and Therapeutics. 22:670-676, 2016.

Swamynathan P, Venugopal P, Kannan S, Thej C, Kolkundar U, Bhagwat S, Ta M, Majumdar AS, Balasubramanian S. Are serum-free and xeno-free culture conditions ideal for large scale clinical grade expansion of Wharton's jelly derived mesenchymal stem cells? A comparative study. Stem Cell Research and Therapy, 5:88, 2014.

Taghizadeh RR, Cetrulo KJ, Cetrulo CL. Wharton’s jelly stem cells: future clinical applications. Placenta, 32:S311-S315, 2011.

Takahashi K. Cellular Reprogramming. Cold Spring Harbor Perspectives in Biology, 2014.

Temple S, Studer L. Lessons Learned from Pioneering Neural Stem Cell Studies. Stem Cell Reports, 8:191-193, 2017.

Thirumala S, Goebel WS, Woods EJ. Clinical grade adult stem cell banking. Organogenesis, 5:143-154, 2009.

Thomson J A, Itskovitz-Eldor J, Shapiro S S, Waknitz M A, Swiergiel J J, Marshall V S, Jones J M. Embryonic stem cell lines derived from human blastocysts. Science, 282:1145-1147, 1998.

Tisato V, Naresh K, Girdlestone J, Navarrete C, Dazzi F. Mesenchymal stem cells of cord blood origin are effective at preventing but not treating graft-versus-host disease. Leukaemia, 21:1992-1999, 2007.

Tkach M and Thery C. Communication by extracellular vesicles: where we are and where we need to go. Cell, 164:(6)1226–1232, 2016.

Toma J G, Akhavan M, Fernandes K J, Barnabé-Heider F, Sadikot A, Kaplan D R, Miller F D. Isolation of multipotent adult stem cells from the dermis of mammalian skin. Nature Cell Biology, 3:778-784, 2001.

Tong CK, Vellasamy S, Tan BC, Abdullah M, Vidyadaran S, Seow HF, Ramasamy R. Generation of mesenchymal stem cell from human umbilical cord tissue using a combination enzymatic and mechanical disassociation method. Cell Biology International, 35:221-226, 2011.

Trivanović D, Kocić J, Mojsilović S, Krstić A, Ilić V, Djordjević IO, Santibanez JF, Jovcić G, Terzić M, Bugarski D. Mesenchymal stem cells isolated from peripheral blood and umbilical cord Wharton's jelly. Serbian Archives of Medicine, 141:178-186, 2013.

Tsagias N, Koliakos I, Karagiannis V, Eleftheriadou M, Koliakos GG. Isolation of mesenchymal stem cells using the total length of umbilical cord for transplantation purposes. Transfusion Medicine, 21:253-261, 2011.

Tsai PC, Fu TW, Chen YM, Ko TL, Chen TH, Shih YH, Hung SC, Fu YS. The therapeutic potential of human umbilical mesenchymal stem cells from Wharton's jelly in the treatment of rat liver fibrosis. Liver Transplantation, 15:484-495, 2009.

Uccelli A, Laroni A, Freedman M S. Mesenchymal stem cells for the treatment of multiple sclerosis and other neurological diseases. Lancet Neurology, 10:649-656, 2011.

Uccelli A, Moretta L, Pistoia V. Mesenchymal stem cells in health and disease. Nature Reviews Immunology, 8:726-736, 2008.

Utikal J, Maherali N, Kulalert W, Hochedlinger K. Sox2 is dispensable for the reprogramming of melanocytes and melanoma cells into induced pluripotent stem cells. Journal of Cell Sciences. 122, 3502–3510, 2009.

Wagner W, Ho A D. Mesenchymal stem cell preparations - comparing apples and oranges. Stem Cell Reviews and Reports, 3:239-248, 2007.

Wagner W, Feldmann Jr RE, Seckinger A, Maurer MH, Wein F, Blake J, Krause U, Kalenka A, Burgers HF, Saffrich R, Wuchter P, Kuschinsky W, Ho AD. The heterogeneity of human mesenchymal stem cell preparations - evidence from simultaneous analysis of proteomes and transcriptomes. Experimental Hematology, 34:536-548, 2006.

Wang D, Feng X, Lu L. Konkel JE, Zhang H, Chen Z, Li X, Gao X, Lu L, Shi S, Chen W, Sun L. A CD8 T cell-IDO axis is required for mesenchymal stem cell suppression of human SLE. Arthritis Rheumatology, 66:2234-2245, 2014.

Wang D, Wang S, Huang S, Zhang Z, Yuan X, Feng X, Lu L, Sun L. Serum IFN-c Predicts the Therapeutic Effect of Mesenchymal Stem Cells Transplantation in Systemic Lupus Erythematosus Patients. Stem Cells Translational Medicine, 6:1777-1785, 2017.

Wang JJ, YE F, Chneg LJ, Shi YJ, Bao J, Sun HQ, Wang W, Zhang P, Bu H. Osteogenic differentiation of mesenchymal stem cells promoted by overexpression of connective tissue growth factor. Journal of Zhejiang University, 10(5):355-367, 2009.

Wang LT, Jiang SS, Ting CH, Hsu PJ, Chang CC, Sytwu HK, Liu KJ, Yen BL. Differentiation of MSCs From Human iPSCs Results in Downregulation of c-Myc & DNA Replication Pathways with Immunomodulation Toward CD4 & CD8 Cells. Stem Cells, 36:903-914, 2018.

Wang XY, Lan Y, He WY, Zhang L, Yao HY, Hou CM, Tong Y, Liu YL, Yang G, Liu XD, Yang X, Liu B, Mao N. Identification of mesenchymal stem cells in aorta-gonad-mesonephros and yolk sac of human embryos. Blood, 111:2436-2443, 2008.

Wang Y, Chen X, Cao W, Shi Y. Plasticity of mesenchymal stem cells in immunomodulation: pathological and therapeutic implications. Nature Immunology, 15:1009-1016, 2014.

Watson N, Divers R, Kedar R, Mehindru A, Mehindru A, Borlongan M C, Borlongan CV. Discarded Wharton jelly of the human umbilical cord: a viable source for mesenchymal stromal cells. Cytotherapy, 17:18-24, 2015.

Weiss M L, Anderson C, Medicetty S, Seshareddy KB, Weiss RJ, Werff IV, Troyer D, McIntosh KR. Immune properties of human umbilical cord Wharton's jelly-derived cells. Stem Cells, 26:2865–2874, 2008.

Weiss M L, Troyer DL. Stem Cells in the Umbilical Cord. Stem Cell Reviews, 2:155-162, 2006.

Weissman IL. Stem cells: units of development, units of regeneration, and units in evolution. Cell, 100:157-168, 2000.

Wernig M, Meissner A, Cassady J P, Jaenisch R. c-Myc is dispensable for direct reprogramming of mouse fibroblasts. Cell Stem Cell, 2:10-12, 2008.

Wernig M, Meissner A, Foreman R, Brambrink T, Ku M, Hochedlinger K, Bernstein BE, Jaenisch R. In vitro reprogramming of fibroblasts into a pluripotent ES-cell-like state. Nature, 448:318-324, 2007.

Wieczorek M, Abualrous ET, Sticht J, Álvaro-Benito M, Stolzenberg S, Noé F, Freund C. Major Histocompatibility Complex (MHC) Class I and MHC Class II Proteins: Conformational Plasticity in Antigen Presentation. Frontiers in Immunology, 8:292, 2017.

Wikstrom P, Lissbrant IF, Stattin P, Egevad L, Bergh A. Endoglin (CD105) is expressed on immature blood vessels and is a marker for survival in prostate cancer. Prostate, 51:268-275, 2002.

Wilmut I, Schnieke AE, McWhir J, Kind AJ, Campbell KH. Viable offspring derived from fetal and adult mammalian cells. Nature, 385: 810-813, 1997.

Wolbank S, van Griensven M, Grillari-Voglauer R, Peterbauer-Scherb A. Alternative sources of adult stem cells: human amniotic membrane. Advances in Biochemical Engineering Biotechnology, 123:1, 2010.

Wong S H, Hamel L, Chevalier S, Philip A. Endoglin expression on human microvascular endothelial cells association with betaglycan and formation of higher order complexes with TGF-beta signalling receptors. European Journal of Biochemistry, 267:5550-5560, 2000.

Wu P, Zhang B, Shi H, Qian H, Xu W. MSC-Exosome: A novel cell-free therapy for cutaneous regeneration. Cytotherapy, 20:291–301, 2018.

Xie HF, Ye M, Feng R, Graf T. Stepwise reprogramming of B cells into macrophages. Cell, 117:663-676, 2004.

Yang H, Xia Y, Lu SQ, Soong TW, Feng ZW. Basic fibroblast growth factor induced neuronal differentiation of mouse bone marrow stromal cells requires FGFR-1, MAPK/ERK, and transcription factor AP-1. Journal of Biological Chemistry, 283:5287-5295, 2008.

Yen BL, Chang CJ, Liu KJ, Chen YC, Hu HI, Bai CH, Yen ML. Brief Report—Human Embryonic Stem Cell-Derived Mesenchymal Progenitors Possess Strong Immunosuppressive Effects Toward Natural Killer Cells as Well as T Lymphocytes. Stem Cells, 27:451-456, 2009.

Yen BL, Huang HI, Chien CC, Jui HY, Ko BS, Yao M, Shun CT, Yen ML, Lee MC, Chen YC. Isolation of multipotent cells from human term placenta. Stem Cells, 23:3-9, 2005.

Yen ML, Hou CH, Peng KY, Tseng PC, Jiang SS, Shun CT, Chen YC, Kuo M L. Efficient derivation and concise gene expression profiling of human embryonic stem cell derived mesenchymal progenitors (EMPs). Cell Transplant, 20:1529-1545, 2011.

Yu J, Vodyanik MA, Smuga-Otto K, Antosiewicz-Bourget J, Frane J L, Tian S, Nie J, Jonsdottir GA, Ruotti V, Stewart R, Slukvin II, Thomson JA. Induced pluripotent stem cell lines derived from human somatic cells. Science, 318:1917-1920, 2007.

Zappia E, Casazza S, Pedemonte E, Benvenuto F, Bonanni I, Gerdoni E, Giunti D, Ceravolo A, Cazzanti F, Frassoni F, Mancardi G, Uccelli A. Mesenchymal stem cells ameliorate experimental autoimmune encephalomyelitis inducing T-cell anergy. Blood, 106:1755-1761, 2005.

Zhang J. “Fluorophores”. Flow Cytometry at Einstein. Albert Einstein College of Medicine (AECOM). n.d. http://www.einstein.yu.edu/research/facilities/facs/page. aspx?id=22637. Accessed: 08 Jan, 2014.

Zhang J, Lv S, Liu X, Song B, Shi L. Umbilical cord mesenchymal stem cell treatment for Crohn’s disease: a randomized controlled clinical trial. Gut and Liver 12:73-78, 2018.

Zhao Q, Gregory CA, Lee RH, Reger RL, Qin L, Hai B, Park MS, Yoon N, Clough B, McNeill E, Prockop DJ, Liu F. MSCs derived from iPSCs with a modified protocol are tumor-tropic but have much less potential to promote tumors than bone marrow MSCs. Proceedings of National Academy of Sciences of the United States of America, 112:530-535, 2015.

Zheng Y, Wang Y, Zhai Z, Zhai Q, Hu SY. Therapeutic effects of human umbilical cord mesenchymal stem cell transplantation on acute graft versus host disease. Chinese Journal of Contemporary Pediatrics, 17:869-872, 2015.

Zhou C, Yang B, Tian Y, Jiao H, Zheng W, Wang J, Guan F. Immunomodulatory effect of human umbilical cord Wharton’s jelly-derived mesenchymal stem cells on lymphocytes. Cellular Immunology, 272:33-38, 2011.

Zhu H, Mitsuhashi N, Klein A, Barsky L W, Weinberg K, Barr M L, Barsky L W, Demetriou A, Wu G D. The role of the hyaluronan receptor CD44 in mesenchymal stem cell migration in the extracellular matrix. Stem Cells, 24:928-935, 2006.

Zimmerlin L, Park TS, Zambidis ET, Donnenberg VS, Donnenberg AD. Mesenchymal stem cell secretome and regenerative therapy after cancer. Biochimie, 95:2235-2245, 2013.

8. PUBLISHED PAPERS

Since I joined Dr Ilic laboratory as a research technician and part-time PhD student, I co-authored 15 publications. Five of them were directly related to my PhD project, whereas for all others I contributed the data as a technician.

Publications directly related to my PhD thesis project:

(1) **Devito L**, Petrova A, Miere C, Codognotto S, Blakely N, Lovatt A, Ogilvie C, Khalaf Y, Ilic D. Cost-effective master cell bank validation of multiple clinical-grade human pluripotent stem cell lines from a single donor. Stem Cells Translational Medicine, 3:1116-1124, 2014.

Through this work I learned the principles of GMP cell culture and generated a research grade of hESC line KCL034 that I used as a positive control for numerous experiments in my thesis.

(2) Badraiq H, **Devito L**, Ilic D. Isolation and expansion of mesenchymal stromal/stem cells from umbilical cord under chemically defined conditions. Methods in Molecular Biology 1283:65-71, 2015.

In this method publication, we described isolation and expansion of MSC under chemically-defined xeno-free conditions (dXF medium). This is described in detail in the thesis (see Results, section 3.1).

(3) **Devito L**, Badraiq H, Galleu A, Taheem DK, Codognotto S, Siow R, Khalaf Y, Briley A, Shennan A, Poston L, McGrath J, Gentleman E, Dazzi F, Ilic D. Wharton's jelly mesenchymal stromal/stem cells derived under chemically defined animal product-free low oxygen conditions are rich in MSCA-1(+) subpopulation. Regenerative Medicine, 9:723-732, 2014.

At the beginning of the project, while I was comparing different culture conditions, I found that expression of MSCA-1 marker is markedly increased only under dXF conditions. This is described in detail in the thesis (see Results, sections 3.1 and 3.2).

(4) Miere C, **Devito L**, Ilic D. Sendai Virus-Based Reprogramming of Mesenchymal Stromal/Stem Cells from Umbilical Cord Wharton's Jelly into Induced Pluripotent Stem Cells. Methods in Molecular Biology, 1357:33-44, 2016.

In this method publication, we described SeV-mediated reprogramming of WJ MSC into iPSC. I used the same approach to reprogram nMSC12 and nMSC13 into iPSC12 and iPSC13, respectively. This is described in detail in the thesis (see Results, sections 3.5 and 3.6).

(5) Ilic D, **Devito L**, Miere C, Codognotto S. Human embryonic and induced pluripotent stem cells in clinical trials. British Medical Bulletin, 116:19-27, 2015.

A review paper describing clinical trials involving hESC and hiPSC. Some of the aspects were discussed in my thesis.

(6) Miere C, Hewitson H, **Devito L**, Wood V, Kadeva N, Cornwell G, Codognotto S, Stephenson E, Ilic D. Generation of KCL018 research grade human embryonic stem cell line carrying a mutation in the DMPK gene. Stem Cell Research 16:342-434, 2016.

(7) **Devito L**, Petrova A, Wood V, Kadeva N, Cornwell G, Codognotto S, Stephenson E, Ilic D. Generation of KCL033 clinical grade human embryonic stem cell line. Stem Cell Research, 16:296-299, 2016.

(8) **Devito L**, Jacquet L, Petrova A, Miere C, Wood V, Kadeva N, Cornwell G, Codognotto S, Stephenson E, Ilic D. Generation of KCL034 clinical grade human embryonic stem cell line. Stem Cell Research, 2016;16:184-288, 2016.

(9) **Devito L**, Wood V, Kadeva N, Cornwell G, Codognotto S, Stephenson E, Ilic D. Generation of KCL039 clinical grade human embryonic stem cell line. Stem Cell Research 16:170-217, 2016.

(10) Canham MA, Van Deusen A, Brison DR, De Sousa PA, Downie J, **Devito L**, Hewitt ZA, Ilic D, Kimber SJ, Moore HD, Murray H, Kunath T. The Molecular Karyotype of 25 Clinical-Grade Human Embryonic Stem Cell Lines. Scientific Reports, 5:17258, 2015.

As a technician, I participated in characterization of multiple hESC lines derived in our laboratory. The work involved the same experiments as I have done for characterization of mu iPSC12 and iPSC13 lines, which are described in detail in the thesis (see Results, section 3.7).

(11) Petrova A, Celli A, Jacquet L, Dafou D, Crumrine D, Hupe M, Arno M, Hobbs C, Cvoro A, Karagiannis P, **Devito L**, Sun R, Adame LC, Vaughan R, McGrath JA, Mauro TM, Ilic D. 3D In vitro model of a functional epidermal permeability barrier from human embryonic stem cells and induced pluripotent stem cells. Stem Cell Reports, 2:675-689, 2014.

(12) Petrova A, Capalbo A, Jacquet L, Hazelwood-Smith S, Dafou D, Hobbs C, Arno M, Farcomeni A, **Devito L**, Badraiq H, Simpson M, McGrath JA, Di WL, Cheng JB, Mauro TM, Ilic D. Induced Pluripotent Stem Cell Differentiation and Three-Dimensional Tissue Formation Attenuate Clonal Epigenetic Differences in Trichohyalin. Stem Cells Development, 25:1366-1375, 2016.

One of the ongoing projects in the lab is bioengineering of 3D model of epidermis using keratinocytes differentiated from hESC and iPSC lines. As the lab technician, I was involved in cell culture aspects of the project.

(13) Cvoro A, **Devito L**, Milton FA, Noli L, Zhang A, Filippi C, Sakai K, Suh JH, H Sieglaff D, Dhawan A, Sakai T, Ilic D, Webb P. A thyroid hormone receptor/KLF9 axis in human hepatocytes and pluripotent stem cells. Stem Cells 33:416-428, 2015.

This was a collaboration project with a group from Houston working on thyroid hormone signalling. Our group provided hESC/iPSC-related data. As the lab technician, I have performed cell culture, including T3-treatment time course, gene expression knock down using siRNA transfections, differentiation into endodermal progenitors as described in Cheng *et al.* (2012), and immunostaining.

(14) Shahbazi MN, Jedrusik A, Vuoristo S, Recher G, Hupalowska A, Bolton V, Fogarty NNM, Campbell A, **Devito L**, Ilic D, Khalaf Y, Niakan KK, Fishel S, Zernicka-Goetz M. Self-organization of the human embryo in the absence of maternal tissues. Nature Cell Biology, 18:700-708, 2016.

(15) Shahbazi MN, Scialdone A, Skorupska N, Weberling A, Recher G, Zhu M, Jedrusik A, **Devito L**, Noli L, Macaulay IC, Buecker C, Khalaf Y, Ilic D, Voet T, Marioni JC, Zernicka-Goetz M. Pluripotent state transitions coordinate morphogenesis in mouse and human embryos. Nature 552:239-243, 2017.

These two publications are coming from ongoing collaboration with a group from Cambridge working on the earliest stages of human development. Since I am trained embryologist, one of my duties as a technician is to take care of supranumerary embryos donated for research. For this collaboration, I was thawing the embryos the embryos used in the experiments in Guy's Assisted Conception Unit and assuring that the documentation is up to HFEA standards.

STEM CELLS TRANSLATIONAL MEDICINE®

EMBRYONIC STEM CELLS/INDUCED PLURIPOTENT STEM (iPS) CELLS

Cost-Effective Master Cell Bank Validation of Multiple Clinical-Grade Human Pluripotent Stem Cell Lines From a Single Donor

LIANI DEVITO,[a,*] ANASTASIA PETROVA,[a,*] CRISTIAN MIERE,[a,*] STEFANO CODOGNOTTO,[a,b] NICOLA BLAKELY,[c] ARCHIE LOVATT,[c] CAROLINE OGILVIE,[d] YACOUB KHALAF,[a,e] DUSKO ILIC[a]

Key Words. Clinical-grade human embryonic stem cell lines • Clinical-grade iPS cell lines • Current good manufacturing practice • Validation • Master cell bank • Human viral pathogens

ABSTRACT

Standardization guidelines for human pluripotent stem cells are still very broadly defined, despite ongoing clinical trials in the U.S., U.K., and Japan. The requirements for validation of human embryonic (hESCs) and induced pluripotent stem cells (iPSCs) in general follow the regulations for other clinically compliant biologics already in place but without addressing key differences between cell types or final products. In order to realize the full potential of stem cell therapy, validation criteria, methodology, and, most importantly, strategy, should address the shortfalls and efficiency of current approaches; without this, hESC- and, especially, iPSC-based therapy will not be able to compete with other technologies in a cost-efficient way. We addressed the protocols for testing cell lines for human viral pathogens and propose a novel strategy that would significantly reduce costs. It is highly unlikely that the multiple cell lines derived in parallel from a tissue sample taken from one donor would have different profiles of endogenous viral pathogens; we therefore argue that samples from the Master Cell Banks of sibling lines could be safely pooled for validation. We illustrate this approach with tiered validation of two sibling clinical-grade hESC lines, KCL033 and KCL034 (stage 1, sterility; stage 2, specific human pathogens; and stage 3, nonspecific human pathogens). The results of all tests were negative. This cost-effective strategy could also be applied for validation of Master Cell Banks of multiple clinical-grade iPSC lines derived from a single donor. STEM CELLS TRANSLATIONAL MEDICINE *2014;3:1116–1124*

[a]Division of Women's Health, Women's Health Academic Centre, King's College London, London, United Kingdom; [b]St8Biologics, QA Consultancy, London, United Kingdom; [c]SGS Vitrology Ltd., Glasgow, United Kingdom; [d]Guy's & St. Thomas' Centre for Preimplantation Genetic Diagnosis and Genetics Centre and [e]Assisted Conception Unit, Guy's & St. Thomas' National Health Services Foundation Trust, London, United Kingdom

[*]Contributed equally.

Correspondence: Dusko Ilic, M.D., Ph.D., Assisted Conception Unit, Guy's Hospital, 11th Floor, Tower Wing, London SE1 9RT, United Kingdom. Telephone: 44-20-7188-0547; E-Mail: dusko.ilic@kcl.ac.uk

Received January 21, 2014; accepted for publication July 7, 2014; first published online in SCTM *EXPRESS* August 13, 2014.

1066-5099/2014/$20.00/0

http://dx.doi.org/10.5966/sctm.2014-0015

INTRODUCTION

Optimism that human embryonic stem cells (hESCs) would provide a virtually unlimited source of selected cell types for future cell therapies and drug screening and development has resulted in considerable progress in stem cell biology since the first hESCs were derived in 1998 [1]. The initial difficulties in obtaining embryos for stem cell research has largely been overcome, especially in the U.K., where a regulatory route map to facilitate clinical research application has been produced relatively quickly [2, 3]. By the end of 2009, more than 1,000 hESC lines had been derived worldwide; however, only a few had been thoroughly characterized [4, 5]. With the discovery of induced pluripotent stem cells (iPSCs) in 2006 [6], interest in hESCs started to wane.

An Investigational New Drug application for the first clinical trial of hESC-based therapy received initial Food and Drug Administration clearance in January 2009. The company, Geron Corp. (Menlo Park, CA, http://www.geron.com), generated a Master Bank from hESC line H1, which was derived as a research grade line in the presence of animal products [1]. The inner cell mass was isolated by immunosurgery with a rabbit antiserum and plated on mitotically inactivated mouse embryonic fibroblasts in a medium supplemented with 20% fetal bovine serum. The Master Bank used for production of hESC-derived oligodendrocyte progenitors GRNOPC1 had to be "re-derived" under current good manufacturing practice (cGMP) conditions and subjected to validation, not only for the presence of human viral pathogens but also for the presence of animal pathogens, significantly increasing the costs.

Similarly, the hESC line MA-09 used in clinical trials for Stargardt's macular dystrophy and age-related macular degeneration was also derived as a research grade line in the presence of animal components [7, 8] and had to undergo a similar process and costly validation for the presence of animal pathogens to be used for cellular therapy.

The first clinical-grade hESC lines were derived at a cGMP facility in Brisbane, Australia, from frozen embryos donated at Sydney IVF Ltd., under sponsorship of the Singapore-based

company ES Cell International Pte. Ltd. (ESI Bio, BioTime, Inc., Alameda, CA, http://www.biotimeinc.com) [9]. To promote the lines, the company was willing to make them easily accessible in a research grade version through the A*STAR Singapore Stem Cell Consortium (SSCC). The intention was that the Stem Cell Bank within the SSCC would expand and distribute the cells under non-cGMP conditions for minimal reimbursement. Despite international efforts and multimillion investments, they did not gain the popularity of the H1 and H9 hESC lines derived by Thomson et al. [1] and the cells were never used in clinical trials. In May 2010, the California-based BioTime acquired ESI, including a bank of six clinical-grade hESC lines. Five of them the company characterized further [10]. BioTime has also recently acquired Geron's hESC portfolio; there might, therefore, be long-term plans for using these cell lines in the clinic.

In the U.K., the Medical Research Council systematically invested in derivation of clinical-grade hESC lines in five centers across the country. Currently, more than 30 such lines have been derived. At King's College London, in our purpose-built cGMP laboratory, we derived, under animal product-free conditions [11–14], eight clinical-grade lines: KCL031–KCL034 and KCL037–KCL040. All eight clinical-grade lines will be available through the U.K. Stem Cell Bank, which will conduct further validation of these lines before releasing them. The lines are also under consideration for placement on the NIH hESC registry [15], which will make them eligible for use in NIH-supported research.

In the next step, following cGMP, we adapted four clinical-grade hESC lines, KCL033, KCL034, KCL037, and KCL040, to feeder-free conditions using methods described previously [12]. However, owing to the high costs of running a cGMP facility and Master Cell Bank validation, we were not able to proceed with all the lines. Of the four lines, KCL040 and KCL037 had haplotypes that matched ~0.016% and ~0.019% of the population, respectively, and were therefore potentially more clinically useful than the other two, which only matched ~0.004% [13]. However, the lines KCL033 and KCL034 were sibling lines, meaning that they were derived from embryos donated by the same couple. In addition, these embryos had been generated and cryopreserved as supernumerary in a single in vitro fertilization (IVF) cycle. Furthermore, the embryos had been thawed at the same time, and the lines were generated in parallel under the same conditions using the same reagents. The embryos were thus coming from a single source and were undergoing all procedures in parallel until initial stock cryopreservation. We, therefore, reasoned that if one line had been positive for any human pathogens, it was highly unlikely that the other line would have a different status. Testing of only one cell line should therefore theoretically be sufficient to exclude or confirm the presence of pathogens in all sibling lines; however, regulations require that all lines should be tested. We therefore considered the strategy of pooling samples from such Master Cell Banks, thereby reducing costs without compromising the detection of human viral pathogens.

Hence, KCL033 and KCL034 were taken further, and Master Cell Banks were generated and validated in vitro for the presence of human viral pathogens. All validation studies were conducted by SGS Vitrology (Glasgow, U.K., http://www.sgs.com), in compliance with the principles of GMP as set out in Directive 2003/94/EC for medicinal products for human use [16] and 91/412/EEC for veterinary medicinal products [17]. In the present study, we describe the strategy, methodology, and outcomes of these in vitro validation studies.

Materials and Methods

Human Samples

The present work was ethically approved (U.K. National Health Service Research Ethics Committee Reference: 06/Q0702/90). The experiments were performed under licenses from the U.K. Human Fertilization and Embryology Authority (license no. R0133) and the U.K. Human Tissue Authority (license no. 22621).

Cell Culture

The methods have been previously described in detail [11–14].

Sterility Testing

Five vials each of KCL033 and KCL034 from the respective Master Cell Banks were pooled and tested for sterility. The presence of microorganisms was assessed after 14 days of incubation at the appropriate temperature. Tryptone soya broth (TSB) was used for the growth of aerobic bacteria and fungi at 20°C–25°C. Fluid thioglycolate (THIO) medium was used for the growth of both anaerobic and aerobic bacteria at 30°C–35°C.

The experiment controls were as follows. Uninoculated TSB and THIO in duplicate served as the negative control (NC) and when inoculated with 1 ml of sterile demineralized water served as the operator/assay technique control. TSB inoculated with 10–100 colony forming units of *Bacillus subtilis*, *Aspergillus brasiliensis*, and *Candida albicans* and THIO inoculated with *Clostridium sporogenes*, *Pseudomonas aeruginosa*, and *Staphylococcus aureus* served as the positive controls (PCs). Environmental monitoring was performed in the sample isolator (settle plates) and before and after manipulation (contact plates).

Sterility testing was performed in accordance with the current requirements of the European Pharmacopoeia, Section 2.6.1 Sterility, U.S. Pharmacopeia <71> Sterility Tests, and International Conference on Harmonisation Topic Q5D guidelines.

Mycoplasma Testing

One vial each of KCL033 and KCL034 from the respective Master Cell Banks were pooled and increased to 5 ml volume by adding sterile Dulbecco's modified Eagle's medium. The pooled sample was sonicated on ice for 2 minutes, increased to a final volume of 15 ml, and tested for *Mycoplasma* without additional treatment.

Vero indicator cell cultures were inoculated with the test material and cultured for 3 days. Then, the cells were mechanically transferred into the chamber slide and cultured for an additional 3 days. At day 6, the cells were stained with DNA-binding Hoechst 33258 fluorescent dye for *Mycoplasma* detection.

Test material was also inoculated into broth known to have nutritive properties for *Mycoplasma* species and either cultured further in broth or plated on agar plates, which were then observed microscopically for typical *Mycoplasma* colony morphology.

Mycoplasma testing was performed in accordance with the current requirements of the European Pharmacopoeia, Section 2.6.7, Mycoplasmas.

Fluorescent-Product Enhanced Reverse Transcriptase Assay for Retroviral Activity

Spent medium from the KCL033 and KCL034 cultures, 8.7 ml each, was pooled and centrifuged at 11,000*g* for 10 minutes at 4°C.

Then, the supernatant was filtered through a 0.45-μm filter. The sample was spiked with 3.0×10^4 retroviral particles (amphotropic murine leukemia virus [A-MLV]) per milliliter, and retroviral particles were purified by ultracentrifugation at 100,000*g* for a minimum of 60 minutes at 4°C. To release reverse transcriptase (RT) activity from the retroviral particles, the pellets were resuspended in disruption buffer. Recovery of retroviral particles in the absence of the test sample was assessed by ultracentrifugation of the same number of A-MLV in culture medium. Aliquots (5 μl) of processed test sample and retrovirus particle recovery control were added to the RT reaction mix containing all reagents necessary for reverse transcription (dNTP, $MgCl_2$, reverse primer, RNase inhibitor) and Brome mosaic virus RNA as a template. The mix also contained activated calf thymus (aCT) DNA to reduce false-positive signals arising from DNA polymerases. To assess the level of DNA polymerase activity, the sample was also analyzed in the absence of aCT DNA. Synthesized cDNA was subsequently amplified using TaqMan (Life Technologies, Carlsbad, CA, http://www.lifetechnologies.com) real-time polymerase chain reaction (PCR). The data were collected and analyzed using an Applied BioSystems 7900HT Fast Real Time PCR System (Applied BioSystems, Foster City, CA, http://www.appliedbiosystems.com). The negative controls included PCR no-template control (PNTC), NC, and medium only control. The positive controls included PC and spike positive control (SPC). SPC consisted of retroviral particles at or near the limit of detection spiked into the test sample before processing. The cycling parameters were as follows: for reverse transcription: 30 minutes at 37°C (reverse transcription) and 5 minutes at 95°C (reverse transcription inactivation), and 5 minutes at 25°C (reaction cooling); for c-DNA PCR: 2 minutes at 50°C (uracil-DNA glycosylase [UNG] activation) and 10 minutes at 95°C (AmpliTaq Gold activation; Life Technologies), followed by 40 cycles of 15 seconds at 95°C (denaturation) and 1 minute at 60°C (annealing/extension).

The methods used were compliant with the current edition of the European Pharmacopoeia, 2.6.21, Nucleic Acid Amplification Techniques.

Real-Time PCR

For detection of the enteroviruses, hepatitis A virus (HAV), and hepatitis C virus (HCV), RNA was extracted using RNA easy kit (Qiagen, Venlo, The Netherlands, http://www.qiagen.com) from 3.0×10^6 cells in 200 μl of phosphate-buffered saline (PBS) per column. Eluted RNA from multiple columns was pooled together. During the RNA extraction procedure, the sample was spiked with cucumber mosaic virus (CrMV) interference control RNA from an unrelated species. From the pooled RNA, 3 μl (67 ng/μl) was used per replicate in testing for pathogens in real-time PCR assays. This is equivalent to approximately 1.2×10^5 cells per reaction assuming 100% recovery from the extraction process.

For detection of sexually transmitted disease (STD) pathogens and all other viruses, DNA was extracted using the QIAamp DNA mini-kit (Qiagen) from either 3.0×10^6 cells (for detection of viruses) or 3.6×10^6 cells (for bacterial pathogen detection) in 200 μl of PBS per column. Eluted DNA from multiple columns was pooled together. During the DNA extraction procedure, the sample was spiked with CrMV interference control DNA from an unrelated species. From the pooled DNA, 3 μl (280 ng/μl for viruses, 238.3 ng/μl for STD pathogens) was used per replicate in testing for pathogens in real-time PCR assays. This is equivalent to approximately 1.2×10^5 cells for viruses and 1.0×10^5 cells for STD pathogens.

Extracted nucleic acids were tested in real-time PCRs containing either CrMV interference control specific primers and probe or pathogen target specific primers and probe. The accumulation of the PCR products was monitored and data collected using an Applied Biosystems 7900HT Fast Real Time PCR System. Real-time PCR controls included PNTC, NC, PC, postspike control, exogenous internal positive control, extraction no-template control, and extraction recovery and contamination control. The cycling parameters were as follows.

For the HAV, HCV, and enteroviruses, we used initial steps of 10 minutes at 50°C (reverse transcription) and 10 minutes at 95°C (reverse transcription inactivation), followed by 40 cycles of 15 seconds at 95°C (denaturation) and 1 minute at 60°C (annealing/extension).

For HIV-1, HIV-2, human T-lymphotropic virus (HTLV) type 1 and 2, hepatitis B virus (HBV), human herpesvirus (HHV)-6, HHV-7, HHV-8, human cytomegalovirus (hCMV), Epstein-Barr virus (EBV; also known as HHV-4), B19 virus, Simian virus 40, human polyomavirus JC, human polyomavirus BK, and *Treponema pallidum*, we used 2 minutes at 50°C (UNG activation) and 10 minutes at 95°C (AmpliTaq Gold activation), followed by 40 cycles of 15 seconds at 95°C (denaturation) and 1 minute at 60°C (annealing/extension). For *Chlamydia* species and *Neisseria gonorrhoeae,* the number of cycles was increased to 50.

The methods used were compliant with the current edition of the European Pharmacopoeia, 2.6.21, Nucleic Acid Amplification Techniques.

In Vitro Assay for Detection of Virus Contaminants Using Indicator Cell Lines

The cell lines used in this assay were normal human fetal lung fibroblasts MRC-5, African green monkey *Cercopithecus aethiops* kidney Vero C1008 (Vero 76, clone E6, Vero E6), and human cervical carcinoma HeLa. The control viruses used in the assay were herpes simplex virus type 1, human adenovirus type 5, and influenza A virus.

KCL033 and KCL034 in frozen culture medium (2×10^6 cells per milliliter) were thawed, pooled together, and centrifuged at low speed. The supernatant (SN) was removed and saved, and the pellet was resuspended in a small volume of SN and subjected to two cycles of freezing and thawing to facilitate release of cell-associated viral particles. Following low-speed centrifugation, the SN was removed and pooled with the original SN. The pooled SN was diluted with appropriate maintenance medium at a ratio of 1:4 and used for inoculation of the indicator cell lines. Subconfluent monolayers of indicator cell lines in T80 flasks were inoculated with the test item or with relevant controls in duplicate (2.5 ml inoculum per flask). MRC-5 cultures were fed on days 7, 14, and 21, VeroC1008 on day 14, and HeLa on days 11, 18, and 25 after inoculation. The HeLa cells were also subcultured on days 7, 14, and 21. The cultures were monitored for 28 days for cell health and evidence of a virus-induced cytopathic effect (CPE). On day 28 after inoculation, the test item cultures and relevant controls were tested for hemadsorption with guinea pig erythrocytes, one half at 2°C–8°C and the other half at 20°C–25°C.

Transmission Electron Microscopy

Cell pellets containing 1×10^7 cells fixed in glutaraldehyde solution were postfixed in OsO_4, stained en bloc in uranyl acetate,

dehydrated in an ethanol series and propylene oxide before being infiltrated to Araldite resin (Huntsman Corp., Salt Lake City, UT, http://www.huntsman.com), and polymerized. Semithin sections (1 μm) were mounted on glass slides, stained with toluidine blue, and examined by light microscopy for general quality of fixation, gross cell morphology, and the presence of mitotic, dead, or dying cells. Ultrathin sections (0.1 μm) were mounted on electron microscope grids and stained with uranyl acetate and lead citrate solutions. A minimum of 100 median cell profiles of the tested cell culture were examined for the presence of viruses, virus-like particles, and other extraneous agents.

RESULTS

Stage 1: Sterility and *Mycoplasma* Testing

Validation of the Master Cell Banks was divided into three stages. In order to proceed to the next stage, the samples had to pass each validation test.

The first stage was to test for any contamination that might have arisen from our handling, despite the continuous monitoring during sample processing in our cGMP-compliant facility. Pooled samples from the KCL033 and KCL034 Master Cell Banks were therefore tested first for sterility, to detect the presence of bacteria, fungi, and *Mycoplasma* species and to ensure that no inhibitory materials were present that would mask the detection of pathogens.

The growth of bacteria or fungi was not detected in the test article after 14 days of incubation. Spiking the test material with either bacteria or fungi resulted in growth at a similar rate as the positive control, indicating that no inhibitory factors were present in the tested sample (Table 1).

Mycoplasma validation was performed in the indicator cell line and liquid (broth) and solid (agar) media known to have nutritive properties for *Mycoplasma* species. Growth was not detected, and no inhibitory factors were present in the tested sample (Table 2A–2C).

Table 1. Sterility testing

Sample	Growth medium	Inoculum	Result
NC			
	TSB	None	No growth detected
	THIO	None	No growth detected
OATC			
	TSB	Water	No growth detected
	THIO	Water	No growth detected
PC			
	TSB	*Bacillus subtilis*	Positive after 3 days
		Aspergillus brasiliensis	Positive after 3 days
		Candida albicans	Positive after 3 days
	THIO	*Clostriduim sporogenes*	Positive after 3 days
		Pseudomonas aeruginosa	Positive after 3 days
		Staphylococcus aureus	Positive after 3 days
KCL033 and KCL034	TSB	None	No growth detected
	THIO	None	No growth detected
Spiked KCL033 and KCL034	TSB	*Bacillus subtilis*	Positive after 3 days
		Aspergillus brasiliensis	Positive after 3 days
		Candida albicans	Positive after 3 days
	THIO	*Clostriduim sporogenes*	Positive after 3 days
		Pseudomonas aeruginosa	Positive after 3 days
		Staphylococcus aureus	Positive after 3 days

Abbreviations: NC, negative control; OATC, operator/assay technique control; PC, positive control; THIO, thioglycollate; TSB, tryptone soya broth.

Stage 2: Detection of Specific Human Pathogens

Having confirmed in stage 1 that our handling did not introduce exogenous pathogens, in the second stage, we tested for the presence of human viral pathogens that might have been inherited from the donor tissue. Two different types of assay were performed: fluorescent-product enhanced reverse transcriptase (F-PERT) for detection of reverse transcriptase, which would indicate retroviral activity, and a series of real-time PCRs for detection of various common human viruses, including *T. pallidum*, *Chlamydia* species, and *N. gonorrhoeae*.

Regulatory guidance recommends the use of reverse transcriptase activity packaged into extracellular retroviral particles as a marker for the potential presence of retroviral contamination. The assays are designed to detect conversion of RNA template to cDNA when retroviral reverse transcriptase is present in the test sample [18–21]. PERT assays are routinely required for cell banks or any product originating from mammalian and avian cell substrates manufactured in a process that does not contain endogenous retroviral activity. The F-PERT assay for KCL033 and KCL034 pooled sample was negative to a sensitivity of approximately 1,000 retroviral particles per reaction or 2,600 particles per milliliter of pooled sample (Table 3).

Screening of embryo donors for STDs, mandatory in the U.S. and most European Union (EU) countries, is not required in the U.K. However, because the U.K., as a member of the EU, follows the EU Tissue and Cells Directive [22–24], we validated our samples for the presence of STD pathogens, in addition to the list of specific human viral pathogens. Real-time PCR, commonly used to detect human viruses in biological materials [20, 21], confirmed that KCL033 and KCL034 were negative for all viruses tested and for *T. pallidum*, *Chlamydia* species, and *N. gonorrhoeae* (Table 4). Negative results were expected for some of the viruses included in the panel (i.e., HIV-1 and -2, HBV, HCV, HTLV-1 and -2, hCMV, EBV), either because the embryo donors were tested before IVF treatment, or because we had previously performed the

Table 2A. *Mycoplasma* testing: indicator cell cuture test

Indicator cells	Fluorescence		Result
	Nuclear	Extranuclear	
NC	Yes	Yes	Negative
KCL033 and KCL034			
Flask A	Yes	Yes	Negative
Flask B	Yes	Yes	Negative
OATC	Yes	Yes	Negative
PC			
Mycoplasma orale	Yes	Yes	Positive
Mycoplasma hyorhinis	Yes	Yes	Positive

Abbreviations: NC, negative control; OATC, operator/assay technique control; PC, positive control.

Table 2B. *Mycoplasma* testing: culture test in broth

Sample	Result
NC	Negative
KCL033 and KCL034	Negative
OATC	Negative
Spiked KCL033 and KCL034 (*Mycoplasma fermentans*)	Positive
PC (*M. fermentans*)	Positive

Abbreviations: NC, negative control; OATC, operator/assay technique control; PC, positive control.

Table 2C. *Mycoplasma* testing: culture test on agar

Sample	Results									
	Plate A					Plate B				
	Day of subculture									
	0	3	7	14	21	0	3	7	14	21
NC	N	N	N	N	N	N	N	N	N	N
KCL033 and KCL034	N	N	N	N	N	N	N	N	N	N
OATC	N	N	N	N	N	N	N	N	N	N
Spiked KCL033 and KCL034 (*Mycoplasma fermentans*)	P	P	P	P	P	P	P	P	P	P
PC (*M. fermentans*)	P	P	P	P	P	P	P	P	P	P

Abbreviations: N, negative (absence of *Mycoplasma*); NC, negative control; OATC, operator/assay technique control; P, positive (presence of *Mycoplasma*); PC, positive control.

test with a non-cGMP service provider at low cost to minimize unnecessary spending.

Stage 3: Detection of Nonspecific Viral and Other Adventitious Contaminants

The assays in stage 2 covered only specific types of human pathogens. In the third stage, we therefore performed two additional tests for the detection of nonspecific viral contaminants: the 28-day in vitro assay and transmission electron microscopy (TEM).

Table 3. F-PERT assay

F-PERT reaction	Result	Assay sensitivity per milliliter[a]
PNTC	−	NA
NC	−	NA
MOC	−	NA
KCL033/034 with aCT	−	2.6×10^3
KCL033/034 without aCT	++++	NA
KCL033/034 SPC	++++	NA
PC	++++	NA

C_T = undetermined after 40 cycles of PCR. $C_T = \leq 39.99$ after 40 cycles of PCR.

[a]Assay sensitivity per milliliter was based on testing 5 μl of KCL033 or KCL034 sample per replicate from the original sample resuspended in 100 μl of disruption buffer, after ultracentrifugation of 7.8 ml of the original sample.

Abbreviations: −, negative to the sensitivity of the assay (i.e., no amplification signals detected; assay sensitivity reported was based on the sample SPC that has amplified in a minimum of three of four replicates); +, potentially positive (amplification signals detected in three or more replicates); aCT, activated calf thymus; F-PERT, fluorescent-product enhanced reverse transcriptase; MOC, medium only control; NC, negative control; PC, positive control; PCR, polymerase chain reaction; PNTC, PCR no-template control; SPC, spike positive control.

The 28-day in vitro assay was designed to meet the general requirements of the tests for extraneous agents in cell culture as described in European Pharmacopoeia, chapters 5.2.3 ("Cell Substrates for Production of Vaccines for Human Use") and 2.6.16 ("Tests for Extraneous Agents in Viral Vaccines for Human Use"), with extension to 28 days to increase the sensitivity of the assay for slow growing viruses, as suggested by the Food and Drug Administration and later accepted by the World Health Organization. MRC-5, Vero C1008, and HeLa cell cultures were inoculated with the pooled samples from the KCL033 and KCL034 Master Cell Banks and monitored for 28 days. None of the cultures inoculated with the test material showed signs of a virus-induced cytopathic effect or hemadsorption with guinea-pig red blood cells. The KCL033 and KCL034 samples were therefore considered negative for the presence of cytopathic or hemadsorbing adventitious virus contaminants (Table 5A–5C).

Regulatory agencies recommend the use of TEM on harvested cells to ascertain the presence of viruses and adventitious agents. TEM can reveal the size, structure, and localization of viral, fungal, bacterial, or *Mycoplasma* contaminants in the sample. Obviously, for this test, KCL033 and KCL034 could not be pooled, because we would not be able to be sure how many cells from each cell line were analyzed in a mixed sample. We tested only KCL034 in the TEM assay and no viruses, virus-like particles, or extraneous agents, including *Mycoplasma*, yeast, fungi, or bacteria were detected in at least 100 random median cell profiles examined (Fig. 1).

We have not tested for extraneous agents that might be present without causing cytopathic or other apparent effects in the cell culture. Such tests are done in vivo, commonly involving embryonated eggs and suckling and adult mice; they generally cost >$12,000 per sample. Multiple cell lines derived in parallel from a tissue sample from a single donor could also be pooled for these tests, as described above for our two clinical-grade hESC lines.

Table 4. Real-time PCR detection of specific human pathogens

Nucleic acid	Pathogen/interference control	Cells/assay/line	DNA/RNA used in assay (ng)	Sensitivity of assay (copies per reaction)	Real-time PCR								
					PNTC	NC	ENTC	ERCC	PSC at DL	PSC >10× DL	PC at DL	PC >10× DL	KCL033 KCL034
DNA													
	CrMV				−	−	−	+++	NA	NA	+++	+++	+++
	Treponema pallidum	8×10^6	714.9	10	−	−	−	−	+++	+++	+++	+++	−
	Chlamydia	8×10^6	714.9	50	−	−	−	−	+++	+++	+++	+++	−
	Neisseria gonorrhoeae	8×10^6	714.9	25	−	−	−	−	+++	+++	+++	+++	−
	HIV-1	18×10^6	840	100	−	−	−	−	+++	+++	+++	+++	−
	HIV-2	18×10^6	840	100	−	−	−	−	+++	+++	+++	+++	−
	HTLV-1 and -2	18×10^6	840	1,000	−	−	−	−	+++	+++	+++	+++	−
	HBV	18×10^6	840	100	−	−	−	−	+++	+++	+++	+++	−
	HHV-6	18×10^6	840	100	−	−	−	−	+++	+++	+++	+++	−
	HHV-7	18×10^6	840	100	−	−	−	−	+++	+++	+++	+++	−
	HHV-8	18×10^6	840	100	−	−	−	−	+++	+++	+++	+++	−
	hCMV	18×10^6	840	100	−	−	−	−	+++	+++	+++	+++	−
	EBV (HHV-4)	18×10^6	840	100	−	−	−	−	+++	+++	+++	+++	−
	Human parvovirus B19	18×10^6	840	1,000	−	−	−	−	+++	+++	+++	+++	−
	SV40	18×10^6	840	100	−	−	−	−	+++	+++	+++	+++	−
	JCV	18×10^6	840	100	−	−	−	−	+++	+++	+++	+++	−
	BKV	18×10^6	840	1,000	−	−	−	−	+++	+++	+++	+++	−
RNA													
	CrMV				−	−	−	+++	NA	NA	+++	+++	+++
	Enterovirus	9×10^6	201	100	−	−	−	−	+++	+++	+++	+++	−
	HAV	9×10^6	201	500	−	−	−	−	+++	+++	+++	+++	−
	HCV	9×10^6	201	50	−	−	−	−	+++	+++	+++	+++	−

Note: 714.9 ng of DNA equals approximately 100,000 cells per reaction, and 840 ng of DNA equals approximately 120,000 cells per reaction (7 pg of DNA equals 1 genome equivalent); 201 ng of RNA equals approximately 150,000 cells per reaction.

Abbreviations: −, no amplification signals detected in all three replicates; +, amplification detected in one of three replicates tested; ++, amplification detected in two of three replicates tested; +++, amplification detected in three of three replicates tested; BKV, human polyomavirus BK; CrMV, cucumber mosaic virus; EBV, Epstein-Barr virus; HAV, hepatitis A virus; HBV, hepatitis B virus; hCMV, human cytomegalovirus; HCV, hepatitis C virus; HHV, human herpesvirus; HTLV, human T-lymphotropic virus; JCV, human polyomavirus JC; DL, predetermined detection limit; ENTC, extraction no-template control; ERCC, extraction recovery and contamination control; NA, not applicable; NC, negative control; PC, positive control; PCR, polymerase chain reaction; PNTC, PCR no-template control; PSC, postspike controls; SV40, simian virus 40;

Table 5A. Controls in the assay with indicator cell lines

Assay	Control	Cell lines			Inoculum
		MRC-5	Vero C1008	HeLa	
CPE					
	Negative control				Tissue culture medium
	Positive control		N/A		HSV-1[a]
		N/A		N/A	Ad5[a]
HAD					
	Negative control		N/A	N/A	Tissue culture medium
	Positive control		N/A	N/A	Inf A[a]

Negative and positive controls for CPE were inoculated on day 0, the same day as inoculation of the test sample; negative and positive controls for HAD were inoculated on day 14.
[a]One hundred median tissue culture infective dose units per flask.
Abbreviations: Ad5, adenovirus type 5; CPE, cytopathic effect; HAD, hemadsorption; HSV-1, herpes simplex virus 1; Inf A, influenza A virus; N/A, not applicable.

Table 5B. Virus-induced cytopathic effect assay results

Sample	Cell lines		
	MRC-5	Vero C1008	HeLa
Negative control	−/−	−/−	−/−
KCL033/KCL034	−/−	−/−	−/−
Positive control			
HSV-1	+/+	N/A	+ / +
Ad5	N/A	+/+	N/A

Abbreviations: −, negative result; +, positive result; −/− and +/+, individual results obtained for duplicate flasks tested; Ad5, adenovirus type 5; HSV-1, herpes simplex virus 1; N/A, not applicable.

Table 5C. HAD assay results

Sample	HAD assay conditions	
	2°C–8°C	20°C–25°C
	gp	
HAD negative (MRC-5 T80 flask)	−	−
HAD positive (Inf A 100 $TCID_{50}$ MRC-5 T80 flask)	+	+
MRC-5		
Negative control	−	−
KCL033/KCL034	−	−
Vero C1008		
Negative control	−	−
KCL033/KCL034	−	−
HeLa		
Negative control	−	−
KCL033/KCL034	−	−

Abbreviations: −, negative result; +, positive result; gp, guinea pig erythrocytes; HAD, hemadsorption; Inf A, influenza A virus; $TCID_{50}$, median tissue culture infective dose.

Discussion

Once human pluripotent stem cell (hPSC) therapy is approved and available, it will have to compete with other technologies over a range of criteria, including costs. Even if the technology is at least as beneficial as established alternatives, the high production costs could become a major obstacle in successful dissemination of the therapy and return of investments for developers and investors. Nevertheless, it is essential for hPSC-based therapy that quality control should be very rigorous for each step, from isolation of the stem cells through to the final differentiated product.

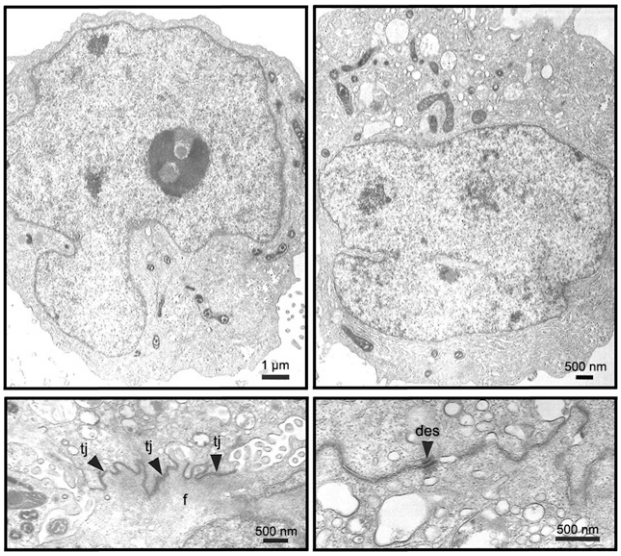

Figure 1. Typical KCL034 transmission electron microscopy cell profiles. The cells were generally adherent, with intercellular connections and a normal range of organelles and nuclei, with sparse heterochromatin and prominent nucleoli. Abbreviations: des, desmosome; f, fibrils; tj, tight junction.

In order to decrease the costs of quality control while maintaining rigorous monitoring, we considered the possibility of mixing multiple lines derived in parallel from tissue of a single donor, before testing for the presence of various human viruses and other adventitious agents. The risks associated with this approach seem very low, because (a) the tissue has been processed under identical environmental conditions, exposed to identical cell culture media and reagents, cryopreserved and stored in the same vacuum flask, and (b) the possibility of introducing any human viruses from the controlled environment of a cGMP-compliant laboratory is rather remote. Therefore, the only source of contamination would be the donor tissue itself. Although possible, it is unlikely that a part of tissue from which one cell line is derived would be positive for some virus or other pathogen and the other part would not. Such a risk might be somewhat higher in the case of embryos harvested during a single IVF cycle than it would be for multiple iPS cell clones obtained from reprogramming of a single batch of donor cells.

Pooling the lines derived from different donors could be considered as potentially providing additional cost savings. However, an important consideration in the testing of pooled lines using PCR methods is the determination of sensitivity. For nucleic acid testing methods, the European Pharmacopoiea 2.6.21 states a requirement of sensitivity at the 95% confidence level. For example, the assay sensitivity for the detection of *T. pallidum* is 10 copies per reaction at 95% confidence, the minimum number of copies detected in 95% of the reactions. Thus, we can follow that the reaction containing 100,000 cells (or 714.9 ng of DNA, based on the estimate that 7 pg of DNA corresponds to 1 genome equivalent)

will detect 10 copies of the pathogen with a sensitivity of 95%, regardless of the number of lines pooled. Therefore, if testing 10 cell lines with 10,000 cells from each cell line in the reaction, all 10 pooled cell lines would need to have 1 copy of *T. pallidum* to give a low-level positive result of 10 copies per reaction at the assay detection limit.

It has been estimated that in the U.S., CMV infects 50%–80% of the adult population [25] and nearly 95% of adults aged 35–40 years have been infected with EBV [26]. When considering the cost of deriving hPSC lines, it would therefore seem vitally important to prescreen potential donors for common viral pathogens such as HIV, HBV, HCV, HTLV, CMV, and EBV, along with screening for other health risks such as hereditary diseases or cancer. This approach would diminish the risk of investing in lines that would not be safe for therapeutic use and might reduce the pathogen burden sufficiently to enable larger scale pooling. This strategy would be impractical for hESC lines owing to donor confidentiality but should be easily applicable when recruiting donors for clinical-grade iPSC lines. Alternatively, screening of biopsied samples in non-GMP facilities before cell line derivation would exclude contaminated material and reduce the overall derivation costs, although the tests would have to be repeated once the cell lines were derived to satisfy regulations.

Conclusion

The requirements for validation of hPSC lines are even more rigorous than for other biological material for human therapy, including adult or fetal stem cells. The paramount issue is to prove the safety of these cells. However, the costs associated with validation of the products could render hESC- and iPSC-based therapy prohibitively expensive. Using two clinical-grade hESC lines, KCL033 and KCL034, derived in parallel from sibling embryos harvested in a single IVF cycle, we demonstrated as a proof-of-principle that multiple cell lines can be safely tested together and thus reduce the validation costs significantly without compromising safety and/or efficiency. This pooling strategy would be especially cost-effective in the case of clinical-grade iPSC lines, because three lines are generally derived from each donor. For example, a clinical iPSC bank from 100 donors with 3 lines from each donor, such as the Clinical iPSC Bank of Kyoto, could save on validation $18 million using our approach of pooling the samples from a single donor.

Acknowledgments

This work was supported by the U.K. Medical Research Council (Grant G0801061) and incentive funds to Y.K. and D.I. We thank the hESC lines derivation team: Victoria Wood, Neli Kadeva, Glenda Cornwell, and Dr. Emma Stephenson. We are especially indebted to the patients who donated embryos and Dr. Peter Braude, who set up the program.

Author Contributions

L.D., A.P., and C.M.: experimental work; S.C., N.B., and A.L.: conception and design, manuscript writing. Y.K.: conception and design, financial support; C.O. and D.I.: conception and design, financial support, manuscript writing.

Disclosure of Potential Conflicts of Interest

N.B. and A.L. have compensated employment with SGS Vitrology.

References

1 Thomson JA, Itskovitz-Eldor J, Shapiro SS et al. Embryonic stem cell lines derived from human blastocysts. Science 1998;282:1145–1147.

2 Stephenson EL, Braude PR, Mason C. International community consensus standard for reporting derivation of human embryonic stem cell lines. Regen Med 2007;2:349–362.

3 Available at http://www.advisorybodies.doh.gov.uk/genetics/gtac/InterimUKSCroutemap120309.pdf.

4 Löser P, Schirm J, Guhr A et al. Human embryonic stem cell lines and their use in international research. Stem Cells 2010;28:240–246.

5 Strulovici Y, Leopold PL, O'Connor TP et al. Human embryonic stem cells and gene therapy. Mol Ther 2007;15:850–866.

6 Takahashi K, Yamanaka S. Induction of pluripotent stem cells from mouse embryonic and adult fibroblast cultures by defined factors. Cell 2006;126:663–676.

7 Schwartz SD, Hubschman JP, Heilwell G et al. Embryonic stem cell trials for macular degeneration: A preliminary report. Lancet 2012;379:713–720.

8 Klimanskaya I, Chung Y, Becker S et al. Human embryonic stem cell lines derived from single blastomeres. Nature 2006;444:481–485.

9 Crook JM, Peura TT, Kravets L et al. The generation of six clinical-grade human embryonic stem cell lines. Cell Stem Cell 2007;1:490–494.

10 Funk WD, Labat I, Sampathkumar J et al. Evaluating the genomic and sequence integrity of human ES cell lines: Comparison to normal genomes. Stem Cell Res (Amst) 2012;8:154–164.

11 Ilic D, Stephenson E, Wood V et al. Derivation and feeder-free propagation of human embryonic stem cells under xeno-free conditions. Cytotherapy 2012;14:122–128.

12 Stephenson E, Jacquet L, Miere C et al. Derivation and propagation of human embryonic stem cell lines from frozen embryos in an animal product-free environment. Nat Protoc 2012;7:1366–1381.

13 Jacquet L, Stephenson E, Collins R et al. Strategy for the creation of clinical grade hESC line banks that HLA-match a target population. EMBO Mol Med 2013;5:10–17.

14 Health Explained: How to make stem cells. BBC News. Available at http://www.bbc.co.uk/news/health-18496355.

15 NIH Human Embryonic Stem Cell Registry. NIH. Available at http://stemcells.nih.gov/research/registry/Pages/Default.aspx.

16 Directive 2002/94/EC of the European Parliament and of the Council of October 08, 2003 laying down the principles and guidelines of good manufacturing practice in respect of medical products for human use and investigational medicinal products for human use. Official Journal of the European Union October 14, 2003;L262:22–26. Available at http://ec.europa.eu/health/files/eudralex/vol-1/dir_2003_94/dir_2003_94_en.pdf.

17 Commission Directive 91/412/EEC of July 23, 1991 laying down the principles and guidelines of good manufacturing practice for veterinary medicinal products. Official Journal of the European Union August 17, 1991;L228:70–73. http://ec.europa.eu/health/files/eudralex/vol-5/dir_1991_412/dir_1991_412_en.pdf.

18 Lovatt A, Black J, Galbraith D et al. High throughput detection of retrovirus-associated reverse transcriptase using an improved fluorescent product enhanced reverse transcriptase assay and its comparison to conventional detection methods. J Virol Methods 1999;82:185–200.

19 Brorson K, Swann PG, Lizzio E et al. Use of a quantitative product-enhanced reverse transcriptase assay to monitor retrovirus levels in mAb cell-culture and downstream processing. Biotechnol Prog 2001;17:188–196.

20 Lovatt A. Applications of quantitative PCR in the biosafety and genetic stability assessment of biotechnology products. J Biotechnol 2002;82:279–300.

21 Xu Y, Brorson K. An overview of quantitative PCR assays for biologicals: Quality and safety evaluation. Dev Biol (Basel) 2003;113:89–98.

22 Directive 2004/23/EC of the European Parliament and of the Council of March 31,

2004 on setting standards of quality and safety for the donation, procurement, testing, processing, preservation, storage and distribution of human tissues and cells. Available at http://eur-lex.europa.eu/LexUriServ/LexUriServ.do?uri=OJ:L:2004:102:0048:0058:EN:PDF.

23 Commission Directive 2006/17/EC of February 8, 2006 implementing Directive 2004/23/EC of the European Parliament and of the Council as regards certain technical requirements for the donation, procurement and testing of human tissues and cells. Available at http://eur-lex.europa.eu/LexUriServ/LexUriServ.do?uri=OJ:L:2006:038:0040:0052:EN:PDF.

24 Commission Directive 2006/86/EC of October 24, 2006 implementing Directive 2004/23/EC of the European Parliament and of the Council as regards traceability requirements, notification of serious adverse reactions and events and certain technical requirements for the coding, processing, preservation, storage and distribution of human tissues and cells. Available at http://eurlex.europa.eu/LexUriServ/LexUriServ.do?uri=OJ:L:2006:294:0032:0050:EN:PDF. Accessed.

25 Cytomegalovirus (CMV) and congenital CMV infection. U.S. Centers for Disease Control and Prevention. Available at http://www.cdc.gov/cmv/overview.html.

26 Epstein-Barr virus and infectious mononucleosis. U.S. Centers for Disease Control and Prevention. Available at http://www.cdc.gov/epstein-barr/index.html.

Methods in Molecular Biology (2015) 1283: 65–71
DOI 10.1007/7651_2014_116

Published online: 24 August 2014

Isolation and Expansion of Mesenchymal Stromal/Stem Cells from Umbilical Cord Under Chemically Defined Conditions

Heba Badraiq, Liani Devito, and Dusko Ilic

Abstract

From a perspective of manufacturer, procurement of bone marrow aspirates for isolation of mesenchymal stromal/stem cells (MSC) is challenging. The MSC isolated from adult donors have lower proliferation capacity than the cells isolated form young donors of pediatric age. To obtain more MSC from young healthy donors for allogeneic therapy on multiple patients, umbilical cord (UC) seems to be the best alternative. Here, we describe an easy, cost-effective and reproducible protocol of isolation of the MSC from Wharton's Jelly (WJ) in UC.

Keywords: Umbilical cord, Mesenchymal stem cells, Explant culture

1 Introduction

The use of animal derived supplements, such as fetal bovine serum (FBS), should be eliminated for clinical grade cells to avoid the risks in transmitting animal pathogens and to avoid immunogenic reactions after clinical transplantations. The optimization of a xeno-free (XF) culture represents a positive step for the future production of these cells in a clinical grade scale. In addition, content and concentration of cytokines, growth, and other soluble factors greatly varies from batch to batch of FBS and even for purpose of basic research, the trend is to culture cells in serum-free medium. Different research groups have established a range of protocols for isolation and characterization of stromal cells from WJ. However, defined XF culture systems allow for a better multipotent differentiation and expansion rates of adipose tissue- and BM-MSCs, serving as a preferred alternative to FBS containing medium for the production of large scale, functionally competent, clinical grade MSCs (1–3).

Isolation of MSCs from WJ has been poorly investigated and the techniques vary depending on the laboratories. The enzymatic treatment with a combination of various collagenases is widely used; however this treatment fluctuates in the literature. Trypsin

and other proteases such as hyaluronidase are frequently added in different concentrations, and the incubation time also changes from 4 to 24 h at room temperature or at 37 °C (4–8). The yield of MSC often varies and enzymes containing no animal product are difficult to obtain and they are expensive.

The method of WJ MSCs isolation from UC explants possesses advantages over the enzymatic method: (a) cell damage by enzymes is avoided, (b) WJ contains growth factors that support the proliferation of MSC, and (c) it is a low cost protocol. The primary cultures obtained by UC explants appear to be heterogeneous (9, 10), with a population of fibroblast-like cells with a different cell shape and size. In our experimental setting, MSCs outgrowing from explants in chemically defined, animal product-free medium were also relatively heterogeneous initially. However, heterogeneity was substantially decreased after the first passage and it was gone after several population doublings (PD), yielding uniform population of the MSC.

2 Materials

2.1 UC

The UC is collected only from patients who gave their informed consent (*see* **Note 1**). Only one UC should be collected at a time to avoid and minimize risk of contamination (*see* **Note 2**). After delivery and inspection of placenta and UC by a nurse, the UC is cut and placed immediately inside a sterile 500-ml bottle containing PBS supplemented with Gentamicin + Amphotericin B (Gibco). The bottle is placed inside the tissue carrier bag and transported to the laboratory (*see* **Note 3**).

2.2 CELLstart-Coated Dishes

Survival of anchorage-dependent cells is determined by signals from their environment. These signals are primarily derived from soluble factors present in serum and from cell interactions with extracellular matrix (ECM). When serum factors are withdrawn, cells can still survive on certain matrices, whereas they undergo apoptosis on others. Fibronectin is the most effective survival-promoting ECM ligand for both primary fibroblasts and endothelial cells after serum withdrawal (11, 12). CELLstart, xeno-free coating reagent, is mostly fibronectin. Cell culture dishes should be coated the day of use following the manufacturer's recommendation (*see* **Note 4**).

2.3 Equipment

1. 100-μl pipetman.
2. 1,000-μl pipetman.
3. Autoclaved surgical tweezers.
4. Biosafety cabinet.

5. Cryobox/"Mr Frosty"/(Nalgene; Cat. No. 5100-001) (*see* **Note 5**).
6. Disposable scalpels (Swann-Morton, Cat. No. 0503).
7. Hemocytometer (Hausser).
8. Phase contrast microscope.
9. Pipette gun.
10. Tissue culture incubator.
11. Tube rack.

2.4 Plasticware and Other Disposables (See Note 6)

1. 100-mm Cell culture dish (Corning, Cat. No. 430293).
2. 100-µl Filter tips (SLS, Cat No. 171403).
3. 1,000-µl Filter tips (SLS, Cat No. 171703).
4. 500-ml Storage bottle (Corning, Cat. No. CLS430282).
5. 75-cm^2 Flask (Corning, Cat No.430641).
6. γ-irradiated individually wrapped polystyrene 5-ml pipettes (Falcon; Cat. No. 357543).
7. γ-irradiated individually wrapped polystyrene 10-ml pipettes (Falcon; Cat. No. 357551).
8. γ-irradiated individually wrapped polystyrene 25-ml pipettes (Falcon; Cat. No. 357525).
9. γ-irradiated 15-ml conical tube (BD Falcon; Cat no. 352096).
10. γ-irradiated 50-ml conical tube (BD Falcon; Cat no. 352070).
11. Cryotube (Thermo Scientific; Cat No. 377224).
12. Isopropyl alcohol (IPA) wipes.
13. Waste container.

2.5 Reagents and Medium

1. CELLstart (Life Technologies, Cat. No. 07930).
2. Cryostor CS10 (STEMCELL Technologies, Cat. No. A10142-01).
3. DMEM (Life Technologies, Cat No. 41965-039).
4. DPBS with Ca^{2+}/Mg^{2+} (Lonza, Cat No. BE17 513F).
5. Gentamicin/Amphotericin B 500X (Gibco/Life Technologies, Cat. No. R-015-10).
6. Isopropanol (Shield Medicare; Cat. No. 3035300).
7. PBS, Ca^{2+}/Mg^{2+}-free (Life Technologies Cat No. 10010-023).
8. Stemgro (Corning, Cat. No. 40-410-KIT).
9. Tryple (Life Technologies, Cat No. 12604-021).

3 Methods

3.1 Receiving the UC

1. Assure that the UC is accompanied with signed donor consent and a proof that the donor has no blood-borne diseases.
2. The UC is received inside a storage bottle containing sterile PBS supplemented with Gentamicin/Amphotericin B (*see* **Note** 7). The bottle should be wiped with IPA cleaning wipes and placed inside the biosafety cabinet.

3.2 Plating UC Explants

1. The cords should be then transferred into a non-coated 100-mm dish.
2. The cord can be cut into 3–5 cm pieces and thoroughly washed with PBS to eliminate any remains of blood (a new storage bottle can be used to wash the cord pieces).
3. Place one piece in a new non-coated 100-mm dish. While holding the UC piece with surgical tweezers, cut it longitudinally with a sterile scalpel to expose the Wharton's jelly (WJ) and then slice it into 0.5–1 cm^2 pieces.
4. Ten to fifteen pieces (explants) can be transferred per dish into a pre-labeled 100-mm dish coated with CELLstart.
5. Plate the umbilical cord explants on the bottom of the plate and wait 2–5 min before covering slowly with 10 ml Stemgro medium supplemented with Gentamicin/Amphotericin B.
6. Set as many explants as possible. Unused UC discard as medical waste.
7. Place dishes into tissue culture incubators at 37 °C.

3.3 MSC Derivation

1. The medium (Stemgro with Gentamicin/Amphotericin B) in explant culture needs to be exchanged every 2–3 days.
2. The cells are ready for subculture about 10–14 days after initial outgrowths were observed.
3. Remove remaining explants and discard them into medical waste.
4. Wash outgrowths in each 10-mm dish with 5 ml PBS, Ca^{2+}/Mg^{2+}-free
5. Add 5 ml TripLE in each 10-mm dish. Incubate 3–5 min at 37 °C. Detach the cells with vigorous pipetting or, if needed, scrape the cells off with cell scraper. Add equal amount of DMEM and transfer into 15- or 50-ml conical tube. Pool cell suspension from up to four plates in one 50-ml tube.
6. Spin down for 5 min at 700 × *g*. Pool pellets from all tubes and resuspend in 10-ml Stemgro with Gentamicin/Amphotericin B.

7. Count cells using a hemocytometer. This number is population doubling (PD) = 0.
8. Plate the cells in T75 coated with CELLstart in 10 ml Stemgro with Gentamicin/Amphotericin B. Approximate density for optimal growth should be ≈7,000 cells/cm^2 (≈525,000 cells/T75). Lesser density may slow cell proliferation (*see* **Note 8**).
9. Change medium every 2–3 days. Use Stemgrow w/o Gentamicin/Amphotericin B (*see* **Note 9**).
10. Once when the cells reach ≥80 % density, repeat steps 4–8 if needed. Target is to have ≈2 × 10^7 cells in total.
11. When the cell number reaches near ≈2 × 10^7, proceed with cryopreservation.

3.4 MSC Cryopreservation

1. For cryopreservation, cell monolayer is washed with PBS and incubated in TrypLE for 3–5 min at 37 °C. TrypLE is then diluted with an equal amount of pre-warmed DMEM. Separate 20 μl for cell counting before centrifuging the cells at 700 × *g* for 5 min.
2. The cell pellet is then resuspended at a concentration of ≈1 × 10^6 cells/ml with Cryostor CS10. Add 0.5 ml in each cryovial (≈500,000 cells in 0.5 ml/vial). Cryovials should be placed inside precooled Mr Frosty (*see* **Note 10**)
3. Place Mr Frosty at −20 °C for 2 h and then in −80 °C for another 2 h. After that, transfer the Cryovials from the freezer into liquid nitrogen dewar.

4 Notes

1. Assure that you have the following information:
   (a) Copy of signed consent.
   (b) Time of delivery.
   (c) Hospital ID number.
   (d) Results of tests for: HIV1/HIV2, HepA, HepB, HepC, HTLV1/2, and Syphilis tests. The mandatory tests are different from country to country; assure that you follow regulations set for your country.
   (e) Ask if there is clean medical history. If not, write down the conditions.
2. UC can be collected from healthy donors either after vaginal delivery or from Caesarean section deliveries. UC obtained from Caesarian sections are sterile and risk of contamination in the culture is low in comparison with UC collected from natural vaginal deliveries.

3. The tissue carrier bag should not be carried in public transport. Private car, hired car, or specialized courier services should be used to transport the tissue carrier bag containing the UC between the collection site and the laboratory.
4. Avoid drying of coated surface.
5. Each isopropanol freezing cryobox can hold 18 cryovials. Check level of isopropanol in each cryobox before usage. If not sufficient, fill it up to the fill line
6. Isopropanol, disposable culture, and plasticware of the equivalent quality can be purchased from different manufacturers without altering the outcome of the procedure.
7. If you are not sure that PBS is supplemented with antibiotic/antimycotic mix, wash the cord 3× in 150 ml of PBS supplemented with antibiotic/antimycotic mix, gently stirring for 5 min each time.
8. Use smaller vessels if needed (i.e., T25).
9. Since all cells were mixed at step 6 (Section 3.3), the medium sample can be taken from any of culture flasks and it will represent the whole population. The following two tests are recommended:
   (a) To assess sterility of the culture, spread 1 ml of spent medium w/o Gentamicin/Amphotericin B in which cells were at least 48 h and spread over agar plate and send to microbiology laboratory for analysis.
   (b) For testing mycoplasma, plate ≈10,000 cells in Maktek dish and stain with Hoechst 24 h later.
10. Do not leave cells in cryopreservant for extended period at room temperature. That will affect their viability upon thawing.

Acknowledgments

The study was supported by the studentship to H.B. from Saudi Arabia government.

References

1. Gottipamula S, Muttigi MS, Chaansa S, Ashwin KM, Priya N, Kolkundkar U, Sundar Raj S, Majumdar AS, Seetharam RN (2013) Large-scale expansion of pre-isolated bone marrow mesenchymal stromal cells in serum-free conditions. J Tissue Eng Regen Med. [Epub ahead of print]
2. Patrikoski M, Juntunen M, Boucher S, Campbell A, Vemuri MC, Mannerstrom B, Miettinen S (2013) Development of fully defined xeno-free culture system for the preparation and propagation of cell therapy-compliant human adipose stem cells. Stem Cell Res Ther 4:27
3. Chase LG, Yang S, Zachar V, Yang Z, Lakshmipathy U, Bradford J, Boucher SE, Vemuri MC (2012) Development and characterization of a clinically compliant xeno-free culture medium in good manufacturing practice for human

multipotent mesenchymal stem cells. Stem Cells Transl Med 1:750–758

4. Fong CY, Richards M, Manasi N, Biswas A, Bongso A (2007) Comparative growth behaviour and characterization of stem cells from human Wharton's jelly. Reprod Biomed Online 15:708–718
5. Fong CY, Subramanian A, Biswas A, Gauthaman K, Srikanth P, Hande MP, Bongso A (2010) Derivation efficiency, cell proliferation, frozen-thaw survival, stem-cell properties, and differentiation of human Wharton's jelly stem cells. Reprod Biomed Online 21:391–401
6. Pereira WC, Khushnooma I, Madkaikar M, Ghosh K (2008) Reproducible methodology for the isolation of mesenchymal stem cells from human umbilical cord and its potential for cardiomyocyte generation. J Tissue Eng Regen Med 2:394–399
7. Weiss ML, Anderson C, Medicetty S, Seshareddy KB, Weiss RJ, Werff IV, Troyer D, McIntosh KR (2008) Immune properties of human umbilical cord Wharton's jelly-derived cells. Stem Cells 26:2865–2874
8. Kadam SS, Tiwari S, Bhonde RR (2009) Simultaneous isolation of vascular endothelial cells and mesenchymal stem cells from the human umbilical cord. In Vitro Cell Dev Biol Anim 45:23–27
9. Conconi MT, Di Liddo R, Tommasini M, Calore C, Parnigotto PP (2011) Phenotype and differentiation potential of stromal populations obtained from various zones of human umbilical cord: an overview. Open Tissue Eng Regen Med J 4:6–20
10. Mark P, Kleinsorge M, Gaebel R, Lux CA, Toelk A, Pittermann E, David R, Steinhoff G, Ma N (2013) Human mesenchymal stem cells display reduced expression of CD105 after culture in serum-free medium. Stem Cells Int 2013:698076
11. Ilic D, Almeida EA, Schlaepfer DD, Dazin P, Aizawa S, Damsky CH (1998) Extracellular matrix survival signals transduced by focal adhesion kinase suppress p53-mediated apoptosis. J Cell Biol 143:547–560
12. Almeida EA, Ilic D, Han Q, Hauck CR, Jin F, Kawakatsu H, Schlaepfer DD, Damsky CH (2000) Matrix survival signaling: from fibronectin via focal adhesion kinase to c-Jun NH(2)-terminal kinase. J Cell Biol 149: 741–754

Methodology

For reprint orders, please contact: reprints@futuremedicine.com

Regenerative Medicine

Wharton's jelly mesenchymal stromal/stem cells derived under chemically defined animal product-free low oxygen conditions are rich in MSCA-1$^+$ subpopulation

Liani Devito[1], Heba Badraiq[1], Antonio Galleu[2], Dheraj K Taheem[3], Stefano Codognotto[1], Richard Siow[4], Yacoub Khalaf[1], Annette Briley[1], Andrew Shennan[1], Lucilla Poston[1], John McGrath[5], Eileen Gentleman[3], Francesco Dazzi[2] & Dusko Ilic*[,1]

[1]Division of Women's Health, Women's Health Academic Centre KHP, King's College London, London, UK
[2]Department of Haemato-Oncology, Rayne Institute, King's College London, UK
[3]Craniofacial Development & Stem Cell Biology, King's College London, UK
[4]Cardiovascular Division, King's College London, UK
[5]St John's Institute of Dermatology, King's College London, London, UK
*Author for correspondence: dusko.ilic@kcl.ac.uk

Aim: Umbilical cord contains, within Wharton's jelly (WJ), multipotent mesenchymal stromal/stem cells (MSCs) of fetal origin that can be isolated and expanded *in vitro* with a minimal manipulation and very high efficiency. Our aim was to develop a highly reproducible protocol that has the unique potential to be scaled up and adapted to cGMP requirements for the use in cellular therapy. **Results:** We found that derivation of WJ MSCs under defined conditions in low oxygen resulted in several folds higher populations of MSCA-1$^+$ cells (6.0–19.2%) when compared with WJ MSCs derived in the presence of serum (0.1–2.8%) or clinical-grade bone marrow (BM) MSCs cultured under atmospheric O_2 (20%). We demonstrate that WJ MSCs derived following our protocol display antiproliferative activity similar to clinical-grade BM MSCs. We also show that these WJ MSCs can be differentiated into adipo-, chondro- and osteogenic lineages. **Conclusion:** Easy accessibility, abundance and genetic 'naivety' make WJ MSCs logistically a more attractive source for clinical applications than BM MSCs.

Keywords: animal product-free culture • chemically defined condition • mesenchymal stem cell • mesenchymal stromal cell • MSCA-1 • umbilical cord • Wharton's jelly

Background

Traditional isolation of mesenchymal stem cells (MSCs) from bone marrow (BM) is dependent on adherence to tissue culture plastic. When mononuclear cells from BM aspirate are plated in a dish, MSCs will attach and in approximately 2 weeks form colonies of fibroblast-like cells that can be propagated *in vitro* in either serum or platelet lysate supplemented culture medium [1]. The method is still widely used even though yield is very low – only about one in 80,000 plated cells are MSCs. Extensive characterization of cell surface markers on BM MSCs led to the discovery of multiple prospective 'markers' that were actually not really MSC-specific, although could enrich yield, if used for purification of BM aspirate before cell plating [2]. Among them, CD271 and MSC antigen-1 (MSCA-1) seem to be the most promising, increasing yield of colony forming units over >100-fold [3–7]. MSCA-1, which was previously associated only with cells of the osteoblasts lineage may, therefore, also represent a marker of multipotent BM stromal stem cells [7].

Donor procurement makes the logistics of obtaining BM as a source of MSCs complicated. Although BM MSCs from adult donors still have satisfactory abilities to be used for regenerative medicine purposes, from the manufacturing prospective, the best donors are in the pediatric age range. In addition, the procedure requires planning and involves some pain for the donor. Therefore, the MSCs therapy field is constantly looking for alternative sources. Among the various options (peripheral blood, placental, amniotic, dental pulp and nasal mucosa, among others), adipose tissue-derived (AD) MSCs have proven to be the most suitable, although a somewhat restricted, source for cell therapies [8]. Since for allogeneic therapy AD MSCs are harvested from people with extra fat tissue undergoing cosmetic surgery, there is a plausible preoccupation that the

Future Medicine part of fsg

abnormal metabolic environment related to excessive body weight bears consequences for these cells, perhaps rendering them unsuitable for clinical use on multiple recipients [9]. Ideally, the cells for allogeneic therapy on multiple recipients should be isolated from a healthy young donor, with a clean, well-documented health history. Cord blood and umbilical cord (UC) are clearly an obvious choice. They are easily obtainable shortly after birth and therefore less likely to contain acquired, potentially deleterious mutations contained in cells derived from adult tissues. Nevertheless, the possible transmission of pathogens from mother to child necessitates a careful screening of donors.

Indeed, in the last few years, stromal cells isolated from UC's Wharton's jelly (WJ), are becoming more and more popular as a potentially promising alternative source for cellular therapy. Their advantage in comparison with BM MSCs is in the number of cells obtainable, extended retention of stem cell properties *in vitro* and the reported presence of surface markers involved in immune tolerance [10–14]. A subpopulation of WJ MSCs expressing CD29, CD73, CD90 and CD105 and negative for CD34, CD45 and HLA-DR displayed low immunogenicity and could be isolated in large numbers form >90% of UC [14]. Earlier studies demonstrated that WJ MSCs secrete IL-6 and VEGF, cytokines known for their role in immunosuppressive activity of MSCs, and are negative for immune response-related co-stimulatory molecules CD40, CD80 and CD86, suggesting further their therapeutic potential [14].

WJ is composed of water (90%), sulphated glycosaminoglycans (GAGs) and a collagen-rich 3D extracellular matrix (ECM) network. The most abundant GAG is hyaluronic acid (~70%), whereas collagen type I and III are more prevalent than IV, VI and VII [15]. The composition of the 3D matrix suggests three distinct zones, sub-amnion, WJ *per se*, and perivascular zone, and even though different types of stromal cells are dispersed in different zones, the term WJ MSCs is often extended to all UC stromal cells [16]. They share common features with MSCs from adult tissues, such as being positive for CD44, CD73, CD90, CD105, α-smooth muscle actin and vimentin [17,18]. In spite of recent surge in publications, there is very little, or no, information about CD271 and MSCA-1 in WJ MSCs.

Methods

UC collection

The National Health Service Research Ethics Committee approved the protocol (12/NE/0371). Following informed consent, UCs were collected from Cesarean section deliveries of otherwise healthy women at the gestational age ≥37 weeks. After delivery and inspection of placenta and UC by a nurse, a 10–20 cm piece of the UC was cut and placed immediately inside a sterile 100-ml bottle. The cord was washed twice to remove remaining blood in warmed PBS supplemented with antibiotics and antimycotic (Life Technologies, NY, USA) and processed for explant culture in ≤4 h.

Plating UC explants

The cords were transferred into a 145-mm dish, cut into three to four smaller pieces and thoroughly washed with PBS. The cord was cut longitudinally with a sterile scalpel to expose WJ and then sliced into 0.5–1 cm^2 pieces. A total of 10–12 blood vessel-free pieces (explants) were transferred, inner side of the explant facing the bottom of the dish, per a pre-labeled 100-mm dish coated with CellSTART (Life Technologies). To facilitate the attachment of the explants to the plastic surface, they were left exposed to air for 5–10 min before adding 15 ml of cell culture medium [19]. The medium was either StemGro® hMSC Medium (Corning) or DMEM supplemented with 10% fetal calf serum (FCS; Hyclone, UT, USA). The plates with explants were then transferred to the incubator (Thermo Scientific Heraeus®, MA, USA) and cultured at 37°C, 5% CO_2, 5% O_2. The initial evaluation of suitable conditions for the long-term WJ MSC cultures under defined low O_2 were performed within a gas environment-regulated workstation (SCItive, Ruskinn Technology, MN, USA) set to 5% O_2, 5% CO_2 and 75% relative humidity.

WJ stromal cells derivation

Explant media was changed every 3 days until cell outgrowth was observed under the microscope. The cells were allowed to expand for an additional 7–10 days before the first passaging.

To passage the cells, cell monolayers were washed with PBS (Invitrogen, Paisley, UK) and incubated in Tryple Select (Invitrogen) for 3–5 min at 37°C. Tryple was then diluted with an equal amount of prewarmed DMEM (Invitrogen). Cells were centrifuged for 5 min and the cell pellet resuspended in complete media for replating or in a freezing solution for cryopreservation. The cells were passaged at 60–80% confluence.

For cell counting, the cells were completely resuspended in growth medium and counted using a hemocytometer (Hausser). Population doublings were calculated according to the formula: PD = [log (A/B)]/0.301, where A is the number of cells that were harvested and B, the number of cells seeded into the plate. The first harvest from explants is termed P0.

Trypan blue was used routinely to assess cell survival when the cells were counted for passaging or flow cytometry analyses.

Cells grown under standard conditions were frozen in 10% DMSO (Sigma-Aldrich, MO, USA) in fetal bovine serum (FBS), whereas cells grown under defined xeno-free (XF) conditions were frozen in Synth-a-Freeze® (Life Technologies) and stored in liquid nitrogen.

Flow cytometry analyses

Expression of cell surface molecules was assessed using a FACS CANTO II (BD, Oxford, UK). To this purpose, 1 × 10^6 cells were resuspended in 100 µl of ice-cold PBS supplemented with 10% FBS then mixed with the appropriate primary antibody 1:50 and then incubated in the dark for 15 min at room temperature. After washing with PBS, the cells were resuspended in 500 µl of ice-cold PBS with 10% FBS. The data were analyzed using the DIVA software. All antibodies used in flow cytometry were purchased from Miltenyi Biotec (Cologne, Germany): PE-conjugated anti-CD34, anti-CD73 and anti-MSCA-1, APC-conjugated anti-CD56, anti-CD29 and anti-CD105, FITC-conjugated anti-CD44, anti-CD90 and anti-CD271, and Vio-Blue-conjugated anti-CD45. Titration was done for each of antibody used and unstained cells were used as negative control. Fluorescence minus one (FMO) was also performed to avoid any nonspecific binding.

Acute myeloid leukemia cell line Katsumi, used as a $CD34^+CD45^+$ control for flow cytometry, was a kind gift from Eric So (King's College London, UK). The cells were cultured in RPMI-1640 medium supplemented with 20% FCS at 37°C, 5% CO_2, 20% O_2.

Clinical grade human BM MSCs were manufactured according to the validated GMP protocol from the BM aspirates of healthy individuals donating BM for their siblings. Donors were consented to release unused materials for research. Briefly, 2 ml of BM unfractionated cell suspension was plated at a density of 10–25 × 10^6/636 cm^2 in α-modified Eagle's medium (αMEM) supplemented with 5% human platelet lysate and incubated for 3 days at 37°C in 5% CO_2. Non-adherent cells were then discarded and the remaining cells left to grow until confluence (90–100%). After usually 3 weeks, MSCs were detached with Trypsin 0.05% and EDTA 4Na 0.2 g/l. BM MSCs were distributed for compassionate use under the hospital exemption scheme (EC No 1394/2007).

Differentiation assay

To assess adipogenenic potential of WJ MSCs derived under defined XF conditions, the cells were cultured first under standard conditions for 3 days. The medium was then replaced with supplemented complete STEMPRO® adipogenesis differentiating medium (GIBCO®, Invitrogen) and changed every 3–4 days for 14 days. The cells were fixed with 4% paraformaldehyde for 30 min and to detect cellular lipids incubated for 20 min in 1:100 dilution of Lipid-TOX™ Green Neutral Lipid Stain. Samples mounted in VECTASHIELD® (Vector, CA, USA) were examined under a Nikon epifluorescence microscope. Nuclei were visualized with Hoechst 33342 (Invitrogen).

To assess chondrogenic potential of WJ MSCs derived under defined XF conditions, cells were seeded at a density of 2 × 10^4 cells/cm^2 and cultured for 21 day in StemGro supplemented with 2 mM L-glutamine, 347 µM L-Proline, 100 nM dexamethasone, 1% insulin–transferrin–selenium solution, 137 µM ascorbate-2-phosphate and 0.38 µM (10 ng/ml) recombinant human TGF-β1/3 (PeproTech, Hamburg, Germany). Medium was changed every 3–4 days. Cells fixed in 4% paraformaldehyde were stained with 1% Alcian Blue solution to detect glycosaminoglycans.

To assess osteogenic potential of WJ MSCs derived under defined XF conditions, the cells were seeded at a density of 2 × 10^4 cells/cm^2 and cultured for 21 day in StemGro supplemented with 2 mM L-glutamine, 100 nM dexamethasone, 50 µM ascorbate-2-phosphate and 2.5 mM β-glycerophosphate. Medium was changed every 3–4 days. Cells fixed in 4% paraformaldehyde were stained with 1% alizarin red solution to detect calcium-containing mineral.

The stained samples were examined under Olympus CK40 inverted phase contrast microscope. Images were recorded with ProgRes CT5 camera (Jenoptik, Thuringia, Germany).

Mitogen-induced proliferation assay

Human peripheral blood mononuclear cells (PBMCs) were isolated from leukocyte cones purchased from the National Blood Service (Colindale, UK). Leukocyte cones were diluted 1/1 with PBS (Invitrogen Life Technologies) and layered on Histopaque (Sigma-Aldrich) for density gradient separation.

PBMCs proliferation assays were performed in 0.2 ml of medium (RPMI supplemented with 10% FBS and penicillin/streptomycin) per well of 96-well flat-bottom plates (Costar®, Sigma-Aldrich). WJ MSCs from four donors derived under defined XF conditions and clinical-grade BM MSCs from three donors were plated overnight at serial dilutions. A total of 5 × 10^5/well PBMCs were then added to MSCs to obtain co-cultures with increasing PBMC/MSC ratios from 10:1 to 80:1. PBMCs were then stimulated with 5 µg/ml phytohemagglutinin (PHA; Sigma-Aldrich) and after 72 h proliferation was measured by incorporation of radiolabeled [^{3}H]-thymidine (TdR) during the final 18 h of incubation. Briefly, cell cultures were pulsed with

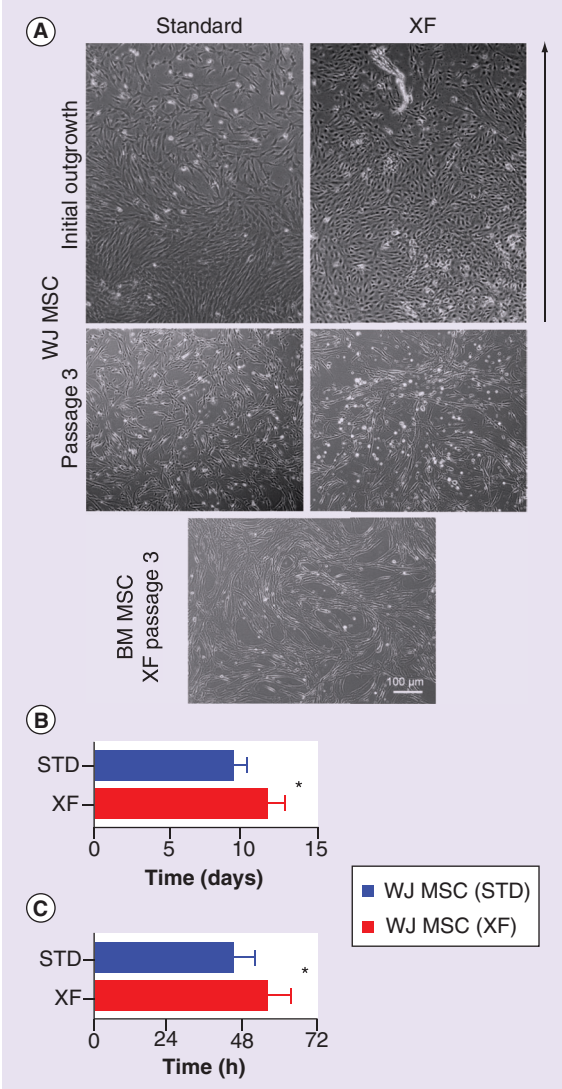

Figure 1. Derivation of mesenchymal stem cells from umbilical cord explants. (A) The cells in initial outgrowth from attached umbilical cord (UC) explants grown under STD conditions (10% fetal calf serum/DMEM) looked more like typical fibroblasts, whereas cells grown under chemically defined XF conditions were less elongated and never as tightly packed as cells in standard culture. Interestingly, after three passages, the WJ MSCs cultured under XF conditions resembled more phenotypically clinical-grade BM MSCs than WJ MSCs cultured under STD conditions. **(B)** First outgrowth from UC explants. The first outgrowth was observed sooner (9.3 ± 0.3 days; n = 7) under STD than under XF conditions (12.1 ± 0.5 days; n = 8). The p-value was analyzed by two-tailed unpaired t-test with significant difference observed (*$p \leq 0.05$). **(C)** Population doubling time of WJ MSC (P1–P2). The mean doubling time of cells derived under STD condition was shorter (40.8 ± 4.8 h; n = 7) than under XF conditions (55.2 ± 2.6 h; n = 7). The p-value was analyzed by a two-tailed unpaired t-test with significant difference between the groups (*$p \leq 0.05$).
BM: Bone marrow; MSC: Mesenchymal stem cell; STD: Standard; WJ: Wharton's jelly; XF: Xeno-free.

0.5 µCi/well of [^{3}H]-TdR (Amersham, UK) 18 h before harvesting onto glass fiber filter mats (Wallac, Perkin-Elmer, MA, USA) using a 96-well plate automated cell harvester (Skatron; Molecular Devices, CA, USA). Scintillation fluid was added and [^{3}H]-TdR incorporation was measured by liquid scintillation spectroscopy on a β-counter (Wallac). The results were expressed in counts per minute (cpm) or percentage of control proliferation for triplicate cultures. Cultures of stimulated PBMCs without MSCs were used as positive control.

Statistical analyses

Statistical analyses to determine differences between STD and XF conditions were carried out by unpaired t-test unless otherwise noted. Differences were considered significant when $p < 0.05$.

Results

WJ MSCs grown from UC explants under XF conditions are morphologically similar to clinical-grade BM MSCs

Overall, after several passages WJ MSCs were spindle shaped with a flat polygonal morphology characteristic of BM MSCs (Figure 1A). Early evidence of WJ MSCs growth from the UC explants was typically observed within 8–11 days (9.3 ± 0.3) following initial plating under standard conditions (STD; 10% FBS/DMEM) and 10 to 14 (12.1 ± 0.5) for chemically defined, XF conditions (Figure 1B). Population doublings were calculated between the two first passages (P1 and P2) to establish the proliferative rate among the conditions used. No significant cell death was observed (>90% of trypan blue-negative cells at any experiment). The assay demonstrated that the cells cultured under STD conditions have a significantly higher proliferative rate than those under XF conditions (40.8 ± 4.8 vs 55.2 ± 2.6 h; n = 7; Figure 1C).

WJ MSCs isolated & grown under XF conditions have capacity of multipotent stem cells

First, we wanted to determine whether the isolated stromal cells (PD 5) have differentiation potential into the three mesenchymal lineages by testing their response to adipogenic, chondrogenic and osteogenic induction media. After 2 weeks of culture in adipogenic medium, we could detect fat droplets, while it took 3 weeks to induce Alcian Blue-positive glycosaminoglycan depositions (cartilage) or mineralized nodules (bone) by Alizarin Red staining (Figure 2A). Control cells cultured under chemically defined XF conditions without the addition of differentiation supplements showed no change in cell morphology and no cells were positive for LipidTOX, Alcian Blue or Alizarin Red (data not shown).

Immunomodulatory potential of WJ MSCs isolated & grown under defined XF conditions

MSCs are known for their ability to exert potent immunosuppressive and immunoregulatory effects on a variety of cell types mediating both adaptive and innate immunities [20]. Next, we compared the immunomodulatory effect of clinical-grade BM MSCs (n = three donors) and WJ MSCs isolated and grown under XF condition (n = four donors) by adding them to PHA-stimulated PBMCs. WJ MSCs inhibited PHA)-stimulated PBMCs proliferation in a dose-dependent manner in a similar fashion as BM MSCs, although there was a significantly higher antiproliferative activity at 1/20 ratio (Figure 2B). These data suggest that WJ MSCs isolated and grown under XF conditions retain similar immunosuppressive activities to the ones originally described in BM MSCs.

WJ MSCs subpopulations profile is dependent on culture conditions

As the next step of characterization, we assessed the effect of chemically defined, animal product-free culture conditions on WJ MSCs surface marker profile (CD29, CD34, CD44, CD45, CD56, CD73, CD90,

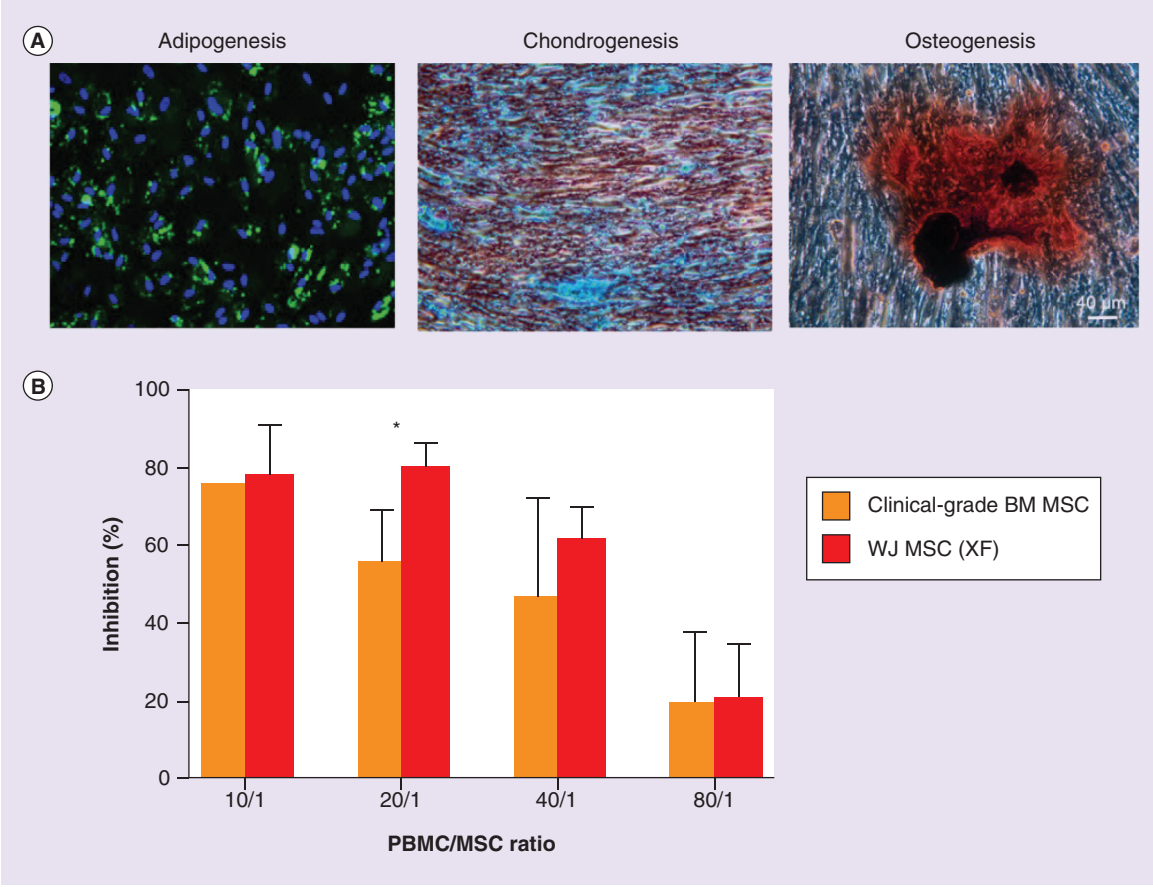

Figure 2. Characteristics of Wharton's jelly mesenchymal stem cells. (A) Adipogenic, chondrogenic and osteogenic differentiation of WJ MSCs. Cells rich in intracellular lipid droplets visualized with a fluorescent LipidTOX™ Green Neutral Lipid Stain indicate successful adipogenic induction. Cartilage proteoglycans detected with 1% Alcian Blue after chondrogenic and calcium phosphate mineral accumulation detected with 1% Alizarin red after osteogenic induction confirmed the multipotent nature of WJ MSCs. **(B)** Immunomodulatory potential of WJ MSCs. WJ MSC (n = four donors) inhibited phytohemagglutinin-stimulated human PBMC proliferation in dose-dependent manner in a similar fashion as BM MSC (n = 3 donors), with significantly higher antiproliferative activity at 20/1 ratio. The relative proliferation at each PBMC/MSC ratio was calculated as percentage of the proliferation obtained in the positive control as described by the following formula: A/B × 100, where A is the proliferation at one specific PBMS/MSC ratio and B is the proliferation of the corresponding PBMC/MSC ratio, but in the absence of phytohemagglutinin (negative control), and C is the proliferation of the positive control. The percentage of inhibition was then calculated by subtracting the percentage of proliferation to 100 (maximum of inhibition). Statistics: two-tailed unpaired t-test. 95% CI; *$p < 0.05$. WJ MSC used in the assay were PD 5–6, whereas BM MSC were at P2 or P3.
BM: Bone marrow; MSC: Mesenchymal stem cell; PBMC: Peripheral blood mononuclear cell; WJ: Wharton's jelly; XF: Xeno-free.

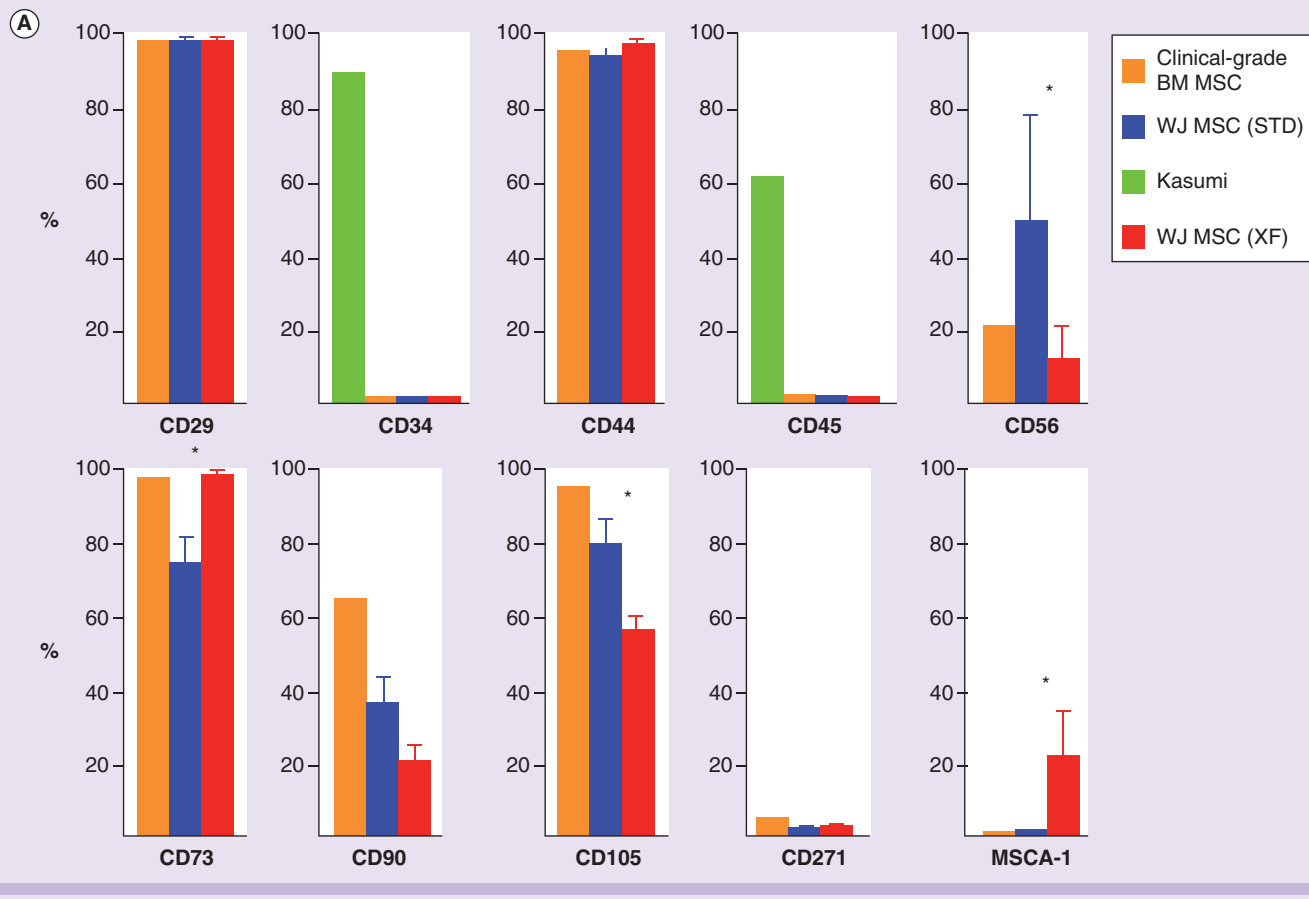
A
%
100
80
60
40
20
CD29
CD34
CD44
CD45
CD56
CD73
CD90
CD105
CD271
MSCA-1
*
Clinical-grade BM MSC
WJ MSC (STD)
Kasumi
WJ MSC (XF)

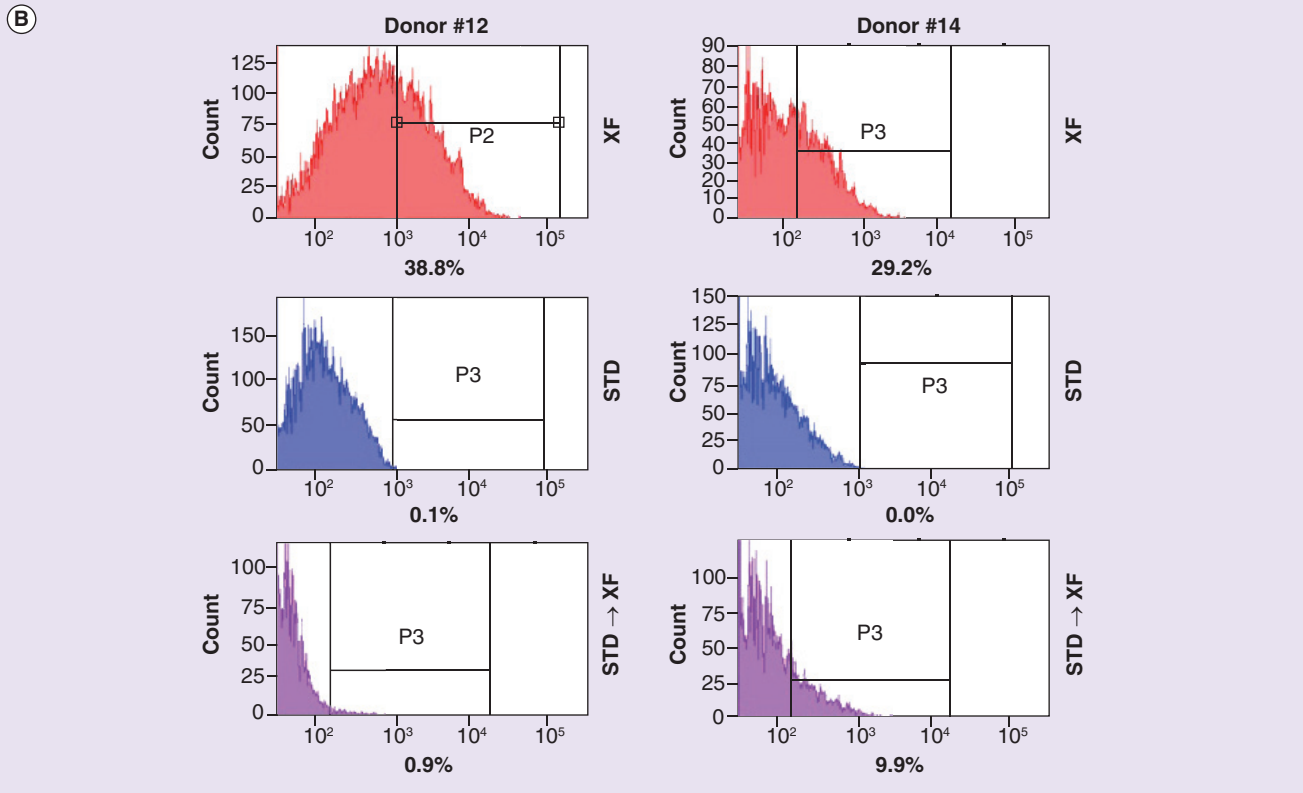
B
Donor #12
Donor #14
Count
P2
P3
XF
STD
STD → XF
38.8%
29.2%
0.1%
0.0%
0.9%
9.9%

CD105, CD271 and MSCA-1) in cells isolated from five donors (Donor ID: #9, #10, #11, #12 and #14). Approximately half of the explants from each UC were cultured under standard (STD) conditions (DMEM supplemented with 10% FCS), whereas the other half were cultured under chemically defined XF conditions. Kasumi cells were used as positive control for hematopoietic markers. Clinical-grade BM MSCs were used for comparison of the expression of cell surface molecules with WJ MSCs derived under STD and XF conditions (Figure 3A).

The profiling of cell surface markers from five independent donors, cultured under two different conditions, confirmed that WJ MSCs isolated in this study expressed all MSC markers seen in BM MSCs. Significant differences in the expression of CD56, CD73, CD105 and MSCA-1 were noted between WJ MSCs cultured under STD and XF conditions. Interestingly, it seems that XF condition favors the expression of the MSCA-1 marker, which was barely detectable in STD conditions or in clinical-grade BM MSCs. Nevertheless, there were large differences in the size of MSCA-1+ subpopulation amongst donors (donor #9 [4.4%] vs the other four donors (13.5–38.8%). Neither age nor any obvious health-related condition could be linked to variations in size of MSCA-1+ population (Figure 3B). Expression profile did not vary over the time spent in culture; there were no difference between cells at PD 4–5 (Figure 3B) and PD 9–11 (data not shown).

Isolation & expansion of MSCA-1+ subpopulation is dependent on culture conditions

To confirm that chemically defined XF culture conditions described here selectively privileged the expansion of MSCA-1+ cells, we transferred WJ MSCs derived and expanded under STD conditions (n = two donors) into defined XF medium for 14 days and assessed the proportion of MSCA-1+ cells. For both donors, the numbers of MSCA-1+ cells increased from 0.1 to 0.9% in donor #12 and from undetectable (0%) to 9.9% in donor #14. Since population doubling time of WJ MSCs under XF conditions is slightly over 2 days (55.2 ± 2.6 h; Figure 1C) and the cells were cultured for only 14 days, this increase is likely due to stimulation of MSCA-1 expression, not higher cell proliferation of already present MSCA-1+ cells. The cells cultured in parallel under STD conditions had no detectable increase of the MSCA1+ subpopulation (data not shown).

Discussion

In this study we characterized the features of MSC isolated from UC explants under chemically defined XF conditions. For isolation of the MSCs, we opted to use an explant technique because aside from being less harsh for cells and less cumbersome for researchers, in the long run it is much more cost effective. In addition, we opted to isolate and expand WJ MSCs under physiological ('hypoxic') culture conditions [21].

Cell outgrowth from the explants was observed sooner under STD than XF conditions. Cells also proliferated faster under STD conditions. Neither result was surprising – STD medium contains FBS, which is by definition rich in growth factors and nutrients that stimulate cell growth and proliferation.

Thorough comparative phenotype analysis between UC tissue in *in vivo* and *in vitro* expanded stromal cells demonstrated protocol-dependent variations in the size of subpopulations positive for multiple

Figure 3. Xeno-free culture conditions induce MSCA-1 expression (see facing page). (A) Expression profile of WJ MSCs' surface markers. XF (red) and STD (blue) were negative for hematopoietic stem cell markers CD34 (mucosialin, gp 105–120) and CD45 (leukocyte common antigen, Ly-5). Similarly to BM MSCs (97.7%), nearly all WJ MSCs from all five donors expressed CD29, regardless of culture conditions (98.4 ± 0.4% of cells under STD vs 98.7 ± 0.3% under XF conditions). CD44 expression also did not differ regardless of donor or culture conditions (BM MSCs: 97.4%, STD: 96.1 ± 1.6%, XF: 98.2 ± 0.5%). In contrast, CD56 expression varied ostensibly from donor to donor (range 5.0–27.6% under XF conditions; range 21.3–82.9% under STD conditions). CD73, ecto-5'-nucleotidase, has been expressed in almost the entire population of clinical-grade BM MSCs (97.9%) and WJ MSCs cultured under XF conditions (98.7 ± 0.3%), whereas WJ MSCs cultured under STD conditions were about 25% less positive for CD73 (74 ± 8.8%). CD90 expression, also known as thymocyte differentiation antigen (Thy-1), was in general lower in WJ MSCs (XF: 20.2 ± 5.6%; STD: 38.6 ± 6.4%) than in BM MSCs (65.3%), varying among donors regardless of the condition of culture (i.e., 7.2% in donor #14 to 33.9% in donor #10 under XF conditions). A higher proportion of BM MSCs were positive for CD105, endoglin, (97.4%) than WJ MSCs. Although CD105+ cells varied amongst donors, it was found generally lower in WJ MSCs cultured under XF conditions (57.6 ± 4.3% in XF vs 80.28 ± 7.7 in STD). CD271, nerve growth factor receptor (NGFR) was detected only in a very small subpopulation of WJ MSCs (0.0–3.9%) regardless of culture conditions. MSCA-1, however, displays a curious pattern. Whereas this marker was barely detectable in BM MSCs (0.1%) and in WJ MSCs cultured under STD conditions (0.13 ± 0.1%), more than 13.5–38.8% of cells were positive under XF conditions. Donor #9 was an exception with only 4.4% MSCA-1+ cells under XF conditions. An unpaired two-tailed t-test was performed for statistical analyses (n = 4; *$p \leq 0.05$). All analyses on WJ MSCs presented here were performed at PD4–5 for each of donors. **(B)** MSCA-1 expression is induced by exposing WJ MSCs to XF conditions. WJ MSCs derived and expanded under STD condition (n = 2 donors) were exposed to XF condition for 14 days (STD–XF), which was sufficient to significantly induce an increase of the MSCA-1+ subpopulation from 0.1 to 0.9% in donor #12 and from 0 to 9.9% in donor #14.
BM: Bone marrow; MSC: Mesenchymal stem cell; STD: Standard; WJ: Wharton's jelly; XF: Xeno-free.

putative MSC markers. After primary culture, however, there were no significant differences between expression of MSC markers in cells isolated by enzymatic digestion and by explant isolation [21,22]. We found that stromal cells cultured on CellSTART-coated dishes in StemGro medium at 5% O_2 have unusually large MSCA-1$^+$ subpopulations, whereas the cells from the same donor derived and cultured under STD conditions (1% FCS/DMEM) had scarcely any. Interestingly, in BM MSCs, expression of MSCA-1 is restricted to CD271 bright population [5,6]. However, this is not the case with WJ MSCs where <5% of cells are CD271$^+$ across multiple donors and regardless of culture conditions (Figure 3A).

MSCA-1 epitope recognized by W8B2 antibody was shown to be identical to a tissue nonspecific alkaline phosphatase (TNAP) ectoenzyme expressed at high levels in liver, bone and kidney as well as in embryonic stem (ES) cells [3]. MSCA-1/TNAP is a repressor of NFκB-inducing kinase (NIK) activity and regulates both the classical and alternative NFκB-mediated signaling [22,23]. In general, alkaline phosphatases dephosphorylate various substrates implicated specifically in the promotion of inflammation and in such a way exhibit potent anti-inflammatory effects [23,24]. TNAP is also involved in skeletal and dental mineralization [24–27], as well as in the brain and activity-dependent neurodevelopmental processes including myelination and synaptogenesis [26,28–30]. Whether presence of large MSCA-1/TNAP$^+$ subpopulations in WJ MSCs might provide an additional benefit in MSC-based cellular therapy of inflammatory diseases such as graft vs host disease [25,27–29], or for development of novel cellular therapies for regeneration of skeletal damage, remains to be investigated.

Multiple factors can influence the behavior of cells *in vitro*. Indeed, mimicking the physical environment of the manipulated tissue *in vitro* may result in better outcomes in both clinical practice and for tissue engineering. For example, *in vitro* fertilization laboratories routinely manipulate human embryos under oxygen tension similar to that of the oviduct and uterine environments because the embryos cultured in low oxygen yield a better quality blastocyst and marked improvement in birth rate [30,31]. Similarly, exposure to sequential high-to-low humidity environments in an air/liquid interface culture mimicking transition from an aquatic environment (amniotic fluid) to the open air *post partum* was essential in generating human epidermal tissue with a normal epidermal permeability barrier equivalent to that of normal skin [32,33]. Hypoxic environments were also superior for long-term expansion of human adipose-derived stem cells [34], and a physiological oxygen environment has also been beneficial for WJ MSCs culture. Moreover, reducing the oxygen concentration from ambient to 5% O_2 increased significantly the yield of MSCs from WJ without affecting their capacity for osteogenic or chondrogenic differentiation [35,36]. Low oxygen also supported a more primitive phenotype of WJ MSCs, which was dependent on hypoxia-inducible factor [37,38].

Conclusion

Several protocols for isolation and scale-up of clinically compliant WJ MSCs have been published [27,39,40]. Our protocol is, however, the first one to combine chemically defined, animal product-free culture conditions with a low oxygen environment. Although it has been suggested that the low oxygen may support expression of pluripotency marker OCT4 [37], we could not confirm this finding under our culture conditions (data not shown). Further studies are needed to confirm the hypothesis that WJ MSCs isolated by this method might have an advantage in replacement of BM and AD MSCs for cellular therapy.

Future perspective

The best donors for allogeneic MSC-based cellular therapy are in the pediatric age range. Logistically, it is difficult to identify suitable child donors and the MSC therapy field is constantly looking for alternative sources. Among the various options, UC is clearly an obvious choice. UC cells are easily obtainable shortly after birth and therefore less likely to contain acquired,

Executive summary

Wharton's jelly mesenchymal stem cells isolated & grown under xeno-free conditions have capacity of multipotent stem cells

- Wharton's jelly (WJ) mesenchymal stem cells (MSCs) derived under defined conditions in low oxygen display adipo-, osteo- and chondro-genic potential typical for MSCs.

Immunomodulatory potential of WJ MSCs isolated & grown under defined xeno-free conditions

- Immunomodulatory potential of WJ MSCs isolated and grown under defined xeno-free conditions is similar to bone marrow MSCs.

Isolation & expansion of MSCA-1$^+$ subpopulation is dependent on culture conditions

- Derivation of WJ MSCs under defined conditions in low oxygen resulted in several folds higher populations of MSCA-1$^+$ cells that can be easily isolated/purified and further expanded.

potentially deleterious mutations that are contained in cells derived from adult tissues. We believe that over time, WJ MSCs will prevail as a source for the cellular therapy. Currently, MSCs used for cellular therapy are, in general, a mixed population of not well-characterized primary cells expanded under conditions that vary from laboratory to laboratory. We hope that our work highlights that the profile of surface markers on MSCs can be changed under different culture conditions and that, therefore, there is a need for standardization of MSCs used for cellular therapy.

Financial & competing interests disclosure

The study was supported by the studentship to H Badraiq from Saudi Arabia government and a studentship to DK Taheem from Orthopaedic Research UK. The authors have no other relevant affiliations or financial involvement with any organization or entity with a financial interest in or financial conflict with the subject matter or materials discussed in the manuscript. This includes employment, consultancies, honoraria, stock ownership or options, expert testimony, grants or patents received or pending, or royalties.

No writing assistance was utilized in the production of this manuscript.

Ethical conduct of research

The authors state that they have obtained appropriate institutional review board approval or have followed the principles outlined in the Declaration of Helsinki for all human or animal experimental investigations. In addition, for investigations involving human subjects, informed consent has been obtained from the participants involved.

References

Papers of special note have been highlighted as:
• of interest; •• of considerable interest

1 Friedenstein AJ, Chailakhjan RK, Lalykina KS. The development of fibroblast colonies in monolayer cultures of guinea-pig bone marrow and spleen cells. *Cell Tissue Kinet.* 3(4), 393–403 (1974).

2 Horwitz EM, Le Blanc K, Dominici M *et al.* Clarification of the nomenclature for MSC: The International Society for Cellular Therapy position statement. *Cytotherapy* 7(5), 393–395 (2005).

3 Jones EA, English A, Kinsey SE *et al.* Optimization of a flow cytometry-based protocol for detection and phenotypic characterization of multipotent mesenchymal stromal cells from human bone marrow. *Cytometry B Clin. Cytom.* 70(6), 391–399 (2006).

4 Sobiesiak M, Sivasubramaniyan K, Hermann C *et al.* The mesenchymal stem cell antigen MSCA-1 is identical to tissue non-specific alkaline phosphatase. *Stem Cells Dev.* 19(5), 669–677 (2010).

5 Bühring HJ, Treml S, Cerabona F, de Zwart P, Kanz L, Sobiesiak M. Phenotypic characterization of distinct human bone marrow-derived MSC subsets. *Ann. NY Acad. Sci.* 1176, 124–134 (2009).

6 Battula VL, Treml S, Bareiss PM *et al.* Isolation of functionally distinct mesenchymal stem cell subsets using antibodies against CD56, CD271, and mesenchymal stem cell antigen-1. *Haematologica* 94(2), 173–184 (2009).

7 Gronthos S, Fitter S, Diamond P, Simmons PJ, Itescu S, Zannettino AC. A novel monoclonal antibody (STRO-3) identifies an isoform of tissue nonspecific alkaline phosphatase expressed by multipotent bone marrow stromal stem cells. *Stem Cells Dev.* 16(6), 953–963 (2007).

•• **Describes MSCA-1 as a potential marker of mesenchymal stem cells, and a MSCA-1-specific antibody is the foundation on which Mesoblast built their business and grew into one of the biggest stem cell companies worldwide.**

8 Pikuła M, Marek-Trzonkowska N, Wardowska A, Renkielska A, Trzonkowski P. Adipose tissue-derived stem cells in clinical applications. *Expert Opin. Biol. Ther.* 13(10), 1357–1370 (2013).

9 Tran TT, Kahn CR. Transplantation of adipose tissue and stem cells: role in metabolism and disease. *Nat. Rev. Endocrinol.* 6(4), 195–213 (2010).

10 La Rocca G, Lo Iacono M, Corsello T, Corrao S, Farina F, Anzalone R. Human Wharton's jelly mesenchymal stem cells maintain the expression of key immunomodulatory molecules when subjected to osteogenic, adipogenic and chondrogenic differentiation *in vitro*: new perspectives for cellular therapy. *Curr. Stem Cell Res. Ther.* 8(1), 100–113 (2013).

11 Troyer DL, Weiss ML. Wharton's jelly-derived cells are a primitive stromal cell population. *Stem Cells* 26(3), 591–599 (2008).

12 Hass R, Kasper C, Böhm S, Jacobs R. Different populations and sources of human mesenchymal stem cells (MSC): a comparison of adult and neonatal tissue-derived MSC. *Cell Commun. Signal.* 14(9), 12 (2011).

13 Lo Iacono M, Anzalone R, Corrao S, Zummo G, Farina F, La Rocca G. Nonclassical type I HLAs and B7 costimulators revisited: analysis of expression and immunomodulatory role in undifferentiated and differentiated MSC isolated from human umbilical cord Wharton's jelly. *Histol. Histopathol.* 26(Suppl. 1), 313 (2011).

14 Weiss ML, Anderson C, Medicetty S *et al.* Immune properties of human umbilical cord Wharton's jelly-derived cells. *Stem Cells* 26(11), 2865–2874 (2008).

15 Sobolewski K, Bańkowski E, Chyczewski L, Jaworski S. Collagen and glycosaminoglycans of Wharton's jelly. *Biol. Neonate* 71(1), 11–21 (1997).

16 Corrao S, La Rocca G, Lo Iacono M, Corsello T, Farina F, Anzalone R. Umbilical cord revisited: from Wharton's jelly myofibroblasts to mesenchymal stem cells. *Histol Histopathol.* 28(10), 1235–1244 (2013).

17 De Kock J, Najar M, Bolleyn J *et al.* Mesoderm-derived stem cells: the link between the transcriptome and their differentiation potential. *Stem Cells Dev.* 21(18), 3309–3323 (2012).

18 Huang YC, Parolini O, La Rocca G, Deng L. Umbilical cord versus bone marrow-derived mesenchymal stromal cells. *Stem Cells Dev.* 21(15), 2900–2903 (2012).

19 Reinisch A, Strunk D. Isolation and animal serum free expansion of human umbilical cord derived mesenchymal stromal cells (MSCs) and endothelial colony forming progenitor cells (ECFCs). *J. Vis. Exp.* 32, 1525 (2009).

20 Marigo I, Dazzi F. The immunomodulatory properties of mesenchymal stem cells. *Semin. Immunopathol.* 33(6), 593–602 (2011).

21 Margossian T, Reppel L, Makdissy N, Stoltz JF, Bensoussan D, Huselstein C. Mesenchymal stem cells derived from Wharton's jelly: comparative phenotype analysis between tissue and *in vitro* expansion. *Biomed. Mater. Eng.* 22(4), 243–54 (2012).

22 Hu WH, Mo XM, Walters WM, Brambilla R, Bethea JR. TNAP, a novel repressor of NF-kappaB-inducing kinase, suppresses NF-kappaB activation. *J. Biol. Chem.* 279(34), 35975–35983 (2004).

23 Pike AF, Kramer NI, Blaauboer BJ, Seinen W, Brands R. A novel hypothesis for an alkaline phosphatase 'rescue' mechanism in the hepatic acute phase immune response. *Biochim. Biophys. Acta.* 1832(12), 2044–2056 (2013).

24 Hessle L, Johnson KA, Anderson HC *et al.* Tissue-nonspecific alkaline phosphatase and plasma cell membrane glycoprotein-1 are central antagonistic regulators of bone mineralization. *Proc. Natl Acad. Sci. USA* 99(14), 9445–9449 (2002).

25 Wennberg C, Hessle L, Lundberg P *et al.* Functional characterization of osteoblasts and osteoclasts from alkaline phosphatase knockout mice. *J. Bone Miner. Res.* 15(10), 1879–1888 (2000).

26 Hanics J, Barna J, Xiao J, Millán JL, Fonta C, Négyessy L. Ablation of TNAP function compromises myelination and synaptogenesis in the mouse brain. *Cell Tissue Res.* 349(2), 459–471 (2012).

27 Capelli C, Gotti E, Morigi M *et al.* Minimally manipulated whole human umbilical cord is a rich source of clinical-grade human mesenchymal stromal cells expanded in human platelet lysate. *Cytotherapy* 13(7), 786–801 (2011).

28 Fonta C, Negyessy L, Renaud L, Barone P. Postnatal development of alkaline phosphatase activity correlates with the maturation of neurotransmission in the cerebral cortex. *J. Comp. Neurol.* 486(2), 179–196 (2005).

29 Tisato V, Naresh K, Girdlestone J, Navarrete C, Dazzi F. Mesenchymal stem cells of cord blood origin are effective at preventing but not treating graft-versus-host disease. *Leukemia* 21(9), 1992–1999 (2007).

30 Noda Y, Goto Y, Umaoka Y, Shiotani M, Nakayama T, Mori T. Culture of human embryos in alpha modification of Eagle's medium under low oxygen tension and low illumination. *Fertil. Steril.* 62(5), 1022–1027 (1994).

31 Waldenström U, Engström AB, Hellberg D, Nilsson S. Low-oxygen compared with high-oxygen atmosphere in blastocyst culture, a prospective randomized study. *Fertil. Steril.* 91(6), 2461–2465 (2009).

32 Sun R, Celli A, Crumrine D *et al.* Lowered humidity produces human epidermalequivalents with enhanced barrier properties. *Tissue Eng. Part C Methods* doi:10.1089/ten.tec.2014.0065 (2014) (Epub ahead of print).

33 Petrova A, Celli A, Jacquet L *et al.* 3D *In vitro* model of a functional epidermalpermeability barrier from human embryonic stem cells and induced pluripotent stem cells.. *Stem Cell Reports* 2(5), 675–689 (2014).

34 Yang S, Pilgaard L, Chase LG *et al.* Defined xenogeneic-free and hypoxic environment provides superior conditions for long-term expansion of human adipose-derived stem cells. *Tissue Eng. Part C Methods* 18(8), 593–602 (2012).

35 López L, Seshareddy K, Trevino E, Cox J, Weiss ML. Evaluating the impact of oxygen concentration and plating density on human Wharton's jelly-derived mesenchymal stromal cells. *Open Tissue Eng. Regen. Med. J.* 4, 82–94 (2011).

36 Nekanti U, Dastidar S, Venugopal P, Totey S, Ta M. Increased proliferation and analysis of differential gene expression in human Wharton's jelly-derived mesenchymal stromal cells under hypoxia. *Int. J. Biol. Sci.* 6(5), 499–512 (2010).

• **Highlights the importance of mimicking physiological conditions as much as possible *in vitro*.**

37 Drela K, Sarnowska A, Siedlecka P *et al.* Low oxygen atmosphere facilitates proliferation and maintains undifferentiated state of umbilical cord mesenchymal stem cells in an hypoxia inducible factor-dependent manner. *Cytotherapy* 16(7), 881–892 (2014).

38 Lavrentieva A, Majore I, Kasper C, Hass R. Effects of hypoxic culture conditions on umbilical cord-derived human mesenchymal stem cells. *Cell Commun. Signal.* 16(8), 18 (2010).

39 Julavijitphong S, Wichitwiengrat S, Tirawanchai N, Ruangvutilert P, Vantanasiri C, Phermthai T. A xeno-free culture method that enhances Wharton's jelly mesenchymal stromal cell culture efficiency over traditional animal serum-supplemented cultures. *Cytotherapy* 16(5), 683–691 (2014).

40 Nekanti U, Mohanty L, Venugopal P, Balasubramanian S, Totey S, Ta M. Optimization and scale-up of Wharton's jelly-derived mesenchymal stem cells for clinical applications. *Stem Cell Res.* 5(3), 244–254 (2010).

Methods in Molecular Biology (2016) 1357: 33–44
DOI 10.1007/7651_2014_163

Published online: 06 August 2015

Sendai Virus-Based Reprogramming of Mesenchymal Stromal/Stem Cells from Umbilical Cord Wharton's Jelly into Induced Pluripotent Stem Cells

Cristian Miere, Liani Devito, and Dusko Ilic

Abstract

In an attempt to bring pluripotent stem cell biology closer to reaching its full potential, many groups have focused on improving reprogramming protocols over the past several years. The episomal modified Sendai virus-based vector has emerged as one of the most practical ones. Here we describe reprogramming of mesenchymal stromal/stem cells (MSC) derived from umbilical cord Wharton's Jelly into induced pluripotent stem cells (iPSC) using genome non-integrating Sendai virus-based vectors. The detailed protocols of iPSC colony cryopreservation (vitrification) and adaption to feeder-free culture conditions are also included.

Keywords: Umbilical cord, MSC, Sendai virus, Reprogramming, iPSC, Vitrification, Adaption to feeder-free culture conditions

1 Introduction

Since its emergence in 2006, reprogramming of somatic cells to pluripotency has revolutionized cell biology by opening new avenues and bypassing many hurdles researchers were struggling with. Significant progress has been made from basic research (1), drug development (2, 3), toxicity screening (4), and disease modeling (5, 6) to promise for cell therapy. The first patient with macular degeneration of retina has been treated with induced pluripotent stem cell (iPSC)-derived retinal pigment epithelium cells in September 2014, in the world's first iPSC clinical trial in Kobe, Japan.

The original proof-of-concept studies used retroviral transduction of four transcription factors, Oct4, Sox2, Klf-4, and c-Myc, later known as the Yamanaka factors, into human dermal fibroblasts (7). After several weeks in culture, colonies with embryonic stem cell (ESC)-like morphology and properties emerged in the culture dish. Known today as iPSC, these cells are the man-made equivalent to ESC. Much research has compared the two cell types (8), in an attempt to further pluripotent stem cell biology and to get closer to the promise of regenerative medicine. Several alternative methods

have been attempted to increase efficiency or bypass problems with the original protocol based on genome-integrating viral vectors and presence of c-Myc oncogene (reviewed in (9)).

The modified Sendai virus method (10) is based on a non-integrating vector that is also replication deficient, so that upon several passages, the newly derived iPSC lines become transgene-free. The reasons for choosing this method include a straightforward, not labor-intensive protocol, the non-integrating nature of the vector, low cytotoxicity elicited in culture, broad range of target cells accessible, and highly reproducible protocol.

The CytoTune®-iPS Sendai Reprogramming Kit (Life Technologies) contains four SeV-based reprogramming vectors, each encoding one of the four Yamanaka factors. The kit has been shown to reprogram several cell types, including human CD34+ cord blood cells (11), nasal epithelial cells (12), dermal fibroblasts (13, 14), peripheral blood mononuclear cells (15), and T-lymphocytes (16).

Mesenchymal stromal/stem cells (MSC) are multipotent stem cells, capable of differentiating into osteoblasts, chondrocytes, and adipocytes. In the human body exist multiple sources of MSC and the most frequently used for clinical applications are bone marrow MSC. They are also present in extraembryonic perinatal tissue, having been isolated from placenta, fetal membrane, Wharton's Jelly (WJ) umbilical cord, cord blood, and amniotic fluid (17). Routinely discarded after birth, these tissues do not pose any ethical problems and are readily available for processing (18).

The characteristics of MSCs include plastic adherence and expression of a set of surface markers including CD90, CD73, and CD105. Although MSCs have been harvested from multiple different tissues, recent evidence points toward different properties based on the tissue of origin. Due to their developmental stage, extraembryonic derived MSCs are considered to have a broader differentiation ability and faster proliferation rate than adult tissue-derived MSCs (19).

Due to their low immunogenicity, one of the main uses of WJ-MSCs could be allogeneic transplantation. The multipotency and immunomodulatory properties make them ideal candidates for this purpose. WJ-MSCs have been reported to be useful in cancer therapy, liver disease, cardiovascular disease, cartilage regeneration, and peripheral nerve repair (reviewed in (17)).

We have recently reported a protocol for derivation of WJ-MSCs under chemically defined (20) and xeno-free conditions (21). Here we describe in detail the reprogramming protocol of WJ-MSC into iPSC using the CytoTune Kit from Life Technologies.

2 Materials

2.1 Feeder Cells

Reprogramming-Qualified Newborn Foreskin Fibroblasts (NuFF; Global Stem, GSC-3006G) (*see* **Note 1**).

2.2 Equipment

1. 100-μl pipettman.
2. 1,000-μl pipettman.
3. Biosafety cabinet.
4. Hemocytometer (Hausser).
5. Phase contrast microscope.
6. Pipette gun.
7. Tissue culture incubator.
8. Tube rack.

2.3 Plasticware and Other Disposables (See Note 2)

1. 75-cm^2 Flask (Corning; Cat. No.430641).
2. Six-well culture plate (Costar-VWR; Cat. No. 734-1596).
3. P60 (60-mm) TC-Treated Culture Dish (Corning; Cat. No. 430166).
4. Open pulled straws for vitrification (MTR; Cat. No. 19050/0050).
5. 0.22-μM syringe filter (VWR; Cat. No. 6896-2502).
6. Four-well dish (Nunc; Cat. No. 1256572).
7. 5-ml cryogenic vial (Nalgene; Cat. No. 5000-0050).
8. 100-μl Filter tips (SLS; Cat. No. 171403).
9. 1,000-μl Filter tips (SLS; Cat. No. 171703).
10. γ-Irradiated individually wrapped polystyrene 5-ml pipettes (Falcon; Cat. No. 357543).
11. γ-Irradiated individually wrapped polystyrene 10-ml pipettes (Falcon; Cat. No. 357551).
12. γ-Irradiated individually wrapped polystyrene 25-ml pipettes (Falcon; Cat. No. 357525).
13. γ-Irradiated 15-ml conical tube (BD Falcon; Cat. No. 352096).
14. Cryotube (Thermo Scientific; Cat No. 377224).
15. Waste container.

2.4 Reagents and Media

1. EmbryoMax® 0.1 % Gelatin Solution (Millipore; Cat. No. ES-006-B).

2. Pluriton™ Reprogramming Medium (Stemgent; Cat. No. 00-700).
3. Recombinant Human Fibroblast Growth Factor (FGF) basic (146 aa) (R&D Systems; Cat. No. 233-FB-025).
4. DMEM, high glucose, Glutamax™, pyruvate (Life Technologies; Cat. No. 31966-021).
5. MEM Non-Essential Amino Acid Solution (100×) (Life Technologies; Cat. No. 11140-035).
6. Fetal Bovine Serum, ES Cell Qualified (Life Technologies; Cat. No. 16141-079).
7. CytoTune®-iPS Sendai Reprogramming Kit (Life Technologies; Cat. No. A1378001).
8. DPBS, Ca^{2+}/Mg^{2+}-free (Life Technologies; Cat. No. 14190).
9. CTS™ TrypLE™ Select (Life Technologies; Cat. No. 12859-01).
10. KnockOut DMEM/F12 (Life Technologies; Cat. No. 12660-012).
11. KnockOut™ Serum replacement (KOSR) (Life Technologies; Cat. No. 10828010).
12. HEPES 1 M Buffer Solution (Life Technologies; Cat. No. 15630-056).
13. Sucrose (Sigma; Cat. No. S0389).
14. Ethylene glycol (Sigma; Cat. No. 10246-6).
15. Dimethyl sulfoxide (DMSO) (VWR; Cat. No. 23500.26).
16. Ethanol, absolute (Sigma; Cat. No. E7023).
17. Rock inhibitor Y-27632 (Sigma; Cat. No. Y0503).
18. Growth Factor Reduced (GFR) Matrigel (BD Biosciences; Cat. No. 354239).
19. PBS-EDTA (Lonza; Cat. No. BE02-017F).
20. TeSR™-E8™ basal medium (STEMCELL Technologies; Cat. No. 05941).
21. TeSR™-E8™ supplement (STEMCELL Technologies; Cat. No. 05942).
22. Alkaline Phosphatase Staining Kit II (Stemgent; Cat. No. 00-0055).
23. ReadyMix™ Taq PCR Reaction Mix (Sigma; Cat. No. P4600).
24. HyperLadder™ 100 bp (BioLine; Cat. No. BIO-33056).
25. Agarose (Life Technologies; Cat. No. 16500).
26. CryoStor CS10 (STEMCELL Technologies; Cat. No. A10142-01).

3 Methods

3.1 Conditioning Medium

1. Coat one T75 flask with 5 ml of 0.1 % Gelatin Solution for 1 h at 37 °C.
2. Plate 3–4 × 10^6 NuFF in 30 ml DMEM supplemented with 5 % FBS for 24 h. Wash the cells thoroughly 3–5x with DMEM without FBS before adding Pluriton medium supplemented with 4 ng/ml bFGF.
3. Change Pluriton medium supplemented with 4 ng/ml bFGF daily for 7–10 days. Keep spent medium at +4 °C.
4. The last day of conditioning, Pool all spent medium and pass through a 0.22-μm filter; aliquot the Pluriton-conditioned medium.
5. Aliquots are kept at −20 °C and should be used within Pluriton expiry date.

3.2 Reprogramming

Day: −2

6. Coat desired number of wells of a six-well plate dish with 0.1 % Gelatin Solution, 1 ml per well, for 1 h at 37 °C.
7. Plate MSC at several different densities (i.e., 1.5, 2.0, 2.5 × 10^5 cells/well) in 2 ml of DMEM high glucose, with Glutamax and pyruvate, supplemented with 10 % FCS and 1× Non-Essential Amino Acids.

Day: −1

8. Change medium.

Day 0

9. Choose 70 % confluent well for reprogramming. The cells from other wells can be collected and snap frozen as cell pellets serving as a negative control in Sendai virus detection RT-PCR later (Section 3.6).
10. Transduce the cells with Sendai virus encoding reprogramming factors at an multiplicity of infection (M.O.I.) of 3 per cell according to the certificate of analysis (*see* **Note 3**). Follow the manufacturer's protocol step by step exactly.

Day: 1–7

11. Refresh medium on a daily basis. High cell death is normal (*see* **Note 4**).

Day: 5

12. Coat with 2 ml of 0.1 % Gelatin Solution, for 1 h at 37 °C, two P60 culture dishes for each well of the six-well dish undergoing reprogramming.

13. Plate 3×10^5 NuFF feeders per P60 in 5 ml of DMEM high glucose, with Glutamax and pyruvate, supplemented with 10 % FCS and 1× Non-Essential Amino Acids.

Day: 7

14. Wash cells undergoing reprogramming with 3 ml of DPBS (Ca^{2+}/Mg^{2+}-free) and incubate in 1 ml TrypLE for 3–5 min at 37 °C. TrypLE is then diluted with 11 ml of pre-warmed DMEM. Mix well and separate cells into three tubes, 4 ml each. Centrifuge the cells at 1,200 rpm for 5 min.
15. Resuspend the cell pellet in 5 ml of conditioned Pluriton medium in each of two tubes and plate cell suspension from one tube into one P60 with NuFF feeders (*see* **Note 5**).
16. Remove supernatant from the third tube and snap freeze cell pellet. This will be your positive control in Sendai virus detection RT-PCR later (Section 3.6)

Day: 8–28

17. Exchange medium daily and allow iPSC colonies to grow and expand in culture.

Day: 18 (*see* **Note 6**)

18. Coat the vessel with 5 ml of 0.1 % Gelatin Solution for 1 h at 37 °C.
19. Plate 2×10^4 NuFF feeders per each well in 0.5 ml of DMEM high glucose, with Glutamax and pyruvate, supplemented with 10 % FCS and 1× Non-Essential Amino Acids.
20. Refresh culture medium every 2–3 days.

Day: 21–28

21. Primary iPSC colonies from one of two P60 dishes with the most uniform and compact cells are manually picked (*see* **Note 7**) and passaged onto NuFF feeder cells in 0.5 ml Pluriton (*see* **Note 8**).
22. The second P60 dish is used for assessing reprogramming efficiency.
23. Collect the cells from the third P60 dish and snap-freeze the cell pellets; use them as a positive control.

3.3 Cryopreservation (Vitrification) and Thawing of Vitrified Colonies

iPSCs cultured on feeder cells were cryopreserved in pieces of about 100–200 cells using the open pulled straw (OPS) vitrification method (22–24).

For vitrification you have to have prepared the following solutions:

ES-HEPES solution

Component	Volume (ml)
KnockOut™ DMEM/F12	15.6
KnockOut™ SR (KOSR)	4.0
HEPES 1 M buffer solution	0.4
	20.0

Mix the components, filter through a 0.22-μM syringe filter and store at 4 °C for up to 7 days.

1 M sucrose solution

1. Mix 3.42 g of sucrose with 6.0 ml ES-HEPES in a 15-ml centrifuge tube and place in the incubator at 37 °C.
2. When the sucrose had fully dissolved, add 2.0 ml of ES-HEPES and 2.0 ml KOSR. Mix well by flipping the tube.
3. Filter the solution through a 0.22-μM syringe filter and store at 4 °C for up to 7 days.

10 % vitrification solution (VS1)

Component	Volume (ml)
ES-HEPES	2.00
Ethylene glycol	0.25
Dimethyl sulfoxide	0.25
	2.50

Mix the components and store at 4 °C for up to 7 days.

20 % vitrification solution (VS2)

Component	Volume (ml)
ES-HEPES	0.75
1 M sucrose	0.75
Ethylene glycol	0.50
Dimethyl sulfoxide	0.50
	2.50

Mix the components and store at 4 °C for up to 7 days.

The procedure goes as follows:

1. Submerge straws in 70 % ethanol for at least 20 min and then allow them to dry in biosafety cabinet.

2. Label a 5-ml cryogenic vial with the cell line identification code, passage number, and the date of freezing, remove the top, and place in a cane. Place the cane into a container with liquid N_2, ensuring that the 5-ml cryogenic vial and most of the cane are submerged.
3. Place 500 μl of ES-HEPES in well #1 of four-well dish, CS1 in well #2, and VS2 in well #3. The well #4 remains empty.
4. Equilibrate the dish in the incubator at 37 °C for 10–15 min.
5. Place the dish in the biosafety cabinet and invert the lid.
6. Place several 30–40 μl drops of each VS1 and VS2 on the inner surface of the inverted lid of the four-well dish in two separate areas.
7. Cut the colonies to be vitrified with a 21 G syringe needle, generating a grid-like pattern, which ensures evenly sized pieces.
8. Detach the pieces from the dish by gentle scraping with the tip of a 200-μl micropipette
9. Transfer the detached pieces into well 1 containing ES-HEPES using a pipette tip primed with ES-HEPES solution.
10. Set timer for 1 min 25 s (*see* **Note 9**). Immediately transfer 4–8 pieces to one of VS1 drops on the lid.
11. When timer reaches 25 s, transfer them to VS2 using a pipette tip primed with VS2 solution.
12. When timer reaches 0, aspirate the pieces into a narrow end of the straw.
13. Hold the straw horizontally with a forceps and dip quickly into liquid N_2 for several seconds and then place into a 5-ml cryogenic vial (*see* **Note 10**).
14. Repeat the procedure until no pieces are left in the well #1.
15. Put lid on the 5-ml cryogenic vial and transfer into dewer with liquid N_2 for extended storage.

Thawing of the vitrified cells:

1. To thaw vitrified cells, you have to have ready four-well dishes with feeder cells (*see* Section 3.2, steps 17–21). A day before thawing replace feeder medium with Pluriton (*see* **Note 8**).
2. Just before thawing, add into the 24-h conditioned medium on feeders Rock inhibitor Y-27632 in a final concentration of 10 μM. Mix well.
3. Place 500 μl of DMEM into each of two wells of four-well dish.
4. Take straw to be thawed form the liquid N2 and place the tip directly into well 1 to release frozen pieces.
5. After 30 s, transfer the pieces into well 2.
6. After 5 min, transfer the cells into well with feeders.

7. Two days later, refresh the medium. There is no need for adding Y-27632.

3.4 Adapting iPSC to Feeder-Free Conditions

1. Thaw GFR-Matrigel stock overnight at 4 °C (*see* **Note 11**).
2. Check for the presence of any gel formation. If there were no visible clumps, GFR-Matrigel stock dilute to a final concentration of 0.34 mg/ml with cold DMEM.
3. Coat one well of a six-well plate with 750 μl of GFR-Matrigel working solution per well for 1 h at 37 °C.
4. Remove the GFR-Matrigel and replace with DMEM until use (*see* **Note 12**).
5. Rinse three to four wells of the iPSC cultured on feeders with 500 μl PBS-EDTA.
6. Incubate the cells with 500 μl PBS-EDTA per well for 3–5 min at 37 °C.
7. When the edges of the colonies visibly detach from the substrate (keep checking under the microscope), remove all PBS-EDTA.
8. Add 500 μl of complete TeSR-E8 supplemented with 10 μM Y-27632 and detach cells by pipetting up and down.
9. Transfer the suspension from all wells of the same cell line into one well of a six-well plate pre-coated with GFR-Matrigel.
10. Rinse the four-well dish wells with another 500 μl of medium and transfer into the same six-well plate well.
11. The following day change the culture medium with complete TeSR-E8 without Y-27632.
12. Passage cells using PBS-EDTA, by adjusting the volumes according to the volume of the plate being used (*see* **Note 13**).

3.5 Assessing Reprogramming Efficiency

We assess reprogramming approximately 20 days after passaging on NuFF feeder cells. Leaving the emerging colonies too long will lead to merger of some of them and will have a negative impact on the efficiency rate observed. We use Alkaline Phosphatase Staining Kit II and follow the manufacturer's recommendation. We count colonies using OpenCFU software.

3.6 Sendai Virus Detection PCR

1. In our experience Sendai virus becomes undetectable in 100 days of continuous cell culture since viral transduction on day 0 of reprogramming. Collect cells at day 100. Extract RNA with any commercially available column-based kit or alternative methods; perform reverse-transcription using any of kits suitable for nanogram-range of RNA. Negative control: non-transduced cells (Section 3.2, step 9); positive control: transduced cells 7 day post transduction (Section 3.2, step 16).

2. Perform end-point PCR with 5 μl of cDNA in 50 μl Ready-Mix™ Taq PCR Reaction Mix.
3. Use the following primers to detect for the presence of Sendai virus vector (10):

β-Actin forward	CAA CCG CGA GAA GAT GAC
β-Actin reverse	AGG AAG GCT GGA AGA GTG
Sendai virus forward	GGA TCA CTA GGT GAT ATC GAG C
Sendai virus reverse	ACC AGA CAA GAG TTT AAG AGA TAT GTA TC

4. Cycling conditions: One cycle of 95 °C for 5 min, [95 °C 30 s, 55 °C 30 s, 72 °C 30 s] for 35 cycles, and one cycle of 72 °C for 5 min.
5. Analyze PCR products on 2 % agarose gel. To determine size of the product, we used 100 bp molecular weight ladder.
6. The expected size of the PCR product is 181 bp for SeV and 455 bp for β-actin.

4 Notes

1. Reprogramming efficiency depends also on quality of the feeders. It is important to choose reprogramming-qualified feeder cells.
2. Disposable culture and plasticware of the equivalent quality can be purchased from different manufacturers without altering the outcome of the procedure.
3. Viral titer varies from vector to vector and from batch to batch of the CytoTune kit. You will have to calculate for each vector independently, the specific volume to add per well.
4. Highest cytotoxicity is observed 48–72 h post transduction.
5. Before plating the cells, wash feeders 2× with DMEM/F12 to remove traces of the FBS.
6. This step does not have to be done exactly at day 18. It could be done a day or two earlier or later, depending on other workload. The main point is that it has to pass 72 h from the plating before the feeders could be used. The dishes with feeders should be used within the maximum of 7–10 days after plating.
7. Dissecting and picking colonies could be done with different tools (needle, Pasteur pipette, loading tip for Western blotting), it depends on personal preferences. Important: change tools between colonies.

8. For this step, we also validated NutriStem™ (Stemgent, Cat. No. 01-005), TeSR™-E8™ with its supplement, and KnockOut DMEM/F12 (Life Technologies, Cat No 10829-018) with its supplement (Life Technologies, Cat No 10828-028).
9. It is essential to do this process quickly, following indicated timing.
10. Do not take the straw out of liquid N_2 while doing that.
11. Work on ice. Precool tubes, pipettes, and tips.
12. Do not let GFR-Matrigel dry or results may vary. Just before use, remove DMEM and plate cells.
13. iPSCs adapted to feeder-free conditions do not require vitrification. They can be treated as any other adherent cells. We cryopreserve them in CryoStor CS10 following the manufacturer's protocol.

Acknowledgments

The study was supported by the studentship to C.M. from the Medical Research Council, UK.

References

1. Loh YH, Yang L, Yang JC et al (2011) Genomic approaches to deconstruct pluripotency. Annu Rev Genomics Hum Genet 12:165–185
2. Inoue H, Yamanaka S (2011) The use of induced pluripotent stem cells in drug development. Clin Pharmacol Ther 89:655–661
3. Egawa N, Kitaoka S, Tsukita K et al (2012) Drug screening for ALS using patient-specific induced pluripotent stem cells. Sci Transl Med 4:145ra104
4. Hou Z, Zhang J, Schwartz MP et al (2013) A human pluripotent stem cell platform for assessing developmental neural toxicity screening. Stem Cell Res Ther 4(Suppl 1):S12
5. Paşca SP, Portmann T, Voineagu I et al (2011) Using iPSC-derived neurons to uncover cellular phenotypes associated with Timothy syndrome. Nat Med 17:1657–1662
6. Miller JD, Ganat YM, Kishinevsky S et al (2013) Human iPSC-based modeling of late-onset disease via progerin-induced aging. Cell Stem Cell 13:691–705
7. Takahashi K, Tanabe K, Ohnuki M et al (2007) Induction of pluripotent stem cells from adult human fibroblasts by defined factors. Cell 131:861–872
8. Narsinh KH, Plews J, Wu JC (2011) Comparison of human induced pluripotent and embryonic stem cells: fraternal or identical twins? Mol Ther 19:635–638
9. Malik N, Rao M (2013) A review of the methods for human iPSC derivation. Methods Mol Biol 997:23–33
10. Fusaki N, Ban H, Nishiyama A (2009) Efficient induction of transgene-free human pluripotent stem cells using a vector based on Sendai virus, an RNA virus that does not integrate into the host genome. Proc Jpn Acad Ser B Phys Biol Sci 85:348–362
11. Nishishita N, Shikamura M, Takenaka C et al (2012) Generation of virus-free induced pluripotent stem cell clones on a synthetic matrix via a single cell subcloning in the naïve state. PLoS One 7(6):e38389
12. Ono M, Hamada Y, Horiuchi Y et al (2012) Generation of induced pluripotent stem cells from human nasal epithelial cells using a Sendai virus vector. PLoS One 7:e42855
13. Kudva YC, Ohmine S, Greder LV et al (2012) Transgene-free disease-specific induced pluripotent stem cells from patients with type 1 and type 2 diabetes. Stem Cells Transl Med 1:451–461

14. Jin ZB, Okamoto S, Xiang P et al (2012) Integration-free induced pluripotent stem cells derived from retinitis pigmentosa patient for disease modeling
15. Merling RK, Sweeney CL, Choi U et al (2013) Transgene-free iPSCs generated from small volume peripheral blood nonmobilized CD34 + cells. Blood 121:e98–e107
16. Wakao H, Yoshikiyo K, Koshimizu U et al (2013) Expansion of functional human mucosal-associated invariant T cells via reprogramming to pluripotency and redifferentiation. Cell Stem Cell 12:546–558
17. Kim DW, Staples M, Shinozuka K et al (2013) Wharton's Jelly-derived mesenchymal stem cells: phenotypic characterization and optimizing their therapeutic potential for clinical applications. Int J Mol Sci 14:11692–11712
18. Marcus AJ, Woodbury D (2008) Fetal stem cells from extra-embryonic tissues: do not discard. J Cell Mol Med 12(3):730–742
19. Pappa KI, Anagnou NP (2009) Novel sources of fetal stem cells: where do they fit on the developmental continuum? Regen Med 4:423–433
20. Badraiq H, Devito L, Ilic D (2014) Isolation and expansion of mesenchymal stromal/stem cells from umbilical cord under chemically defined conditions. Methods Mol Biol [Epub ahead of print]
21. Devito L, Badraiq H, Galleu A et al (2014) Wharton's Jelly MSC derived under chemically defined animal product-free low oxygen conditions are rich in MSCA-1+ subpopulation. Regen Med (in press)
22. Reubinoff BE, Pera MF, Vajta G et al (2001) Effective cryopreservation of human embryonic stem cells by the open pulled straw vitrification method. Hum Reprod 16:2187–2194
23. Ilic D, Stephenson E, Wood V et al (2012) Derivation and feeder-free propagation of human embryonic stem cells under xeno-free conditions. Cytotherapy 14:122–128
24. Stephenson E, Jacquet L, Miere C et al (2012) Derivation and propagation of human embryonic stem cell lines from frozen embryos in an animal product-free environment. Nat Protoc 7:1366–1381

British Medical Bulletin, 2015, **116**:19–27
doi: 10.1093/bmb/ldv045
Advance Access Publication Date: 17 November 2015

Human embryonic and induced pluripotent stem cells in clinical trials

Dusko Ilic[†,*], Liani Devito[†], Cristian Miere[†], and Stefano Codognotto[‡]

[†]Stem Cell Laboratories, Guy's Assisted Conception Unit, Division of Women's Health, Faculty of Life Sciences and Medicine, King's College London, London, UK, and [‡]ST8Biologics, London, UK

*Correspondence address: Assisted Conception Unit, 11th Floor Tower Wing, Guy's Hospital, London SE1 9RT, UK. E-mail: dusko.ilic@kcl.ac.uk

Accepted 6 October 2015

Abstract

Background: Human embryonic and induced pluripotent stem cells (hESC and hiPSC) have tremendous potential for clinical implementation. In spite of all hurdles and controversy, clinical trials in treatment of spinal cord injury, macular degeneration of retina, type 1 diabetes and heart failure are already ongoing.

Sources of data: ClinicalTrials.gov database, International Clinical Trials Registry Platform, PubMed and press releases and websites of companies and institutions working on hESC- and iPSC-based cellular therapy.

Areas of agreement: The initial results from multiple clinical trials demonstrate that hESC-based therapies are safe and promising.

Areas of controversy: Are iPSC cells safe in the clinical application? Is there a room for both hESC and iPSC in the future clinical applications?

Growing points: Increasing number of new clinical trials.

Areas timely for developing research: Development of hESC- and/or iPSC-based cellular therapy for other diseases.

Key words: human embryonic stem cells (hESC), human induced pluripotent stem cells (hiPSC), macular degeneration, spinal cord injury, diabetes, heart repair

Introduction

Since they were isolated for the first time,[1] human embryonic stem cells (hESC) remain at the centre of controversy. Whereas scientists clearly have seen their potential in the treatment of debilitating disease, the regulators and public became widely divided, from

being very supportive to seeking a regulatory ban on hESC research. In spite of all the obstacles, the hESC-based therapies moved to clinical trials very quickly. Only 12 years later, the first patient has been treated with hESC-based cellular therapy. Just to remind you, the first antibody was commercially produced in 1978, and the first antibody-based treatment was approved in 1998. It took 20 years to reach that step and we knew a lot of about antibodies already. About hESC we did not know anything. 'The new kid on the block', human induced pluripotent stem cells (hiPSC) seemed to hold even more potential than hESC.[2–4]

The review article is aiming to provide an overview of the studies conducted in human subjects using hESC- or iPSC-based cellular therapies in treatment of diseases (Table 1).

Spinal cord injury

Geron

Geron (CA, USA; www.geron.com) is considered to be the pioneer in the business of hESC and regenerative medicine. For years Geron opened new areas of research and development and took a lead in bringing hESC towards therapeutic application. The company exclusively licensed fundamental hESC-related patents from Wisconsin Alumni Research Foundation and learned how to manufacture several different types of functional cells derived from hESC. In collaboration with researchers at the University of California, Irvine, Geron had shown that in animal models hESC-derived oligodendrocyte progenitor cells (GRNOPC1) could improve functional locomotor behaviour after implantation in the injury site 7 days after injury. Histological analysis also provided evidence for the engraftment and function of these cells.[5] The reliability and reproducibility of their differentiation protocols for these specific hESC-derived GRNOPC1 cells were probably behind the decision to embark on a risky task: repair of spinal cord injury.

After the completion of extensive animal toxicology testing, including 24 separate studies in rats and mice, that required more than five billion GRNOPC1 cells, Geron filed a 21 000 page Investigational New Drug (IND) application with the FDA containing data from the animal and *in vitro* testing of the cells to ensure the highest possible degree of

Table 1 Ongoing clinical trials with hESC and iPSC

Indication	Cell source	Institution	Country	Start date	Finish date	Subjects
Spinal cord injury	hESC	Geron	USA	October 2010	July 2013	5
		Asterias	USA	March 2015	June 2018	13
Immunotherapy vaccine for lung cancer	hESC	Asterias	UK	Not defined	Not defined	Not defined
Geographic atrophy secondary to myopic macular degeneration	hESC	Ocata	USA	April 2014	April 2015	Not defined
Stargardt macular degeneration of retina	hESC	Ocata	USA	July 2012	December 2030	13
			UK	November 2011	December 2015	16
Dry macular degeneration of retina	hESC	Ocata	USA	July 2012	December 2030	13
		Cell Cure Neurosciences	Israel	April 2015	August 2017	15
	iPSC	RIKEN CBD	Japan	October 2013	Not defined	6
Wet macular degeneration of retina	hESC	The London Project to Cure Blindness	UK	August 2015	October 2016	10
Diabetes type I	hESC	ViaCyte	USA	September 2014	August 2017	40
Heart failure	hESC	APHP	France	June 2013	June 2017	6

safety of the product before initiating human clinical trials. In January 2009, Geron received FDA clearance to begin the world's first human clinical trial of a hES cell-based therapy. On news of the FDA approval, stocks jumped from $4.81 to $8.05 (68%). However, a few weeks later, when the company realized that its worldwide license for its stem cell technology was not valid in Europe, shares plummeted 16.7%, from $1.30 down to $6.47 in midday trading in New York. The same month a group in Israel reported that following neural stem cell transplantation in Russia, the unexpected development of a multifocal brain tumour in the recipient. Although this was nothing to do with Geron's trial, it caused their stock value to drop further.[6] In August 2009 Geron announced that its IND had been placed on clinical hold by the FDA pending the agency's review of new nonclinical animal study data submitted by the company. In this study, the injected animals developed a higher frequency of microscopic cysts in the regenerating injury site. A year later, on July 30, 2010, the FDA notified the company that the clinical hold had been lifted and the Phase I clinical trial of GRNOPC1 in patients with acute spinal cord injury could proceed.

The first patient was treated at the Shepherd Center in Atlanta in October 2010. Data on the first two patients with neurologically complete American Spinal Injury Association (ASIA) impairment scale grade A thoracic spinal cord injuries were presented at the two conferences in June 2011. According to Geron's press release, these patients received GRNOPC1 at a dose of 2 million cells, 7–14 days post-injury, delivered by injection into the lesion site between T3 and T10, using a specially designed syringe-positioning device. None had either surgical complication during or after procedure, nor adverse events related to the injection procedures or to GRNOPC1. Low-dose tacrolimus was given for temporary immune suppression from the time of injection for 46 days, at which point the dose was tapered and withdrawn completely at 60 days. Initial analyses showed no evidence of immune responses to GRNOPC1 through until Day 90, which includes the 30-day period after complete withdrawal of immune-suppression. There was also no evidence of cavitation in the spinal cord at the injury site on MRI through until Day 180. Following this report, Geron received clearance from the FDA to expand eligibility criteria to include patients with injuries down to T11. In addition, the FDA approved that the current 30-day period between subjects in the trial could be reduced to 10 days. In October 2011, safety data on four patients presented at two symposia showed that the results were fulfilling all expectations.

So, why then was Geron switching gears and closed the promising GRNOPC1 clinical trial only a month later, in November 2011, and ostensibly giving up on their stem cell programme, which was one of the most innovative in the world? The answer is simple: money. Although the prime goal of the clinical trial was safety, public expectations were driven by a Geron's short movie of a rat with a spinal cord injury that could walk after being treated with GRNOPC1. No matter how many times the Company emphasized that their trial was specifically only about safety, almost everyone expected that the treated patients would walk shortly after the GRNOPC1 injection. Of course, this did not happen and Geron's stock started to slide. With each new patient enrolled and each day that passed it became clear that there would be no miracle, and from January till September 2011 shares dropped nearly 60%.

As a medium size enterprise, Geron did not have readily available resources to bring a potential drug from bench to bedside. For example, they conducted in total 28 animal studies, involving >3500 rodents and pigs. In the recent economic climate, without government or Big Pharma wading in to help cope with enormous regulatory and manufacturing costs, small and medium enterprises are incapable of bringing a new drug to market. The fact that even if injection of GRNOPC1 cells could make people walk, the costs would leave no room for profit, did not help Geron's case. In order to survive, lack of investment and support forced the company to do the only sensible thing: temporarily close their stem cell programme. Their action has brought to light ethical and social questions about prematurely ended trials and compromising the contract between participants and trial sponsor.[7]

In total, they treated five patients 21–32 year-old, four males and one female. All participants received 2×10^6 GRNOPC1 cells within 2 weeks of injury. None of them developed antibodies or cellular immune response to GRNOPC1 through a year post treatment even though some had complete HLA mismatch with GRNOPC1; the closes match was 5 out of 10 alleles. The treatment *per se* caused no serious adverse events. However, no motor or sensory neurological changes were observed.

Asterias

In January 2013, Geron entered into Asset Contribution Agreement with BioTime (CA, USA; www.biotimeinc.com) and its subsidiary Asterias Biotherapeutics (http://asteriasbiotherapeutics.com). The transactions were closed 10 months later with Geron contributing to Asterias both intellectual property and tangible assets related to its discontinued hESC programmes. Asterias received multiple lots of OPC1 cells used in the clinical trial as well as multiple lots of hESC manufacturing cell banks from which additional lots of OPC1 cells could be made.

In May 2014, Asterias received USD 14.3 million as a strategic partnership award from the California Institute for Regenerative Medicine (CIRM) to reinitiate clinical development of hESC-derived OPC1 cells, now renamed AST-OPC1, in a dose-escalating trial. Additional USD 13 million was raised shortly after in an equity financing. With enough money on the account and a green light from the US FDA, Asterias has initiated a Phase 1/2a open-label, single-arm dose-escalation clinical trial and the first patient was treated in Atlanta in June 2015. With the third patient treated in Chicago in August 2015, the trial finalized initial low-dose (2×10^6 cells) safety cohort. The study, conducted at a total of up to eight centres in the United States, will test three sequential escalating doses with highest being 20×10^6 cells. The AST-OPC1cells will be administered in 13 patients with sub-acute, C-5 to C-7, neurologically complete cervical spinal cord injury. These patients are quadriplegic, have lost all sensation and movement below their injury site. AST-OPC1 will be administered 14–30 days post-injury. Additional information on this study, including trial sites, can be found at www.clinicaltrials.gov (ID: NCT02302157) and at the SCiStar Study Website www.scistarstudy.com

Immunotherapy vaccine for lung cancer

In addition to OPC1 and spinal cord injury, Geron contributed to Asterias all the documents related to antigen-presenting dendritic cells GRNVAC1 and GRNVAC2. GRNVAC2, now called AST-VAC2, is hESC-derived cancer vaccine designed to stimulate patients' immune systems to attack telomerase, a protein that is expressed in majority of cancers but is rarely expressed in normal adult cells (http://www.businesswire.com/news/home/20140911006326/en/BioTime-Subsidiary-Asterias-Biotherapeutics-Cancer-Research-UK#.VbR2Y3iyXTR). The vaccine was developed following successful early phase clinical trials of a similar, autologous vaccine GRNVAC1, now called AST-VAC1. GRNVAC1 were autologous mature dendritic cells transfected with mRNA encoding human telomerase reverse transcriptase (hTERT) and a portion of the lysosome-associated membrane protein LAMP-1. Dendritic cell-based telomerase immunotherapy GRNVAC1 showed telomerase-specific immune responses in 55% of acute myeloid leukaemia and 95% of prostate cancer patients. In September 2014, Asterias teamed up with the UK charity Cancer Research UK and its development and commercialization arm Cancer Research Technology to bring AST-VAC2 into clinical trials in patients with non-small lung cancer.

Macular degeneration of retina

Ocata (former Advanced Cell Technologies)

Ocata Therapeutics (MA, USA; https://www.ocata.com) reported derivation of retinal pigment epithelial (RPE) cells from hESC more than 10 years ago.[8] At that time, the report did not catch much attention and nobody could predict that this would be actually the seminal paper for what is today considered the first hESC-based therapy that successfully demonstrated clinical benefits in clinical trials.[9–11] Two years later, the group showed reproducible generation

of RPE cells from 18 different hESC lines.[12,13] Furthermore, RPE cells derived from one of the hESC lines were tested in animal model of retinal disease—the Royal College of Surgeons rat, in which photoreceptor loss is caused by a defect in the adjacent retinal pigment epithelium. The improvement in visual performance of treated rats was stunning and in November 2009, the company filed an IND with the US FDA to treat patients with Stargardt's macular dystrophy. The US FDA cleared application a year later, in November 2010. The IND to treat dry age-related macular degeneration (AMD), was cleared by the FDA in January 2011. Shortly after, in July 2011, the first two patients, a 77-year-old woman with dry AMD and a 27-year-old woman with Stargardt's macular dystrophy were enrolled at the Jules Stein Eye Institute at the University of California, Los Angeles, and about 50 000 RPE cells were administered into one eye of each patient. Additional information on these studies can be found at www.clinicaltrials.gov (ID: NCT01344993, NCT01345006).

About the same time, in June 2011, EMEA granted orphan medicinal product designation to their hESC-derived RPE cells and in January 2012, the first European patient suffering from Stargardt's macular degeneration was treated at the Moorfields Eye Hospital in London. Additional information on this study can be found at www.clinicaltrials.gov (ID: NCT01469832).

Each of the three studies will enrol 16 patients in five cohorts: four low vision cohorts will contain three patients each, whereas one better vision cohort will contain four patients. In the low vision cohorts, the patients will be transplanted with 50 000 (cohort 1), 100 000 (cohort 2), 150 000 (cohort 3) or 200 000 (cohort 4) hESC-derived RPE cells, whereas the cohort with better vision patients (cohort 2a) was transplanted with 100 000 cells. Each cohort will be enrolled sequentially, with the exception of the better vision cohort, which may be enrolled in parallel with the other cohorts.

Although the results are preliminary and the number of treated patients is still too small, the initial data are encouraging. Among 18 patients treated so far, visual acuity improved in ten, remained the same in seven and worsen in one.[10] In addition, it seemed that in dry AMD the improvement in visual acuity has a dose trend—more cells injected, better vision. This had not been observed in Stargardt's macular degeneration patients. Immunosuppression has been given to the participants in the trials for total of 13 weeks, one week before the treatment and 12 weeks after. Regardless, no signs of rejection were evident in follow up.

The company also reported the data from two Asian patients with dry AMD and two with Stargardt's macular degeneration and one year and follow up.[11] No serious safety issues were noted and visual acuity improved in three patients, whereas in one remained stable. Asian patients may carry different risk alleles for retinal disorders and the report suggested that hESC-derived RPE cells seemed to be safe for them too.

Long-term follow up of 15 years for both dry AMD and Stargardt's macular dystrophy trials in the USA are registered as separate studies at www.clinicaltrials.gov, NCT02463344 and NCT02445612 respectively. The first visit of extended follow up will be 12 months post-injection. In addition, Ocata is embarking on a trial in patients with geographic atrophy secondary to myopic macular degeneration (ID: NCT02122159 at www.clinicaltrials.gov).

The first patient with dry AMD has been enrolled in the Phase 2 clinical trial in September 2015.

Cell Cure Neurosciences

Cell Cure Neurosciences (Israel; http://www.cellcureneurosciences.com) was funded as a subsidiary of Singapore-based ES Cell International. In 2010, through acquisition of ES Cell International, BioTime (CA, USA; www.biotimeinc.com) acquired a majority in Cell Cure. Cell Cure generated under xeno-free conditions a proprietary formulations of hESC-derived RPE cells OpRegen® and OpRegen-Plus® and it has an exclusive license agreement with Israeli pharmaceutical giant Teva Pharmaceutical Industries (http://www.tevapharm.com) to develop and commercialize the hESC-derived RPE for the treatment of dry AMD. In October 2014, Cell Cure filled an IND application with the US FDA to initiate Phase I1/2a clinical trial of OpRegen in patients with

geographic atrophy, the severe type of AMD. Only a month later the US FDA gave them the green light. The clinical trial running in Hadassah Ein Kerem University Hospital in Jerusalem is now recruiting the patients. The study will enrol 15 patients, divided in four cohorts, which will, following vitrectomy, receive 50 000–500 000 RPE cells into subretinal space. Additional information on this study can be found at www.clinicaltrials.gov (ID: NCT02286089).

The US FDA has granted Fast Track designation for OpRegen in September 2015.

The London Project to Cure Blindness

As the result of a partnership between the Moorfields Eye Hospital (www.moorfields.nhs.uk), the University College London Institute of Ophthalmology (www.ucl.ac.uk/ioo), the National Institute for Health Research (NIHR; www.nihr.ac.uk) and Pfizer (NY, USA; www.pfizer.com) under umbrella named the London Project to Cure Blindness (www.thelondonproject.org), the first patient with wet AMD was treated in August 2015 and there have been no complications to date. The trial will recruit 10 patients in total over a period of 18 months. Each patient will be followed for a year to assess the safety and stability of the cells and whether there is an effect in restoring vision.

More recently, The London Project has secured funding to examine the use of iPSC technology for transplantation.

RIKEN CBD

Following a successful launching of clinical trials with hESC-derived RPE cells, Japanese researcher Masayo Takahashi from Riken Centre for Developmental Biology in Kobe (http://www.cdb.riken.jp/en/), seized the opportunity and initiated the first-in-man study with iPSC-derived RPE cells. Rigorous *in vitro* and preclinical experiments in animals were satisfactory enough for the Japanese Ministry of Health, Labour and Welfare to give the green light in July 2013 to the open-label study, designed to evaluate safety of the autologous iPSC-derived RPE cell sheets in patients with wet AMD. Enrolment started the next month. The iPSC were generated from a 4-mm skin biopsy from upper arm, differentiated into RPE cells and prepared as cell sheets for transplantation. An estimate for the entire process, Quality Control (QC) included, has been 10 months for each participant. Post-transplantation patients will be monitored each month for 6 months and then every 2 months up to one year. Follow up examinations will occur once a year for the next 3 years.

The study is planning to enrol six participants. The first three will be transplanted with the 1.3 mm × 3 mm RPE sheet, whereas the following three will receive either larger sheet or multiple smaller sheets. In case of multiple sheets, the maximum number per participant will be three. The first patient, a 70-year-old female received the treatment in September 2014. The patient did not receive any immunosuppression and 6 month later there were still no signs of rejection or other adverse effects. However, the study was temporarily halted in March 2015, when the investigators found three single nucleotide variations (SNVs) and three copy-number variants (CNVs) present in the second patient iPSC and not detectable in the original fibroblasts. Additional information on the study can be found at http://www.riken-ibri.jp/AMD/english/index.html, the International Clinical Trials Registry Platform (ICTRP; http://www.who.int/ictrp/en/) under ID: JPRN-UMIN000011929 and at the Japan Primary Registries Network (JPRN; http://www.umin.ac.jp/ctr/index.htm) under ID: UMIN000011929. The promising result and availability of the iPSC lines homozygous for HLA haplotype[14–16] is taking the trial toward different direction—use of allogeneic iPSC lines.

Type 1 diabetes

Viacyte (former Novocell)

Viacyte (CA, USA; www.viacyte.com), a privately held company, invested more than a decade to bring hESC-based therapy for type 1 diabetes from bench to patients with a goal of achieving long-term insulin independence without immune suppression. The company was founded in 1999 under name Novocell and merged with CyThera and Bresagen in 2004. Mimicking pancreatic organogenesis *in vitro*, they

were able to deduce a protocol to differentiate hESC into pancreatic hormone-expressing endocrine cells.[17] These cells, when implanted into mice, reacted to glucose stimulation; human insulin and C-peptide were detected in sera at levels similar to those of mice transplanted with approximately 3000 human islets.[18] Using surface markers, they were able to separate pancreatic hormone-expressing endocrine cells into different subtypes. Enriched pancreatic endoderm, CD142+ cells, when transplanted into mice, gave rise to all pancreatic lineages, including functional insulin-producing cells, demonstrating that they are indeed pancreatic progenitors.[19] Next, the company developed manufacturing process on a scale amenable to clinical entry. The cells produced in such a way, upon implantation in mice, formed neo-pancreatic tissue sufficient to protect against streptozotocin-induced hyperglycaemia.[20,21] In parallel, the company developed Encaptra®, an encapsulating drug delivery system made from porous cell-impermeable membrane. The company filed an IND and device master file with the US FDA in July 2014. The application was approved relatively quickly, only a month later, and the first patient was implanted with hESC-derived islet replacement product candidate in October 2014 at University of California San Diego. The second site at the University of Alberta Hospitals in Edmonton in Canada was opened in July 2015.

The product candidate, called VC-01™, is placed under patient's skin and actually represents Encaptra-250 pouch/device filled with hESC-derived pancreatic precursor cells PEC-01™. After surgical implantation, the cells differentiate further into fully functioning insulin-producing β-cells, as well as to other endocrine cell types that make up the normal human pancreatic islet. The Phase 1/2 open-label, dose-escalation study will enrol about 40 participants with a diagnosis of type 1 diabetes mellitus for at least 3 years. All the patients will be C-peptide negative and thus have essentially no ability to produce insulin. They will be divided into two cohorts. The first cohort is sub-therapeutic and each of six participants will receive two VC-01 implants, placed in the lower back, aiming to evaluate safety and tolerability. The patients in the second cohort will receive four to six dose-ranging VC-01 implants to achieve efficacy. The participants will be also implanted with sentinels, Encaptra-20 pouches, which can be periodically withdrawn from the patients and analysed. Their size is about 10-folds smaller than VC-01 implant, which is about half the size of business card (http://www.ipscell.com/2015/03/viacyte/). Additional information on this study can be found at www.clinicaltrials.gov (ID: NCT02239354). Therapy development was supported substantially by the CIRM (www.cirm.ca.gov) and JDRF (www.jdrf.org), a global organization focussed on type 1 diabetes research.

Heart failure

APHP

The world-first hESC-based trial for the heart repair commenced in autumn 2014 in France under the sponsorship of the Assistance Publique – Hôpitaux de Paris (APHP; http://www.aphp.fr). The study is planning to recruit six patients who have severe left ventricular systolic dysfunction with left ventricular ejection fraction (LVEF) ≤35% and history of myocardial infarction, older than 6 months, with a residual akinesia involving more than 2 out of 16 contiguous segments. A fibrin patch embedding hESC-derived cardiac-committed CD15+ ISL-1+ progenitors will be transplanted into epicardium of the infarcted area and covered with an autologous pericardial flap. The flap is designed to provide nutrients to the underlying graft with the idea of improving viability of embedded cells.[22] The objective of this study is to assess both the feasibility and safety of this approach. Efficacy will be assessed on the following end points: left ventricular function, viability of the grafted area, functional status and major adverse cardiovascular events.

The first patient, a 68-year-old insulin-dependent diabetic woman, with an indication for a surgical anterior myocardial revascularization, has received in addition to planned coronary artery bypass, also a fibrin patch embedded with hESC-derived cardiac-committed CD15+ ISL-1+ progenitors. At 3-month follow-up time point, the patient showed marked improvement.

Echocardiographic LVEF improved from 26 to 36%. At the time of the treatment, the patient had New York Heart Association (NYHA) Class III symptoms, whereas after the treatment the symptoms matched NYHA Class I. Furthermore, the akinetic infarct zone, under the patch, has become moderately hypokinetic.[23] Additional information on this study can be found at www.clinicaltrials.gov (ID: NCT02057900).

Conclusion

In spite of significant challenges, hESC and iPSC-based cellular therapies are reaching clinical application in an extraordinary short time, especially given challenges and obstacles that at certain time seemed to be insurmountable. To fully realize their potential, first is necessary to demonstrate their safety and only then efficacy. This can be achieved only by careful planning and with adequate resources in a regulatory-friendly environment. Initial data from all trials are promising and they are likely to incite new trials for other diseases. One of the closest to the clinical trial might be Parkinson's disease.

References

1. Thomson JA, Itskovitz-Eldor J, Shapiro SS, et al. Embryonic stem cell lines derived from human blastocysts. *Science* 1998;282:1145–7.
2. Takahashi K, Yamanaka S. Induction of pluripotent stem cells from mouse embryonic and adult fibroblast cultures by defined factors. *Cell* 2006;126:663–76.
3. Takahashi K, Tanabe K, Ohnuki M, et al. Induction of pluripotent stem cells from adult human fibroblasts by defined factors. *Cell* 2007;131:861–72.
4. Yu J, Vodyanik MA, Smuga-Otto K, et al. Induced pluripotent stem cell lines derived from human somatic cells. *Science* 2007;318:1917–20.
5. Keirstead HS, Nistor G, Bernal G, et al. Human embryonic stem cell-derived oligodendrocyte progenitor cell transplants remyelinate and restore locomotion after spinal cord injury. *J Neurosci* 2005;25:4694–705.
6. Amariglio N, Hirshberg A, Scheithauer BW, et al. Donor-derived brain tumor following neural stem cell transplantation in an ataxia telangiectasia patient. *PLoS Med* 2009;6:e1000029.
7. Scott CT, Magnus D. Wrongful termination: lessons from the geron clinical trial. *Stem Cells Transl Med* 2014;3:1398–401.
8. Klimanskaya I, Hipp J, Rezai KA, et al. Derivation and comparative assessment of retinal pigment epithelium from human embryonic stem cells using transcriptomics. *Cloning Stem Cells* 2004;6:217–45.
9. Schwartz SD, Hubschman JP, Heilwell G, et al. Embryonic stem cell trials for macular degeneration: a preliminary report. *Lancet* 2012;379:713–20.
10. Schwartz SD, Regillo CD, Lam BL, et al. Human embryonic stem cell-derived retinal pigment epithelium in patients with age-related macular degeneration and Stargardt's macular dystrophy: follow-up of two open-label phase 1/2 studies. *Lancet* 2015;385:509–16.
11. Song WK, Park KM, Kim HJ, et al. Treatment of macular degeneration using embryonic stem cell-derived retinal pigment epithelium: preliminary results in Asian patients. *Stem Cell Reports* 2015;4:860–72.
12. Lund RD, Wang S, Klimanskaya I, et al. Human embryonic stem cell-derived cells rescue visual function in dystrophic RCS rats. *Cloning Stem Cells* 2006;8:189–99.
13. Lu B, Malcuit C, Wang S, et al. Long-term safety and function of RPE from human embryonic stem cells in preclinical models of macular degeneration. *Stem Cells* 2009;27:2126–35.
14. Saito MK, Matsunaga A, Takasu N, et al. Donor recruitment and eligibility criteria for HLA-homozygous iPSC bank in Japan. In: Ilic D (ed). *Stem Cell Banking*. New York: Springer, 2014,67–76.
15. Wilmut I, Leslie S, Martin NG, et al. Development of a global network of induced pluripotent stem cell haplobanks. *Regen Med* 2015;10:235–8.
16. Neofytou E, O'Brien CG, Couture LA, et al. Hurdles to clinical translation of human induced pluripotent stem cells. *J Clin Invest* 2015;125:2551–7.
17. D'Amour KA, Bang AG, Eliazer S, et al. Production of pancreatic hormone-expressing endocrine cells from human embryonic stem cells. *Nat Biotechnol* 2006;24:1392–401.
18. Kroon E, Martinson LA, Kadoya K, et al. Pancreatic endoderm derived from human embryonic stem cells generates glucose-responsive insulin-secreting cells in vivo. *Nat Biotechnol* 2008;26:443–52.
19. Kelly OG, Chan MY, Martinson LA, et al. Cell-surface markers for the isolation of pancreatic cell types derived from human embryonic stem cells. *Nat Biotechnol* 2011;29:750–6.

20. Schulz TC, Young HY, Agulnick AD, et al. A scalable system for production of functional pancreatic progenitors from human embryonic stem cells. *PLoS One* 2012;7:e37004.
21. Schulz TC. Concise review: manufacturing of pancreatic endoderm cells for clinical trials in type 1 diabetes. *Stem Cells Transl Med* 2015;4:927–31.
22. Puymirat E, Geha R, Tomescot A, et al. Can mesenchymal stem cells induce tolerance to cotransplanted human embryonic stem cells? *Mol Ther* 2009;17:176–82.
23. Menasché P, Vanneaux V, Hagège A, et al. Human embryonic stem cell-derived cardiac progenitors for severe heart failure treatment: first clinical case report. *Eur Heart J* 2015;36:2011–7.

Stem Cell Research 16 (2016) 342–344

Contents lists available at ScienceDirect

Stem Cell Research

journal homepage: www.elsevier.com/locate/scr

Lab Resource: Stem Cell Line

Generation of KCL018 research grade human embryonic stem cell line carrying a mutation in the *DMPK* gene

Cristian Miere, Heema Hewitson, Liani Devito, Victoria Wood, Neli Kadeva, Glenda Cornwell, Stefano Codognotto, Emma Stephenson, Dusko Ilic *

Stem Cell Laboratories, Division of Women's Health, Faculty of Life Sciences and Medicine, King's College London and Assisted Conception Unit, Guys' Hospital, London, United Kingdom

ARTICLE INFO

Article history:
Received 30 December 2015
Received in revised form 5 January 2016
Accepted 12 January 2016
Available online 15 January 2016

ABSTRACT

The KCL018 human embryonic stem cell line was derived from an embryo donated for research that carried an autosomal dominant mutation affecting one allele of the *DMPK* gene encoding the dystrophia myotonica protein kinase (2200 trinucleotide repeats; 14 for the normal allele). The ICM was isolated using laser microsurgery and plated on γ-irradiated human foreskin fibroblasts. Both the derivation and cell line propagation were performed in an animal product-free environment. Pluripotent state and differentiation potential were confirmed by in vitro assays.

Resource table

Name of stem cell line	KCL018
Institution	King's College London, London UK
Derivation team	Neli Kadeva, Victoria Wood, Glenda Cornwell, Stefano Codognotto, Emma Stephenson
Contact person and email	Dusko Ilic, email: dusko.ilic@kcl.ac.uk
Type of resource	Biological reagent: cell line
Sub-type	Human pluripotent stem cell line
Origin	Human embryo
Key marker expression	Pluripotent stem cell markers: NANOG, OCT4, TRA-1-60, TRA-1-81, alkaline phosphatase (AP) activity
Authentication	Identity and purity of line confirmed
Link to related literature (direct URL links and full references)	1) Ilic, D., Stephenson, E., Wood, V., Jacquet, L., Stevenson, D., Petrova, A., Kadeva, N., Codognotto, S., Patel, H., Semple, M., Cornwell, G., Ogilvie, C., Braude, P., 2012. Derivation and feeder-free propagation of human embryonic stem cells under xeno-free conditions. Cytotherapy. 14 (1), 122–128. doi: 10.3109/14,653,249.2011.623692 http://www.ncbi.nlm.nih.gov/pubmed/22029654 2) Stephenson, E., Jacquet, L., Miere, C., Wood, V., Kadeva, N., Cornwell, G., Codognotto, S., Dajani, Y., Braude, P., Ilic, D., 2012. Derivation and propagation of human embryonic stem cell lines from frozen embryos in an animal product-free environment. Nat. Protoc. 7 (7), 1366–1381. doi: 10.1038/nprot.2012.080 http://www.ncbi.nlm.nih.gov/pubmed/22722371
Information in public databases	KCL018 is a National Institutes of Health (NIH) registered hESC line NIH Registration Number: 0218 NIH Approval Number: NIHhESC-13-0218 http://grants.nih.gov/stem_cells/registry/current.htm?id=658
Ethics	The hESC line KCL018 is derived under license from the UK Human Fertilisation and Embryology Authority (research license numbers: R0075 and R0133) and also has local ethical approval (UK National Health Service Research Ethics Committee Reference: 06/Q0702/90). Informed consent was obtained from all subjects and the experiments conformed to the principles set out in the WMA Declaration of Helsinki and the NIH Belmont Report. No financial inducements are offered for donation.

Resource details

Consent signed	Aug 12, 2009
Embryo thawed	Aug 23, 2009
UK Stem Cell Bank Deposit Approval	Sep 23, 2010 Reference: SCSC10-30
Sex	Female 46, XX
Grade	Research
Disease status (Fig. 1)	Mutation affecting one allele of the *DMPK* gene encoding dystrophia myotonica protein kinase (~2200 CTG repeats; 14 for the normal allele) associated with Myotonic dystrophy Type 1 (Ilic et al., 2012)
Karyotype (aCGH)	No copy number changes detected
DNA fingerprint	Allele sizes (in bp) of 17 microsatellite markers specific for chromosomes 13, 18 and 21 (Ilic et al., 2012)
Viability testing	Pass
Pluripotent markers (immunostaining) (Fig. 2)	NANOG, OCT4, TRA-1-60, TRA-1-81, AP activity (Ilic et al., 2012)
Three germ layers	Endoderm: AFP (α-fetoprotein); Ectoderm: TUBB3

* Corresponding author.
E-mail address: dusko.ilic@kcl.ac.uk (D. Ilic).

http://dx.doi.org/10.1016/j.scr.2016.01.004

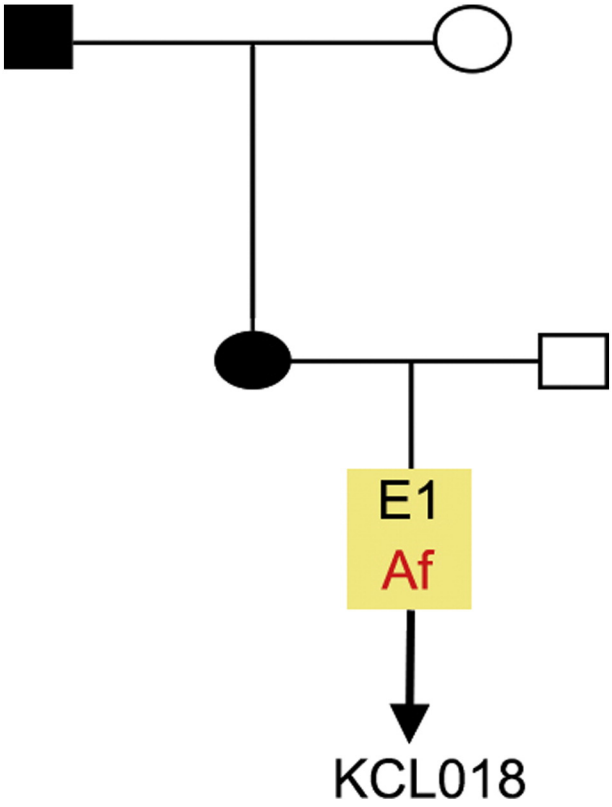

Fig. 1. Genetic pedigree tree. The couple undergoing IVF had only on embryo in this particular cycle. The embryo carried the mutation and was donated for research.

differentiation in vitro (immunostaining) (Fig. 3)	(tubulin, β3 class III); Mesoderm: ACTA2 (actin, α2, smooth muscle) (Ilic et al., 2012)
Sibling lines available	No

We generated KCL018 clinical grade hESC line following protocols, established previously (Ilic et al., 2012; Stephenson et al., 2012). The expression of the pluripotency markers was tested after freeze/thaw cycle (Ilic et al., 2012). Differentiation potential into three germ layers was verified in vitro (Ilic et al., 2012).

Materials and methods

Consenting process

We distribute Patient Information Sheet (PIS) and consent form to the in vitro fertilization (IVF) patients if they opted to donate to research embryos that were stored for 5 or 10 years. They mail signed consent back to us and that might be months after the PIS and consent were mailed to them. If in the meantime new versions of PIS/consent are implemented, we do not send these to the patients or ask them to resign; the whole process is done with the version that was given them initially. The PIS/consent documents (PGD-V.6) were created on Aug. 10, 2007. HFEA Code of Practice that was in effect at the time of document creation: Edition 7 — R.1 (http://www.hfea.gov.uk/2999.html). The donor couple signed the consent on Oct. 15, 2009. HFEA Code of Practice that was in effect at the time of donor signature: Edition 8 — R.1. HFEA Code of Practice Edition 7 — R.1 was in effect until Dec. 09, 2007 and Edition 8 — R.1 was in effect: Oct. 01, 2009–Apr. 06, 2010.

Embryo culture and micromanipulation

Embryo culture and laser-assisted dissection of inner cell mass (ICM) were carried out as previously described in details (Ilic et al., 2012; Stephenson et al., 2012). The cellular area containing the ICM was then washed and transferred to plates containing mitotically inactivated human neonatal foreskin fibroblasts (HFF).

Cell culture

ICM plated on mitotically inactivated HFF were cultured as described (Ilic et al., 2012; Stephenson et al., 2012). TE cells were removed mechanically from outgrowth (Ilic et al., 2007; Ilic et al., 2010). hESC colonies were expanded and cryopreserved at the third passage.

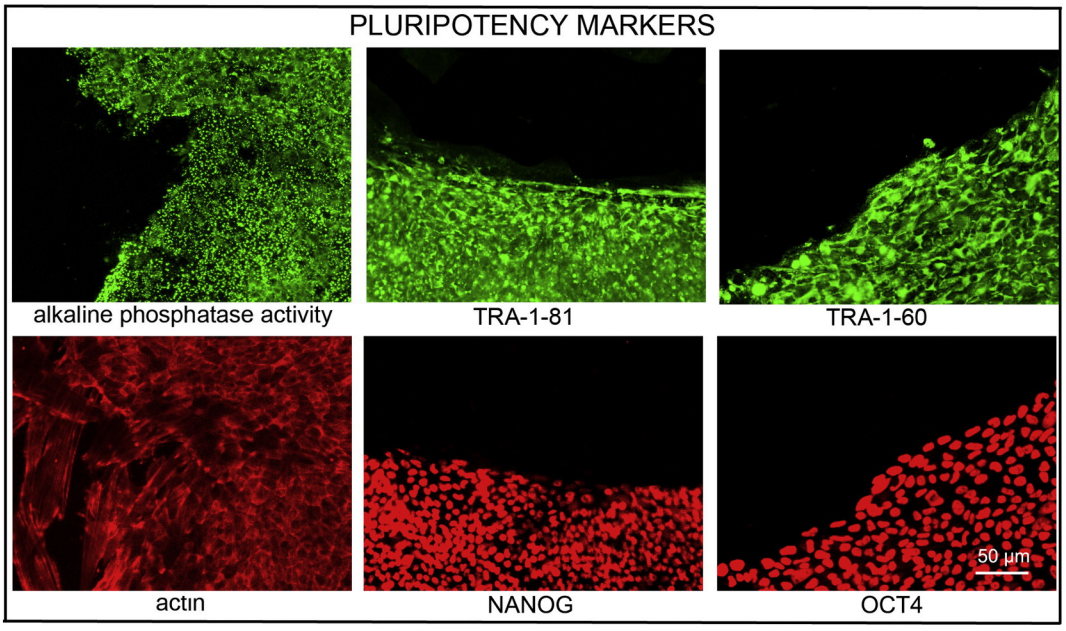

Fig. 2. Expression of pluripotency markers. Pluripotency is confirmed by immunostaining (Oct4, Nanog, TRA-1-60, TRA-1-81) and alkaline phosphatase (AP) activity assay. Actin stress fibers, visualized with rhodamine-phalloidin (red), are present in both feeders and hES cell colonies, whereas AP activity (green) is detected only in hES cells. Scale bar, 50 µm.

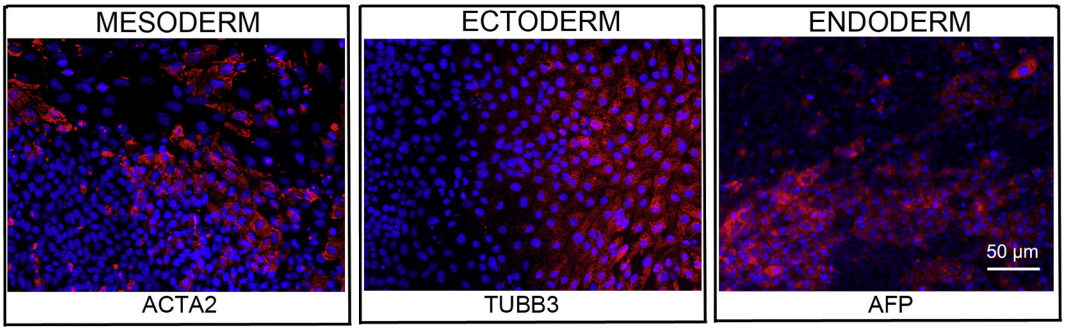

Fig. 3. Differentiation of three germ layers in vitro is confirmed by detection of markers: smooth muscle actin (red) for mesoderm, β-III tubulin (red) for ectoderm and α-fetoprotein (red) for endoderm. Nuclei are visualized with Hoechst 33,342 (blue). Scale bar, 50 µm.

Viability test

Straws with the earliest frozen passage (p. 2–3) are thawed and new colonies are counted three days later. These colonies are then expanded up to passage 8, at which point cells were part frozen and part subjected to standard battery of tests (pluripotency markers, in vitro and in vivo differentiation capability, genetics, sterility, mycoplasma).

Pluripotency markers

Pluripotency was assessed using two different techniques: enzymatic activity assay [alkaline phosphatase (AP) assay] and immunostaining as described (Ilic et al., 2012; Stephenson et al., 2012).

Genotyping

DNA was extracted from hES cell cultures using a Chemagen DNA extraction robot according to the manufacturer's instructions. Amplification of polymorphic microsatellite markers was carried out as described (Ilic et al., 2012). Allele sizes were recorded to give a unique fingerprint of each cell line.

Array comparative genomic hybridization (aCGH)

aCGH was performed as described in details (Ilic et al., 2012).

Chr	Marker	Allele 1	Allele 2
	D13S252	299	299
	D13S305	443	458
13	D13S325	289	297
	D13S628	429	450
	D13S634	397	417
	D18S386	383	386
	D18S390	372	372
	D18S391	209	217
18	D18S535	482	486
	D18S819	408	424
	D18S976	479	479
	D18S978	219	219
	D21S11	244	251
	D21S1409	216	224
21	D21S1411	308	308
	D21S1435	184	188
	D21S1437	331	335

Author disclosure statement

There are no competing financial interests in this study.

Acknowledgments

This work was supported by the UK Medical Research Council grants G0701172 and G0801061. We thank Dr. Yacoub Khalaf, Director of the Assisted Conception Unit of Guy's and St Thomas' NHS Foundation Trust and his staff for supporting the research program. We are especially indebted to Prof Peter Braude and to the patients who donated embryos.

References

Ilic, D., Stephenson, E., Wood, V., Jacquet, L., Stevenson, D., Petrova, A., Kadeva, N., Codognotto, S., Patel, H., Semple, M., Cornwell, G., Ogilvie, C., Braude, P., 2012. Derivation and feeder-free propagation of human embryonic stem cells under xeno-free conditions. Cytotherapy 14 (1), 122–128.

Ilic, D., Caceres, E., Lu, S., Julian, P., Foulk, R., Krtolica, A., 2010. Effect of karyotype on successful human embryonic stem cell derivation. Stem Cells Dev. 19 (1), 39–46.

Ilic, D., Genbacev, O., Krtolica, A., 2007. Derivation of hESC from intact blastocysts. Curr. Protoc. Stem Cell Biol. (Chapter 1: Unit 1 A.2).

Stephenson, E., Jacquet, L., Miere, C., Wood, V., Kadeva, N., Cornwell, G., Codognotto, S., Dajani, Y., Braude, P., Ilic, D., 2012. Derivation and propagation of human embryonic stem cell lines from frozen embryos in an animal product-free environment. Nat. Protoc. 7 (7), 1366–1381.

Stem Cell Research 16 (2016) 296–299

Contents lists available at ScienceDirect

Stem Cell Research

journal homepage: www.elsevier.com/locate/scr

Lab Resource: Stem Cell Line

Generation of KCL033 clinical grade human embryonic stem cell line

Liani Devito, Anastasia Petrova, Victoria Wood, Neli Kadeva, Glenda Cornwell, Stefano Codognotto, Emma Stephenson, Dusko Ilic *

Stem Cell Laboratories, Division of Women's Health, Faculty of Life Sciences and Medicine, King's College London and Assisted Conception Unit, Guys' Hospital, London, United Kingdom

ARTICLE INFO

Article history:
Received 28 December 2015
Accepted 29 December 2015
Available online 15 January 2016

ABSTRACT

The KCL033 human embryonic stem cell line was derived from a normal healthy blastocyst donated for research. The ICM was isolated using laser microsurgery and plated on γ-irradiated human foreskin fibroblasts. Both the derivation and cell line propagation were performed in an animal product-free environment and under current Good Manufacturing Practice (cGMP) standards. Pluripotent state and differentiation potential were confirmed by in vitro assays. The line was also validated for sterility and specific and non-specific human pathogens.

1. Resource table

Name of stem cell line	KCL033
Institution	King's College London, London, UK
Derivation team	Neli Kadeva, Victoria Wood, Glenda Cornwell, Stefano Codognotto, Emma Stephenson
Contact person and email	Dusko Ilic, email: dusko.ilic@kcl.ac.uk
Date archived/stock date	Aug 17, 2011
Type of resource	Biological reagent: cell line
Sub-type	Human pluripotent stem cell line
Origin	Human embryo
Key marker expression	Pluripotent stem cell markers: NANOG, OCT4, TRA-1-60, TRA-1-81, alkaline phosphatase (AP) activity
Authentication	Identity and purity of line confirmed
Link to related literature (direct URL links and full references)	1) Jacquet, L., Stephenson, E., Collins, R., Patel, H., Trussler, J., Al-Bedaery, R., Renwick, P., Ogilvie, C., Vaughan, R., Ilic, D., 2013. Strategy for the creation of clinical grade hESC line banks that HLA-match a target population. EMBO Mol. Med. 5 (1), 10–17. doi: 10.1002/emmm.201201973 http://www.ncbi.nlm.nih.gov/pubmed/23161805 2) Canham, A., Van Deusen, A., Brison, D.R., De Sousa, P., Downie, J., Devito, L., Hewitt, Z.A., Ilic, D., Kimber, S.J., Moore, H.D., Murray, H., Kunath, T., 2015. The molecular karyotype of 25 clinical-grade human embryonic stem cells lines. *Sci. Rep.* 5, 17258. doi: 10.1038/srep17258 http://www.ncbi.nlm.nih.gov/pubmed/26607962 3) Ilic, D., Stephenson, E., Wood, V., Jacquet, L., Stevenson, D., Petrova, A., Kadeva, N., Codognotto, S., Patel, H., Semple, M., Cornwell, G., Ogilvie, C., Braude, P., 2012. Derivation and feeder-free propagation of human embryonic stem cells under xeno-free conditions. Cytotherapy. 14 (1), 122–128. doi: 10.3109/14653249.2011.623692 http://www.ncbi.nlm.nih.gov/pubmed/22029654 4) Stephenson, E., Jacquet, L., Miere, C., Wood, V., Kadeva, N., Cornwell, G., Codognotto, S., Dajani, Y., Braude, P., Ilic, D., 2012. Derivation and propagation of human embryonic stem cell lines from frozen embryos in an animal product-free environment. Nat. Protoc. 7 (7), 1366–1381. doi: 10.1038/nprot.2012.080 http://www.ncbi.nlm.nih.gov/pubmed/22722371 5) Devito, L., Petrova, A., Miere, C., Codognottom S., Blakely, N., Lovatt, A., Ogilvie, C., Khalaf, Y., Ilic, D., 2014. Cost-effective master cell bank validation of multiple clinical-grade human pluripotent stem cell lines from a single donor. Stem Cells Transl. Med. 3(10), 1116–1124. doi: 10.5966/sctm.2014-0015 http://www.ncbi.nlm.nih.gov/pubmed/25122690
Information in public databases	KCL033 is a National Institutes of Health (NIH) registered hESC line NIH Registration Number: NIHhESC-14-0267 http://grants.nih.gov/stem_cells/registry/current.htm?id=653
Ethics	The hESC line KCL033 is derived under license from the UK Human Fertilisation and Embryology Authority (research license numbers: R0075 and R0133) and also has local ethical approval (UK National Health Service Research Ethics

* Corresponding author.

http://dx.doi.org/10.1016/j.scr.2015.12.047

Committee Reference: 06/Q0702/90).
Informed consent was obtained from all subjects and the experiments conformed to the principles set out in the WMA Declaration of Helsinki and the NIH Belmont Report. No financial inducements are offered for donation.

2. Resource details

Consent signed	May 26, 2009
Embryo thawed	Jul 11, 2011
UK stem cell bank deposit approval	Mar 08, 2012 Reference: SCSC12-54
Sex	Female 46, XX
Grade	Clinical
Disease status	Healthy/Unaffected
Karyotype (aCGH)	No copy number changes detected.
SNP array	Gain in regions 5p14.3 and 12p11.21 (Canham et al., 2015)
DNA fingerprint	Allele sizes (in bp) of 16 microsatellite markers specific for chromosomes 13, 18 and 21 (Jacquet et al., 2013)
HLA typing	HLA-A 11,29; B 44,51; Bw 4; C 04,16; DRB1 04,07; DRB4 01; DQB1 02,03 (Jacquet et al., 2013; Canham et al., 2015)
Viability testing	Pass
Mycoplasma	Negative
Sterility	Pass
Pluripotent markers (immunostaining) (Fig. 1)	NANOG, OCT4, TRA-1-60, TRA-1-81
Three germ layers differentiation in vitro (immunostaining) (Fig. 2)	Endoderm: AFP Ectoderm: TUBB3 (tubulin, beta 3 class III) Mesoderm: ACTA2 (actin, alpha 2, smooth muscle)
Sibling lines available	KCL032, KCL034

We generated KCL033 clinical grade hESC line following protocols, established previously (Ilic et al., 2012; Stephenson et al., 2012), and now adapted to cGMP conditions. The expression of the pluripotency markers was tested after freeze/thaw cycle (Fig. 1). Differentiation potential into three germ layers was verified in vitro (Fig. 2).

Molecular karyotyping identified a novel 2.4 Mb gain on chromosome 5p14.3 and a gain on chromosome 12p11.21, which was also found in KCL040.

The gain on chromosome 5p14.3 containing a single gene, *CDH18* (Cadherin-18), was also present in one of two sibling cell lines, KCL032, but not in KCL034, a third sibling. A duplication of this size has not been reported to date, but its presence in two sibling hESC lines strongly suggests that it was inherited from one of the parents rather than by acquisition during hESC derivation and culture (Canham et al., 2015). The 2498.8 bp gain starts at bp 19086546 and ends at bp 21585311 as referred to Human Genome Build 38.

The gain on chromosome 12p11.21 contains no genes and it has been also reported in at least 14 submissions at Database of Genomic Variants (DGV; http://dgv.tcag.ca), which has collected structural variations in more than 14,000 healthy individuals from worldwide population (MacDonald et al., 2014). Estimated frequency in the human population is 4.70% (Canham et al., 2015).

Validation for sterility and specific and non-specific human pathogens (Devito et al., 2014) conformed that the cells in the Master Bank were sterile, mycoplasma-free, and negative for *Treponema pallidum*, chlamydia, *Neisseria gonorrhoeae*, human immunodeficiency virus-1 and 2 (HIV-1 and -2), human T-lymphotropic virus types-1 and 2 (HTLV-1 and 2), hepatitis A, B and C (HAV, HBV and HCV), human herpes simplex virus HHV-4 (Epstein–Barr virus, EBV), -6, -7, and -8, human cytomegalovirus (hCMV), human parvovirus B19, SV40, JCV, BKV, enterovirus, HAV, HCV, nonspecific viral and other adventitious contaminants.

We also generated research grade of KCL033 line that is adapted to feeder-free conditions.

3. Materials and methods

3.1. Consenting process

We distribute Patient Information Sheet (PIS) and consent form to the in vitro fertilization (IVF) patients if they opted to donate to research embryos that were stored for 5 or 10 years. They mail signed consent back to us and that might be months after the PIS and consent were mailed to them. If in meantime new versions of PIS/consent are implemented, we do not send these to the patients or ask them to re-sign; the whole process is done with the version that was given them initially. The PIS/consent documents (FRO-V.6) were created on Dec. 18, 2008. HFEA Code of Practice that was in effect at the time of document creation: Edition 7 — R.4 (http://www.hfea.gov.uk/2999.html). The donor couple signed the consent on May 26, 2009. HFEA Code of Practice that was in effect at the time of donor signature: Edition 7 — R.4. HFEA Code of Practice Edition 7 — R.4 was in effect: 02 Oct. 2008–30 Sep. 2009.

3.2. Embryo culture and micromanipulation

Embryo culture and laser-assisted dissection of inner cell mass (ICM) were carried out as previously described in detail (Ilic et al., 2012; Stephenson et al., 2012). The cellular area containing the ICM was then washed and transferred to plates containing mitotically inactivated human neonatal foreskin fibroblasts (HFF).

3.3. Cell culture

ICM plated on mitotically inactivated HFF were cultured as described (Ilic et al., 2012; Stephenson et al., 2012). TE cells were removed mechanically from the outgrowth (Ilic et al., 2007; Ilic et al., 2010). hES colonies were expanded and cryopreserved at the third passage.

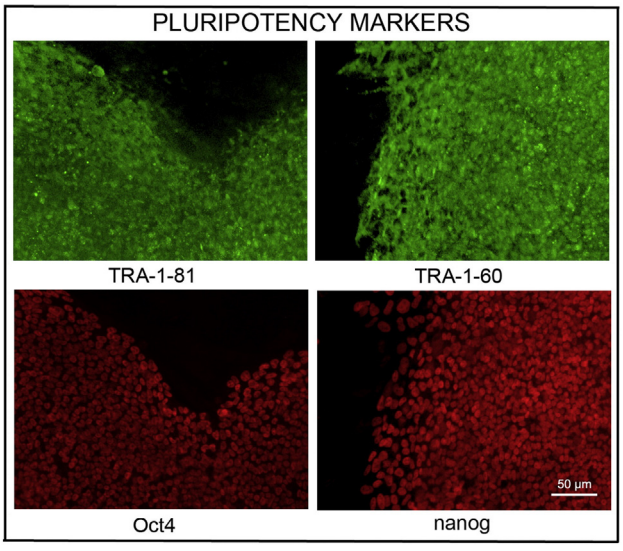

Fig. 1. Expression of pluripotency markers. Pluripotency is confirmed by immunostaining (Oct. 4, Nanog, TRA-1-60, TRA-1-81). Scale bar, 50 µm.

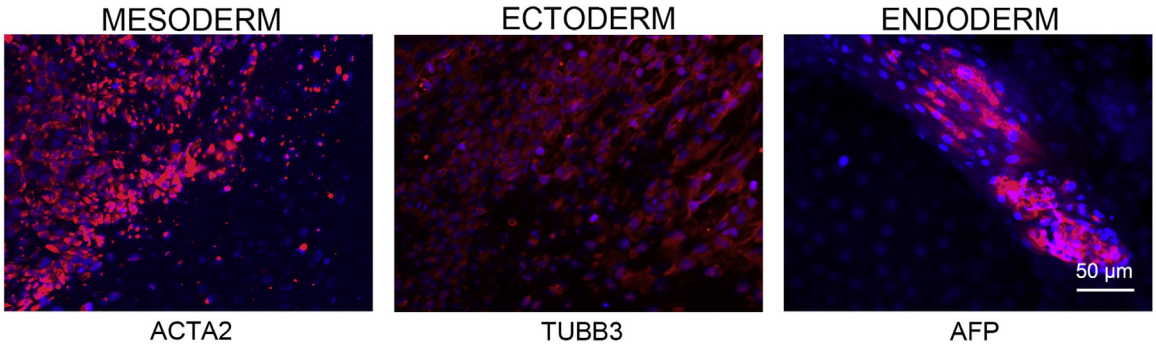

Fig. 2. Differentiation of three germ layers in vitro is confirmed by detection of markers: smooth muscle actin (ACTA2, red) for mesoderm, β-III tubulin (TUBB3, red) for ectoderm and α-fetoprotein (AFP, red) for endoderm. Nuclei are visualized with Hoechst 33342 (blue). Scale bar, 50 μm.

3.4. Viability test

Straws with the earliest frozen passage (p. 2–3) are thawed and new colonies are counted three days later. These colonies are then expanded up to passage 8, at which point cells were part frozen and part subjected to standard battery of tests (pluripotency markers, in vitro and in vivo differentiation capability, genetics, sterility, mycoplasma).

3.5. Pluripotency markers

Pluripotency was assessed with immunostaining for pluripotency markers as described (Ilic et al., 2012; Stephenson et al., 2012).

3.6. Differentiation

Spontaneous differentiation into three germ layers was assessed in vitro and in vivo as described (Petrova et al., 2014; Stephenson et al., 2012).

3.7. Genotyping

DNA was extracted from hES cell cultures using a Chemagen DNA extraction robot according to the manufacturer's instructions. Amplification of polymorphic microsatellite markers was carried out as described (Ilic et al., 2012). Allele sizes were recorded to give a unique fingerprint of each cell line.

3.8. Array comparative genomic hybridization (aCGH)

aCGH was performed as described in detail (Ilic et al., 2012).

3.9. Whole-genome single nucleotide polymorphism (SNP) array

SNP array was performed as described in detail (Canham et al., 2015).

3.10. HLA typing

HLA-A, -B and -DRB1 typing was performed with a PCR sequence-specific oligonucleotide probe (SSOP; Luminex, Austin, TX, USA) hybridization protocol at the certified Clinical Transplantation Laboratory, Guy's and St Thomas' NHS Foundation Trust and Serco Plc. (GSTS) Pathology (Guy's Hospital, London, UK) as described (Jacquet et al., 2013). HLA typing was also performed independently by other group (Canham et al., 2015).

3.11. Validation for sterility and specific and non-specific human pathogens

Validation for sterility and specific and non-specific human pathogens was performed as described (Devito et al., 2014). All validation studies were conducted by SGS Vitrology (Glasgow, U.K., http://www.sgs.com), in compliance with the principles of GMP as set out in Directive 2003/94/EC for medicinal products for human use (Directive 2003/94/EC, 2003) and 91/412/EEC for veterinary medicinal products (Directive 91/412/EEC, 1991).

Sterility testing was performed in accordance with the current requirements of the European Pharmacopoeia, Section 2.6.1 Sterility, U.S. Pharmacopeia, 71. Sterility Tests, and International Conference on Harmonisation Topic Q5D guidelines.

Mycoplasma testing was performed in accordance with the current requirements of the European Pharmacopoeia, Section 2.6.7, Mycoplasmas.

All PCR-based assays used were compliant with the current edition of the European Pharmacopoeia, 2.6.21, Nucleic Acid Amplification Techniques.

Author disclosure statement

There are no competing financial interests in this study.

Acknowledgments

This work was supported by the UK Medical Research Council grants G0701172 and G0801061. We thank Dr. Yacoub Khalaf, Director of the Assisted Conception Unit of Guy's and St Thomas' NHS Foundation Trust and his staff for supporting the research program. We are especially indebted to Prof Peter Braude and patients who donated the embryos.

References

Canham, A., Van Deusen, A., Brison, D.R., De Sousa, P., Downie, J., Devito, L., Hewitt, Z.A., Ilic, D., Kimber, S.J., Moore, H.D., Murray, H., Kunath, T., 2015. The molecular karyotype of 25 clinical-grade human embryonic stem cells lines. Sci. Rep. 5, 17258.

Devito, L., Petrova, A., Miere, C., Codognottom S., Blakely, N., Lovatt, A., Ogilvie, C., Khalaf, Y., Ilic, D., 2014. Cost-effective master cell bank validation of multiple clinical-grade human pluripotent stem cell lines from a single donor. Stem Cells Transl Med. 3(10), 1116–1124.

Directive 2002/94/EC, 2003. Laying down the principles and guidelines of good manufacturing practice in respect of medical products for human use and investigational medicinal products for human use. Off. J. Eur. Union L262, 22–26 (of the European Parliament and of the Council of October 08, October 14; 2003;. Available at http://ec.europa.eu/health/files/eudralex/vol-1/dir_2003_94/dir_2003_94_en.pdf).

Directive 91/412/EEC, 1991. Laying down the principles and guidelines of good manufacturing practice for veterinary medicinal products. Off. J. Eur. Union L228, 70–73 (of July 23, August 17, 1991; Available at: http://ec.europa.eu/health/files/eudralex/vol-5/dir_1991_412/dir_1991_412_en.pdf).

Ilic, D., Genbacev, O., Krtolica, A., 2007. Derivation of hESC from intact blastocysts. Curr. Protoc. Stem Cell Biol. (Chapter 1: Unit 1 A.2).

Ilic, D., Caceres, E., Lu, S., Julian, P., Foulk, R., Krtolica, A., 2010. Effect of karyotype on successful human embryonic stem cell derivation. Stem Cells Dev. 19 (1), 39–46.

Ilic, D., Stephenson, E., Wood, V., Jacquet, L., Stevenson, D., Petrova, A., Kadeva, N., Codognotto, S., Patel, H., Semple, M., Cornwell, G., Ogilvie, C., Braude, P., 2012. Derivation and feeder-free propagation of human embryonic stem cells under xeno-free conditions. Cytotherapy 14 (1), 122–128.

Jacquet, L., Stephenson, E., Collins, R., Patel, H., Trussler, J., Al-Bedaery, R., Renwick, P., Ogilvie, C., Vaughan, R., Ilic, D., 2013. Strategy for the creation of clinical grade hESC line banks that HLA-match a target population. EMBO Mol. Med. 5 (1), 10–17.

MacDonald, J.R., Ziman, R., Yuen, R.K.C., Feuk, L., Scherer, S.W., 2014. The database of genomic variants: a curated collection of structural variation in the human genome. Nucleic Acids Res. 42, D986–D992.

Petrova, A., Celli, A., Jacquet, L., Dafou, D., Crumrine, D., Hupe, M., Arno, M., Hobbs, C., Cvoro, A., Karagiannis, P., Devito, L., Sun, R., Adame, L.C., Vaughan, R., McGrath, J.A., Mauro, T.M., Ilic, D., 2014. 3D In vitro model of a functional epidermal permeability barrier from human embryonic stem cells and induced pluripotent stem cells. Stem Cell Rep. 2 (5), 675–689.

Stephenson, E., Jacquet, L., Miere, C., Wood, V., Kadeva, N., Cornwell, G., Codognotto, S., Dajani, Y., Braude, P., Ilic, D., 2012. Derivation and propagation of human embryonic stem cell lines from frozen embryos in an animal product-free environment. Nat. Protoc. 7 (7), 1366–1381.

Stem Cell Research 16 (2016) 184–188

Contents lists available at ScienceDirect

Stem Cell Research

journal homepage: www.elsevier.com/locate/scr

Lab Resource: Stem Cell Line

Generation of KCL034 clinical grade human embryonic stem cell line

Liani Devito, Laureen Jacquet, Anastasia Petrova, Cristian Miere, Victoria Wood, Neli Kadeva, Glenda Cornwell, Stefano Codognotto, Emma Stephenson, Dusko Ilic *

Stem Cell Laboratories, Division of Women's Health, Faculty of Life Sciences and Medicine, King's College London and Assisted Conception Unit, Guys' Hospital, London, United Kingdom

ARTICLE INFO

Article history:
Received 28 December 2015
Accepted 29 December 2015
Available online 3 January 2016

ABSTRACT

The KCL034 human embryonic stem cell line was derived from a normal healthy blastocyst donated for research. The ICM was isolated using laser microsurgery and plated on γ-irradiated human foreskin fibroblasts. Both the derivation and cell line propagation were performed in an animal product-free environment and under current Good Manufacturing Practice (cGMP) standards. Pluripotent state and differentiation potential were confirmed by in vitro assays. The line was also validated for sterility, specific and non-specific human pathogens.

Resource table

Name of stem cell line	KCL034
Institution	King's College London, London UK
Derivation team	Neli Kadeva, Victoria Wood, Glenda Cornwell, Stefano Codognotto, Emma Stephenson
Contact person and email	Dusko Ilic, email: dusko.ilic@kcl.ac.uk
Date archived/ stock date	Aug. 08, 2011
Type of resource	Biological reagent: cell line
Sub-type	Human pluripotent stem cell line
Origin	Human embryo
Key marker expression	Pluripotent stem cell markers: NANOG, OCT4, TRA-1-60, TRA-1-81, alkaline phosphatase (AP) activity
Authentication	Identity and purity of line confirmed
Link to related literature (direct URL links and full references)	1) Jacquet, L., Stephenson, E., Collins, R., Patel, H., Trussler, J., Al-Bedaery, R., Renwick, P., Ogilvie, C., Vaughan, R., Ilic, D., 2013. Strategy for the creation of clinical grade hESC line banks that HLA-match a target population. EMBO Mol. Med. 5 (1), 10–17. doi: 10.1002/emmm.201201973 http://www.ncbi.nlm.nih.gov/pubmed/23161805 2) Canham, A., Van Deusen, A., Brison, D.R., De Sousa, P., Downie, J., Devito, L., Hewitt, Z.A., Ilic, D., Kimber, S.J., Moore, H.D., Murray, H., Kunath, T., 2015. The molecular karyotype of 25 clinical-grade human embryonic stem cells lines. *Sci. Rep.* 5, 17258. doi: 10.1038/srep17258 http://www.ncbi.nlm.nih.gov/pubmed/26607962 3) Ilic, D., Stephenson, E., Wood, V., Jacquet, L., Stevenson, D., Petrova, A., Kadeva, N., Codognotto, S., Patel, H., Semple, M., Cornwell, G., Ogilvie, C., Braude, P., 2012. Derivation and feeder-free propagation of human embryonic stem cells under xeno-free conditions. Cytotherapy. 14 (1), 122–128. doi: 10.3109/14653249.2011.623692 http://www.ncbi.nlm.nih.gov/pubmed/22029654 4) Stephenson, E., Jacquet, L., Miere, C., Wood, V., Kadeva, N., Cornwell, G., Codognotto, S., Dajani, Y., Braude, P., Ilic, D., 2012. Derivation and propagation of human embryonic stem cell lines from frozen embryos in an animal product-free environment. Nat. Protoc. 7 (7), 1366–1381. doi: 10.1038/nprot.2012.080 http://www.ncbi.nlm.nih.gov/pubmed/22722371 5) Devito, L., Petrova, A., Miere, C., Codognottom S., Blakely, N., Lovatt, A., Ogilvie, C., Khalaf, Y., Ilic, D., 2014. Cost-effective master cell bank validation of multiple clinical-grade human pluripotent stem cell lines from a single donor. Stem Cells Transl. Med. 3(10), 1116–1124. doi: 10.5966/sctm.2014–0015 http://www.ncbi.nlm.nih.gov/pubmed/25122690 6) Devito, L., Petrova, A., Miere, C., Codognottom S., Blakely, N., Lovatt, A., Ogilvie, C., Khalaf, Y., Ilic, D., 2014. Cost-effective master cell bank validation of multiple clinical-grade human pluripotent stem cell lines from a single donor. Stem Cells Transl. Med. 3(10), 1116–1124. doi: 10.5966/sctm.2014–0015 http://www.ncbi.nlm.nih.gov/pubmed/25122690 7) Petrova, A., Celli, A., Jacquet, L., Dafou, D., Crumrine, D., Hupe, M., Arno, M., Hobbs, C., Cvoro, A., Karagiannis, P., Devito, L., Sun, R., Adame, L.C., Vaughan, R., McGrath, J.A., Mauro, T.M., Ilic, D., 2014. 3D In vitro model of a functional epidermal permeability barrier from human embryonic stem cells and induced pluripotent stem cells. Stem Cell Reports. 2(5), 675–689. doi: 10.1016/j.stemcr.2014.03.009 http://www.ncbi.nlm.nih.gov/pubmed/24936454 8) Cvoro, A., Devito, L., Milton, F.A., Noli, L., Zhang, A., Filippi, C., Sakai, K., Suh, J.H., Sieglaff, D., Dhawan, A., Sakai, T., Ilic, D., Webb, P., 2015. A thyroid hormone receptor/KLF9 axis in human hepatocytes and pluripotent stem cells. Stem Cells. 33(2), 416–428. doi: 10.1002/stem.1875 http://www.ncbi.nlm.nih.gov/pubmed/25330987
Information in public databases	KCL034 is a National Institutes of Health (NIH) registered hESC line NIH Registration Number: NIHhESC-14-0268 http://grants.nih.gov/stem_cells/registry/current.htm?id=654

* Corresponding author.
E-mail address: dusko.ilic@kcl.ac.uk (D. Ilic).

http://dx.doi.org/10.1016/j.scr.2015.12.034

Ethics	The hESC line KCL034 is derived under licence from the UK Human Fertilisation and Embryology Authority (research licence numbers: R0075 and R0133) and also has local ethical approval (UK National Health Service Research Ethics Committee Reference: 06/Q0702/90). Informed consent was obtained from all subjects and the experiments conformed to the principles set out in the WMA Declaration of Helsinki and the NIH Belmont Report. No financial inducements are offered for donation.

Resource details

Consent signed	May 26, 2009
Embryo thawed	Jul. 11, 2011
UK Stem Cell Bank Deposit Approval	Mar. 08, 2012 Reference: SCSC12-54
Sex	Male 46, XY
Grade	Clinical
Disease status	Healthy/unaffected
Karyotype (aCGH)	No copy number changes detected.
SNP Array	Gain in region 6p22.1 (Canham et al., 2015)
DNA fingerprint	Allele sizes (in bp) of 16 microsatellite markers specific for chromosomes 13, 18 and 21 (Jacquet et al., 2013)
HLA typing	HLA-A 11,29; B 44,51; Bw 4; C 04,16; DRB1 04,07; DRB4 01; DQB1 02,03 (Jacquet et al., 2013; Canham et al., 2015)
Viability testing	Pass
Mycoplasma	Negative
Sterility	Pass
Pluripotent markers (immunostaining) (Fig. 1)	NANOG, OCT4, TRA-1-60, TRA-1-81, AP activity
Three germ layers differentiation in vitro (immunostaining) (Fig. 2)	Endoderm: AFP Ectoderm: TUBB3 (tubulin, beta 3 class III) Mesoderm: ACTA2 (actin, alpha 2, smooth muscle)
Three germ layer differentiation in vivo (teratomas) (Fig. 3)	Endoderm: AFP, GATA4 Ectoderm: TUBB3, GFAP (glial fibrillary acidic protein) Mesoderm: DES (desmin), Alcian Blue and periodic acid–Schiff (PAS)-stained cartilage
Targeted differentiation (Fig. 4)	Endoderm: definitive endoderm — GATA4 (Cvoro et al., 2015). Ectoderm: keratinocytes — p63, KRT14 (Petrova et al., 2014) Mesoderm: cardiomyocytes — TNNT2
Sibling lines available	KCL032, KCL033

We generated KCL034 clinical grade hESC line following protocols, established previously (Ilic et al., 2012; Stephenson et al., 2012), and now adapted to cGMP conditions. The expression of the pluripotency markers was tested after freeze/thaw cycle (Fig. 1). Differentiation potential into three germ layers was verified in vitro (Fig. 2), in vivo (Fig. 3) and with targeted differentiation into specific endoderm, ectoderm and mesoderm cell types (Fig. 4).

Molecular karyotyping identified a gain on chromosome 6p22.1. The gain on chromosome 5p14.3 containing the following genes: *HIST1H2BL*, *HIST1H2AI*, *HIST1H3H*, *HIST1H2AJ*, *HIST1H2BM*, *HIST1H4J*, *HIST1H4K*, *HIST1H2AK*, *HIST1H2BN*, *HIST1H2AL*, *HIST1H1B*, *HIST1H3I*, *HIST1H4L*, *HIST1H3J*, *HIST1H2AM*, *HIST1H2BO*, *OR2B2* and *OR2B6* (Canham et al., 2015). The 330.8 kb gain starts at bp 27627265 and ends at bp 27958049 as referred to Human Genome Build 38. This duplication that contained part of the Histone 1 gene cluster was not fully present on the database of genomic variants (DGV; http://dgv.tcag.ca), which has collected structural variations in more than 14,000 healthy individuals from worldwide population (MacDonald et al., 2014). It is probable that this gain represents a benign event as other histone clusters have been shown to be preferentially duplicated during evolution (Canham et al., 2015; Braastad et al., 2004).

Validation for sterility and specific and non-specific human pathogens (Devito et al., 2014) conformed that the cells in Master Bank were sterile, mycoplasma-free, and negative as well as for Treponema pallidum, Chlamydia, Neisseria gonorrhoeae, Human immunodeficiency virus-1 and 2 (HIV-1 and -2), Human T-lymphotropic virus type-1 and 2 (HTLV-1 and 2), Hepatitis A, B and C (HAV, HBV and HCV), Human herpes simplex virus HHV-4 (Epstein–Barr virus, EBV), -6, -7, and -8, Human cytomegalovirus (hCMV), human parvovirus B19, SV40, JCV, BKV, Enterovirus, HAV, HCV, nonspecific viral and other adventitious contaminants.

We also generated research grade of KCL034 line that is adapted to feeder-free conditions.

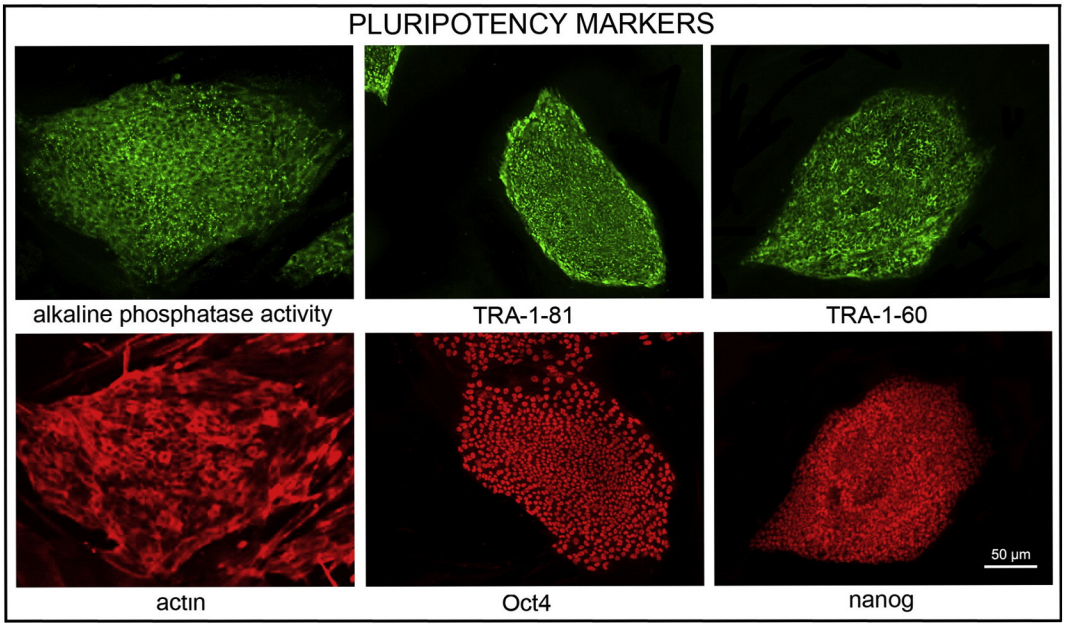

Fig. 1. Expression of pluripotency markers. Pluripotency is confirmed by immunostaining (Oct4, Nanog, TRA-1-60, TRA-1-81) and alkaline phosphatase (AP) activity assay. Actin stress fibers, visualized with rhodamine–phalloidin (red), are present in both feeders and hES cell colonies, whereas AP activity (green) is detected only in hES cells. Scale bar, 50 µm.

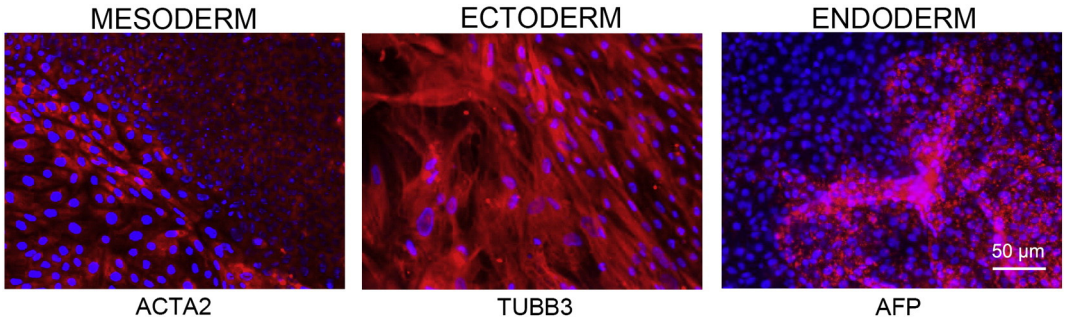

Fig. 2. Differentiation of three germ layers in vitro is confirmed by detection of markers: smooth muscle actin (ACTA2, red) for mesoderm, β-III tubulin (TUBB3, red) for ectoderm and α-fetoprotein (AFP, red) for endoderm. Nuclei are visualized with Hoechst 33342 (blue). Scale bar, 50 μm.

Materials and methods

Consenting process

We distribute Patient Information Sheet (PIS) and consent form to the in vitro fertilization (IVF) patients if they opted to donate to research embryos that were stored for 5 or 10 years. They mail signed consent back to us and that might be months after the PIS and consent were mailed to them. If in meantime new versions of PIS/consent are implemented, we do not send these to the patients or ask them to re-sign; the whole process is done with the version that was given them initially. The PIS/consent documents (FRO-V.6) were created on Dec. 18, 2008. HFEA Code of Practice that was in effect at the time of document creation: Edition 7 — R.4 (http://www.hfea.gov.uk/2999.html). The donor couple signed the consent on May 26, 2009. HFEA Code of Practice that was in effect at the time of donor signature: Edition 7 — R.4. HFEA Code of Practice Edition 7 — R.4 was in effect: 02 Oct. 2008–30 Sep. 2009.

Embryo culture and micromanipulation

Embryo culture and laser-assisted dissection of inner cell mass (ICM) were carried out as previously described in details (Ilic et al., 2012; Stephenson et al., 2012). The cellular area containing the ICM was then washed and transferred to plates containing mitotically inactivated human neonatal foreskin fibroblasts (HFF).

Cell culture

ICM plated on mitotically inactivated HFF were cultured as described (Ilic et al., 2012; Stephenson et al., 2012). TE cells were removed mechanically from outgrowth (Ilic et al., 2007, 2010). hES colonies were expanded and cryopreserved at the third passage.

Viability test

Straws with the earliest frozen passage (p. 2–3) are thawed and new colonies are counted three days later. These colonies are then expanded up to passage 8, at which point cells were part frozen and part subjected to standard battery of tests (pluripotency markers, in vitro and in vivo differentiation capability, genetics, sterility, mycoplasma).

Pluripotency markers

Pluripotency was assessed using two different techniques: enzymatic activity assay [alkaline phosphatase (AP) assay] and immunostaining as described (Ilic et al., 2012; Stephenson et al., 2012).

Differentiation

Spontaneous differentiation into three germ layers was assessed in vitro and in vivo as described (Petrova et al., 2014; Stephenson

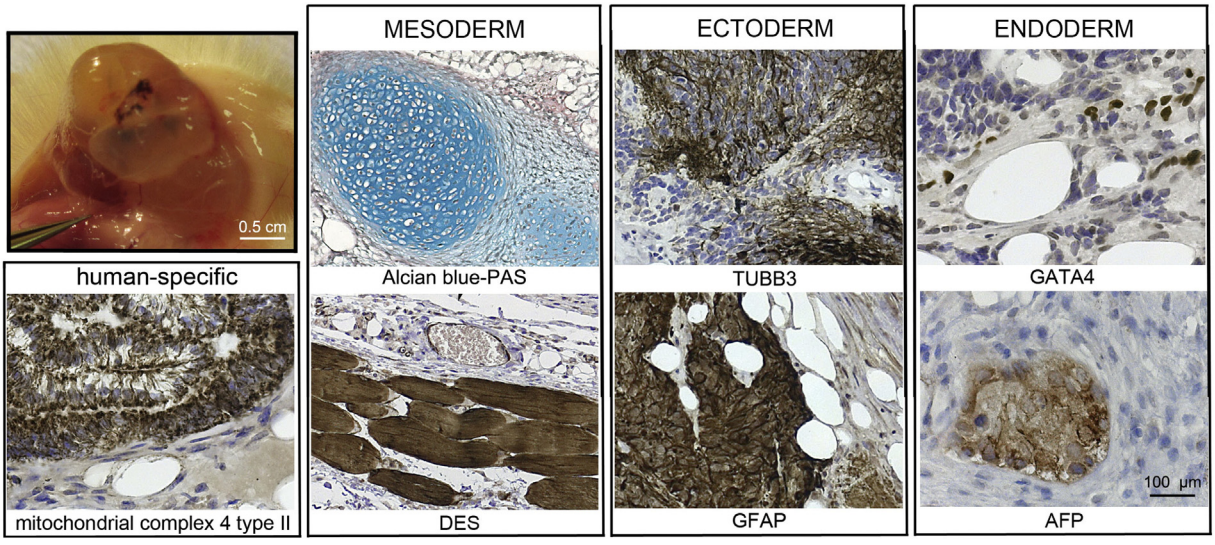

Fig. 3. Differentiation of three germ layers in vivo. Teratomas were encapsulated and did not invade surrounding tissue. Sections are counterstained with hematoxylin and eosin and specific stains are brown (immunohistochemistry) or light blue (Alcian blue). Germ layer markers: Alcian blue–PAS-stained cartilage and DES for mesoderm, TUBB3 and GFAP for ectoderm, GATA4 and AFP for endoderm. Positive immunostaining for complex IV type II marker confirms the human origin of the tumor (adjacent section of the one stained for desmin). Scale bars are 100 μm.

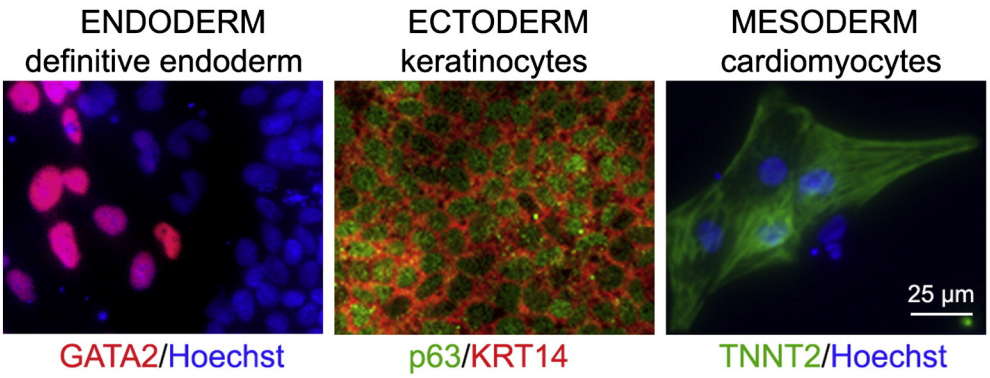

Fig. 4. Targeted differentiation into specific cell types of endoderm (definitive endoderm), extoderm (keratinocytes) and mesoderm (cardiomyocytes). Definitive endoderm: GATA2 (red), nuclei (blue). Ectoderm: p63 (red), KRT14 (green), nuclei (blue). Mesoderm: TNNT2 (green), nuclei (blue). Scale bar, 125 μm.

et al., 2012). Targeted differentiation in cardiomyocytes (Jacquet et al., 2015; Laflamme et al., 2007) and definitive endoderm (Cvoro et al., 2015; Cheng et al., 2012), keratinocytes (Petrova et al., 2014), followed the protocols described earlier. Nuclei are visualized with Hoechst 33342.

Genotyping

DNA was extracted from hESC cultures using a Chemagen DNA extraction robot according to the manufacturer's instructions. Amplification of polymorphic microsatellite markers was carried out as described (Ilic et al., 2012). Allele sizes were recorded to give a unique fingerprint of each cell line.

Array comparative genomic hybridization (aCGH)

aCGH was performed as described in details (Ilic et al., 2012).

Whole-genome single nucleotide polymorphism (SNP) array

SNP array was performed as described in details (Canham et al., 2015).

HLA typing

HLA-A, -B and -DRB1 typing was performed with a PCR sequence-specific oligonucleotide probe (SSOP; Luminex, Austin, TX, USA) hybridization protocol at the certified Clinical Transplantation Laboratory, Guy's and St Thomas' NHS Foundation Trust and Serco Plc. (GSTS) Pathology (Guy's Hospital, London, UK) as described (Jacquet et al., 2013). HLA typing was also performed independently by other group (Canham et al., 2015).

Validation for sterility and specific and non-specific human pathogens

Validation for sterility and specific and non-specific human pathogens was performed as described (Devito et al., 2014). All validation studies were conducted by SGS Vitrology (Glasgow, U.K., http://www.sgs.com), in compliance with the principles of GMP as set out in Directive 2003/94/EC for medicinal products for human use (Directive 2003/94/EC, 2003) and 91/412/EEC for veterinary medicinal products (Directive 91/412/EEC, 1991).

Sterility testing was performed in accordance with the current requirements of the European Pharmacopoeia, Section 2.6.1 Sterility, U.S. Pharmacopeia, 71. Sterility Tests, and International Conference on Harmonisation Topic Q5D guidelines.

Mycoplasma testing was performed in accordance with the current requirements of the European Pharmacopoeia, Section 2.6.7, Mycoplasmas.

All PCR-based assays used were compliant with the current edition of the European Pharmacopoeia, 2.6.21, Nucleic Acid Amplification Techniques.

Author disclosure statement

There are no competing financial interests in this study.

Acknowledgments

This work was supported by the UK Medical Research Council grants G0701172 and G0801061. We thank Dr. Yacoub Khalaf, Director of the Assisted Conception Unit of Guy's and St Thomas' NHS Foundation Trust and his staff for supporting the research program. We are especially indebted to Prof Peter Braude and patients who donated embryos.

References

Braastad, C.D., Hovhannisyan, H., Van Wijnen, A.J., Stein, J.L., Stein, G.S., 2004. Functional characterization of a human histone gene cluster duplication. Gene 342 (1), 35–40.
Canham, A., Van Deusen, A., Brison, D.R., De Sousa, P., Downie, J., Devito, L., Hewitt, Z.A., Ilic, D., Kimber, S.J., Moore, H.D., Murray, H., Kunath, T., 2015. The molecular karyotype of 25 clinical-grade human embryonic stem cells lines. Sci. Rep. 5, 17258.
Cheng, X., Ying, L., Lu, L., Galvão, A.M., Mills, J.A., Lin, H.C., Kotton, D.N., Shen, S.S., Nostro, M.C., Choi, J.K., Weiss, M.J., French, D.L., Gadue, P., 2012. Self-renewing endodermal progenitor lines generated from human pluripotent stem cells. Cell Stem Cell 10 (4), 371–384.
Cvoro, A., Devito, L., Milton, F.A., Noli, L., Zhang, A., Filippi, C., Sakai, K., Suh, J.H., Sieglaff, D., Dhawan, A., Sakai, T., Ilic, D., Webb, P., 2015. A thyroid hormone receptor/KLF9 axis in human hepatocytes and pluripotent stem cells. Stem Cells 33 (2), 416–428. http://dx.doi.org/10.1002/stem.1875 http://www.ncbi.nlm.nih.gov/pubmed/25330987.
Devito, L., Petrova, A., Miere, C., Codognottom, S., Blakely, N., Lovatt, A., Ogilvie, C., Khalaf, Y., Ilic, D., 2014. Cost-effective master cell bank validation of multiple clinical-grade human pluripotent stem cell lines from a single donor. Stem Cells Transl. Med. 3 (10), 1116–1124.
Directive 2003/94/EC of the European Parliament and of the Council, 2003. Laying down the principles and guidelines of good manufacturing practice in respect of medical products for human use and investigational medicinal products for human use. Off. J. Eur. Union L262, 22–26 (Available at http://ec.europa.eu/health/files/eudralex/vol-1/dir_2003_94/dir_2003_94_en.pdf October 08 October 14, 2003).
Directive 91/412/EEC, 1991. Laying down the principles and guidelines of good manufacturing practice for veterinary medicinal products. Off. J. Eur. Union L228, 70–73 (Available at: http://ec.europa.eu/health/files/eudralex/vol-5/dir_1991_412/dir_1991_412_en.pdf July 23 August 17, 1991).
Ilic, D., Genbacev, O., Krtolica, A., 2007. Derivation of hESC from intact blastocysts. Curr. Protoc. Stem Cell Biol. (Chapter 1: Unit 1A.2).
Ilic, D., Caceres, E., Lu, S., Julian, P., Foulk, R., Krtolica, A., 2010. Effect of karyotype on successful human embryonic stem cell derivation. Stem Cells Dev. 19 (1), 39–46.
Ilic, D., Stephenson, E., Wood, V., Jacquet, L., Stevenson, D., Petrova, A., Kadeva, N., Codognotto, S., Patel, H., Semple, M., Cornwell, G., Ogilvie, C., Braude, P., 2012. Derivation and feeder-free propagation of human embryonic stem cells under xeno-free conditions. Cytotherapy 14 (1), 122–128.
Jacquet, L., Stephenson, E., Collins, R., Patel, H., Trussler, J., Al-Bedaery, R., Renwick, P., Ogilvie, C., Vaughan, R., Ilic, D., 2013. Strategy for the creation of clinical grade hESC line banks that HLA-match a target population. EMBO Mol. Med. 5 (1), 10–17.
Jacquet, L., Neueder, A., Földes, G., Karagiannis, P., Hobbs, C., Jolinon, N., Mioulane, M., Sakai, T., Harding, S.E., Ilic, D., 2015. Three Huntington's Disease Specific Mutation-Carrying Human Embryonic Stem Cell Lines Have Stable Number of CAG Repeats upon In Vitro Differentiation into Cardiomyocytes. PLoS One 10, e0126860. http://

dx.doi.org/10.1371/journal.pone.0126860 http://www.ncbi.nlm.nih.gov/pubmed/25993131.

Laflamme, M.A., Chen, K.Y., Naumova, A.V., Muskheli, V., Fugate, J.A., Dupras, S.K., Reinecke, H., Xu, C., Hassanipour, M., Police, S., O'sullivan, C., Collins, L., Chen, Y., Minami, E., Gill, E.A., Ueno, S., Yuan, C., Gold, J., Murry, C.E., 2007. Cardiomyocytes derived from human embryonic stem cells in pro-survival factors enhance function of infarcted rat hearts. Nat. Biotechnol. 25 (9), 1015–1024.

MacDonald, J.R., Ziman, R., Yuen, R.K.C., Feuk, L., Scherer, S.W., 2014. The database of genomic variants: a curated collection of structural variation in the human genome. Nucleic Acids Res. 42, D986–D992.

Petrova, A., Celli, A., Jacquet, L., Dafou, D., Crumrine, D., Hupe, M., Arno, M., Hobbs, C., Cvoro, A., Karagiannis, P., Devito, L., Sun, R., Adame, L.C., Vaughan, R., McGrath, J.A., Mauro, T.M., Ilic, D., 2014. In vitro model of a functional epidermal permeability barrier from human embryonic stem cells and induced pluripotent stem cells. Stem Cell Reports 2 (5), 675–689. http://dx.doi.org/10.1016/j.stemcr.2014.03.009 http://www.ncbi.nlm.nih.gov/pubmed/24936454.

Stephenson, E., Jacquet, L., Miere, C., Wood, V., Kadeva, N., Cornwell, G., Codognotto, S., Dajani, Y., Braude, P., Ilic, D., 2012. Derivation and propagation of human embryonic stem cell lines from frozen embryos in an animal product-free environment. Nat. Protoc. 7 (7), 1366–1381.

Stem Cell Research 16 (2016) 345–348

Contents lists available at ScienceDirect

Stem Cell Research

journal homepage: www.elsevier.com/locate/scr

Lab Resource: Stem Cell Line

Generation of KCL036 research grade human embryonic stem cell line carrying a mutation in the *HTT* gene

Laureen Jacquet [a], Heema Hewitson [a], Victoria Wood [a], Neli Kadeva [a], Glenda Cornwell [a], Stefano Codognotto [a], Carl Hobbs [b], Emma Stephenson [a], Dusko Ilic [a,*]

[a] Stem Cell Laboratories, Division of Women's Health, Faculty of Life Sciences and Medicine, King's College London and Assisted Conception Unit, Guys' Hospital, London, United Kingdom
[b] Histology Laboratory, Wolfson Centre for Age-Related Diseases, Faculty of Life Sciences and Medicine, King's College London, London, United Kingdom

ARTICLE INFO

Article history:
Received 31 December 2015
Received in revised form 16 January 2016
Accepted 8 February 2016
Available online 10 February 2016

ABSTRACT

The KCL036 human embryonic stem cell line was derived from an embryo donated for research that carried an autosomal dominant mutation affecting one allele of the *HTT* gene encoding huntingtin (38 trinucleotide repeats; 14 for the normal allele). The ICM was isolated using laser microsurgery and plated on γ-irradiated human foreskin fibroblasts. Both the derivation and cell line propagation were performed in an animal product-free environment. Pluripotent state and differentiation potential were confirmed by in vitro and in vivo assays.

Resource table

Name of stem cell line	KCL036
Institution	King's College London, London UK
Derivation team	Neli Kadeva, Victoria Wood, Glenda Cornwell, Stefano Codognotto, Emma Stephenson
Contact person and email	Dusko Ilic, email: dusko.ilic@kcl.ac.uk
Date archived/ stock date	Nov 22, 2011
Type of resource	Biological reagent: cell line
Sub-type	Human pluripotent stem cell line
Origin	Human embryo
Key marker expression	Pluripotent stem cell markers: NANOG, OCT4, TRA-1-60, TRA-1-81, alkaline phosphatase (AP) activity
Authentication	Identity and purity of line confirmed
Link to related literature (direct URL links and full references)	1) Ilic, D., Stephenson, E., Wood, V., Jacquet, L., Stevenson, D., Petrova, A., Kadeva, N., Codognotto, S., Patel, H., Semple, M., Cornwell, G., Ogilvie, C., Braude, P., 2012. Derivation and feeder-free propagation of human embryonic stem cells under xeno-free conditions. Cytotherapy. 14 (1), 122–128. doi: 10.3109/14,653,249.2011.623692 http://www.ncbi.nlm.nih.gov/pubmed/22029654 2) Stephenson, E., Jacquet, L., Miere, C., Wood, V., Kadeva, N., Cornwell, G., Codognotto, S., Dajani, Y., Braude, P., Ilic, D., 2012. Derivation and propagation of human embryonic stem cell lines from frozen embryos in an animal product-free environment. Nat. Protoc. 7 (7), 1366–1381. doi: 10.1038/nprot.2012.080 http://www.ncbi.nlm.nih.gov/pubmed/22722371

(*continued*)

Name of stem cell line	KCL036
Information in public databases	3) Jacquet, L., Neueder, A., Földes, G., Karagiannis, P., Hobbs, C., Jolinon, N., Mioulane, M., Sakai, T., Harding, S.E., Ilic, D., 2015. Three Huntington's Disease Specific Mutation-Carrying Human Embryonic Stem Cell Lines Have Stable Number of CAG Repeats upon In Vitro Differentiation into Cardiomyocytes. PLoS One. 10(5), e0126860. http://www.ncbi.nlm.nih.gov/pubmed/25993131 KCL036 is a National Institutes of Health (NIH) registered hESC line NIH Registration Number: 0241 NIH Approval Number: NIHhESC-13-0241 http://grants.nih.gov/stem_cells/registry/current.htm?id=668
Ethics	The hESC line KCL036 is derived under license from the UK Human Fertilisation and Embryology Authority (research license numbers: R0075 and R0133) and also has local ethical approval (UK National Health Service Research Ethics Committee Reference: 06/Q0702/90). Informed consent was obtained from all subjects and the experiments conformed to the principles set out in the WMA Declaration of Helsinki and the NIH Belmont Report. No financial inducements are offered for donation.

Resource details

Consent signed	Jul 21, 2011
Embryo thawed	Oct 23, 2011
UK Stem Cell Bank Deposit Approval	Sep 13, 2012 Reference: SCSC12-28

(*continued on next page*)

* Corresponding author.

http://dx.doi.org/10.1016/j.scr.2016.02.026

(*continued*)

Consent signed	Jul 21, 2011
Sex	Male 46, XY
Grade	Research
Disease status (Fig. 1)	Mutation affecting one allele of the *HTT* gene encoding huntingtin (~38 CAG repeats; 14 for the normal allele) associated with Huntington's disease (Ilic et al., 2015)
Karyotype (aCGH)	Decreased copy number at 2q37.3 (242,930,599–242,948,040) and at 3q25.1 (151,368,847–151,542,568). The imbalances are considered to be benign copy number variants. The chromosome 3 imbalance was not called by software.
DNA fingerprint	Allele sizes (in bp) of 17 microsatellite markers specific for chromosomes 13, 18 and 21 (Jacquet et al., 2015)
Viability testing	Pass
Pluripotent markers (immunostaining) (Fig. 2)	NANOG, OCT4, TRA-1-60, TRA-1-81, AP activity (Jacquet et al., 2015)
Three germ layers differentiation in vitro (immunostaining) (Fig. 3)	Endoderm: AFP (α-fetoprotein); Ectoderm: TUBB3 (tubulin, β3 class III); Mesoderm: ACTA2 (actin, α2, smooth muscle) (Jacquet et al., 2015)
Three germ layer differentiation in vivo (teratomas) (Fig. 4)	Endoderm: AFP, GATA4. Ectoderm: TUBB3, GFAP (glial fibrillary acidic protein). Mesoderm: DES (desmin), Alcian Blue and periodic acid–Schiff (PAS)-stained cartilage (Jacquet et al., 2015)
Targeted differentiation (Fig. 5)	Cardiomyocytes: TNNT2 (cardiac troponin T) immunostaining
Sibling lines available	None

We generated KCL036 research grade hESC line following protocols established previously (Ilic et al., 2012; Stephenson et al., 2012; Jacquet et al., 2013). The expression of the pluripotency markers was tested after freeze/thaw cycle (Fig. 2; Jacquet et al., 2015). Differentiation potential into three germ layers was verified in vitro (Fig. 3 and Fig. 5; Jacquet et al., 2015) and in vivo (Fig. 4; Jacquet et al., 2015).

Validation for sterility and specific and non-specific human pathogens confirmed that the cells in Master Bank were sterile, mycoplasma-free, and negative for human immunodeficiency virus 1 (HIV-1), Human T-lymphotropic virus type 1 (HTLV-1), hepatitis B and C (HBV and HCV), human herpes simplex virus HHV-4 (Epstein–Barr virus, EBV), and human cytomegalovirus (hCMV).

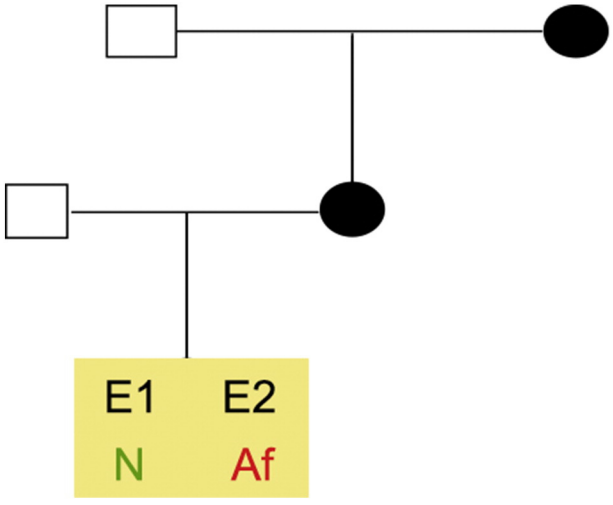

Fig. 1. Genetic pedigree tree. The couple undergoing IVF had 16 embryos in this particular cycle. Three embryos were normal, whereas those that carried the mutation in *HTT* were donated for research. We derived hESC lines from two of them.

We also generated research grade of KCL036 line that is adapted to feeder-free conditions (Jacquet et al., 2015).

Materials and methods

Consenting process

We distribute patient information sheets (PIS) and consent forms to the in vitro fertilization (IVF) patients if they opted to donate to research embryos that were stored for 5 or 10 years. They mail signed consent back to us and that might be months after the PIS and consent were mailed to them. If in the meantime new versions of PIS/consent are implemented, we do not send these to the patients or ask them to re-sign; the whole process is done with the version that was given them initially. The PIS/consent documents (PGD-V.9) were created on Feb. 09, 2011. HFEA Code of Practice that was in effect at the time of document creation: Edition 8—R.2 (http://www.hfea.gov.uk/2999.html). The donor couple signed the consent on Jul. 21, 2011. HFEA Code of Practice that was in effect at the time of donor signature: Edition 8—R.3. HFEA Code of Practice Edition 8—R.2 was in effect: Apr. 07, 2010–Apr. 06, 2011. HFEA Code of Practice Edition 8—R.3 was in effect: Apr. 07, 2011–Oct. 01, 2011.

Embryo culture and micromanipulation

Embryo culture and laser-assisted dissection of inner cell mass (ICM) were carried out as previously described in details (Ilic et al., 2012; Stephenson et al., 2012). The cellular area containing the ICM was then washed and transferred to plates containing mitotically inactivated human neonatal foreskin fibroblasts (HFF).

Cell culture

ICM plated on mitotically inactivated HFF were cultured as described (Ilic et al., 2012; Stephenson et al., 2012). TE cells were removed mechanically from outgrowth (Ilic et al., 2007; Ilic et al., 2010). hESC colonies were expanded and cryopreserved at the third passage.

Viability test

Straws with the earliest frozen passage (p.2–3) are thawed and new colonies are counted 3 days later. These colonies are then expanded up to passage 8, at which point cells were part frozen and part subjected to standard battery of tests (pluripotency markers, in vitro and in vivo differentiation capability, genetics, sterility, mycoplasma).

Pluripotency markers

Pluripotency was assessed using two different techniques: enzymatic activity assay [alkaline phosphatase (AP) assay] and immunostaining as described (Ilic et al., 2012; Stephenson et al., 2012).

Differentiation

Spontaneous differentiation into three germ layers was assessed in vitro and in vivo (Jacquet et al., 2015) as described (Ilic et al., 2012; Stephenson et al., 2012; Petrova et al., 2014). Targeted differentiation in cardiomyocytes followed the protocols described earlier (Jacquet et al., 2015; Laflamme et al., 2007).

Genotyping

DNA was extracted from hESC cultures using a Chemagen DNA extraction robot according to the manufacturer's instructions.

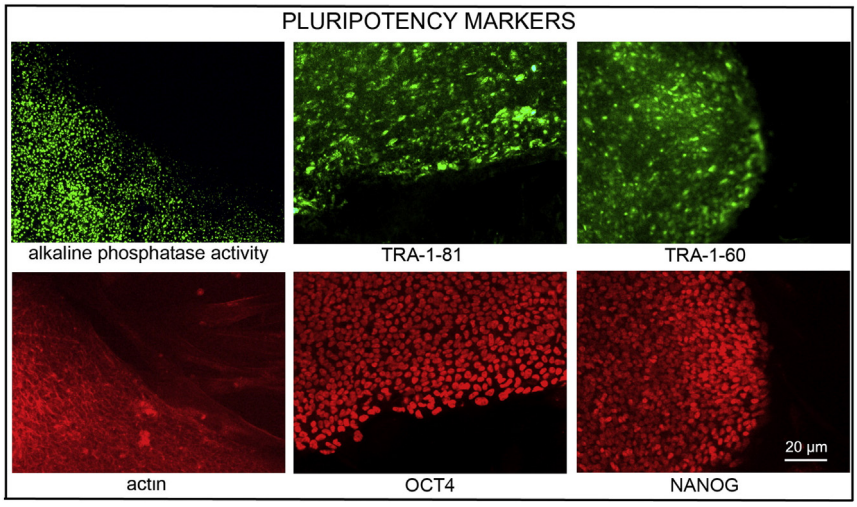

Fig. 2. Expression of pluripotency markers. Pluripotency is confirmed by immunostaining (Oct4, Nanog, TRA-1-60, TRA-1-81) and alkaline phosphatase (AP) activity assay. Scale bar, 20 µm.

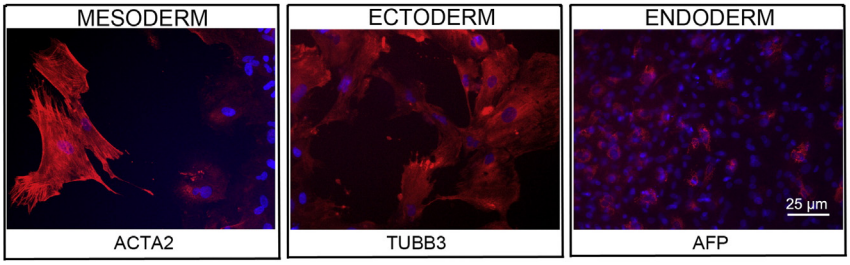

Fig. 3. Differentiation of three germ layers in vitro is confirmed by detection of markers: smooth muscle actin (ACTA2, red) for mesoderm, β-III tubulin (TUBB3, red) for ectoderm, and α-fetoprotein (AFP, red) for endoderm. Nuclei are visualized with Hoechst 33342 (blue). Scale bar, 25 µm.

Amplification of polymorphic microsatellite markers was carried out as described (Ilic et al., 2012). Allele sizes were recorded to give a unique fingerprint of each cell line.

Array comparative genomic hybridization (aCGH)

aCGH was performed as described in details (Ilic et al., 2012).

Special pathology

The Doctors Laboratory London (UK) tested the line for HIV1, HepB, HepC, CMV, and EBV by PCR.

Author disclosure statement

There are no competing financial interests in this study.

Acknowledgments

This work was supported by the UK Medical Research Council grants G0701172 and G0801061. We thank Dr. Yacoub Khalaf, Director of the Assisted Conception Unit of Guy's and St Thomas' NHS Foundation Trust and his staff for supporting the research program. We are especially indebted to Prof Peter Braude and to the patients who donated embryos.

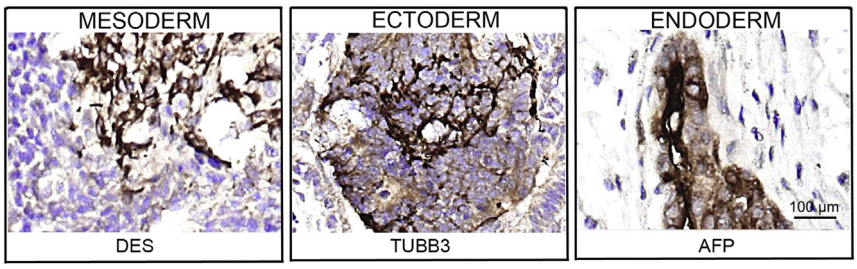

Fig. 4. Differentiation of three germ layers in vivo. Teratomas were encapsulated and did not invade surrounding tissue. Sections are counterstained with hematoxylin and eosin and specific stains are brown (immunohistochemistry). Germ layer marker: DES for mesoderm, TUBB3 for ectoderm, and AFP for endoderm. Scale bars are 100 µm.

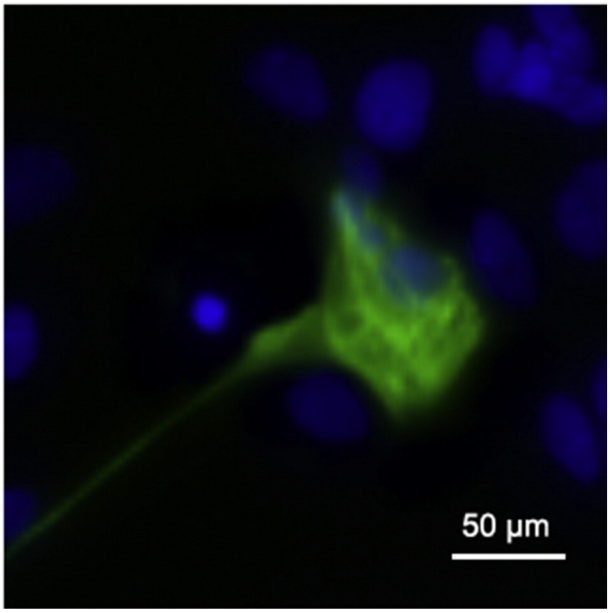

Fig. 5. TNNT2 (green) immunostaining on day 30 of cardiac differentiation. Nuclei are visualized with Hoechst 33342 (blue). Scale bar, 50 µm.

References

Ilic, D., Stephenson, E., Wood, V., Jacquet, L., Stevenson, D., Petrova, A., Kadeva, N., Codognotto, S., Patel, H., Semple, M., Cornwell, G., Ogilvie, C., Braude, P., 2012. Derivation and feeder-free propagation of human embryonic stem cells under xeno-free conditions. Cytotherapy 14 (1), 122–128.

Ilic, D., Caceres, E., Lu, S., Julian, P., Foulk, R., Krtolica, A., 2010. Effect of karyotype on successful human embryonic stem cell derivation. Stem Cells Dev. 19 (1), 39–46.

Ilic, D., Genbacev, O., Krtolica, A., 2007. Derivation of hESC from intact blastocysts. Curr. Protoc. Stem. Cell Biol. (Chapter 1: Unit 1 A.2).

Jacquet, L., Neueder, A., Földes, G., Karagiannis, P., Hobbs, C., Jolinon, N., Mioulane, M., Sakai, T., Harding, S.E., Ilic, D., 2015. Three Huntington's disease specific mutation-carrying human embryonic stem cell lines have stable number of CAG repeats upon in vitro differentiation into cardiomyocytes. PLoS ONE 10 (5), e0126860.

Jacquet, L., Stephenson, E., Collins, R., Patel, H., Trussler, J., Al-Bedaery, R., Renwick, P., Ogilvie, C., Vaughan, R., Ilic, D., 2013. Strategy for the creation of clinical grade hESC line banks that HLA-match a target population. EMBO Mol. Med. 5 (1), 10–17.

Laflamme, M.A., Chen, K.Y., Naumova, A.V., Muskheli, V., Fugate, J.A., Dupras, S.K., Reinecke, H., Xu, C., Hassanipour, M., Police, S., O'sullivan, C., Collins, L., Chen, Y., Minami, E., Gill, E.A., Ueno, S., Yuan, C., Gold, J., Murry, C.E., 2007. Cardiomyocytes derived from human embryonic stem cells in pro-survival factors enhance function of infarcted rat hearts. Nat. Biotechnol. 25 (9), 1015–1024.

Petrova, A., Celli, A., Jacquet, L., Dafou, D., Crumrine, D., Hupe, M., Arno, M., Hobbs, C., Cvoro, A., Karagiannis, P., Devito, L., Sun, R., Adame, L.C., Vaughan, R., McGrath, J.A., Mauro, T.M., Ilic, D., 2014. 3D in vitro model of a functional epidermal permeability barrier from human embryonic stem cells and induced pluripotent stem cells. Stem Cell Rep. 2 (5), 675–689.

Stephenson, E., Jacquet, L., Miere, C., Wood, V., Kadeva, N., Cornwell, G., Codognotto, S., Dajani, Y., Braude, P., Ilic, D., 2012. Derivation and propagation of human embryonic stem cell lines from frozen embryos in an animal product-free environment. Nat. Protoc. 7 (7), 1366–1381.

SCIENTIFIC REPORTS

OPEN

The Molecular Karyotype of 25 Clinical-Grade Human Embryonic Stem Cell Lines

Received: 07 August 2015
Accepted: 27 October 2015
Published: 26 November 2015

Maurice A. Canham[1], Amy Van Deusen[1], Daniel R. Brison[2], Paul A. De Sousa[3,4], Janet Downie[3], Liani Devito[5], Zoe A. Hewitt[6], Dusko Ilic[5], Susan J. Kimber[7], Harry D. Moore[6], Helen Murray[3] & Tilo Kunath[1]

The application of human embryonic stem cell (hESC) derivatives to regenerative medicine is now becoming a reality. Although the vast majority of hESC lines have been derived for research purposes only, about 50 lines have been established under Good Manufacturing Practice (GMP) conditions. Cell types differentiated from these designated lines may be used as a cell therapy to treat macular degeneration, Parkinson's, Huntington's, diabetes, osteoarthritis and other degenerative conditions. It is essential to know the genetic stability of the hESC lines before progressing to clinical trials. We evaluated the molecular karyotype of 25 clinical-grade hESC lines by whole-genome single nucleotide polymorphism (SNP) array analysis. A total of 15 unique copy number variations (CNVs) greater than 100 kb were detected, most of which were found to be naturally occurring in the human population and none were associated with culture adaptation. In addition, three copy-neutral loss of heterozygosity (CN-LOH) regions greater than 1 Mb were observed and all were relatively small and interstitial suggesting they did not arise in culture. The large number of available clinical-grade hESC lines with defined molecular karyotypes provides a substantial starting platform from which the development of pre-clinical and clinical trials in regenerative medicine can be realised.

Since the derivation of human embryonic stem cells (hESCs) from blastocysts in 1998[1], and the more recent production of human induced pluripotent stem cells (iPSCs) from adult tissues[2], anticipation has been growing with regard to their potential as cell therapies for a number of incurable conditions. As with any new medicine, Good Manufacturing Practice (GMP) is required to produce hESC/iPSC-derived cell products for clinical use in humans[3]. However, while over 1200 hESC lines have been established and reported worldwide[4], the majority are suitable only for research purposes due to the sourcing of embryonic material, derivation process and subsequent handling procedures. Frequently, derivation and culture methods employ mouse feeder cells or poorly defined media containing animal-based products[1,5], which may render these cell lines unusable as a starting material for any cell-based clinical application.

In recent years, there have been advances in the derivation of hESC lines whereby fully defined media devoid of animal-derived products is used[6,7], and the traditional mouse feeders have been replaced with GMP-qualified human feeders[8–10] or recombinant human proteins as a substrate on which to culture

[1]MRC Centre for Regenerative Medicine, Institute for Stem Cell Research, School of Biological Sciences, The University of Edinburgh, UK. [2]Department of Reproductive Medicine, St. Mary's Hospital, Central Manchester NHS Foundation Trust, Manchester Academic Health Sciences Centre, Manchester, UK. [3]Roslin Cells Limited, Nine Edinburgh BioQuarter, Edinburgh, UK. [4]Centre for Clinical Brain Sciences and MRC Centre for Regenerative Medicine, The University of Edinburgh, UK. [5]Stem Cell Laboratories, Guy's Assisted Conception Unit, Division of Women's Health, Faculty of Life Sciences and Medicine, King's College London, London, UK. [6]Centre for Stem Cell Biology, Department of Biomedical Science, The University of Sheffield, Sheffield, UK. [7]Faculty of Life Sciences, The University of Manchester, Manchester, UK. Correspondence and requests for materials should be addressed to T.K. (email: tilo.kunath@ed.ac.uk)

Derivation Centre	EUTCD Grade Cell Lines	Number
King's College London[1]	**KCL031**, **KCL032**, **KCL033**, **KCL034**, **KCL037**, **KCL038**, **KCL039**, **KCL040**	8
The University of Manchester	**Man11**, **Man12**, *Man13*, *Man14*, *Man15*, *Man16*	6
Newcastle University	*NCL14*	1
Roslin Cells Ltd, Edinburgh	**RC9**, **RC11**, *RC12*, *RC13*, *RC14*, *RC15*, *RC16*, **RC17**	8
The University of Sheffield	*MasterShef1*, **MasterShef2**, **MasterShef3**, **MasterShef4**, **MasterShef5**, *MasterShef6*, **MasterShef7**, **MasterShef8**, **MasterShef10**, **MasterShef11**, **MasterShef12**, **MasterShef13**, **MasterShef14**, *Shef3.2,* **Shef6.1**	15
Total		**38**

Table 1. List of 38 EUTCD compliant (clinical-grade) hESC lines. The 25 hESC lines analysed by SNP analysis are shown in bold. [1]All eight (8) of the KCL hESC lines are listed on the NIH Stem Cell Registry (escr.nih.gov) making them available for NIH-funded projects in the USA.

hESCs[11–14]. Furthermore, animal-based enzymes and guinea pig complement used to isolate the inner cell mass for hESC derivation have been replaced with mechanical isolation or laser microdissection[15–19]. These efforts have culminated in the derivation of approximately 50 clinical-grade hESC lines from various centres across the world[20–23] (www.mrc.ac.uk/research/facilities/stem-cell-bank; stemcells.nih.gov).

Remarkably, 38 of these lines have been derived among five different centres in the United Kingdom through funding from the Medical Research Council (MRC), Scottish Enterprise, the North West Development Agency and the Juvenile Diabetes Research Foundation. The MRC launched an initiative in 2005 to provide infrastructure funding to UK *in vitro* fertilization (IVF) units to provide GMP-compliant embryos for hESC line derivation and further funded the Human Embryonic Stem Cell Co-ordinators (hESCCO) network, subsequently the National Clinical hESC Forum. This allowed the derivation centres to work with the Human Fertilisation and Embryology Authority and the UK Stem Cell Bank to establish common parameters for patient consent, screening and embryo procurement for the derivation of clinical-grade hESC lines. Ultimately this farsighted policy has yielded a cohort of hESC lines which have benefited from the shared implementation of GMP-compliant IVF laboratory standards, hESC derivation procedures and ethical principles for donor consenting[24]. A list of clinical-grade hESC lines conforming to the European Union Tissue and Cells Directives (Directives 2004/23/EC and 2006/17/EC) is shown in Table 1. These directives introduced common safety and quality standards across European member states to ensure that all tissues and cells used in patient treatment are traceable from donor to recipient, thus implementing key principles of GMP.

The value of a large number of different cell lines as starting material for clinical applications is three-fold: (a) different hESC lines have varying propensities to generate specific cell lineages during *in vitro* differentiation[25], (b) hESC lines may harbour or acquire genetic anomalies potentially excluding them from clinical use[26], and (c) in order to accommodate human leucocyte antigen (HLA) matching to a broad section of potential patients a sizeable number of hESC lines would be required. It has been estimated that approximately 150 different lines with particular HLA haplotypes would be required to cover ~93% of potential UK recipients[27]. With the advent of iPSC technology, the latter issue will be addressed by derivation of hiPSC lines from individuals homozygous for common HLA loci. An international effort is currently underway to address this[28], but the issues of line-to-line variation and genetic stability of hESC and iPSC lines will remain[29].

In accordance with GMP standards applicable to the sourcing and the application of raw materials used during production processes, such as hESC/iPSC cell derivation and differentiation into desired cell types, there is emerging evidence that equal scrutiny should be undertaken to account for the genetic health of cells at all stages of production[3,30]. Some characteristics of self-renewal and multipotency that define pluripotent stem cells (PSCs) are also shared by tumour stem cells[31]. This has been exemplified by the identification of non-random genetic changes, particularly gains of chromosomes 12, 17 and X, common to embryonal carcinoma cell lines and PSCs following prolonged culture[26,32]. Moreover, recent studies using high-resolution single nucleotide polymorphism (SNP) analysis of PSCs have shown copy number variations (CNVs) that can lead to gene expression alterations functionally linked to cancer[33]. One such microduplication associated with oncogenic transformation was detected on chromosome 20q11.21[34,35]. A comprehensive survey of 125 different PSC lines from many different laboratories across the world showed that about one third of lines acquired a culture-induced genomic variation upon prolonged culture, the most common of which was chromosome 20q11.21 microduplication[36]. The anti-apoptotic gene, *BCL2L1*, within this region has been shown to be a driver of growth advantage[36,37]. In addition to anomalies acquired during self-renewal, the process of *in vitro* differentiation from genetically healthy PSCs can also lead to genomic instability[38].

However, most CNVs are benign and relatively large duplications and deletions (>100 kb) are common in healthy individuals[39]. Such parent-of-origin CNVs will also be present in blastocysts and hESC lines derived from them. The ideal way to determine if a CNV identified in a hESC line is naturally occurring is to genotype the parents of the donated blastocyst. This is indeed possible in cases involving

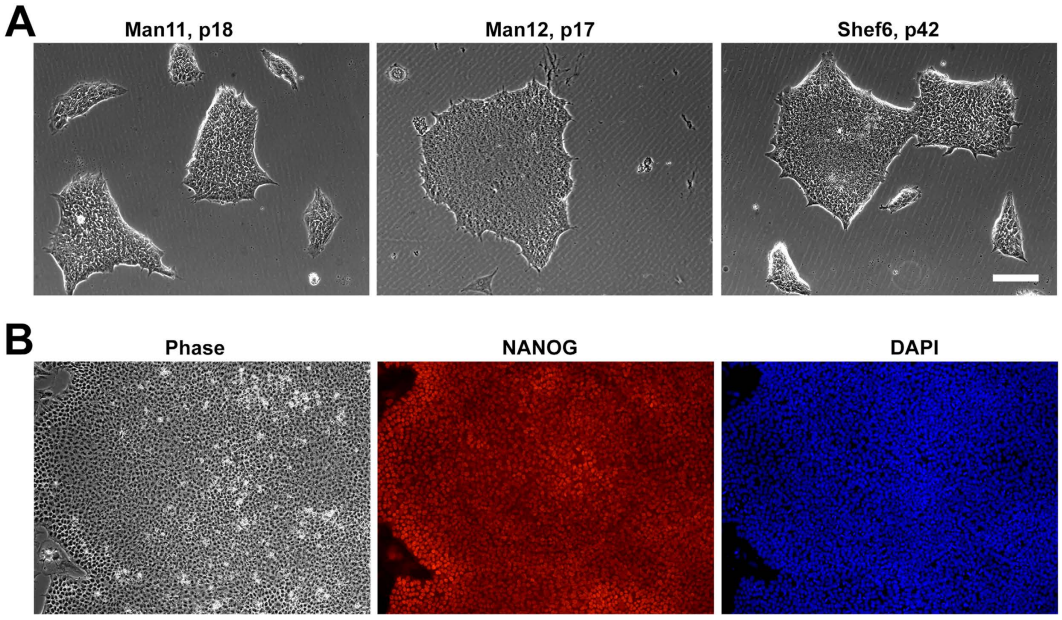

Figure 1. Culture of 3 clinical-grade hESC lines. (**A**) Man11, Man12, and Shef6 hESCs were cultured in Laminin-521 in Essential 8 medium prior to collection of genomic DNA. (**B**) Human ESC lines maintained expression of the pluripotent marker, NANOG, during expansion. Scale bar, 90 μm.

preimplantation genetic diagnosis[40]. However, the vast majority of blastocysts, including all within the UK, are donated under conditions that prohibit access to parental DNA. An alternative method to determine if a particular CNV observed in a hESC cell line might be parent-of-origin is to compare it to known CNVs present on the Database of Genomic Variants (DGV)[41]. The DGV has catalogued a collection of published CNVs from over 14,300 healthy individuals. Although not exhaustive, the collection is highly curated and covers a significant number of CNVs and other genomic structural variants known to exist in the general population. However, if a hESC CNV is found to be present on this database it does not exclude the possibility that it is a *de novo* genomic alteration that arose during development of the blastocyst or during establishment and maintenance of the cell line.

As well as CNVs, copy-neutral loss of heterozygosity (CN-LOH) represent another form of genomic structural variation characterised by a stretch of homozygosity along part of a chromosome[42]. If the affected alleles contain recessive mutations or lie within regions of the genome subject to imprinting, there can be either a net loss or a net gain of gene function and expression[42]. CN-LOH regions can also be due to the presence of persistent ancestral recombination 'cold spots' or be the consequence of recent consanguinity[43,44]. While these changes would be considered parent-of-origin if found in hESC lines, there are examples of somatic or acquired CN-LOH regions found during the progression of many cancers, particularly those of haematopoietic origin[45]. Whole genome SNP arrays are useful to detect CN-LOH events instead of regions, and regions greater than 1 Mb in length warrant further investigation[42].

In this study, we sought to examine the genetic integrity of 25 clinical-grade hESC lines utilising whole-genome SNP genotyping analysis. While karyology is sufficient for establishing genetic normalcy within current regulatory standards, advances in technology and an increasing cytogenetic knowledge base demand higher resolution investigation of cell lines and cell products designed for clinical use.

Results and Discussion

Human ES cell lines were cultured in feeder-free conditions prior to the isolation of genomic DNA (Fig. 1). The DNA from 25 hESC lines (Table 1) was assayed for single nucleotide polymorphisms (SNPs) using the Illumina HumanCytoSNP-12 array and data was analysed for large CNVs with GenomeStudio and KaryoStudio software. Our SNP analysis of 25 clinical-grade hESC lines found 15 unique CNVs greater than 100 kb and 3 CN-LOH regions greater than 1 Mb in size among 16 hESC lines, with results summarised in Table 2. Nine clinical-grade hESC lines did not harbour any structural genomic variants of this size. The percentage of cell lines we found to have CNVs greater than 100 kb (72%) is in agreement with the percentage of healthy individuals (~70%) in the population found to harbour CNVs of at least this size[39]. Additionally, the percentage of cell lines with CN-LOH events between 2.5 and 5 Mb (12%) is similar to the percentage of individuals in outbred populations with CN-LOH of this size range[43]. Since we have restricted our search to large structural changes, we are reporting a considerably lower number of CNVs and CN-LOH regions identified in other studies that have examined hESC or hiPSC lines[33,36,46]. Approximately 5%–10% of the normal human genome contains CNVs averaging a few kilobases in

hESC Line	Passage	Detected Region	Variation	Start (bp)[1]	End (bp)	Length (kb)	# SNPs	*Genes*
KCL031	21	8q24.23	Loss[2]	136718037	136837768	119.7	20	NONE
KCL032	7	5p14.3	Gain	19086546	21585311	2498.8	252	*CDH18*
KCL033	17	5p14.3	Gain	19031726	21440254	2408.5	256	*CDH18*
KCL033	17	12p11.21	Gain[2]	31116366	31248444	132.1	19	NONE
KCL034	19	6p22.1	Gain	27627265	27958049	330.8	13	*HIST1H2BL; HIST1H2AI; HIST1H3H; HIST1H2AJ; HIST1H2BM; HIST1H4J; HIST1H4K; HIST1H2AK; HIST1H2BN; HIST1H2AL; HIST1H1B; HIST1H3I; HIST1H4L; HIST1H3J; HIST1H2AM; HIST1H2BO; OR2B2; OR2B6*
KCL037	8	18q23	Gain	78611768	79153453	541.7	84	*SALL3; ATP9B*
KCL040	21	2q11.1-11.2	CN-LOH	94871756	98412364	3540.6	345	*TEKT4; MAL; MRPS5; ZNF514; ZNF2; PROM2; KCNIP3; FAHD2A; TRIM43; ANKRD36C; GPAT2; ADRA2B; ASTL; DUSP2; STARD7; TMEM127; CIAO1; SNRNP200; ITPRIPL1; NCAPH; NEURL3; ARID5A; KANSL3; FER1L5; LMAN2L; CNNM4; CNNM3; ANKRD23; ANKRD39; SEMA4C; FAM178B; FAHD2B; ANKRD36; ANKRD36B; COX5B; ACTR1B; ZAP70; TMEM131; VWA3B; CNGA3*
KCL040	21	12p11.21	Gain[2]	31116366	31248444	132.1	19	NONE
KCL040	21	16p11.2	Loss[2]	32491547	33993220	1501.7	34	*TP53TG3; TP53TG3C; TP53TG3B*
Man11	21	15q25.3	Gain[2]	85376921	85597560	220.6	39	*AKAP13*
MasterShef2	18	17q21.31	Gain[2]	46138530	46710944	572.4	22	*KANSL1; LRRC37A; ARL17B; LRRC37A2; ARL17A; NSF*
MasterShef3	22	6q27	Gain[2]	167908790	168175598	266.8	59	*MLLT4; KIF25; FRMD1*
MasterShef3	22	17p11.2	Gain	21358248	21593333	235.1	31	*KCNJ12; C17orf51*
MasterShef5	37	12q21.31-21.33	CN-LOH	85929477	89347087	3417.6	397	*MGAT4C; C12orf50; C12orf29; CEP290; TMTC3; KITLG*
MasterShef7	16	14q21.3	Gain	46731743	47047175	315.4	18	*MDGA2*
MasterShef7	16	16p11.2	Gain	29672266	30188484	516.2	94	*QPRT; C16orf54; ZG16; KIF22; MAZ; PRRT2; PAGR1; MVP; CDIPT; SEZ6L2; ASPHD1; KCTD13; TMEM219; TAOK2; HIRIP3; INO80E; DOC2A; C16orf92; FAM57B; ALDOA; PPP4C; TBX6; YPEL3; GDPD3; MAPK3; CORO1A*
MasterShef11	17	19p12	Loss[2,3]	20423851	20532555	108.7	9	NONE
Shef6	45	8p22	Gain	14634612	15188066	553.5	93	*SGCZ*
RC9	17	8q24.23	Loss[2]	136718037	136837768	119.7	20	NONE
RC11	18	2p16.2-16.1	CN-LOH	53624707	57243565	3618.9	499	*GPR75-ASB3; CHAC2; ERLEC1; GPR75; PSME4; ACYP2; TSPYL6; C2orf73; SPTBN1; EML6; RTN4; CLHC1; RPS27A; MTIF2; CCDC88A; CFAP36; SMEK2; PNPT1; EFEMP1; CCDC85A*
RC17	17	12p13.31	Gain[2]	7847740	7992065	144.3	20	*SLC2A14; SLC2A3*
KCL038	9	NONE						
KCL039	8	NONE						
Man12	20	NONE						
MasterShef4	35	NONE						
MasterShef8	19	NONE						
MasterShef10	22	NONE						
MasterShef12	16	NONE						
MasterShef13	11	NONE						
MasterShef14	13	NONE						

Table 2. Summary of SNP array analysis of clinical-grade hESC lines. [1]Nucleotide numbers refer to Human Genome Build 38. [2]denotes that the frequency of this CNV in the human population has been estimated (Supplementary Table S2). [3]denotes a homozygous deletion.

length[47], and high resolution arrays can produce large data sets dominated by such naturally occurring small events[48,49]. Thus, we chose to use the HumanCytoSNP-12 array and KaryoStudio software, tailored to identify CNVs greater than 75 kb and CN-LOH regions greater than 1 MB, a resolution adequate for common molecular cytogenetic interpretation and applicable in a clinically relevant setting[42,49–51].

Of the 15 unique CNVs detected, 12 were heterozygous duplications, 2 were heterozygous deletions, and 1 was a homozygous deletion (Table 2). We asked whether these structural genomic variants were

likely to be parent-of-origin CNVs, that is, naturally occurring, or if they could have arisen during the hESC derivation process or during expansion in culture. We first checked each CNV on the DGV (http://dgv.tcag.ca) to determine whether the CNVs have been previously observed in healthy individuals[41,52].

Amongst the 15 large hESC CNVs, we found 10 had clear evidence of being present in healthy individuals. For example, a duplication of 267 kb on chromosome 6q27 observed in MasterShef3 containing 3 protein-encoding genes—*MLLT4, KIF25, FRMD1*—was represented on the DGV and has been reported in the healthy population at a frequency of over 1 in 50 individuals (Fig. 2A)[48,51,53]. RC17 hESCs harboured a single 144 kb duplication on chromosome 12p13.31 encompassing the *SLC2A14* and *SLC2A3* genes (Fig. 2B). Although this is close to the *NANOG* locus, we do not believe it confers a growth advantage since this CNV is commonly found (1 in 25) in healthy individuals[39,51,54]. A 132 kb duplication on chromosome 12p11.21 was detected in both KCL033 and KCL040 hESC lines (Supplementary Fig. S1). This region does not contain any protein-coding genes, and there are at least 14 submissions of this duplication on the DGV[39,51,53–55]. Man11, MasterShef2, and MasterShef7 also harboured genomic duplications of greater than 100 kb that are represented on the DGV (Supplementary Fig. S1). Man11 harboured a 220 kb gain on chromosome 15q25.3 that has been reported several times[39,51,56]. This duplication contains one gene, *AKAP13,* and this CNV was not found in the sibling hESC line, Man12. One of the CNVs detected in MasterShef7, a 315 kb duplication present on chromosome 14q21.3, contains a single gene, *MDGA,* and this CNV is also present on the DGV[51]. A 572 kb gain on chromosome 17q21.31 encompassing 5 genes in MasterShef2 was also found to be present in the normal population at high frequency (9.8%)[53].

Both heterozygous deletions and the homozygous deletion were found to be naturally occurring in the human population. Two unrelated cell lines, KCL031 and RC9 hESCs harboured the same 120 kb deletion on chromosome 8q24.23 (Fig. 3). This CNV is estimated to have a frequency of about 1 in 26 people and has been reported numerous times to occur in healthy individual[39,48,51,53,55,56]. This region does not contain any protein-coding genes. KCL040 and MasterShef11 also possessed genomic deletions greater than 100 kb that were present on the DGV (Supplementary Fig. S2). KCL040 harbours a previously reported 1.5 Mb deletion on chromosome 16p11.2 that contains 3 related genes[56,57]. MasterShef11 has a 109 kb homozygous deletion on chromosome 19p12 that has been widely reported to occur in healthy individuals (~1 in 9) and does not contain any genes[39,48,51,55,56].

We identified a novel 2.4 Mb gain on chromosome 5p14.3, containing a single gene, *Cadherin-18*, that was present in two sibling cell lines, KCL032 and KCL033 (Fig. 4), but not in KCL034, a third sibling line[20,58]. A duplication of this size has not been reported to date, but its presence in two sibling hESC lines strongly suggests it was inherited from one of the parents of the donated blastocysts rather than by acquisition of an identical CNV during hESC derivation and culture.

The remaining 5 CNVs, all duplications, were not fully represented on the DGV. For example, a 516 kb duplication was detected on chromosome 16 in MasterShef7 hESCs that encompassed over 20 genes (Fig. 5). A similarly sized duplication of this region has not been reported to date, but the DGV is not exhaustive and this CNV may represent a novel, but rare naturally-occurring genomic variant. This duplication is not known to confer a selective growth advantage, and has not been reported to be associated with hESC culture adaptation[36]. We also checked this CNV on the DECIPHER database[59] of microdeletion and microduplication clinical syndromes to determine if it was associated with a known disorder. This CNV was not associated with a described clinical syndrome, nor were any of the other 14 CNVs identified here.

The four other unique CNVs that were not fully represented on the DGV were present in KCL034, KCL037, MasterShef3, and Shef6 hESC lines (Supplementary Fig. S3). KCL034 harboured a duplication of a 331 kb region on chromosome 6 (chr6q22.1) that contained part of the Histone 1 gene cluster. While this region was not fully present on the DGV, it is probable that this gain represents a benign event as other histone clusters have been shown to be preferentially duplicated during evolution[60]. A 542 kb gain on chromosome 18q23 in KCL037 containing two coding genes, *SALL3* and *ATP9B*, has not been previously reported. However, a smaller duplication covering the same two genes has been observed[51]. A 235 kb duplication was detected on chromosome 17 in MasterShef3 hESCs. Although, a duplication of this size is not present on the DGV, four slightly smaller duplications of the region have been reported[39,51,53,55]. A 553 kb gain on chromosome 8p22 in Shef6 hESCs within an intron of the *SGCZ* gene is an unreported novel structural duplication, but a deletion of this region has been observed[51]. While the 5 novel CNVs detected in our study were not fully present on the DGV, they were also not on the 'ESC-associated' culture-adaptation list of CNVs from the International Stem Cell Initiative survey of 125 different hESC and hiPSC lines[36]. Based on the available evidence, these CNVs likely represent novel, but rare, structural variants found in the human population. However, we do not know the health status of the individuals that may harbour these novel CNVs, so we cannot assume they are benign. Furthermore, we cannot definitively exclude the possibility that these CNVs arose during blastocyst development or during the early stages of hESC line derivation.

In addition to the 15 CNVs identified, our analysis detected 3 regions of CN-LOH greater than 1 MB among three different hESC lines, KCL040, MasterShef5, and RC11 (Table 2 and Fig. 6). All three regions ranged in size between 3.4 and 3.7 Mb, two of which were on chromosome 2 and the other on chromosome 12. Due to their interstitial nature and relatively small genetic size, it is unlikely any of these CN-LOH regions would represent examples of acquired CN-LOH. The vast majority of CN-LOH events

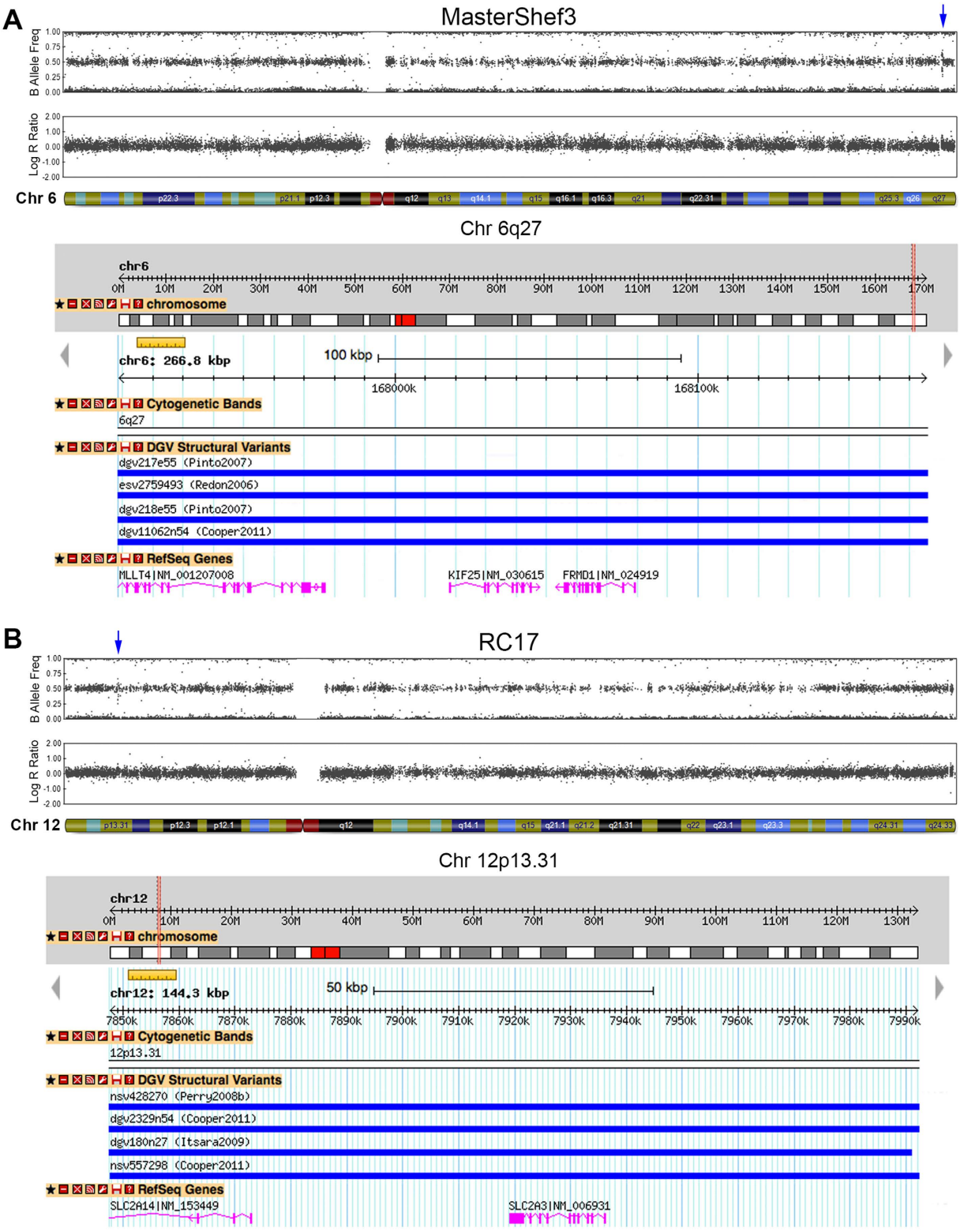

Figure 2. Duplications found in hESC lines that are present on the DGV. (**A**) Chromosome 6 ideograms from SNP array analysis of MasterShef3 revealed a 267 kb duplication near the telomere, which contained 3 genes, *MLLT4, KIF25,* and *FRMD1*. Duplications of this size, or greater, have been reported and annotated on the DGV with an estimated frequency of 2.82% in the human population. (**B**) A 144 kb duplication was observed on chromosome 12p13.31 of RC17 hESCs. This region contained two genes, *SCL2A14* and *SLC2A3*, and is represented on the DGV (3.9% frequency in humans).

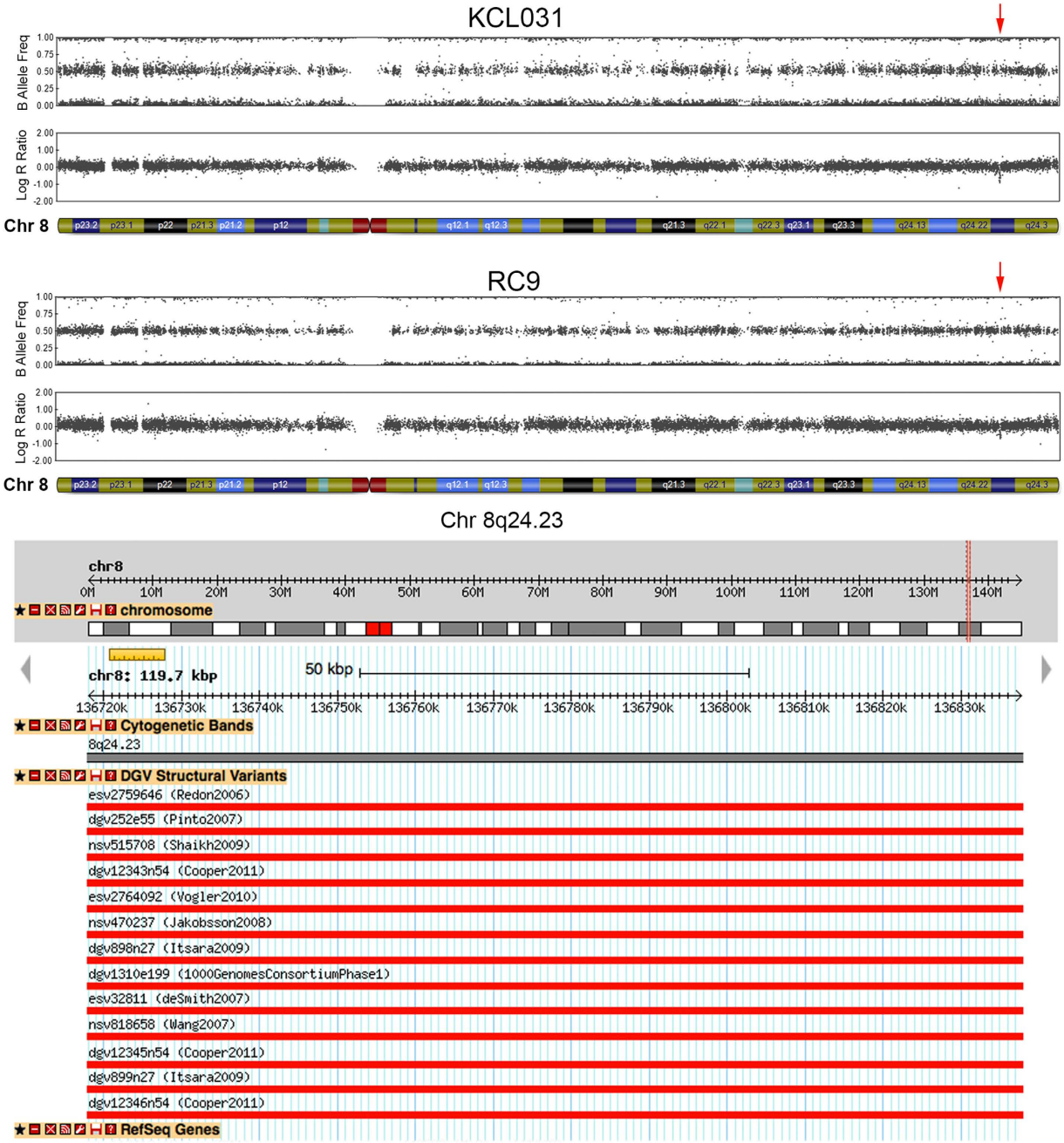

Figure 3. A common deletion observed in two unrelated hESC lines. Chromosome 8 ideograms from SNP array analysis of KCL031 and RC9 hESC lines revealed a 120 kb deletion on chromosome 8q24.23 (red arrow). This deletion is relatively common in the human population (3.85%), and does not contain any protein-coding genes.

documented in cancers are telomeric in nature and while examples of acquired interstitial CN-LOH do exist[61,62], the double recombination event required to achieve this would be difficult to explain for sizes less than 25 Mb[63,64]. Since hESCs are known to maintain monoallelic expression in some imprinted regions[65], we cross-referenced the 3 CN-LOH regions we identified to the Genomic Imprinting database (http://www.geneimprint.com)[66]. None of the CN-LOH regions reside in known imprinted regions, although *CCDC85A* in the CN-LOH of RC11 is predicted, but not validated, to be an imprinted gene on this database.

While none of the CNV and CN-LOH regions observed in the hESCs appear to harbour genomic anomalies associated with culture adaptation at the passages reported here (Table 2), we have detected the presence of the culture-adapted microduplication on chromosome 20q11.21 at higher passages of 4

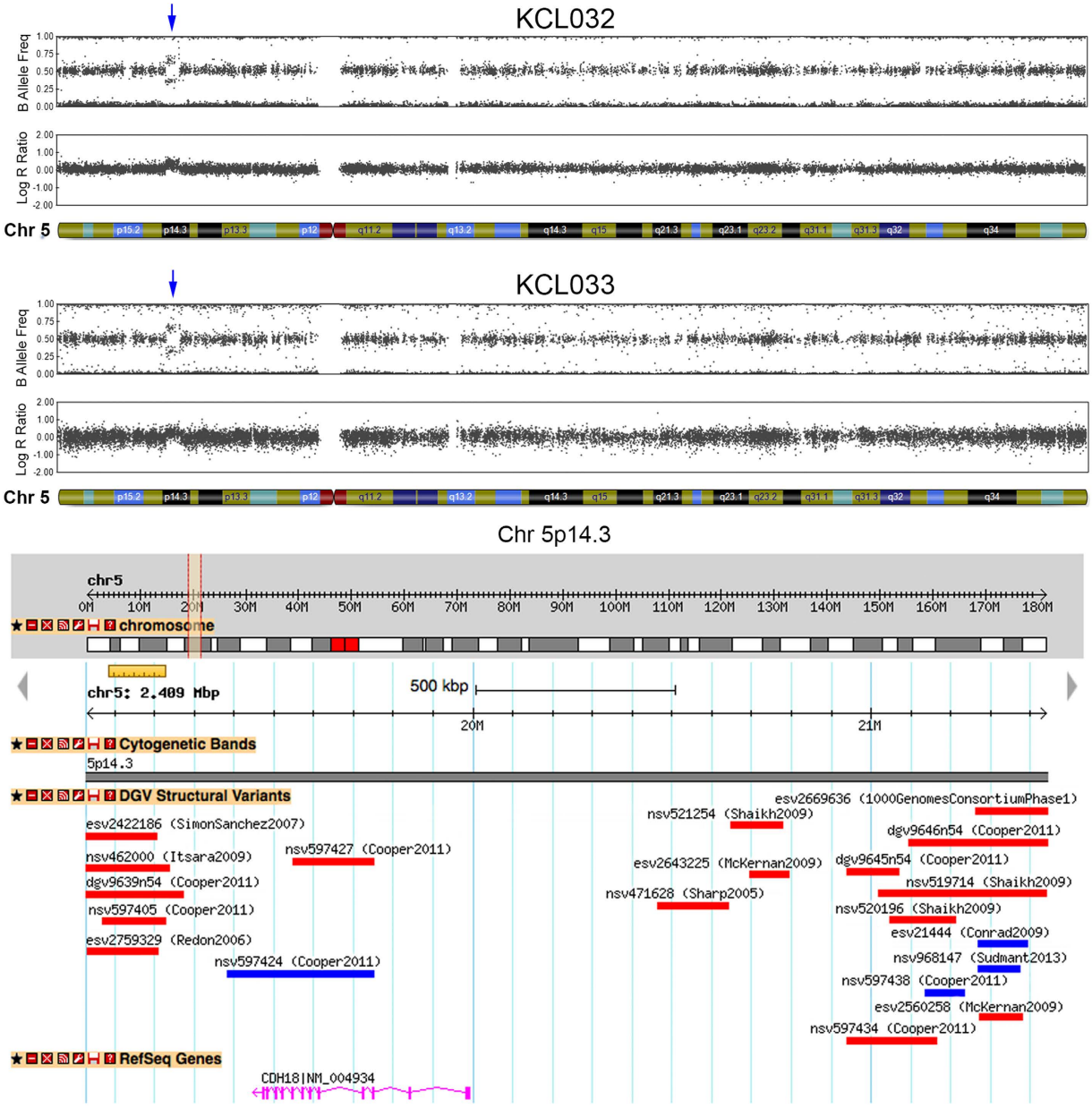

Figure 4. An identical duplication found in sibling KCL hESC lines, but not present on the DGV. Chromosome 5 ideograms from SNP array analysis of KCL032 and KCL033 hESC lines with the common CNV indicated by blue arrows. This 2.4 Mb duplication on chromosome 5p14.3 included the *CDH18* gene. A duplication of this size was not present on the DGV, but a smaller duplication (nsv597424) covering most of the *CDH18* exons was present, and a number of smaller deletions have been observed in this region. Only published CNVs greater than 100 kb are represented here.

clinical-grade hESC lines. This microduplication was reported to be found in ~20% of research-grade hESC lines[36,37]. Thus, it is with prudence that each cell line should be re-evaluated frequently and certainly before the production of any differentiated cell product[67]. These results also illustrate that the heterogeneity of molecular karyotypes in the human population will be reflected in the cell lines produced from human embryos. A perfect genome is unlikely to exist, so an appreciation of human genomic diversity will lend itself to a more measured interpretation of molecular karyotype and genome sequencing data of cell lines destined for clinical use.

Our molecular karyotypic evaluation of 25 clinical-grade hESC lines has established a valuable platform for the development and manufacture of cell therapy products for clinical application in regenerative medicine.

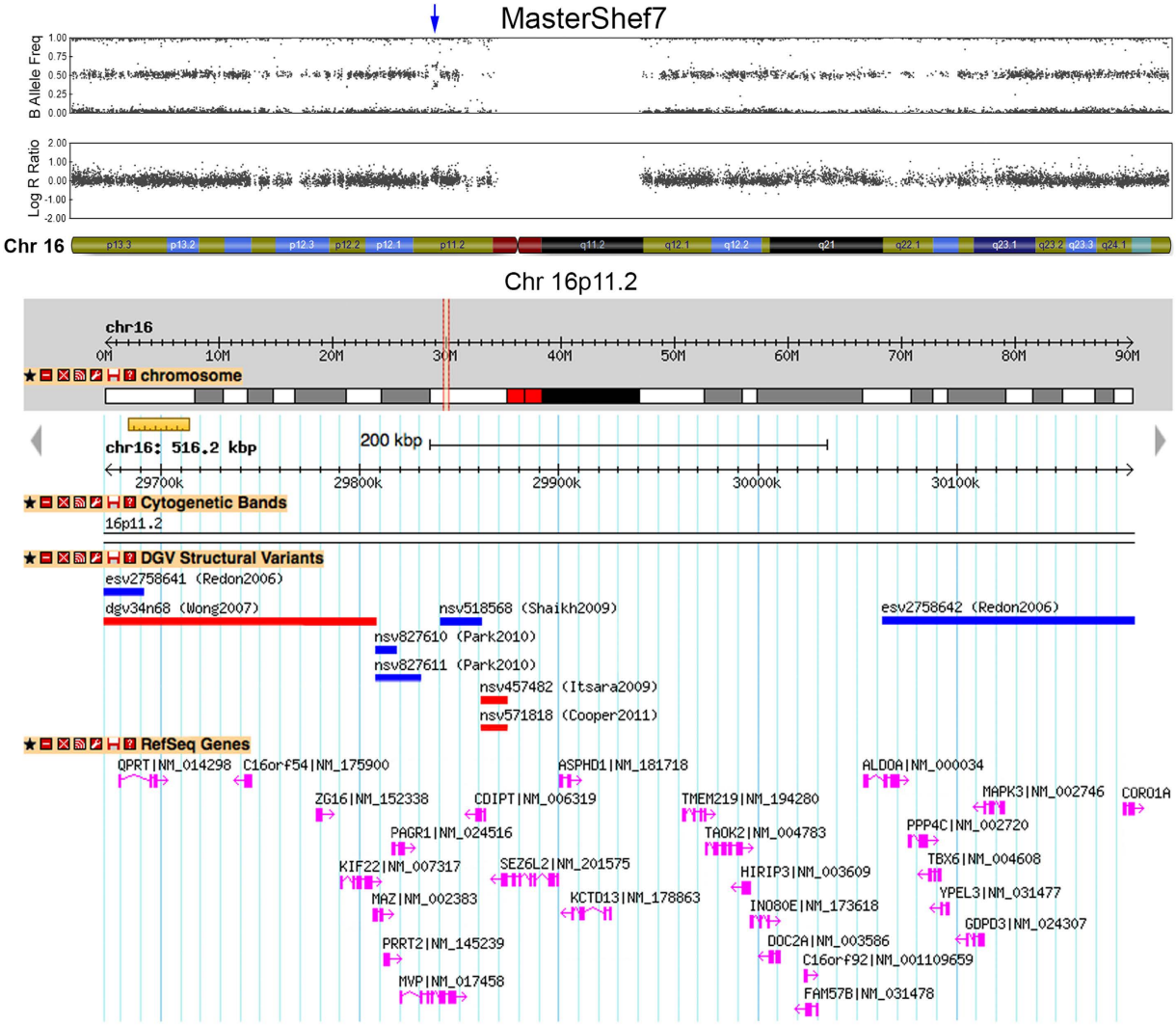

Figure 5. A novel duplication observed in MasterShef7. A 516 kb duplication on chromosome 16p11.2 was detected in MasterShef7 by SNP array analysis. This region contained 26 protein-coding genes, and a duplication of this size has not been reported to date. Smaller duplications have been observed in this region, including a duplication (esv2758642) spanning 7 of the genes. Only published CNVs greater than 10 kb are represented here.

Materials and Methods

Clinical-grade hESC Samples. Approval for the use of all hESC lines used in this study was granted by the MRC Steering Committee for the UK Stem Cell Bank and for the Use of Stem Cell Lines. The following clinical-grade hESC lines were kindly provided by the following derivation centres: The University of Sheffield (12 lines) MasterShef2, MasterShef3, MasterShef4, MasterShef5, MasterShef7, MasterShef8, MasterShef10, MasterShef11, MasterShef12, MasterShef13, MasterShef14 and Shef6; King's College London (8 lines) KCL031, KCL032, KCL033 KCL034, KCL037, KCL038, KCL039, and KCL040; Roslin Cells Ltd (3 lines) RC9, RC11, and RC17; and Central Manchester NHS Foundation Trust/The University of Manchester (2 lines) Man11 and Man12. Most of the cell samples were provided as frozen cell pellets, which were directly processed for genomic DNA isolation. However, Man11 and Man12, sibling hESC lines, were provided as cryopreserved hESC lines, and Shef6 was obtained directly from the UK Stem Cell Bank (UKSCB Accession No. R-05-031). These three lines were thawed and cultured in Essential 8 media (Life Technologies) on Laminin-521 substrate (Biolamina) for less than 10 passages before pelleting by centrifugation for genomic DNA isolation. Human ES cell morphology and pluripotent marker, NANOG, expression were maintained during this expansion (Fig. 1). NANOG immunostaining was performed with anti-NANOG antibody (1:500) from R&D Systems (cat no. AF1997).

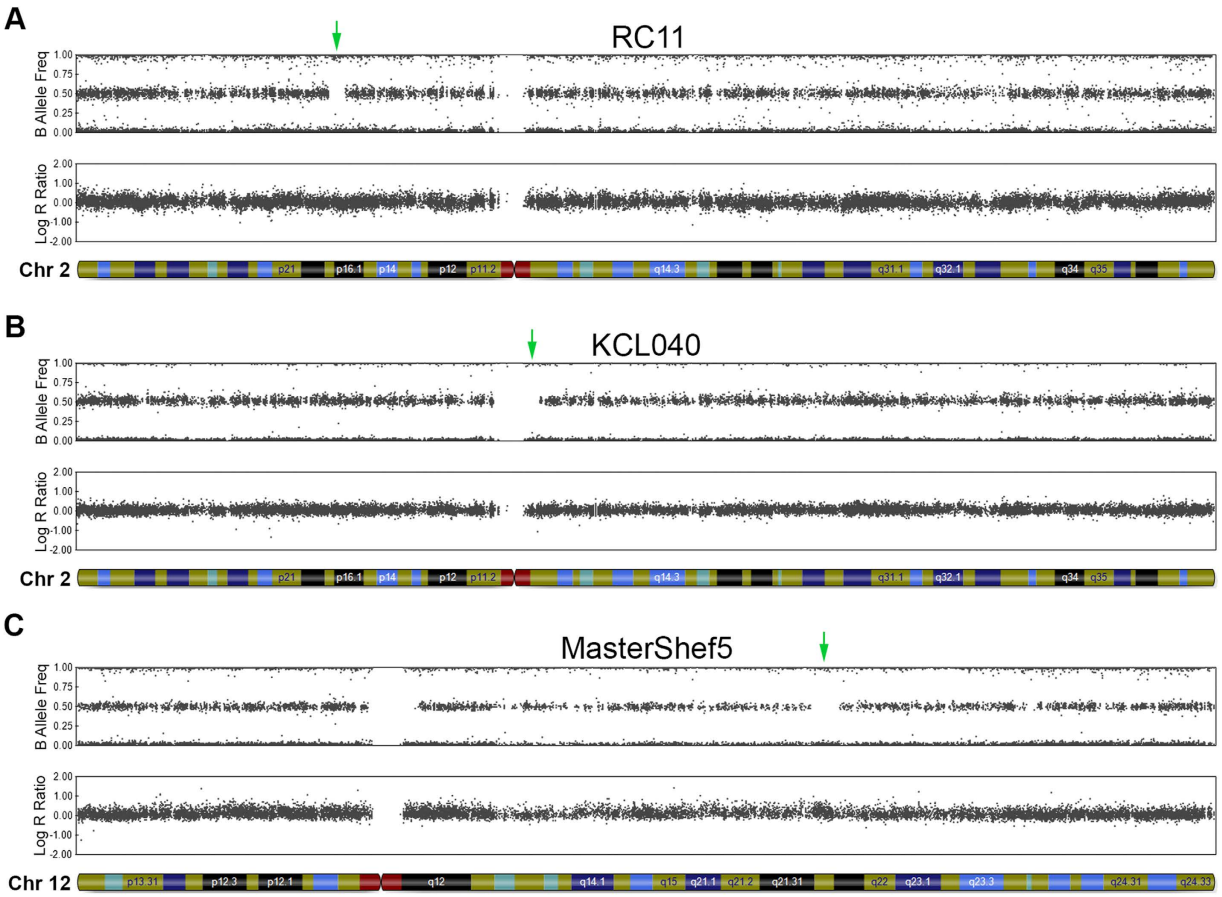

Figure 6. Interstitial CN-LOH regions detected in clinical-grade hESC lines. Chromosome ideograms from SNP array analysis showing CN-LOH regions indicated by green arrows: (**A**) A 3.6 Mb region on chromosome 2p16.2-16.1 in RC11. (**B**) A 3.5 Mb region on chromosome 2q11.1-11.2 in KCL040. (**C**) A 3.4 Mb region around chromosome 12q21.31-21.33 in MasterShef5.

Isolation of Genomic DNA. Genomic DNA was isolated from cell pellets using the MasterPure™ Complete DNA and RNA Purification Kit (Epicentre) according to the manufacturer's instructions. Briefly, cell pellets were lysed with Tissue and Cell Lysis Solution, followed by Proteinase K and RNase A treatment. Proteins were precipitated with MPC Protein Precipitation Reagent and removed by centrifugation. Genomic DNA was precipitated with isopropanol, pelleted by centrifugation and then resuspended in TE buffer to a final concentration of 50 ng/μl. Purity was checked by spectrophotometry using the NanoDrop 1000 spectrophotometer (Thermo Fisher Scientific).

HLA typing. All samples were subjected to HLA typing at the Histocompatibility and Immunogenetics (H&I) Laboratory of the Scottish National Blood Transfusion Service (SNBTS). The HLA typing data (Supplementary Table S1) was used for identification purposes by comparing it to the HLA typing data for each cell line provided by the hESC derivation centres. The H&I Laboratory at SNBTS is accredited through Clinical Pathology Accreditation (UK) Ltd (CPA), and all CPA labs are subjected to UK National External Quality Assessment Schemes (UK NEQAS).

Genotyping and Analysis. Genomic DNA samples were assayed using the Illumina HumanCytoSNP-12 v2.1 BeadChip, at either AROS (Aarhus, Denmark) or the Wellcome Trust Clinical Research Facility (Edinburgh, UK). The data have been deposited in NCBI's Gene Expression Omnibus and are accessible through GEO Series accession number GSE68508. Genotyping was initially assessed using GenomeStudio genotyping module (v1.94, Illumina). KaryoStudio (v1.4, Illumina) was employed to perform automatic normalisation and to identify genomic aberrations utilising default settings of the built-in cnvPartition algorithm (3.07, Illumina) to generate B-allele frequency and smoothened Log R ratio plots for detected regions. These parameters are designed to detect CNVs greater than 75 kb and CN-LOH regions larger than 1 MB with a confidence value greater than 35. All identified duplication and deletions were first cross-matched to the Database of Genomic Variants (DGV; http://dgv.tcag.ca) to identify naturally-occurring structural variations in the human genome[41,52]. We also determined the

estimated frequency of 8 common CNVs in the human population (Supplementary Table S2) by accessing the DGV Gold Standard track of a highly curated and accurate CNV map of the human genome[47]. All CNVs were inputted into the DECIPHER database (https://decipher.sanger.ac.uk/) to determine if they were associated with any clinical syndromes[59]. The CN-LOH regions were cross-referenced with the Genomic Imprinting database (http://www.geneimprint.com) to determine if the genomic variants occurred in known imprinted regions[66]. CNVs that were not identified on the DGV were then checked against a list of ES cell-associated culture adaptation genomic variants published by the International Stem Cell Initiative[36].

References

1. Thomson, J. A. *et al.* Embryonic stem cell lines derived from human blastocysts. *Science* **282,** 1145–1147 (1998).
2. Takahashi, K. *et al.* Induction of pluripotent stem cells from adult human fibroblasts by defined factors. *Cell* **131,** 861–872 (2007).
3. Unger, C., Skottman, H., Blomberg, P., Sirac Dilber, M. & Hovatta, O. Good manufacturing practice and clinical-grade human embryonic stem cell lines. *Hum. Mol. Genet.* **17,** R48–R53 (2008).
4. Fraga, A. M., Souza de Araújo, É. S., Stabellini, R., Vergani, N. & Pereira, L. V. A survey of parameters involved in the establishment of new lines of human embryonic stem cells. *Stem Cell Rev and Rep* **7,** 775–781 (2011).
5. Ludwig, T. E. *et al.* Derivation of human embryonic stem cells in defined conditions. *Nat. Biotechnol.* **24,** 185–187 (2006).
6. Rajala, K. *et al.* A defined and xeno-free culture method enabling the establishment of clinical-grade human embryonic, induced pluripotent and adipose stem cells. *PLoS ONE* **5,** e10246 (2010).
7. Chen, G. *et al.* Chemically defined conditions for human iPSC derivation and culture. *Nat. Methods* **8,** 424–429 (2011).
8. Prathalingam, N. *et al.* Production and validation of a good manufacturing practice grade human fibroblast line for supporting human embryonic stem cell derivation and culture. *Stem Cell Res Ther* **3,** 12 (2012).
9. Richards, M., Fong, C.-Y., Chan, W.-K., Wong, P.-C. & Bongso, A. Human feeders support prolonged undifferentiated growth of human inner cell masses and embryonic stem cells. *Nature biotechnology* **20,** 933–936 (2002).
10. Ellerström, C. *et al.* Derivation of a xeno-free human embryonic stem cell line. *Stem Cells* **24,** 2170–2176 (2006).
11. Rodin, S. *et al.* Clonal culturing of human embryonic stem cells on laminin-521/E-cadherin matrix in defined and xeno-free environment. *Nat Commun* **5,** (2014).
12. Rodin, S. *et al.* Long-term self-renewal of human pluripotent stem cells on human recombinant laminin-511. *Nat. Biotechnol.* **28,** 611–615 (2010).
13. Nakagawa, M. *et al.* A novel efficient feeder-free culture system for the derivation of human induced pluripotent stem cells. *Sci Rep* **4,** (2014).
14. Lu, H. F. *et al.* A defined xeno-free and feeder-free culture system for the derivation, expansion and direct differentiation of transgene-free patient-specific induced pluripotent stem cells. *Biomaterials* **35,** 2816–2826 (2014).
15. Ström, S. *et al.* Mechanical isolation of the inner cell mass is effective in derivation of new human embryonic stem cell lines. *Hum. Reprod.* **22,** 3051–3058 (2007).
16. Ström, S., Holm, F., Bergström, R., Strömberg, A.-M. & Hovatta, O. Derivation of 30 human embryonic stem cell lines–improving the quality. *In Vitro Cell. Dev. Biol. Anim.* **46,** 337–344 (2010).
17. Hovatta, O. Derivation of human embryonic stem cell lines, towards clinical quality. *Reprod. Fertil. Dev.* **18,** 823–828 (2006).
18. Turetsky, T. *et al.* Laser-assisted derivation of human embryonic stem cell lines from IVF embryos after preimplantation genetic diagnosis. *Human Reproduction* **23,** 46–53 (2008).
19. Liu, W. *et al.* Derivation and characterization of human embryonic stem cell lines from poor quality embryos. *J Genet Genomics* **36,** 229–239 (2009).
20. Jacquet, L. *et al.* Strategy for the creation of clinical grade hESC line banks that HLA-match a target population. *EMBO Mol Med* **5,** 10–17 (2012).
21. Hewitt, Z. A., Amps, K. J. & Moore, H. D. Derivation of GMP raw materials for use in regenerative medicine: hESC-based therapies, progress toward clinical application. *Clin. Pharmacol. Ther.* **82,** 448–452 (2007).
22. Tannenbaum, S. E. *et al.* Derivation of xeno-free and GMP-grade human embryonic stem cells–platforms for future clinical applications. *PLoS ONE* **7,** e35325 (2012).
23. Crook, J. M. *et al.* The Generation of Six Clinical-Grade Human Embryonic Stem Cell Lines. *Cell Stem Cell* **1,** 490–494 (2007).
24. Murdoch, A. *et al.* The procurement of cells for the derivation of human embryonic stem cell lines for therapeutic use: recommendations for good practice. *Stem Cell Reviews and Reports* **8,** 91–99 (2011).
25. Osafune, K. *et al.* Marked differences in differentiation propensity among human embryonic stem cell lines. *Nat. Biotechnol.* **26,** 313–315 (2008).
26. Baker, D. E. C. *et al.* Adaptation to culture of human embryonic stem cells and oncogenesis *in vivo*. *Nat. Biotechnol.* **25,** 207–215 (2007).
27. Taylor, C. J. *et al.* Banking on human embryonic stem cells: estimating the number of donor cell lines needed for HLA matching. *Lancet* **366,** 2019–2025 (2005).
28. Turner, M. *et al.* Toward the development of a global induced pluripotent stem cell library. *Cell Stem Cell* **13,** 382–384 (2013).
29. Bock, C. *et al.* Reference Maps of human ES and iPS cell variation enable high-throughput characterization of pluripotent cell lines. *Cell* **144,** 439–452 (2011).
30. Stephenson, E. *et al.* Safety paradigm: genetic evaluation of therapeutic grade human embryonic stem cells. *Journal of The Royal Society Interface* **7,** S677–S688 (2010).
31. Lee, A. S., Tang, C., Rao, M. S., Weissman, I. L. & Wu, J. C. perspective. *Nat. Med.* **19,** 998–1004 (2013).
32. Draper, J. S. *et al.* Recurrent gain of chromosomes 17q and 12 in cultured human embryonic stem cells. *Nat. Biotechnol.* **22,** 53–54 (2004).
33. Närvä, E. *et al.* High-resolution DNA analysis of human embryonic stem cell lines reveals culture-induced copy number changes and loss of heterozygosity. *Nat. Biotechnol.* **28,** 371–377 (2010).
34. Spits, C. *et al.* Recurrent chromosomal abnormalities in human embryonic stem cells. *Nat. Biotechnol.* **26,** 1361–1363 (2008).
35. Lefort, N. *et al.* Human embryonic stem cells reveal recurrent genomic instability at 20q11.21. *Nat. Biotechnol.* **26,** 1364–1366 (2008).
36. Amps, K. *et al.* Screening ethnically diverse human embryonic stem cells identifies a chromosome 20 minimal amplicon conferring growth advantage. *Nat. Biotechnol.* **29,** 1132–1144 (2011).
37. Avery, S. *et al.* BCL-XL Mediates the Strong Selective Advantage of a 20q11.21 Amplification Commonly Found in Human Embryonic Stem Cell Cultures. *Stem Cell Reports* **1,** 379–386 (2013).
38. Laurent, L. C. *et al.* Dynamic Changes in the Copy Number of Pluripotency and Cell Proliferation Genes in Human ESCsand iPSCs during Reprogramming and Time in Culture. *Cell Stem Cell* **8,** 106–118 (2011).

39. Itsara, A. *et al.* Population analysis of large copy number variants and hotspots of human genetic disease. *Am. J. Hum. Genet.* **84,** 148–161 (2009).
40. Ben-Yosef, D. *et al.* Genomic Analysis of hESC Pedigrees Identifies *De Novo* Mutations and Enables Determination of the Timing and Origin of Mutational Events. *Cell Rep* **4,** 1288–1302 (2013).
41. MacDonald, J. R., Ziman, R., Yuen, R. K. C., Feuk, L. & Scherer, S. W. The Database of Genomic Variants: a curated collection of structural variation in the human genome. *Nucleic Acids Res.* **42,** D986–92 (2014).
42. Kearney, H. M., Kearney, J. B. & Conlin, L. K. Diagnostic implications of excessive homozygosity detected by SNP-based microarrays: consanguinity, uniparental disomy, and recessive single-gene mutations. *Clin. Lab. Med.* **31,** 595–613–ix (2011).
43. McQuillan, R. *et al.* Runs of Homozygosity in European Populations. *The American Journal of Human Genetics* **83,** 359–372 (2008).
44. Gibson, J., Morton, N. E. & Collins, A. Extended tracts of homozygosity in outbred human populations. *Hum. Mol. Genet.* **15,** 789–795 (2006).
45. Makishima, H. & Maciejewski, J. P. Pathogenesis and consequences of uniparental disomy in cancer. *Clin. Cancer Res.* **17,** 3913–3923 (2011).
46. Hussein, S. M. *et al.* Copy number variation and selection during reprogramming to pluripotency. *Nature* **470,** 58–62 (2012).
47. Zarrei, M., MacDonald, J. R., Merico, D. & Scherer, S. W. A copy number variation map of the human genome. *Nat. Rev. Genet.* **16,** 172–183 (2015).
48. Redon, R. *et al.* Global variation in copy number in the human genome. *Nature* **444,** 444–454 (2006).
49. Bernardini, L. *et al.* High-resolution SNP arrays in mental retardation diagnostics: how much do we gain? *Eur. J. Hum. Genet.* **18,** 178–185 (2010).
50. Vermeesch, J. R. *et al.* Guidelines for molecular karyotyping in constitutional genetic diagnosis. *Eur. J. Hum. Genet.* **15,** 1105–1114 (2007).
51. Cooper, G. M. *et al.* A copy number variation morbidity map of developmental delay. *Nat. Genet.* **43,** 838–846 (2011).
52. Iafrate, A. J. *et al.* Detection of large-scale variation in the human genome. *Nat. Genet.* **36,** 949–951 (2004).
53. Pinto, D., Marshall, C., Feuk, L. & Scherer, S. W. Copy-number variation in control population cohorts. *Hum. Mol. Genet.* **16 Spec No. 2,** R168–73 (2007).
54. Perry, G. H. *et al.* Copy number variation and evolution in humans and chimpanzees. *Genome Res.* **18,** 1698–1710 (2008).
55. Vogler, C. *et al.* Microarray-based maps of copy-number variant regions in European and sub-Saharan populations. *PLoS ONE* **5,** e15246 (2010).
56. Shaikh, T. H. *et al.* High-resolution mapping and analysis of copy number variations in the human genome: a data resource for clinical and research applications. *Genome Res.* **19,** 1682–1690 (2009).
57. de Smith, A. J. *et al.* Array CGH analysis of copy number variation identifies 1284 new genes variant in healthy white males: implications for association studies of complex diseases. *Hum. Mol. Genet.* **16,** 2783–2794 (2007).
58. Devito, L. *et al.* Cost-effective master cell bank validation of multiple clinical-grade human pluripotent stem cell lines from a single donor. *Stem Cells Transl Med* **3,** 1116–1124 (2014).
59. Firth, H. V. *et al.* DECIPHER: Database of Chromosomal Imbalance and Phenotype in Humans Using Ensembl Resources. *Am. J. Hum. Genet.* **84,** 524–533 (2009).
60. Braastad, C. D., Hovhannisyan, H., van Wijnen, A. J., Stein, J. L. & Stein, G. S. Functional characterization of a human histone gene cluster duplication. *Gene* **342,** 35–40 (2004).
61. Gupta, M. *et al.* Novel regions of acquired uniparental disomy discovered in acute myeloid leukemia. *Genes Chromosomes Cancer* **47,** 729–739 (2008).
62. Stephens, K. *et al.* Interstitial uniparental isodisomy at clustered breakpoint intervals is a frequent mechanism of NF1 inactivation in myeloid malignancies. *Blood* **108,** 1684–1689 (2006).
63. O'Keefe, C., McDevitt, M. A. & Maciejewski, J. P. Copy neutral loss of heterozygosity: a novel chromosomal lesion in myeloid malignancies. *Blood* **115,** 2731–2739 (2010).
64. Kryh, H. *et al.* Comprehensive SNP array study of frequently used neuroblastoma cell lines; copy neutral loss of heterozygosity is common in the cell lines but uncommon in primary tumors. *BMC Genomics* **12,** 443 (2011).
65. Rugg-Gunn, P. J., Ferguson-Smith, A. C. & Pedersen, R. A. Epigenetic status of human embryonic stem cells. *Nat. Genet.* **37,** 585–587 (2005).
66. Falls, J. G., Pulford, D. J., Wylie, A. A. & Jirtle, R. L. Genomic imprinting: implications for human disease. *Am. J. Pathol.* **154,** 635–647 (1999).
67. Peterson, S. E. & Loring, J. F. Genomic Instability in Pluripotent Stem Cells: Implications for Clinical Applications. *Journal of Biological Chemistry* **289,** 4578–4584 (2014).

Acknowledgements

This work was funded by a Medical Research Council RMRC project grant (MR/K017276/1) and The Cure Parkinson's Trust. T.K. is a Parkinson's UK Senior Research Fellow. Z.A.H. and H.D.M. were funded by MRC grant G0801059. Derivation of Man11 and Man12 was supported by several MRC grants to D.R.B. and S.J.K. and the NIHR Welcome Manchester Clinical Research Facility. We thank Victoria Robertson for HLA typing of hESC lines, and we thank Prof Peter Andrews, Dr Paul Travers, Dr Ronnie Wright, and Dr David Turner for critical comments on the manuscript.

Author Contributions

M.A.C. and T.K. designed the study and wrote the paper. M.A.C. and A.V.D. performed experiments, and M.A.C. and T.K. performed data analysis. D.R.B., P.A.D.S., J.D., L.D., Z.A.H., D.I., S.J.K., H.D.M. and H.M. provided samples and edited the manuscript.

Additional Information

Supplementary information accompanies this paper at http://www.nature.com/srep

Competing financial interests: The authors declare no competing financial interests.

How to cite this article: Canham, M. A. *et al.* The Molecular Karyotype of 25 Clinical-Grade Human Embryonic Stem Cell Lines. *Sci. Rep.* **5**, 17258; doi: 10.1038/srep17258 (2015).

SUPPLEMENTARY INFORMATION

The Molecular Karyotype of 25 Clinical-Grade Human Embryonic Stem Cell Lines

Maurice A. Canham, Amy Van Deusen, Daniel R. Brison, Paul De Sousa, Janet Downie, Liani Devito, Zoe A. Hewitt, Dusko Ilic, Susan J. Kimber, Harry D. Moore, Helen Murray, Tilo Kunath

Supplementary Table S1

Cell Line	HLA-I				HLA-II				
	A	B	Bw	C	DRB1	DRB3	DRB4	DRB5	DQB1
KCL031	02, 24	51, 52	4	12, 14	11, 15	02		01	03, 06
KCL032	02, 11	15, 51	4, 6	03, 04	04, 13	03	01		03, 06
KCL033	11, 29	44, 51	4	04, 16	04, 07		01		02, 03
KCL034	11, 29	44, 51	4	04, 16	04, 07		01		02, 03
KCL037	02, 03	35, 40	6	03, 04	01, 13	03			05, 06
KCL038	03, 11	07, 15	6	03, 07	14, 15	02		01	05, 06
KCL039	01, 24	35, 49	4, 6	04, 07	03	01/02			02
KCL040	03, 24	07, 15	6	03, 07	04, 15		01	01	03, 06
Man11	02, 24	35, 44	4, 6	04, 05	04, 11	02	01		03
Man12	01, 02	37, 44	4	05, 06	04		01		03
MasterShef2	01, 68	44	4	07	01, 11	01/02/03			03, 05
MasterShef3	02, 24	40, 44	4, 6	03, 05	04, 15		01	01	03, 06
MasterShef4	01, 08	44	4, 6	05, 07	03, 15	01		01	02, 06
MasterShef5	03, 24	27	4	02	03, 11	02			03, 02
MasterShef7	01, 29	08, 44	4, 6	07, 16	03, 07	01	01		02
MasterShef8	03, 23	14, 44	4, 6	04, 08	07, 13	03	01		02, 06
MasterShef10	01, 03	07, 27	4, 6	01, 07	04, 15		01	01	03, 06
MasterShef11	02, 03	07	6	07	15			01	06
MasterShef12	01, 03	38, 40	4, 6	02, 12	03, 13	01, 02			02, 06
MasterShef13	02, 11	18, 44	4, 6	05, 12	11, 15	02		01	03, 06
MasterShef14	03, 26	07, 38	4, 6	07, 12	09, 13	01	01		03, 06
Shef6	02, 23	15, 44	4, 6	03, 04	04, 07		01		02, 03
RC9	01, 02	07, 08	6	07	01, 15			01	05, 06
RC11	01, 24	07, 08	6	07	03, 15	01		01	02, 06
RC17	01, 03	07, 08	6	07	03, 11	01, 02			02, 03

Supplementary Table S1: HLA typing of 25 clinical-grade hESC lines. Two-digit HLA typing was performed on genomic DNA isolated from 25 hESC lines.

Supplementary Table S2

Human ESC Line(s)	Region	Variation	GSSV No.	NR_freq
KCL031 and RC9	8q24.23	Loss	gssv179004	3.85%
KCL033 and KCL040	12p11.21	Gain	gssv32361	4.70%
KCL040	16p11.2	Loss	gssv62559	5.14%
Man11	15q25.3	Gain	gssv58152	0.30%
MasterShef2	17q21.31	Gain	gssv71248	9.82%
MasterShef3	6q27	Gain	gssv157263	2.82%
MasterShef11	19p12	Loss	gssv81932	10.94%
RC17	12p13.31	Gain	gssv32355	3.90%

Supplementary Table S2: Common CNVs in the human population. The accession number of the DGV Gold Standard CNV (gssv no.) and the estimated frequency (NR_freq) in the human population are listed.

Supplementary Figure S1A

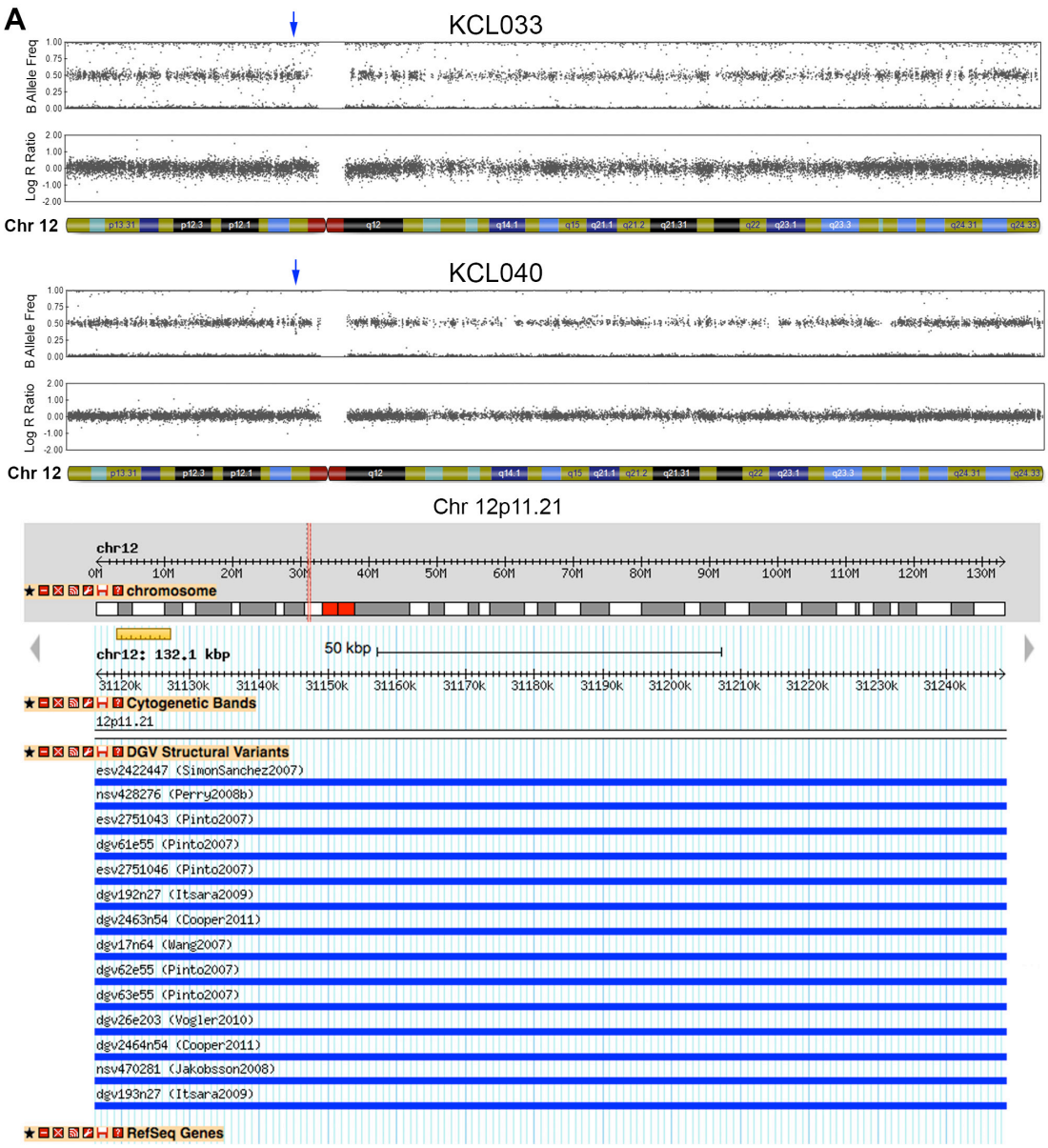

Supplementary Figure S1B,C

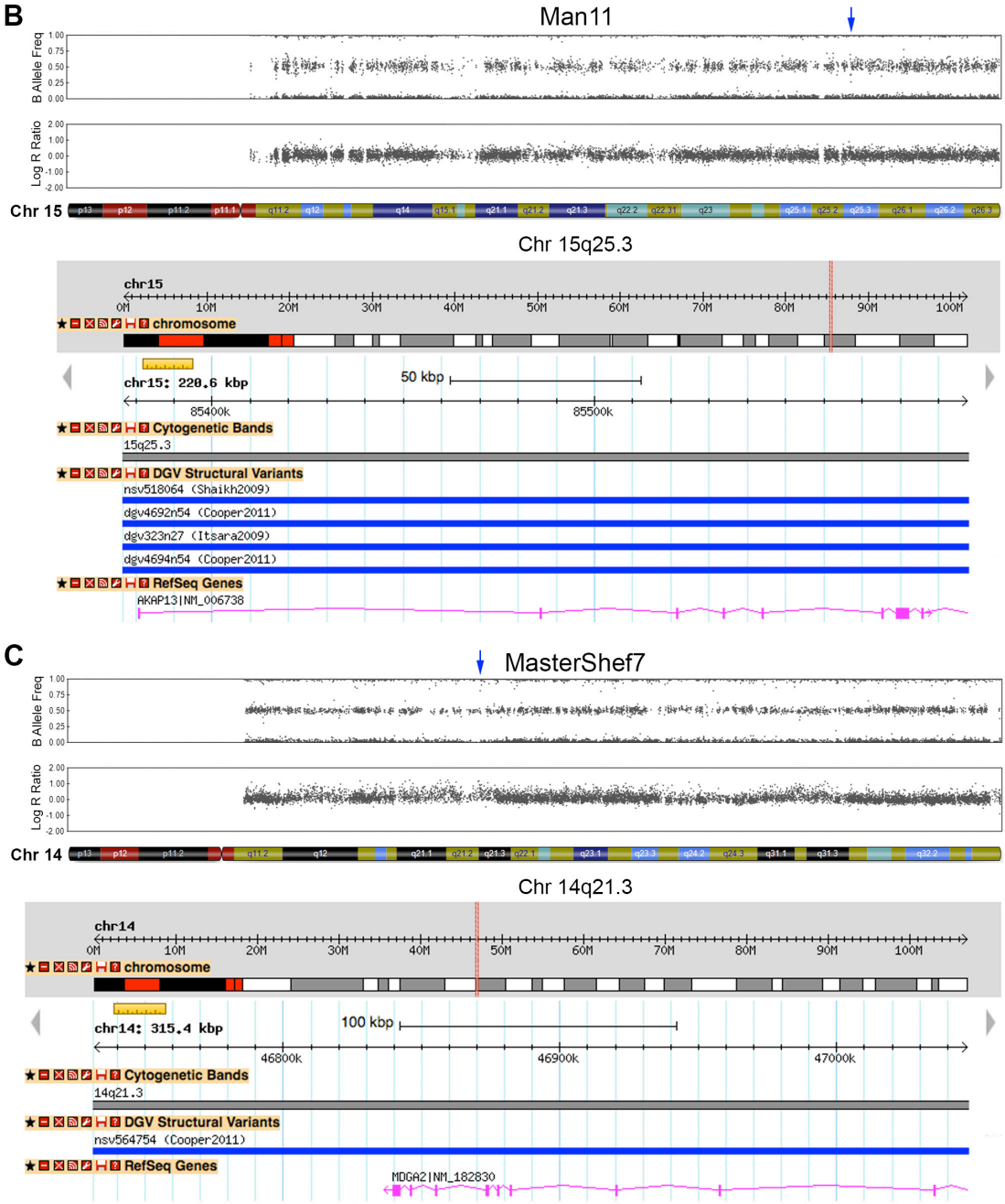

Supplementary Figure S1D

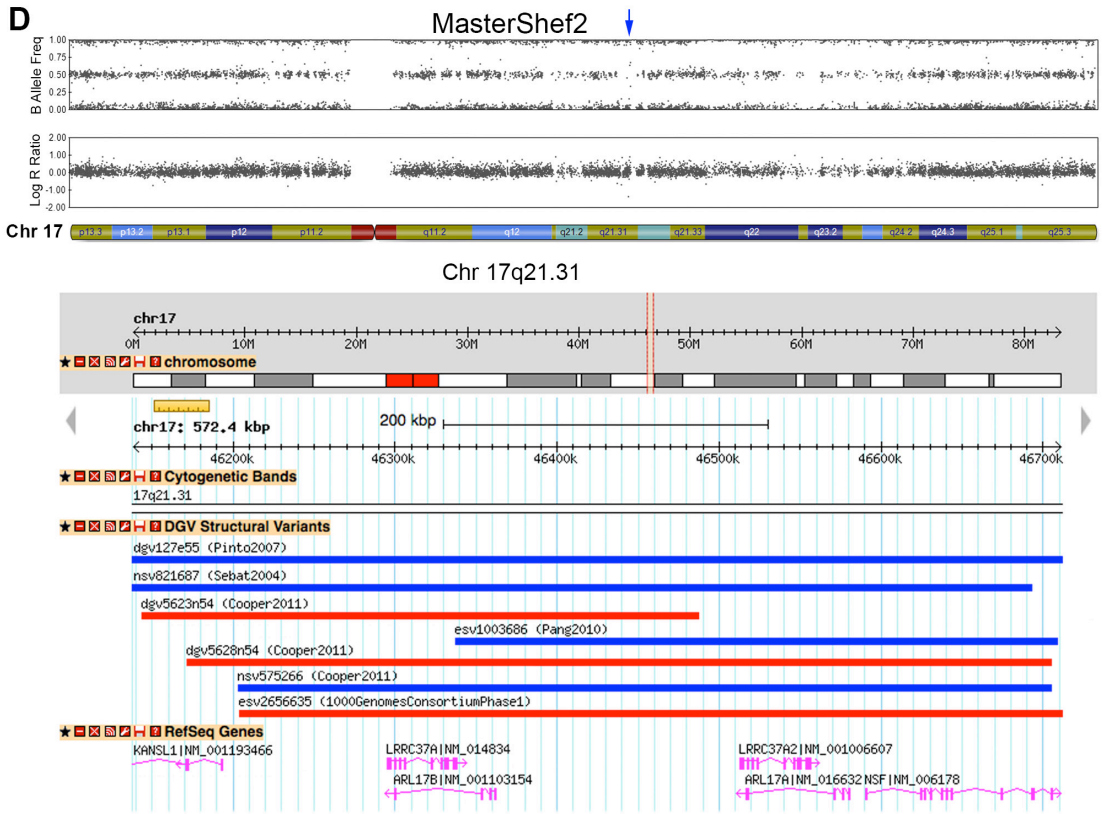

Supplementary Figure S1: Duplications found in hESC lines that are present on the DGV. (A) A 132.1 kb duplication on chromosome 12p11.21 was observed in two unrelated hESC lines, KCL033 and KCL040. This region does not contain any protein-coding genes, and is well represented on the DGV and relatively common (4.7%). (B) A 220.6 kb duplication was observed in Man11 hESCs spanning most of the *AKAP13* gene, but was not present in the sibling line Man12. This is a known CNV and is present on the DGV at a low frequency (0.3%). (C) A 315.4 kb duplication on chromosome 14q21.1 was observed in MasterShef7 hESCs. This CNV is not apparent in the whole chromosome 14 ideogram, but is significantly called by the KaryoStudio software. The region contains the *MDGA2* gene and is represented on the DGV by one entry. (D) A 572.4 kb duplication on chromosome 17q21.31 was observed in MasterShef2 hESCs. This CNV contained 5 coding genes, and a number of duplications and deletions have been reported on the DGV within this region and is common (9.82%).

Supplementary Figure S2A

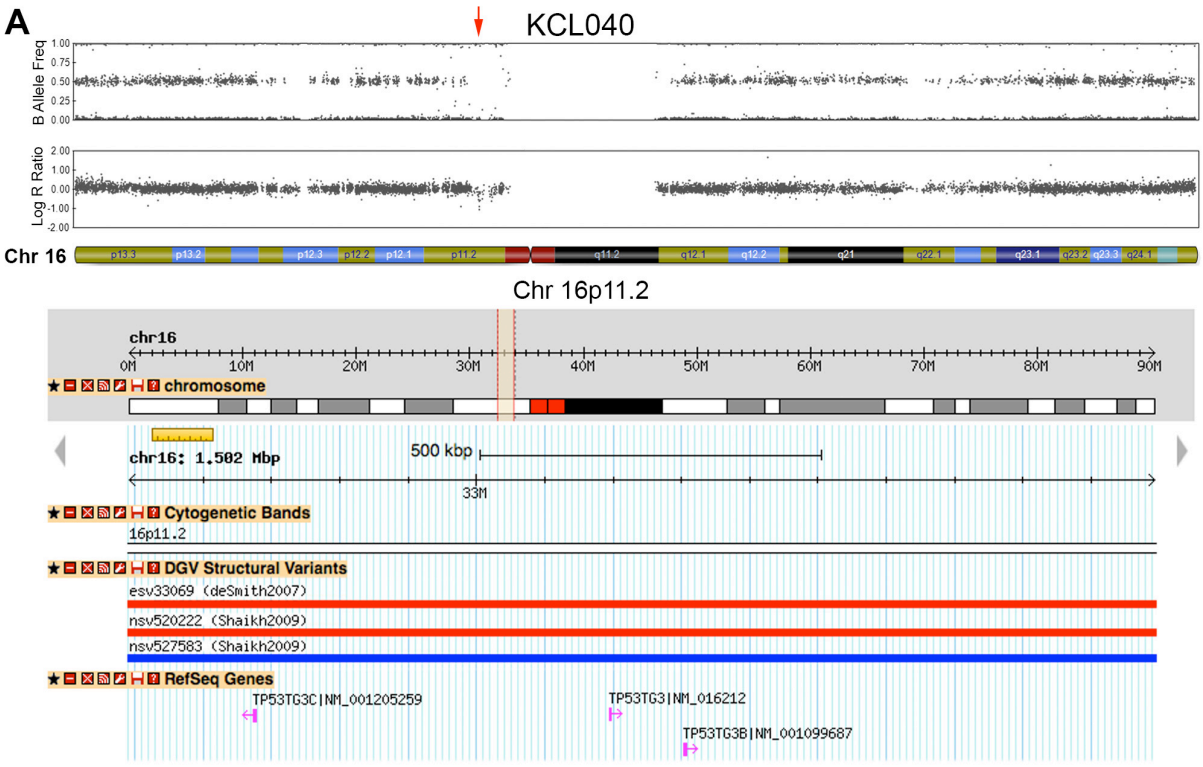

Supplementary Figure S2B

Supplementary Figure S2: Deletions found in hESC lines that are present on the DGV. (A) A 1.5 Mb deletion was observed on chromosome 16p11.2 of KCL040 hESCs containing 3 protein-coding genes. Two deletions and one duplication of this region have been reported and are present on the DGV at a relatively common frequency of 5.14%. (B) A homozygous deletion of 108.7 kb was observed on chromosome 19p12 in MasterShef11 hESCs. This region has been frequently observed to be deleted and duplicated in the human population (10.94%), and it does not contain any coding genes.

Supplementary Figure S3A,B

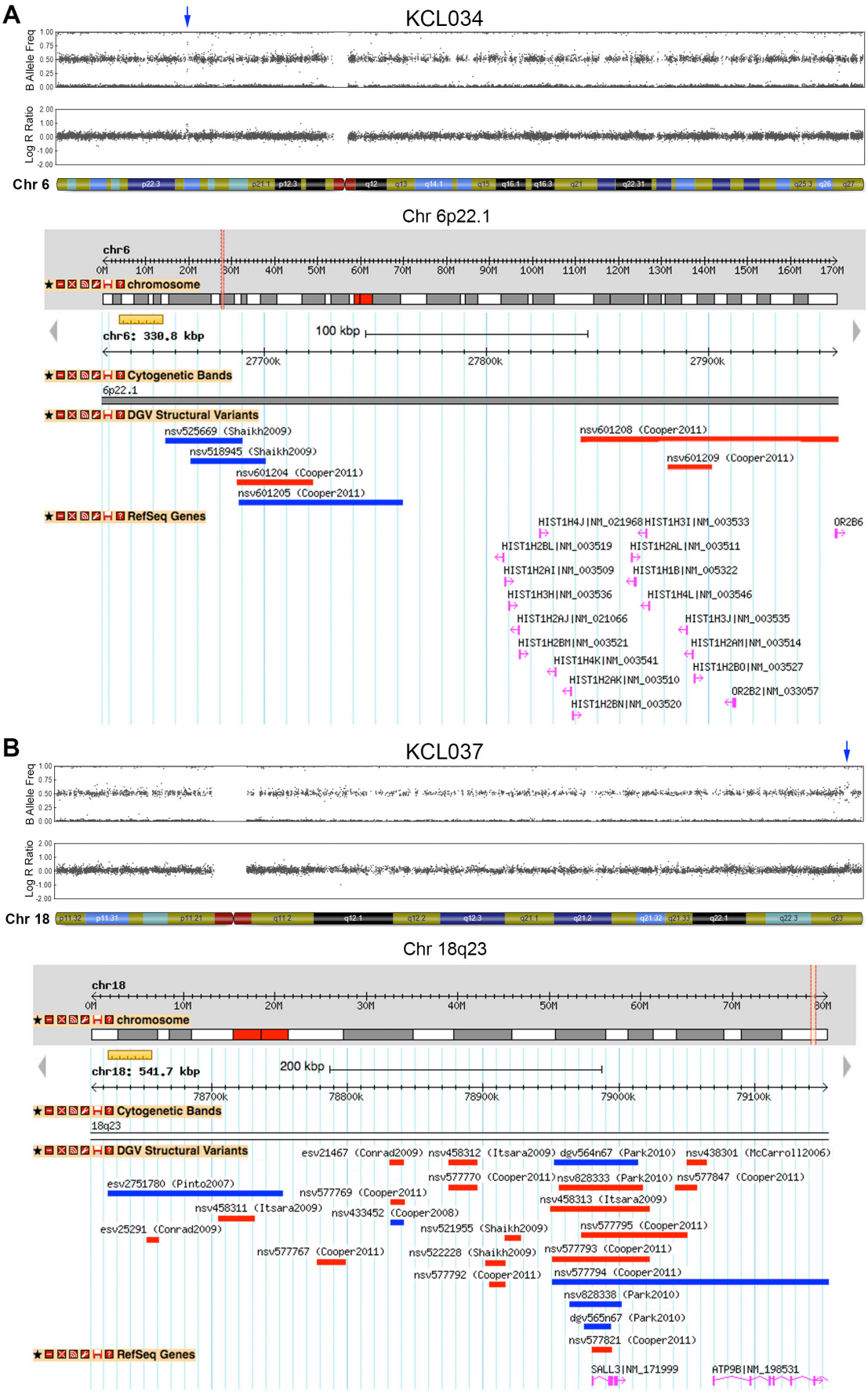

Supplementary Figure S3C,D

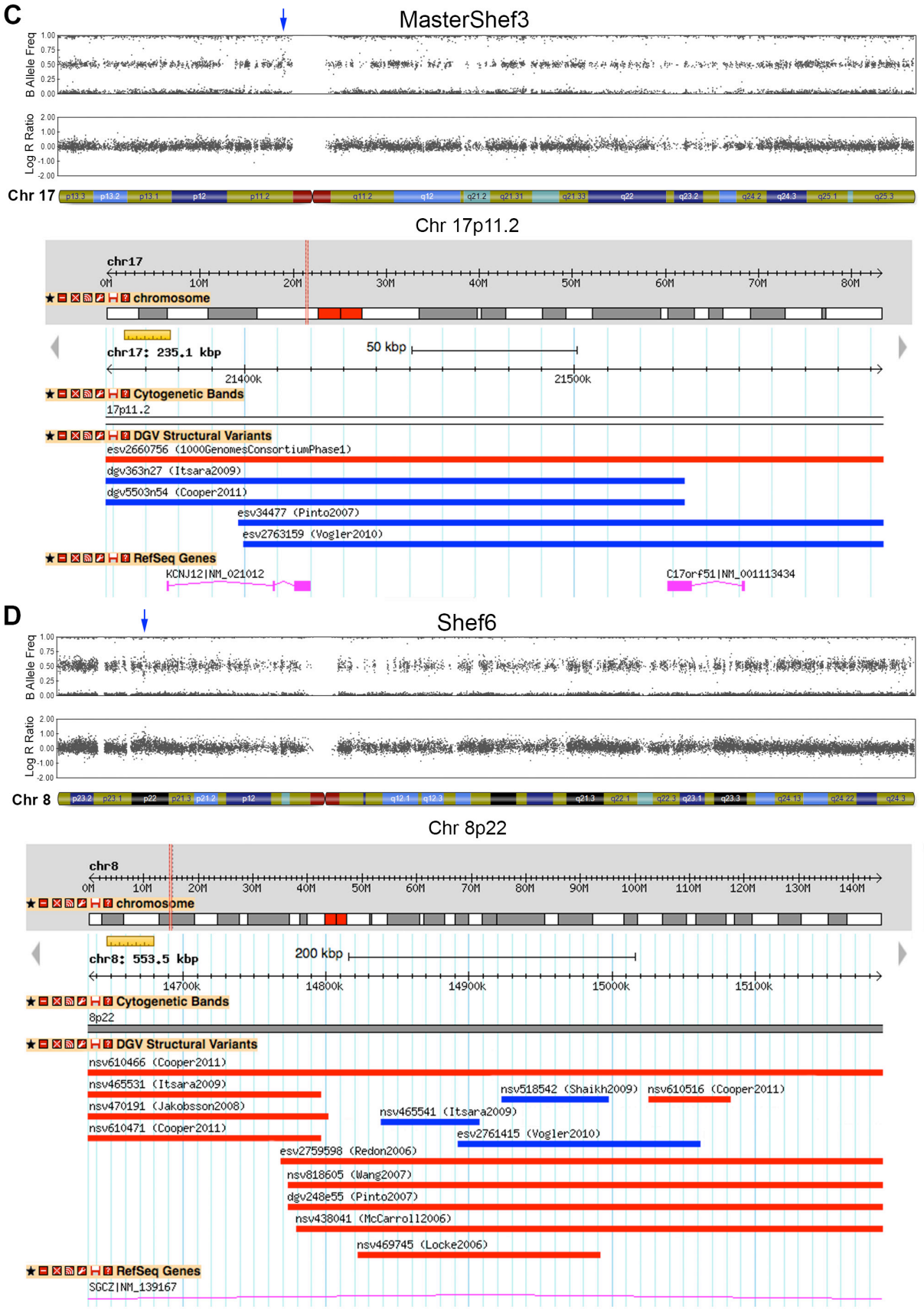

Supplementary Figure S3: Duplication in hESCs that are not fully represented on the DGV. (A) A 330.8 kb duplication on chromosome 6p22.1, containing part of the Histone 1 gene cluster, was detected in KCL034 hESCs. A duplication of this size has not been reported, but a deletion (nsv601208) spanning most of the Histone 1 cluster has been observed. (B) A 541.7 kb duplication on chromosome 18q23 was found in KCL037 hESCs. Although a duplication of this size has not been reported, a smaller duplication (nsv577794) spanning the two coding genes in the region has been observed. Only published CNVs larger that 10 kb are represented on this plot. (C) MasterShef3 harboured a 235.1 kb duplication on chromosome 17p11.2 spanning the *KCNJ12* and *C17ORF51* genes. Although a duplication of this size has not been reported, a deletion of this region is on the DGV (esv2660756), as well as several duplications covering the majority of this CNV. (D) A 553.5 kb duplication was detected within an intron of *SGCZ* on chromosome 8p22 in Shef6 hESCs. Small duplications within this CNV have been reported, and a full deletion of the region is present on the DGV (nsv610466).

Stem Cell Reports
Article

ISSCR

OPEN ACCESS

3D In Vitro Model of a Functional Epidermal Permeability Barrier from Human Embryonic Stem Cells and Induced Pluripotent Stem Cells

Anastasia Petrova,[1,2,9] Anna Celli,[3] Laureen Jacquet,[1] Dimitra Dafou,[4,10] Debra Crumrine,[3] Melanie Hupe,[3] Matthew Arno,[5] Carl Hobbs,[6] Aleksandra Cvoro,[7] Panagiotis Karagiannis,[2] Liani Devito,[1] Richard Sun,[3] Lillian C. Adame,[3] Robert Vaughan,[8] John A. McGrath,[2] Theodora M. Mauro,[3,*] and Dusko Ilic[1,*]

[1]Stem Cell Laboratory, Assisted Conception Unit, Division of Women's Health, Women's Health Academic Centre, King's College London, London SE1 9RT, UK
[2]St John's Institute of Dermatology, King's College London, London SE1 9RT, UK
[3]Department of Dermatology, Veteran Affairs Medical Center, University of California, San Francisco, San Francisco, CA 94121, USA
[4]Division of Genetics and Molecular Medicine, King's College London School of Medicine, Guy's Hospital, London SE1 9RT, UK
[5]Genomics Centre, King's College London, London SE1 9NH, UK
[6]Histology Laboratory, Wolfson Centre for Age-Related Diseases, School of Biomedical Sciences, King's College London, London SE1 1UL, UK
[7]Genomic Medicine, The Methodist Hospital Research Institute, Houston, TX 77030, USA
[8]Clinical Transplantation Laboratory, GSTS and MRC Centre for Transplantation, King's College London, King's Health Partners, London SE1 9RT, UK
[9]Present address: Immunobiology Unit, Institute of Child Health, University College London, London WC1N 1EH, UK
[10]Present address: School of Biology, Department of Genetics, Development and Molecular Biology, Aristotle University, 54124 Thessaloniki, Greece
*Correspondence: maurot@derm.ucsf.edu (T.M.M.), dusko.ilic@kcl.ac.uk (D.I.)
http://dx.doi.org/10.1016/j.stemcr.2014.03.009

SUMMARY

Cornification and epidermal barrier defects are associated with a number of clinically diverse skin disorders. However, a suitable in vitro model for studying normal barrier function and barrier defects is still lacking. Here, we demonstrate the generation of human epidermal equivalents (HEEs) from human embryonic stem cells (hESCs) and induced pluripotent stem cells (iPSCs). HEEs are structurally similar to native epidermis, with a functional permeability barrier. We exposed a pure population of hESC/iPSC-derived keratinocytes, whose transcriptome corresponds to the gene signature of normal primary human keratinocytes (NHKs), to a sequential high-to-low humidity environment in an air/liquid interface culture. The resulting HEEs had all of the cellular strata of the human epidermis, with skin barrier properties similar to those of normal skin. Such HEEs generated from disease-specific iPSCs will be an invaluable tool not only for dissecting molecular mechanisms that lead to epidermal barrier defects but also for drug development and screening.

INTRODUCTION

The major function of the skin is to form a permeability barrier between an organism and its external environment. Integrity and cohesion of the "bricks and mortar" structure of the outermost layer of epidermis, the stratum corneum (SC), is essential for terrestrial life, the survival of which ultimately depends on maintenance of permeability barrier homeostasis (Elias, 1983; Kalinin et al., 2002; Segre 2003). The SC is composed of corneocytes ("bricks") encased in a lipid-rich extracellular matrix (ECM; "mortar") (Nemes and Steinert, 1999).

Corneocytes, which are composed of keratin microfibrils surrounded by cornified envelopes (CEs), are the final products of a linear keratinocyte differentiation pathway from a mitotically active stratum basale (SB) through a transcriptionally active stratum spinosum (SS) and a stratum granulosum (SG) that transitions into anucleate SC cells. The CEs are formed from precursor proteins directly beneath the plasma membrane. Following membrane disintegration, Ca^{2+} influx activates transglutaminase, which irreversibly crosslinks CE proteins around filaggrin-associated keratin filaments. These CEs combine with secreted and processed lipids to form a functional epidermal barrier.

The lipids are packaged into lamellar bodies in the SG cells. The lamellar body, with all its contents, is secreted in response to barrier perturbation. The secreted lipids of the SC are processed into lamellar membranes (Figures 1A and 1B). Lamellar bodies also contain proteolytic enzymes and antimicrobial peptides, which when secreted along with lipid contribute to permeability barrier function (reviewed in Elias, 2012).

Ichthyoses and atopic dermatitis are due to polymorphisms or mutations in genes that control keratinocyte differentiation, cornification, or lipid metabolism. These changes lead to defects in epidermal permeability barrier homeostasis that range from mild (can be easily mistaken for normal dry skin) to life threatening (Segre 2006; Smith et al., 2006; Richard, 2004). Although ichthyosis-like diseases are also present in animals and can be mimicked in transgenic mouse models, there are still no suitable in vitro models for these diseases.

Human epidermal equivalents (HEEs) are in-vitro-generated 3D models that are widely used in experimental settings. However, their utility for addressing the mechanisms

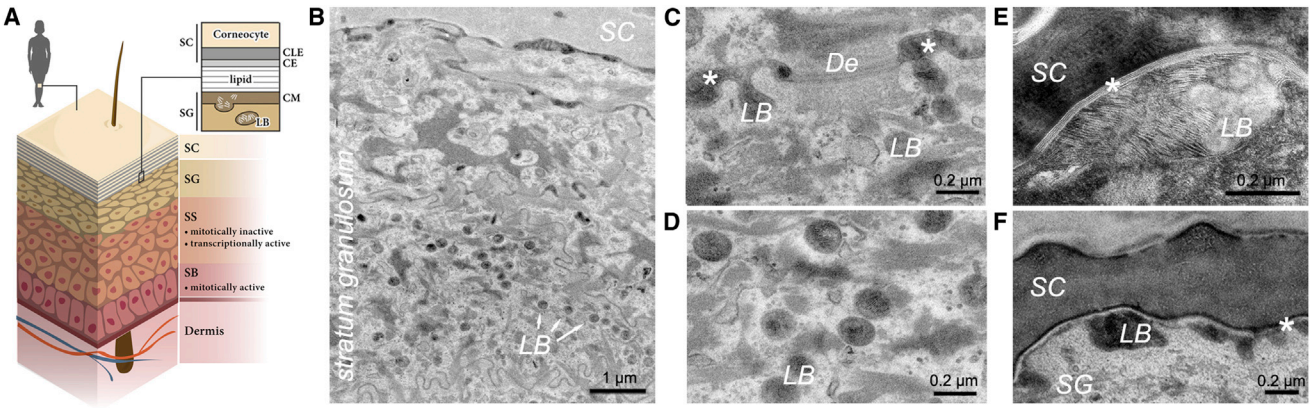

Figure 1. Epidermal Permeability Barrier within the SC of Normal Human Skin

(A) Schematic drawing of normal human skin, depicting the epidermal permeability barrier within the SC.

(B–F) TEM demonstrates the components of a competent permeability barrier in normal human skin. Lipids are packaged into lamellar bodies (LBs) in the SG cells.

(B) LBs (arrows) are present in the uppermost SG cells. These LBs are not discrete droplets, but rather are part of a tubular network extending from the Golgi.

(C) LBs, with all their contents, are secreted into extracellular space (asterisks) between the uppermost SG cells. De, desmosome.

(D) Close-up of LB morphology.

(E) Lipid from LBs is processed into lipid bilayers (asterisk) by SC enzymes that require acidity, thus forming lipid structures that are impermeable to passage of water and ions.

(F) Ceramide-based lipids bind to the CE (asterisk), forming the cornified lipid envelope (CLE).

Scale bars are noted in each panel.

of various skin disorders, or for drug development and testing, has been limited by the fact that previously engineered HEEs do not form a fully developed epidermal barrier. In spite of advances in HEE engineering, such as integrating melanocytes (Nissan et al., 2011), macrophages (Linde et al., 2012), or dermal fibroblasts (Itoh et al., 2013) and pluristratified epidermis, issues involving the generation of a functional permeability barrier in vitro remain unresolved. Further, in vitro studies have been limited by the fact that only a limited number of HEEs can be generated from one sample of epidermis, and the primary keratinocytes generated from this sample may contain previously unidentified polymorphisms in genes that modify epidermal growth, differentiation, or barrier development. HEEs generated from immortalized keratinocytes develop even less well than those generated from primary keratinocytes (Götz et al., 2012). Therefore, in order to develop a HEE model that can be produced in an unlimited number of genetically identical units, we turned to human embryonic stem cells (hESCs) and induced pluripotent stem cells (iPSCs), primary cells that are capable of infinite proliferation and whose genetic footprint can be fully characterized.

We demonstrate here that by following an integrated, highly reproducible four-step protocol, we were able to differentiate hESCs/iPSCs into keratinocytes with gene-expression profiles similar to those of normal human keratinocytes (NHKs, i.e., primary keratinocytes isolated from biopsies of normal healthy skin). These hESC/iPSC-derived keratinocytes were then used to generate HEEs in an air/liquid interface culture exposed to sequential a high-to-low humidity environment. HEEs generated from hESC/iPSC-derived keratinocytes have a functional permeability barrier similar to native human skin and are indistinguishable from HEEs generated from NHKs under the same condition. We are not aware of any other protocols resulting in this functional endpoint.

RESULTS

Reprogramming

Since the first iPSCs were derived, different reprogramming approaches aimed at increasing their efficiency and minimizing the potential for DNA damage have been developed (reviewed in Bellin et al., 2012; Robinton and Daley 2012). We used a nonintegrating, nonviral, synthetic, modified mRNA system (Yakubov et al., 2010; Warren et al., 2010) to reprogram human newborn fibroblasts (Figure S1 available online). In our hands, the reprogramming efficiency was ~0.76% (Figures 2A and S2), which is lower than that reported by Warren et al. (2010). We chose two iPSC clones, iKCL004 and iKCL011, that had a population doubling time (PDT) similar to that of KCL034, a clinical-grade

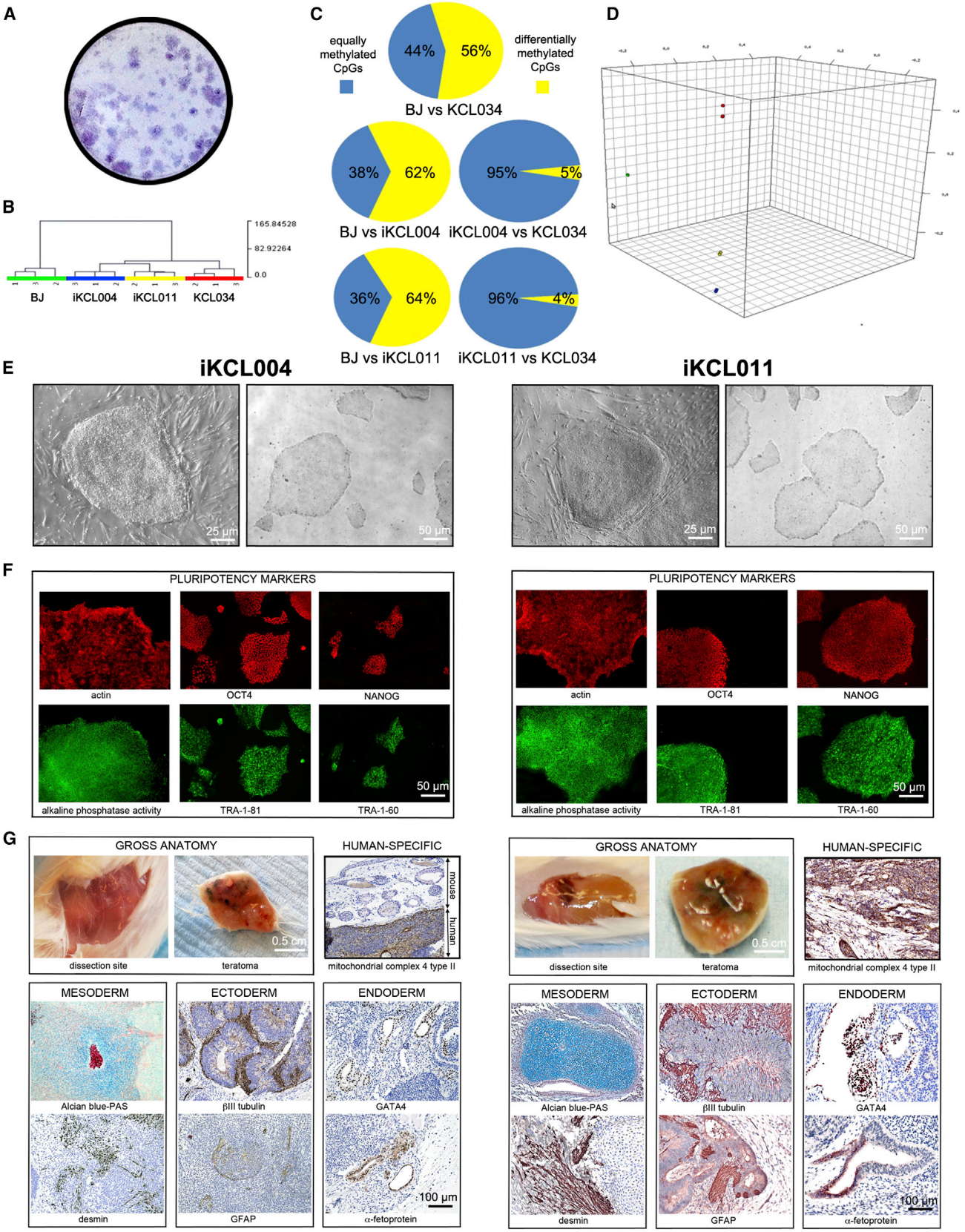

(legend on next page)

hESC line that we used as a control throughout all experiments. Both iKCL004 and iKCL011 had a methylation signature of PSCs, expressed pluripotency markers, and were able to differentiate into cells of all three germ layers in vivo (Figures 2B–2G and S3). Array comparative genomic hybridization (CGH) did not detect any copy number changes, using Promega male as a standard, over an extended period of cell culture (>3 months) under feeder-free conditions.

Efficient and Reproducible Differentiation of hESCs and iPSCs into Keratinocytes

To recapitulate epidermogenesis, in the first step of keratinocyte differentiation, which we termed "induction," we transferred a clinical-grade hESC line (KCL034) and two iPSC lines (iKCL004 and iKCL011) from 5% O_2 to atmospheric O_2, and exposed them to 25 ng/ml BMP4 and 1 μM of the carboxylic acid form of vitamin A, all-*trans* retinoic acid (ATRA), for 7 days (Figure 3A). The lines did not respond similarly to induction. Both iPSC lines expressed higher mRNA levels of the epidermal markers integrin β4 (*ITGB4*) and keratin 14 (*KRT14*), suggesting differentiation toward an epidermal lineage, whereas hESC line KCL034 seemed to remain "undecided," having similar mRNA levels of these two epidermal markers and a neural marker, oligodendrocyte lineage transcription factor 2 (*OLIG2*; Figure 3B). In the next step, termed "selection," we used native 3D decellularized human dermal fibroblast (HDF) ECM as a growth-supporting platform. This was done to mimic basement membrane (BM), which is formed soon after epidermal induction during embryogenesis (Figure S4). A week later, we purified epidermal progenitor stem cells based on their preferential adherence to collagen IV (Murray et al., 1979; Bickenbach and Roop, 1999). During the next "enrichment" step of our differentiation protocol, the purified cells gave rise to a homogeneous population of keratin 14 $(K14)^+p63^+$ colonies, which was further amplified in the final "expansion" step of the protocol (Figure 3C). p63 is a transcription factor that plays a major role in maintaining the proliferative potential of epithelial progenitors (reviewed in Blanpain and Fuchs, 2007). Whereas plating of cells on 3D HDF ECM rapidly increased *p63* mRNA expression, pluripotent markers, such as the transcription factors *Oct4* and *nanog*, steadily decreased during differentiation (Figure 3D). K18, which is expressed earliest during embryonic development, and with its binding partner K8 can serve as a marker of simple epithelium, was expressed at higher levels only during the induction and selection steps, suggesting that the cells subjected to our differentiation protocol were following a fate similar to that which occurs for epidermal morphogenesis during embryonic development. This four-step protocol was highly reproducible. *KRT14* expression increased steadily during differentiation and there were no significant differences among the three lines in multiple rounds of the differentiation process (Figure 3E). The PD of hESC/IPSC-derived keratinocytes did not differ much from that of NHKs over a period of 5 weeks in culture (Figure 3F).

hESC/iPSC-Derived Keratinocytes Are Very Similar to Primary NHKs

Next, we compared enriched and expanded populations (T3) of hESC/iPSC-derived keratinocytes with NHKs from different donors in several different ways, and did not find any major discrepancies. Differences in the expression levels of *KRT14* and *p63* in multiple T3 populations of hESC/iPSC-derived keratinocytes (n = 9; three biological repeats for each of three lines) and NHKs from three donors were not statistically significant (Figure 4A). Flow-cytometry analysis of NHK and T3 populations of hESC/iPSC-derived keratinocytes using K14 and integrin β4 as markers did not identify any marked difference in the percentage of double-positive (DP) cells; 95% of NHK, 87.8% of

Figure 2. Generation and Characterization of Normal Human iPSCs

(A) Trypan blue staining of colonies in one well of a six-well dish. The average reprogramming efficiency from two independent experiments was ~0.76%.

(B–D) DNA methylation analyses. Hierarchical clustering (B), methylation portrait (C), and principal component analysis (D) suggest that both iKCL004 and iKCL011 have the methylation signature of PSCs. BJ, parental HFFs. n = 3 biological replicates (rounds of differentiation) for each cell line.

(D) Undifferentiated iKCL004 and iKCL011 cultured on HFF feeders and under feeder-free conditions display the typical morphology of PSCs.

(E) Expression of pluripotency markers is confirmed by alkaline phosphatase (AP) activity assay and immunostaining for NANOG, OCT4, TRA-160, and TRA-1-81 in iKCL004 and iKCL011 lines.

(F) Differentiation of iKCL004 and iKCL011 into all three germ layers in vivo is confirmed by detection of specific markers. Teratomas were encapsulated and did not invade surrounding tissues. All sections were stained with hematoxylin and eosin (H&E). Specific stains are brown (immunohistochemistry) or light blue (Alcian). Positive staining for mitochondrial complex IV type II confirms the human origin of the teratoma tissue. Germ layer markers: Alcian blue/periodic acid Schiff (PAS)-stained cartilage and desmin for mesoderm, βIII tubulin and glial fibrillary acidic protein (GFAP) for ectoderm, and GATA4 and α-fetoprotein for endoderm.

See also Figures S1–S3.

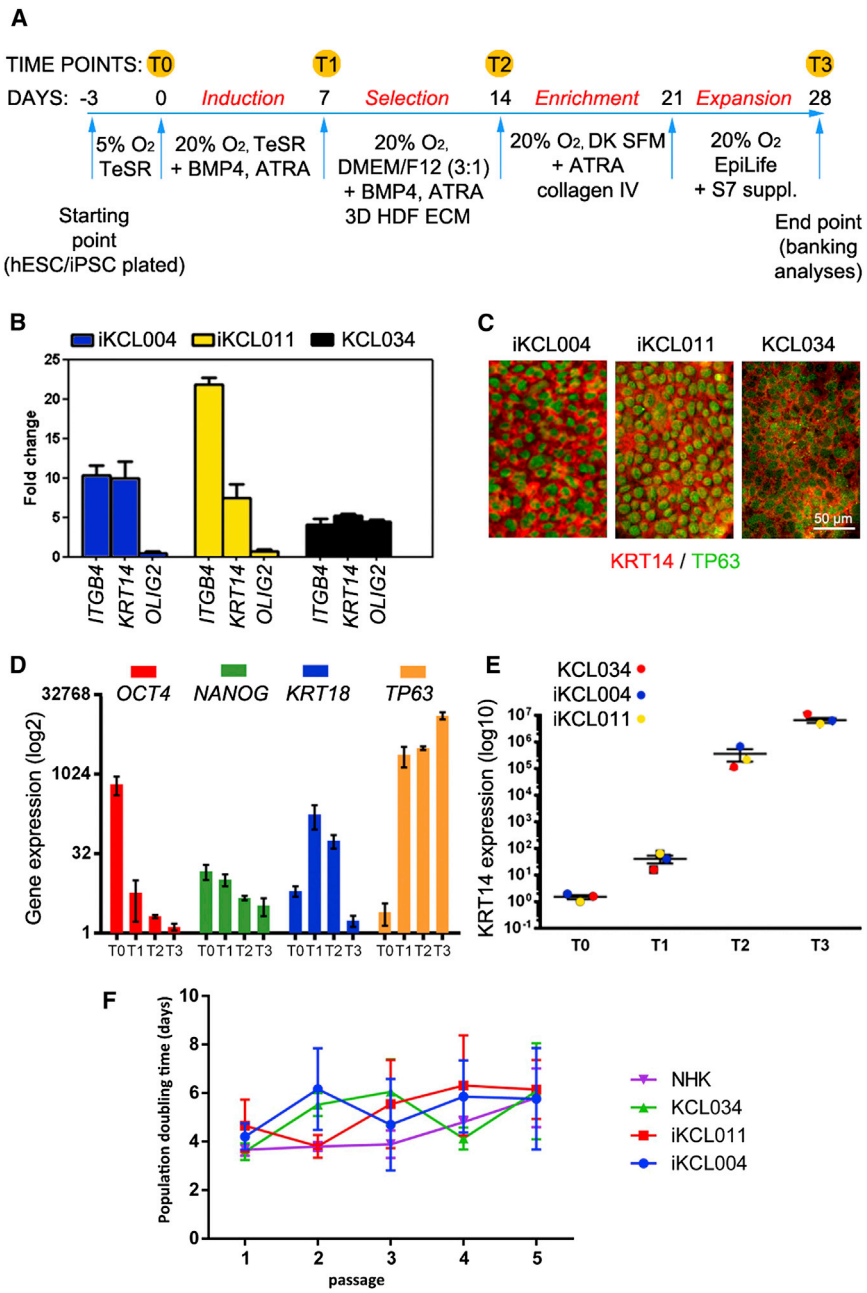

Figure 3. Efficient and Reproducible Differentiation of hESCs and iPSCs into Keratinocytes

(A) Schematic of the differentiation protocol. T0 (day 0), T1 (day 7), T2 (day 14), and T3 (day 28) represent time points at which the cells were switched to a new culture condition and/or collected for analyses.

(B) qPCR analysis measuring the expression of differentiation markers (epidermal: *ITGB4* and *KRT14*; neural: *OLIG2*) suggests a difference in commitment toward epidermal lineage at time point T1. n = 9 for each cell line; each of three rounds of differentiations (biological replicates) had three technical replicates.

(C) Diversity is lost at later stages, and cell colonies at the enrichment step are uniformly positive for keratinocyte markers K14 (red) and p63 (green).

(D) qPCR analyses measuring expression of differentiation markers at T0, T1, T2, and T3 of the differentiation protocol. Expression of pluripotency markers *OCT4* and *NANOG* is diminished by the end of differentiation, whereas *KRT18* and *p63* mRNA levels reflect stages during epidermogenesis. n = 9 for each cell line; each of three rounds of differentiations (biological replicates) had three technical replicates.

(E) Levels of *KRT14* mRNA expressed during three rounds of differentiation at four different time points for each of lines demonstrate the reproducibility of the protocol. Absolute quantification was performed using the ddCt method. GOI expression was normalized to the geometrical mean of two HK genes (*GAPDH* and *EIF4A2*). The SEM was calculated for mean expression in KCL034, iKCL004, and iKCL011. n = 9 for each cell line; each of three biological replicates/rounds of differentiations had three technical replicates.

(F) The proliferation rate of hESC/iPSC-derived keratinocytes shows no marked difference compared with freshly isolated primary NHKs over a period of 5 weeks. Statistical significance was calculated for each passage using two-way ANOVA with Sidak's multiple comparison test. Data are presented as a blank adjusted mean with SD (n = 3 biological replicates for each cell line).

See also Figure S4.

KCL034 T3, 95.4% of iKCL004 T3, and 86% of iKCL011 T3 were K14$^+$/integrin β4$^+$ (Figures 4B and S5). Finally, we used the HumanHT-12 Expression BeadChip whole-genome expression array, which provides coverage for more than 47,000 transcripts and known splice variants, to compare the transcriptomes of undifferentiated hESCs/iPSCs (T0), hESC/iPSC-derived keratinocytes (T3), and NHKs from two different donors. The T0 and T3 transcriptomes were analyzed as biological replicates from three independent differentiation runs for each of three cell lines (KCL034, iKCL004, and iKCL011). Principal component analysis identified an expected pattern: hESC/iPSC-derived keratinocytes at T3 were grouped together with NHKs and were dissimilar to undifferentiated hESCs/iPSCs at T0

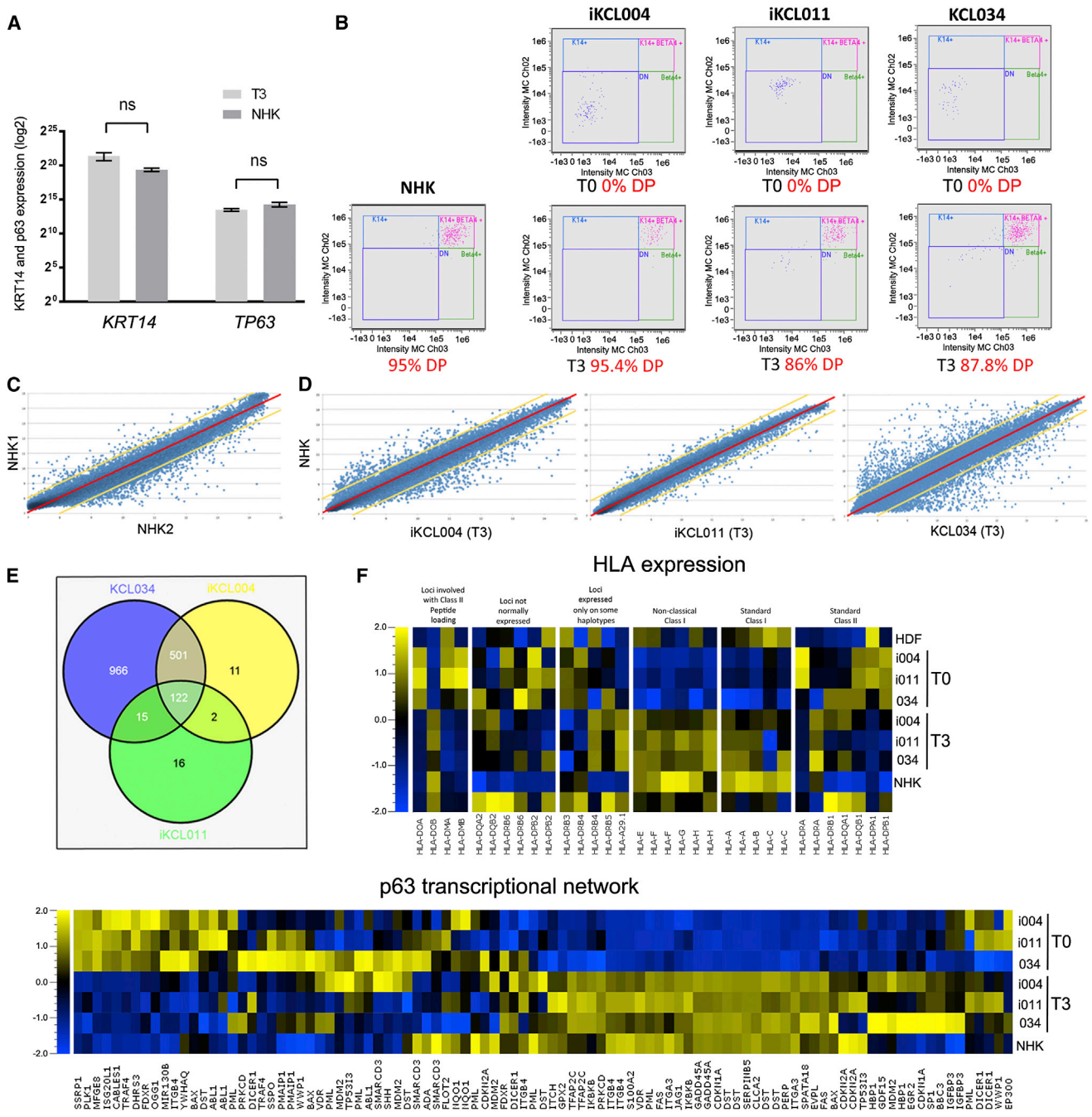

Figure 4. Profiling of hESC/iPSC-Derived Keratinocytes

(A) qPCR analyses measuring expression of *KRT14* and *p63* in hESC/iPSC-derived keratinocytes at T3 (n = 9; three rounds of differentiation for each of three lines) and NHKs (n = 2) found no significant difference between the two groups. Multiple t tests. Statistical significance was determined using the Holm-Sidak method. For *KRT14*, p = 0.120881; for *p63*, p = 0.155472.

(B) Populations of hESC/iPSC-derived keratinocytes at T3 have a similar percentage of $K14^+$/integrin $\beta4^+$ cells as NHKs. The percentage is an average from three rounds of differentiation for each of the three lines. At T0, no $K14^+$/integrin $\beta4^+$ cells were detected. Fluorescence-activated cell sorting (FACS) images represent one of the three rounds.

(C and D) Scatterplots showing the relative expression of all genes on the chip.

(C) Global gene-expression profiles of NHKs from two donors (NHK1 and NHK2) shown as a scatterplot against each other.

(legend continued on next page)

(Figure S6). As an average of three biological replicates, the transcriptome of iKCL011-derived keratinocytes at T3 was closer to the transcriptome of NHKs than to keratinocytes derived from iKCL004 or KCL034. A scatter analysis of gene expression in NHKs from two different donors (NHK1 and NHK2) found that 939 transcripts (2.00%) differed by >2-fold (Figure 4C). An average of these two was then compared with an average of three biological replicates from each of the three lines at T3. The keratinocytes derived from iKCL011 differed by >2-fold in only 155 transcripts (0.33%) from NHKs by >2-fold, whereas iKCL004 (636 transcripts, 1.35%) and KCL034 (1,604 transcripts, 3.41%) were more distinct (Figure 4D). Among all transcripts that were different from NHKs, only 122 (0.26%) were common to all hESC/iPSC-derived keratinocytes at T3 (Figure 4E). We profiled these 122 transcripts using the GeneGo database (Thomson Reuters) for Pathway Maps, Process Networks, Gene Ontology Networks, and Disease Biomarkers list, and found that 34 (0.07%) of them might have relevance to keratinocyte biology (Tables S1–S5, S6, and S7).

We also looked at how reprogramming and differentiation changed human leukocyte antigen (HLA) gene expression (Figure 4F). Although parental HDFs do express HLA class I, the reprogrammed clonal lines iKCL004 and iKCL011 do not, similarly to hESC line KCL034. Differentiation into keratinocytes changed the global pattern. Notably, HLA class I genes were turned on, implying that the recipients of epidermis generated from the hESC-derived keratinocytes as an off-shelf product would be in need of immunosuppressive therapy, whereas that may not be the case with iPSC-based autografts.

hESC-derived keratinocytes exhibit an epidermal transcription program, and p63 is considered to be the main transcription regulator of epidermogenesis and essential for epidermal commitment of hESCs (Blanpain and Fuchs, 2007; Aberdam et al., 2007; Medawar et al., 2008; Pozzi et al., 2009; Crum and McKeon 2010; Vanbokhoven et al., 2011). Therefore, we compared the expression profiles of 96 genes that, according to the NCI Pathway Interaction Database, constitute the p63 transcriptional network. Of these genes, only three (*ADA* [OMIM: 608958], *SMARCD3* [OMIM: 601737], and *YWHAQ* [OMIM: 609009] had ≥2-fold higher expression in NHK from two donors than in all biological replicates of hESC/iPSC-derived keratinocytes at T3. Similarly, only three of those 96 genes (*BBC3* or *PUMA* [OMIM: 605854], *CDKN1A* or *p21* [OMIM: 116899], and *SP1* [OMIM: 189906]) had ≥2-fold higher expression in hESC/iPSC-derived keratinocytes at T3 than in NHKs from two donors. None of these six genes are known to be essential for epidermogenesis, although they may be indirectly involved.

HEEs with a Functional Epidermal Permeability Barrier Generated In Vitro

Molecular characterization suggested that our highly reproducible protocol for differentiating hESCs/iPSCs into keratinocytes yields a fairly pure population of cells that are very similar to NHK. To test the capability of hESC/iPSC-derived keratinocytes to generate multilayered epithelium in vitro, we used the HEE model developed by R.S., A.C., D.C., M.H., L.C., S.D. Peckenpacker, K. Park, Y. Uchida, K.R. Feingold, P.M. Elias, D.I., and T.M.M. (unpublished data). The HEEs generated using this protocol developed in vitro all of the cellular strata seen in the human epidermis. Since they also developed normal barrier properties in vitro, there was no need to implant the organotypic cultures into immunodeficient mice, which is a commonly used technique (Del Rio et al., 2002). We assessed the integrity of the stratifying cultures by measuring the transepithelial electric resistance (TEER), which indicates changes in the transcellular and paracellular permeability of epithelial/epidermal in vitro cell cultures. Within 2 weeks, the TEER in all cultures reached >1,000 Ω, indicating the formation of a permeability barrier and multilayered epithelia (Figures 5A and 5B).

Differentiation markers were normally expressed and located (Figures 6A–6D). Since our system does not contain mixed fibroblast-keratinocytes cultures, the basement membrane zone (BMZ) generated by this system cannot

(D) Global gene-expression profiles of hESC/iPSC-derived keratinocytes at T3 (average of n = 3 biological replicates/rounds of differentiation for each line) shown in scatterplots against NHKs (average of n = 2). Normalized linear expression levels for each probe are plotted as XY coordinates for each sample. Yellow lines indicate boundaries of a 2-fold relative expression difference.
(E) Venn diagram of the transcripts with a 2-fold relative expression difference from NHKs in KCL034-, iKCL004-, and iKCL011-derived keratinocytes at T3 shows that 122 out of >47,000 were common to all three lines.
(F) Heatmaps showing relative expression patterns across multiple samples for specific gene lists. HLA genes were selected by text searching for "HLA" within the "Gene Symbol" annotation, and p63-related genes were identified from the p63 transcriptional network in the NCI Pathway Interaction database. The colors of the heatmaps indicate high (yellow) or low (blue) expression relative to the average for that gene across the samples. The values are the average of three independent runs for KCL034, iKCL004, and iKCL011 at T0 and T3. Transcripts for NHKs from two different donors are shown independently on the HLA heatmap, and as an average on the p63 transcriptional network heatmap.
See also Figures S5 and S6, and Tables S1–S5, S6, and S7.

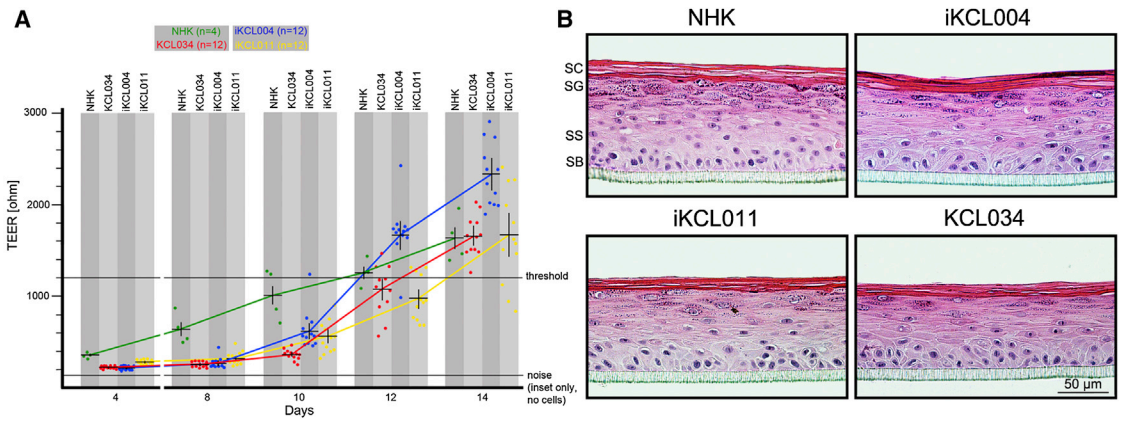

Figure 5. Pluristratified HEEs Generated In Vitro from hESCs and iPSCs

(A) The TEER during HEE formation over a period of 14 days reflects permeability barrier formation (n = 4 for NHK, n = 12 for each of lines; each point represents an average of measurements from three different spots). Error bars represent SD. Only 14-day-old HEE cultures that displayed a TEER of >1,200 ohm cm^2 were used for subsequent analyses unless indicated otherwise.

(B) H&E staining demonstrates normal morphology with the presence of all epidermal layers regardless of the source of keratinocyte population. SB, stratum basale; SS, stratum spinosum.

be equivalent to the BMZ of human skin. Nevertheless, in our 3D cultures, basal-layer keratinocytes were secreting ECM proteins, such as laminin, and assembling a BMZ-like structure (Figures 6E and 6F).

Next, we examined the epidermal permeability barrier. Lipid secretion appeared normal. Lamellar bodies and extensive intercellular bilayers were detected in all cultures (Figure 7A). The endoplasmatic reticulum (ER) Ca^{2+} store, which is essential for normal keratinocyte signaling and differentiation (Callewaert et al., 2003; Celli et al., 2012), was detectable at day 8 of the culture (Figure 7B). Typically, the Ca^{2+} gradient for normal epidermis has low levels in the SB and lowest levels in the SS, followed by an increase in extra- and intracellular Ca^{2+} that peaks within the SG (Elias et al., 2002). In terminally differentiated air-lifted cultures at day 14, HEEs generated from NHKs and hESC (KCL034)-derived keratinocytes had the greatest density of Ca^{2+} precipitates in the SG, whereas precipitates were somewhat more diffuse in HEEs generated from iPSC-derived keratinocytes (Figure 7C). However, the lanthanum perfusion assay, which is used to depict pathways of water movement through epidermis, demonstrated a functional permeability barrier in all cultures: the passage of electron-dense lanthanum tracer was blocked by the epidermal lipid barrier at the SG/SC interface and was not detected in the SC (Figure 7D).

DISCUSSION

We have described a stepwise protocol for manufacturing in vitro HEEs, with all of the cellular strata and apparently normal barrier properties seen in the human epidermis, from hESCs and iPSCs.

When manipulating the cellular fate of pluripotent cells in vitro, it is crucial to have a thorough understanding of the embryonic morphogenesis of the target tissue in order to achieve efficient production of the desired cell type (Hay et al., 2008; Cheng et al., 2012). Epidermal morphogenesis and homeostasis are relatively well described (Blanpain and Fuchs, 2009; Simpson et al., 2011). After gastrulation, the embryo surface emerges as a single layer of neuroectoderm, which will ultimately specify the nervous system and skin epithelium. This decision is guided by Wnt signaling, which blocks the ability of the ectoderm to respond to fibroblast growth factors (FGFs). In the absence of FGF signaling, the cells express bone morphogenetic proteins (BMPs) and become fated to develop into epidermis. In contrast, neural fate develops when, in the absence of a Wnt signal, the ectoderm is able to receive and translate activating cues by FGFs, which then attenuate BMP signaling through inhibitory cues (Chang and Hemmati-Brivanlou, 1998; Stern, 2005). Similarly to our protocol, most of the published protocols for differentiation of PSCs (either mouse or human) into keratinocytes follow this strategy (referenced in Figure S6). We introduced a step in which we purified epidermal progenitor stem cells based on their preferential adherence to collagen IV (Murray et al., 1979; Bickenbach and Roop, 1999). In our hands, this step, which is a kind of physiological purification step that puts a minimal stress on the cells, resulted not only in a higher yield of hESC/iPSC-derived keratinocytes but also in a purified population that was highly homogeneous and similar to NHKs (Figure 2). Homogeneous

populations of keratinocytes differentiated from disease-specific iPSCs would be advantageous for addressing the effects of such mutations on keratinocyte biology (Mildner et al., 2010; Simpson et al., 2010).

Although a link between the level of ambient humidity and barrier development has been described in both animals (Hanley et al., 1997; Kömüves et al., 1999) and human premature infants (Agren et al., 2006), and then recapitulated in vitro with NHKs (Thakoersing et al., 2010), the exact molecular mechanism is still unclear. A limited number of studies have addressed the relationship between environmental humidity and barrier function in postnatal epidermis (Takei et al., 2013; Katagiri et al., 2003; Sato et al., 2002; Denda et al., 1998), and the results warrant further work. Regardless, the model that we describe here would have an unprecedented advantage for elucidating the molecular mechanisms of barrier development, perturbation, and recovery, as well as how mutations of genes involved in cornification and lipid metabolism affect permeability barrier homeostasis (Mildner et al., 2010; Simpson et al., 2010).

Previous HEE models have developed some barrier properties (Gschwandtner et al., 2013; Thakoersing et al., 2012; Ponec et al., 2001). The technique presented here is an advance from previously published HEEs because it is able to produce a HEE that not only shows morphologic changes associated with barrier establishment but also demonstrates the essential functional properties seen in skin with a functional barrier. The HEEs described above provide an effective block against water permeation, as evidenced by their ability to block lanthanum and form a calcium gradient. Further, this 3D model of HEEs with a functional permeability barrier is highly reproducible and has the potential to be easily scaled up and adapted to cGMP requirements for the use in regenerative and aesthetic medicine, as well as drug development. The recent (March 2013) European Union ban on the import and sale of cosmetics containing ingredients tested on animals will increase the demand for efficient and cost-effective alternative in vitro models that would not compromise consumer safety. HEEs with a functional permeability barrier generated completely in vitro from either hESCs or iPSCs, as described here, might present the best available answer (Küchler et al., 2013).

EXPERIMENTAL PROCEDURES

mRNA Synthesis and Modifications

The intronless coding sequences (CDSs) of *OCT4*, *SOX2*, *KLF4*, *c-MYC*, and *LIN28* were retrieved from the National Center for Biotechnology Information (NCBI). As previously described by Warren et al. (2010), a KOZAK translational initiation signal was added in the 5′ UTR, whereas the 3′ UTR was terminated with an alpha-globin-driven oligo(dT) sequence for templated addition of a polyA tail. The CDSs were then codon optimized with the use of GeneOptimizer expert software (GENEART/Life Technologies). Codon optimization allows more efficient transcription by avoiding RNA secondary structures, adjusting GC content, and removing splice-sites. The gene encoding the destabilized enhanced GFP (*d2EGFP*) codon from pRVGP-d2EGFP vector (Addgene) and optimized *OCT4*, *SOX2*, *KLF4*, *c-MYC*, and *LIN28* CDSs were synthesized and subcloned (GENEART/Life Technologies) into the pTNT plasmid vector, which was specifically designed for in vitro expression (Promega). Plasmids were linearized with BamHI. PCR templates were generated from the linearized plasmids using the same upstream primers for all six constructs and six different gene-specific, downstream T120-heeled reverse primers for addition of the poly(A) tail. Quality control of the PCR reaction was performed by capillary electrophoresis (Agilent Bioanalyzer). The templates were transcribed with T7 polymerase and further modified according to Warren et al. (2010). Modifications included the complete substitution of 5-methylcytidine (5mC) for cytidine and the substitution of pseudouridine (psi) for uridine to increase mRNA viability and ectopic protein expression. Furthermore, to promote efficient translation and increase mRNA half-life, a synthetic 5′ guanine cap 3′-0-Me-m7G(5′) ppp(5′)G was added and 5′-triphosphates were eliminated by Antarctic phosphatase treatment. The DNA template was removed with DNase, and single-strand RNA (ssRNA) was purified with spin columns. Quality control of the purified ssRNA product was performed by capillary electrophoresis (Agilent Bioanalyzer; Figure S1). An "mRNA cocktail" containing *OCT4*, *SOX2*, *KLF4*, *C-MYC*, *LIN28*, and d*2eGFP* in molar ratios of 3:1:1:1:1:1 at a final concentration of 100 ng/μl was prepared (AmsBio), aliquoted for single use, and frozen in single-use aliquots.

Reprogramming

Mitotically inactivated foreskin fibroblasts (NuFF from donor 11; AmsBio) were used as feeder cells and plated at a density of 2.5×10^5/well of a six-well dish coated with CELLstart (Life Technologies). Human neonatal foreskin fibroblasts BJ (ATCC, CRL-2522) were plated onto feeders 24 hr later at a density of 7,000/well. For each four wells to be transfected, 25 μl of RNAiMAX (Sigma), a lipofectamine transfection reagent, was diluted in 225 μl of Opti-MEM (Life Technologies) and mixed with 50 μl of mRNA cocktail diluted in 200 μl Opti-MEM. The complex was incubated at room temperature for 15 min before 120 ml was added dropwise into each of four wells to be transfected. The culture medium was refreshed 4 hr later with complete Pluriton medium (Stemgent) supplemented with 300 ng/ml B18R (eBioscience). Transfection was repeated for 17 consecutive days. On days 6–17, Pluriton was preconditioned with NuFF feeders for 24 hr and supplemented with 300 ng/ml B18R and 0.5 mM Na-butyrate. On days 18–21, potential iPSC colonies were left to expand in complete Pluriton with no other supplements. Ten colonies were picked based on morphology on day 21, transferred onto human foreskin fibroblast (HFF) feeders in KOSR-XF medium (Life Technologies), and expanded. Two clones with a similar growth rate, iKCL004 and iKCL011, were further characterized. The cells were cultured at 5% O_2, 37°C, 5% CO_2 throughout the reprogramming.

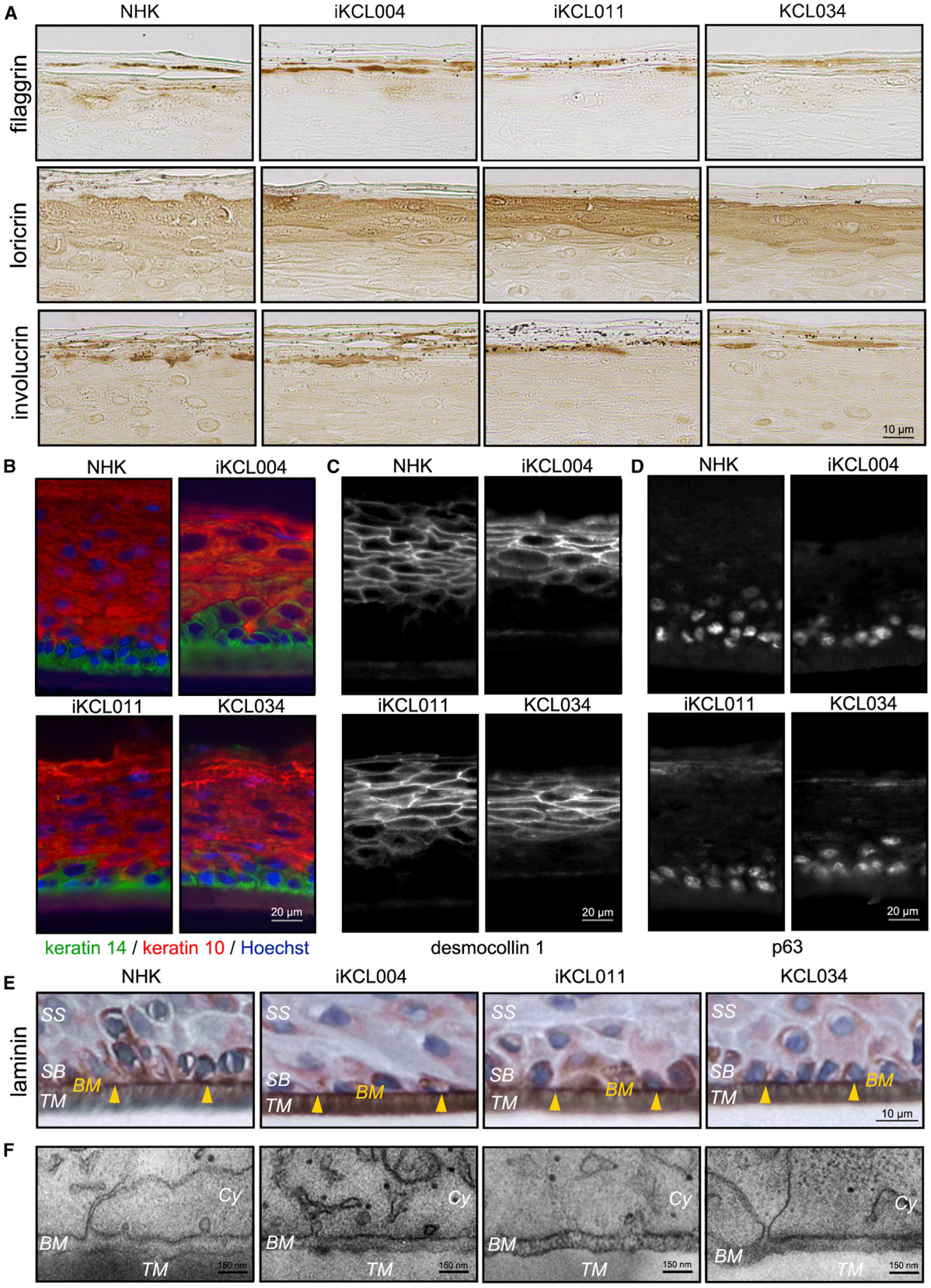

(legend on next page)

Characterization and Culture of PSCs

hESC line KCL034 was derived and characterized as previously described (Jacquet et al., 2013; Stephenson et al., 2012). Expression of pluripotency markers and capability to differentiate into cells of three germ layers were confirmed for both iKCL004 and iKCL011 by methods that are routinely used for hESC lines in our derivation center.

PSC lines were cultured under standard feeder-free conditions on BD Matrigel hESC-qualified matrix (Becton Dickinson) in mTESR1 medium (StemCell Technologies) under hypoxic (5% O_2) conditions.

Methylation Assay

Genomic DNA was isolated from BJ parental fibroblasts (negative control), KCL034 (positive control), iKCL004, and iKCL011. Each sample of 500 ng DNA was bisulfite treated (EZ Zymo DNA Kit) according to the manufacturer's recommendations optimized for 450k array. Epigenome-wide methylation (>480,000 CpG sites) was analyzed using the Infinium Human Methylation 450 BeadChip Kit (Illumina) in biological triplicates for each line. GenoSplice Technology performed quality control, processing, and further analyses of the data.

3D HDF ECM

Preparation of decellularized 3D ECM was performed as previously described (Ilic et al., 2012).

Differentiation Protocol

To induce differentiation, undifferentiated PSCs were transferred into a 20% O_2 atmosphere environment and treated with mTESR1 basal media supplemented with 1 μM ATRA (Sigma-Aldrich) and 25 ng/ml BMP4 (R&D) for 7 days (*Induction*). To select for cells with early acquisition of ectodermal fate, the cells were harvested and replated onto freshly prepared 3D HDF ECM at a density of 5–10 × 10^3 cells per cm^2 and grown in Dulbecco's modified Eagle's medium/Ham F12 (3:1; Life Technologies) supplemented with 1 μM ATRA and 25 ng/ml BMP4 for a further 7 days (*Selection*). To enrich for putative epidermal progenitors, rapid adhesion to type IV collagen-coated dishes was used, and the rapidly adhering cells were cultured in defined keratinocyte-SFM supplemented with 1 μM ATRA for 7 days (*Enrichment*). After that, the cells were cultured in EpiLife medium (Life Technologies) for a further 7 days (*Expansion*) before final harvest and analysis.

Proliferation Assay

All three lines and NHKs were seeded in six-well plates in triplicates at a constant density of 4 × 10^5 per well. Every 7 days, cells were harvested and the total number was counted. The cells were then subcultured at the density described above. This cycle was repeated for five passages. Average PDs were calculated for each line and control at each passage according to the following formula:

PD = (log 2) − 1(logNt − logN0), where Nt = cell number at harvest and N0 = cell number plated (4 × 10^5). The total PD level was calculated as the cumulative of average PDs for five passages. The PDT was calculated according to the following formula: PDT = I/PD, where I = interval (days) between the passages (7).

Immunostaining

Samples were processed as previously described (Ilic et al., 2007; Stephenson et al., 2012). The following antibodies were used: rabbit anti-K14, rabbit anti-filaggrin, rabbit anti-involucrin, and rabbit anti-loricrin (all from Covance); rabbit anti-laminin (DAKO); mouse anti-p63 (Santa Cruz Biotechnology); rabbit anti-fibronectin, mouse anti-collagen IV, mouse anti-collagen VII, and rabbit anti-desmocollin 1 (all from Sigma-Aldrich); and rabbit anti-p63, mouse anti-K10, and rabbit anti-collagen I (all from Abcam). Secondary antibodies were obtained from Jackson ImmunoResearch and Life Technologies.

Flow Cytometry with Confocal Imaging

Cells were incubated with PE-conjugated rat anti-CD104 (integrin β4) antibody (BD PharMingen) for 1 hr, washed, fixed with 4% (v/v) paraformaldehyde, and permeabilized with 0.1% Triton X-100 in PBS. The samples were then incubated with fluorescein isothiocyanate (FITC)-conjugated mouse anti-K14 antibody (Abcam) for 1 hr, washed and incubated with Hoescht 33342 (Life Technologies) for 5 min. To set the gating, fluorescence minus one (FMO) and single-stained compensation controls were also prepared. For acquisition, 1 × 10^6 cells/per sample were resuspended in 100 μl of 1% BSA/PBS. The data were acquired on an ImageStream^X analyzer and analyzed with IDEAS software (Amnis).

Quantitative RT-PCR

Data for quantitative PCR (qPCR) analysis were collected from three independently performed differentiation rounds for each of the cell lines. Total RNA extraction was performed at T0, T1, T2, and T3 time points using the RNeasy kit (QIAGEN). For cDNA preparation, the QuantiTect Reverse Transcription Kit (-QIAGEN) was used. The primers are listed in Figure S7. KAPA SYBR FAST Universal 2× qPCR Master Mix (Kapa Biosystems) was used to set up the qPCR and run on a real-time PCR 7900HT system (Applied Biosystems). All reactions were run in triplicates. The data were collected and analyzed using GUSB and β-actin

Figure 6. The Distribution of Epidermal Markers in HEEs Mirrors that in Human Skin

(A) Immunostaining for three markers of keratinocyte terminal differentiation: filaggrin, loricrin, and involucrin. Each of these markers is expressed at the appropriate site, denoting normal epidermal differentiation.

(B–D) Immunostaining for K14 (basal layer) and K10 (suprabasal layers) (B), desmocollin 1 (suprabasal layers) (C), and p63 (basal layer in general) (D) demonstrates normal epithelial stratification in all HEE cultures.

(E and F) Basal layer keratinocytes express laminin (E) and form BMZ-like structure (F). BM, basement membrane; Cy, cytoplasm; SB, stratum basale; TM, transwell membrane. Yellow arrowheads point to laminin-positive staining of BM.

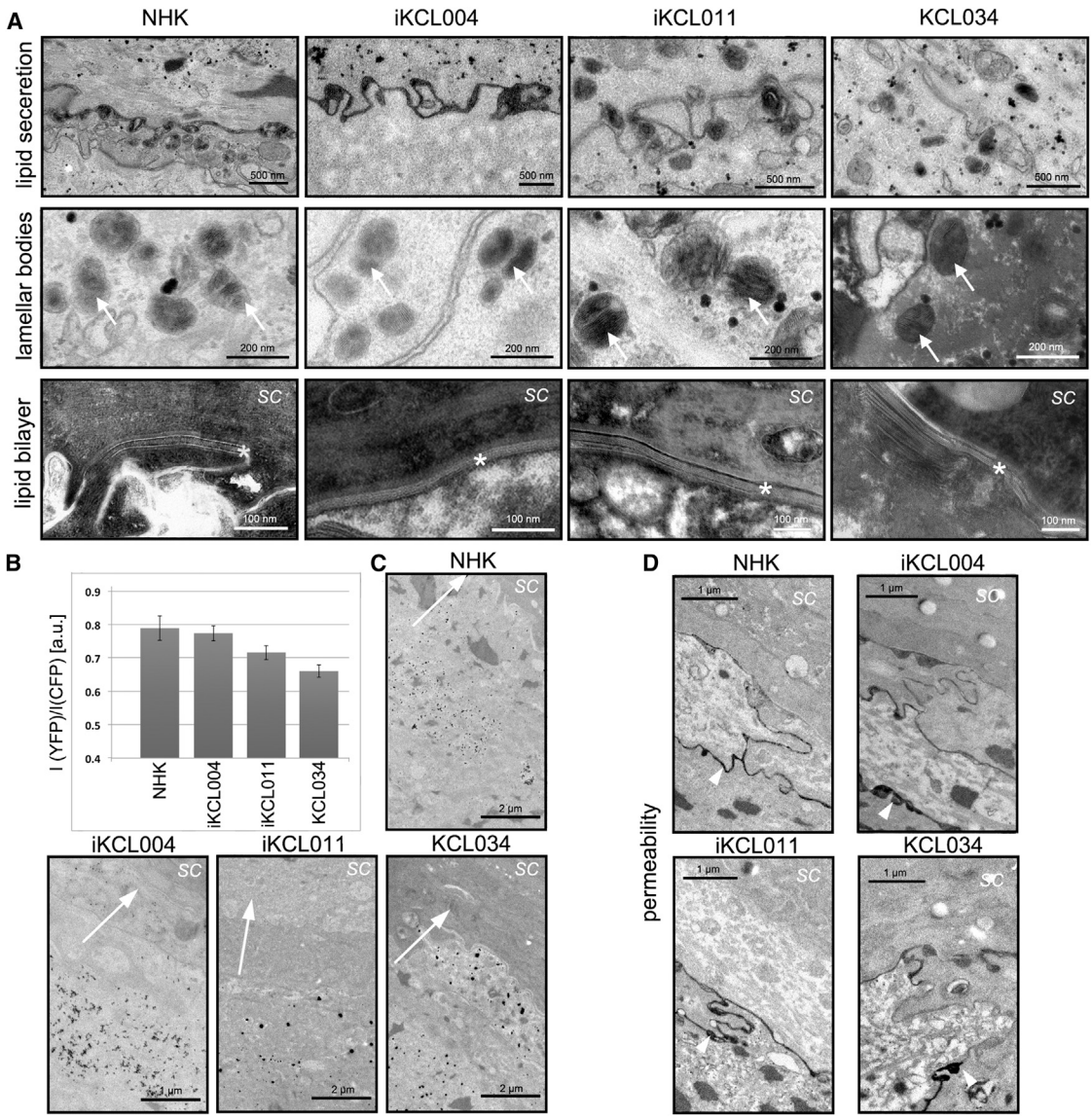

Figure 7. HEE with a Functional Permeability Barrier

(A) Lipid bilayer formation assessed with TEM. Arrows, lamellar bodies; asterisks, lipid bilayers. Upper row: normal lipid secretion between the SG and SC is seen in all cultures. Middle row: LBs are seen in the SG of all cultures (arrows). LB morphology was normal in all cultures, although it appeared slightly smudged in KCL034. Bottom row: lipid was successfully processed into lipid bilayers (asterisks) in all cultures. Like LB morphology, lipid bilayer morphology was normal in all cultures, although it seems slightly disrupted in KCL034.

(B) ER Ca^{2+} sequestration at day 7 of HEE culture in cells transfected with the ER-targeted Ca^{2+} sensor D1ER. Data are presented as the mean of the intensity ratio (I) between the yellow-channel (higher Ca^{2+}) and blue-channel (lower Ca^{2+}) images (I(yfp)/I(cfp)) ± SEM. Higher ratios denote higher Ca^{2+} stores in the ER. n = 10–14 cells from two biological replicates in each group. Significance was calculated using a one-way ANOVA. Distributions with $p < 0.05$ were assumed to be statistically different based on unpaired t tests between the populations.

(C) The epidermal Ca^{2+} gradient captured on TEM as electron-dense Ca^{2+} deposits at day 14. Arrows indicate the direction from the basal layer toward the SC. Ca^{2+} precipitates (black deposits) denote the presence of Ca^{2+} in the tissue. Precipitates are seen in the viable SG but are absent from the SC, denoting a functional barrier to the passage of water and ions.

(D) Permeability barrier integrity assessed by lanthanum perfusion. Lanthanum is visualized as electron-dense deposits in the extracellular spaces of the viable SG (arrowheads), demonstrating that lanthanum and, by extension, water and other small ions can pass between keratinocytes in this stratum. In contrast, lanthanum spreads along the base of the SC, but cannot penetrate further into the SC because a functioning lipid barrier is blocking its movement upward. All cultures demonstrated a functional permeability barrier.

or GAPDH as the reference genes. The results were analyzed and quantified using the ddCT method.

Whole-Genome Gene-Expression Array

Total RNA from T3 cell populations and control primary NHKs were reverse transcribed into cDNA using SuperScript III Reverse Transcriptase (Life Technologies). In vitro transcription of biotin-labeled antisense RNA (aRNA) was performed with the TargetAmp-Nano labeling kit (Epicenter), and purification was performed with the RNeasy Mini Kit (QIAGEN). The quality and quantity of the resultant biotin-labeled aRNAs were assessed using a Bioanalyzer (Agilent) and Qubit Fluorometer (Life Technologies). A total amount of 750 ng of biotin-labeled aRNA in a 5 μl volume was then used for the HumanHT-12 Expression BeadChip whole-genome, gene-expression direct hybridization assay system (Illumina) according to the manufacturer's instructions and run on the iScan system (Illumina).

HEEs

A suspension of 0.25 × 10^6 neonatal NHKs or hESC/iPSC-derived keratinocytes was seeded on a CELLstart CTS (Invitrogen)-coated 12-well 0.4 μm PET Millicell Hanging Cell Culture Insert (Millipore) in CnT.BM.1 medium with CnT-07 supplement (CELLnTEC). Three days after seeding, the medium was switched to CnT-BM.3 medium with CnT-02-3DF with supplement (CELLnTEC). On day 4, the HEEs were air exposed by feeding the insert from bottom of the well only. HEEs were grown in a humidified (×100% relative humidity) or dry (30%–50% relative humidity) incubator at 37°C (R.S., A.C., D.C., M.H., L.C., S.D. Peckenpacker, K. Park, Y. Uchida, K.R. Feingold, P.M. Elias, D.I., and T.M.M., unpublished data). The TEER was measured with an epithelial voltohmmeter (EVOM; World Precision Instruments).

ER Ca^{2+} Sequestration

Cells were transfected with the ER-targeted cameleon-based Ca^{2+} sensor D1ER (a gift from Dr. Amy Palmer; Palmer and Tsien, 2006) using the lipid-based *Trans*IT transfection reagent (Mirus) at a 1:3 DNA/*Trans*IT ratio. Transfection complexes were assembled 30 min prior to cell plating by adding 1 μl D1ER (at a 1.3 μg/μl concentration) and 3 μl transfection reagent per 100 μl serum-free OptiMem. Cells were resuspended in low-calcium 154 CF medium supplemented with 0.03 mM Ca^{2+} (GIBCO) at a density of 0.5 × 10^6 cells per 1.5 ml. Transfection complexes were added to the suspension at a 100 μl:1 ml complex/cell suspension ratio and gently mixed by pipetting. The cells were then plated into 12-well inserts precoated with CELLstart at a 0.5 × 10^6 cells per insert density and left with the transfection complexes overnight. The medium was then switched to CnT.BM.1 medium with CnT-07 supplement (CELLnTEC) for 3 days. Dual-channel fluorescence measurements were recorded using a Zeiss LSM Meta confocal system (Zeiss).

Transmission Electron Microscopy

Samples were processed for transmission electron microscopy (TEM) as previously described (Ilic et al., 2007; Tu et al., 2012).

ACCESSION NUMBERS

The methylation data have been deposited in the Gene Expression Omnibus under accession number GSE55006, and expression array data have been deposited under accession number GSE55898.

SUPPLEMENTAL INFORMATION

Supplemental Information includes seven figures and seven tables and can be found with this article online at http://dx.doi.org/10.1016/j.stemcr.2014.03.009.

ACKNOWLEDGMENTS

For help and support, we thank H. Navsaria and G. Damodaran (Cell and Tissue Engineering, Centre for Cutaneous Research, Queen Mary, University of London), W.-L. Di (Institute of Child Health, University College London), S. Minger (GE Healthcare), and the staffs of the San Francisco Veteran Affairs Medical Center, the Genomics and Flow Cytometry facilities, and the Biomedical Research Centre at Guy's Hospital. We also thank C. Ogilvie from the Genetics Centre at Guy's Hospital for a critical reading of the manuscript. This work was supported in part by grants from the Medical Research Council UK (G0801061 to D.I.), the NIH (R21 ARO61583 and R01 AR051930), the Research Service of the Department of Veterans Affairs (to T.M.M.), and the Dystrophic Epidermolysis Bullosa Research Association (DebRA) (to J.A.M.). A.P. was a DebRA-supported PhD student.

Received: November 19, 2013
Revised: March 25, 2014
Accepted: March 26, 2014
Published: April 24, 2014

REFERENCES

Aberdam, D., Gambaro, K., Rostagno, P., Aberdam, E., de la Forest Divonne, S., and Rouleau, M. (2007). Key role of p63 in BMP-4-induced epidermal commitment of embryonic stem cells. Cell Cycle *6*, 291–294.

Agren, J., Sjörs, G., and Sedin, G. (2006). Ambient humidity influences the rate of skin barrier maturation in extremely preterm infants. J. Pediatr. *148*, 613–617.

Bellin, M., Marchetto, M.C., Gage, F.H., and Mummery, C.L. (2012). Induced pluripotent stem cells: the new patient? Nat. Rev. Mol. Cell Biol. *13*, 713–726.

Bickenbach, J.R., and Roop, D.R. (1999). Transduction of a preselected population of human epidermal stem cells: consequences for gene therapy. Proc. Assoc. Am. Physicians *111*, 184–189.

Blanpain, C., and Fuchs, E. (2007). p63: revving up epithelial stem-cell potential. Nat. Cell Biol. *9*, 731–733.

Blanpain, C., and Fuchs, E. (2009). Epidermal homeostasis: a balancing act of stem cells in the skin. Nat. Rev. Mol. Cell Biol. *10*, 207–217.

Callewaert, G., Parys, J.B., De Smedt, H., Raeymaekers, L., Wuytack, F., Vanoevelen, J., Van Baelen, K., Simoni, A., Rizzuto, R., and Missiaen, L. (2003). Similar $Ca^{(2+)}$-signaling properties in keratinocytes and

in COS-1 cells overexpressing the secretory-pathway Ca(2+)-ATPase SPCA1. Cell Calcium *34*, 157–162.

Celli, A., Mackenzie, D.S., Zhai, Y., Tu, C.-L., Bikle, D.D., Holleran, W.M., Uchida, Y., and Mauro, T.M. (2012). SERCA2-controlled Ca^2+-dependent keratinocyte adhesion and differentiation is mediated via the sphingolipid pathway: a therapeutic target for Darier's disease. J. Invest. Dermatol. *132*, 1188–1195.

Chang, C., and Hemmati-Brivanlou, A. (1998). Cell fate determination in embryonic ectoderm. J. Neurobiol. *36*, 128–151.

Cheng, X., Ying, L., Lu, L., Galvão, A.M., Mills, J.A., Lin, H.C., Kotton, D.N., Shen, S.S., Nostro, M.C., Choi, J.K., et al. (2012). Self-renewing endodermal progenitor lines generated from human pluripotent stem cells. Cell Stem Cell *10*, 371–384.

Crum, C.P., and McKeon, F.D. (2010). p63 in epithelial survival, germ cell surveillance, and neoplasia. Annu. Rev. Pathol. *5*, 349–371.

Del Rio, M., Larcher, F., Serrano, F., Meana, A., Muñoz, M., Garcia, M., Muñoz, E., Martin, C., Bernad, A., and Jorcano, J.L. (2002). A preclinical model for the analysis of genetically modified human skin in vivo. Hum. Gene Ther. *13*, 959–968.

Denda, M., Sato, J., Masuda, Y., Tsuchiya, T., Koyama, J., Kuramoto, M., Elias, P.M., and Feingold, K.R. (1998). Exposure to a dry environment enhances epidermal permeability barrier function. J. Invest. Dermatol. *111*, 858–863.

Elias, P.M. (1983). Epidermal lipids, barrier function, and desquamation. J. Invest. Dermatol. Suppl. *80*, 44s–49s.

Elias, P.M. (2012). Structure and function of the stratum corneum extracellular matrix. J. Invest. Dermatol. *132*, 2131–2133.

Elias, P.M., Ahn, S.K., Denda, M., Brown, B.E., Crumrine, D., Kimutai, L.K., Kömüves, L., Lee, S.H., and Feingold, K.R. (2002). Modulations in epidermal calcium regulate the expression of differentiation-specific markers. J. Invest. Dermatol. *119*, 1128–1136.

Götz, C., Pfeiffer, R., Tigges, J., Blatz, V., Jäckh, C., Freytag, E.M., Fabian, E., Landsiedel, R., Merk, H.F., Krutmann, J., et al. (2012). Xenobiotic metabolism capacities of human skin in comparison with a 3D epidermis model and keratinocyte-based cell culture as in vitro alternatives for chemical testing: activating enzymes (Phase I). Exp. Dermatol. *21*, 358–363.

Gschwandtner, M., Mildner, M., Mlitz, V., Gruber, F., Eckhart, L., Werfel, T., Gutzmer, R., Elias, P.M., and Tschachler, E. (2013). Histamine suppresses epidermal keratinocyte differentiation and impairs skin barrier function in a human skin model. Allergy *68*, 37–47.

Hanley, K., Jiang, Y., Elias, P.M., Feingold, K.R., and Williams, M.L. (1997). Acceleration of barrier ontogenesis in vitro through air exposure. Pediatr. Res. *41*, 293–299.

Hay, D.C., Zhao, D., Fletcher, J., Hewitt, Z.A., McLean, D., Urruticoechea-Uriguen, A., Black, J.R., Elcombe, C., Ross, J.A., Wolf, R., and Cui, W. (2008). Efficient differentiation of hepatocytes from human embryonic stem cells exhibiting markers recapitulating liver development in vivo. Stem Cells *26*, 894–902.

Ilic, D., Mao-Qiang, M., Crumrine, D., Dolganov, G., Larocque, N., Xu, P., Demerjian, M., Brown, B.E., Lim, S.T., Ossovskaya, V., et al. (2007). Focal adhesion kinase controls pH-dependent epidermal barrier homeostasis by regulating actin-directed Na^+/H^+ exchanger 1 plasma membrane localization. Am. J. Pathol. *170*, 2055–2067.

Ilic, D., Stephenson, E., Wood, V., Jacquet, L., Stevenson, D., Petrova, A., Kadeva, N., Codognotto, S., Patel, H., Semple, M., et al. (2012). Derivation and feeder-free propagation of human embryonic stem cells under xeno-free conditions. Cytotherapy *14*, 122–128.

Itoh, M., Umegaki-Arao, N., Guo, Z., Liu, L., Higgins, C.A., and Christiano, A.M. (2013). Generation of 3D skin equivalents fully reconstituted from human induced pluripotent stem cells (iPSCs). PLoS ONE *8*, e77673.

Jacquet, L., Stephenson, E., Collins, R., Patel, H., Trussler, J., Al-Bedaery, R., Renwick, P., Ogilvie, C., Vaughan, R., and Ilic, D. (2013). Strategy for the creation of clinical grade hESC line banks that HLA-match a target population. EMBO Mol Med *5*, 10–17.

Kalinin, A.E., Kajava, A.V., and Steinert, P.M. (2002). Epithelial barrier function: assembly and structural features of the cornified cell envelope. Bioessays *24*, 789–800.

Katagiri, C., Sato, J., Nomura, J., and Denda, M. (2003). Changes in environmental humidity affect the water-holding property of the stratum corneum and its free amino acid content, and the expression of filaggrin in the epidermis of hairless mice. J. Dermatol. Sci. *31*, 29–35.

Kömüves, L.G., Hanley, K., Jiang, Y., Katagiri, C., Elias, P.M., Williams, M.L., and Feingold, K.R. (1999). Induction of selected lipid metabolic enzymes and differentiation-linked structural proteins by air exposure in fetal rat skin explants. J. Invest. Dermatol. *112*, 303–309.

Küchler, S., Strüver, K., and Friess, W. (2013). Reconstructed skin models as emerging tools for drug absorption studies. Expert Opin. Drug Metab. Toxicol. *9*, 1255–1263.

Linde, N., Gutschalk, C.M., Hoffmann, C., Yilmaz, D., and Mueller, M.M. (2012). Integrating macrophages into organotypic co-cultures: a 3D in vitro model to study tumor-associated macrophages. PLoS ONE *7*, e40058.

Medawar, A., Virolle, T., Rostagno, P., de la Forest-Divonne, S., Gambaro, K., Rouleau, M., and Aberdam, D. (2008). DeltaNp63 is essential for epidermal commitment of embryonic stem cells. PLoS ONE *3*, e3441.

Mildner, M., Jin, J., Eckhart, L., Kezic, S., Gruber, F., Barresi, C., Stremnitzer, C., Buchberger, M., Mlitz, V., Ballaun, C., et al. (2010). Knockdown of filaggrin impairs diffusion barrier function and increases UV sensitivity in a human skin model. J. Invest. Dermatol. *130*, 2286–2294.

Murray, J.C., Stingl, G., Kleinman, H.K., Martin, G.R., and Katz, S.I. (1979). Epidermal cells adhere preferentially to type IV (basement membrane) collagen. J. Cell Biol. *80*, 197–202.

Nemes, Z., and Steinert, P.M. (1999). Bricks and mortar of the epidermal barrier. Exp. Mol. Med. *31*, 5–19.

Nissan, X., Larribere, L., Saidani, M., Hurbain, I., Delevoye, C., Feteira, J., Lemaitre, G., Peschanski, M., and Baldeschi, C. (2011). Functional melanocytes derived from human pluripotent stem cells engraft into pluristratified epidermis. Proc. Natl. Acad. Sci. USA *108*, 14861–14866.

Palmer, A.E., and Tsien, R.Y. (2006). Measuring calcium signaling using genetically targetable fluorescent indicators. Nat. Protoc. *1*, 1057–1065.

Ponec, M., Gibbs, S., Pilgram, G., Boelsma, E., Koerten, H., Bouwstra, J., and Mommaas, M. (2001). Barrier function in reconstructed epidermis and its resemblance to native human skin. Skin Pharmacol. Appl. Skin Physiol. *14* (*Suppl 1*), 63–71.

Pozzi, S., Zambelli, F., Merico, D., Pavesi, G., Robert, A., Maltère, P., Gidrol, X., Mantovani, R., and Vigano, M.A. (2009). Transcriptional network of p63 in human keratinocytes. PLoS ONE *4*, e5008.

Richard, G. (2004). Molecular genetics of the ichthyoses. Am. J. Med. Genet. C. Semin. Med. Genet. *131C*, 32–44.

Robinton, D.A., and Daley, G.Q. (2012). The promise of induced pluripotent stem cells in research and therapy. Nature *481*, 295–305.

Sato, J., Denda, M., Chang, S., Elias, P.M., and Feingold, K.R. (2002). Abrupt decreases in environmental humidity induce abnormalities in permeability barrier homeostasis. J. Invest. Dermatol. *119*, 900–904.

Segre, J. (2003). Complex redundancy to build a simple epidermal permeability barrier. Curr. Opin. Cell Biol. *15*, 776–782.

Segre, J.A. (2006). Epidermal barrier formation and recovery in skin disorders. J. Clin. Invest. *116*, 1150–1158.

Simpson, C.L., Kojima, S., and Getsios, S. (2010). RNA interference in keratinocytes and an organotypic model of human epidermis. Methods Mol. Biol. *585*, 127–146.

Simpson, C.L., Patel, D.M., and Green, K.J. (2011). Deconstructing the skin: cytoarchitectural determinants of epidermal morphogenesis. Nat. Rev. Mol. Cell Biol. *12*, 565–580.

Smith, F.J., Irvine, A.D., Terron-Kwiatkowski, A., Sandilands, A., Campbell, L.E., Zhao, Y., Liao, H., Evans, A.T., Goudie, D.R., Lewis-Jones, S., et al. (2006). Loss-of-function mutations in the gene encoding filaggrin cause ichthyosis vulgaris. Nat. Genet. *38*, 337–342.

Stephenson, E., Jacquet, L., Miere, C., Wood, V., Kadeva, N., Cornwell, G., Codognotto, S., Dajani, Y., Braude, P., and Ilic, D. (2012). Derivation and propagation of human embryonic stem cell lines from frozen embryos in an animal product-free environment. Nat. Protoc. *7*, 1366–1381.

Stern, C.D. (2005). Neural induction: old problem, new findings, yet more questions. Development *132*, 2007–2021.

Takei, K., Denda, S., Kumamoto, J., and Denda, M. (2013). Low environmental humidity induces synthesis and release of cortisol in an epidermal organotypic culture system. Exp. Dermatol. *22*, 662–664.

Thakoersing, V.S., Ponec, M., and Bouwstra, J.A. (2010). Generation of human skin equivalents under submerged conditions-mimicking the in utero environment. Tissue Eng. Part A *16*, 1433–1441.

Thakoersing, V.S., Gooris, G.S., Mulder, A., Rietveld, M., El Ghalbzouri, A., and Bouwstra, J.A. (2012). Unraveling barrier properties of three different in-house human skin equivalents. Tissue Eng. Part C Methods *18*, 1–11.

Tu, C.-L., Crumrine, D.A., Man, M.-Q., Chang, W., Elalieh, H., You, M., Elias, P.M., and Bikle, D.D. (2012). Ablation of the calcium-sensing receptor in keratinocytes impairs epidermal differentiation and barrier function. J. Invest. Dermatol. *132*, 2350–2359.

Vanbokhoven, H., Melino, G., Candi, E., and Declercq, W. (2011). p63, a story of mice and men. J. Invest. Dermatol. *131*, 1196–1207.

Warren, L., Manos, P.D., Ahfeldt, T., Loh, Y.H., Li, H., Lau, F., Ebina, W., Mandal, P.K., Smith, Z.D., Meissner, A., et al. (2010). Highly efficient reprogramming to pluripotency and directed differentiation of human cells with synthetic modified mRNA. Cell Stem Cell *7*, 618–630.

Yakubov, E., Rechavi, G., Rozenblatt, S., and Givol, D. (2010). Reprogramming of human fibroblasts to pluripotent stem cells using mRNA of four transcription factors. Biochem. Biophys. Res. Commun. *394*, 189–193.

Stem Cell Reports, Volume *2*

Supplemental Information

3D In Vitro Model of a Functional Epidermal Permeability Barrier from Human Embryonic Stem Cells and Induced Pluripotent Stem Cells

Anastasia Petrova, Anna Celli, Laureen Jacquet, Dimitra Dafou, Debra Crumrine, Melanie Hupe, Matthew Arno, Carl Hobbs, Aleksandra Cvoro, Panagiotis Karagiannis, Liani Devito, Richard Sun, Lillian C. Adame, Robert Vaughan, John A. McGrath, Theodora M. Mauro, and Dusko Ilic

Inventory of Supplemental Information

Figure S6 (related to Figure 4)

(A-B**)** Expression level averages shown for the sample groups in a principal component analysis plot

(C) Distance measures between groups of samples

Figure S7 (related to Experimental procedures)

Primer sequences

Table S1 (related to Figure 4)

Pathway Map analysis

Table S2 (related to Figure 4)

Process Networks analysis

Table S3 (related to Figure 4)

Gene Ontology Processes analysis

Table S4 (related to Figure 4)

Diseases by Biomarkers analysis

Table S5 (related to Figure 4)

Genes relevant to keratinocyte biology in a group of the 122 transcripts

Table S6 (related to Figure 4)

Genes that were 2-folds or greater expressed higher in NHK

Table S7 (related to Figure 4)

Genes that were 2-folds or greater expressed higher in NHK

Supplementary references (related to Discussion)

Protocols of differentiation of pluripotent stem cells, either mouse or human, into keratinocytes that share similar strategy with our protocol

SUPPLEMENTAL INFORMATION

Figure S1 (related to Figure 2)

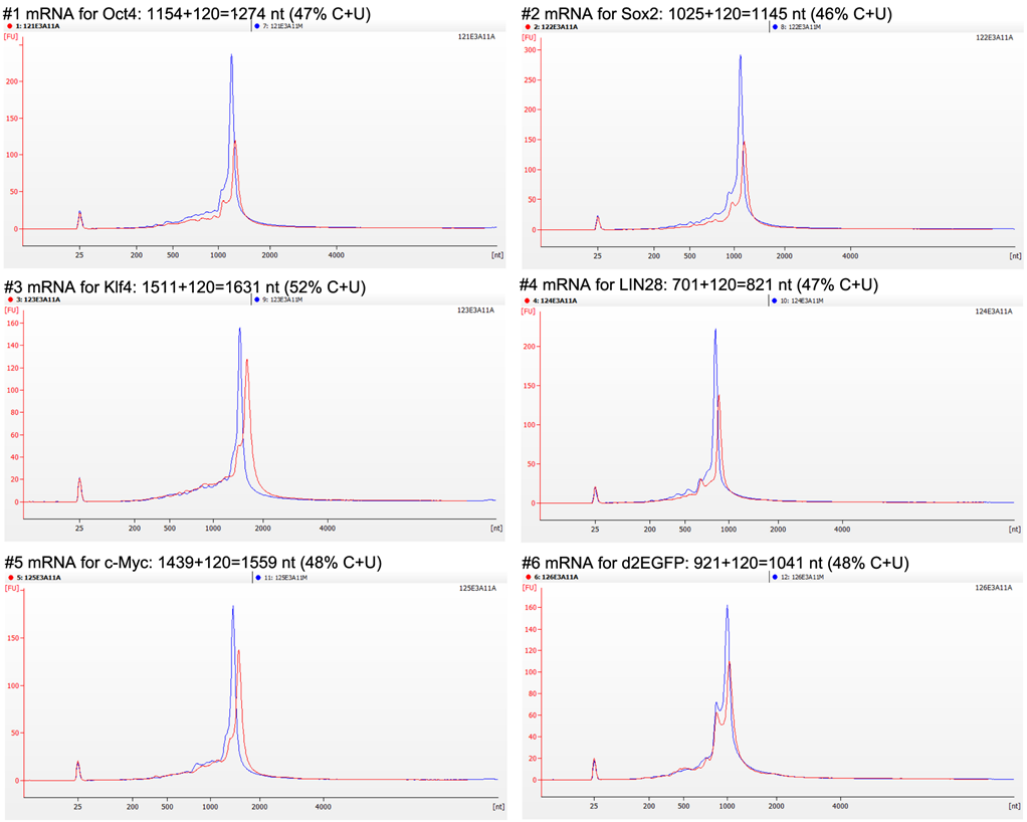

Synthetic modified mRNA quality control. All transcripts were generated with and without the required modifications. All RNA profiles show an overlay of unmodified RNAs (red tracing) and of fully modified RNAs (blue tracing). The successful incorporation of modified nucleotides is evident by an apparent small shift to lower molecular weight. The long dA:dT segment results in some sequence-context dependent “stuttering” of T7 RNA polymerase, quite similar to the physiological situation where mRNAs carry poly(A) tails of variable lengths. The high percentage (100%) of modified m5CTP and pseudo-UTP did not lead to premature termination with short products. Homogeneous highly modified in-vitro-transcribed mRNA products with 5’-cap, internal m5C and Pseudo-U and 3’-A120 tailproducts were obtained in sufficient yields.

Figure S2 (related to Figure 2)

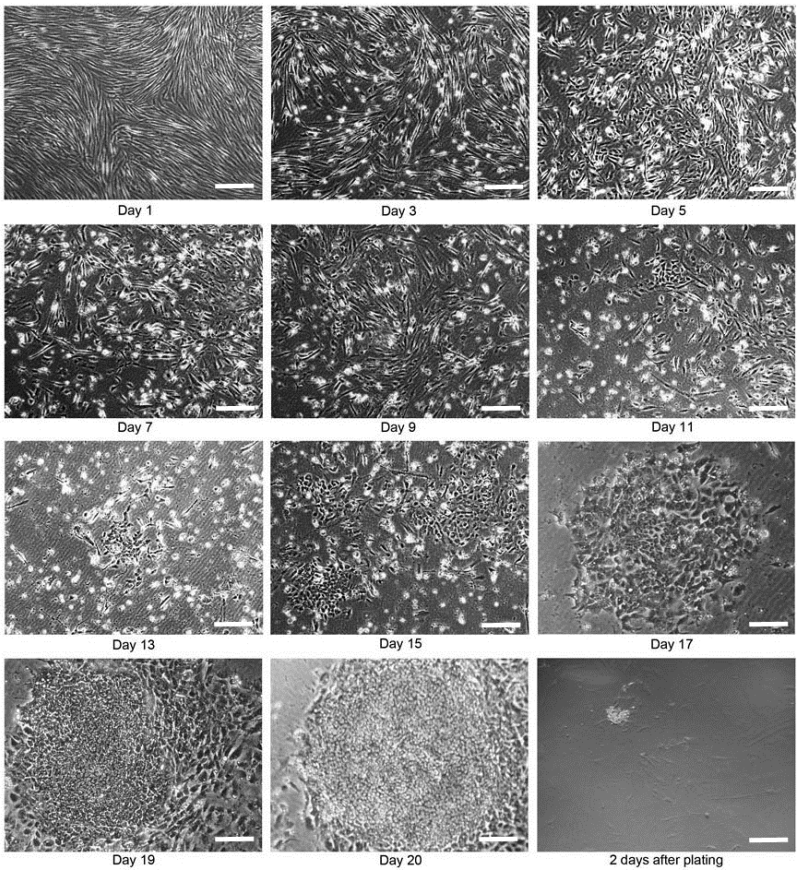

Representative morphology of BJ fibroblasts plated on NuFF-feeders undergoing mRNA reprogramming. Day 1: Healthy cells after the first transfection. Day 3: Cell loss and cell rounding indicate high apoptotic rate. Day 5: Cells start undergoing MET and adopt an epithelial morphology. Day 7 and 9: Increase in cell death. Surviving cells are transitioning. Day 11: First sign of compaction and colony formation. Day 13: Increased compaction. Cells become smaller and more hESC-like. Day 15. Increase in colony size. Day 17: Last transfection. Only reprogrammed cells survived all 17 transfections and colonies keep increasing in size. Day 19: Cells are fed with NuFF-conditioned Pluriton. Colony center (arrow) keeps compacting as cells continue to reprogram and adopt morphology typical for hESC. Day 20: The colony center is ready for picking and being plated on HFF-feeders in complete KOSR medium. Two days after plating: All the colonies plated have attached start to expand. Scale bar in all panels is 50 μm, except Day 17, where is 12.5 μm.

Figure S3 (related to Figure 2)

	BJ		iKCL004		iKCL011	
Marker	**Allele 1**	**Allele 2**	**Allele 1**	**Allele 2**	**Allele 1**	**Allele 2**
D13S252	299	299	298	298	299	299
D13S325	289	293	289	293	289	293
D13S628	454	457	454	457	454	457
D13S634	403	415	403	415	403	415
D18S386	381	386	381	386	380	386
D18S390	368	376	368	376	368	376
D18S391	217	217	217	217	218	218
D18S535	486	490	486	490	486	491
D18S819	408	416	407	416	407	415
D18S976	472	481	472	480	472	481
D18S978	207	211	207	211	207	211
D21S11	245	245	245	245	245	245
D21S1409	216	224	216	224	216	224
D21S1411	308	328	308	328	308	328
D21S1435	180	184	180	184	181	185
D21S1446	311	325	311	325	312	326

Genotyping. Microsatellite markers specific for chromosomes 13, 18, 21, X and Y were amplified. The sex chromosome markers were consistent with a male complement. The allele sizes in bp for markers on chromosomes 13, 18, and 21 are listed in the tables. The occasional 1bp size difference is due to the size differentiation by capillary electrophoresis.

Figure S4 (related to Figure 3)

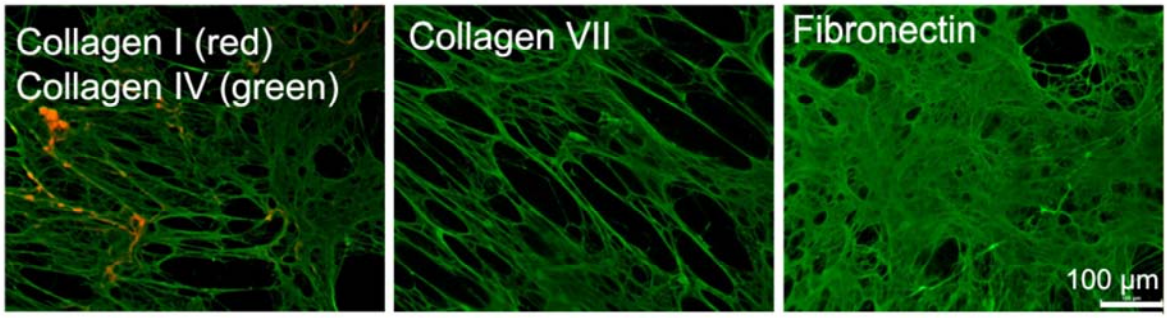

Basement membrane ECM components fibronectin, collagen I, IV and VII are also expressed and assembled in 3D HDF ECM.

Figure S5 (related to Figure 4)

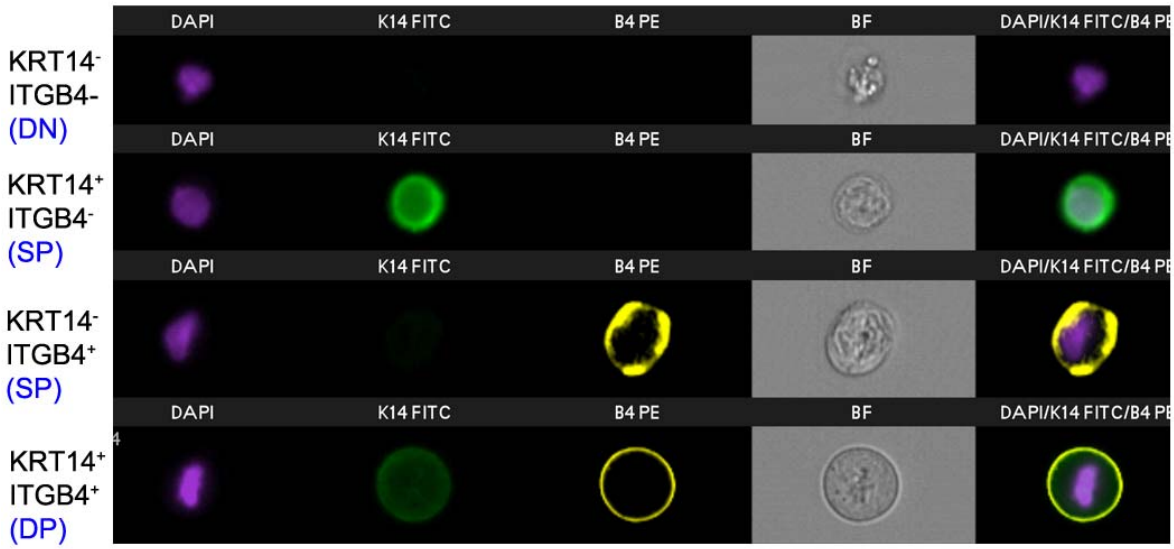

Confocal images of cells undergoing flow cytometry. DN, double negative ($K14^-$/integrin $\beta4^-$); SP, single positive (either $K14^+$/integrin $\beta4^-$ or $K14^-$/integrin $\beta4^+$); DP double positive ($K14^+$/integrin $\beta4^+$).

Figure S6 (related to Figure 4)

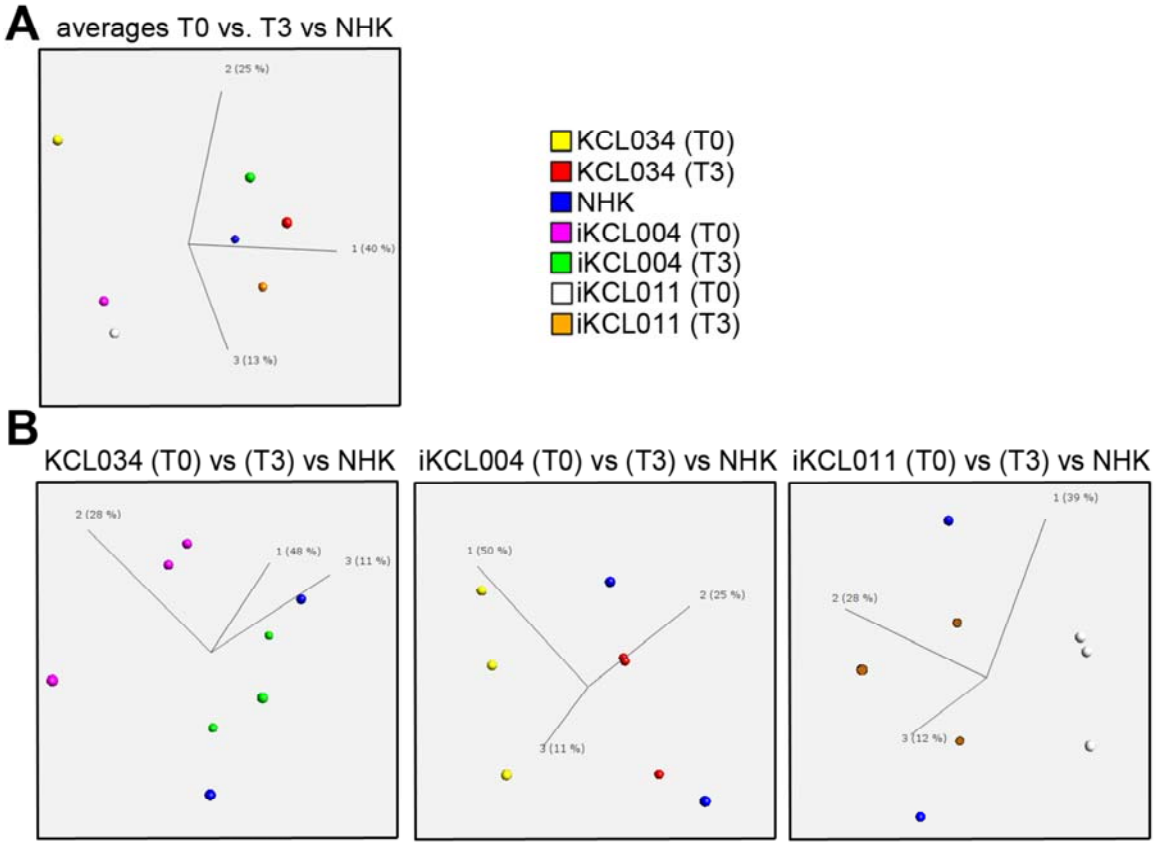

C

	NHK	iKCL011 (T3)	iKCL004 (T3)	KCL034 (T3)
NHK	0	283.92	320.28	345.16
iKCL011 (T3)	283.92	0	318.65	317.05
iKCL004 (T3)	320.28	318.65	0	249.49
KCL034 (T3)	345.16	317.05	249.49	0

(A-C**)** Expression level averages shown for the sample groups in a principal component analysis plot (A and B). A single sphere represents each group and its 3D position is dictated by its value for each of the three main or principal components in the data. These components are represented by three axes. Each axis label indicates the proportion of the variability in the data represented by that component. (C) Distance measures between groups of samples. Euclidean distances for samples were calculated using Omics Explorer (Qlucore).

Figure S7 (related to Experimental Procedures)

Gene	Primer sequence
ACTB	Forward: 5′-CCATGTACGTTGCTATCCAG-3′ Reverse: 5′-CCTCGTAGATGGGCACAG-3′
GAPDH	Forward: 5’-GAAGGTGAAGGTCGGAGTC-3’ Reverse: 5’-GAAGATGGTGATGGGATTTC-3’
GUSB	Forward: 5′-AAACGATTGCAGGGTTTCAC -3′ Reverse: 5′-CTCTCGTCGGTGACTGTTCA -3′
ITGB4	Forward: 5′-GGGTCCAGGAAGATCCATTT-3 Reverse: 5′-AGTCGCAATACGGGTACAGG-3′
KRT14	Forward: 5’GGCCTGCTGAGATCAAAGAC-3’ Reverse: 5’-TGTCTCATACTTGGTGCGGA-3’
KRT18	Forward: 5’-AAGGCCTACAAGCCCAGATT -3’ Reverse:5’-CAGTGTGGTGCTCTCCTCAA-3’
NANOG	Forward: 5’AATACCTCAGCCTCCAGCAGATG-3’ Reverse: 5’-TGCGTCACACCATTGCTATTCTTC-3’
OLIG2	Forward: 5′-GAAACTACCCCACCGACTCA-3′ Reverse: 5′-ACCCAAACTGTTTCCACAGC-3′
OCT4	Forward: 5′- GCCGTGAAGCTGGAGAAG -3′ Reverse: 5′- GTGTATATCCCAGGGTGATCC-3′
TAp63	Forward: 5′-GTCATTTGATTCGAGTAGAGGGG-3′ Reverse: 5′-CTGGGGTGGCTCATAAGGT-3′

The Primer3 website (http://frodo.wi.mit.edu/) was used to design the primers. The optimal annealing and extension temperature of the DNA Polymerase contained in the SYBR® Green PCR Master Mix (Roche) is 60°C, hence primers had to be chosen that were compatible with reagents to be used. Specificity of the primer pairs for relevant genes was verified by performing nucleotide alignment searches using BLAST.

Table S1 (related to Figure 4)

Enrichment by Pathway Maps

#	Maps	Total	pValue	Min FDR	p-value	FDR	In Data
1	Cytoskeleton remodeling_Keratin filaments	36	5.883E-05	0.0085892	5.883E-05	8.589E-03	4
2	Cell adhesion_ECM remodeling	52	2.519E-04	0.01839008	2.519E-04	1.839E-02	4
3	Immune response_Antiviral actions of Interferons	52	3.659E-03	0.16473062	3.659E-03	1.647E-01	3
4	Development_Keratinocyte differentiation	56	4.513E-03	0.16473062	4.513E-03	1.647E-01	3
5	Immune response_IFN alpha/beta signaling pathway	24	8.958E-03	0.24703051	8.958E-03	2.470E-01	2
6	Chemotaxis_Leukocyte chemotaxis	75	1.015E-02	0.24703051	1.015E-02	2.470E-01	3
7	Development_G-CSF-induced myeloid differentiation	30	1.380E-02	0.28519618	1.380E-02	2.852E-01	2
8	GTP-XTP metabolism	90	1.659E-02	0.28519618	1.659E-02	2.852E-01	3
9	Androstenedione and testosterone biosynthesis and metabolism p.2	35	1.852E-02	0.28519618	1.852E-02	2.852E-01	2
10	Androstenedione and testosterone biosynthesis and metabolism p.2/ Rodent	36	1.953E-02	0.28519618	1.953E-02	2.852E-01	2

Classification of 122 transcripts with 2-fold relative expression difference from NHK in all hESC/iPSC-derived keratinocytes at T3 using GeneGo database (Thomson Reuters) for Pathway Maps ranked using an enrichment score (p-value). Groups that have a relevance to keratinocyte biology are highlighted in yellow.

Table S2 (related to Figure 4)

Enrichment by Process Networks

#	Networks	Total	pValue	Min FDR	p-value	FDR	In Data
1	Inflammation_Interferon signaling	110	9.587E-09	9.2032E-07	9.587E-09	9.203E-07	11
2	Proteolysis_Connective tissue degradation	119	2.570E-06	0.00012337	2.570E-06	1.234E-04	9
3	Proteolysis_ECM remodeling	85	2.074E-05	0.00066363	2.074E-05	6.636E-04	7
4	Cell adhesion_Cell-matrix interactions	211	1.196E-03	0.02453835	1.196E-03	2.454E-02	8
5	Cytoskeleton_Intermediate filaments	81	1.278E-03	0.02453835	1.278E-03	2.454E-02	5
6	Inflammation_Kallikrein-kinin system	185	2.482E-03	0.03970433	2.482E-03	3.970E-02	7
7	Development_Ossification and bone remodeling	157	4.843E-03	0.06641205	4.843E-03	6.641E-02	6
8	Immune response_Innate immune response to RNA viral infection	84	9.981E-03	0.10981602	9.981E-03	1.098E-01	4
9	Proliferation_Negative regulation of cell proliferation	184	1.030E-02	0.10981602	1.030E-02	1.098E-01	6
10	Immune response_Th17-derived cytokines	98	1.683E-02	0.16152697	1.683E-02	1.615E-01	4

Classification of 122 transcripts with 2-fold relative expression difference from NHK in all hESC/iPSC-derived keratinocytes at T3 using GeneGo database (Thomson Reuters) for Process Networks ranked using an enrichment score (p-value). Groups that have a relevance to keratinocyte biology are highlighted in yellow.

Table S3 (related to Figure 4)

Enrichment by GO Processes

#	Processes	Total	pValue	Min FDR	p-value	FDR	In Data
1	cellular response to type I interferon	87	4.241E-18	5.8044E-15	4.241E-18	5.804E-15	15
2	response to type I interferon	88	5.087E-18	5.8044E-15	5.087E-18	5.804E-15	15
3	type I interferon-mediated signaling pathway	86	1.347E-16	1.0245E-13	1.347E-16	1.024E-13	14
4	response to organic substance	3073	4.805E-16	2.7413E-13	4.805E-16	2.741E-13	57
5	response to cytokine stimulus	809	8.840E-16	4.0345E-13	8.840E-16	4.034E-13	30
6	response to virus	316	4.876E-15	1.8544E-12	4.876E-15	1.854E-12	20
7	defense response	1465	7.409E-15	2.2929E-12	7.409E-15	2.293E-12	38
8	response to chemical stimulus	4787	8.038E-15	2.2929E-12	8.038E-15	2.293E-12	70
9	response to metal ion	426	1.267E-14	3.2119E-12	1.267E-14	3.212E-12	22
10	epidermis development	631	6.978E-14	1.4477E-11	6.978E-14	1.448E-11	25

Classification of 122 transcripts with 2-fold relative expression difference from NHK in all hESC/iPSC-derived keratinocytes at T3 using GeneGo database (Thomson Reuters) for Gene Ontology Processes ranked using an enrichment score (p-value). Groups that have a relevance to keratinocyte biology are highlighted in yellow.

Table S4 (related to Figure 4)

Enrichment by Diseases (by Biomarkers)

#	Diseases	Total	pValue	Min FDR	p-value	FDR	In Data
1	Stomach Neoplasms	5686	4.728E-15	3.4835E-12	4.728E-15	3.483E-12	81
2	Stomach Diseases	5714	6.357E-15	3.4835E-12	6.357E-15	3.483E-12	81
3	Carcinoma, Bronchogenic	3044	4.532E-14	1.2954E-11	4.532E-14	1.295E-11	56
4	Bronchial Neoplasms	3047	4.728E-14	1.2954E-11	4.728E-14	1.295E-11	56
5	Carcinoma, Non-Small-Cell Lung	2887	8.271E-14	1.655E-11	8.271E-14	1.655E-11	54
6	Salivary Gland Diseases	708	9.060E-14	1.655E-11	9.060E-14	1.655E-11	27
7	Neoplasms, Ductal, Lobular, and Medullary	1683	2.604E-13	4.0775E-11	2.604E-13	4.077E-11	40
8	Connective Tissue Diseases	1946	3.041E-13	4.1661E-11	3.041E-13	4.166E-11	43
9	Mesothelioma	241	3.431E-13	4.1783E-11	3.431E-13	4.178E-11	17
10	Neoplasms, Mesothelial	243	3.925E-13	4.3018E-11	3.925E-13	4.302E-11	17

Classification of 122 transcripts with 2-fold relative expression difference from NHK in all hESC/iPSC-derived keratinocytes at T3 using GeneGo database (Thomson Reuters) for Disease Biomarkers list, ranked using an enrichment score (p-value). None of them had a relevance to keratinocyte biology.

Table S5 (related to Figure 4)

GO processes	Pathway		Networks	
Epidermis development	Cytoskeleton remodeling Keratin filaments	Cell Adhesion ECM remodeling	Cell adhesion Cell-matrix interaction	Cytoskleton Intermediate filaments
AKR1C3	*KRT1*	*KLK1*	*90K*	*ACTIN*
COL5A1	*KRT7*	*KLK3*	*COL5A1*	*KRT1*
COL5A2	*PPL*	*SPARC*	*COL5A2*	*KRT7*
CDSN	*VIM*	*VCAN*	*LGALS1*	*PPL*
COX2			*LAMB1*	*VIM*
FLG			*LAMC2*	
FLG2			*VCAN*	
IBP				
KLK5				
KLK7				
KRT1				
KRT31				
LAMC2				
PPL				
PTHrP				
SPRR1B				
SPRR2D				
SPRR2E				
SPRR2F				
SPRR3				
TXNIP				
Tissue kallikreins				

Genes relevant to keratinocyte biology in a group of the 122 transcripts.

Table S6 (related to Figure 4).

Genes that were 2-folds or greater expressed higher in NHK than in hESC/iPSC-derived keratinocytes at T3 (n=3 independent differentiation rounds for each of the line).

Table S7 (related to Figure 4)

Genes that were 2-folds or greater expressed in hESC/iPSC-derived keratinocytes at T3 than in NHK (n=3 independent differentiation rounds for each of the lines).

Supplementary references:

Aberdam, E., Barak, E., Rouleau, M., de LaForest, S., Berrih-Aknin, S., Suter, D.M., Krause, K.H., Amit, M., Itskovitz-Eldor, J., and Aberdam, D. (2008). A pure population of ectodermal cells derived from human embryonic stem cells. Stem Cells. *26*, 440-444.

Bilousova, G., Chen, J., and Roop, D.R. (2011). Differentiation of mouse induced pluripotent stem cells into a multipotent keratinocyte lineage. J. Invest. Dermatol. *131*, 857-864.

Guenou, H., Nissan, X., Larcher, F., Feteira, J., Lemaitre, G., Saidani, M., Del Rio, M., Barrault, C.C., Bernard, F.X., Peschanski, M., et al. (2009). Human embryonic stem-cell derivatives for full reconstruction of the pluristratified epidermis: a preclinical study. Lancet. *374*,1745-1753.

Hewitt, K.J., Shamis, Y., Carlson, M.W., Aberdam, E., Aberdam, D., and Garlick, J.A. (2009). Three-dimensional epithelial tissues generated from human embryonic stem cells. Tissue Eng Part A. *15*, 3417-3426.

Itoh, M., Kiuru, M., Cairo, M.S., and Christiano, A.M. (2011). Generation of keratinocytes from normal and recessive dystrophic epidermolysis bullosa-induced pluripotent stem cells. Proc. Natl. Acad. Sci. USA. *108*, 8797-8802.

Iuchi, S., Dabelsteen, S., Easley, K., Rheinwald, J.G., and Green, H. (2006). Immortalized keratinocyte lines derived from human embryonic stem cells. Proc. Natl. Acad. Sci. USA. *103*, 1792-1797.

Ji, L., Allen-Hoffmann, B.L., de Pablo, J.J., Palecek, S.P. (2006). Generation and differentiation of human embryonic stem cell-derived keratinocyte precursors. Tissue Eng. *12*, 665-679.

Metallo, C.M., Azarin, S.M., Moses, L.E, Ji, L., de Pablo, J.J. and Palecek, S.P. (2010). Human embryonic stem cell-derived keratinocytes exhibit an epidermal transcription program and undergo epithelial morphogenesis in engineered tissue constructs. Tissue Eng. Part A *16*, 213-23.

Selekman, J.A., Grundl, N.J., Kolz, J.M., and Palecek, S.P. (2013). Efficient Generation of Functional Epithelial and Epidermal Cells from Human Pluripotent Stem Cells Under Defined Conditions. Tissue Eng. Part C Methods. [Epub ahead of print]

van de Kamp, J., Kramann, R., Anraths, J., Schöler, H.R., Ko, K., Knüchel, R., Zenke, M., Neuss, S., and Schneider, R.K. (2012). Epithelial morphogenesis of germline-derived pluripotent stem cells on organotypic skin equivalents in vitro. Differentiation. *83*, 138-147.

Yoshida, S., Yasuda, M., Miyashita, H., Ogawa, Y., Yoshida, T., Matsuzaki, Y., Tsubota, K., Okano, H., Shimmura, S. (2011). Generation of stratified squamous epithelial progenitor cells from mouse induced pluripotent stem cells. PLoS One. *6*, e28856.

STEM CELLS AND DEVELOPMENT
Volume 25, Number 18, 2016

DOI: 10.1089/scd.2016.0156

Induced Pluripotent Stem Cell Differentiation and Three-Dimensional Tissue Formation Attenuate Clonal Epigenetic Differences in Trichohyalin

Anastasia Petrova,[1–3,*] Antonio Capalbo,[4,*] Laureen Jacquet,[1,*] Simon Hazelwood-Smith,[5] Dimitra Dafou,[5,†] Carl Hobbs,[6] Matthew Arno,[7] Alessio Farcomeni,[8] Liani Devito,[1] Heba Badraiq,[1] Michael Simpson,[5] John A McGrath,[2] Wei-Li Di,[3] Jeffrey B Cheng,[9] Theodora M Mauro,[9] and Dusko Ilic[1]

The epigenetic background of pluripotent stem cells can influence transcriptional and functional behavior. Most of these data have been obtained in standard monolayer cell culture systems. In this study, we used exome sequencing, array comparative genomic hybridization (CGH), miRNA array, DNA methylation array, three-dimensional (3D) tissue engineering, and immunostaining to conduct a comparative analysis of two induced pluripotent stem cell (iPSC) lines used in engineering of 3D human epidermal equivalent (HEE), which more closely approximates epidermis. Exome sequencing and array CGH suggested that their genome was stable following 3 months of feeder-free culture. While the miRNAome was also not affected, $\approx 7\%$ of CpG sites were differently methylated between the two lines. Analysis of the epidermal differentiation complex, a region on chromosome 1 that contains multiple genes involved in skin barrier maturation (including trichohyalin, *TCHH*), found that in one of the iPSC clones (iKCL004), TCHH retained a DNA methylation signature characteristic of the original somatic cells, whereas in other iPSC line (iKCL011), the *TCHH* methylation signature matched that of the human embryonic stem cell line KCL034. The difference between the two iPSC clones in *TCHH* methylation did not have an obvious effect on its expression in 3D HEE, suggesting that differentiation and tissue formation may mitigate variations in the iPSC methylome.

Introduction

Reprogramming somatic cells back to a pluripotent state, similar to embryonic stem cells (ESCs), initially required insertion of reprogramming transgenes and their viral vectors into the host genome [1]. Previous studies demonstrated that the effect of reprogramming on terminally differentiated somatic cells was strikingly similar to that seen in neoplastic transformation. Profound epigenetic changes led to pluripotent plasticity and indefinite self-renewal of cells that were previously committed to differentiation and had a limited proliferation capacity. Although reprogramming-associated point mutations might arise during the initial stages of conversion [2], it instead appears that these point mutations are predominantly a consequence of cloning individual cells with different mutation histories [3]. In addition, induced pluripotent stem cell (iPSC) clones might carry not only epigenetic memory of their parental somatic cell origin [4] but also have a unique pattern of DNA methylation as a result of nonuniform epigenome transformation during reprogramming [5–7]. Specific genetic and epigenetic footprints influence the molecular and functional properties of each iPSC clone. Altered gene expression and distinct differentiation propensity among early passage iPSC clones are likely to be largely attenuated through continuous passaging [7]. In contrast, human pluripotent stem cells, both human ESC (hESC) and especially iPSC, kept for

[1]Assisted Conception Unit, Stem Cell Laboratory, Division of Women's Health, Women's Health Academic Centre, King's College London, London, United Kingdom.
[2]St John's Institute of Dermatology, King's College London, London, United Kingdom.
[3]Immunobiology Unit, Institute of Child Health, University College London, London, United Kingdom.
[4]GENERA, Centers for Reproductive Medicine, Rome, Italy.
[5]Division of Genetics and Molecular Medicine, King's College London, London, United Kingdom.
[6]Histology Laboratory, Wolfson Centre for Age-Related Diseases, King's College London, London, United Kingdom.
[7]Genomics Centre, King's College London, London, United Kingdom.
[8]Statistics Section, Department of Public Health and Infectious Diseases, Sapienza–University of Rome, Rome, Italy.
[9]Department of Dermatology, Veteran Affairs Medical Center, University of California San Francisco, San Francisco, California.
*These three authors contributed equally to this work.
[†]Current affiliation: Department of Genetics, Developmental and Molecular Biology, School of Biology, Aristotle University, Thessaloniki, Greece.

extended period of time in culture are prone to genomic instability [8,9]. It is unknown to what extent the cellular genetic and epigenetic makeup or culture conditions contribute to genomic instability over time.

We reprogrammed human foreskin BJ fibroblasts (HFFs) into iPSC using modified synthetic mRNA. Two iPSC clones, iKCL004 and iKCL011, that we used to build human skin equivalents [human epidermal equivalent (HEE)] with a functional permeability barrier [10] showed subtle differences, which prompted us to investigate in depth the genetic and epigenetic footprint of both lines. Since the focus of our work was keratinocyte differentiation culminating in the stratum corneum derived epidermal permeability barrier, we concentrated on the epidermal differentiation complex (EDC) on chromosome 1, which contains multiple genes involved in epidermal cornification [11–19]. One of our clinical grade lines, KCL034, was used as a control in most analyses [20].

Materials and Methods

Reprogramming

Human neonatal foreskin fibroblasts BJ (ATCC, CRL-2522) were reprogrammed using modified synthetic mRNA as described [10]. At day 2–17 of reprogramming, some cells also were treated with 1 μM pifithrin-α. Two clones with a similar growth rate, one derived in the absence (iKCL004) and one in the presence of 1 μM pifithrin-α (iKCL011), were further characterized; pluripotency marker expression and differentiation into three germ layers in vitro and in vivo (teratomas) revealed no obvious difference between the lines [10].

Cell culture

Undifferentiated hESC line KCL034 and iPSC lines, iKCL004 and iKCL011, were cultured under standard feeder-free conditions on Matrigel (Becton Dickinson) in mTeSR1 medium (STEMCELL Technologies) under hypoxic (5% O_2) conditions. Differentiation into keratinocytes and generation of HEEs were described previously [10]. Transepithelial electrical resistance was measured with epithelial voltohmmeter EVOM (World Precision Instruments) as described [10,21]. Normal human keratinocytes (NHK) were cultured in EpiLife (Life Technologies). Human neonatal foreskin fibroblasts BJ were cultured in Dulbecco's modified Eagle's medium supplemented with 10% fetal bovine serum (Hyclone).

Quantitative reverse transcriptase–polymerase chain reaction

Total RNA was extracted using the RNeasy Mini Kit (QIAGEN) following the manufacturer's instructions. A 20-min DNase I (Qiagen) treatment step was included to eliminate the potential contamination of genomic DNA. cDNA was generated by reverse transcription of total RNA (350 ng) using the RT2 First Strand Kit (Qiagen) following the manufacturer's instruction. The quantitative reverse transcriptase–polymerase chain reaction (qPCR) consisted of 3 μL of cDNA diluted 1:10 in water, 6.25 μL of RT2 Real Time SYBR® Green qPCR Master Mix (Qiagen), and 400 nM of each primer for a final volume of 12.5 μL. qPCR cycling conditions were as follows: one cycle 95°C for 10 min; 40 cycles 95°C for 15 s, 61°C for 30 s followed by melt curve acquisition from 59°C to 95°C with 0.5°C increment. The *BAX* (Fw: CGGGTTGTCGCCCTTTTC TA; Rv: CGGGGATTGATCAGACACGTA) and *p21* (Fw: GC ACTTTGATTAGCAGCGGA; Rv: AAGACAACTACTCCC AGCCC) primers were designed using Primer3 software. The GAPDH and ACTB primers were from PrimerDesign Ltd. All samples were analyzed in triplicate, Ct values were determined, and the expression was calculated by the $2^{-\Delta\Delta Ct}$ method. GAPDH and ACTB were used for internal normalization.

Array comparative genomic hybridization

Array comparative genomic hybridization (CGH) was performed following strict protocols for each of the different steps as provided by the manufacturers of the reagents. CGH Labeling Kit (Enzo Life Sciences) was used to label 1 μg DNA. Post labeling, DNA was purified with QIAquick PCR Purification Kit (Qiagen). Labeling efficiency and yield were assessed by spectrophotometry (NanoDrop). For hybridization, washing, and scanning of arrays, we used an Agilent 4×44K platform. Image quantification, array quality control (QC), and aberration detection were performed using feature extraction and DNA Analytics software packages (Agilent); 95% of array data were required to pass QC. The ADM-2 algorithm at threshold 6 (with a three-probe sliding window providing a mean detection interval of 200 kb) was used for aberration calling.

Exome sequencing

Exome sequencing was undertaken using genomic DNA extracted from BJ parental fibroblasts before and after reprogramming (two clones: iKCL004 and iKCL011). Libraries were prepared using the SureSelect Human All Exon Capture v4 (Agilent) and sequenced with 100-bp paired end reads on the HiSeq platform (Illumina).

The resulting sequence reads were aligned to the reference genome (hg19) with NovoAlign (Novocraft Technologies). Duplicate reads, resulting from PCR clonality or optical duplicates, and reads mapped to multiple locations were excluded from downstream analysis. Single-nucleotide substitutions and small insertions or deletions were identified and quality filtered within the SAMtools software package and in-house software tools. Variants were annotated with respect to genes and transcripts with the ANNOVAR tool.

To identify differentially arising new mutations, we undertook a series of pairwise comparisons with the VarScan 2 tool. Comparison was limited to protein coding regions and associated splice sites of genes defined by the GENCODE project and sites at which >20 reads were observed in all three samples (~90% of the targeted exome).

The resulting differentially called variants were filtered with the following criteria to retain high quality changes; presence of the new allele in >20% of reads in the sample in which the variant was identified, absence of any reads representing the alternative allele in the other two samples. Variants located within repeat elements or segmentally duplicated regions were excluded as likely alignment artifacts. The sequence alignments spanning each candidate variant were checked manually using the Integrative Genomics Viewer 2.3.

miRNA expression analysis

miRNA expression was evaluated in biological triplicates of undifferentiated hESC and iPSC using TaqMan Array

MicroRNA Cards (Panel A and Panel B; Applied Biosystems). The cards contain primer sets for 736 human miRNA sequences (667 unique miRNAs), two sequences from Arabidopsis, eight measurements of MammU6, and 22 RNU sequences.

The cell samples were collected in 200 μL of total volume of lysis buffer. MicroRNA isolation and purification were conducted through the TaqMan miRNA ABC (Anti-miRNA Bead Capture) Purification Kit (Applied Biosystems). This system is designed for rapid and specific purification of human miRNAs. The Human Panel A or Panel B v3.0 Beads are superparamagnetic Dynabeads® covalently bound to a unique set of 377 anti-miRNA oligonucleotides for each panel. The miRNA isolation relies on hybridization of endogenous miRNAs to the corresponding anti-miRNA oligonucleotides attached to the beads. The purification protocol was followed according to the manufacturers' instructions. The bead hybridization and the miRNA elution steps were conducted on the Thermomixer® R (Eppendorf). All the washing steps were performed through the DynaMag™-2 magnet (Applied Biosystems), to clear up the solution from DNA, proteins, contaminants, and residual binding solution, while keeping the miRNAs bound to the beads. MicroRNAs were eluted in 20 μL of final volume, to concentrate them in the smallest possible volume. The cDNA was then generated using the specific Megaplex RT Primer pools A and B v3.0 (Applied Biosystems), which include 377 primer sets for each specific miRNA isolated in the previous step, according to the manufacturer protocol. Preamplification was performed according to manufacturer instructions and protocol using the specific Megaplex PreAmp Primer pools A and B v3.0 (Applied Biosystems). Briefly, 25 μL of preamplification products were added to 425 μL nuclease-free water and mixed with 450 μL TaqMan Universal Master Mix II, No UNG, then dispensed into the 384 wells by centrifugation on a Heraeus Megafuge 40 (Thermo Scientific) with the proper TaqMan Low Density Arrays card adapters. The reactions were incubated in a 384-well plate at 95°C for 10 min followed by 40 cycles of 95°C for 15 s and at 60°C for 1 min on a ViiA™ 7 Real-Time PCR System (Applied Biosystems).

Raw data were analyzed using SDS software (Applied Biosystems), and Ct values were used as a readout. Manual inspection of all amplification plots was performed and miRNAs were excluded from the analysis if: Ct values were too high (above 35, indicating a miRNA expression too low for accurate detection) or if amplification was not achieved in at least two samples (biological replicates). Data were processed through the RealTime StatMiner 5.0 software (Integromics).

Presence/absence indicators were compared among groups through a logistic mixed model, with a slide specific intercept to capture any overdispersion. The *P*-values arising from Wald tests on the group indicator coefficients were then adjusted using Benjamini–Hochberg (BH) correction. The global false discovery rate (FDR) was guaranteed below the rate of 5%. We then proceeded to compare expression levels after Loess normalization as this normalization approach has been shown to effectively reduce standard deviations, increase sensitivity and improve accuracy of differential miRNA expression detection, and increase interplatform concordance [22]. Once again we controlled for multiplicity using BH correction. Effect sizes of miRNAs relative concentration were measured by means of fold changes. Pearson's correlation was used to generate a heatmap for intragroup correlation plot among all biological samples.

Hierarchical clustering analysis exploiting complete linkage clustering method and Euclidean distance similarity measure was performed on fold changes using KCL034 cell lines as a calibrator to compare similarity of miRNA expression profile between iPSC and hESC lines. A Volcano plot was generated using significance versus fold change on the *y*- and *x*-axes, respectively.

Whole epigenome methylation array

Epigenome-wide methylation (>480,000 CpG sites) was analyzed using Infinium Human Methylation 450 BeadChip Kit (Illumina) in biological triplicates of 500 ng bisulfite treated DNA for each: BJ parental fibroblasts (negative control), KCL034 (positive control), iKCL004, and iKCL011 line. GenoSplice Technology performed QC of the data, their processing, and further analyses. Microarray data have been deposited in the NCBI Gene Expression Omnibus (GEO) with the accession number GSE55006.

Whole genome gene-expression array

Total RNA from undifferentiated hESC and iPSC, as well as control primary (NHK) and hESC/iPSC-differentiated keratinocytes (NHK), was reverse transcribed into cDNA using SuperScript III Reverse Transcriptase (Life Technologies). A total amount of 750 ng of biotin-labeled aRNA in a 5 μL volume was then used for HumanHT-12 Expression BeadChip whole-genome gene expression direct hybridization assay system (Illumina) according to manufacturer's instructions, run on iScan system (Illumina) and analyzed as described [10]. All samples were analyzed as biological replicates from three independent experiments. Microarray data have been deposited in the NCBI GEO with the accession number GSE55898.

Immunostaining

Immunostaining has been performed as previously described [23,24]. The following antibodies were used: rabbit anti-KRT14 (Covance), -Oct4 (Santa Cruz Biotechnology), -Sox2 (GeneTex), -LCE2B (Bioss), -p63 (Abcam), mouse anti-cMyc (Santa Cruz Biotechnology), -Klf4 (ATGen), -TCHH (ImmuQuest), and goat anti-LIN28 (R&D Systems). Secondary antibodies were purchased from Jackson ImmunoResearch. Actin stress fibers were visualized with rhodamine-conjugated phalloidin and DNA with a nuclear stain Hoechst 33342, both from Life Technologies.

Results

Reprogramming had no effect on mutation rate and genomic stability of iKCL004 and iKCL011 lines

We first reprogrammed HFFs using synthetic modified mRNA and following a modified version of the protocol originally described by Warren et al. [25]. mRNA transfection efficiency was on average >75% (Fig. 1A, B). We increased the B18R concentration from 200 to 300 ng/mL to further suppress the innate immune response triggered with the exogenous mRNA cocktail. We also added B18R to the medium 4 h prior the first transfection to precondition the cells. Regardless, a regime of daily transfection had a deleterious effect on the cells; the vast majority did not survive (Fig. 1C). At day 4 of reprogramming, we assessed the

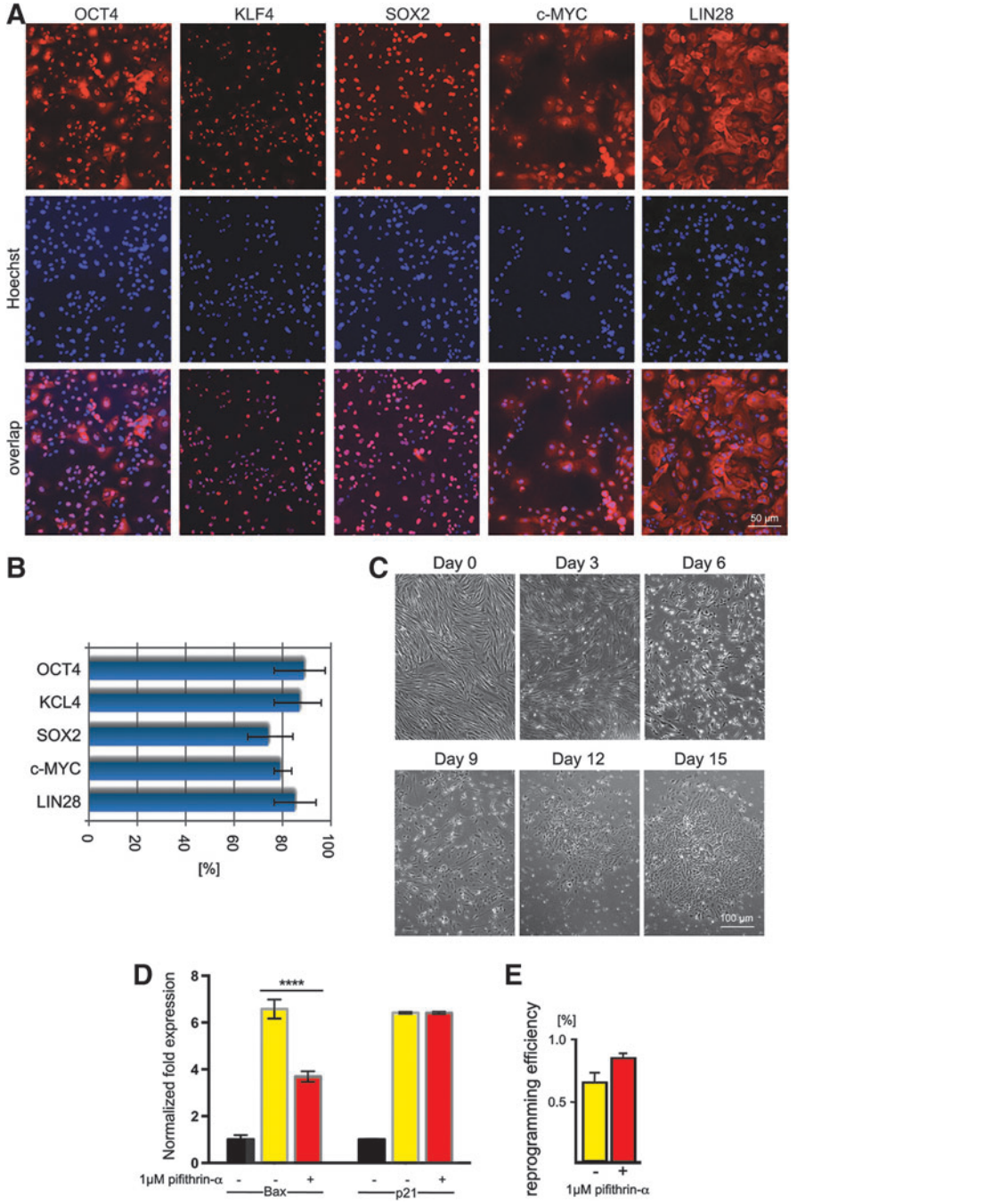

FIG. 1. Reprogramming HFFs using synthetic modified mRNA. **(A)** Synthetic modified mRNAs are translated into proteins. Cells transfected with mRNA cocktail expressing reprogramming factors Klf4, cMyc, Oct4, LIN28, and Sox2. The 15-h time point was chosen for analysis as it corresponds to the average peak expression time post-transfection of the different reprogramming factors [25]. **(B)** More than 75% cells express reprogramming factors 15 h after mRNA transfection. The cells were fixed and immunostained for Oct4, Klf4, Sox2, c-Myc, and LIN28 15 h post-transfection with mRNA reprogramming cocktail. Nuclei were visualized with Hoechst 33342. Total cell number was calculated. Data are presented as the mean of cells positive for Oct4, Klf4, Sox2, c-Myc, and LIN28 ± standard error of the mean ($n = 3$). **(C)** Daily transfection had a deleterious effect on the cells; vast majority did not survive. Day 0: the cells before the first transfection demonstrate normal morphology and density. Day 3: decreased cell density and cell rounding indicate a high apoptotic rate. Day 6: massive apoptosis is seen. Surviving cells start undergoing mesenchymal epithelial transformation and adopt an epithelial morphology. Day 9: surviving cells continue to transition to an epithelial morphology. Day 12: first signs of compaction and colony formation are noted. Day 15: increased compaction. Cells become smaller and more hESC like. **(D)** Inhibitory effect of pifithrin-α on p53-mediated transcription. qPCR expression analyses of the two p53 target genes, *BAX*, and *p21* at Day 4 of reprogramming showed decrease in *BAX*, but not *p21* mRNA levels ($n = 3$ biological replicates). Transfected samples are compared with the negative control (untransfected BJ cells). Data are given by normalized mean ± standard error of the mean ($n = 3$); statistical significance was calculated by two-way analysis of variance with Tukey post hoc test. $^{****}P < 0.0001$. **(E)** An average reprogramming efficiency from two independent experiments was calculated as number of trypan blue positive colonies per total number of cells plated per well of six-well dish. HFF, human foreskin fibroblast; hESC, human embryonic stem cell; qPCR, quantitative reverse transcriptase–polymerase chain reaction.

inhibitory effect of pifithrin-α on p53-mediated transcription using qPCR. Transcription of two p53 target genes BAX and CDKN1A (known as p21) was elevated > sixfold in cells subjected to daily mRNA transfections, suggesting that p53 activation is induced by reprogramming itself. Pifithrin-α treated cells had reduced levels of BAX, but no effect on p21 transcription was observed (Fig. 1D). Daily mRNA transfections caused massive cell death in both conditions, although cell survival seemed to be somewhat higher in the presence of pifithrin-α. Although reprogramming efficiency was about 30% higher in the presence of 1 μM pifithrin-α (0.86% vs. 0.66%), in our hands, it was still lower than the reprogramming efficiency reported by Warren et al. [25] regardless of the p53 inhibition (Fig. 1E).

Harsh conditions in cell culture might result in survival of clones that carry growth-promoting mutation(s) associated with tumorigenesis. To assess the genomic integrity of our lines, we subjected iKCL004 and iKCL011 to array CGH at two different time points, one at early passages (<10) and the other about 3 months after the lines were adapted to the feeder-free culture. Even though it is widely known that extended periods of cell culture under feeder-free conditions are linked to higher rates of chromosomal abnormalities in pluripotent stem cells, especially iPSC [8,9], we did not

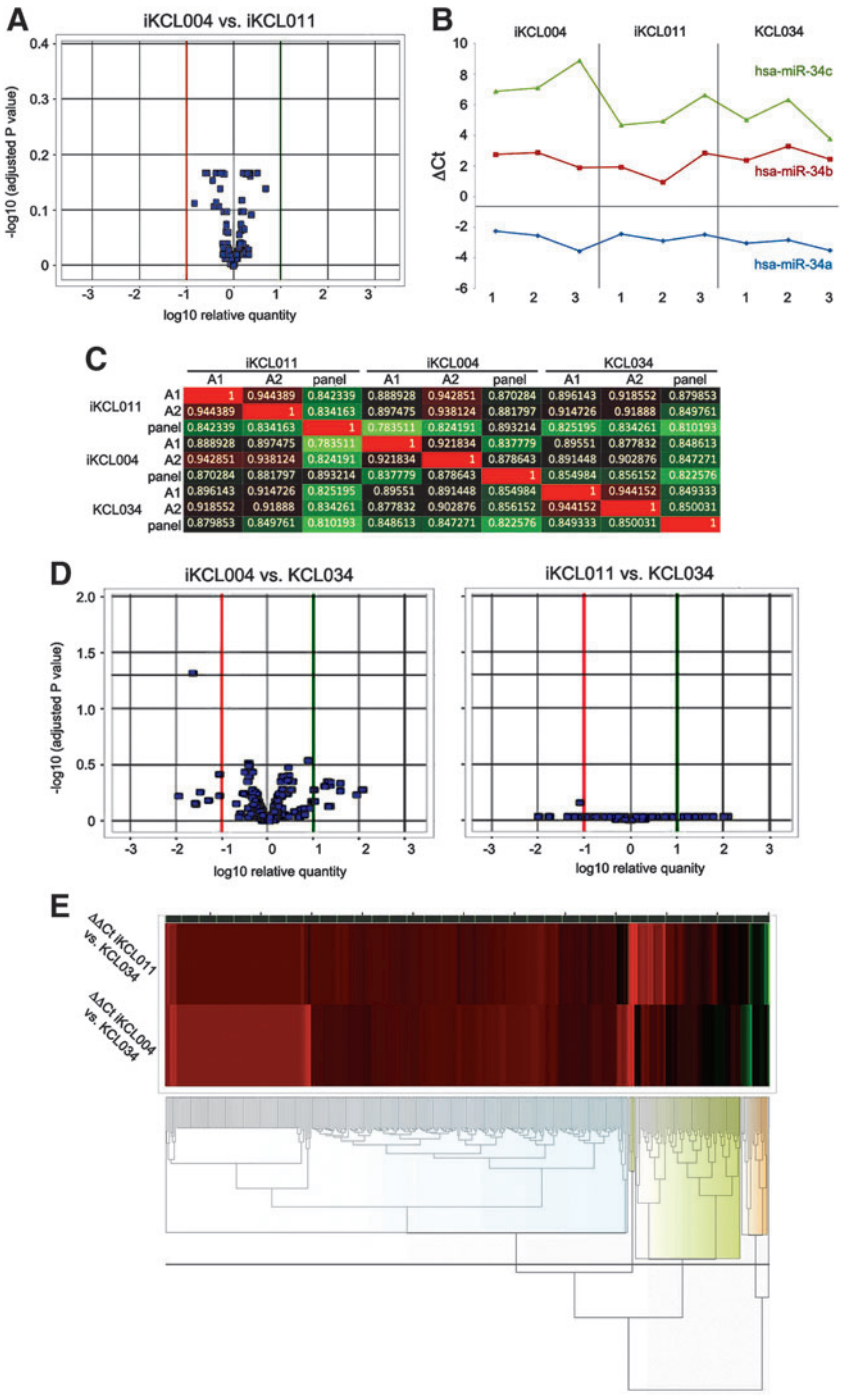

FIG. 2. hESC/iPSC miRNA profiling. **(A)** Volcano plot showing no significant miRNA differentially expressed between two iPSC lines ($n = 3$ biological replicates per group). Significance versus fold change on the *y*- and *x*-axes, respectively, is plotted. *Horizontal black lines* represent the statistical significance threshold. *Green* and *red lines* represent the upper and lower fold changes thresholds, respectively. (**B**) Correlation heatmap among the profiles of miRNA expression of all the samples analyzed (three biological replicates per each of two iPSC and one hESC line). Superior to the heatmap and on the *left* of it three biological replicates and their relative grouping are reported. The color intensity varies in function of the Pearson correlation index ranging from *green* to *red* for a lower or a higher correlation, respectively. The proper numerical value of correlation between each couple of sample is reported within the squares at the intersections. (**C**) Volcano plot showing no significant miRNA differentially expressed between two iPSC lines, iKCL004 and iKCL011, and a control hESC line KCL034. (**D**) Hierarchical clustering of fold-change values obtained from the comparison of the two iPSC lines against hESC line used as a calibrator. The analysis was performed exploiting complete linkage, Euclidean distance, and *z*-score normalization, and the heatmaps, beside reporting four clusters of genes showing a similar behavior (highlighted by the four groups of dendograms with the same colored halo below the heatmaps), do not reveal significant differences among the samples analyzed. **(E)** Hierarchical clustering of fold-change values obtained from the comparison of the two iPSC lines against hESC line used as a calibrator. The analysis was performed exploiting complete linkage, Euclidean distance, and *z*-score normalization and the heatmaps, beside reporting four clusters of genes showing a similar behavior (highlighted by the four groups of dendograms with the same colored halo below the heatmaps), do not reveal significant differences among the samples analyzed. iPSC, induced pluripotent stem cell.

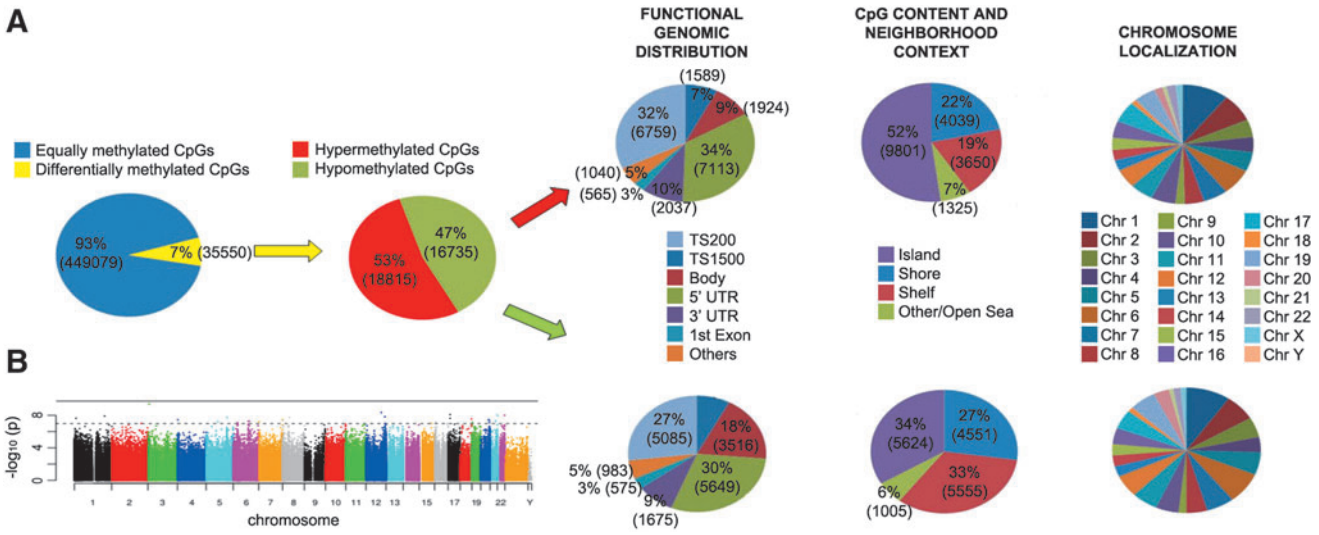

FIG. 3. Whole epigenome methylation profile. **(A)** Comparative analysis of iKCL004 and iKCL011 methylome found that 35,550 (7%) of CpGs are differently methylated between the two lines. Nearly a half of them were hypermethylated (18,815 or 53%) and the other half was hypomethylated (16,737 or 47%). Nearly twice more hypomethylated sites (3,516 or 18%) were found in body than hypermethylated sites (1,924 or 9%). Both hyper- and hypomethylated CpG sites were predominantly distributed in islands, shores, and shelves, across all chromosomes. **(B)** Manhattan plot, color-coded by chromosomes.

detect any copy number changes using array CGH in either iKCL004 or iKCL011 over 3 months of culture on Matrigel in mTeSR1 medium [10], suggesting that the genome of both lines is relatively stable. Next, we subjected iKCL004, iKCL011, and parental BJ fibroblast to exome sequencing. The comparative analysis did not identify any alleles that had arisen during the reprogramming, which suggested that the rate of mutation was not substantially affected during reprogramming of BJ fibroblasts.

miRNAome is similar in both iPSC lines

Recently, it has been demonstrated that miRNAs can contribute to iPSC somatic donor memory [26]. Therefore, we evaluated miRNA expression in biological triplicates of iKCL004 and iKCL011 using TaqMan Array MicroRNA Cards containing primer sets for 736 human miRNA sequences. This miRNA profiling technology is a medium throughput approach that holds the advantage of high

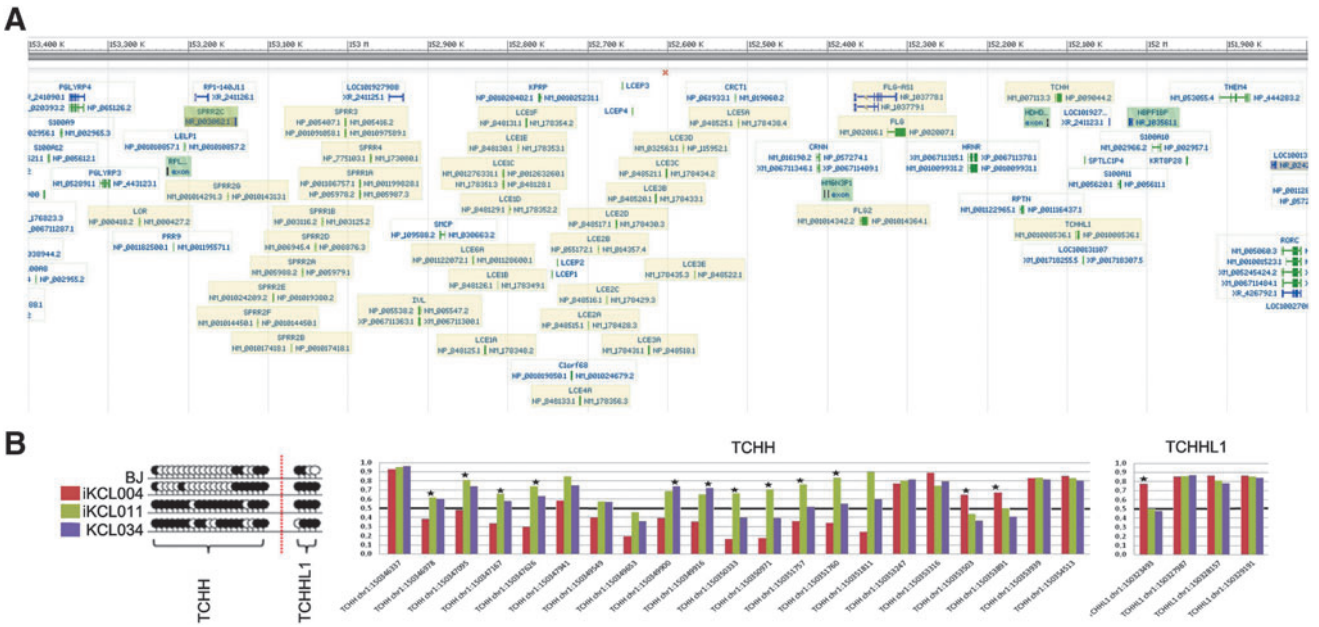

FIG. 4. DNA methylation of EDC genes. **(A)** EDC on chromosome 1. *Pale yellow* background indicates genes involved in keratinocyte terminal differentiation which with methylation we analyzed individually. **(B)** DNA methylation of TCHH family shown as lollipop diagram and bar charts. In the lollipop diagram, *black circles* represent CpG sites that have Beta value ≥0.5 and *white circles* represent CpG sites with Beta value <0.5. The difference of 0.4 (40%) is considered significant (*star*) in a bar chart diagram. EDC, epidermal differentiation complex; TCHH, trichohyalin.

accuracy thanks to the use of single assay TaqMan chemistry [27]. After filtering, as described in ''Materials and Methods'' section, and Loess-based normalization, we compared 383 miRNA expressed in iKCL004 and iKCL011. We found that the average fold change was 0.9998, with a confidence interval 0.995–1.004, $P=0.702$. Kendall's Tau rank correlation coefficient was 0.860, $P<0.0001$ (if the two rankings are the same, the value is 1 and if they are completely independent, the value is 0). No miRNA was flagged as differentially expressed after multiplicity correction with Benjamini–Hochberg FDR method at the 5% level (Fig. 2A).

Considering that even minimal cellular variation of miRNA concentration can be biologically significant, we next repeated every single miRNA analysis at the 10% and 20% levels, which are less stringent. Even with these larger values for the Type I error, no miRNA was selected as statistically significant in any analysis.

We then analyzed the relative expression miRNA profiles of iKCL004 and iKCL011 against the hESC line KCL034 to see if one of the two iPSC lines was more similar to hESC. Pearson's correlation showed high similarity between all cell samples analyzed (>0.78; Fig. 2B). No significance was found between miRNA signature of KCL034 compared with iKCL011 and iKCL004 (Fig. 2C, E).

iKCL004 and iKCL011 have a different methylation signature

During reprogramming, to acquire pluripotency potential, the DNA of somatic cells undergoes a global epigenetic transformation. Variability of methylation in iPSC lines very often influences the molecular and functional properties of iPSC lines [2,7,28]. Although epigenome-wide methylation analysis suggested that both iKCL004 and iKCL011 display the methylation signature of pluripotent stem cells [10], about 7% of CpG sites (35,550 out of >480,000) were differentially methylated (difference >0.2) between iKCL004 and iKCL011, suggesting that these iPSC lines are likely to harbor spots of aberrant epigenetic reprogramming (Fig. 3A, B). Although the differences in DNA methylation signature appeared to have no effect on miRNA expression profile (Fig. 2), they may influence the differentiation propensity of these two iPSC lines.

Since our group is primarily interested in differentiation of hESC and hiPSC into keratinocytes, especially the formation of the epidermal permeability barrier, we next focused on the EDC on chromosome 1. EDC is a ≈2-Mb region at chromosome band 1q21, which contains multiple conserved gene encoding stratum corneum proteins [11–19] (Fig. 4A). We found no difference in DNA methylation of regions associated with either late cornified envelope or small proline-rich region (SPRR) families, as well as with filaggrin, filaggrin 2, involucrin, and loricrin (Supplementary Table S1; Supplementary Figs. S1–S3;

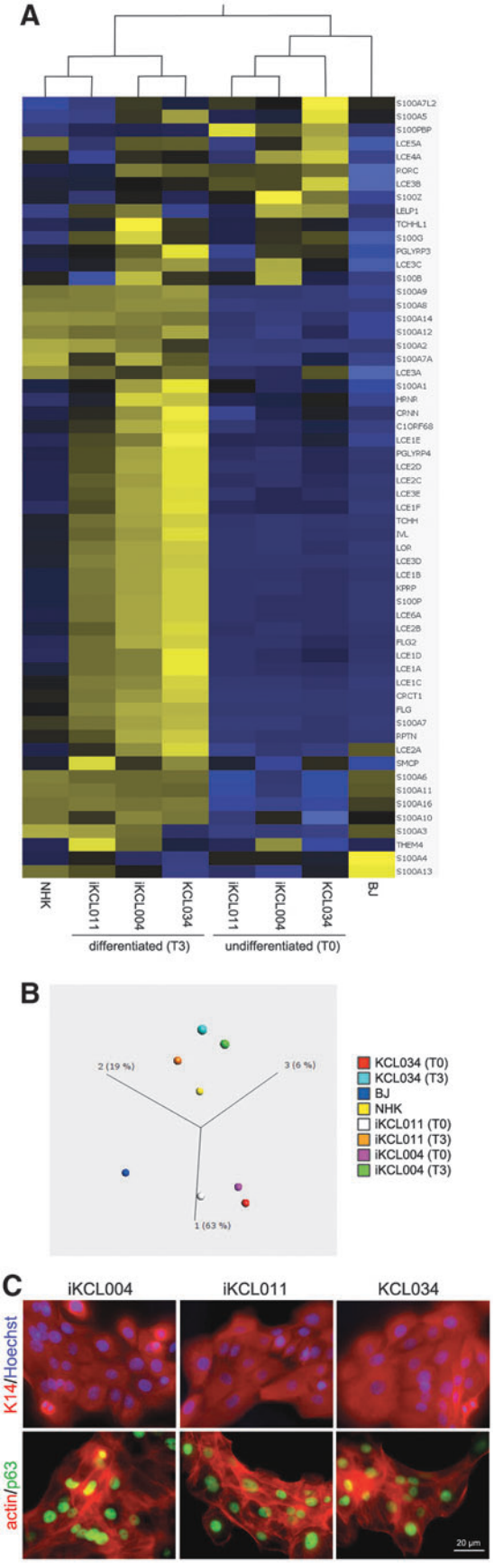

FIG. 5. hESC/iPSC-derived keratinocytes. **(A, B)** Heatmap and principal component analysis of EDC genes in undifferentiated (T0) hESC (KCL034) and iPSC (iKCL004 and iKCL011), hESC/iPSC-derived keratinocytes (T3), and NHK and fibroblasts (BJ) parental to iPSC lines. **(C)** KRT14 and p63 expression in hESC/iPSC-derived keratinocytes suggest that they would be comparable with cells in basal layer of epidermis. NHK, normal human keratinocytes.

Supplementary Data are available online at www.liebertpub.com/scd). However, in iKCL004, but not in iKCL011, trichohyalin (TCHH) retained a DNA methylation signature characteristic of somatic cell origin (Fig. 4B). TCHH, an intermediate filament-associated protein, similar to involucrin, is transiently expressed during late stages of skin development, as well as in development of the inner root sheath of the hair follicle [29–32].

TCHH expression pattern in HEE resembles neonatal, not adult, skin

Next, we investigated whether the difference in methylation signature of TCHH in iKCL004 had an effect on expression of EDC genes and hESC/iPSC differentiation into keratinocytes. We compared the transcriptome of EDC genes in undifferentiated hESC/iPSC (T0), hESC/iPSC-derived keratinocytes (T3), and NHK from skin biopsies of two donors. The T0 and T3 transcriptomes were analyzed as biological replicates from three independent sets of differentiation experiments. Heatmaps showing relative expression for EDC genes and the principal component analysis clearly demonstrate that (i) hESC/iPSC-derived keratinocytes at T3 cluster together with NHK; and that (ii) no significant difference was observed between iKCL004 and iKCL011 (Fig. 5A, B). hESC/iPSC-derived keratinocytes, in general, express keratin 14 (KRT14) and TP63 (p63) (Fig. 5C), which are markers of keratinocytes in the stratum basale of human epidermis. No TCHH expression at protein level was detected in any of the samples (data not shown), which suggested that aberrant DNA methylation of TCHH gene did not affect hESC/iPSC differentiation into keratinocytes and did not induce its expression in $KRT14^{+}/p63^{+}$ cells.

TCHH is not normally seen in interfollicular adult skin, but is found only in the stratum granulosum (SG) of neonatal skin [30]. To examine TCHH expression in a neonatal model of SG cells, we generated multilayered HEEs from the hESC/iPSC-derived keratinocytes and primary human foreskin keratinocytes following our high-to-low humidity protocol [10,21]. All resulting HEEs, regardless of the keratinocytes' origin, had a similar TCHH expression, which resembled the pattern seen in the neonatal skin (Fig. 6). The data suggest that a difference between two iPSC clones in DNA methylation of TCHH gene did not have an obvious effect at TCHH expression pattern in three-dimensional (3D) HEEs.

Discussion

Exome sequencing of both iPSC lines and parental HFFs BJ confirmed that the reprogramming used to generate these cells did not lead to increased number of mutations. Moreover, both lines were genetically identical to their parental line. Karyotype of both iPSC lines was stable over the extended periods of in vitro culture under feeder-free conditions. Cytogenetic resilience of iKCL004 and iKCL011 lines might arise from particular aspects of cell culture, as well as reflect a genetic predisposition to chromosomal stability/instability, commonly noted with hESC lines [8,9,33,34]. hESC is derived from embryos created by in vitro fertilization, often from donors that have problems with fertility. Prevalence of balanced structural chromosomal abnormalities in patients seeking assisted conception is higher than in general population and it is reasonable to speculate that undiagnosed genetic mutations might be underlying cause of infertility, and consequently, genomic instability in the hESC lines.

Although ideally, hiPSC should be functionally and molecularly indistinguishable from hESC, often that is not the case [35]. These differences may manifest only upon differentiation, not in the pluripotent state; miRNA profile [36] and residual DNA methylation [28] are likely to influence differentiation propensity. For example, upon induction of keratinocyte differentiation with bone morphogenic protein 4 and all-trans retinoic acid, none of the three lines used in the study (iKCL004, iKCL011, and KCL034) responded equally [10]. Over time, by end of the differentiation, these differences were diminished, probably through selection and purification by selective attachment to collagen IV-coated surface as described [10]. Indeed, the miRNA profile of both iPSC lines, iKCL004 and iKCL011, was not significantly different from control hESC KCL034 line (Fig. 2). Interestingly, epigenome-wide methylation (>480,000 CpG sites) analysis using Infinium Human Methylation 450 BeadChip Kit found more differences between iKCL004 and iKCL011 (7%) than between either iKCL004 and KCL034 (5%) or iKCL011 and KCL034 (4%) (Fig. 3) [10].

Differently methylated CpG sites are in general randomly scattered across the genome. Within one gene, DNA methylation often is significantly different on only one or two CpG sites (Supplementary Table S1; Supplementary Figs. S1–S3).

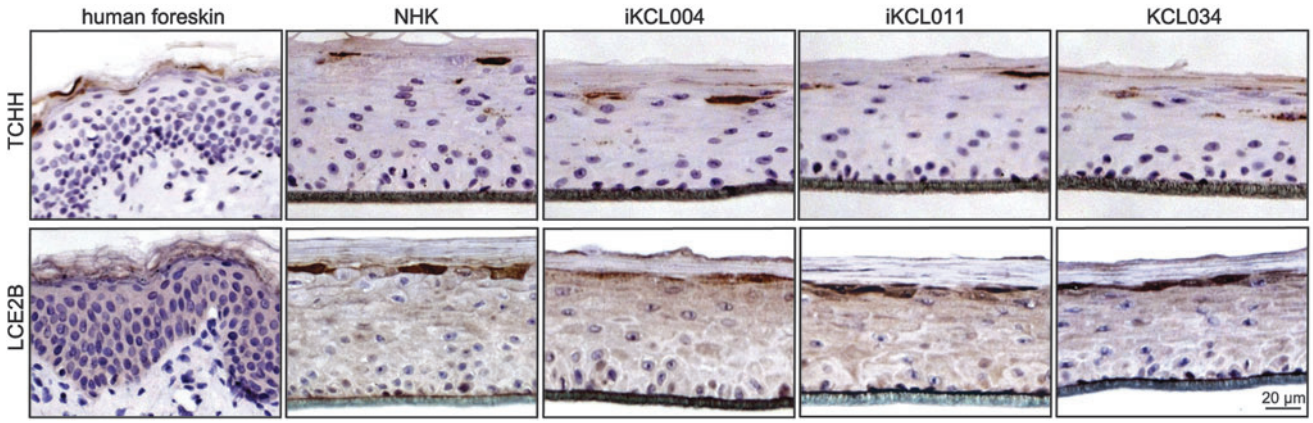

FIG. 6. The expression pattern of TCHH in human epidermal equivalents is similar to human neonatal skin. Localization in the granular layer corresponds to expression of other proteins involved in cornification such as LCE2B.

One of the few genes in which DNA methylation was significantly different on most of its CpG sites (12 out of 21) was *TCHH* (Supplementary Table S1; Fig. 4). TCHH is normally expressed in the inner root sheet and medulla of hair follicles and transiently in the SG and corneum of the epidermis during late stages of fetal skin development [30]. It is also present in isolated cells of the SG of some regions of epidermis (Supplementary Fig. S4) [37]. While in normal skin, TCHH expression correlates with expression of filaggrin, this correlation is lost in psoriatic skin [38]. By forming multiple complex cross-links with itself and other structural proteins, including epiplakin, involucrin, and SPRRs, TCHH is important for the mechanical strength of the hair follicle and epithelial tissues such as hard palate or filiform papillae of the tongue [39]. TCHH is also thought to be a potential major autoantigen in alopecia areata [40]. CpG sites within *TCHH* were mostly hypomethylated in HFFs and hypermethylated in the hESC KCL034 line (Fig. 4). TCHH methylation pattern suggested that iKCL004 retained methylation signature of the parental fibroblasts, whereas iKCL011 matched the hESC line. We found, however, no differences in TCHH expression pattern in HEE (Fig. 6) suggesting that DNA methylation of the *TCHH* gene in establishing an iPSC population may not play an essential role.

The data presented in this study highlight our limited understanding of the epigenetic heterogeneity. It is generally considered that faithful genetic and epigenetic reprogramming is critical to obtain fully naive ''ground state'' of pluripotency.'' Indeed, DNA methylation defects have been linked to multiple human diseases [41]. However, as there are significant differences among the genomes of healthy human individuals that do not affect normal fetal and postnatal growth, it is quite plausible that the same rule can also be applied for the epigenome–DNA methylation status may not be equally important for regulation of all genes. Differentiation and tissue formation may, in some cases, attenuate variations in iPSC methylome. These findings should enhance future research using these 3D cultures, since iPSC methylome differences produced by the transformation and culture techniques do not result in phenotypic variation.

Acknowledgments

This work was supported, in part, by grants from the Medical Research Council UK (G0801061 to D.I.), the NIH (R21 ARO61583 and R01 AR051930), the Research Service of the Department of Veterans Affairs (to T.M.M.), and the Dystrophic Epidermolysis Bullosa Research Association (DebRA) (to J.A.M.). A.P. was a DebRA-supported PhD student. We thank Prof Caroline Ogilvie from the Genetics Center at Guy's Hospital for a critical reading of the article.

Author Disclosure Statement

No competing financial interests exist.

References

1. Takahashi K and S Yamanaka. (2006). Induction of pluripotent stem cells from mouse embryonic and adult fibroblast cultures by defined factors. Cell 126:663–676.
2. Sugiura M, Y Kasama, R Araki, Y Hoki, M Sunayama, M Uda, M Nakamura, S Ando and M Abe. (2014). Induced pluripotent stem cell generation-associated point mutations arise during the initial stages of the conversion of these cells. Stem Cell Rep 2:52–63.
3. Young MA, DE Larson, CW Sun, DR George, L Ding, CA Miller, L Lin, KM Pawlik, K Chen, et al. (2012). Background mutations in parental cells account for most of the genetic heterogeneity of induced pluripotent stem cells. Cell Stem Cell 10:570–582.
4. Kim K, R Zhao, A Doi, K Ng, J Unternaehrer, P Cahan, H Huo, YH Loh, MJ Aryee, et al. (2011). Donor cell type can influence the epigenome and differentiation potential of human induced pluripotent stem cells. Nat Biotechnol 29:1117–1119.
5. Ohi Y, H Qin, C Hong, L Blouin, JM Polo, T Guo, Z Qi, SL Downey, PD Manos, et al. (2011). Incomplete DNA methylation underlies a transcriptional memory of somatic cells in human iPS cells. Nat Cell Biol 13:541–549.
6. Lister R, M Pelizzola, YS Kida, RD Hawkins, JR Nery, G Hon, J Antosiewicz-Bourget, R O'Malley, et al. (2011). Hotspots of aberrant epigenomic reprogramming in human induced pluripotent stem cells. Nature 471:68–73.
7. Polo JM, S Liu, ME Figueroa, W Kulalert, S Eminli, KY Tan, E Apostolou, M Stadtfeld, Y Li, et al. (2010). Cell type of origin influences the molecular and functional properties of mouse induced pluripotent stem cells. Nat Biotechnol 28:848–855.
8. Stephenson E, CM Ogilvie, H Patel, G Cornwell, L Jacquet, N Kadeva, P Braude and D Ilic. (2010). Safety paradigm: genetic evaluation of therapeutic grade human embryonic stem cells. J R Soc Interface 7:S677–S688.
9. Liang G and Y Zhang. (2013). Genetic and epigenetic variations in iPSCs: potential causes and implications for application. Cell Stem Cell 13:149–159.
10. Petrova A, A Celli, L Jacquet, D Dafou, D Crumrine, M Hupe, M Arno, C Hobbs, A Cvoro, et al. (2014). 3D in vitro model of a functional epidermal permeability barrier from human embryonic stem cells and induced pluripotent stem cells. Stem Cell Rep 2:675–689.
11. Jackson B, CM Tilli, MJ Hardman, AA Avilion, MC MacLeod, GS Ashcroft and C Byrne. (2005). Late cornified envelope family in differentiating epithelia—response to calcium and ultraviolet irradiation. J Invest Dermatol 124:1062–1070.
12. Contzler R, B Favre, M Huber and D Hohl. (2005). Cornulin, a new member of the ''fused gene'' family, is expressed during epidermal differentiation. J Invest Dermatol 124:990–997.
13. Marshall D, MJ Hardman, KM Nield and C Byrne. (2001). Differentially expressed late constituents of the epidermal cornified envelope. Proc Natl Acad Sci U S A 98:13031–13036.
14. South AP, A Cabral, JH Ives, CH James, G Mirza, I Marenholz, D Mischke, C Backendorf, J Ragoussis and D Nizetic. (1999). Human epidermal differentiation complex in a single 2.5 Mbp long continuum of overlapping DNA cloned in bacteria integrating physical and transcript maps. J Invest Dermatol 112:910–918.
15. Lioumi M, CA Ferguson, PT Sharpe, T Freeman, I Marenholz, D Mischke, C Heizmann and J Ragoussis. (1999). Isolation and characterization of human and mouse ZIRTL, a member of the IRT1 family of transporters, mapping within the epidermal differentiation complex. Genomics 62:272–280.
16. Zhao XP and JT Elder. (2002). Evidence for local control of gene expression in the epidermal differentiation complex. Exp Dermatol 11:406–412.

17. Zhao XP and JT Elder. (1997). Positional cloning of novel skin-specific genes from the human epidermal differentiation complex. Genomics 45:250–258.
18. Marenholz I, A Volz, A Ziegler, A Davies, I Ragoussis, BP Korge and D Mischke. (1996). Genetic analysis of the epidermal differentiation complex (EDC) on human chromosome 1q21: chromosomal orientation, new markers, and a 6-Mb YAC contig. Genomics 37:295–302.
19. Mischke D, BP Korge, I Marenholz, A Volz and A Ziegler. (1996). Genes encoding structural proteins of epidermal cornification and S100 calcium-binding proteins form a gene complex (''epidermal differentiation complex'') on human chromosome 1q21. J Invest Dermatol 106:989–992.
20. Devito L, A Petrova, C Miere, S Codognotto, N Blakely, A Lovatt, C Ogilvie, Y Khalaf and D Ilic. (2014). Cost-effective master cell bank validation of multiple clinical-grade human pluripotent stem cell lines from a single donor. Stem Cell Transl Med 3:1116–1124.
21. Sun R, A Celli, D Crumrine, M Hupe, LC Adame, SD Pennypacker, K Park, Y Uchida, KR Feingold, et al. (2015). Lowered humidity produces human epidermal equivalents with enhanced barrier properties. Tissue Eng Part C Methods 21:15–22.
22. Meyer SU, S Kaiser, C Wagner, C Thirion and MW Pfaffl. (2012). Profound effect of profiling platform and normalization strategy on detection of differentially expressed microRNAs—a comparative study. PLoS One 7:e38946.
23. Ilic D, M Mao-Qiang, D Crumrine, G Dolganov, N Larocque, P Xu, M Demerjian, BE Brown, ST Lim, et al. (2007). Focal adhesion kinase controls pH-dependent epidermal barrier homeostasis by regulating actin-directed Na+/H+ exchanger 1 plasma membrane localization. Am J Pathol 170:2055–2067.
24. Stephenson E, L Jacquet, C Miere, V Wood, N Kadeva, G Cornwell, S Codognotto, Y Dajani, P Braude and D Ilic. (2012). Derivation and propagation of human embryonic stem cell lines from frozen embryos in an animal product-free environment. Nat Protoc 7:1366–1381.
25. Warren L, PD Manos, T Ahfeldt, YH Loh, H Li, F Lau, W Ebina, PK Mandal, ZD Smith, et al. (2010). Highly efficient reprogramming to pluripotency and directed differentiation of human cells with synthetic modified mRNA. Cell Stem Cell 7:618–630.
26. Vitaloni M, J Pulecio, J Bilic, B Kuebler, L Laricchia-Robbio and JC Izpisua Belmonte. (2014). MicroRNAs contribute to induced pluripotent stem cell somatic donor memory. J Biol Chem 289:2084–2098.
27. Wang B, P Howel, S Bruheim, J Ju, LB Owen, O Fodstad and Y Xi. (2011). Systematic evaluation of three microRNA profiling platforms: microarray, beads array, and quantitative real-time PCR array. PLoS One 6:e17167.
28. Kim K, A Doi, B Wen, K Ng, R Zhao, P Cahan, J Kim, MJ Aryee, H Ji, et al. (2010). Epigenetic memory in induced pluripotent stem cells. Nature 467:285–290.
29. Steinert PM and LN Marekov. (1999). Multiple roles for trichohyalin in the inner root sheath. Exp Dermatol 8:331–332.
30. Lee SC, JB Lee, JP Kook, JJ Seo, KI Nam, SS Park and YP Kim. (1999). Expression of differentiation markers during fetal skin development in humans: immunohistochemical studies on the precursor proteins forming the cornified cell envelope. J Invest Dermatol 112:882–886.
31. Lee SC, M Wang, OW McBride, JE O'Keefe, IG Kim and PM Steinert. (1993). Human trichohyalin gene is clustered with the genes for other epidermal structural proteins and calcium-binding proteins at chromosomal locus 1q21. J Invest Dermatol 100:65–68.
32. Mlitz V, B Strasser, K Jaeger, M Hermann, M Ghannadan, M Buchberger, L Alibardi, E Tschachler and L Eckhart. (2014). Trichohyalin-like proteins have evolutionarily conserved roles in the morphogenesis of skin appendages. J Invest Dermatol 134:2685–2692.
33. Hanson C and G Caisander. (2005). Human embryonic stem cells and chromosome stability. APMIS 113:751–755.
34. Catalina P, R Montes, G Ligero, L Sanchez, T de la Cueva, C Bueno, PE Leone and P Menendez. (2008). Human ESCs predisposition to karyotypic instability: is a matter of culture adaptation or differential vulnerability among hESC lines due to inherent properties? Mol Cancer 7:76.
35. Chin MH, MJ Mason, W Xie, S Volinia, M Singer, C Peterson, G Ambartsumyan, O Aimiuwu, L Richter, et al. (2009). Induced pluripotent stem cells and embryonic stem cells are distinguished by gene expression signatures. Cell Stem Cell 5:111–123.
36. Neveu P, MJ Kye, S Qi, DE Buchholz, DO Clegg, M Sahin, IH Park, KS Kim, GQ Daley, et al. (2010). MicroRNA profiling reveals two distinct p53-related human pluripotent stem cell states. Cell Stem Cell 7:671–681.
37. O'Keefe EJ, EH Hamilton, SC Lee and P Steinert. (1993). Trichohyalin: a structural protein of hair, tongue, nail, and epidermis. J Invest Dermatol 101:65S–71S.
38. Ishida-Yamamoto A, Y Hashimoto, M Manabe, WM O'Guin WM, BA Dale and H Iizuka. (1997). Distinctive expression of filaggrin and trichohyalin during various pathways of epithelial differentiation. Br J Dermatol 137:9–16.
39. Steinert PM, DA Parry and LN Marekov. (2003). Trichohyalin mechanically strengthens the hair follicle: multiple cross-bridging roles in the inner root sheath. J Biol Chem 278:41409–41419.
40. Leung MC, CW Sutton, DA Fenton and DJ Tobin. (2010). Trichohyalin is a potential major autoantigen in human alopecia areata. J Proteome Res 9:5153–5163.
41. Robertson KD. (2005). DNA methylation and human disease. Nat Rev Genet 6:597–610.

Address correspondence to:
Dusko Ilic
Assisted Conception Unit
Stem Cell Laboratory
11th Floor, Tower Wing, Guy's Hospital
London SE1 9RT
United Kingdom

E-mail: dusko.ilic@kcl.ac.uk

Received for publication June 3, 2016
Accepted after revision July 26, 2016
Prepublished on Liebert Instant Online July 26, 2016

Supplementary Data

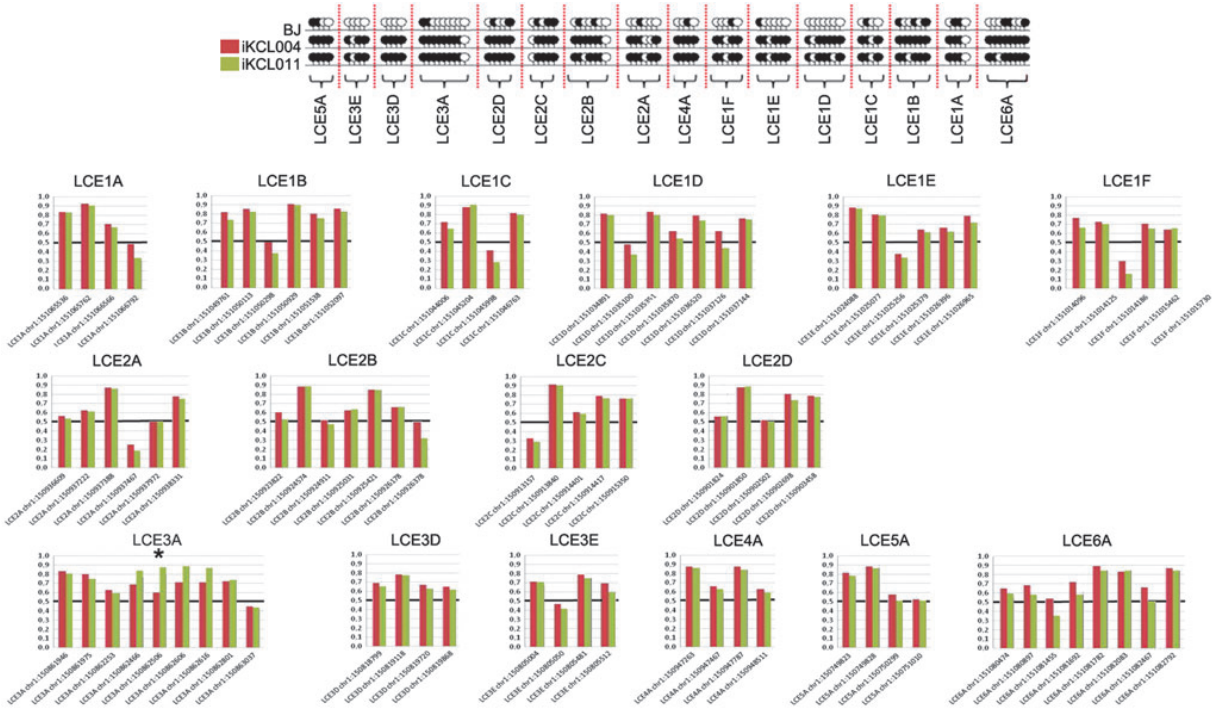

SUPPLEMENTARY FIG. S1. DNA methylation of *LCE* family. DNA methylation of *LCE* gene family shown as lollipop diagram and bar charts. In lollipop diagram, *black circles* represent CpG sites that have Beta value ≥0.5 and *white circles* represent CpG sites with Beta value <0.5. The difference of 0.4 (40%) is considered significant (*star*) in bar chart diagram. LCE, late cornified envelope.

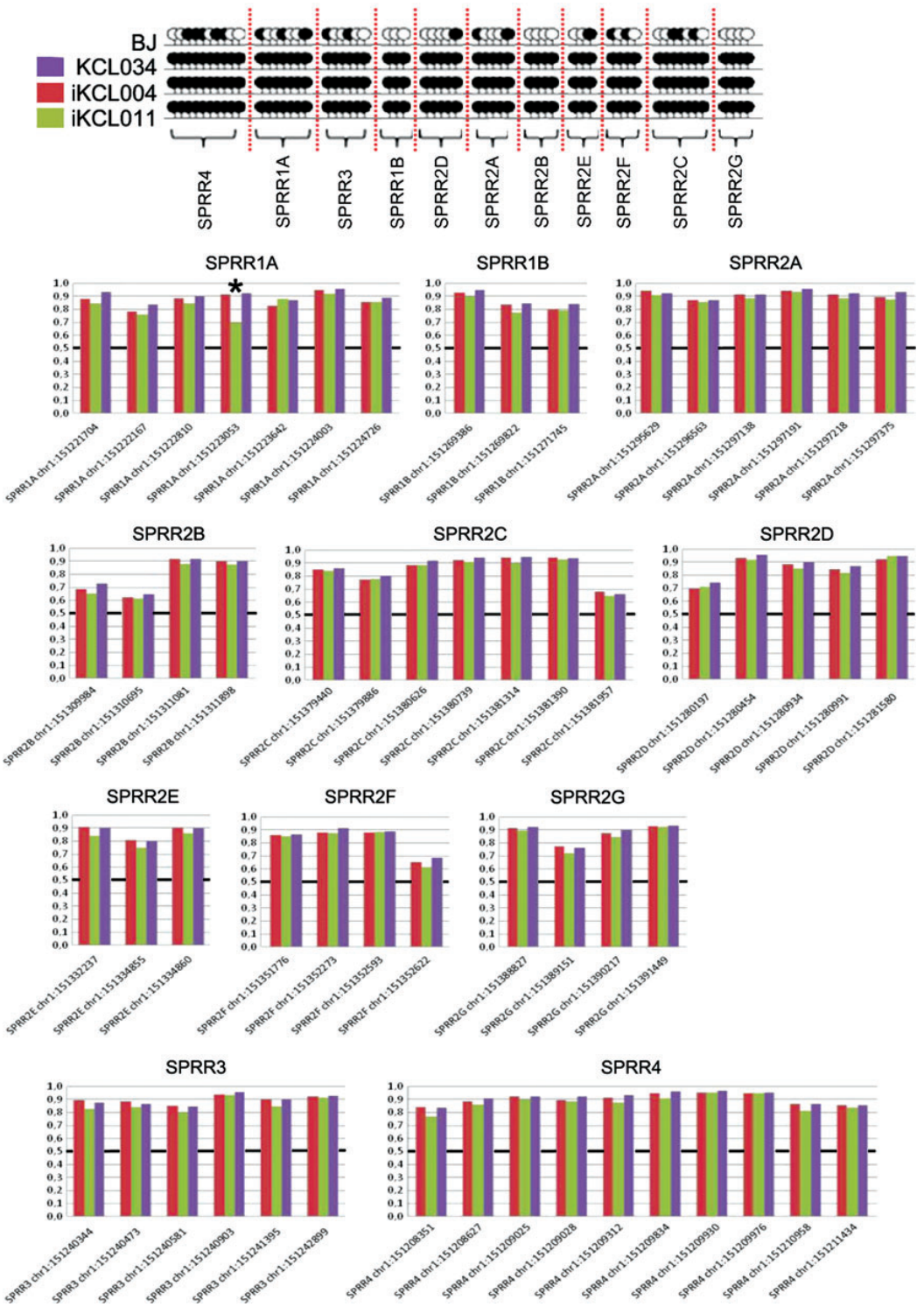

SUPPLEMENTARY FIG. S2. DNA methylation of *SPRR* family. DNA methylation of *SPRR* gene family shown as lollipop diagram and bar charts. In lollipop diagram, *black circles* represent CpG sites that have Beta value ≥0.5 and *white circles* represent CpG sites with Beta value <0.5. The difference of 0.4 (40%) is considered significant (*star*) in bar chart diagram. SPRR, small proline-rich regions.

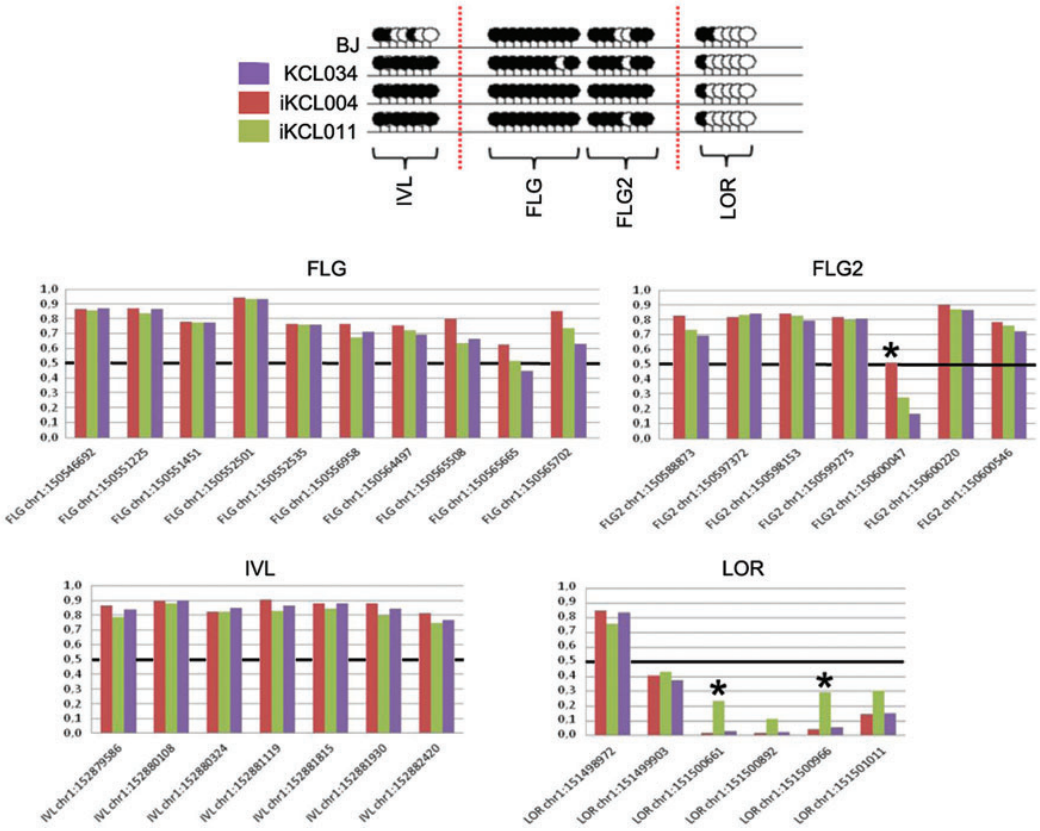

SUPPLEMENTARY FIG. S3. DNA methylation of *LOR*, *INV*, and *FLG* family. DNA methylation of genes encoding loricrin, involucrin, and filaggrin family shown as lollipop diagram and bar charts. In lollipop diagram, *black circles* represent CpG sites that have Beta value ≥0.5 and *white circles* represent CpG sites with Beta value <0.5. The difference of 0.4 (40%) is considered significant (*star*) in bar chart diagram.

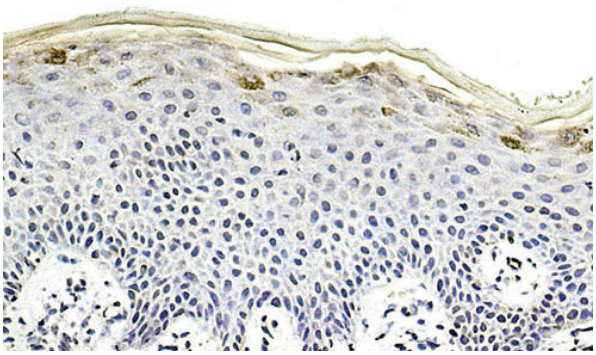

SUPPLEMENTARY FIG. S4. TCHH expression in adult epidermis. Isolated cells of the stratum granulosum were positive for TCHH in some regions of adult epidermis. TCHH, trichohyalin.

Supplementary Table S1. Average Beta values of CpG Methylation in Parental BJ Fibroblast, iKCL004, iKCL011, and KCL034

CpG sites that have Beta value ≥0.5 are highlighted pink, whereas CpG sites with Beta value <0.5 are highlighted green.

			Average Beta Value			
Illumina Target ID	Methylation Site Coordinate (hg18)	Gene Name	BJ	iKCL004	iKCL011	KCL034
cg05388137	chr1:150323493	TCHHL1	0.54	0.78	0.50	0.48
cg10827479	chr1:150327987	TCHHL1	0.73	0.85	0.86	0.87
cg08918985	chr1:150328157	TCHHL1	0.32	0.86	0.81	0.78
cg01925883	chr1:150329191	TCHHL1	0.32	0.86	0.85	0.84
cg16689481	chr1:150346337	TCHH	0.85	0.92	0.95	0.96
cg15973171	chr1:150346978	TCHH	0.33	0.38	0.62	0.61
cg14661959	chr1:150347095	TCHH	0.17	0.48	0.81	0.74
cg04938315	chr1:150347167	TCHH	0.25	0.34	0.66	0.58
cg05523911	chr1:150347626	TCHH	0.21	0.30	0.74	0.63
cg04986781	chr1:150347941	TCHH	0.39	0.58	0.85	0.75
cg03438305	chr1:150349549	TCHH	0.15	0.40	0.58	0.57
cg05464302	chr1:150349653	TCHH	0.04	0.19	0.46	0.36
cg10234068	chr1:150349900	TCHH	0.14	0.40	0.69	0.74
cg24645670	chr1:150349916	TCHH	0.08	0.35	0.65	0.72
cg24880024	chr1:150350333	TCHH	0.10	0.16	0.66	0.40
cg05642734	chr1:150350971	TCHH	0.07	0.17	0.71	0.39
cg18287591	chr1:150351757	TCHH	0.10	0.36	0.76	0.52
cg20795569	chr1:150351760	TCHH	0.08	0.34	0.83	0.55
cg00584000	chr1:150351811	TCHH	0.11	0.24	0.90	0.60
cg20592707	chr1:150353247	TCHH	0.54	0.77	0.80	0.81
cg26685752	chr1:150353316	TCHH	0.75	0.89	0.75	0.80
cg02211983	chr1:150353503	TCHH	0.35	0.65	0.44	0.36
cg22603037	chr1:150353891	TCHH	0.30	0.67	0.50	0.41
cg11166365	chr1:150353939	TCHH	0.79	0.83	0.83	0.82
cg23021650	chr1:150354513	TCHH	0.72	0.85	0.83	0.80
cg10321714	chr1:150546692	FLG	0.77	0.87	0.86	0.87
cg01880149	chr1:150551225	FLG	0.73	0.87	0.84	0.87
cg07548383	chr1:150551451	FLG	0.70	0.78	0.78	0.77
cg12136906	chr1:150552501	FLG	0.86	0.94	0.93	0.93
cg03465714	chr1:150552535	FLG	0.64	0.76	0.76	0.76
cg22719314	chr1:150556958	FLG	0.74	0.77	0.67	0.71
cg19855573	chr1:150564497	FLG	0.61	0.75	0.72	0.69
cg13447818	chr1:150565508	FLG	0.70	0.80	0.64	0.67
cg10500702	chr1:150565665	FLG	0.53	0.62	0.51	0.45
cg26390526	chr1:150565702	FLG	0.68	0.85	0.74	0.63
cg20825532	chr1:150588873	FLG2	0.75	0.83	0.73	0.69
cg07134486	chr1:150597372	FLG2	0.77	0.82	0.83	0.84
cg20694572	chr1:150598153	FLG2	0.51	0.84	0.83	0.79
cg17542852	chr1:150599275	FLG2	0.42	0.82	0.80	0.81
cg03957898	chr1:150600047	FLG2	0.24	0.51	0.27	0.16
cg23812489	chr1:150600220	FLG2	0.77	0.90	0.87	0.87
cg03439811	chr1:150600546	FLG2	0.69	0.78	0.76	0.72

cg05248781	chr1:150749823	LCE5A	0.57	0.82	0.78	0.75
cg16320885	chr1:150749828	LCE5A	0.74	0.88	0.86	0.90
cg01868128	chr1:150750299	LCE5A	0.27	0.58	0.51	0.47
cg00011513	chr1:150751010	LCE5A	0.16	0.53	0.51	0.49
cg23724738	chr1:150805004	LCE3E	0.31	0.71	0.71	0.67
cg07476201	chr1:150805050	LCE3E	0.18	0.47	0.42	0.38
cg24000437	chr1:150805481	LCE3E	0.27	0.79	0.75	0.75
cg23110514	chr1:150805512	LCE3E	0.28	0.69	0.60	0.64
cg22519158	chr1:150818799	LCE3D	0.44	0.69	0.65	0.66
cg20676475	chr1:150819118	LCE3D	0.38	0.78	0.77	0.76
cg02054568	chr1:150819720	LCE3D	0.42	0.67	0.63	0.65
cg18116418	chr1:150819868	LCE3D	0.24	0.65	0.62	0.57
cg26135325	chr1:150861946	LCE3A	0.63	0.83	0.81	0.80
cg20634798	chr1:150861975	LCE3A	0.60	0.80	0.75	0.76
cg27206522	chr1:150862253	LCE3A	0.30	0.63	0.59	0.59
cg26466858	chr1:150862466	LCE3A	0.26	0.69	0.84	0.77
cg13071333	chr1:150862506	LCE3A	0.07	0.60	0.88	0.80
cg08732526	chr1:150862606	LCE3A	0.33	0.71	0.89	0.91
cg09895009	chr1:150862616	LCE3A	0.38	0.71	0.87	0.89
cg07821297	chr1:150862801	LCE3A	0.43	0.72	0.74	0.73
cg16046605	chr1:150863037	LCE3A	0.35	0.45	0.44	0.42
cg11680857	chr1:150901824	LCE2D	0.48	0.56	0.56	0.89
cg22044308	chr1:150901850	LCE2D	0.69	0.88	0.88	0.90
cg16361876	chr1:150902502	LCE2D	0.22	0.52	0.50	0.51
cg21312148	chr1:150902698	LCE2D	0.28	0.80	0.74	0.72
cg01433225	chr1:150903458	LCE2D	0.59	0.78	0.77	0.79
cg13844662	chr1:150913157	LCE2C	0.19	0.33	0.29	0.29
cg00406188	chr1:150913840	LCE2C	0.66	0.91	0.90	0.90
cg03960217	chr1:150914401	LCE2C	0.25	0.61	0.59	0.56
cg26919735	chr1:150914417	LCE2C	0.56	0.79	0.76	0.76
cg06198390	chr1:150915350	LCE2C	0.51	0.76	0.76	0.77
cg19371339	chr1:150923822	LCE2B	0.22	0.60	0.53	0.43
cg08279693	chr1:150924574	LCE2B	0.65	0.89	0.89	0.90
cg24332770	chr1:150924911	LCE2B	0.12	0.52	0.47	0.42
cg25098401	chr1:150925031	LCE2B	0.45	0.62	0.64	0.63
cg21754343	chr1:150925421	LCE2B	0.56	0.85	0.85	0.85
cg18855143	chr1:150926178	LCE2B	0.46	0.66	0.66	0.67
cg06619428	chr1:150926378	LCE2B	0.34	0.50	0.32	0.26
cg22616525	chr1:150936609	LCE2A	0.17	0.56	0.53	0.46
cg13974761	chr1:150937222	LCE2A	0.09	0.62	0.61	0.56
cg13705774	chr1:150937388	LCE2A	0.61	0.87	0.86	0.87
cg13697387	chr1:150937467	LCE2A	0.05	0.25	0.18	0.15
cg08166767	chr1:150937972	LCE2A	0.09	0.50	0.50	0.41
cg16354520	chr1:150938331	LCE2A	0.15	0.78	0.75	0.73
cg20823091	chr1:150947263	LCE4A	0.47	0.88	0.86	0.90
cg21846488	chr1:150947467	LCE4A	0.38	0.66	0.63	0.59

cg00981443	chr1:150947787	LCE4A	0.57	0.88	0.84	0.84
cg04221650	chr1:150948511	LCE4A	0.13	0.63	0.59	0.53
cg23413307	chr1:151014096	LCE1F	0.31	0.77	0.66	0.67
cg26302157	chr1:151014125	LCE1F	0.19	0.73	0.70	0.67
cg13493250	chr1:151014186	LCE1F	0.16	0.30	0.16	0.13
cg01915081	chr1:151015462	LCE1F	0.52	0.71	0.65	0.65
cg21535199	chr1:151015730	LCE1F	0.39	0.64	0.66	0.62
cg14528310	chr1:151024088	LCE1E	0.77	0.88	0.87	0.87
cg25610428	chr1:151025077	LCE1E	0.19	0.81	0.80	0.81
cg14792160	chr1:151025256	LCE1E	0.16	0.38	0.34	0.19
cg21065959	chr1:151025379	LCE1E	0.36	0.64	0.61	0.62
cg16987735	chr1:151026396	LCE1E	0.10	0.66	0.62	0.62
cg15923484	chr1:151026965	LCE1E	0.33	0.79	0.72	0.73
cg01406203	chr1:151034891	LCE1D	0.34	0.82	0.80	0.86
cg22365757	chr1:151035100	LCE1D	0.02	0.48	0.37	0.31
cg12725323	chr1:151035351	LCE1D	0.49	0.84	0.80	0.84
cg11583211	chr1:151035870	LCE1D	0.13	0.62	0.54	0.51
cg11835200	chr1:151036520	LCE1D	0.27	0.80	0.74	0.67
cg15531099	chr1:151037126	LCE1D	0.18	0.62	0.44	0.42
cg24325314	chr1:151037144	LCE1D	0.30	0.76	0.75	0.77
cg16011217	chr1:151044006	LCE1C	0.21	0.72	0.65	0.53
cg08895932	chr1:151045204	LCE1C	0.64	0.88	0.91	0.89
cg24304714	chr1:151045998	LCE1C	0.08	0.41	0.29	0.24
cg11067224	chr1:151046763	LCE1C	0.43	0.82	0.80	0.76
cg21434954	chr1:151049761	LCE1B	0.59	0.82	0.74	0.77
cg19250709	chr1:151050113	LCE1B	0.48	0.86	0.82	0.82
cg08878744	chr1:151050298	LCE1B	0.17	0.50	0.37	0.31
cg03881934	chr1:151050929	LCE1B	0.67	0.91	0.89	0.93
cg07090653	chr1:151051538	LCE1B	0.34	0.80	0.75	0.75
cg12449852	chr1:151052097	LCE1B	0.50	0.86	0.83	0.83
cg01975957	chr1:151065536	LCE1A	0.48	0.84	0.83	0.83
cg06221609	chr1:151065762	LCE1A	0.78	0.93	0.90	0.92
cg07330196	chr1:151066566	LCE1A	0.54	0.71	0.67	0.72
cg14696820	chr1:151066792	LCE1A	0.11	0.49	0.34	0.31
cg22124859	chr1:151080474	LCE6A	0.23	0.65	0.59	0.55
cg09417355	chr1:151080897	LCE6A	0.13	0.68	0.58	0.53
cg16265542	chr1:151081455	LCE6A	0.04	0.54	0.35	0.33
cg26531371	chr1:151081692	LCE6A	0.52	0.72	0.58	0.63
cg08101739	chr1:151081782	LCE6A	0.54	0.89	0.84	0.85
cg00998782	chr1:151082083	LCE6A	0.48	0.83	0.84	0.87
cg13366738	chr1:151082467	LCE6A	0.14	0.66	0.51	0.49
cg23624133	chr1:151082792	LCE6A	0.57	0.87	0.84	0.85
cg02060465	chr1:151208351	SPRR4	0.25	0.84	0.77	0.84
cg08948808	chr1:151208627	SPRR4	0.13	0.88	0.86	0.91
cg11066776	chr1:151209025	SPRR4	0.70	0.92	0.90	0.92
cg24316982	chr1:151209028	SPRR4	0.66	0.90	0.89	0.92

cg02202484	chr1:151209312	SPRR4	0.65	0.91	0.87	0.93
cg08763351	chr1:151209834	SPRR4	0.44	0.95	0.91	0.96
cg19602452	chr1:151209930	SPRR4	0.91	0.95	0.95	0.97
cg16738827	chr1:151209976	SPRR4	0.83	0.95	0.95	0.95
cg09902062	chr1:151210958	SPRR4	0.14	0.86	0.81	0.86
cg18805469	chr1:151211434	SPRR4	0.48	0.86	0.84	0.85
cg00922841	chr1:151221704	SPRR1A	0.50	0.88	0.85	0.93
cg06101324	chr1:151222167	SPRR1A	0.09	0.78	0.76	0.84
cg04505023	chr1:151222810	SPRR1A	0.36	0.89	0.85	0.90
cg04546999	chr1:151223053	SPRR1A	0.57	0.91	0.70	0.92
cg27569034	chr1:151223642	SPRR1A	0.37	0.83	0.88	0.87
cg07909128	chr1:151224003	SPRR1A	0.37	0.95	0.92	0.96
cg04841371	chr1:151224726	SPRR1A	0.52	0.86	0.85	0.89
cg24667326	chr1:151240344	SPRR3	0.55	0.89	0.83	0.88
cg04138756	chr1:151240473	SPRR3	0.27	0.88	0.84	0.86
cg25856811	chr1:151240581	SPRR3	0.11	0.85	0.80	0.85
cg13444842	chr1:151240903	SPRR3	0.79	0.94	0.93	0.96
cg21543102	chr1:151241395	SPRR3	0.49	0.90	0.85	0.90
cg20671415	chr1:151242899	SPRR3	0.29	0.93	0.91	0.93
cg18771659	chr1:151269386	SPRR1B	0.46	0.93	0.90	0.95
cg24884084	chr1:151269822	SPRR1B	0.02	0.84	0.78	0.84
cg02919982	chr1:151271745	SPRR1B	0.42	0.80	0.79	0.84
cg01011918	chr1:151280197	SPRR2D	0.41	0.69	0.71	0.75
cg14826683	chr1:151280454	SPRR2D	0.42	0.93	0.92	0.96
cg10812889	chr1:151280934	SPRR2D	0.04	0.88	0.85	0.90
cg03943115	chr1:151280991	SPRR2D	0.04	0.84	0.82	0.87
cg18087023	chr1:151281580	SPRR2D	0.62	0.92	0.95	0.95
cg14966325	chr1:151295629	SPRR2A	0.51	0.94	0.91	0.92
cg18766755	chr1:151296563	SPRR2A	0.09	0.87	0.86	0.87
cg04993112	chr1:151297138	SPRR2A	0.29	0.91	0.89	0.92
cg22014834	chr1:151297191	SPRR2A	0.73	0.94	0.93	0.96
cg09169531	chr1:151297218	SPRR2A	0.33	0.91	0.88	0.92
cg26059632	chr1:151297375	SPRR2A	0.25	0.89	0.87	0.93
cg20612962	chr1:151309984	SPRR2B	0.17	0.69	0.65	0.73
cg13950674	chr1:151310695	SPRR2B	0.21	0.62	0.61	0.65
cg08009265	chr1:151311081	SPRR2B	0.45	0.92	0.88	0.92
cg06400319	chr1:151311898	SPRR2B	0.49	0.90	0.88	0.90
cg27631593	chr1:151332237	SPRR2E	0.34	0.91	0.84	0.90
cg08555657	chr1:151334855	SPRR2E	0.46	0.81	0.75	0.80
cg00152644	chr1:151334860	SPRR2E	0.54	0.90	0.86	0.90
cg04121973	chr1:151351776	SPRR2F	0.80	0.86	0.85	0.86
cg03449150	chr1:151352273	SPRR2F	0.05	0.88	0.88	0.91
cg22946974	chr1:151352593	SPRR2F	0.73	0.88	0.89	0.89
cg22204954	chr1:151352622	SPRR2F	0.35	0.65	0.62	0.69
cg13401840	chr1:151379440	SPRR2C	0.30	0.85	0.84	0.86
cg00891995	chr1:151379886	SPRR2C	0.13	0.77	0.78	0.80

cg00535683	chr1:151380626	SPRR2C	0.54	0.88	0.88	0.92
cg25212571	chr1:151380739	SPRR2C	0.62	0.92	0.91	0.94
cg07804289	chr1:151381314	SPRR2C	0.13	0.94	0.90	0.95
cg10119001	chr1:151381390	SPRR2C	0.54	0.94	0.93	0.94
cg23606417	chr1:151381957	SPRR2C	0.40	0.68	0.65	0.66
cg03969260	chr1:151388827	SPRR2G	0.41	0.91	0.89	0.92
cg06034133	chr1:151389151	SPRR2G	0.35	0.77	0.72	0.77
cg11267802	chr1:151390217	SPRR2G	0.03	0.87	0.85	0.90
cg20141817	chr1:151391449	SPRR2G	0.43	0.93	0.92	0.93
cg27626424	chr1:151498972	LOR	0.58	0.85	0.76	0.84
cg05001111	chr1:151499903	LOR	0.55	0.41	0.44	0.37
cg08611411	chr1:151500661	LOR	0.04	0.02	0.23	0.03
cg21860629	chr1:151500892	LOR	0.03	0.02	0.12	0.02
cg11534293	chr1:151500966	LOR	0.04	0.04	0.30	0.06
cg10228283	chr1:151501011	LOR	0.28	0.15	0.30	0.15
cg21419383	chr1:152879586	IVL	0.61	0.86	0.79	0.84
cg02889647	chr1:152880108	IVL	0.72	0.89	0.88	0.90
cg15059851	chr1:152880324	IVL	0.50	0.82	0.82	0.85
cg25082710	chr1:152881119	IVL	0.45	0.91	0.83	0.86
cg05440289	chr1:152881815	IVL	0.79	0.88	0.84	0.88
cg15486123	chr1:152881930	IVL	0.48	0.88	0.80	0.84
cg02855850	chr1:152882420	IVL	0.31	0.81	0.75	0.77

STEM CELLS®

EMBRYONIC STEM CELLS/INDUCED PLURIPOTENT STEM CELLS

A Thyroid Hormone Receptor/KLF9 Axis in Human Hepatocytes and Pluripotent Stem Cells

ALEKSANDRA CVORO,[a] LIANI DEVITO,[b] FLORA A. MILTON,[a] LAILA NOLI,[b] AIJUN ZHANG,[a] CELINE FILIPPI,[c,d] KEIKO SAKAI,[e] JI HO SUH,[a] DOUGLAS H. SIEGLAFF,[a] ANIL DHAWAN,[d] TAKAO SAKAI,[e] DUSKO ILIC,[b] PAUL WEBB[a]

Key Words. Thyroid receptor • Krüppel-like factor 9 • Induced pluripotent stem cell • Human embryonic stem cell • Notch

ABSTRACT

Biological processes require close cooperation of multiple transcription factors that integrate different signals. Thyroid hormone receptors (TRs) induce Krüppel-like factor 9 (KLF9) to regulate neurogenesis. Here, we show that triiodothyronine (T3) also works through TR to induce KLF9 in HepG2 liver cells, mouse liver, and mouse and human primary hepatocytes and sought to understand TR/KLF9 network function in the hepatocyte lineage and stem cells. Knockdown experiments reveal that KLF9 regulates hundreds of HepG2 target genes and modulates T3 response. Together, T3 and KLF9 target genes influence pathways implicated in stem cell self-renewal and differentiation, including Notch signaling, and we verify that T3 and KLF9 cooperate to regulate key Notch pathway genes and work independently to regulate others. T3 also induces KLF9 in human embryonic stem cells (hESCs) and human induced pluripotent stem cells (hiPSC) and this effect persists during differentiation to definitive endoderm and hiPSC-derived hepatocytes. Microarray analysis reveals that T3 regulates hundreds of hESC and hiPSC target genes that cluster into many of the same pathways implicated in TR and KLF9 regulation in HepG2 cells. KLF9 knockdown confirms that TR and KLF9 cooperate to regulate Notch pathway genes in hESC and hiPSC, albeit in a partly cell-specific manner. Broader analysis of T3 responsive hESC/hiPSC genes suggests that TRs regulate multiple early steps in ESC differentiation. We propose that TRs cooperate with KLF9 to regulate hepatocyte proliferation and differentiation and early stages of organogenesis and that TRs exert widespread and important influences on ESC biology. STEM CELLS *2015;33:416–428*

[a]Genomic Medicine, Houston Methodist Research Institute, Houston, Texas, USA; [b]Stem Cell Laboratory, Assisted Conception Unit, Division of Women's Health, King's College London, London, United Kingdom; [c]Guy's and St. Thomas NHS Foundation Trust and King's College Biomedical Research Centre, London, United Kingdom; [d]Institute of Liver Studies, King's College London, London, United Kingdom; [e]Department of Molecular and Clinical Pharmacology, Institute of Translational Medicine, The University of Liverpool, Liverpool, United Kingdom

Correspondence: Paul Webb, Ph.D., Genomic Medicine, Houston Methodist Research Institute, 6670 Bertner Avenue, Houston, Texas 77030, USA. Telephone: 713-441-2516; Fax: 713-441-2178; e-mail: PWebb@houstonmethodist.org

Received February 12, 2014; accepted for publication September 13, 2014; first published online in STEM CELLS *EXPRESS* October 21, 2014.

1066-5099/2014/$30.00/0

http://dx.doi.org/10.1002/stem.1875

INTRODUCTION

Thyroid hormone (TH) receptors (TRs α and β) belong to the nuclear receptor superfamily. TRs occupy thyroid response elements and alter expression of genes in response to the active form of TH (T3). Primary events involved in TH-dependent changes in gene expression are well understood; T3 induces TR conformational changes that facilitate interactions with coregulators which enhance or repress TR-regulated gene transcription [1, 2]. Downstream consequences of TR-dependent induction of genes that encode other transcription factors (TFs) and interplay between TRs and these TFs are less clear.

The Krüppel-like factors (KLFs) are a family of conserved zinc finger TFs that act as transcriptional activators or repressors in a context-dependent manner and are implicated in transcriptional networking and regulation of balance between pluripotency, self-renewal, and differentiation in mouse embryonic stem cells (mESCs) [3, 4]. Expression of one member of this family, Krüppel-like factor 9 (KLF9), is often associated with differentiated states or early stages of differentiation processes [5–7]. Furthermore, TR actions on neurite extension and branching and neuronal differentiation of mammalian and amphibian cells are mediated by induction of KLF9 [5, 8, 9]. Thus, at least one crucial developmental effect of TR signaling involves KLF9. In mESC, simultaneous depletion of three KLFs, KLF2, KLF4, and KLF5 inhibits self-renewal and triggers cell differentiation [10]. KLF9 and KLF4 bind to the Notch1 gene and exert opposite effects on its transcription, thereby influencing the Notch signaling pathway [6]. Notch signaling works with Wnt, FGF, TGFβ/BMP, and Hedgehog signaling pathways [11–15] and converges upon a core transcriptional network that involves Oct4, Nanog, and Sox2 to regulate stem cell maintenance, differentiation, and cellular homeostasis [16]. Thus, alterations in KLF9 levels could greatly influence cell differentiation processes through changes in Notch signaling and other pathways.

There are reasons to suspect that the TR/KLF9 axis is active in many cellular contexts, in addition to neural development. First TRs and KLF9 are detected in multiple tissue types and differentiating cells at different stages of development [4, 17–19]. Second, T3 induces KLF9 in non-neuronal cell types such as epithelial and erythroid cells [20, 21]. Third, TRs and KLF9 play similar roles in particular tissues; both TRα and KLF9 are active in intestinal stem cell regulation [22–24]. Thus, some T3 actions that are ascribed to TR could be results of KLF9 induction. Presently, little is known about the existence and possible roles of TR/KLF9 networking in non-neuronal contexts.

In this study, we show that TR can induce KLF9 in multiple cell types of hepatocyte origin and stem cells and sought to understand roles of the TR/KLF9 signaling network in these contexts using in vitro cell models. We demonstrate that TR activation leads to KLF9 induction in HepG2 cells, nontransformed liver cells, human induced pluripotent stem cells (hiPSC), and in human embryonic stem cells (hESCs) and this effect persists during hiPSC and hESC differentiation to definitive endoderm and mature hepatocytes. Dissection of TR/KLF9 effects reveals important roles in key signaling pathways, including the Notch pathway, in HepG2 and ESCs. T3 effects upon KLF9 in ESCs occur in the context of widespread TR-dependent effects on genes that are implicated in early stages of ESC differentiation. Our data therefore suggest that the TR/KLF9 axis plays important roles throughout several stages of the hepatocyte lineage and in the choice between stem cell renewal and differentiation.

Materials and Methods

Reagents

Triiodothyronine (T3) was from Sigma-Aldrich (Sigma, St. Louis, MO, http://www.sigmaaldrich.com).

Cell Culture

Human HepG2 cells expressing TRα (HepG2-TRα) or TRβ (HepG2-TRβ) were maintained as described [25]. hESC line KCL034 and hiPSC lines iKCL004 and iKCL011 were maintained in either TeSR2 (Stem Cell Technologies, Vancouver, BC; http://www.stemcell.com/) or Nutristem medium (Stemgent, Cambridge, MA, https://www.stemgent.com) on Matrigel-coated six-well plates in the absence of feeder cells. Matrigel-coated plates were prepared by incubating 1 ml of 0.33 mg/ml growth factor reduced Matrigel (BD Biosciences, San Jose, CA, 354230, http://www.bdbiosciences.com) in Dulbecco's modified Eagle's medium (DMEM)/F-12 (Life Technologies, Carlsbad, CA, http://www.lifetechnologies.com) per well for 1 hour at 37°C.

Animals

Experiments were approved by Methodist Hospital IACUC following NIH guidelines for ethical use of animals in biomedical research. C57B/6J mice were purchased from Jackson Laboratory (Bar Harbor, ME, http://www.jax.org) at 9 weeks of age. Animals were maintained on a 12:12 hours light dark cycle, with food and water available ad libitum and were divided into two groups ($n = 4$): control and T_3. Animals were treated for 3 days by oral gavage $\pm$ 1 mg/kg T_3. Three days after, animals were killed and liver tissue collected for RNA purification.

Isolation of Primary Mouse Hepatocytes

Primary mouse hepatocytes were isolated from male C57B/6J mice using Life Technologies Protocol (Life Technologies, Carlsbad, CA, http://www.lifetechnologies.com), plated in collagen-coated plates (Invitrogen, Carlsbad, CA, http://www.invitrogen.com/) and incubated at 37°C for 2–3 hours using Williams' Medium E, + 5 ml penicillin-streptomycin ($\times$100), and 5% fetal bovine serum (FBS). Medium was then changed to HepatoZYME-SFM (Invitrogen, Carlsbad, CA, http://www.invitrogen.com/). Cells were treated with 1 nM, 10 nM, or 100 nM T3 for 16 hours.

Primary Human Hepatocytes

Primary human hepatocytes were a gift from Prof. Dhawan, Hepatocyte Biology and Transplantation Group, King's College London. Hepatocytes were isolated from donor organs rejected for transplantation and consented for research. The research was undertaken with full institutional ethical approval and conducted according to the principles of the Declaration of Helsinki. The procedure is based on papers by Berry and Friend, modified by Seglen, on hepatocyte isolation from rat livers [26, 27]. Briefly, liver is perfused with 500 ml oxygenated HBSS-EGTA (Lonza, Walkersville, MD, www.lonza.com) prior to perfusion with oxygenated EMEM (Lonza, Walkersville, MD, www.lonza.com) supplemented with collagenase-P for 15 minutes. Tissue is filtered and centrifuged at 50*g* for 5 minutes twice. The pellet contains hepatocytes separated from nonparenchymal cells and dead cells and are used fresh or cryopreserved in University of Wisconsin solution supplemented with 10% DMSO and 4% glucose, using a controlled-rate freezer.

Endoderm Differentiation

hESC (KCL034) and hiPSC (iKCL004 and iKCl011) were differentiated as a monolayer into definitive endoderm [28]. Undifferentiated cells, at 80% confluence, were induced to differentiate by culturing in RPMI-based serum-free medium + 10% serum-free defined medium (SFD), Wnt3a (40 ng/ml), and Activin A (100 ng/ml) for 1 day. For the next 2 days, media were switched to RPMI supplemented with BMP4 (0.5 ng/ml), basic fibroblast growth factor (bFGF) (10 ng/ml), Activin A (100 ng/ml), and vascular endothelialgrowth factor (VEGF) (10 ng/ml). The last 2 days, cells were maintained in SFD + BMP4 (0.5 ng/ml), bFGF (10 ng/ml), Activin A (100 ng/ml), and VEGF (10 ng/ml). SFD serum-free medium consists of 75% Iscove's modified Dulbecco's medium (IMDM) (Invitrogen, Carlsbad, CA, http://www.invitrogen.com/), 25% Ham's F-12 (Mediatech, Inc., Cellgro, Manassas, VA 20109, http://www.cellgro.com), 0.5$\times$ N2-Supplememt (Gibco/Life Technologies, Carlsbad, CA, http://www.lifetechnologies.com/ipac/en/home/brands/gibco.html), 0.5$\times$ B27 without retinoic acid, 0.1% bovine serum albumin (BSA) (Sigma, St. Louis, MO, http://www.sigmaaldrich.com), 50 μg/ml ascorbic acid, and 4.5×10^{-4} M monothioglycerol.

Precommercial iCell highly purified iPSC-derived human hepatocytes (iHep) were purchased from Cellular Dynamics International (CDI; Madison, WI, http://www.cellulardynamics.com). Cells were maintained according to iCell Hepatocytes User's Guide (CDI; Madison, WI, http://www.cellulardynamics.com).

Quantitative Real-Time PCR

Total RNA was prepared using the RNeasy mini-kits (Qiagen, Venlo, Limburg, http://www.qiagen.com). For HepG2, Aurum

Total RNA kit (Bio-Rad, Hercules, CA, http://www.bio-rad.com/) was used. Reverse transcription reactions were performed using 1 μg total RNA with an iScript cDNA Synthesis kit (Bio-Rad, Hercules, CA, http://www.bio-rad.com). Quantitative real-time PCR (qPCR) was performed with the Roche LightCycler 480 RT PCR Instrument using SYBR Green Mastermix (Roche, Mannheim, Germany, www.roche.com). Primer sequences are available per request. Data were collected and analyzed using comparative threshold cycle method with β-actin and 18S rRNA as reference. Experiments were performed at least three times, and mean $\pm$ SD was calculated and statistical analysis was performed using Prism curve-fitting program (GraphPad Prism, version 6.01).

RNA Interference

HepG2-TRβ cells were plated in 10% FBS-DMEM/F-12 media and grown to 50% confluence. Cells were transfected with TRβ or KLF9 ON-TARGET plus SMART pool siRNA (Dharmacon, Waltham, MA, http://www.thermoscientificbio.com/Dharmacon/) at 50 nM final concentration. Positive and negative nontargeting control siRNAs were also from Dharmacon. After 3 days, cells were treated with 100 nM T3 for 8 or 24 hours and RNA or protein prepared.

hESC (KCL034) and hiPSC (iKCL004 and iKCL011) were plated at 125,000/well of six-well dish and transfected with 5 μM nontargeting control or siKLF9 with DharmaFECT1 according to manufacturer's protocol 2 days later. Cells were exposed to 100 nM T3 for 18 hours 2 (for RNA) or 3 (for protein isolation) days post-transfection.

Western Blotting

Total proteins were separated with 4%–12% gradient Bis-Tris gels (Invitrogen, Grand Island, NY, http://www.invitrogen.com/), transferred to polyvinylidene fluoride (PVDF) membranes (Bio-Rad, Hercules, CA, http://www.bio-rad.com/), and incubated with anti-KLF9 antibody (Santa Cruz Biotechnology, Dallas, TX, www.scbt.com) followed by anti-mouse IgG Ab conjugated with HRP (Santa Cruz Biotechnology, Santa Cruz Biotechnology, Dallas, TX, www.scbt.com). A Luminata Classico Western HRP Substrate (EMD Millipore, Billerica, MA, www.millipore.com) was used for protein detection.

Microarray Analysis

Human HT-12_v4 whole genome expression arrays were from Illumina (Illumina, San Diego, CA, http://www.illumina.com/). cRNA synthesis and labeling were performed using Illumina TotalPrep-96 RNA Amplification Kit (Ambion/Life Technologies, Carlsbad, CA, http://www.lifetechnologies.com/us/en/home/brands/ambion.html). Labeling in vitro transcription reaction was performed at 37°C for 14 hours. Biotinylated cRNA samples were hybridized to arrays at 58°C for 18 hours according to manufacturer's protocol. Arrays were scanned using BeadArray Reader.

Unmodified microarray data obtained from GenomeStudio were background-subtracted and quantile-normalized using the lumi package [29] and analyzed with the limma package [30] within R [31]. Effect of KLF9 knockdown was determined through comparison between non-T3 treated control and KLF9 knockdown. T3-response was determined by comparing cells treated with T3 for 8 or 24 hours against their respective untreated controls. All analyses were corrected for multiple hypothesis testing [32], and effects determined as significant when more than or equal to twofold with an adjusted *p*-value $\leq$.05. To facilitate comparisons among datasets, all data were uploaded into a SQLite3 database (http://www.sqlite.org/).

Pathway Enrichment Analysis (GeneCodis)

We used the GeneCodis analysis (http://genecodis.cnb.csic.es/) to identify enriched pathways and functional themes. GeneCodis integrates different information resources (GO, Panther pathways, SwissProt, etc.), searches, and arranges gene set annotation by statistical significance [33–35]. Genes of interest, defined as at least twofold differentially expressed according to microarray, were uploaded as standard human gene symbols and genes in the interaction network with false discovery rate (FDR) $<$0.05 were taken into consideration.

GeneMANIA

We used GeneMANIA (http://www.genemania.org) to find genes related to input genes, using a very large set of functional interaction data [36–38]. Inputs were differentially expressed genes underlying specific functional themes and pathways as identified by GeneCodis. We focus analysis on high confidence physical interactions (from various protein interaction databases included in GeneMANIA) and pathway interactions (from Reactome pathway database).

Ingenuity Pathway Analysis

Data were also analyzed using ingenuity pathway analysis (Ingenuity Systems; IPA, Redwood City, CA, http://www.ingenuity.com). Genes of interest, defined as at least twofold differentially expressed, were uploaded. Each gene identifier was mapped to its corresponding gene object in the ingenuity pathways knowledge base (IPKB). The IPKB, containing a large network of curated molecular interactions and pathways, was searched to find subnetworks enriched in genes of interest.

Immunostaining

hESC/iPSC-derived definitive endoderm cells grown as a monolayer were fixed in 3.8% paraformaldehyde for 20 minutes, permeabilized in 0.5% Triton X-100/phosphate buffered saline (PBS) for 5 minutes, washed in PBS, and incubated with goat anti-GATA4 polyclonal Ab (R&D Systems cat. no. 2606; Minneapolis, MN; www.rndsystems.com) overnight at +4°C. Samples were washed, incubated with rhodamine X-conjugated donkey anti-goat IgG antibodies, and washed again 3$\times$ in PBS. In the second wash 10 μg/ml Hoechst 33342 (Life Technologies, Carlsbad, CA, http://www.lifetechnologies.com) was added to visualize nuclei. Samples were mounted in Vectashield (Vector Laboratories, Burlingame, CA; www.vectorlabs.com) and analyzed with an epifluorescence microscope (Nikon, model E50i) equipped with Retiga 400R cooled monochrome camera (QImaging, Surrey, BC; www.qimaging.com). Images were processed using AdobePhotoshop CS5 software.

Results

T3 Activates KLF9 in Hepatocytes

Our previous analysis of T3 response in parental HepG2 and HepG2 cells that stably express either TRα or TRβ [25] suggested that KLF9 is a T3 inducible-target in this cell

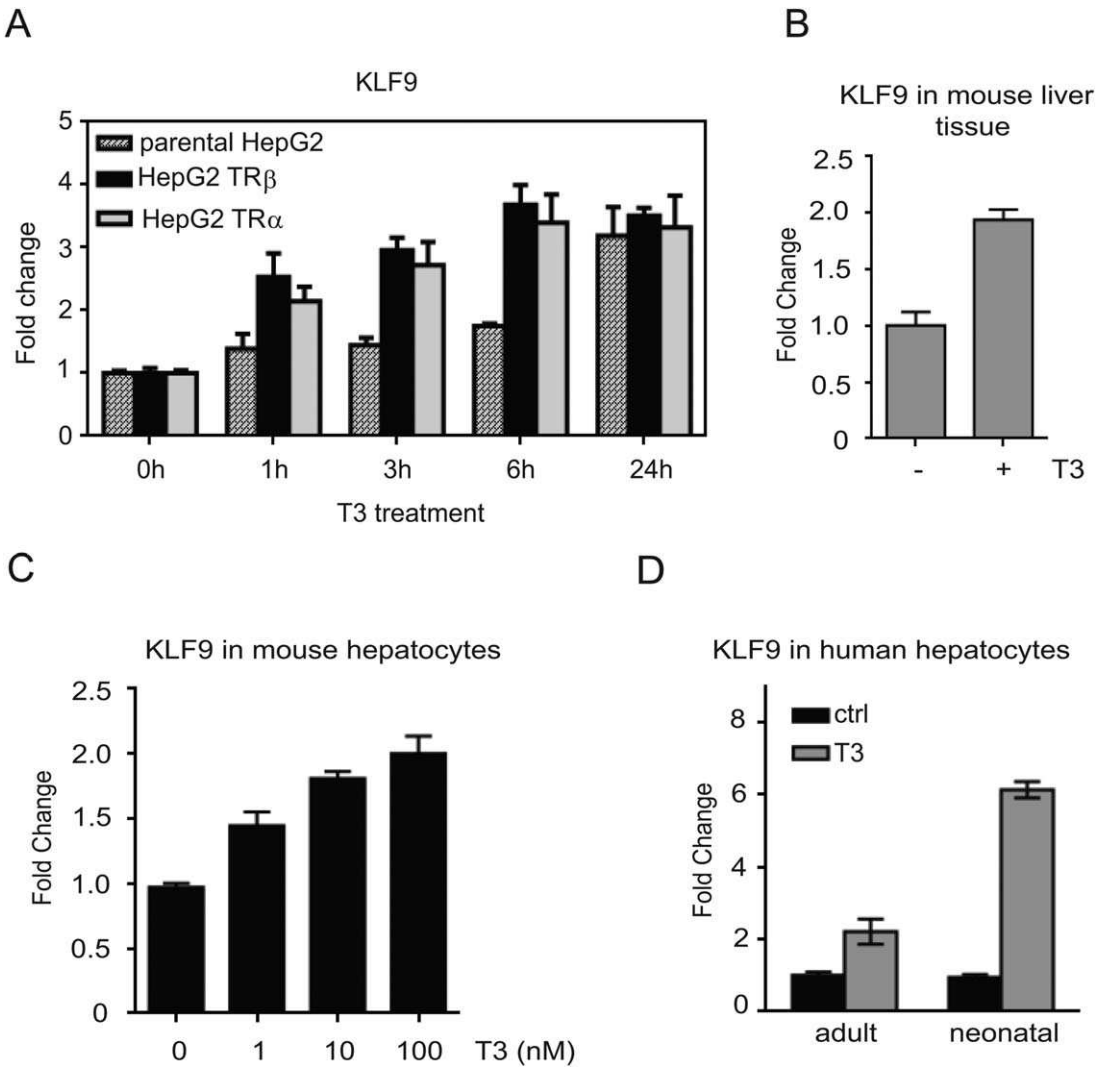

Figure 1. T3 induces KLF9 in HepG2 cells and in hepatocytes. **(A)**: Parental HepG2, HepG2-TRβ, and HepG2-TRα cells were treated with 100 nM T3 for the indicated times and KLF9 mRNA levels were determined by quantitative real-time PCR (qPCR). **(B–D)**: Expression of KLF9 after T3 treatment was assessed by qPCR in mice liver tissue (B), in isolated mice hepatocytes treated with increasing concentrations of T3 (C), and human hepatocytes isolated from neonatal and adult livers (D).

background. We used qRT-PCR to verify T3-activation of KLF9 in these cells (Fig. 1A). T3 response was observed at 24 hours in parental HepG2, which express very low levels of TRβ [39] (Fig. 1A) but more rapid T3 induction was observed in both HepG2-TR cell lines, occurring within one hour of T3 treatment and maintained up to 24 hours (Fig. 1A). T3-induction of KLF9 persisted after pretreatment with protein synthesis inhibitor cycloheximide (CHX) in HepG2-TRβ cells (Supporting Information Fig. S1A). Thus, T3 induction of KLF9 is a direct effect that does not require new protein synthesis. The specific role for TRβ was confirmed by siRNA (Supporting Information Fig. S1B, S1C).

Since HepG2 cells are a liver carcinoma cell line, we verified the effect of T3 on KLF9 expression in mouse liver. We treated 9 weeks old C57/Bl6 male mice $\pm$ T3 by daily oral gavage. After 3 days, we isolated livers and showed that T3 induced KLF9 about twofold (Fig. 1B). We confirmed that KLF9 was not expressed in cholangiocytes, as judged by absence of colocalization with the cholangiocyte marker CK19 (Supporting Information Fig. S2). We also confirmed that T3 induced KLF9 in mouse primary hepatocytes in a dose-dependent fashion (Fig. 1C) and that T3 treatment of human primary hepatocytes (adult and neonatal) resulted in an increase in KLF9 expression (Fig. 1D). Thus, the TR/KLF9 axis is active in transformed and nontransformed hepatocytes.

KLF9 Regulates Multiple Genes in HepG2 and Influences T3 Response

To define roles of KLF9 and the TR/KLF9 network in HepG2, we used siRNA to silence KLF9 expression in HepG2-TRβ cells. We verified that KLF9 levels were reduced in specific siRNA treated cells versus cells that were treated with control siRNA (97% reduction of mRNA and protein) (Supporting Information Fig. S3A). Although KLF9 levels were almost completely suppressed, some T3 induction of KLF9 persisted (Supporting Information Fig. S3B).

Microarray analysis revealed 368 genes that displayed more than twofold change after KLF9 knockdown, with 226 downregulated and 142 upregulated (Fig. 2A). Effects were confirmed by qRT-PCR analysis of representatives of both classes of gene (downregulated Lama1 and Aldoc, upregulated Snord 3A and 3D, Fig. 2B). Thus, KLF9 regulates large numbers of genes in HepG2 and can act as a transactivator and transrepressor.

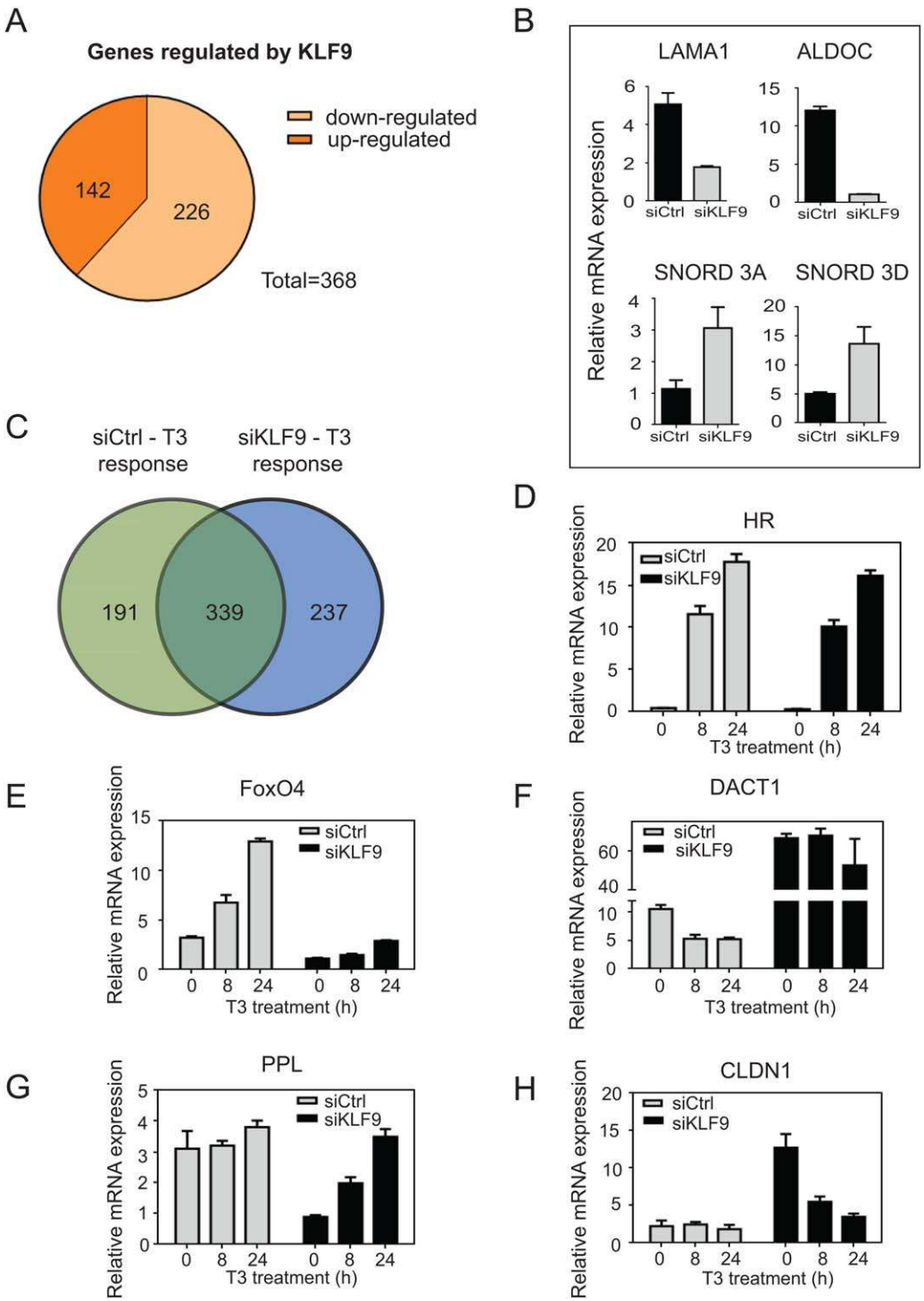

Figure 2. TR/KLF9 axis regulates multiple genes in HepG2 cells. **(A)**: Differential gene regulation in HepG2-TRβ cells after KLF9 silencing revealed by microarray analysis. Microarray data obtained from human Illumina HT-12_v4 gene chips from control versus KLF9 knockdown were analyzed using Limma package within R. Effects determined to be significant when more than or equal to twofold with an adjusted p-value $\leq$ .05. **(B)**: Effects of KLF9 knockdown confirmed at representatives of both classes of gene by quantitative real-time PCR. **(C)**: Differential gene regulation by T3 in control and siKLF9 cells revealed by microarray analysis. **(D–H)**: Cells were treated with 100 nM T3 and qRT-PCR was performed to verify patterns of KLF9-dependency of T3 response. Data are represented as mean $\pm$ SD. Microarray data are deposited in the Gene Expression Omnibus; http://www.ncbi.nlm.nih.gov/geo/query/acc.cgi?token=sxkvckgwhxmfdgx&acc=GSE54699; accession number GSE54699.

To understand whether KLF9 knockdown might influence T3 response, we treated siControl and siKLF9 HepG2-TRβ cells with T3 for 8 and 24 hours and performed microarray analysis. In accordance with previous results, 530 genes displayed T3 response (more than twofold) in siControl HepG2 cells, with more genes displaying T3 response at 24 hours (Supporting

Table 1. Pathway enrichment analysis of KLF9-dependent transcriptome. Canonical pathways obtained from GeneCodis using Panther pathways database. Gene co-occurrence annotation found by GeneCodis for the genes differentially expressed (FC $>$ 2, $p < .05$ corrected for multiple testing) between siCtrl versus siKLF9 HepG2-TRβ samples (KLF9 pathways) and integration of KLF9 targeted and TR/KLF9 targeted pathways. *p*-Values have been obtained through hypergeometric analysis (Hyp) corrected by FDR method (Hyp*).

NGR	NG	Hyp	Hyp*	Annotations (panther pathways)
KLF9 pathways				
91	7	1.86E-05	0.00011164	P00052: TGF-beta signaling pathway
66	5	0.0003218	0.00096552	P00003: Alzheimer disease-amyloid secretase pathway
109	5	0.0030787	0.00461811	P00021: FGF signaling pathway
280	8	0.0039947	0.00479375	P00057:Wnt signaling pathway
107	5	0.0028423	0.00568463	P00006: Apoptosis signaling pathway
198	6	0.0092045	0.00920453	P00031: Inflammation mediated by chemokine and cytokine signaling pathway
TR/KLF9 pathways				
91	9	4.60E-05	0.00103529	P00052: TGF-beta signaling pathway
280	16	7.02E-05	0.00105367	P00057: Wnt signaling pathway
107	9	0.000162	0.00182779	P00006: Apoptosis signaling pathway
66	7	0.000207	0.00186532	P00003: Alzheimer disease-amyloid secretase pathway
70	8	4.28E-05	0.00192706	P00016: Cytoskeletal regulation by Rho GTPase
114	9	0.000262	0.0019674	P00018: EGF receptor signaling pathway
118	9	0.000339	0.00218076	P00004: Alzheimer disease-presenilin pathway
36	5	0.000483	0.00271783	P00045: Notch signaling pathway
109	8	0.000924	0.00415905	P00021: FGF signaling pathway
72	6	0.002094	0.00589054	P00019: Endothelin signaling pathway
96	7	0.001980	0.00594038	P00036: Interleukin signaling pathway
198	10	0.003794	0.00898646	P00031: Inflammation mediated by chemokine and cytokine signaling pathway
69	5	0.008789	0.0146485	P04393: Ras Pathway
126	6	0.029072	0.0408832	P00029:Huntington disease
128	6	0.031068	0.0411201	P00047: PDGF signaling pathway

NGR: Number of annotated genes in the reference list; NG: Number of annotated genes in the input list; Hyp: Hypergeometric pValue; Hyp* Corrected hypergeometric pValue.

Information Table S1). Comparison of genes that responded to KLF9 knockdown or T3 in siControl cells revealed significant overlap between datasets, with 68 genes regulated by both factors (Supporting Information Fig. S4). More surprisingly, KLF9 knockdown also altered the pattern of T3 response. Numbers of T3 responsive genes were similar in control and KLF9 knockdown cells (530 and 576 genes, respectively, Supporting Information Table S1). While most T3 responsive genes were unaffected by KLF9 knockdown (339 genes displayed similar responses in control and KLF9 knockdown cells), 191 T3 target genes displayed reduced T3 response after KLF9 knockdown and 237 genes gained T3 response (Fig. 2C). We confirmed that genes that responded to T3 in the presence and absence of KLF9 were truly KLF9 independent (HR, Fig. 2D). We also confirmed positive and negative T3 responses that were dependent upon KLF9 (FoxO4 and DACT1; Fig. 2E, 2F) and T3 responses that emerged after KLF9 knockdown (PPL and CLDN1, Fig. 2G, 2H). We also detected genes that showed changes in overall expression after KLF9 knockdown, but retained similar T3 response (alkaline phosphatase, intestinal (ALPI), Supporting Information Fig. S5). Thus, T3 and KLF9 display overlapping effects upon gene expression in HepG2 and many T3 responses are modulated by KLF9.

TR/KLF9 Axis Regulates Key Signaling Pathways

To define roles of defined KLF9 target genes in HepG2 we used GeneCodis software analysis (http://genecodis.cnb.csic.es) [33–35] to examine functions of genes that displayed altered expression after KLF9 knockdown. Candidate genes were assigned to pathways and processes listed in Table 1 (upper section) and Supporting Information Table S2, respectively, with differentially expressed genes listed in Supporting Information Tables S3, S4. The main KLF9-dependent pathways were TGFβ signaling, Alzheimer's disease-amyloid secretase pathway, FGF and Wnt signaling (Table 1). The most important processes were signal transduction, cell adhesion, aging, and cell differentiation (Supporting Information Table S2).

We also analyzed T3 responsive pathways and processes (Supporting Information Table S5). Interestingly, only two of the top six KLF9-dependent pathways (TGFβ and FGF pathway) and three processes (transmembrane transport, cell death, and protein folding) were purely KLF9-responsive. Other KLF9 responsive pathways and processes were also flagged as T3 responsive (Table 1-green, Supporting Information Table S2-green).

Analysis of an integrated gene set that included KLF9 responsive gene targets (Fig. 2A) and T3-regulated gene targets with altered response to KLF9 knockdown (Fig. 2C) yielded more statistically enriched pathways (Table 1, lower section) and processes (Supporting Information Table S6). Together, T3 and KLF9 are active in the Notch pathway as well as the EGF, Ras, and platelet-derived growth factor (PDGF) regulated pathways (Table 1-blue). Furthermore, T3 and KLF9 influenced processes such as cell proliferation and metabolic pathways (Supporting Information Table S6-blue; differentially expressed genes in Supporting Information Tables S7, S8). Thus, there are overlaps between KLF9- and T3-dependent pathways and processes in HepG2, and TR and KLF9 cooperate to influence signaling pathways that would not be identified by consideration of actions of either T3 or KLF9 alone.

TR/KLF9 Axis Regulates Multiple Components of the Notch Pathway

Since Notch signaling emerged as a major target pathway regulated by T3 and KLF9 and because Notch signaling also plays important roles in liver development and regeneration, we

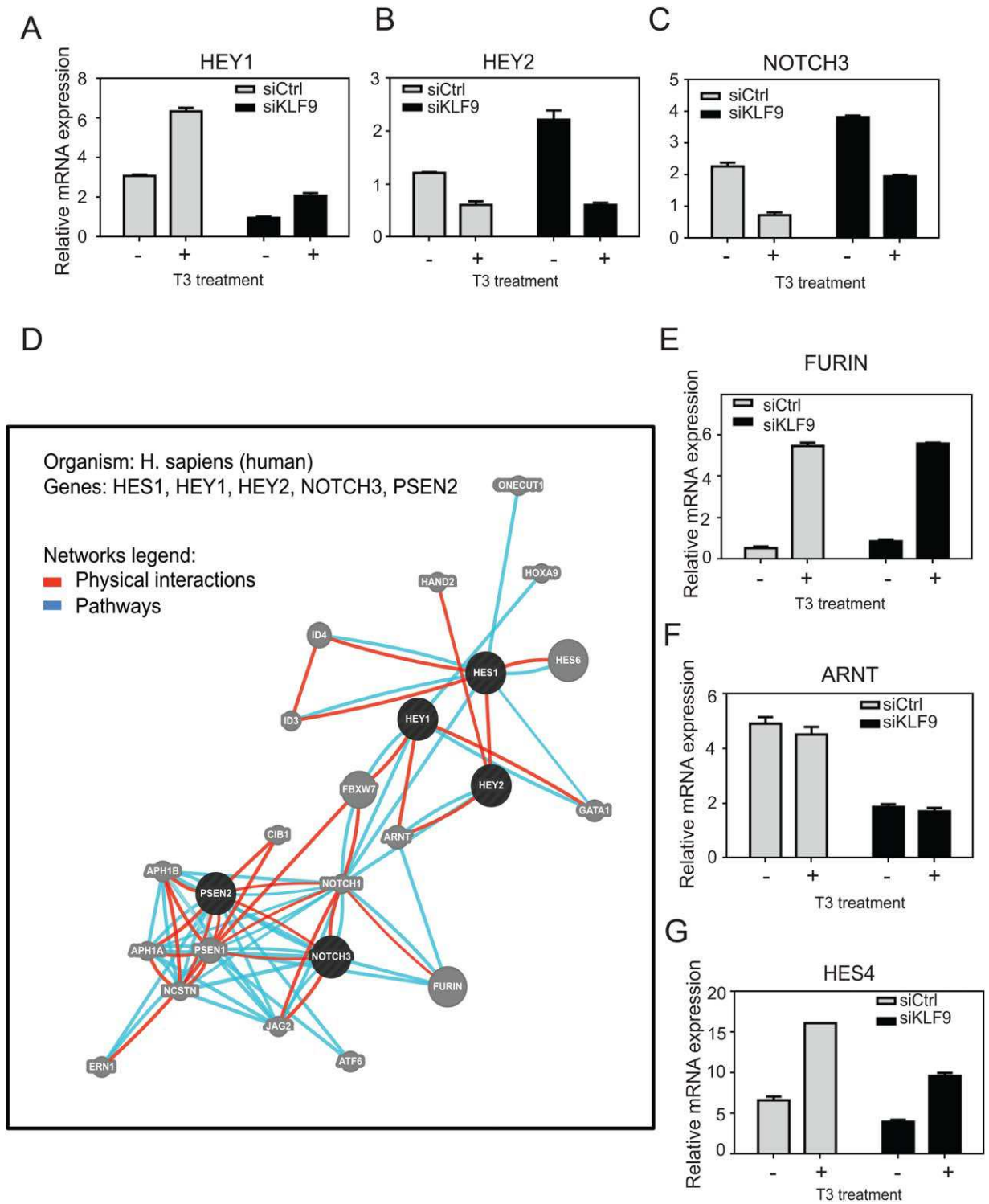

Figure 3. TR/KLF9 axis and the Notch pathway. **(A–C)**: Cells were treated with 100 nM T3 and qRT-PCR was performed to verify TR/KLF9-dependency of identified Notch pathway genes. **(D)**: Network of interactions among Notch pathway KLF9 targets, as retrieved by the GeneMania. Circles represent genes and connecting lines represent interactions between genes. GeneMania retrieved known and predicted interactions between these genes and added extra genes (gray circles) that are strongly connected to query genes. **(E–G)**: Quantitative real-time PCR verification of genes identified by GeneMania as part of TR/KLF9-Notch network. All data are represented as mean ± SD.

explored links between T3, KLF9, and Notch in HepG2. We verified regulation patterns of the five flagged T3/KLF9 target genes with qRT-PCR (HEY1, HEY2, NOTCH3, PSEN2, and HES1) (Table 1, Supporting Information Table S7). This confirmed that HEY1, HEY2, and NOTCH3 all displayed T3 response and that expression levels of these genes were changed by KLF9 knockdown (Fig. 3A–3C). Furthermore, PSEN2 and HES1 transcript levels were, respectively, greatly reduced and elevated by KLF9 knockdown (not shown).

We next performed GeneMania analysis to identify Notch networking partners (http://www.genemania.org); this approach uncovers genes related to input genes, using a large set of functional interaction data [36–38]. We generated the network using a query of the five Notch signaling components identified as T3 and/or KLF9 regulated (Fig. 3A–3C, Supporting Information Table S7). We focused analysis only on high confidence pathway interactions (reactome pathway database; Fig. 3D, blue lines) and physical interactions (various protein interaction databases; GeneMANIA; Fig. 3D, red lines). This strategy uncovered tight networking of the 5 input genes with 20 associated genes. Of these 20 genes, three were also flagged as T3 and/or KLF9 targets in microarray analysis (ID3, Furin, ARNT), underscoring links between TR/KLF9 and Notch. We used qRT-PCR to confirm that ID3 exhibited strong regulation by T3 and KLF9 response (not shown) and that Furin and ARNT were responsive only to T3 and KLF9, respectively (Fig. 3E, 3F). A limited survey of additional genes implicated in Notch signaling revealed that KLF9 and T3 also cooperate to regulate HES4 (Fig. 3G). Thus, T3 and KLF9 regulate multiple Notch pathway genes in HepG2 and TR/KLF9 targets are involved in multiple aspects of Notch signaling (Discussion).

TR/KLF9 Axis Is Active in Embryonic Stem Cells and Definitive Endoderm

Since TR regulates KLF9 in hepatocytes, we asked whether TR might also regulate KLF9 during differentiation along the hepatocyte lineage in culture. We assessed KLF9 expression in two hiPSC lines, iKCL004 and iKCL011 [40] and the hESC line KCL034 [41] (Fig. 4A). While KLF9 is detectable in all three cell lines (iKCL004, iKCL011, and KCL034), its expression was profoundly reduced in comparison to dermal BJ fibroblasts from which the iPSCs were reprogrammed (Fig. 4A). Even though TRα was the predominant TR isoform in these cell lines (Supporting Information Fig. S6), T3 treatment for 6 and 18 hours resulted in robust increase in KLF9 mRNA in all three pluripotent stem cell lines, but not BJ fibroblasts (Fig. 4A).

We differentiated lines into definitive endoderm [28]. As expected, expression of pluripotency markers Nanog and Oct4 decreased during definitive endoderm differentiation and endoderm markers MIXL1 and SOX17 emerged (Supporting Information Fig. S7A). We also confirmed that the majority of cells turned into endoderm by GATA4+ immunostaining (Supporting Information Fig. S7B). TRα remained the prevalent isoform during this process (Supporting Information Fig. S6) and T3 treatment again induced KLF9 in definitive endoderm from all stem cell lines (Fig. 4B).

Finally, we asked whether TR/KLF9 axis is active in highly purified terminally differentiated hiPSC-derived hepatocytes. Like mature hepatocytes, these cells predominantly expressed TRβ (Supporting Information Fig. S6) and, here, T3 also increased KLF9 expression (Fig. 4C). Thus, T3 induces KLF9 in human ESCs and at early and late stages of hepatocyte differentiation in vitro in a manner that is independent of TR subtype.

T3 Exhibits Cell-Specific Effects on Notch Genes in ESCs

To explore TR function in ESCs, we performed microarray analysis on KCL034, iKCL004, and BJ lines treated with T3 for 6 hours. The analysis revealed 820 and 826 genes changed in KCL034 and iKCL004, respectively, and no change in BJ cells (Supporting Information Table S9).

Analysis of T3 target genes using GeneCodis analysis confirmed that T3 regulates many key pathways previously recognized as targets of TR or the TR/KLF9 axis in HepG2, including Notch, Wnt, and FGF (Supporting Information Table S10) along with others such as angiogenesis, cadherin, and endothelin pathways. However, closer investigation of T3 effects upon individual Notch pathway genes revealed differences from HepG2. HEY2 and HES4 appeared as T3 targets in ESCs, as seen in HepG2 (Supporting Information Table S11), but Notch3, HEY1, and FURIN did not respond to T3 in any of pluripotent stem cell lines tested (not shown). Conversely, several Notch genes responded to T3 in stem cells and not in HepG2 (HES5, LFNG, and DLK1) (Fig. 4H, Supporting Information Fig. S8). Thus, T3 displays cell-specific effects upon key Notch pathway genes.

KLF9-Dependency of Notch Genes in ESCs

To determine whether KLF9 might regulate Notch signaling in human pluripotent stem cells, we silenced KLF9 in iKCL004, iKCL011 and KCL034 cells (Fig. 4D, 4E). RNA and Western analysis showed an average of 85%, 75%, and 72% knockdown of KLF9 in iKCL004, iKCL011, and KCL034, respectively, relative to scrambled siRNA control (Fig. 4D) with T3-dependent induction of KLF9 also significantly reduced (Fig. 4E). In these cells, KLF9 knockdown reduced basal levels and T3 response of T3/KLF9 targets HES4 and HES5 (Fig. 4F, 4H). Additionally, PSEN2 and ARNT, pure KLF9-targets in HepG2 cells (Fig. 3), also exhibited similar pure KLF9-dependency in stem cells (Fig. 4G and not shown). There was no change in the expression of T3 target genes LFNG and DLK1 after KLF9 knockdown (not shown). Thus, TR and KLF9 cooperate to regulate key Notch pathway genes in stem cell lines, and work independently to regulate others, but precise effects are cell type specific (Discussion).

T3-Dependent Changes in Differentiation-Related Gene Expression in Stem Cells

To gain insight into T3 regulated biological processes in ESCs, we performed IPA (version Fall 2013) to determine functional pathways of identified genes. IPA scans input genes to identify networks using the IPKB for interactions between "target genes" and known and hypothetical interacting genes stored in the IPA software (in our study, input genes were differently expressed after T3 treatment). This revealed that T3 target genes clustered into categories related to embryonic development and differentiation (Table 2).

We used qRT-PCR to confirm selected T3 responses. T3 induces important differentiation-related genes such as HHEX, one of the earliest markers of anterior endoderm, which gives rise to foregut organs such as the liver, ventral pancreas, thyroid, and lungs [42], HAND1, a TF that is critical for the development of three embryologically distinct lineages: trophoblast of the placenta, extraembryonic mesoderm derivatives and cardiomyocytes [43], and the octamer TF POU3F1, which participates in cell fate determination [44] (Fig. 5A). Conversely, T3 represses the crucial ES pluripotency regulator Nanog (Fig. 5B, 5C). Thus, T3 triggers changes in genes involved in ESC differentiation.

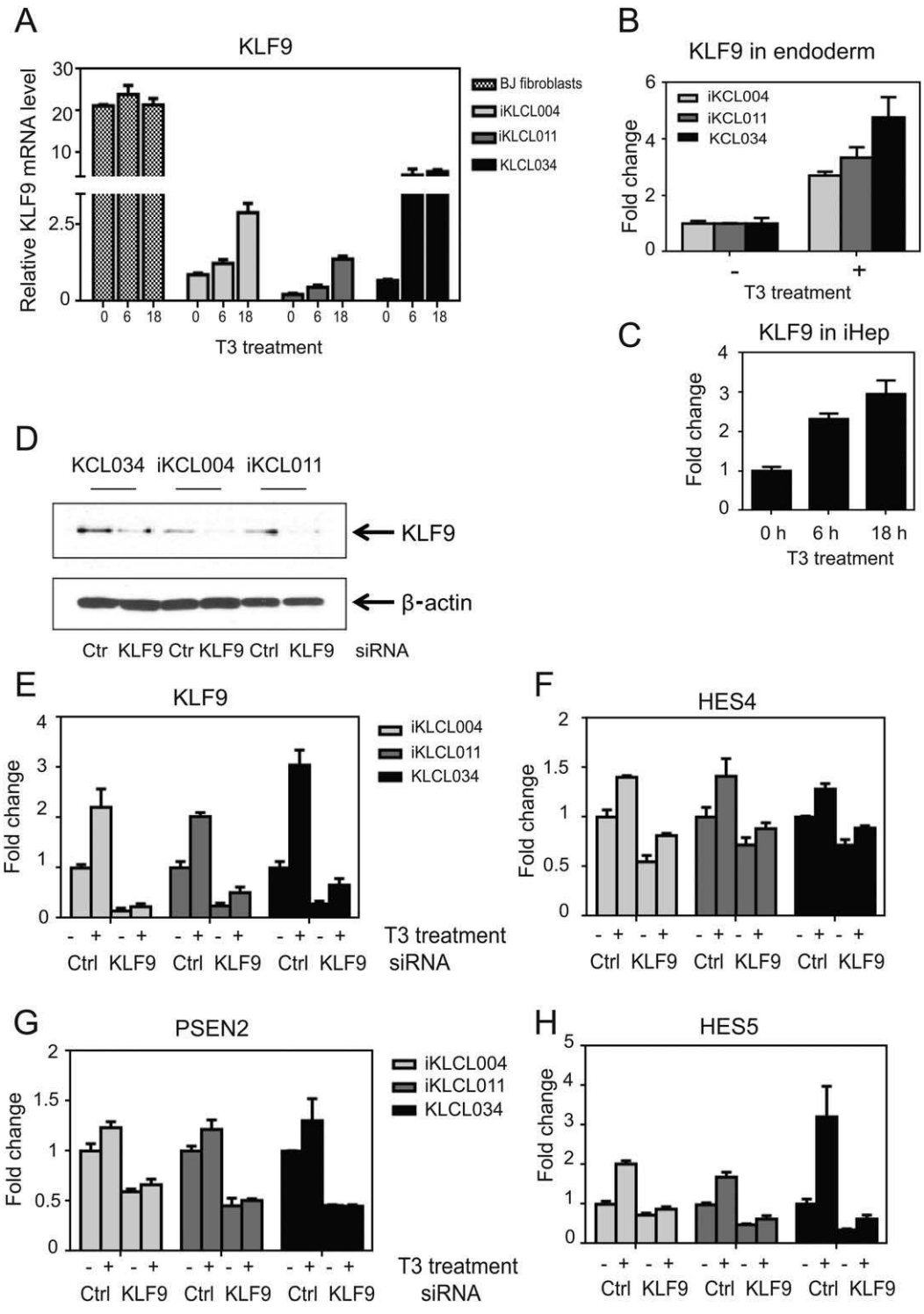

Figure 4, Webb P.

Figure 4. TR/KLF9 axis is active in embryonic stem cells, definitive endoderm, and human induced pluripotent stem cell (hiPSC)-derived hepatocytes. **(A–C)**: Quantitative real-time PCR (qPCR) analysis of KLF9 expression levels −/+T3 in BJ fibroblasts, iKCL004, iKCL011, and KCL034 cells (A), endoderm differentiated from iKCL004, iKCL011, and KCL034 (B), and terminally differentiated hiPSC-derived hepatocytes (C). KLF9 mRNA levels were expressed as fold change. All data are represented as mean ± SD. **(D–H)**: TR/KLF9 axis is involved in regulation of Notch signaling in hiPSC and human embryonic stem cell. (D): Western blot for KLF9 from cell lysates from iKCL004, iKCL011, and KCL034 transfected with Ctrl or KLF9 siRNA. (E–H): iKCL004, iKCL011, and KCL034 cells transfected with Ctrl or KLF9 siRNA were treated with 100 nM T3 for 18 hours. KLF9, HES4, PSEN2, and HES5 mRNA levels were determined by qPCR. The data are presented as fold change of mRNA levels in Ctrl nontreated samples. All data are represented as mean ± SD.

Discussion

It is important to understand how TR-dependent cascades of alternate TFs contribute to T3 regulation of physiologic processes. This study was initially prompted by our observation that TRs regulate KLF9 in HepG2 liver cells and nontransformed hepatocytes. Previous studies implicate KLF9 in regulation of the balance of cellular renewal and differentiation and TR-dependent induction of KLF9 in neural development [5, 8, 9], but the role of their cooperation in hepatocytes is unknown. TR activation regulates hepatocyte proliferation and development [45, 46] and, conversely, induces regression of carcinoma-induced hepatic nodules and reduce incidence of hepatocarcinoma [47, 48]. Moreover, KLF9 regulates the balance between cell differentiation and self-renewal [6, 9]. Thus, investigation of the TR/KLF9 axis in hepatocytes could yield insights into the ways that TRs influence liver regeneration and cancer.

We used the HepG2 system to define TR/KLF9 effects in a hepatocyte background. siRNA knockdown revealed hundreds of KLF9-dependent genes in this cell type with 10%–15% of T3 regulated genes identified in this study, and previous studies [25, 49], also being KLF9 targets (Supporting Information Fig. S4). KLF9 knockdown also reduced T3 response of a large proportion of TR target genes (Fig. 2C). Thus, we suggest that some T3 responsive HepG2 target genes are regulated indirectly through induction of KLF9. In this regard, 35% of T3 responses in HepG2 cells are indirect, as judged by sensitivity to the protein synthesis inhibitor CHX [25]. Inspection of this CHX sensitive dataset reveals many genes flagged as KLF9 targets in this study (not shown).

Surprisingly, some genes displayed emergent T3 response after KLF9 knockdown. We have not assessed mechanisms of this effect, but we note that KLF9 knockdown often results in large alterations of basal expression of this gene class (Fig. 2G, 2H). Thus, we suggest that emergent T3 responses may occur at genes that display close to maximal KLF9 response in HepG2; T3-dependent increases in remaining low levels of KLF9 that persist after siRNA treatment are sufficient to partly rescue effects of KLF9 knockdown.

The fact that large numbers of genes respond to T3 and KLF9 in HepG2 allowed us to define pathways that, respectively, depend upon T3, KLF9, and T3+KLF9. KLF9 target genes are active in pathways implicated in stem cell pluripotency and differentiation, including TGFβ, FGF, and Wnt (Table 1, Fig. 5D). Analysis of an integrated dataset of KLF9- and T3-target genes flagged additional pathways, including Notch, crucial for liver development and regeneration [50–56]. Detailed analysis of T3+KLF9 targets in the Notch pathway revealed multiple genes coordinately regulated by T3 and KLF9 (HEY1, HEY2, HES4, Notch3, and ID3) and others that were purely regulated by T3 (Furin) or KLF9 (PSEN2 and ARNT).

Given connections between TR, KLF9, and Notch signaling in hepatocytes, we determined whether T3 also regulates KLF9 during hepatocyte differentiation from ESCs. Unexpectedly, T3 induced KLF9 in ESCs and hiPSC derived from BJ fibroblasts, but not BJ fibroblasts themselves, and this effect persisted throughout differentiation to definitive endoderm and mature hepatocytes (Fig. 4). Microarray analysis revealed more than 800 T3-regulated genes in hiPSC and these genes cluster into many of the pathways recognized as TR/KLF9 responsive in HepG2, including Notch, FGF, and Wnt. Silencing of KLF9 in hESC and hiPSC confirmed that the TR/KLF9 axis regulates Notch pathway genes in ESCs, as seen in HepG2, albeit in cell-type-specific fashion. Thus, the TR/KLF9 axis is active in ESCs, remains active through early and late stages of hepatocyte differentiation, and plays important cell-specific roles in regulation of ESC Notch signaling genes.

Our studies do not yet allow us to precisely define how T3 and KLF9 affect Notch-dependent behavior of different cell types. We note, however, that T3 and/or KLF9 regulate genes involved in upstream Notch signaling events (Notch3, Furin, and PSEN2), members of the HES/HEY family of TFs that are downstream targets of the Notch pathway and a gene that is part of noncanonical Notch pathways (ARNT) (Supporting Information Fig. S9) [57–59]. Thus, TR and KLF9 regulate multiple branches of the Notch pathway and the fact that T3 and KLF9 cooperate to regulate genes of the HES/HEY family, which constitute outputs of Notch signaling, in a cell-type-specific manner suggests that T3 and KLF9 could influence Notch pathway activity in a cell type-specific manner. HEY/HES TFs are differentially and specifically expressed in different cell types [60], display an oscillatory expression pattern, and control timing of biological events [61, 62]. Thus, TR/KLF9-dependent changes in HES/HEY expression could have

Table 2. Functional categorization of T3 target genes in KCL034 and iKCL004 cells; pathway enrichment determination using ingenuity pathway analysis identify enriched development-related functional themes The number of genes and statistical values are shown for each cell line. Microarray data have been deposited in NCBI's gene expression omnibus; http://www.ncbi.nlm.nih.gov/geo/query/acc.cgi?tacc=GSE58273; accession number GSE58273

	KCL034		IKCL004	
Function	**NG**	***p*-Value**	**NG**	***p*-Value**
Gene expression	126	1.39E-10	103	7.08E-06
Transcription	146	7.90E-10	124	4.56E-06
Cellular development				
Cell differentiation	178	1.09E-17	160	3.69E-14
Cell proliferation	271	1.02E-14	248	4.34E-12
Cell commitment	16	9.05E-05	16	4.39E-05
Cell cycle	73	2.87E-04	71	1.28E-04
Cell morphology	155	4.40E-10	154	6.62E-12
Cell death	242	6.23E-11	213	3.48E-07
Cell viability	104	5.55E-08	84	2.96E-04
Embryonic development				
Development of body axis	86	1.96E-09	81	5.51E-09
Development of head	80	1.38E-09	76	2.31E-09
Lung development	33	8.85E-07	25	2.20E-08
Development of sensory organ	51	5.03E-07	51	7.57E-08
Cardiogenesis	39	1.56E-07	27	4.14E-04
Development of abdomen	28	1.15E-07	46	3.39E-06
Movement of neural crest cells	11	6.95E-06	29	5.22E-07
Eye development	42	1.88E-06	30	2.46E-06
Mesoderm development	31	1.59E-05	31	5.25E-04
Cell movement of embryonic cells	32	7.17E-04	32	4.03E-04
Development of epidermis	17	6.96E-04	22	7.73E-07
Skin development	34	6.35E-04	34	4.35E-08
Development of atrium	6	2.46E-04	6	1.76E-04
Development of lymphatic system component	32	1.68E-04	30	2.83E-04
Development of brain	39	1.30E-04	45	1.85E-07
Development of forebrain	23	1.11E-04	21	3.30E-04

NG, Number of annotated genes in the input list.

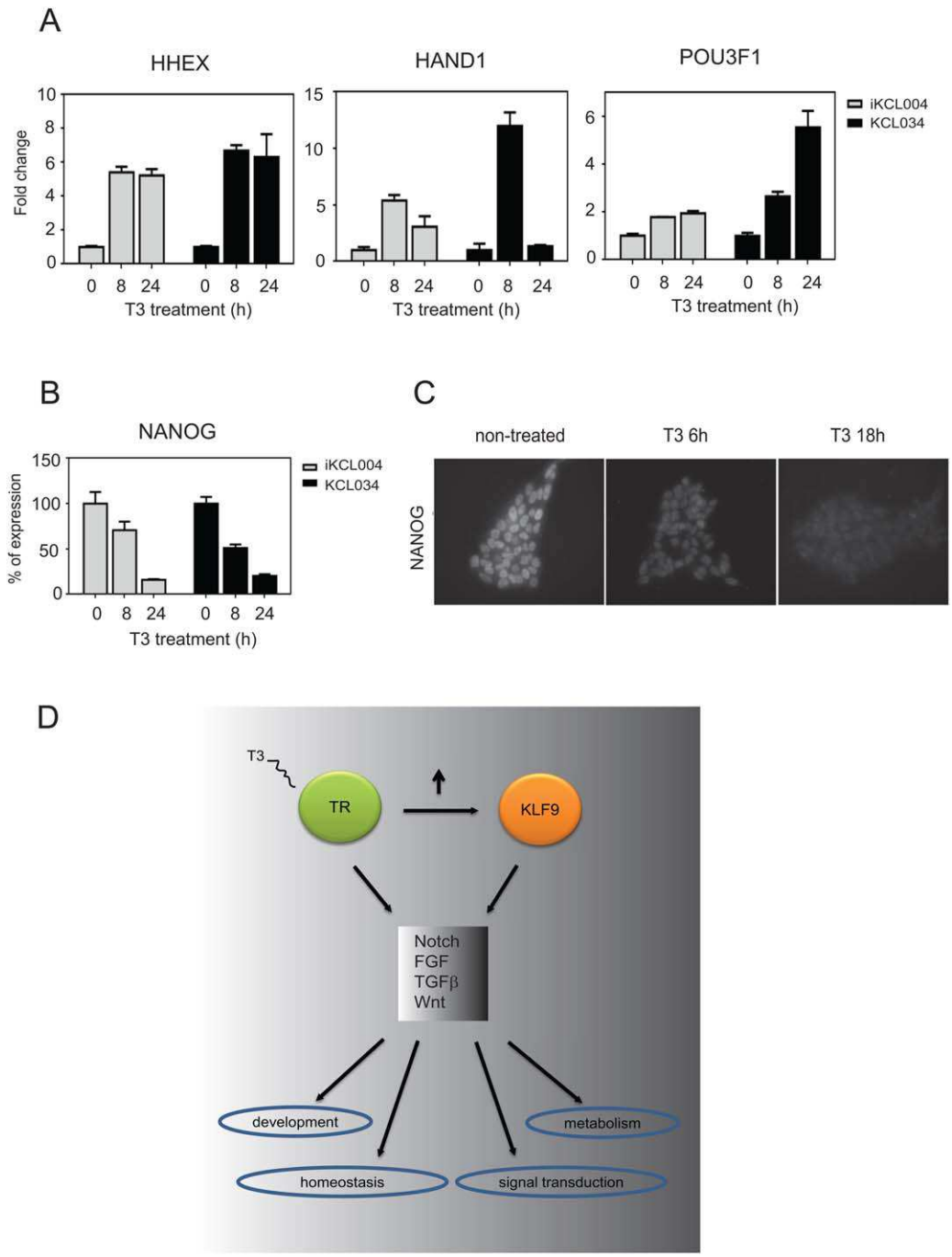

Figure 5. Analysis of representative gene expression in KCL034 and iKCL004 cells. (A): T3-induced expression of HHEX, HAND1, and POU3F1 in iKCL004 and KCL034. (B, C): Nanog display T3-dependent reduction in expression levels in KCL034 and iKCL004 as verified by qPCR (B) and confirmed by immunostaining in KCL034 cells (C). **(D)**: A model for TR/KLF9 action. TR activates transcription of KLF9 and both transcription factors modulate each other's activity in multiple pathways leading to cell-specific responses to different signals. Abbreviation: TR, thyroid hormone receptor.

profound influences on cell fate, depending on cell type and context.

While we focused on TR/KLF9-dependent effects upon the Notch signaling pathway, such effects must be considered in the context of widespread effects on differentiation-related pathways (Fig. 5D). Indeed, IPA-based analysis of TR function in ESCs provides strong evidence of T3 involvement in crucial development-related processes (Table 2), suggesting that TR may orchestrate transitions from the embryonic to adult transcription programs (Fig. 5A–5C). While more experiments will be needed to dissect mechanisms and consequences of these effects, our data suggest that TR/KLF9 axis could orchestrate key biological processes during differentiation through direct transcription regulation or through signaling pathways such as Notch (Supporting Information Fig. S9). It is not clear how the TR/KLF9 axis influences dysregulated Notch signaling that occurs in pathological conditions such as congenital disorders, metabolic syndrome, and cancer [11, 12, 63]. We propose

that it will be important to examine roles of KLF9 and Notch pathway genes in T3-dependent enhancement of liver proliferation and inhibition of hepatocarcinoma proliferation using gene ablation or knockdown.

Conclusions

TRs and KLF9 work together to regulate multiple genes and important developmental processes. The TR/KLF9 axis is active in ESCs and cell types that are representative of the hepatocyte lineage and influences Notch signaling. Better understanding of synergy between TR and KLF9 is crucial for understanding decisions between stemness and differentiation and to uncover regulatory patterns of cell homeostasis. Given the likely importance of KLF9 and Notch signaling in regulation of the balance between proliferation and differentiation, we propose that it will be important to further explore how the TR/KLF9 axis regulates hepatocellular cancer development and important physiological processes such as liver regeneration.

Acknowledgments

This work was supported by UO1 GM094614 subcomponent and RC4 DK090849 to P.W. L.N. has studentship from Saudi Arabia government.

Author Contributions

A.C.: conception and design, collection and assembly of data, data analysis and interpretation, and manuscript writing; L.D., F.A.M., L.N., A.Z., C.F., K.S., J.H.S., and D.H.S.: collection and assembly of data; A.D. and T.S.: provision of study material; D.I.: data analysis and interpretation; P.W.: manuscript writing, financial support, and final approval of manuscript.

Disclosure of Potential Conflicts of Interest

The authors indicate no potential conflicts of interest.

References

1 Yen PM. Physiological and molecular basis of thyroid hormone action. Physiol Rev 2001;81:1097–1142.

2 Cheng SY, Leonard JL, Davis PJ. Molecular aspects of thyroid hormone actions. Endocr Rev 2010;31:139–170.

3 Lomberk G, Urrutia R. The family feud: Turning off Sp1 by Sp1-like KLF proteins. Biochem J 2005;392:1–11.

4 McConnell BB, Yang VW. Mammalian Kruppel-like factors in health and diseases. Physiol Rev 2010;90:1337–1381.

5 Hoopfer ED, Huang L, Denver RJ. Basic transcription element binding protein is a thyroid hormone-regulated transcription factor expressed during metamorphosis in *Xenopus laevis*. Dev Growth Differ 2002;44:365–381.

6 Ying M, Sang Y, Li Y et al. Krüppel-like family of transcription factor 9, a differentiation-associated transcription factor, suppresses Notch1 signaling and inhibits glioblastoma-initiating stem cells. Stem Cells. 2011;29:20–31.

7 Kimura H, Fujimori K. Activation of early phase of adipogenesis through Krüppel-like factor KLF9-mediated, enhanced expression of CCAAT/enhancer-binding protein β in 3T3-L1 cells. Gene 2014;534:169–176.

8 Denver RJ, Ouellet L, Furling D et al. Basic transcription element binding protein is a thyroid hormone-regulated gene in the developing central nervous system: Evidence for a role in neurite outgrowth. J Biol Chem 1999;274:23128–23134.

9 Dugas JC, Ibrahim A, Barres BA. The T3-induced gene KLF9 regulates oligodendrocyte differentiation and myelin regeneration. Mol Cell Neurosci 2012;50:45–57.

10 Jiang J, Chan YS, Loh YH et al. A core Klf circuitry regulates self-renewal of embryonic stem cells. Nat Cell Biol 2008;10:353–360.

11 Katoh M. Networking of WNT, FGF, Notch, BMP, and Hedgehog signaling pathways during carcinogenesis. Stem Cell Rev 2007;3:30–38.

12 Katoh M. Network of WNT and other regulatory signaling cascades in pluripotent stem cells and cancer stem cells. Curr Pharm Biotechnol 2011;12:160–170.

13 Lum L, Beachy PA. The Hedgehog response network: Sensors, switches, and routers. Science 2004;304:1755–1759.

14 Varga AC, Wrana JL. The disparate role of BMP in stem cell biology. Oncogene 2005;24:5713–5721.

15 Dailey L, Ambrosetti D, Mansukhani A et al. Mechanisms underlying differential responses to FGF signaling. Cytokine Growth Factor Rev 2005;16:233–247.

16 Schnerch A, Cerdan C, Bhatia M. Distinguishing between mouse and human pluripotent stem cell regulation: The best laid plans of mice and men. Stem Cells 2010;28:419–430.

17 Martin KM, Metcalfe JC, Kemp PR. Expression of Klf9 and Klf13 in mouse development. Mech Dev 2001;103:149–151.

18 Bookout AL, Jeong Y, Downes M et al. Anatomical profiling of nuclear receptor expression reveals a hierarchical transcriptional network. Cell 2006;126:789–799.

19 Wallis K, Dudazy S, van Hogerlinden M et al. The thyroid hormone receptor α1 protein is expressed in embryonic postmitotic neurons and persists in most adult neurons. Mol Endocrinol 2010;24:1904–1916.

20 Ohguchi H, Tanaka T, Uchida A et al. Hepatocyte nuclear factor 4alpha contributes to thyroid hormone homeostasis by cooperatively regulating the type 1 iodothyronine deiodinase gene with GATA4 and Kruppel-like transcription factor 9. Mol Cell Biol 2008;28:3917–3931.

21 Gamper I, Koh KR, Ruau D. GAR22: A novel target gene of thyroid hormone receptor causes growth inhibition in human erythroid cells. Exp Hematol 2009;37:539–548.

22 Simmen FA, Xiao R, Velarde MC et al. Dysregulation of intestinal crypt cell proliferation and villus cell migration in mice lacking Krüppel-like factor 9. Am J Physiol Gastrointest Liver Physiol 2007;292:G1757–1769.

23 Kress E, Samarut J, Plateroti M. Thyroid hormones and the control of cell proliferation or cell differentiation: Paradox or duality? Mol Cell Endocrinol 2009;313:36–49.

24 Kress E, Skah S, Sirakov M et al. Cooperation between the thyroid hormone receptor TRalpha1 and the WNT pathway in the induction of intestinal tumorigenesis. Gastroenterology 2010;138:1863–1874.

25 Lin JZ, Sieglaff DH, Yuan C et al. Gene specific actions of thyroid hormone receptor subtypes. PLoS One 2013;8:e52407.

26 Berry MN, Friend DS. High-yield preparation of isolated rat liver parenchymal cells: A biochemical and fine structural study. J Cell Biol 1969;43:506–520.

27 Seglen PO. Preparation of isolated rat liver cells. In: Prescott DM, ed. Methods in Cell Biology. Vol 19. New York: Academic Press, 1976:29–83.

28 Cheng X, Ying L, Lu L et al. Self-renewing endodermal progenitor lines generated from human pluripotent stem cells. Cell Stem Cell 2012;10:371–384.

29 Du P, Kibbe WA, Lin SM. Lumi: A pipeline for processing Illumina microarray. Bioinformatics 2008;24:1547–1548.

30 Smyth GK. Limma: Linear models for microarray data. In: Gentleman R, Carey V, Dudoit S et al., eds. Bioinformatics and Computational Biology Solutions using R and Bioconductor. New York: Springer, 2005:397–420.

31 Team RDC. R: A Language and Environment for Statistical Computing. Vienna, Austria: R Foundation for Statistical Computing, 2009.

32 Benjamini Y, Hochberg Y. Controlling the false discovery rate: A practical and powerful approach to multiple testing. J R Stat Soc B 1995;57:289–300.

33 Tabas-Madrid D, Nogales-Cadenas R, Pascual-Montano A. GeneCodis3: A non-redundant and modular enrichment analysis tool for functional genomics. Nucleic Acids Res 2012;40:W478–W483.

34 Nogales-Cadenas R, Carmona-Saez P, Vazquez M et al. GeneCodis: Interpreting gene lists through enrichment analysis and integration of diverse biological information. Nucleic Acids Res 2009;37:W317–W322.

35 Carmona-Saez P, Chagoyen M, Tirado F et al. GENECODIS: A web-based tool for finding significant concurrent annotations in gene lists. Genome Biol 2007;8:R3.
36 Mostafavi S, Ray D, Warde-Farley D et al. GeneMANIA: A real-time multiple association network integration algorithm for predicting gene function. Genome Biol 2008;9(suppl 1):S4.
37 Warde-Farley D, Donaldson SL, Comes O et al. The GeneMANIA prediction server: Biological network integration for gene prioritization and predicting gene function. Nucleic Acids Res 2010; 38:W214–W220.
38 Zuberi K, Franz M, Rodriguez H et al. GeneMANIA prediction server 2013 update. Nucleic Acids Res 2013;41:W115–122.
39 Yuan C, Lin JZ, Sieglaff DH et al. Identical gene regulation patterns of T3 and selective thyroid hormone receptor modulator GC-1. Endocrinology 2012;153:501–511.
40 Petrova A, Celli A, Jacquet L et al. 3D in vitro model of a functional epidermal permeability barrier from human embryonic stem cells and induced pluripotent stem cells. Stem Cell Rep 2014;2:675–689.
41 Jacquet L, Stephenson E, Collins R et al. Strategy for the creation of clinical grade hESC line banks that HLA-match a target population. EMBO Mol Med 2013;5:10–17.
42 Rankin SA, Kormish J, Kofron M et al. A gene regulatory network controlling hhex transcription in the anterior endoderm of the organizer. Dev Biol 2011;351:297–310.
43 Smart N, Dube KN, Riley PR. Identification of Thymosin β 4 as an effector of Hand1-mediated vascular development. Nat Commun 2010;1:46.
44 Katoh Y, Katoh M. Hedgehog signaling, epithelial-to-mesenchymal transition and miRNA. Int J Mol Med 2008;22:271–275.
45 Pibiri M, Ledda-Columbano GM, Cossu C et al. Cyclin D1 is an early target in hepatocyte proliferation induced by thyroid hormone (T3). FASEB J 2001;15:1006–1013.
46 López-Fontal R, Zeini M, Través PG et al. Mice lacking thyroid hormone receptor Beta show enhanced apoptosis and delayed liver commitment for proliferation after partial hepatectomy. PLoS One 2010;14:e8710.
47 Ledda-Columbano GM, Perra A, Loi R et al. Cell proliferation induced by triiodothyronine in rat liver is associated with nodule regression and reduction of hepatocellular carcinomas. Cancer Res 2000; 60:603–609.
48 Perra A, Kowalik MA, Pibiri M et al. Thyroid hormone receptor ligands induce regression of rat preneoplastic liver lesions causing their reversion to a differentiated phenotype. Hepatology 2009;49:1287–1296.
49 Chan IH, Privalsky ML. Isoform-specific transcriptional activity of overlapping target genes that respond to thyroid hormone receptors alpha1 and beta1. Mol Endocrinol 2009;23:1758–1775.
50 Tanimizu N, Miyajima A. Notch signaling controls hepatoblast differentiation by altering the expression of liver-enriched transcription factors. J Cell Sci 2004;117:3165–3174.
51 Wang T, You T, Tao K et al. Notch is the key factor in the process of fetal liver stem/progenitor cells differentiation into hepatocytes. Dev Growth Differ 2012;54:605–617.
52 Ortica S, Tarantino N, Aulner N et al. The 4 Notch receptors play distinct and antagonistic roles in the proliferation and hepatocytic differentiation of liver progenitors. FASEB J 2014;28:603–614.
53 Artavanis-Tsakonas S, Rand MD, Lake RJ. Notch signaling: Cell fate control and signal integration in development. Science 1999; 284:770–776.
54 Liu J, Sato C, Cerletti M et al. Notch signaling in the regulation of stem cell self-renewal and differentiation. Curr Top Dev Biol 2010;92:367–409.
55 Bigas A, Espinosa L. Hematopoietic stem cells: To be or Notch to be. Blood 2012;119: 3226–3235.
56 Koch U, Lehal R, Radtke F. Stem cells living with a Notch. Development 2013;140: 689–704.
57 Chin MT, Maemura K, Fukumoto S et al. Cardiovascular basic helix loop helix factor 1, a novel transcriptional repressor expressed preferentially in the developing and adult cardiovascular system. J Biol Chem 2000;275: 6381–6387.
58 Fischer A, Gessler M. Delta-Notch—And then?. Protein interactions and proposed modes of repression by Hes and Hey bHLH factors. Nucleic Acids Res 2007;35:4583–4596.
59 Medina M, Dotti CG. RIPped out by presenilin-dependent gamma-secretase. Cell Signal 2003;15:829–841.
60 Katoh M, Katoh M. Integrative genomic analyses on HES/HEY family: Notch-independent HES1, HES3 transcription in undifferentiated ES cells, and Notch-dependent HES1, HES5, HEY1, HEY2, HEYL transcription in fetal tissues, adult tissues, or cancer. Int J Oncol 2007;31:461–466.
61 Kageyama R, Ohtsuka T, Kobayashi T. The Hes gene family: Repressors and oscillators that orchestrate embryogenesis. Development 2007;134:1243–1251.
62 Kobayashi T, Mizuno H, Imayoshi I et al. The cyclic gene Hes1 contributes to diverse differentiation responses of embryonic stem cells. Genes Dev 2009;23:1870–1875.
63 Boulter L, Govaere O, Bird TG et al. Macrophage-derived Wnt opposes Notch signaling to specify hepatic progenitor cell fate in chronic liver disease. Nat Med 2012;18: 572–579.


See www.StemCells.com for supporting information available online.

TECHNICAL REPORT

nature cell biology

Self-organization of the human embryo in the absence of maternal tissues

Marta N. Shahbazi[1,5], Agnieszka Jedrusik[1,5], Sanna Vuoristo[1,5], Gaelle Recher[1,6], Anna Hupalowska[1], Virginia Bolton[2], Norah M. E. Fogarty[3], Alison Campbell[4], Liani G. Devito[2], Dusko Ilic[2], Yakoub Khalaf[2], Kathy K. Niakan[3], Simon Fishel[4] and Magdalena Zernicka-Goetz[1,7]

Remodelling of the human embryo at implantation is indispensable for successful pregnancy. Yet it has remained mysterious because of the experimental hurdles that beset the study of this developmental phase. Here, we establish an *in vitro* system to culture human embryos through implantation stages in the absence of maternal tissues and reveal the key events of early human morphogenesis. These include segregation of the pluripotent embryonic and extra-embryonic lineages, and morphogenetic rearrangements leading to generation of a bilaminar disc, formation of a pro-amniotic cavity within the embryonic lineage, appearance of the prospective yolk sac, and trophoblast differentiation. Using human embryos and human pluripotent stem cells, we show that the reorganization of the embryonic lineage is mediated by cellular polarization leading to cavity formation. Together, our results indicate that the critical remodelling events at this stage of human development are embryo-autonomous, highlighting the remarkable and unanticipated self-organizing properties of human embryos.

The development of a human embryo from a fertilized egg begins with a series of cleavage divisions and morphogenetic rearrangements that lead to the formation of a free-floating blastocyst. This blastocyst comprises three distinct cell lineages: embryonic tissue (epiblast) and two extra-embryonic tissues (hypoblast and trophectoderm) that, after implantation into the uterus, will give rise to the yolk sac and placenta respectively. This pre-implantation period has been extensively studied using methods that pioneered *in vitro* fertilization[1,2] (IVF). However, on the seventh day of development, the human embryo must implant into the uterus of the mother to survive, to establish the body plan and to generate the germ layers. The failure of an embryo to implant is a major cause of early pregnancy loss[3] and yet the cellular and molecular changes that take place in the human embryo at this stage remain unknown. This is because experiments *in vivo* are not feasible and there has been no system to culture human embryos *ex vivo*.

Monkey embryos have been used as a model for human embryo development[4,5] and the co-culture of human blastocysts and endometrial cells[6] has provided an experimental system to model post-implantation morphogenesis. However, the extent to which these systems recapitulate post-implantation development of the human embryo remains an open question. Moreover, the potential of human blastocysts for self-organization has never been explored.

Here, to shed light on the early post-implantation phases of human development, we have adapted our recently established protocol for mouse embryos[7,8]. The culture system we have established allows human embryos to undergo the pre- to post-implantation transition *in vitro*, in the absence of any maternal tissues. By comparing human embryos developing *in vitro* and the Carnegie series of *in vivo* developing human embryos[9], we have identified that the key hallmarks of human embryogenesis take place in the absence of any maternal tissues, uncovering the self-organizing properties of human embryos at this stage.

RESULTS

Establishment of a method to culture human embryos through implantation stages *in vitro*

To gain understanding of the developmental events undertaken by the implanting human embryo, we reasoned that we needed an *in vitro* culture system that would recapitulate these processes. To this end, we adapted the culture conditions we had previously established for mouse embryos at comparable stages[7]. Supernumerary pre-implantation human embryos (at either cleavage or blastocyst

[1]Mammalian Embryo and Stem Cell Group, University of Cambridge, Department of Physiology, Development and Neuroscience, Downing Street, Cambridge CB2 3DY, UK. [2]Faculty of Life Sciences and Medicine, King's College London, Women's Health Academic Centre, Assisted Conception Unit, Guy's Hospital, Great Maze Pond, London SE1 9RT, UK. [3]Human Embryo and Stem Cell Laboratory, Francis Crick Institute, Mill Hill Laboratory, London NW7 1AA, UK. [4]CARE Fertility Group, John Webster House, 6 Lawrence Drive, Nottingham Business Park, Nottingham NG8 6PZ, UK. [5]These authors contributed equally to this work. [6]Present address: Bioimaging and Optofluidics group, IOGS, CNRS & University of Bordeaux Rue Francois Mitterand, 33400 Talence, France.
[7]Correspondence should be addressed to M.Z.-G. (e-mail: mz205@cam.ac.uk)

Received 25 February 2016; accepted 29 March 2016; published online 4 May 2016; corrected online 17 May 2016; DOI: 10.1038/ncb3347

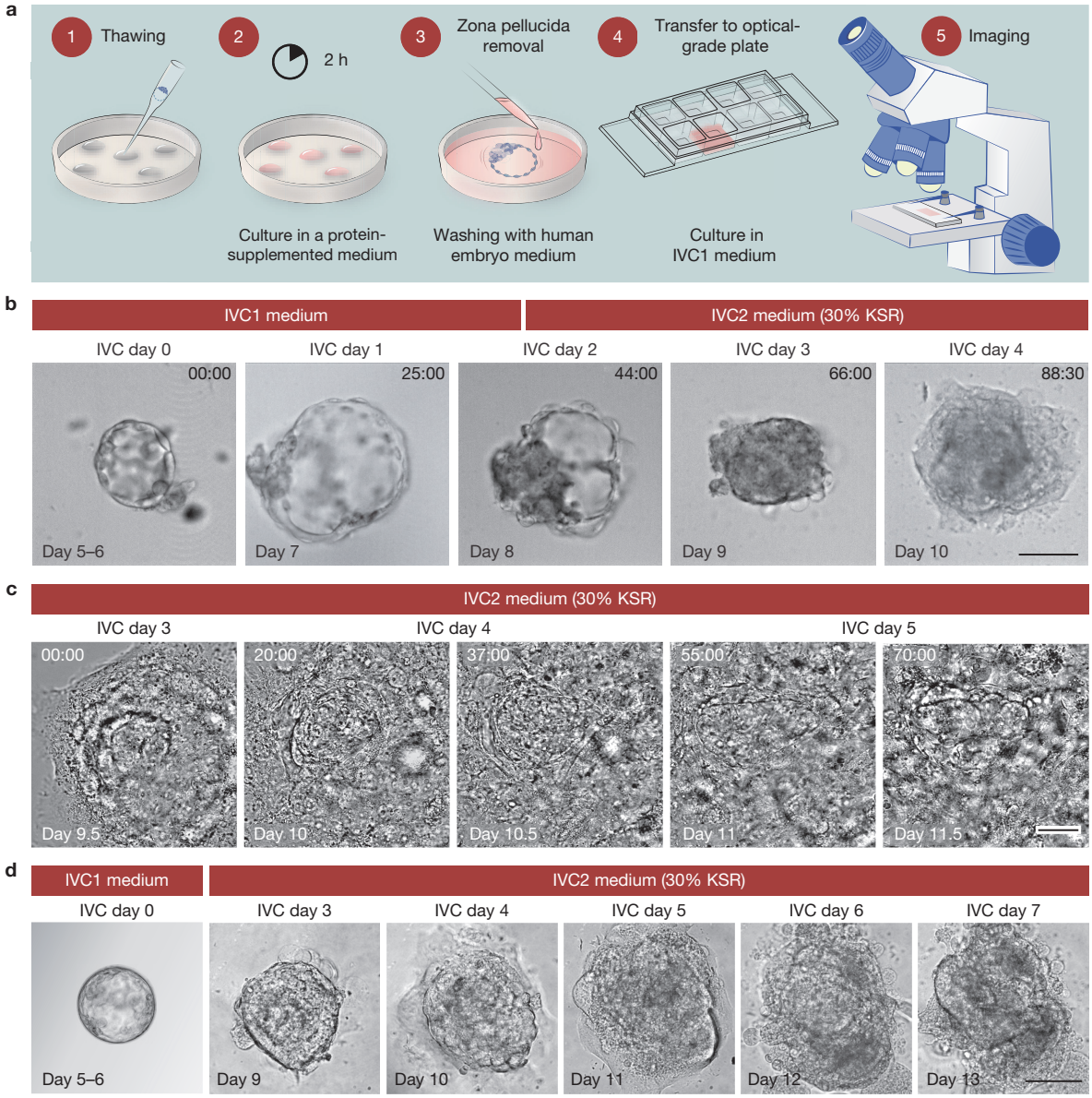

Figure 1 Establishment of an *in vitro* system to study human implantation and early post-implantation morphogenesis. (**a**) Human embryos were thawed and cultured until the blastocyst stage (day 5–6 of development). The zona pellucida was removed and embryos were transferred to plates in IVC1 medium for imaging. (**b–d**) On the second day of culture, medium was changed for IVC2 with 30% KnockOut Serum Replacement (KSR). Shown are representative bright-field images of human blastocysts developing *in vitro* until day 12–13. All scale bars, 100 μm. These data involved the assessment of a total of 5 embryos collected across 3 experiments, out of which 3 showed correct development.

stage) donated for this project were thawed and placed in culture medium to recover, before the zona pellucida was removed (Methods). Embryos were scored by morphological criteria and those showing abnormalities (fragmented blastomeres or developmentally arrested) were discarded. We first plated human blastocysts on optical-grade dishes in 21% O_2 and in *in vitro* culture medium 1 (IVC1), which was replaced by *in vitro* culture medium 2 (IVC2) after 48 h (Fig. 1a,b)[7]. Time-lapse microscopy revealed that human blastocysts cultured in IVC1 underwent a series of contractions and expansions reflecting collapse and subsequent enlargement of the blastocyst cavity (Supplementary Video 1), as observed in IVF clinics[10]. However, by the end of day 7, the blastocyst cavity completely collapsed and embryos attached to the dish (Fig. 1b–d). At this time the attached embryos started to grow and this growth continued until day 12–13 (Fig. 1c,d and Supplementary Video 2). We previously found that either human cord serum or KnockOut Serum Replacement (KSR) in IVC2 permits peri-implantation mouse development[11]. Here we show human embryos develop in medium supplemented with KSR up to day 13 (Fig. 1b–d). The experiment was stopped at this point because the internationally recognized ethical limit for human embryo culture is up to day 14 or to the first signs of development of the primitive streak[12].

The trend in IVF clinics over recent years has been to culture pre-implantation human embryos in hypoxic conditions (5% O_2), as this favours embryo survival[13] and inhibits differentiation in embryonic

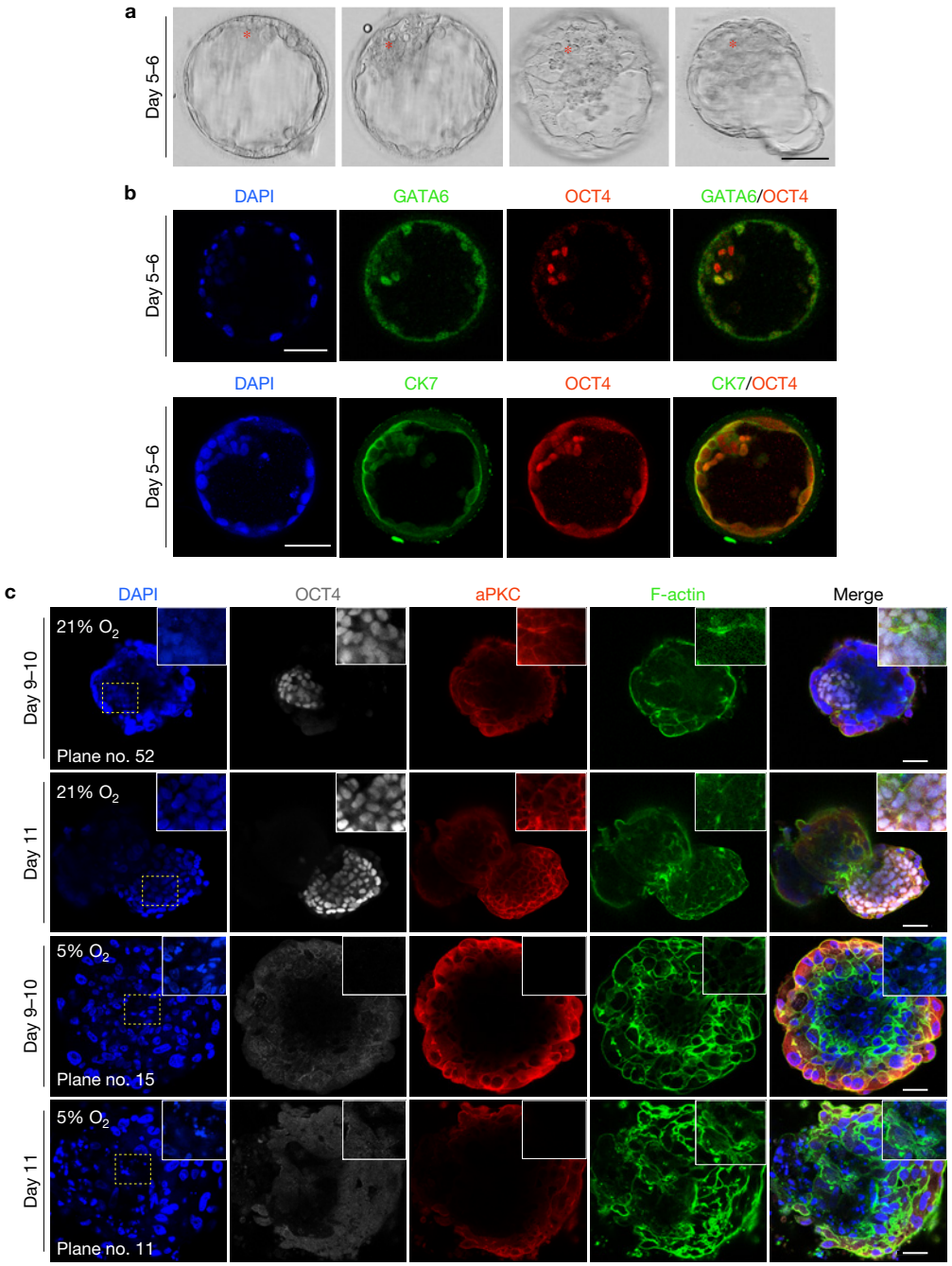

Figure 2 Preservation of the pluripotent lineage in human embryos cultured through implantation stages *in vitro*. (**a**) Bright-field images of day 5–6 blastocysts. Asterisks indicate the inner cell mass. (**b**) Day 5–6 blastocysts were fixed and immunostained for lineage markers. Representative confocal *Z* sections of human blastocysts stained for OCT4 and GATA6, and OCT4 and CK7. (**c**) Human embryos cultured in either 21% or 5% O_2 were analysed at the indicated time points. Representative confocal *Z* sections of human embryos stained for OCT4, aPKC and F-actin. Note the absence of OCT4-expressing cells and the presence of fragmented nuclei in the embryos cultured in 5% O_2. All scale bars, 50 μm. These data involved the assessment of a total of 59 embryos in 21% O_2 (out of which 29 embryos preserved the epiblast) and 20 embryos in 5% O_2 (out of which none preserved the epiblast) collected across 3 experiments.

stem cells[14,15]. To investigate whether hypoxic conditions offer any advantage to human embryos cultured through implantation, we compared development of embryos cultured in 21% O_2 to ones cultured in 5% O_2 in terms of preservation of the pluripotent lineage. Initially, day 5–6 pre-implantation blastocysts had a group of inside pluripotent cells as indicated by the presence of the transcription factor OCT4 (Fig. 2a,b). However, after 4 days in culture, whereas 49% of embryos ($N = 59$) cultured in 21% O_2 maintained a cluster of epiblast cells showing expression of the pluripotency factor OCT4, none of the embryos cultured in hypoxic conditions ($N = 20$) had OCT4-expressing cells (Supplementary Table 1). In contrast, cells of embryos in hypoxic conditions showed signs of cell death (Fig. 2c).

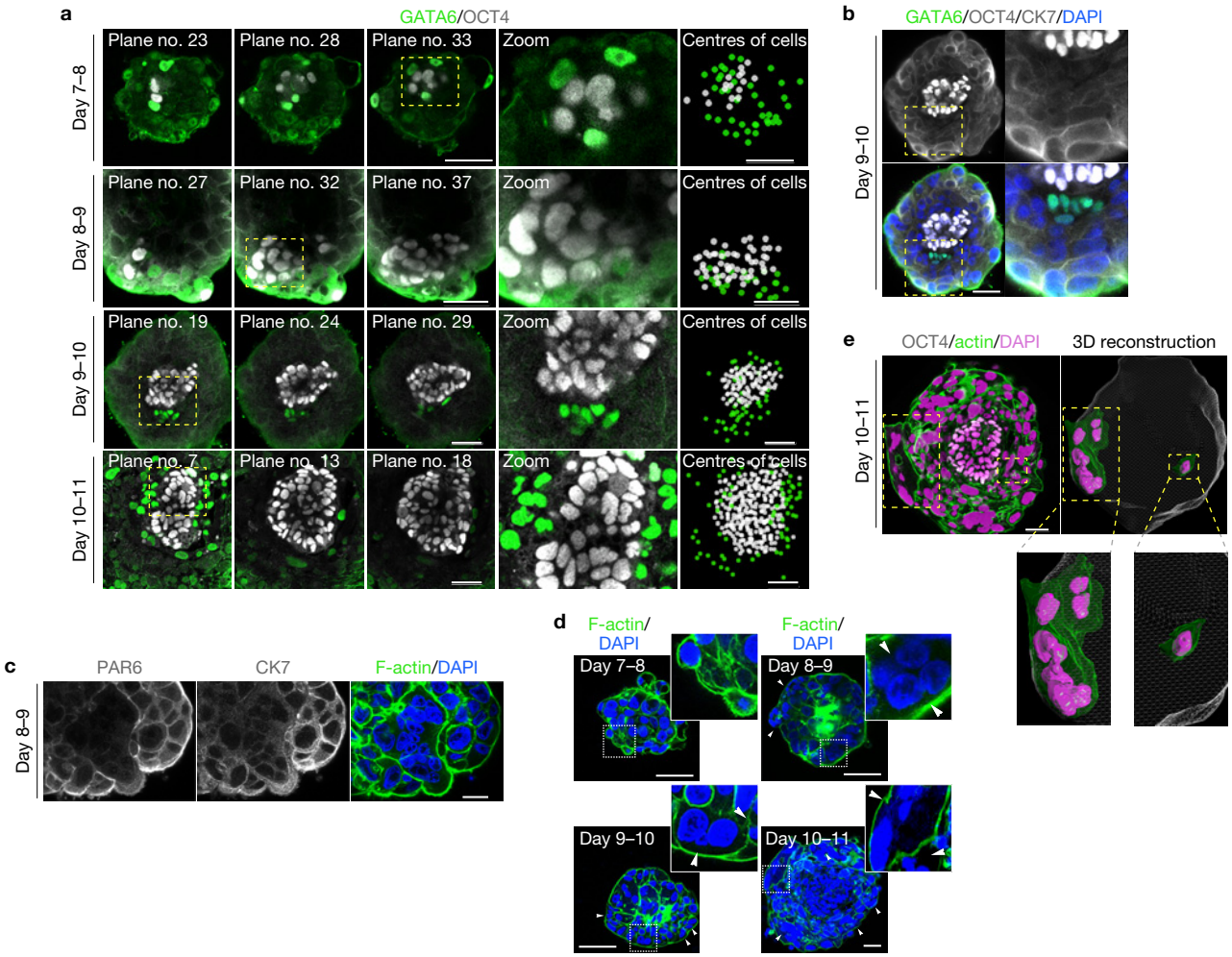

Figure 3 Analysis of embryonic and extra-embryonic lineages in human embryos cultured through implantation stages *in vitro*. Human embryos developing *in vitro* until day 11 were fixed and stained at the indicated time points. (**a**) Representative confocal *Z* sections of human embryos stained for OCT4 and GATA6. Right panels show the centre of all OCT4-expressing (white) and GATA6-expressing (green) cells. All positive cells were counted regardless of the fluorescence intensity value. (**b**) Representative confocal *Z* section of a day 9–10 embryo stained for OCT4, GATA6 and CK7. (**c**) Representative confocal *Z* section of a day 8–9 embryo stained for PAR6 and CK7. (**d**) Representative confocal *Z* section of human embryos stained for F-actin and DAPI. Arrowheads point to multinucleated cells. (**e**) 3D reconstruction of the cellular and nuclear shape of representative trophectoderm cells. Note that cells in close proximity to the epiblast have a single nucleus, whereas cells in the periphery of the embryo are multinucleated. All yellow rectangles indicate the regions in the embryos that are shown with higher magnification. All scale bars, 50 μm. These data involved the assessment of a total of 59 embryos collected across 6 experiments, out of which 29 showed preservation of the embryonic lineage.

This suggests that preservation of the epiblast *in vitro* beyond day 7 might benefit from higher O_2 concentrations possibly because of the increase in embryo size, which may decrease the O_2 pressure in the core of the embryo. Hypoxia clearly has a complex influence on embryonic development and its effects need to be better understood in the intrauterine milieu to determine exactly how it affects both mouse and human embryogenesis[16]. As a result of these findings, here we cultured human embryos beyond day 7 in 21% O_2, which we show permits further development of the pluripotent lineage *in vitro*.

Development of the embryonic and extra-embryonic lineages during human post-implantation morphogenesis *in vitro*

To gain temporal understanding of the cellular and developmental events through early post-implantation development, we fixed and immunostained human embryos at different time points of culture. We used KnockOut Serum Replacement to supplement the medium as it permits a more reproducible time course of development than human cord serum[7]. We have focused on development between days 7 and 11, because during these 5 days the embryo undergoes a major reorganization that is necessary for subsequent gastrulation[9]. Shortly after attachment (day 7–8 of development), we observed a clear separation between embryonic (OCT4-expressing, epiblast) and extra-embryonic (GATA6-expressing, hypoblast) cells, the respective progenitors for the fetus and yolk sac (Fig. 3a), whereas in the unattached blastocysts, this segregation of epiblast and hypoblast progenitors had not yet taken place (Fig. 2b). This contrasts with mouse embryos, where the epiblast and the hypoblast-equivalent (the primitive endoderm) segregate already before implantation[17]; but agrees with observations in human embryos[18–22]. We found that at day 7–8, the epiblast was formed by a cluster of about 20 OCT4-expressing

cells surrounded by approximately 50 GATA6-expressing hypoblast cells (Fig. 3a and Supplementary Table 2). By day 8–9, GATA6-expressing hypoblast cells preferentially localized to one side of the epiblast, as occurs in human embryos developing *in vivo*[9]. This spatial organization was maintained throughout subsequent developmental stages (from day 9 to day 11; Fig. 3a and Supplementary Fig. 1a and Supplementary Videos 3 and 4). By day 11, the number of OCT4-expressing epiblast cells had significantly increased to an average of 328 cells, whereas the number of GATA6-expressing hypoblast cells increased up to 79 (Supplementary Table 2).

To analyse development of trophectoderm, the progenitors of the placenta, we followed cytokeratin 7 (CK7), which is highly expressed in trophoblast derivatives[23]. We found that the trophectoderm cells surrounding the epiblast and hypoblast (Fig. 3b) presented a polarized epithelial phenotype, evident from the localization of the apical determinant PAR6 (Fig. 3c). From day 8 onwards, we noted the presence of CK7-expressing multinucleated cells in the outermost region of the embryo (Fig. 3d). To determine their exact position with respect to the epiblast–hypoblast cluster, we performed a three-dimensional (3D) reconstruction of cellular shapes, based on the computational segmentation of membranes and nuclei (Fig. 3e). This revealed two trophectoderm subpopulations: cells in proximity to the epiblast–hypoblast bilayer had a single nucleus, whereas those in the periphery of the embryo were multinucleated and exhibited characteristic lacunae (Fig. 3e and Supplementary Video 5). On the basis of the expression of CK7, their position and their cellular and nuclear shape, these two cell populations are likely to correspond to the cytotrophoblast and syncytiotrophoblast respectively, indicating that the development of post-implantation trophoblast derivatives can be recapitulated in the absence of any maternal tissue. Together these results demonstrate that the development of all three lineages progresses as human embryos develop *in vitro*.

Human epiblast polarization and pro-amniotic cavity formation

Next, we focused on the development of the epiblast because it undergoes its first major reorganization at implantation. One of the hallmarks of epiblast transformation is the acquisition of a polarized phenotype and the formation of a lumen, the prospective pro-amniotic cavity[9,24], essential for the subsequent development of the body plan. However, the cellular mechanisms underlying lumen formation in humans remain unknown. Whereas some reports in higher primates point towards cell death within the epiblast as the main driver of lumen formation[25], alternative reports suggest folding of the epiblast[26], or a change of polarity in epiblast cells[4]. Importantly, these hypotheses are based on the observations of rhesus monkey embryos by electron microscopy as, so far, it has not been possible to definitively identify cell types and their features in human embryos at implantation. We found that at day 7–8 of development, the epiblast was a cluster of cells showing no signs of polarization (Fig. 4a and Supplementary Figs 1b and 2). However, by day 8–9, a group of OCT4-expressing epiblast cells became radially organized around a small central lumen. These cells were apico-basally polarized in 31% of the embryos (Supplementary Table 1), as determined by the polarized apical localization of actin and aPKC (the principal kinase of the apical Par polarity complex; Fig. 4a and Supplementary Fig. 1b). The formation of a small lumen at the exact site of incipient apical polarization indicates the onset of pro-amniotic cavity formation within the epiblast. Importantly, we did not observe any apoptotic cell, cellular debris or any other indication of cell death in the incipient pro-amniotic cavity (Supplementary Fig. 3). These results indicate that the epiblast becomes polarized by day 9 of *in vitro* development and suggest that apoptosis is not the mechanism driving lumenogenesis in human embryos.

Human bilaminar disc formation

The next expected remodelling event is the formation of the amniotic epithelium and the epiblast disc. In contrast to the mouse, in which the amnion is formed at gastrulation, the amnion is expected to form in humans shortly after implantation with those epiblast cells adjacent to the hypoblast acquiring a columnar shape, and those in contact with cytotrophoblast differentiating into squamous and flat amniotic epithelium. At this stage, both tissues line the pro-amniotic cavity[24]. We observed that as development of embryos progressed *in vitro*, the epiblast and the pro-amniotic cavity expanded in size (Fig. 4a,b and Supplementary Fig. 4 and Supplementary Table 2 and Supplementary Video 6), indicative of embryo growth. At day 10–11 of development, we could detect two morphologically distinct groups of OCT4-expressing cells. 3D reconstructions of cellular shapes revealed that OCT4-expressing cells located near the hypoblast had a columnar morphology whereas opposite-facing OCT4-expressing cells had a distinct squamous and flat shape (Fig. 4c and Supplementary Video 7). Moreover, these flat OCT4-expressing cells were in close proximity to cells with a higher nuclear volume (on average 2.5 times bigger than epiblast cells), a feature characteristic of trophoblast cells. These observations suggest that the two types of OCT4-expressing cells may represent the epiblast disc and the prospective amniotic epithelium.

Human prospective yolk sac formation

The next expected event of human embryo development is the reorganization of hypoblast cells to give rise to a second cavity, the primary yolk sac[9,27], which will provide the blood supply to the developing fetus. Remarkably, we found that human embryos developing *in vitro* established a second cavity at day 11 of development (Supplementary Video 8). This cavity was localized below the epiblast and was surrounded by GATA6-expressing cells, highlighting its hypoblast origin (Fig. 4d,e and Supplementary Video 9). Thus, both expression of characteristic lineage markers as well as morphological features suggest that formation of the prospective yolk sac can be also recapitulated in human embryos developing *in vitro* (Fig. 4f).

Human pluripotent stem cells (hPSCs) recapitulate the events of polarization and lumenogenesis

As the above results revealed that epiblast polarization and lumen formation are the first features of epiblast morphogenesis after implantation, we next investigated the molecular pathways that could be responsible for this critical remodelling. Given the ethical restrictions and the limited number of human embryos available for functional studies, we turned to human embryonic stem cells (hESCs) and human induced pluripotent stem cells (hiPSCs) as alternative models. First, to determine whether the extracellular matrix (ECM) participates in inducing epiblast polarization and lumen formation, we cultured individual hESCs in 3D Matrigel. We found that surrounding

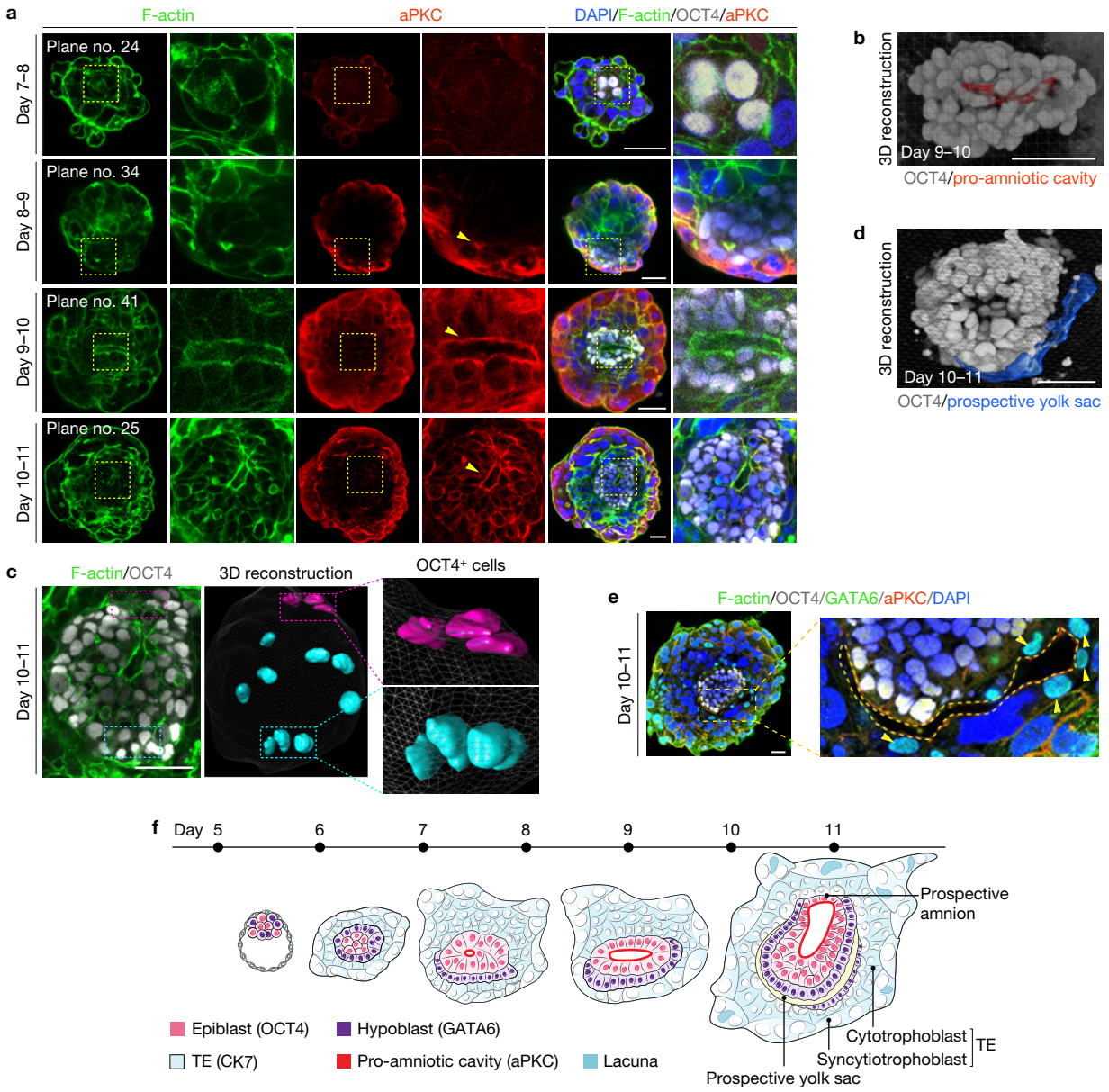

Figure 4 Remodelling of the epiblast in human embryos cultured through implantation stages. Human embryos developing *in vitro* until day 11 were fixed and stained at the indicated time points. (**a**) Representative confocal *Z* sections of human embryos stained for F-actin, aPKC and OCT4. Arrowheads indicate the incipient pro-amniotic cavity. (**b**) 3D reconstruction of the pro-amniotic cavity (shown in red). The nuclei of OCT4-expressing epiblast cells are shown in grey. (**c**) 3D reconstruction of the cellular shape of representative OCT4-expressing epiblast cells. (**d**) 3D reconstruction of the prospective yolk sac (shown in blue). The nuclei of OCT4-expressing epiblast cells are shown in grey. (**e**) Day 10–11 embryo stained for F-actin, OCT4, GATA6 and aPKC. Note the presence of GATA6-expressing cells on both sides of the cavity (arrowheads). The prospective yolk sac is indicated with a dashed line. (**f**) Model of human embryo implantation morphogenesis based on our results and the Carnegie series. The main remodelling events that take place during this transition are: segregation of epiblast and hypoblast progenitors (day 7); polarization and pro-amniotic cavity formation in the epiblast (day 8–10); differentiation of the trophectoderm (TE) into cytotrophoblast and syncytiotrophoblast cells (day 8–10); formation of the prospective amniotic epithelium, the prospective yolk sac and the bilaminar disc (day 10–11). All rectangles indicate the regions in the embryos that are shown with higher magnification. All scale bars, 50 μm. These data involved the assessment of a total of 59 embryos collected across 6 experiments, out of which 9 showed pro-amniotic cavity formation.

cells with ECM enabled lumen formation by 24 h after cell plating, and so it was sufficient to have two sister cells from a single cell division for this to take place (Fig. 5a), in agreement with other recent observations[28]. As the hESCs continued to divide, they self-organized around a central lumen. These hESC cysts were apico-basally polarized, as demonstrated by the polarized localization of aPKC (Fig. 5a), PAR6 (Fig. 5b), centrosomes (Fig. 5c) and the Golgi (Fig. 5d). They retained expression of pluripotency markers such as OCT4 (Fig. 5a), mimicking the preservation of OCT4 in the epiblast of *in vitro*-cultured human embryos (Fig. 3). To confirm these results, we next plated hiPSCs into 3D Matrigel as we did with hESCs. We found that hiPSCs also polarized and began to form

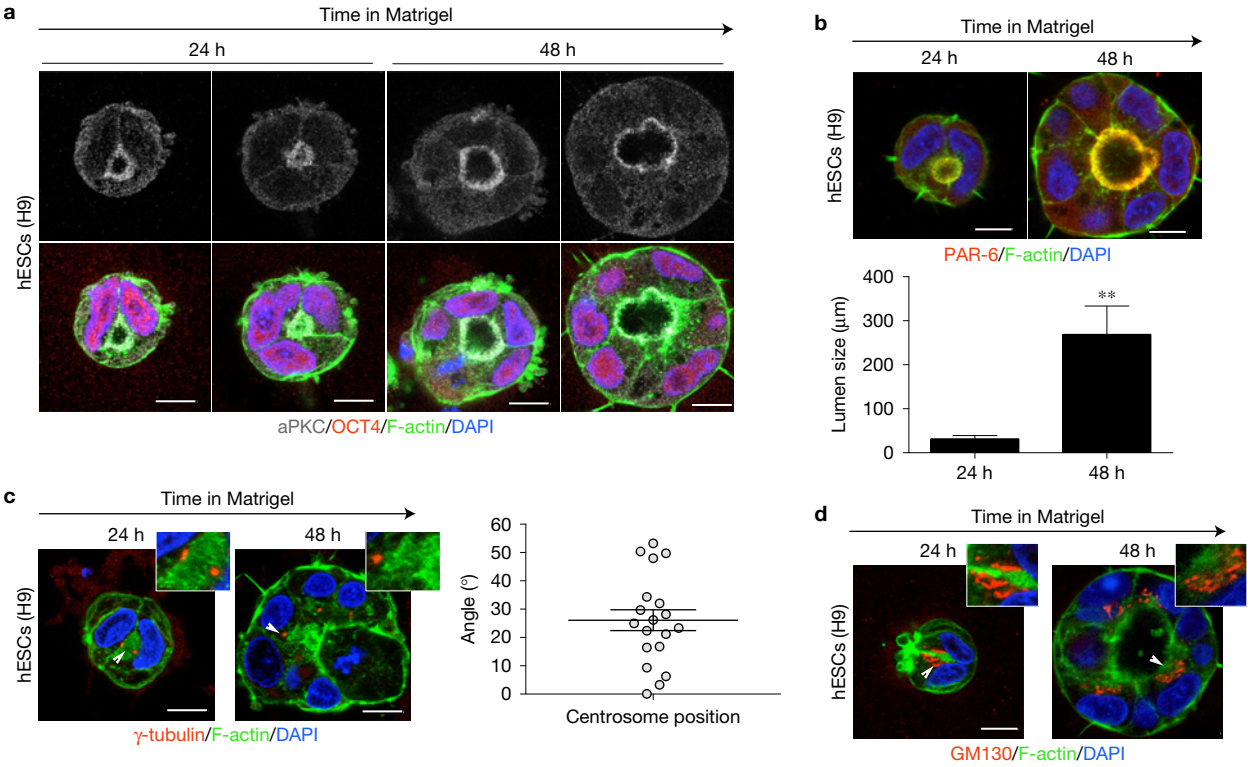

Figure 5 Self-organization of hESCs in response to ECM signalling. hESCs were plated in a 3D matrix of Matrigel and analysed at the indicated time points. (**a**) hESCs stained for OCT4 as a marker of pluripotency, aPKC as a marker of apical polarization and F-actin to reveal the general organization of the cells. (**b**) hESCs stained for PAR-6 and F-actin. The size of the lumen was quantified. Data are shown as average ± s.e.m. Note the increase in lumen size with time ($n=10$ hESC cysts per time point). Unpaired two-tailed Student's t test with Welch's correction, $^{**}P=0.0049$. (**c**) hESCs stained for the centrosome marker γ-tubulin and F-actin. Arrowheads indicate the polarized apical localization of the centrosome. The nucleus centrosome angle with respect to the nucleus–nucleus axis is shown. Each dot represents an individual centrosome. Data are shown as average ± s.e.m. ($n=19$ centrosomes). (**d**) hESCs stained for the Golgi marker GM130 and F-actin. Arrowheads indicate the polarized apical localization of the Golgi. All scale bars, 10 μm. These data involved the assessment of a minimum of 10 hESC cysts per panel, all of which showed the indicated phenotype. Images are representative of a minimum of 2 independent experiments per panel.

lumens between two cells, while retaining OCT4 expression (Fig. 6a). Lumens formed on the apical side of polarized cells that exhibited apical microvilli and a polarized distribution of aPKC, PAR6 and the Golgi (Fig. 6a–c). This polarized organization was preserved in the presence of the ROCK inhibitor Y-27632 (Fig. 6d), commonly used to avoid cell death at the time of plating of hPSCs. We could also detect lumen-directed secretion of the anti-adhesive protein podocalyxin (PODXL), implicated in lumen formation through charge repulsion[29,30] (Fig. 6e,f). The observation that hPSC cysts develop lumens between two cells as they become polarized suggests that lumen formation is not a consequence of cell death. To test this possibility directly, we treated hiPSCs with a caspase 3 inhibitor to prevent cell death[8] and found that polarization and lumen formation were not affected (Fig. 6g,h). Taken together, our results indicate that lumen formation is a consequence of cellular polarization and not cell death and lead us to suggest that similar molecular pathways may drive lumenogenesis in human embryos soon after implantation.

DISCUSSION

Implantation is a milestone in human development, as this is the time when the embryo undergoes major remodelling, which is absolutely required for correct gastrulation and therefore successful body formation and pregnancy outcome. However, so far, the absence of an *in vitro* culture system to visualize and model this critical developmental transition has severely limited our understanding of human embryogenesis. Here, we have established a system for the *in vitro* culture of human embryos that offers a unique opportunity to understand human development after implantation. This system has allowed us to uncover the main morphogenetic events that normally occur after human embryo implantation including: epiblast and hypoblast segregation; epiblast polarization; formation of the pro-amniotic cavity and the bilaminar disc; appearance of the prospective amniotic ectoderm; appearance of yolk sac; and differentiation of the trophoblast into cytotrophoblast and syncytiotrophoblast (Fig. 4f). Although this system may not be able to fully recapitulate all of the complex aspects of human embryogenesis *in vivo*, it has allowed us to reveal a remarkable self-organizing capacity of human blastocysts that has been previously unknown. The next stage in human development corresponds to primitive streak formation but for ethical reasons we are obliged to stop our cultures at day 14 of development or before the primitive streak formation[12]. Thus, our studies have focused on the key events of pre-gastrulation stages.

Our results indicate that the formation of the pro-amniotic cavity in the human embryo is not triggered by apoptosis, as suggested[25],

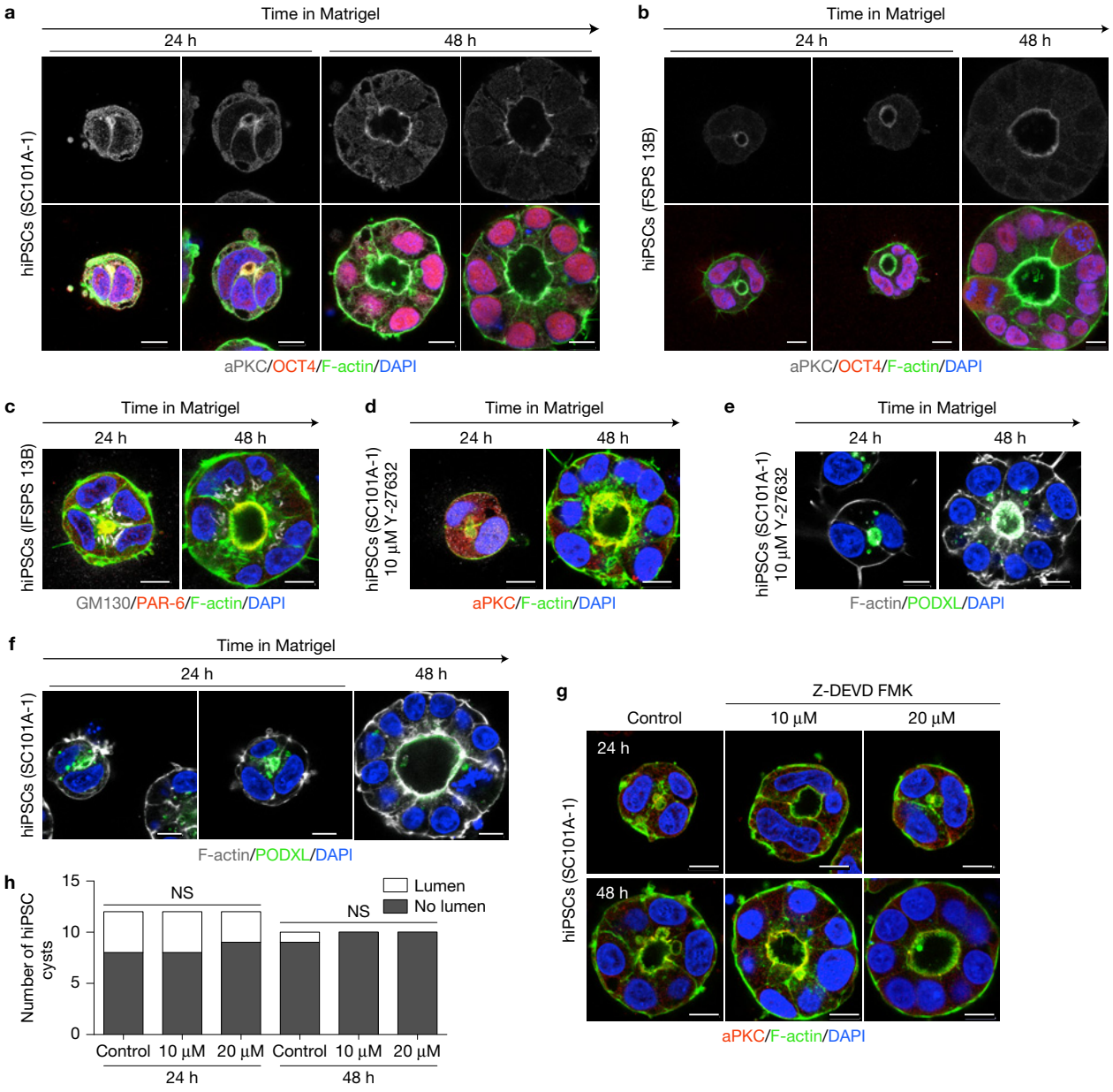

Figure 6 Self-organization of hiPSCs in response to ECM signalling. hiPSCs were plated in a 3D matrix of Matrigel and analysed at the indicated time points. (**a**,**b**) hiPSCs stained for aPKC, OCT-4 and F-actin. (**c**) hiPSCs stained for PAR-6, GM130 and F-actin. (**d**) hiPSCs cultured in the presence of the ROCK inhibitor Y-27632 and stained for aPKC and F-actin. (**e**,**f**) hiPSCs cultured in the presence (**e**) or absence (**f**) of ROCK inhibitor, and stained for PODXL and F-actin. (**g**) hiPSCs were treated with the caspase 3 inhibitor Z-DEVD FMK and lumen formation was analysed 24 and 48 h after plating by staining for aPKC and F-actin. (**h**) Quantification of lumen formation in the presence of Z-DEVD FMK. Data are shown as a contingency table. Fisher's exact test. NS, not significant ($n=12$ hiPSC cysts per condition, 24 h time point; $n=10$ hiPSC cysts per condition, 48 h time point). Data presented in this figure involved the assessment of a minimum of 10 hESC cysts per panel and per condition across a minimum of 2 independent experiments per panel.

but by the epiblast's polarization, as proposed in monkey embryos[4]. Owing to the limitations to perform functional studies in human embryos, we have used hPSCs as an alternative model to test this hypothesis, and demonstrate that the ECM participates in inducing cell polarization and lumen formation through polarized secretion (hollowing) and not programmed cell death (cavitation). This is similar to the mechanism of epiblast polarization we have recently found to operate in mouse embryos[8]. Thus, remarkably, despite the significant differences in embryo morphology between these different mammalian species, the initial steps of post-implantation embryogenesis are evolutionarily conserved.

One of the most intriguing aspects of human implantation development is the differentiation of the epiblast into the epiblast disc and the amniotic epithelium[24]. Interestingly, we could not recapitulate formation of the amniotic epithelium in our 3D hPSC culture possibly because this developmental process requires interaction with extra-embryonic tissues present in the whole embryo. It will be of interest to determine the signalling pathways required for modelling amnion

formation *in vitro*. Indeed, we anticipate that future studies using the *in vitro* culture systems we report here for both human embryos and hPSCs will shed new light on the cellular and molecular mechanisms of this mysterious and yet critical stage of human development, which will be of basic and clinical importance. □

METHODS

Methods and any associated references are available in the online version of the paper.

Note: Supplementary Information is available in the online version of the paper

ACKNOWLEDGEMENTS

We are grateful to the patients donating their embryos, colleagues in the M.Z.-G. laboratory, C. Lee (Gurdon Institute), and embryologists at the CARE, Bourn Hall (K. Elder and P. Snell) and Kings College Guy's Hospital IVF clinics for help and discussions. We thank P. Braude, D. Glover and C. Ogilvie for insightful discussion and I. Bedzhov for help in a pilot experiment. This work was supported by the Wellcome Trust grant to M.Z.-G. Work in the K.K.N. laboratory was supported by The Francis Crick Institute, which receives its core funding from Cancer Research UK, the Medical Research Council and the Wellcome Trust. M.N.S. was initially supported by a Ramon Areces Spanish Foundation Fellowship, and subsequently by an EMBO Postdoctoral Fellowship. S.V. was supported by a Post Doc Pool Grant from the Finnish Cultural Foundation. G.R. was supported by a Newton Fellowship.

AUTHOR CONTRIBUTIONS

M.N.S., A.J. and S.V. carried out all experiments and data analyses. G.R. analysed microscopy data and generated 3D reconstructions. A.H. prepared illustrations and contributed experimentally. N.M.E.F. and K.K.N. helped with human embryo cultures and contributed experimentally, and L.G.D. helped with human embryo cultures. A.C., S.F., D.I., Y.K. and K.K.N. oversaw and provided human embryos for these studies. M.Z.-G. conceived the project and supervised the study. M.N.S. and M.Z.-G. wrote the manuscript with help from all of the authors.

COMPETING FINANCIAL INTERESTS

The authors declare no competing financial interests.

Published online at http://dx.doi.org/10.1038/ncb3347
Reprints and permissions information is available online at www.nature.com/reprints

1. Edwards, R. G., Bavister, B. D. & Steptoe, P. C. Early stages of fertilization *in vitro* of human oocytes matured *in vitro*. *Nature* **221,** 632–635 (1969).
2. Edwards, R. G., Steptoe, P. C. & Purdy, J. M. Fertilization and cleavage *in vitro* of preovulator human oocytes. *Nature* **227,** 1307–1309 (1970).
3. Koot, Y. E., Teklenburg, G., Salker, M. S., Brosens, J. J. & Macklon, N. S. Molecular aspects of implantation failure. *Biochim. Biophys. Acta* **1822,** 1943–1950 (2012).
4. Enders, A. C., Schlafke, S. & Hendrickx, A. G. Differentiation of the embryonic disc, amnion, and yolk sac in the rhesus monkey. *Am. J. Anat.* **177,** 161–185 (1986).
5. Pera, M. F. & Trounson, A. O. Human embryonic stem cells: prospects for development. *Development* **131,** 5515–5525 (2004).
6. Weimar, C. H., Post Uiterweer, E. D., Teklenburg, G., Heijnen, C. J. & Macklon, N. S. *In-vitro* model systems for the study of human embryo-endometrium interactions. *Reprod. Biomed. Online* **27,** 461–476 (2013).
7. Bedzhov, I., Leung, C. Y., Bialecka, M. & Zernicka-Goetz, M. *In vitro* culture of mouse blastocysts beyond the implantation stages. *Nat. Protoc.* **9,** 2732–2739 (2014).
8. Bedzhov, I. & Zernicka-Goetz, M. Self-organizing properties of mouse pluripotent cells initiate morphogenesis upon implantation. *Cell* **156,** 1032–1044 (2014).
9. Hertig, A. T., Rock, J. & Adams, E. C. A description of 34 human ova within the first 17 days of development. *Am. J. Anat.* **98,** 435–493 (1956).
10. Hur, Y. S. *et al.* Effect of artificial shrinkage on clinical outcome in fresh blastocyst transfer cycles. *Clin. Exp. Reprod. Med.* **38,** 87–92 (2011).
11. Morris, S. A. *et al.* Dynamics of anterior-posterior axis formation in the developing mouse embryo. *Nat. Commun.* **3,** 673 (2012).
12. Pera, M. F. *et al.* What if stem cells turn into embryos in a dish? *Nat. Methods* **12,** 917–919 (2015).
13. Gardner, D. K. The impact of physiological oxygen during culture, and vitrification for cryopreservation, on the outcome of extended culture in human IVF. *Reprod. Biomed. Online* **32,** 137–141 (2015).
14. Covello, K. L. *et al.* HIF-2α regulates Oct-4: effects of hypoxia on stem cell function, embryonic development, and tumor growth. *Genes Dev.* **20,** 557–570 (2006).
15. Ezashi, T., Das, P. & Roberts, R. M. Low O_2 tensions and the prevention of differentiation of hES cells. *Proc. Natl Acad. Sci. USA* **102,** 4783–4788 (2005).
16. Rivera-Perez, J. A., Jones, V. & Tam, P. P. Culture of whole mouse embryos at early postimplantation to organogenesis stages: developmental staging and methods. *Methods Enzymol.* **476,** 185–203 (2010).
17. Bedzhov, I., Graham, S. J., Leung, C. Y. & Zernicka-Goetz, M. Developmental plasticity, cell fate specification and morphogenesis in the early mouse embryo. *Phil. Trans. R. Soc. B* **369** (2014).
18. Roode, M. *et al.* Human hypoblast formation is not dependent on FGF signalling. *Dev. Biol.* **361,** 358–363 (2012).
19. Teklenburg, G. *et al.* Cell lineage specific distribution of H3K27 trimethylation accumulation in an *in vitro* model for human implantation. *PLoS ONE* **7,** e32701 (2012).
20. Niakan, K. K. & Eggan, K. Analysis of human embryos from zygote to blastocyst reveals distinct gene expression patterns relative to the mouse. *Dev. Biol.* **375,** 54–64 (2013).
21. O'Leary, T. *et al.* Tracking the progression of the human inner cell mass during embryonic stem cell derivation. *Nat. Biotechnol.* **30,** 278–282 (2012).
22. Niakan, K. K., Han, J., Pedersen, R. A., Simon, C. & Pera, R. A. Human pre-implantation embryo development. *Development* **139,** 829–841 (2012).
23. Haigh, T., Chen, C., Jones, C. J. & Aplin, J. D. Studies of mesenchymal cells from 1st trimester human placenta: expression of cytokeratin outside the trophoblast lineage. *Placenta* **20,** 615–625 (1999).
24. Dobreva, M. P., Pereira, P. N., Deprest, J. & Zwijsen, A. On the origin of amniotic stem cells: of mice and men. *Int. J. Dev. Biol.* **54,** 761–777 (2010).
25. Hill, J. P. The developmental history of the primates. *Phil. Trans. R. Soc. Lond. B* **221,** 45–178 (1932).
26. Luckett, W. P. The development of primordial and definitive amniotic cavities in early Rhesus monkey and human embryos. *Am. J. Anat.* **144,** 149–167 (1975).
27. Palis, J. & Yoder, M. C. Yolk-sac hematopoiesis: the first blood cells of mouse and man. *Exp. Hematol.* **29,** 927–936 (2001).
28. Taniguchi, K. *et al.* Lumen formation is an intrinsic property of isolated human pluripotent stem cells. *Stem Cell Rep.* **5,** 954–962 (2015).
29. Bryant, D. M. *et al.* A molecular switch for the orientation of epithelial cell polarization. *Dev. Cell* **31,** 171–187 (2014).
30. Bryant, D. M. & Mostov, K. E. From cells to organs: building polarized tissue. *Nat. Rev. Mol. Cell Biol.* **9,** 887–901 (2008).

METHODS

Ethics statement. Human embryo experiments were performed in three different groups under three different licences obtained from the Human Fertilization and Embryology Authority (HFEA):

(1) License reference R0193-1-a (University of Cambridge). Cryopreserved human embryos were donated to this project, entitled 'Filming of human implantation *in vitro*', after an informed consent of couples undergoing IVF treatments. Before giving consent, people donating embryos were provided with all of the necessary information about the research project and conditions that apply within the licence and HFEA Code of Practice. In addition, an independent ethic approval was obtained from the 'Human Biology Research Ethics Committee' of the University of Cambridge.

(2) License reference R0075 (Kings College London, Guy's Hospital). Informed consent was obtained from all subjects and the experiments conformed to the principles set out in the WMA Declaration of Helsinki and the NIH Belmont Report. No financial inducements are offered for donation. This project has also a local ethical approval (UK National Health Service Research Ethics Committee Reference: 06/Q0702/90).

(3) License reference R0162 (The Francis Crick Institute). Informed consent was obtained from all couples that donated spare embryos following IVF treatment. Before giving consent, people donating embryos were provided with all of the necessary information about the research project, an opportunity to receive counselling and the conditions that apply within the licence and the HFEA Code of Practice. No financial inducements are offered for donation. This project also has ethical approval from the UK National Health Services Research Ethics Committee Reference: 04/Q0108/99.

In the three locations involved in this project, all of the experiments on human embryos were performed under the HFEA Codes of Practice and the Human Fertilization and Embryology Act 1990 practices. Human embryos were not maintained in culture past 14 days or appearance of the primitive streak.

Human embryonic stem cell work complies with the regulations of the UK Code of Practice for the Use of Human Stem Cell Lines and UK Stem Cell Bank Steering committee. An ethical approval for this project was obtained from the UK Stem Cell Steering Committee.

Human embryo thawing and zona pellucida removal. Human blastocysts (day 5 and day 6) were thawed using Kitazato Thawing Media Kit VT802 (91182; Kitazato Dibimed), or Quinn's Advantage Thaw Kit (ART-8016; LifeGlobal Group) depending on the protocol used for freezing and following the manufacturer's instructions. Cleavage-stage embryos (day 1, day 2 and day 3) were thawed using Embryo Thawing Pack (10984010; Origio) and cultured in drops of human embryo culture medium (LGGG-020; LifeGlobal Group) supplemented with 10% (vol/vol) protein supplement (LPGS-605; LifeGlobal Group) under mineral oil (9305; Irvine Scientific) until blastocyst stage. The zona pellucida of each blastocyst-stage embryo was removed by brief exposure to acidic Tyrode's solution (T1788; Sigma-Aldrich), embryos were washed in the human embryo culture medium (LGGG-020; LifeGlobal Group), or SAGE 1-Step (67010060A; LifeGlobal Group), and transferred to *in vitro* culture medium (see below).

Human embryo *in vitro* culture from pre- to post-implantation stage. The *in vitro* culture procedure is illustrated in Fig. 1a. Day 5–6 human blastocysts devoid of zona pellucida were cultured on 8-well IbiTreat μ-plates (IB-80826; Ibidi GmbH) with *in vitro* culture media at 37 °C, in 21% O_2/5% CO_2 or when indicated in 5% O_2/5% CO_2. For the first 48 h the embryos were cultured in *in vitro* culture medium 1 (IVC1; see below)[7]. On *in vitro* culture day 2 (embryo day 7–8 post fertilization), 50% of the culture medium was replaced with *in vitro* culture medium 2 (IVC2; see below)[7]. From *in vitro* culture day 3 on, IVC2 medium was used and medium was refreshed on a daily basis. The detailed composition of the media used is outlined below:

IVC1. Advanced DMEM/F12 (12634-010; Thermo Fischer Scientific) supplemented with 20% (vol/vol) heat-inactivated FBS (produced in house, Stem Cell Institute, the University of Cambridge or 35-015-CV; Corning), 2 mM L-glutamine (25030; Thermo Fisher Scientific), penicillin (25 units ml^{-1})/streptomycin (25 μg ml^{-1}) (15070-063; Thermo Fischer Scientific), 1X ITS-X (10 mg l^{-1} insulin, 5.5 mg l^{-1} transferrin, 0.0067 mg l^{-1} sodium selenite, 2 mg l^{-1} ethanolamine; 51500-056; Thermo Fisher Scientific), 8 nM β-oestradiol (E8875; Sigma-Aldrich), 200 ng ml^{-1} progesterone (P0130; Sigma-Aldrich) and 25 μM *N*-acetyl-L-cysteine (A7250; Sigma-Aldrich).

Defined IVC2. Advanced DMEM/F12, supplemented with 30% (vol/vol) KnockOut Serum Replacement (10828010; Thermo Fisher Scientific), 2 mM L-glutamine, penicillin (25 units ml^{-1})/streptomycin (25 μg ml^{-1}), 1X ITS-X, 8 nM β-oestradiol, 200 ng ml^{-1} progesterone, and 25 μM *N*-acetyl-L-cysteine. The same catalogue numbers and suppliers apply as above.

A step-by-step protocol of the *in vitro* culture of human embryos through implantation stages can be found at Nature Protocol Exchange[31].

Human embryo time-lapse imaging. Time-lapse phase-contrast images were acquired using spinning-disc confocal microscopy (3i Intelligent Imaging Innovations) and a Zeiss 0.55 NA ×20 (EC PlnN) objective; and wide-field microscopy (3i Intelligent Imaging Innovations) and a Zeiss Plan-Apo Chromat 0.75 NA ×20 objective. The embryos were imaged in a humidified chamber with 21% O_2. A *Z*-range of 120 μm with 5 μm intervals was scanned every 30 min. The images were processed using Fiji (http://fiji.sc/Fiji).

Immunofluorescence of human embryos. Embryos were fixed with 4% paraformaldehyde (PFA) for 20 min at room temperature, washed with phosphate buffered saline (PBS), and permeabilized by 0.5% Triton X-100 in PBS at room temperature for 20 min. Embryos were blocked with 10% FBS (produced in house, Stem Cell Institute)/3% (w/vol) bovine serum albumin (A3311; Sigma-Aldrich) in PBS, at room temperature for 4 h. The primary antibodies mouse monoclonal anti-Oct3/4 (C-10; sc-5279; Santa Cruz Biotechnology; 1:200), rabbit polyclonal anti-aPKC (C-20; Sc-216; Santa Cruz Biotechnology; 1:200), goat monoclonal anti-GATA6 (clone 222228; mab1700; R&D Systems; 1:200), rabbit polyclonal anti-PARD6B (M-64; sc-67393; Santa Cruz Biotechnology; 1:200) and mouse monoclonal anti-cytokeratin 7 (OVTL 12-30; sc-52322; Santa Cruz Biotechnology; 1:200) were diluted in 3% (w/vol) bovine serum albumin (as above)/0.1% Tween20 (P9416; Sigma-Aldrich) in PBS and incubated at 4 °C overnight. Samples were incubated with the following fluorescence-conjugated secondary antibodies: donkey anti-mouse AlexaFluor 568, donkey anti-rabbit AlexaFluor 647, donkey anti-goat AlexaFluor 488 from Thermo Fisher Scientific. All secondary antibodies were diluted 1:500 in 3% (w/vol) bovine serum albumin (as above)/0.1% Tween20 (P9416; Sigma-Aldrich) in PBS. F-actin was stained with AlexaFluor 488 phalloidin (A12379; Thermo Fisher Scientific; 1:200) and nuclei were stained with DAPI (D3571; Thermo Fisher Scientific; 1:1,000).

Human pluripotent stem cell culture. hESC line H9 and hiPSC line FSPS 13B were kindly provided by L. Vallier (Stem Cell Institute, Anne McLaren Laboratory, Cambridge, UK). The hiPSC line SC101A-1 (System Biosciences)[32] was kindly provided by M. Lancaster (MRC Laboratory of Molecular Biology, Cambridge, UK). These hPSCs were maintained on Geltrex (A15696-01; Thermo Fisher Scientific)-coated culture plates in complete serum-free defined hPSC culture media, either Essential 8 (E8; A1517001; Thermo Fisher Scientific) or mTeSR 1 (05850; Stem Cell Technologies). Authentication of the cell lines was performed on the basis of pluripotent gene expression. No cell lines used in this study were found in the database of commonly misidentified cell lines that is maintained by ICLAC and NCBI Biosample and they were not routinely tested for mycoplasma.

3D culture of hPSCs. hPSCs were suspended as single cells using StemPro Accutase Cell Dissociation Reagent (A11105-1; Thermo Fisher Scientific) and plated following a 3D on-top protocol as previously described[33]. Briefly, IbiTreat μ-plates (IB-80826; Ibidi GmbH) were coated with Matrigel Basement Membrane Growth Factor Reduced (354230; Corning) and 2×10^4 cells were plated in either E8 or mTeSR 1 medium. After 5 min and on attachment of the cells to the Matrigel layer, the medium was removed and either fresh E8 or mTeSR 1 medium supplemented with 5% Matrigel was added on top. When indicated, 10 μM ROCK inhibitor Y-27632 (Y0503; Sigma-Aldrich) or 10/20 μM caspase 3 inhibitor Z-DEVD-FMK (1143-5; BioVision) was added to the medium.

A step-by-step protocol of the 3D culture of hPSCs can be found at Nature Protocol Exchange[31].

Immunofluorescence of 3D cultured hPSCs. hPSCs embedded in Matrigel were fixed with either 4% PFA at room temperature or ice-cold methanol at −20 °C for 15 min. The samples were permeabilized with 0.3% Triton X-100–0.1 M glycine in PBS for 20 min. The primary antibodies mouse monoclonal anti-Oct3/4 (as above, 1:200), rabbit polyclonal anti-aPKC (as above, 1:200), rabbit polyclonal anti-PARD6B (as above, 1:200), mouse monoclonal anti-GM130 (clone 35/GM130; 610822; BD Biosciences; 1:200), mouse monoclonal anti−γ−tubulin (clone GTU-88; T5326; Sigma, 1:500) and mouse monoclonal anti-PODXL (clone 222328; MAB1658; R&D Systems; 1:200) were diluted in blocking buffer (1% bovine serum albumin—A3311; Sigma-Aldrich—and 0.1% Tween) and incubated at 4 °C overnight. Samples were washed three times with PBS–0.1% Tween and incubated with AlexaFluor-conjugated secondary antibodies (as above).

Imaging. The images of the fixed samples were acquired using an inverted SP5 confocal microscope (Leica Microsystems) and Leica 1.3 NA 40× oil (HC PL APO), Leica 1.4 NA 63× oil (HC PL APO) and Leica 1.3 NA 63× glycerol (HCX PL APO) objectives. The images were processed using Fiji (http://fiji.sc), UCSF Chimera (https://www.cgl.ucsf.edu/chimera) and MovIT visualization software (BioEmergences, http://bioemergences.iscpif.fr)[34].

DOI: 10.1038/ncb3347

Statistics and reproducibility. The exact number of embryos analysed in the different conditions, as well as the number of embryos that exhibited a polarized epiblast, is indicated in Supplementary Table 1.

No statistical method was used to predetermine sample size. Given the nature of the work (mostly descriptive), no statistical comparisons were done between different embryos. Embryos that showed abnormalities (fragmented blastomeres or developmentally arrested) were excluded from the analysis. The investigators were not blinded to allocation during experiments and outcome assessment.

Figure 1 involved the assessment of 5 embryos collected across 3 independent experiments. Out of these 5 embryos 3 showed a correct development.

Figure 2 involved the assessment of 20 embryos cultured in 5% O_2 and collected across 3 independent experiment. All 20 embryos lacked the pluripotent lineage (phenotype shown in the image). Embryos were randomly assigned to either 5% O_2 or 21% O_2.

Figures 3 and 4 involved the assessment of 59 embryos collected across 6 independent experiments. Briefly, 29 embryos preserved a cluster of pluripotent cells; and out of these 29 embryos, 9 had an organized epiblast.

Figures 5 and 6 involved the assessment of a minimum of 10 hPSC cysts per panel and condition. These were collected across a minimum of 2 independent experiments per panel.

Qualitative data are presented in the form of a contingency table (Fig. 6h). These data were analysed using a Fisher's exact test.

Quantitative data are presented as mean ± s.e.m. The normality of the data was analysed with a D'Agostino–Pearson normality test. Data presented in Fig. 5b showed a normal distribution with significantly different variances. This was analysed using an unpaired two-tailed Student's *t*-test with Welch's correction.

31. Vuoristo, S., Jedrusik, A., Shahbazi, M. N. & Zernicka-Goetz, M. Culture of human embryos through implantation stages *in vitro*. *Protoc. Exch.* http://dx.doi.org/10.1038/protex.2016.017 (2016).
32. Lancaster, M. A. *et al.* Cerebral organoids model human brain development and microcephaly. *Nature* **501,** 373–379 (2013).
33. Lee, G. Y., Kenny, P. A., Lee, E. H. & Bissell, M. J. Three-dimensional culture models of normal and malignant breast epithelial cells. *Nat. Methods* **4,** 359–365 (2007).
34. Faure, E. *et al.* A workflow to process 3D+time microscopy images of developing organisms and reconstruct their cell lineage. *Nat. Commun.* **7,** 8674 (2016).

Corrigendum: Self-organization of the human embryo in the absence of maternal tissues

Marta N. Shahbazi, Agnieszka Jedrusik, Sanna Vuoristo, Gaelle Recher, Anna Hupalowska, Virginia Bolton, Norah M. E. Fogarty, Alison Campbell, Liani G. Devito, Dusko Ilic, Yakoub Khalaf, Kathy K. Niakan, Simon Fishel and Magdalena Zernicka-Goetz

Nature Cell Biology http://dx.doi.org/10.1038/ncb3347 (2016); published online 4 May 2016; corrected online 17 May 2016

In the version of this Technical Report originally published online, in Fig. 1d (which presents pilot *in vitro* culture experiments) it erroneously stated that 20% HCS was used in the IVC2 medium; it should have stated that 30% KSR was used. This error arose by a miscommunication between the postdoctoral fellow who contributed to the pilot *in vitro* culture experiments and prepared the media, and the postdoctoral fellow who performed the experiments. The composition of the media has been verified based on the laboratory notebooks that describe the media preparation. This error has been corrected in the labels and caption of Fig. 1d, in the description of the results in the main text, and in the Methods section, in all versions of the Technical Report.

nature cell biology

DOI: 10.1038/ncb3347

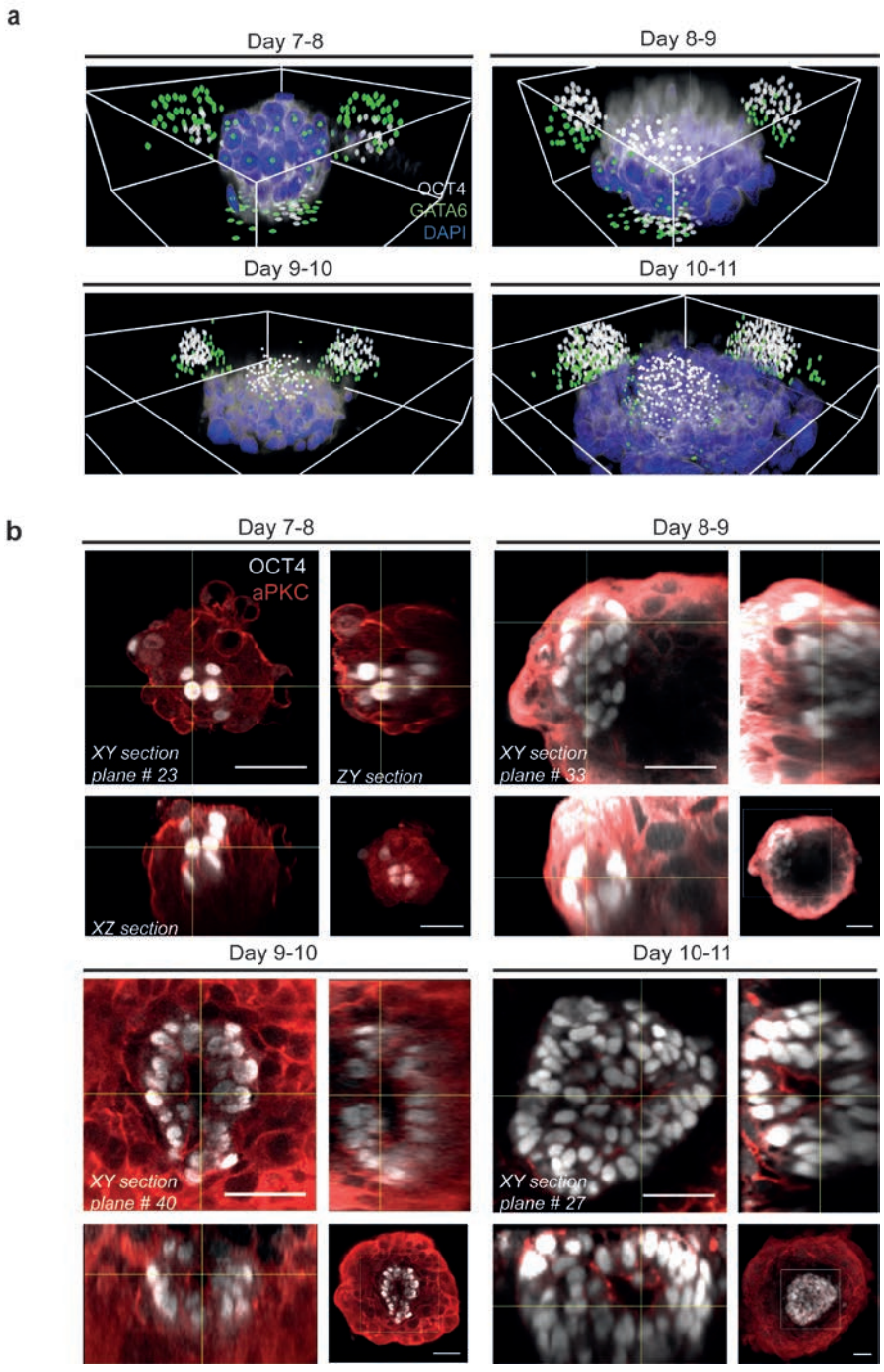

Supplementary Figure 1 3D analysis of embryonic and extra-embryonic lineages in human embryos cultured through implantation stages. Related to Figures 3 and 4. Human blastocysts developing *in vitro* until day 11 were fixed and stained at indicated time points. **a,** 3D rendering of DAPI stain overlaid with the centre of OCT4-expressing and GATA6-expressing cells. Dots are projected at the back of the volume. **b,** Orthogonal views of embryos at different developmental stages stained for aPKC and OCT4. Note the presence of a small pro-amniotic cavity at day 8-9, which is enlarged as development proceeds. All scale bars, 50 μm.

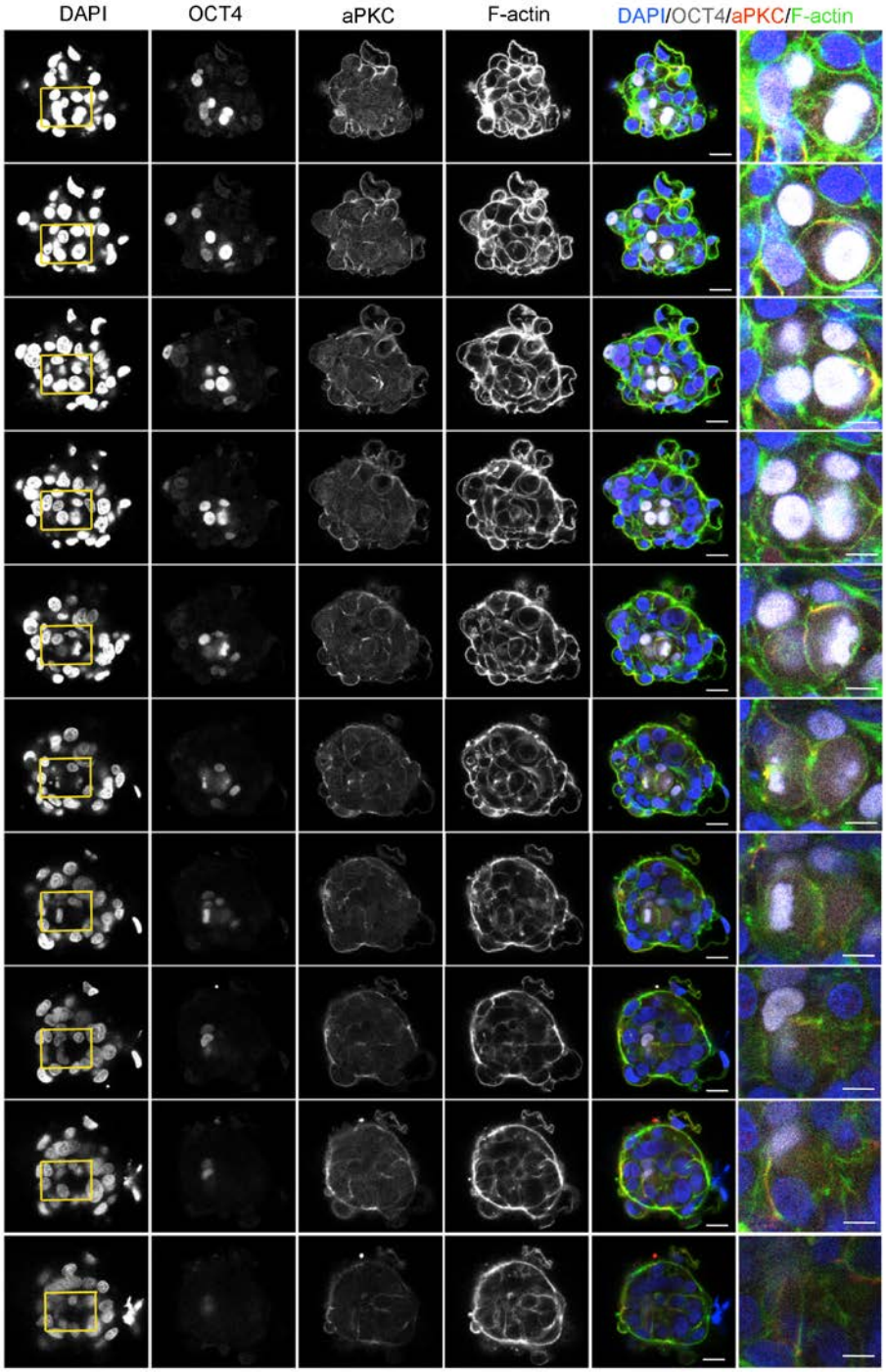

Supplementary Figure 2 Confocal Z-sections of a day 7-8 human embryo. Related to Figure 4. Day 7-8 human embryo stained for OCT4, aPKC and F-actin. The different images correspond to representative confocal Z sections. Scale bar, 20 μm. Boxes indicate the magnified area (scale bar, 10 μm).

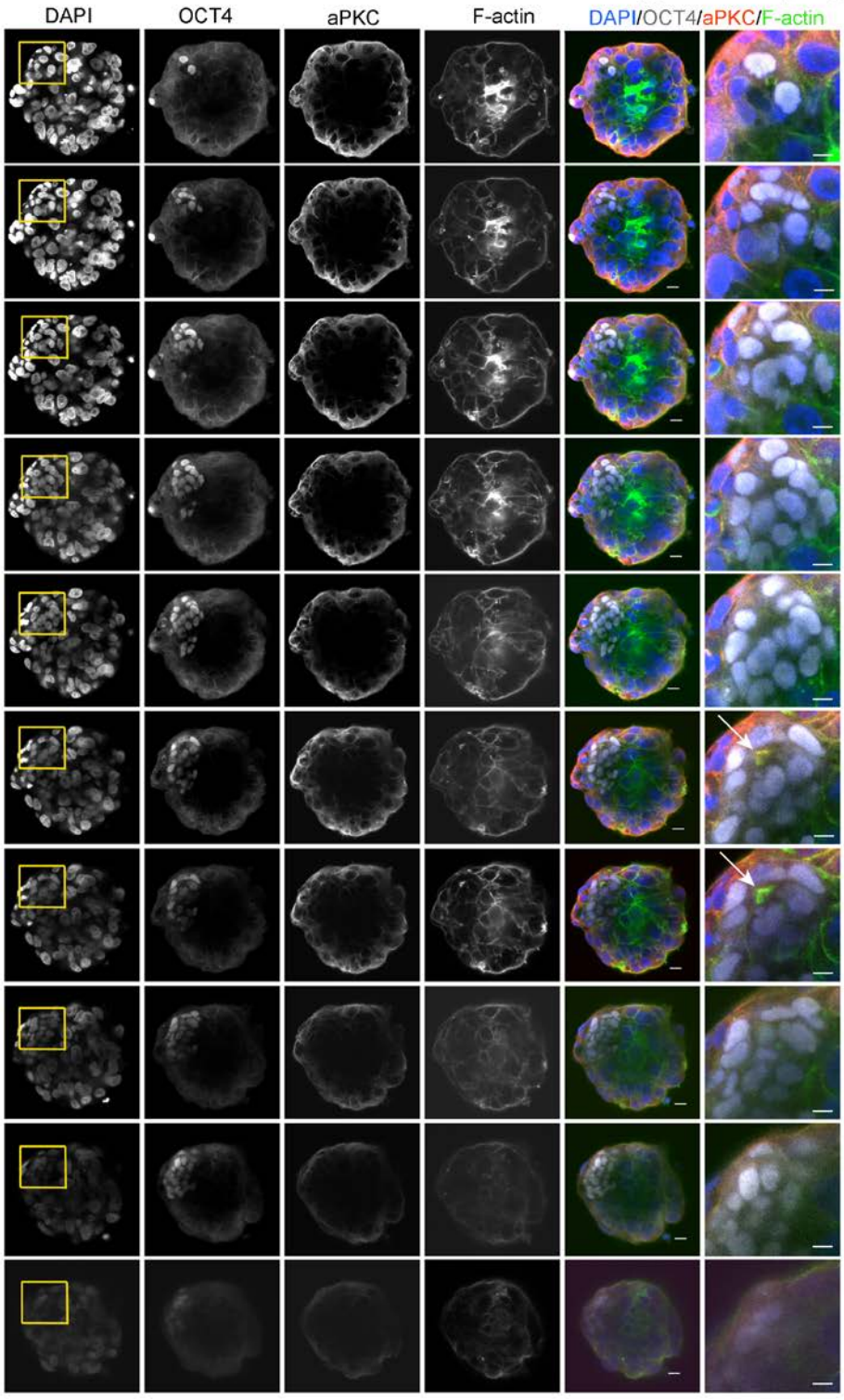

Supplementary Figure 3 Confocal Z-sections of a day 8-9 human embryo. Related to Figure 4. Day 8-9 human embryo stained for OCT4, aPKC and F-actin. The different images correspond to representative confocal Z sections. The arrow indicates the presence of a lumen. Scale bar, 20 μm. Boxes indicate the magnified area (scale bar, 10 μm).

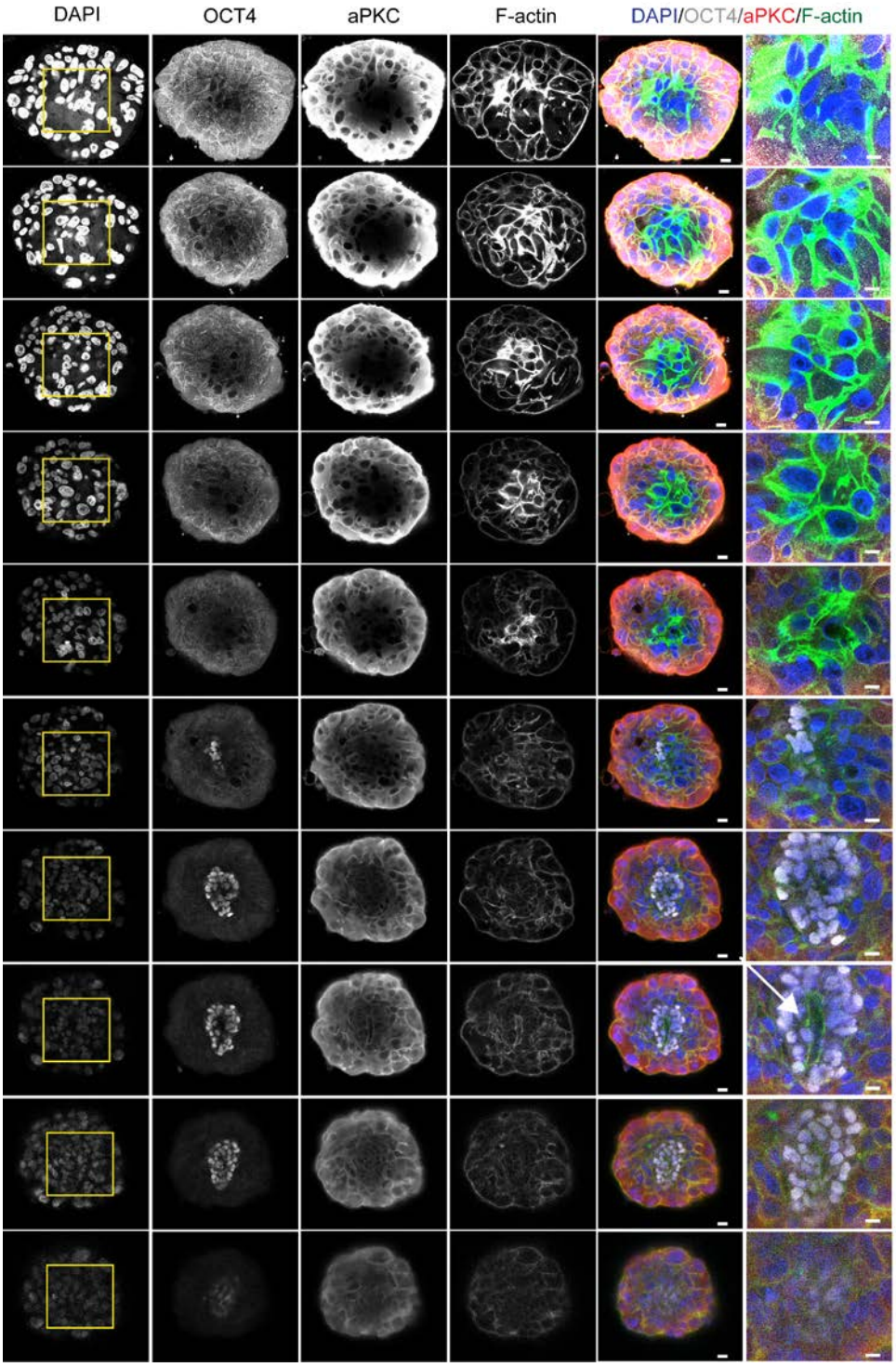

Supplementary Figure 4 Confocal Z-sections of a day 9-10 human embryo. Related to Figure 4. Day 9-10 human embryo stained for OCT4, aPKC and F-actin. The different images correspond to representative confocal Z sections. The arrow indicates the presence of a lumen surrounded by radially organised OCT4-expressing epiblast cells. Scale bar, 20 µm. Boxes indicate the magnified area (scale bar, 10 µm).

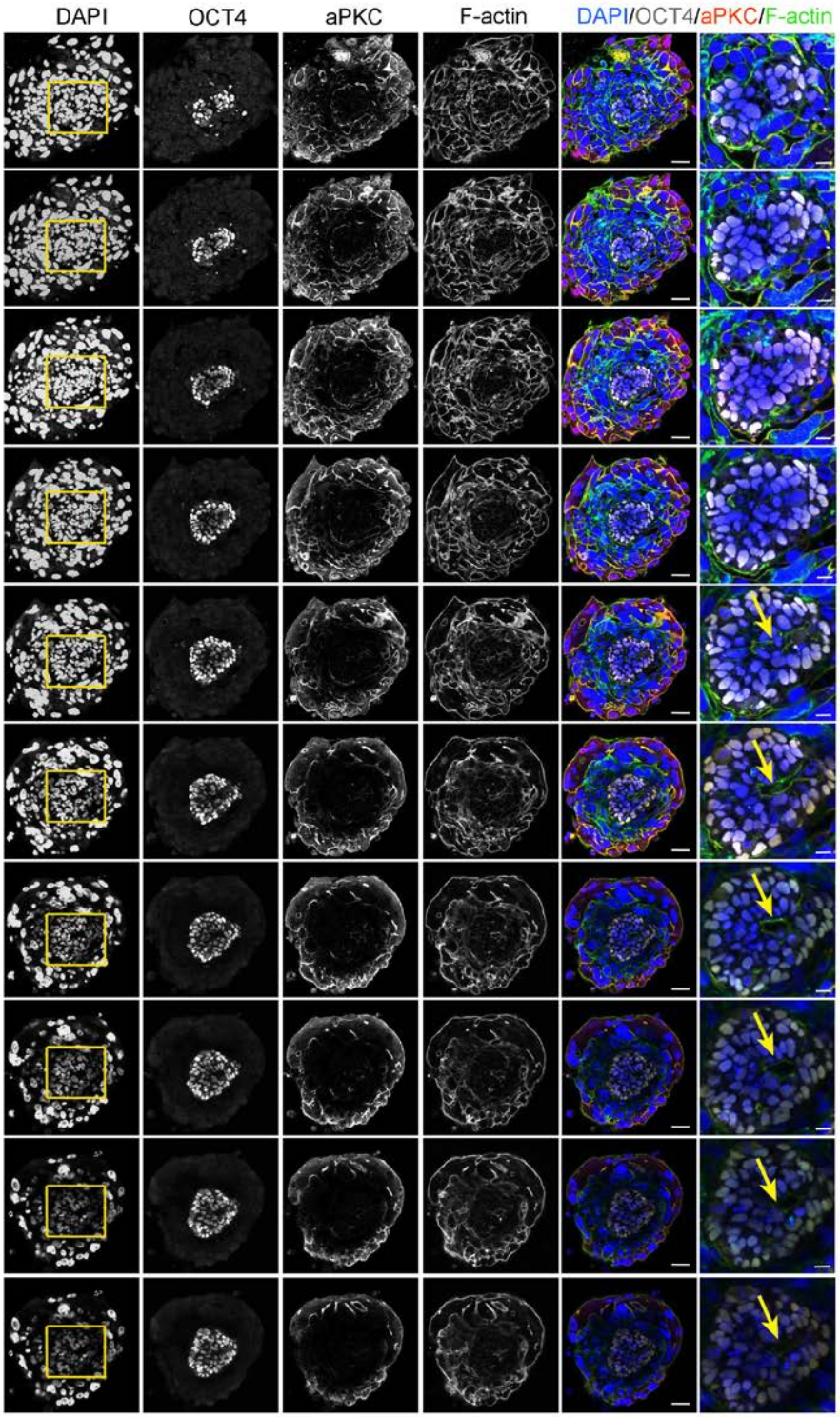

Supplementary Figure 5 Confocal Z-sections of a day 10-11 human embryo. Related to Figure 4. Day 10-11 human embryo stained for OCT4, aPKC and F-actin. The different images correspond to representative confocal Z sections. The arrow indicates the presence of a small lumen surrounded by radially organised OCT4-expressing epiblast cells. Scale bar, 50 µm. Boxes indicate the magnified area (scale bar, 20 µm).

Supplementary Table 1:
Summary of human embryos cultured in this study. Note the lack of epiblast lineage in embryos cultured in hypoxic conditions

Conditions	Embryos analysed	Pluripotent lineage	Pro-amniotic cavity formation
21% O2 (normoxia)	59	No epiblast: 30 (51%); Epiblast: 29 (49%)	Non-polarized epiblast: 20 (69%); Polarized epiblast: 9 (31%)
5% O2 (hypoxia)	20	No epiblast: 20 (100%); Epiblast: 0 (0%)	NA

Supplementary Table 2:
Average number of epiblast and hypoblast cells in human embryos at different stages of implantation development in vitro

Age of the embryo (days)	Number of OCT4+ cells	Number of GATA6+ cells
Day 7-8	17	46
Day 8-9	26	57
Day 9-10	86	61
Day 10-11	328	79

Supplementary Video Legends

Supplementary Video 1 Development of a day 5 human blastocyst in the *in vitro* culture system up to day 9-10. Related to Figure 1**.** A day 5 human embryo was cultured in the *in vitro* culture system for approximately 100 hrs. Bright field images were taken every 30 min to record its development. Scale bar, 100 μm.

Supplementary Video 2 Development of a day 9 human blastocyst in the *in vitro* culture system up to day 12. Related to Figure 1**.** A day 9 human embryo was cultured in the *in vitro* culture system for approximately 72 hrs. Bright field images were taken every 30 min to record its development. Scale bar, 100 μm.

Supplementary Video 3 3D reconstruction of embryonic lineages in a day 9-10 human embryo cultured *in vitro***.** Related to Figure 3. Nuclei are shown in blue, OCT4 in grey and GATA6/F-actin in green.

Supplementary Video 4 3D reconstruction of embryonic lineages in a day 10-11 human embryo cultured *in vitro***.** Related to Figure 3. Nuclei are shown in blue, OCT4 in grey and GATA6/F-actin in green.

Supplementary Video 5 3D reconstruction of the cellular and nuclear shape of representative trophectoderm cells at day 10-11. Related to Figure 3. Nuclei are shown in magenta and membranes in green. Note that cells in close proximity to the epiblast have a single nucleus, whereas cells in the periphery of the embryo are multinucleated.

Supplementary Video 6 3D reconstruction of the pro-amniotic cavity at day 9-10. Related to Figure 4. The nuclei of OCT4-expressing epiblast cells is shown in grey and the pro-amniotic cavity in red.

Supplementary Video 7 3D reconstruction of the cellular shape of representative OCT4-expressing epiblast cells at day 10-11. Related to Figure 4. Epiblast cells in close proximity to GATA6-expressing hypoblast cells are shown in green (note the columnar shape characteristic of cells within the epiblast disc). Epiblast cells in close proximity to cytotrophoblast cells are shown in magenta (note the squamous shape characteristic of amniotic cells).

Supplementary Video 8 3D reconstruction of the prospective yolk sac at day 10-11. Related to Figure 4. The nuclei of OCT4-expressing epiblast cells is shown in grey and the prospective yolk sac in blue.

Supplementary Video 9 3D reconstruction of the hypoblast derived cells and their position with respect to the prospective yolk sac at day 10-11**.** Related to Figure 4. Nuclei of OCT4-expressing epiblast cells are shown in grey, GATA6/F-actin is shown in green and the prospective yolk sac in blue.

LETTERS
https://doi.org/10.1038/s41556-017-0017-8

nature cell biology

Segregation of mitochondrial DNA heteroplasmy through a developmental genetic bottleneck in human embryos

Vasileios I. Floros[1,2], Angela Pyle[3], Sabine Dietmann[4], Wei Wei[1,2], Walfred W. C. Tang[5], Naoko Irie[5], Brendan Payne[4], Antonio Capalbo[6,7], Laila Noli[8,9], Jonathan Coxhead[4], Gavin Hudson[4], Moira Crosier[10], Henrik Strahl[11], Yacoub Khalaf[8,9], Mitinori Saitou[12,13], Dusko Ilic[8,9], M. Azim Surani[5] and Patrick F. Chinnery[1,2]*

Mitochondrial DNA (mtDNA) mutations cause inherited diseases and are implicated in the pathogenesis of common late-onset disorders, but how they arise is not clear[1,2]. Here we show that mtDNA mutations are present in primordial germ cells (PGCs) within healthy female human embryos. Isolated PGCs have a profound reduction in mtDNA content, with discrete mitochondria containing ~5 mtDNA molecules. Single-cell deep mtDNA sequencing of in vivo human female PGCs showed rare variants reaching higher heteroplasmy levels in late PGCs, consistent with the observed genetic bottleneck. We also saw the signature of selection against non-synonymous protein-coding, tRNA gene and D-loop variants, concomitant with a progressive upregulation of genes involving mtDNA replication and transcription, and linked to a transition from glycolytic to oxidative metabolism. The associated metabolic shift would expose deleterious mutations to selection during early germ cell development, preventing the relentless accumulation of mtDNA mutations in the human population predicted by Muller's ratchet. Mutations escaping this mechanism will show shifts in heteroplasmy levels within one human generation, explaining the extreme phenotypic variation seen in human pedigrees with inherited mtDNA disorders.

The 16.5-kilobase human mitochondrial genome (mtDNA) encodes 37 genes essential for the synthesis of 13 polypeptide subunits of the respiratory chain, the final common pathway of oxidative metabolism[1]. In humans, mtDNA is inherited exclusively down the maternal line. Diploid cells typically contain 1–10,000 mtDNA molecules partitioned between a network of fusing and budding mitochondria. Exposed to a potent source of oxygen free radicals and lacking protective histone proteins, mtDNA is particularly vulnerable to mutation, creating a mixed population of wild-type and mutated mtDNA within a cell (heteroplasmy)[2]. MtDNA mutations accumulate in non-dividing (post mitotic) cells during life, with high levels observed in late-onset human disorders including Alzheimer's disease and Parkinson's disease. Although the overall tissue mutation burden is low, very high levels within single cells lead to bioenergetic failure and ultimately cause cell death[1]. These findings raise the possibility that mtDNA mutations contribute to the pathogenesis of several common human diseases, and also play a part in the ageing process itself[3], but the origin of these mutations has not been clear.

Age-associated mtDNA mutations were assumed to arise in somatic tissues during life, but deep sequencing of maternal relatives raised the possibility that low-level mtDNA heteroplasmic point mutations are inherited down the maternal line[4]. To determine whether this is the case, we developed methods to isolate pure primordial germ cells (PGCs) from first trimester karyotypically normal human female embryos (Fig. 1). Anatomical regions containing migrating PGCs were dissected from fresh 4-week embryos, and genital ridges were isolated from 5–8-week embryos. Single-cell suspensions were then labelled with fluorochrome-conjugated antibodies against putative human germ cell surface markers, and sorted using fluorescence-activated cell sorting (FACS). Tissue non-specific alkaline phosphatase (TNAP) histochemistry[5], VASA immunocytochemistry[6] (Supplementary Fig. 1) and germ-cell-specific transcripts (Supplementary Figs. 1 and 2)[7] were used to determine the proportion of PGCs after FACS sorting at appropriate developmental stages. Highly purified (>97%) PGCs were isolated in 4-week (Carnegie stage, CS12) embryos using a combination of TNAP, stage-specific embryonic antigen 4 (SSEA4) and the PGC-associated cell-surface marker CD38; and for weeks 5–8 (CS16/17–CS20/21), we used TNAP and c-KIT antibodies (Fig. 1b).

After cell lysis, mtDNA was amplified in overlapping 2-kilobase fragments to minimize potential contamination from nuclear-encoded mitochondrial insertions (NumtS), before > 5,000-fold depth re-sequencing. NumtS contamination was further minimized by filtering-out all variants with a minor allele frequency (MAF) < 1%. Sequencing of a cloned mtDNA template showed no variants present at ≥ 1% MAF (Supplementary Fig. 3). However, we observed mtDNA single-nucleotide variants at > 1% heteroplasmy in PGCs isolated from all 12 embryos studied (Fig. 2a),

[1]MRC-Mitochondrial Biology Unit, University of Cambridge, Cambridge, UK. [2]Department of Clinical Neurosciences, Cambridge Biomedical Campus, University of Cambridge, Cambridge, UK. [3]Wellcome Trust Centre for Mitochondrial Research, Institute of Genetic Medicine, Newcastle University, Newcastle upon Tyne, UK. [4]Wellcome Trust-Medical Research Council Stem Cell Institute, University of Cambridge, Cambridge, UK. [5]Wellcome Trust Cancer Research UK Gurdon Institute, University of Cambridge, Cambridge, UK. [6]GENERA, Centre for Reproductive Medicine, Clinica Valle Giulia, Rome, Italy. [7]GENETYX, Reproductive Genetics Laboratory, Marostica, Italy. [8]Division of Women's Health, Faculty of Life Sciences and Medicine, King's College London, London, UK. [9]Assisted Conception Unit, Guy's Hospital, London, UK. [10]Human Developmental Biology Resource, Institute of Genetic Medicine, Newcastle University, Newcastle upon Tyne, UK. [11]Centre for Bacterial Cell Biology, Institute for Cell and Molecular Biosciences, Newcastle University, Newcastle upon Tyne, UK. [12]Department of Anatomy and Cell Biology, Graduate School of Medicine, Kyoto University, Kyoto, Japan. [13]JST, ERATO, Kyoto, Japan. Vasileios I. Floros and Angela Pyle contributed equally to this work. *e-mail: pfc25@cam.ac.uk

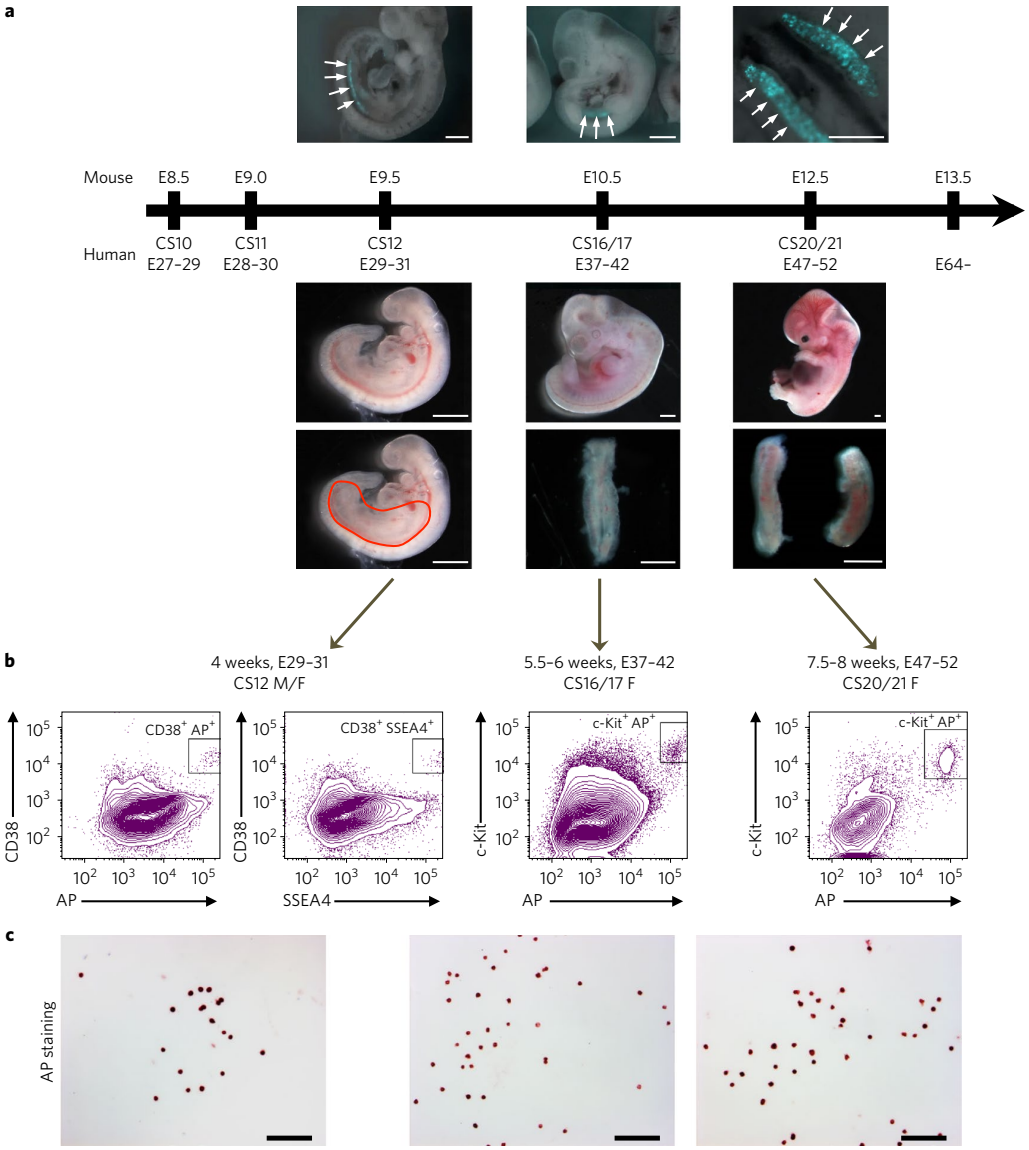

Fig. 1 | Isolation of a pure population of human primordial germ cells (PGCs). a, Human and mouse developmental time points used in this study. Top: *Prdm1* (*Blimp1*)-mVenus and *Dppa3* (*Stella*)-eCFP (*BVSC*) mouse embryos (E9.5 and E10.5) and gonads (E12.5)[17]. The arrows show the fluorescent mouse PGCs subsequently isolated by fluorescent sorting. Scale bars, from left to right, 0.5 mm, 1 mm and 0.5 mm. Bottom: fresh human female embryos showing the lower core-body dissected area (outlined in red) for 4-week (Carnegie stage (CS)12) embryos (left), and dissected female embryonic gonads for 5.5–6-week (CS16/17) and 8-week (CS20/21) embryos (middle and right). Scale bars, 1 mm. **b**, Isolation of human PGCs by fluorescent sorting: for 4-week (CS12) dissected embryos, using a triple-positive combination for TNAP, stage-specific embryonic antigen 4 (SSEA4) and CD38; and for weeks 5–8 (CS16/17 to CS20/21), using gonadal tissue double-positive for TNAP and c-Kit. The boxes in the FACS plots show the sorted cell population. **c**, The purity of isolated hPGCs was validated by alkaline phosphatase (AP) activity staining showing > 97% positive cells. Scale bars, 100 µm. See also Fig. 4a–c and Supplementary Figs. 1 and 2. Observations for **b** and **c** were independently replicated three times at each developmental stage.

which did not map to known human NumtS[8]. This shows that low-level mtDNA heteroplasmy is present within the female germ line in healthy humans. The variants were predominantly nucleotide transitions, which are less prone to in vitro sequencing error and less likely to be due to oxidative damage[9], and are consistent with errors during in vivo DNA synthesis by mtDNA polymerase ϒ or the deamination of cytidine and adenosine[10].

We also observed a change in the mutation spectrum from CS12 to CS20/21 (Fig. 2a). For protein-coding genes, there was a decrease in the proportion of non-synonymous variants (non-synonymous/synonymous ratio, $P = 0.02$) and a corresponding change in the codon bias (Fig. 2b,c). We also saw a decrease in the mutation rate per base pair for transfer RNA genes (Fig. 2d), which are hallmarks of selection against potentially deleterious mtDNA variants. Similar patterns have been seen in mice[11,12], but the timing and mechanism of the selection was not known. On the basis of our observations, this occurs at an early stage in the developing human female germ line during PGC specification and migration. We were surprised to see some evidence of selection against variants in the non-coding mtDNA D-loop (Fig. 2d), but these did not appear to be evenly distributed. CS12

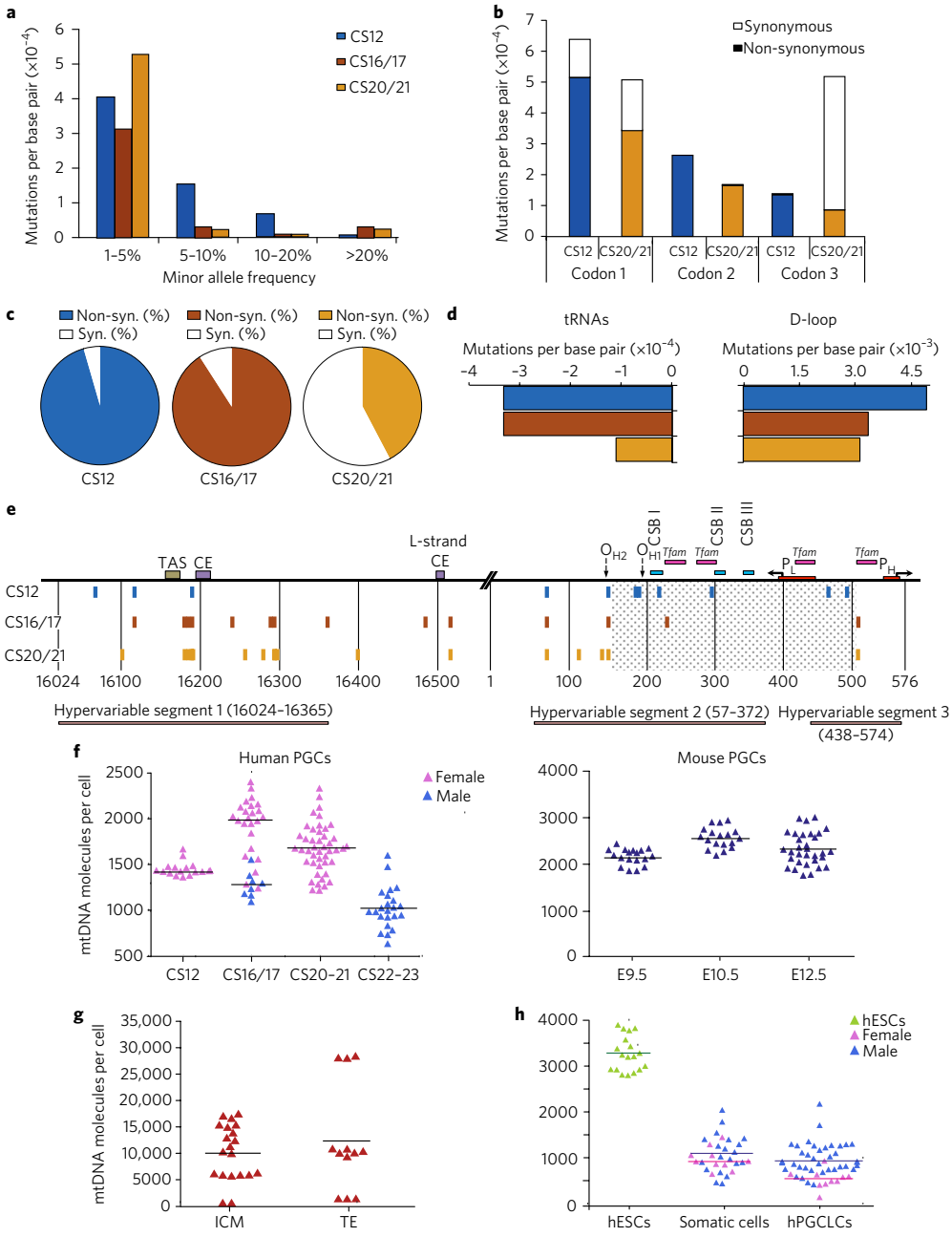

Fig. 2 | Mitochondrial DNA variants in human primordial germ cells. a–**e**, MtDNA variants exceeding the assay detection threshold (minor allele frequency) of >1% during human primordial germ cell (PGC) development. Data were derived from $n=80$ single cells sorted from two CS12 embryos, $n=240$ cells sorted from four CS16/17 embryos, and $n=360$ cells sorted from six CS20/21 embryos. **a**, Frequency distribution of mtDNA variants at sequential stages of germline development. **b**, Codon positions affected by the coding region mutations (no codon bias for CS12, P is not significant; significant codon bias for CS20/21, $P=0.005$; Fisher's exact text, two-sided). **c**, Proportion of non-synonymous (shaded) variants and synonymous (white) (dN/dS, $P=0.02$, Fisher's exact text, two-sided). **d**, Evidence of selection against mtDNA variants in tRNA genes ($P=0.03$, Fisher's exact text, two-sided) and the non-coding displacement (D)-loop ($P=0.003$) between CS12 and CS20/21. **e**, Position of the variants detected in the non-coding mtDNA D-loop region. **f**, MtDNA content of single in vivo PGCs from human (left, $n=117$) and *Blimp1*-mVenus and *Stella*-eCFP (*BVSC*) mouse (right, $n=68$) embryos. Each data point represents the mtDNA content in a single cell corresponding to the mean value from the independent qPCR measurements. Source data are available in Supplementary Table 6. **g**, MtDNA content of single human inner cell mass (ICM, $n=20$) and trophectoderm (TE, $n=12$) cells from five embryos in vivo. Each data point represents the mtDNA content in a single cell corresponding to the mean value from the independent qPCR measurements. Source data are available in Supplementary Table 6. **h**, MtDNA content of single human embryonic stem cells (hESCs, $n=18$), somatic cells ($n=30$) and human primordial germ-cell like cells (hPGCLC, $n=48$) isolated in vitro[7,21]. Two independent PGCLC inductions were performed for both the male (WIS2) and female (H9) ESC lines, with cells analysed at day 5/6. Source data are available in Supplementary Table 6. Each data point represents the mtDNA content in a single cell corresponding to the mean value from the independent qPCR measurements. Horizontal lines in **f**–**h** represent the mean values.

PGCs contained variants in conserved regions not present in CS20/21 PGCs (Fig. 2e), consistent with selection against variants in regions involved in mtDNA transcription and replication[13].

Given that the majority of the mtDNA variants were present at low heteroplasmy levels (Fig. 2a), below the conventional threshold required for a biochemical effect, it was not immediately apparent how the selection could occur. To explore the potential mechanism, we measured the absolute amount of mtDNA in the human PGCs at different stages of development in vivo, and then sequenced individual late-stage PGCs to look for evidence of variant segregation. First, we studied human oocytes from three healthy donors, which contained a mean of 1.22×10^6 mtDNA molecules (s.d. = 189,742, $n=3$)[14]. This was in keeping with previous measurements[15] and confirmed assay reliability. The amount of mtDNA in human PGCs from 14 embryos in vivo was ~1,000-fold less than in oocytes (CS12 mtDNA copies: median 1,425, mean 1,446, s.d. = 77) (Fig. 2f), consistent with a human genetic bottleneck. The mtDNA levels in female and male PGCs were similar, as previously seen in mice[16], and resembled new measurements made in *Blimp1*–mVenus and *Stella*–eCFP [*BVSC*] mice[17] (Fig. 2f; mouse embryonic day (E)9.5 corresponds to human CS12 and mouse E12.5 corresponds to human CS20/21). This validates previous findings in mice with different nuclear genetic backgrounds[16,18,19], and shows a similar mechanism in both humans and mice. However, the lower amount of mtDNA we observed in human PGCs (human/mouse: CS12/E9.5, $P<0.0001$; CS16–17/E10.5, $P<0.0001$; CS20–21/E12.5, $P<0.0001$) predicts a 'tighter' genetic bottleneck in humans than in mice, and thus the more rapid segregation of heteroplasmy. This is in accordance with observations in human and mouse pedigrees where more dramatic shifts in heteroplasmy are seen in humans (see Fig. 4a in ref. [20]).

It is not technically possible to isolate human PGCs from earlier stages because the cells are collected from clinical samples. However, to gain further insight we also measured mtDNA levels in single cells from both the human inner cell mass (ICM) and trophectoderm cells (Fig. 2g). Although we saw a wide range of mtDNA levels in ICM cells, the mean level (9,794, s.d. = 5,661) was more than fivefold greater than in PGCs. We then studied embryonic stem cells (hESCs) and human PGC-like cells (hPGCLCs)[7,21] that are derived from the embryonic epiblast in vitro, thus allowing us to estimate the amount of mtDNA at an intermediate stage of human germ cell development (Fig. 2h). hESCs (mean = 3,264, s.d. = 378) contained less mtDNA than ICM cells, and hPGCLCs (mean = 896, s.d. = 368) contained less mtDNA than hESCs ($P=8.9\times10^{-33}$). These findings are in keeping with a post-implantation mtDNA bottleneck. The female hPGCLCs (mean = 533, s.d. = 203) contained significantly less mtDNA than male hPGCLCs (mean = 991, s.d. = 342, $P=1.5\times10^{-5}$), and less mtDNA than both male (mean = 1102, s.d. = 426, $P=2.2\times10^{-16}$) and female (mean = 972, s.d. = 248, $P=2.2\times10^{-16}$) somatic cells isolated from the same in vitro system but not expressing germ-cell markers. These findings suggest a more stringent mtDNA bottleneck in the human female germ line.

Returning to the PGCs isolated in vivo, next we analysed the subcellular distribution of mtDNA molecules within the developing human female germ line. We used the dissector method to measure the number of mitochondria in human PGCs on adjacent-section electron micrographs (Fig. 3a), validating our results with super-resolution whole-cell imaging using Nikon structured illumination microscopy in three dimensions (N-SIM; Supplementary Videos 1 and 2 and Fig. 3b). The number of mitochondria did not change between CS12 and CS20–21, allowing us to estimate the number of mtDNA per mitochondrion at ~5 per organelle in human PGCs. The reduction in mtDNA content after fertilization of the oocyte (Fig. 2f), and associated intracellular compartmentalization of mtDNA (Fig. 3a,b), has important implications for the distribution of mtDNA heteroplasmy between individual organelles. Assuming that mutated mtDNA molecules are randomly distributed between mitochondria, higher levels of heteroplasmy within a cell will be associated with a greater proportion of mitochondria containing very high levels (>80%) of a specific mutation (Fig. 3c). For example, if the average level within a cell is 40–50% mutant, then 10–20% of the organelles will contain > 80% mutant mtDNA, exceeding the threshold required to cause a biochemical defect for pathogenic mutations[1,2]. In this context, ~10–20% of the organelles would be dysfunctional and potentially vulnerable to removal by mitochondrial quality-control mechanisms, removing mutated mtDNA through selection at the organellar level. To determine whether this is plausible, we performed deep mtDNA sequencing on individual late-stage in vivo PGCs (Fig. 3d,e). This showed much higher percentage levels of mtDNA heteroplasmy within individual germ cells, reaching up to 47% mutant. Thus, following the bottleneck, high levels of mtDNA mutations are found in single PGCs, and are predicted to reach very high levels in individual mitochondria (Fig. 3c). The most likely explanation for the observed change in codon bias seen between CS12 and CS20–21 (Fig. 2b) is the rapid segregation of variants above and below the assay detection threshold (1% MAF) due to the genetic bottleneck (Fig. 2a,c), rather than de novo mutation events per se. In this context, even a subtle bias against deleterious variants would tend to suppress them below the detection threshold, whilst allowing non-functional variants to segregate freely to high levels (Fig. 3d).

To cast light on the possible mechanism of selection, we performed RNA sequencing (RNA-seq) on week-4–9 human PGCs. Unsupervised hierarchical clustering of gene expression and principal component analysis (PCA) of transcriptome confirmed strong expression of germ-cell-specific transcripts (Fig. 4a–c). Importantly, we also observed a distinct transcript profile for the nuclear-encoded mitochondrial proteins (MitoCarta2.0)[22] in the early stages of PGC development (Fig. 4d). PCA of both the nuclear-encoded and the mtDNA-encoded transcripts showed that the most dramatic changes were during the early stages of germ cell development, with mitochondrial genes forming a cluster distinct from late gonadal PGC genes, such as *DAZL* and *DDX4* (Supplementary Fig. 4). The mtDNA-encoded transcripts had the highest scores on PC1, accounting for 92% of the total variance (Fig. 4e). This is consistent with the developmental progression of mtDNA gene expression during PGC development. In contrast, genes involved in the canonical glycolysis pathway had opposing trends on PC1 (Supplementary Figs. 4 and 5). Although based solely on transcript analysis, these findings suggest that PGCs become less dependent on glycolytic metabolism and more dependent on oxidative metabolism as they develop. As a consequence, non-synonymous mtDNA mutations are progressively more likely to have phenotypic consequences during germ cell development. The proliferation of PGCs between CS12 and CS20/21 requires considerable mtDNA replication, inevitably introducing new mutations through Υ polymerase errors. These new mutations are more likely to be synonymous (Fig. 2) and have no functional consequence. The switch from glycolytic to oxidative metabolism provides an explanation for these findings, by exposing functional variants to the selective effects during this critical time period of PGC development.

Germline mtDNA selection at the organelle level has been proposed in mammals[12,23] and *Drosophila*[24,25], but it is not known how this occurs. One possibility is that mitochondria depolarize when the proportion of mutated respiratory chain subunits is high, activating intracellular surveillance systems mediated by Pink1 and Parkin, and leading to the selective removal of damaged organelles containing mutant mtDNA by mitophagy[26,27]. Alternatively, impaired mtDNA replication in ATP-deficient organelles[28] could lead to the preferential turnover of mitochondria containing wild-type genomes; or the transport of mitochondria may be compromised in deficient organelles, preventing their coalescence around

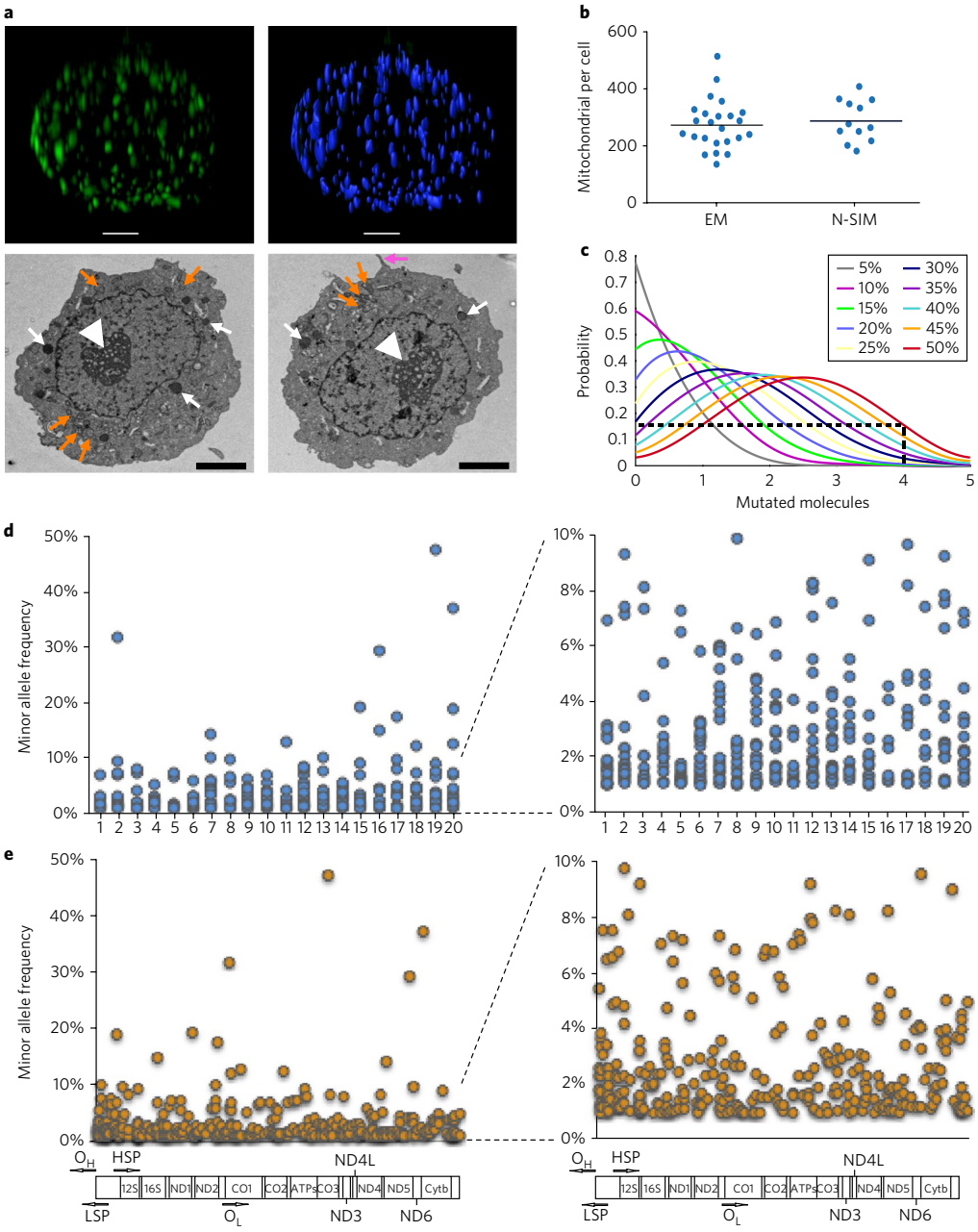

Fig. 3 | Morphology and deep sequencing of single human primordial germ cells in vivo. a, Top: N-SIM image of a human PGC labelled with anti-TOM20 (Supplementary Video 1) with mitochondria identified and counted by IMARIS (Supplementary Video 2). Scale bars, 2 μm. Bottom: transmission electron micrographs characteristic of human PGCs[40]. The white arrowheads indicate the nucleoli. The white arrows indicate chromatin, electron-dense glycogen particles and lipid droplets; the pink arrow, pseudopodia in the migratory stage (CS12) PGCs (right image only); and the orange arrows, round discrete mitochondria around the nucleus. Scale bars, 2 μm. Similar observations made from three independent experiments. **b**, Number of mitochondria in human primordial germ cells. Left (electron micrograph, $n = 24$ cells): mitochondrial count per cell using the dissector method and serial-section electron micrographs. Right (N-SIM, $n = 12$ cells): super-resolution microscopy. Each data point represents a measurement from a single PGC. Electron micrograph: mean = 275.9, median = 272, s.d. = 87.76. N-SIM: mean = 288.8, median = 272, s.d. = 72.12. The horizontal bar represents the mean value. **c**, Probability of an individual mitochondrion containing mutated mtDNA molecules as a function of the overall heteroplasmy level within the cell. Binomial distributions assuming five molecules/mitochondrion that are randomly distributed between organelles. For cells containing 40–50% mutant mtDNA, many mitochondria are likely to contain four or more mutated molecules (> 80%). If deleterious, these high levels will potentially depolarize the cell, triggering mitophagy, or inhibit mtDNA replication within that organelle, potentially leading to selection against mutations at the organellar level. **d**, Minor allele frequency (MAF) of mtDNA variants in 20 single human PGCs from three CS20/21 embryos detected by deep sequencing (left panel). The right panel shows the same data with the *y* axis scaled from 1–10% MAF. In both panels, the detection threshold was set at MAF > 1%. **e**, Position of the variants from single human PGCs within the mitochondrial genome (left panel). The right panel shows the same data with the *y* axis scaled from 1–10% MAF. In both panels, the detection threshold was set at MAF > 1%.

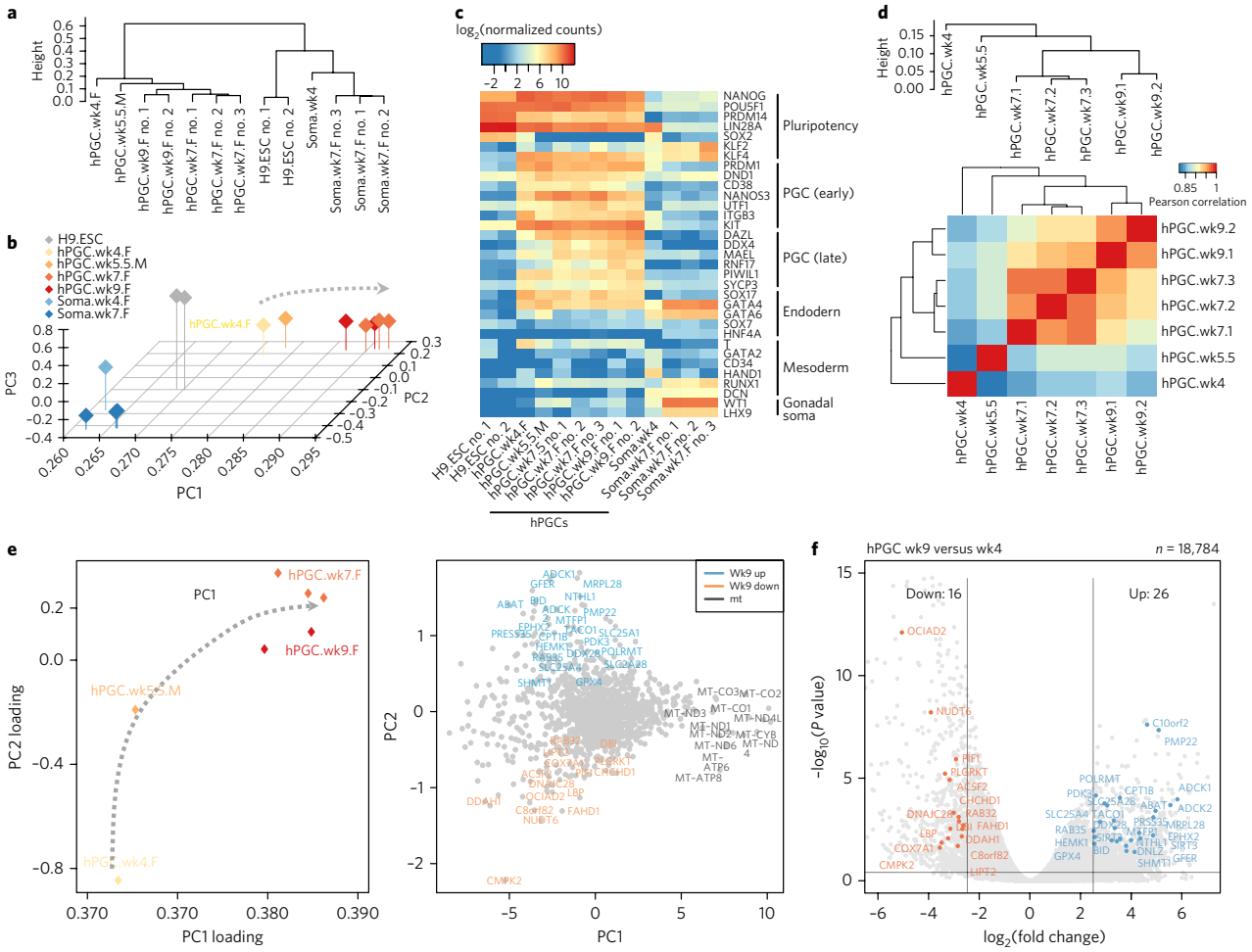

Fig. 4 | Transcriptome analysis of human primordial germ cells. Analysis of $n=13$ transcriptomes. **a**, Unsupervised hierarchical clustering of RNA-seq expression profiles in H9 embryonic stem cells (ESCs), week 4, week 7 and week 9 female (F) human PGCs and week 5.5 male (M) hPGCs, and gonadal somatic cells (soma) showing clustering of gene expression consistent with the appropriate developmental stage (see also Supplementary Fig. 4). Results from a single analysis of the entire transcriptome data set. **b**, PCA of RNA-seq gene expression in hPGC samples. The dotted arrow indicates developmental progression along PC1. **c**, Heat map showing expression of key PGC-associated transcripts (early and late) and of pluripotency, mesoderm, endoderm and gonadal somatic markers. **d**, Correlation of transcription profiles of human PGCs of various stages for nuclear-encoded mitochondrial transcripts predicted by MitoCarta2.0 (see Methods; Pearson's correlation, two-sided) and mtDNA-encoded transcripts. Only genes with normalized reads counts with ($\log_2$(normalized counts) > 2.5) were used for analysis. Expression levels were averaged over biological replicates. The number of biological replicates at each developmental stage is shown in the cluster diagram shown in **a** generated from a total of 13 separate transcriptomes. This shows a progressive change in transcriptome profiles for mitochondrial genes in a sequential manner during PGC development. **e**, Two-dimensional PCA of RNA-seq gene expression (PC2 against PC1) for mitochondrial nuclear-encoded and mtDNA-encoded genes (MitoCarta2.0) at the different stages of hPGCs (left), with a corresponding plot of the PC scores on PC2 and PC1 (right). Gene names are colour-coded to illustrate upregulated expression in hPGCs.wk9 (purple), and downregulated expression in hPGs.wk9 (red) when compared with the hPGCs.wk4 sample (see also **f**, Supplementary Figs. 4 and 5 and Supplementary Table 4). The arrow line indicates potential mitochondrion-related-transcript progression for each developmental stage from migratory hPGC.w4 to gonadal hPGC.wk9. **f**, Volcano plot showing differentially expressed genes (from MitoCarta2.0 list) between week 9 ($n=2$ independent replicates) and week 4 (this measurement was performed once) hPGCs ($\log_2$(fold change) > 2.5, $P<0.05$, DEseq two-sided; see Methods). See also Supplementary Figs. 4 and 5 and Supplementary Table 4. Note that the week-9 PGCs included in the RNA-seq analysis were from a slightly later developmental stage than CS20/21, reflecting the clinical samples that were available.

the Balbiani body where intense mtDNA replication occurs[18]. In our data, specific genes that were upregulated >2.5-fold (Fig. 4f) included *POLRMT, C10orf2*, *SLC25A4* and *MRPL28*, which play a key role in mtDNA replication and gene expression (Supplementary Table 4), similarly seen in the PCA (Supplementary Fig. 4). Thus, mtDNA variants influencing mtDNA replication and expression will also be more likely to have an effect as PGCs develop, providing a possible explanation for the signature of selection we observed against tRNA and D-loop variants between CS12 and CS21 (Fig. 2d,e).

We also saw low levels of mtDNA somatic cells in vitro (Fig. 2h) and in vivo (Fig. 5a), in keeping with a somatic cell bottleneck, as previously observed in mice[19]. We also detected mtDNA variants in the somatic cells in vivo at similar levels to PGCs (Fig. 5b), but the

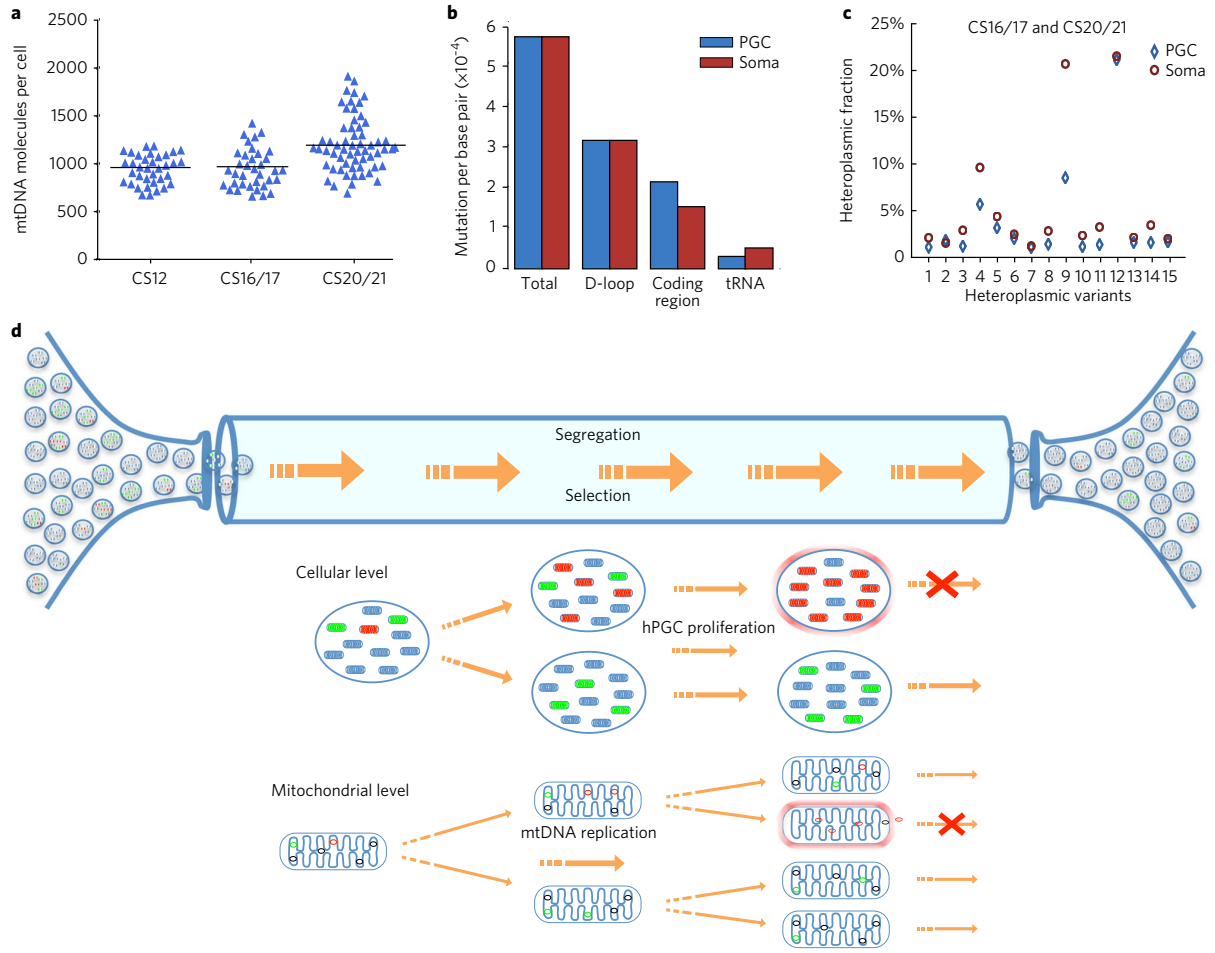

Fig. 5 | Mitochondrial DNA analysis of somatic cells in vivo and mechanisms of selection. a, MtDNA content of single human somatic cells in vivo at the same stage as the female PGCs shown in Figs. 1 and 2 (CS12 $n=36$, CS16/17 $n=36$; CS20/21 $n=60$). Each data point represents the mtDNA content in a single cell corresponding to the mean value from the independent qPCR measurements from 12 embryos. The horizontal bar represents the mean value. Source data are available in Supplementary Table 6. **b**, Mutation frequency for human female PGCs and corresponding somatic cells (soma) in developing human embryos (CS12–20/21) in vivo. The data are derived from 12 embryos. **c**, Segregation of the same heteroplasmic mtDNA variants detected in somatic cells and PGCs from the same embryo at CS16/17 and CS20/21 ($n=15$ variants) in vivo. Variants in the somatic cells had a higher heteroplasmy level than the PGCs ($P=0.03$, Fisher's exact test, two-sided), which was not the case at CS12. Source data available are in Supplementary Table 6. **d**, In vivo PGCs contain ~300 discrete mitochondria that each contain 5 mtDNA molecules. In vitro data suggest that the amount of mtDNA may be even lower in female germ cells at an earlier stage. Some of the mtDNA molecules are mutated with either neutral (green) or deleterious (red) mutations. Between CS12 and CS20/21, the number of cells increases from ~3000 to ~80,000, accompanied by a massive proliferation of mtDNA molecules within the migrating PGCs. As the mitochondria replicate, the mutations will be copied. The random segregation of mtDNA molecules during mitochondrial fission will generate daughter mitochondria with either high or low levels of the original mutation. If the mutation is deleterious, then it will be selected against. This could be because it compromises ATP synthesis and activates surveillance systems that remove defective mitochondria, or because it compromises mtDNA replication, and thus prevents that particular mitochondrion from being copied. Both of these mechanisms can act in concert at both the cellular and mitochondrial levels.

segregation pattern appeared to be different. Some of the mtDNA variants were detected in both the PGCs and the somatic cells from the same embryo, but by the later stages ($n=15$ shared variants, CS16–17 and CS20–21), the somatic cells contained higher heteroplasmy levels ($P=0.034$, Fig. 5c). Although based on limited data, this suggests that a less stringent mtDNA bottleneck is present in somatic cells within human embryos, and that mtDNA variants are less constrained by selection in somatic tissues than in the germ line.

With rudimentary DNA repair mechanisms and negligible intermolecular recombination, uniparentally inherited genomes have limited means of removing de novo mutations. If left unchecked, the relentless accumulation of mtDNA mutations would eventually lead to 'mutational meltdown' through Muller's ratchet, and extinction of the species[29]. The mtDNA genetic bottleneck has probably evolved to counteract this process, exposing potentially deleterious mutations to selective forces. On the basis of our findings, in humans this occurs early during germline development (Fig. 5d). However, if a mutation is sufficiently mild to escape germline selection, the same genetic bottleneck can have disastrous consequences. First observed in Holstein cows[30], dramatic shifts in heteroplasmy levels have been observed within one generation. In humans, healthy mothers harbouring a low-level heteroplasmic mtDNA mutation can have offspring with high levels of heteroplasmy and a severe multisystem disease. Pedigree analyses are consistent with a

human mtDNA bottleneck[31], but there has been no direct evidence in humans. Here we show that a human mtDNA genetic bottleneck exists, and is narrower than the bottleneck in mice[16,18] (Fig. 2f). Reducing the amount of mtDNA during this critical time of germ cell development will expose variants to selection acting at the cellular, organellar or mtDNA level, because this coincides with germ cells expressing transcripts for oxidative phorphorylation as they proliferate and migrate to form the gonad. Harnessing the underlying cell biology could help prevent human mtDNA disease, which currently affects ~1 in 11,000. Moreover, given the potential role of mtDNA mutations in common age-related disorders[32], preventing their transmission may have a wider impact by promoting healthy ageing in future generations.

Methods

Methods, including statements of data availability and any associated accession codes and references, are available at https://doi.org/10.1038/s41556-017-0017-8.

Received: 19 December 2016; Accepted: 27 November 2017;
Published online: 15 January 2018

References

1. Vafai, S. B. & Mootha, V. K. Mitochondrial disorders as windows into an ancient organelle. *Nature* **491**, 374–383 (2012).
2. Stewart, J. B. & Chinnery, P. F. The dynamics of mitochondrial DNA heteroplasmy: implications for human health and disease. *Nat. Rev. Genet.* **16**, 530–542 (2015).
3. Wallace, D. C. Colloquium paper: bioenergetics, the origins of complexity, and the ascent of man. *Proc. Natl. Acad. Sci. USA* **107**, 8947–8953 (2011).
4. Payne, B. A. et al. Universal heteroplasmy of human mitochondrial DNA. *Hum. Mol. Genet.* **22**, 384–390 (2013).
5. Hanley, N. A. et al. SRY, SOX9, and DAX1 expression patterns during human sex determination and gonadal development. *Mech. Dev.* **91**, 403–407 (2000).
6. Anderson, R. A., Fulton, N., Cowan, G., Coutts, S. & Saunders, P. T. Conserved and divergent patterns of expression of DAZL, VASA and OCT4 in the germ cells of the human fetal ovary and testis. *BMC Dev. Biol.* **7**, 136 (2007).
7. Irie, N. et al. SOX17 is a critical specifier of human primordial germ cell fate. *Cell* **160**, 253–268 (2015).
8. Dayama, G., Emery, S. B., Kidd, J. M. & Mills, R. E. The genomic landscape of polymorphic human nuclear mitochondrial insertions. *Nucleic Acids Res.* **42**, 12640–12649 (2014).
9. Kennedy, S. R., Salk, J. J., Schmitt, M. W. & Loeb, L. A. Ultra-sensitive sequencing reveals an age-related increase in somatic mitochondrial mutations that are inconsistent with oxidative damage. *PLoS. Genet.* **9**, e1003794 (2013).
10. Copeland, W. C. & Longley, M. J. Mitochondrial genome maintenance in health and disease. *DNA Repair* **19**, 190–198 (2014).
11. Stewart, J. B., Freyer, C., Elson, J. L. & Larsson, N. G. Purifying selection of mtDNA and its implications for understanding evolution and mitochondrial disease. *Nat. Rev. Genet.* **9**, 657–662 (2008).
12. Freyer, C. et al. Variation in germline mtDNA heteroplasmy is determined prenatally but modified during subsequent transmission. *Nat. Genet.* **44**, 1282–1285 (2012).
13. Falkenberg, M., Larsson, N. G. & Gustafsson, C. M. DNA replication and transcription in mammalian mitochondria. *Annu. Rev. Biochem.* **76**, 679–699 (2007).
14. Pyle, A. et al. Extreme-depth re-sequencing of mitochondrial DNA finds no evidence of paternal transmission in humans. *PLoS. Genet.* **11**, e1005040 (2015).
15. Craven, L. et al. Pronuclear transfer in human embryos to prevent transmission of mitochondrial DNA disease. *Nature* **465**, 82–85 (2010).
16. Cree, L. M. et al. A reduction of mitochondrial DNA molecules during embryogenesis explains the rapid segregation of genotypes. *Nat. Genet.* **40**, 249–254 (2008).
17. Ohinata, Y., Sano, M., Shigeta, M., Yamanaka, K. & Saitou, M. A. Comprehensive, non-invasive visualization of primordial germ cell development in mice by the Prdm1-mVenus and Dppa3-ECFP double transgenic reporter. *Reproduction* **136**, 503–514 (2008).
18. Wai, T., Teoli, D. & Shoubridge, E. A. The mitochondrial DNA genetic bottleneck results from replication of a subpopulation of genomes. *Nat. Genet.* **40**, 1484–1488 (2008).
19. Cao, L. et al. The mitochondrial bottleneck occurs without reduction of mtDNA content in female mouse germ cells. *Nat. Genet.* **39**, 386–390 (2007).
20. Wonnapinij, P., Chinnery, P. F. & Samuels, D. C. Previous estimates of mitochondrial DNA mutation level variance did not account for sampling error: comparing the mtDNA genetic bottleneck in mice and humans. *Am. J. Hum. Genet.* **86**, 540–550 (2010).
21. Kobayashi, T. et al. Principles of early human development and germ cell program from conserved model systems. *Nature* **546**, 416–420 (2017).
22. Calvo, S. E., Clauser, K. R. & Mootha, V. K. MitoCarta2.0: an updated inventory of mammalian mitochondrial proteins. *Nucleic Acids Res.* **44**, D1251–D1257 (2016).
23. Stewart, J. B. et al. Strong purifying selection in transmission of mammalian mitochondrial DNA. *PLoS. Biol.* **6**, e10 (2008).
24. Ma, H., Xu, H. & O'Farrell, P. H. Transmission of mitochondrial mutations and action of purifying selection in *Drosophila melanogaster*. *Nat. Genet.* **46**, 393–397 (2014).
25. Hill, J. H., Chen, Z. & Xu, H. Selective propagation of functional mitochondrial DNA during oogenesis restricts the transmission of a deleterious mitochondrial variant. *Nat. Genet.* **46**, 389–392 (2014).
26. Chen, Y. & Dorn, G. W. 2nd PINK1-phosphorylated mitofusin 2 is a Parkin receptor for culling damaged mitochondria. *Science* **340**, 471–475 (2013).
27. Narendra, D. P. et al. PINK1 is selectively stabilized on impaired mitochondria to activate Parkin. *PLoS. Biol.* **8**, e1000298 (2010).
28. Fukuoh, A. et al. Screen for mitochondrial DNA copy number maintenance genes reveals essential role for ATP synthase. *Mol. Syst. Biol.* **10**, 734 (2014).
29. Muller, H. J. The relation of recombination to mutational advance. *Mutat. Res.* **1**, 2–9 (1964).
30. Upholt, W. B. & Dawid, I. B. Mapping of mitochondrial DNA of individual sheep and goats: rapid evolution in the D loop region. *Cell* **11**, 571–583 (1977).
31. Chinnery, P. F. et al. The inheritance of mtDNA heteroplasmy: random drift, selection or both? *Trends Genet.* **16**, 500–505 (2000).
32. Keogh, M. & Chinnery, P. F. Hereditary mtDNA heteroplasmy: a baseline for aging? *Cell. Metab.* **18**, 463–464 (2013).
40. Funkuda, T. Ultrastructure of primordial germ cells in human embryo. *Virchows Arch. B Cell. Pathol.* **20**, 85–89 (1976).

Acknowledgements

P.F.C. is a Wellcome Trust Senior Fellow in Clinical Science (101876/Z/13/Z), and a UK NIHR Senior Investigator, who receives support from the Medical Research Council Mitochondrial Biology Unit (MC_UP_1501/2), the Medical Research Council (UK) Centre for Translational Muscle Disease research (G0601943) and the National Institute for Health Research (NIHR) Biomedical Research Centre based at Cambridge University Hospitals NHS Foundation Trust and the University of Cambridge. The views expressed are those of the author(s) and not necessarily those of the NHS, the NIHR or the Department of Health. W.W.C.T. is supported by a Croucher Foundation studentship, and M.A.S. by a Wellcome Investigator Award.

Author contributions

V.I.F. developed methods and isolated the in vivo human and mouse PGCs, and performed the microscopy; S.D. performed RNA-seq bioinformatic analysis; A.P. and W.W.C.T. carried out the real-time PCR assays; W.W.C.T. performed the RNA-seq experiments and N.I. derived and isolated the hESCs, hPGCLCs and in vitro somatic cells; W.W. performed additional informatic and statistical analysis; A.C. and L.N. isolated the human inner cell mass and trophectoderm cells, overseen by D.I. and Y.K. J.C. carried out the library preparation and deep sequencing; M.C. helped with the human tissue dissection; H.S. helped with the super-resolution microscopy; B.P. performed the technical validation of the deep sequencing protocol; M.S. provided the *BVSC* mouse; G.H. advised on the NGS data analysis; M.A.S. supervised the RNA-seq experiments and real-time PCR expression assays and advised on the project; P.F.C. supervised the project, designed experiments, analysed the data and wrote the paper. All authors contributed to the manuscript.

Competing interests

The authors declare no competing financial interests.

Additional information

Supplementary information is available for this paper at https://doi.org/10.1038/s41556-017-0017-8.

Reprints and permissions information is available at www.nature.com/reprints.

Correspondence and requests for materials should be addressed to P.F.C.

Publisher's note: Springer Nature remains neutral with regard to jurisdictional claims in published maps and institutional affiliations.

Methods

Isolation of single cells. Ethically approved human embryonic tissue samples were provided by the Human Developmental Biology Resource (HDBR), Newcastle University, UK. For CS12 embryos, the lower section (see Fig. 1) was dissected in phosphate-buffered saline (PBS) from intact healthy embryos from healthy donors. For CS16 to CS21 embryos, genital ridges from individual embryos were dissected in PBS and the surrounding mesonephric tissue was removed. The dissected tissue was dissociated to a single-cell suspension with 350 µl in the case of CS12 and 200 and 250 µl in the case of CS16/7 and CS20/1, respectively, of 5 U ml^{-1} Liberase DL Research Grade (Roche) at 37 °C for 20–35 min (depending on the stage/size of the tissue). The dissociated sample was then washed with 750–800 µl of cold Flow Cytometry Staining Buffer (FCSB) (R&D Systems) and the solution was passed through a 50 µm cell strainer. Twenty microlitres was removed for the cell count using a Tali Image Cytometer (Life Technologies), before the cell suspension was centrifuged at 300*g* for 5 min at 4 °C. Cells were suspended in cold FCSB and incubated with 5 µl of Brilliant Violet 421-conjugated anti-human CD38 (Biolegend, 303526), 20 µl of Alexa Fluor 647-conjugated SSEA-4 (BD Pharmingen, 560796) and 5 µl of Alexa Fluor 488-conjugated anti-alkaline phosphatase (BD Pharmingen, 561495) in the case of CS12 embryonic tissue, and 5 µl of Brilliant Violet 421-conjugated anti-human CD117 (c-Kit) (Biolegend, 313216) and 5 µl of Alexa Fluor 488-conjugated anti-alkaline phosphatase (BD Pharmingen, 561495) in the case of CS16/7 and CS20/1 gonadal tissue for 30 min at 4 °C. Cells were the washed with 1 ml of FCSB and centrifuged at 300*g* for 5 min at 4 °C. Cells were suspended in fresh cold FACB and sorted using a FACS Aria II (BD Biosciences). To determine the right antibody combination for isolation of pure human PGCs, different cell populations were sorted onto Polysine Microscope Adhesion Slides (Thermo Fisher Scientific) and left to settle in a humidified chamber at room temperature for 20–30 min before being fixed with 4% PFA for 5 min at room temperature. Purity for each sorted population was tested with alkaline phosphatase staining using Leukocyte Alkaline Phosphatase Kit (Sigma-Aldrich). Greater than 97% pure samples were used for downstream analysis. Initially, gender was determined by PCR as described in ref. [33] and then verified by karyotype analysis. Somatic cells were isolated at the same time using the same protocols, and inner cell mass and trophectoderm cells were manually dissected from in vitro-fertilized human day-6 embryos as described previously[34]. In vitro human embryonic stem cells (hESCs), human primordial germ cell-like cells (hPGCLCs) and somatic cells were cultured, induced and isolated as described previously[7,21]. Two independent PGCLC inductions were performed for both the male (WIS2) and female (H9) ESC lines. Single cells were isolated by FACS using the NANOS3-tdTomato knock-in reporter and the cell surface marker for tissue non-specific alkaline phosphatase (TNAP) in the WIS line, and TNAP/CD38 double positivity in the h9 line. The somatic cells were isolated during the same FACS sort and were negative for these markers. All cell lines were regularly checked for mycoplasma infection.

The work with the human day-6 embryos was performed under licence from the UK Human Fertilisation and Embryology Authority (research license numbers: R0075 and R0133) and also has local ethical approval (UK National Health Service Research Ethics Committee Reference: 06/Q0702/90). Informed consent was obtained from all subjects and the experiments conformed to the principles set out in the WMA Declaration of Helsinki and the NIH Belmont Report. No financial inducements are offered for donation. The study is compliant with all relevant ethical regulations regarding research involving human participants.

Measuring mtDNA content. *Lysis of PGCs.* PGCs collected in 96-well plates at 40 or 80 cells per well (Life Technologies) were lysed for 16 h in 50 mM Tris-HCl, pH 8.5, with 0.5% Tween 20 and 200 ng ml^{-1} proteinase K, at 55 °C, followed by heat inactivation at 95 °C for 10 min.

Lysis of single PGCs. PGCs collected in 96-well plates at a single cell per well (Life Technologies) were lysed for 30 min in 4 µl of 50 mM Tris-HCl, pH 8.5, with 0.5% Tween 20 and 200 ng ml^{-1} proteinase K, at 37 °C, followed by heat inactivation at 80 °C for 15 min.

Quantification of mtDNA copy number. Quantitative real-time PCR (qPCR) was performed on a CFX96 Touch Real-Time PCR Detection System (Bio-Rad). Human mtDNA copy number was calculated by absolute quantification using a singleplex Taqman assay targeting the mitochondrial *MT-ND1* gene (Supplementary Table 1a). Mouse mitochondrial DNA copy number was calculated by absolute quantification using a singleplex Taqman assay targeting the mitochondrial *MT-ND5* gene (Supplementary Table 1b). Standard curves using PCR-generated templates were used for absolute quantification. Samples and standards were measured in triplicate.

Somatic cells, human inner cell mass, trophectoderm, human embryonic stem cells, human primordial germ cell-like cells, and in vitro somatic cells. MtDNA levels were measured using the same protocols as for the PGCs.

Immunocytochemistry. PGCs were sorted on Polysine Microscope Adhesion Slides (Thermo Fisher Scientific) and left to settle in a humidified chamber at room temperature for 20–30 min before fixation with 4% PFA for 10 min at room temperature, washed three times with PBS, 0.1% Tween-20, (5 min each wash) and incubated for 20 min with PBS, 0.3% Triton-X buffer, and washed three times with PBS, 0.1% Tween-20 (5 min each wash). Cells were subsequently blocked for 1 h with PBS, 2.5% BSA, 0.1% Tween-20 and 5% normal goat serum at room temperature followed by staining with DDX4 (VASA) mouse monoclonal IgG1 antibody (Selleckchem) diluted 1:200 in the blocking solution at 4 °C overnight. The slides were then washed three times with PBS, 0.1% Tween-20 (5 min each wash) and incubated with Alexa fluorophore-conjugated secondary antibody (Molecular Probes) 1:500 diluted in PBS, 0.1% Tween-20 for 1 h at room temperature in the dark, washed three times in PBS, 0.1% Tween-20 (5 min each wash) and once in PBS for 5 min. Finally, the glass-bottom dishes were mounted in ProLong Gold Antifade Mountant with DAPI (Molecular Probes) and imaged using a Zeiss Axio Imager Z1/Apotome Microscope.

Electron microscopy. PGCs were collected in 1.5 ml microcentrifuge tubes containing 2.5% electron-microscopy-grade glutaraldehyde (TAAB Laboratories Equipment) in Sorenson's phosphate buffer 0.2 M pH 7.4 (Electron Microscopy Sciences) and stored at 4 °C overnight. The cells were enrobed in low-melting-point agarose (4%) to form a small block. After secondary fixation in 2% osmium tetroxide (Agar Scientific), the cells were dehydrated in graded acetone, embedded in epoxy resin (TAAB) and polymerized at 60 °C. Semi-thin sections (0.5 µm) were taken from the resin block and stained with toluidine blue to identify the first cells. As soon as cells were found in the block, ultrathin serial sections (70 nm) were taken and collected on copper washer grids (Gilder Grids). Serial sections were taken for approximately 150 µm to ensure that there would be at least 6 whole cells sectioned. The grids were stained with uranyl acetate and lead citrate (Leica UK) and viewed on a Philips CM100 TEM (FEI). Cells that were completely sectioned were imaged from each sample and mitochondria counted using the dissector technique[35]. Pairs of images 140 nm apart were taken at several levels through each cell. Each pair is comprised of a 'reference' and 'look-up' section. The number of mitochondria that are hit by the reference section but not by the look-up section is counted. To increase efficiency, the roles of the reference and look-up sections can be reversed. If the volume of the dissector is known, then the number density Nv can be obtained. The volume of the dissector equals the area of cell profile multiplied by the distance between the paired sections. Multiplying number density by cell volume gives mitochondrial number.

Super-resolution microscopy. PGCs were collected in 35-mm-diameter glass-bottom dishes (glass no. 1.5, 0.170 ± 0.005 mm, high-tolerance coverslip; MatTek) and left to settle in a humidified chamber at room temperature for 20–30 min before being fixed with 4% PFA for 10 min at room temperature. Dishes were washed three times with TBS (pH 7.6), 0.1% Tween-20 (5 min each wash) and then permeabilized for 10 min using TBS, 0.1% sodium citrate, 0.2% Triton-X buffer, before being washed three times with TBS, 0.1% Tween-20 (5 min each wash). Cells were subsequently blocked for 1 h with TBS, 0.3 M glycine, 2.5% BSA, 5% normal goat serum, 0.1% Tween-20 buffer at room temperature followed by staining with TOM20 mouse monoclonal IgG2a antibody (F-10), sc-17764 (Santa Cruz Biotechnology) diluted 1:1,000 in the blocking solution at 4 °C overnight. The glass-bottom dishes were then washed three times with TBS, 0.1% Tween-20 (5 min each wash) and incubated with Alexa fluorophore-conjugated secondary antibody (Molecular Probes) 1:1,000 diluted in TBS, 0.1% Tween-20 for 1 h at room temperature in the dark, washed three times in PBS, 0.1% Tween-20 (5 min each wash) and once in TBS for 5 min. Finally, the glass-bottom dishes were mounted in ProLong Gold Antifade Mountant with DAPI (Molecular Probes) and imaged using a Nikon Structured Illumination Microscope.

Image segmentation analysis for measuring mitochondrion content. Three-dimensional reconstruction of super-resolution *z*-stack images was rendered using NIS-Elements software (Nikon). Mitochondrion content count and visualization of PGCs were performed using Imaris software (Bitplane).

Ultradeep sequencing and variant analysis. Details of collected samples are given in Supplementary Table 2. PGCs and somatic cells were sorted and lysed in 96-well plates as described above and mtDNA was amplified using PrimeSTAR GXL DNA polymerase (error rate = 0.00108%, Takara Bio) in nine overlapping fragments (Supplementary Table 1c) for grouped cells or in two overlapping fragments (Supplementary Table 1d) for the single cells. The specificity of mtDNA amplification was assessed using DNA extracted from Rho0 cell lines previously shown to be devoid of mtDNA[4]. There was no template amplification after > 40 PCR cycles, confirming that the primers amplified only mtDNA and not nuclear-mitochondrial sequences. No PCR products were generated with any of the primers. Amplified products were assessed by gel electrophoresis, against DNA-positive and DNA-negative controls. Each amplicon was individually purified using Agencourt AMPure XP beads (Beckman-Coulter), quantified using a Qubit 2.0 fluorimeter (Life Technologies) and amplicons from the same sample were pooled. Libraries were prepared for Next Generation Sequencing (NGS) using the Illumina Nextera XT DNA sample preparation kit (Illumina), and pooled amplicons were 'tagmented', amplified, cleaned, normalized and pooled

in equimolar concentrations for library preparation. The library was sequenced using MiSeq Reagent Kit v3.0 (Illumina) in paired-end, 250 bp reads. Post-run FASTQ files were analysed using an in-house-developed bioinformatic pipeline. Reads were aligned to the rCRS (NC_012920) using BWA v0.7.4 invoking –mem[36]. Aligned reads were sorted and indexed using Samtools v0.1.8[37] and duplicate reads were removed using Picard v1.85 (http://broadinstitute.github.io/picard/). Variant calling was performed in tandem using VarScan v2.3.1[38] (minimum depth = 1,500, supporting reads = 10, base-quality = > 30, mapping quality = > 20 and variant threshold = 1.0%). Variants were annotated using ANNOVAR v529[39]. Heteroplasmic variants are defined as > 1% minor allele frequency. Our previous work using this method showed that variants present at > 1% heteroplasmy were highly likely to have been present in the original DNA sample, and unlikely to be artefacts. In-house Perl scripts were used to extract base/read quality data and coverage data. In addition, low-quality variants, present in low-complexity regions, were not included in the analysis. Sequencing a cloned mtDNA template with the same protocol showed minimal background sequencing error (Supplementary Fig. 3).

RNA-seq library preparation. PGCs were sorted into 100 µl of extraction buffer of PicoPure RNA Isolation Kit (Applied Biosystems) and RNA was extracted following the manufacturer's protocol. The Ovation RNA-Seq System V2 (Nugen) was used for reverse transcription and amplification of total RNA (0.5 to 2 ng) into cDNA. Fragments of 250 bp were generated by sonication of amplified cDNA using the Covaris S220 Focused-ultrasonicators. Subsequently, using the Ovation Rapid DR Multiplex System (Nugen) and 500 ng of fragmented cDNA, an RNA-seq library was prepared. Quantification of the library was carried out by qPCR using the KAPA Library Quantification Kit (Kapa Biosystems) using the QuantStudio 6 Flex Real-Time PCR System (Applied Biosystems). Libraries were sequenced by the HiSeq 2000/2500 sequencing system (Illumina) with single-end 50 bp read length. Every four indexed libraries were multiplexed to one lane of a flowcell, resulting in > 40 million single-end reads per sample.

RNA-seq analysis. After removal of adaptor sequence and low-quality reads, RNA-seq reads were mapped to the human reference genome (UCSC GRCh37/hg19) using TopHat2 v2.0.13 (http://ccb.jhu.edu/software/tophat) guided by ENSEMBL gene models. The annotations of transcripts were based on Ensembl (Release 74) considering protein-coding, long-noncoding RNA and processed transcripts. Using featureCounts, the raw counts per transcripts were obtained. The counts for nuclear-encoded transcripts were normalized, and statistical tests for differential expression of transcripts were performed by using the R Bioconductor DESeq package (www.bioconductor.org). To account for the profound reduction in mtDNA content, mitochondrial transcript counts were normalized by the set of DESeq-scaling factors obtained for nuclear-encoded transcripts before evaluating their differential abundance. Further normalization of expression-normalized transcript counts was carried out by transcript length (per kilobase). Hierarchical clustering plots were generated with the R 'hclust' functions using Ward's method. Principal components were computed by singular value decomposition with the R 'prcomp' function on scaled DESeq-normalized expression values. Only the 80% most highly expressed transcripts were used for clustering and PCA. By selecting the most equivalent time points in human PGC development, mitochondrial genes that were significantly differentially expressed ($\log_2$(fold change) > 2.5 or < −2.5 and P value < 0.05) between hPGCs (week 7 or 9) and hPGCs (week 4) were compiled and highlighted in the plots of the principal component (PC) scores for each gene (Fig. 5e). Human mitochondrion-related genes were adopted from MitoCarta2.0 inventory.

Quantitative PCR with reverse transcription (RT–qPCR). Total RNA from sorted PGCs or somatic cells was extracted by the PicoPure RNA Isolation Kit (Applied Biosystems). cDNA was synthesized and amplified using Ovation RNA-Seq System V2 (Nugen). RT–qPCR reactions were set up with SYBR Green JumpStart Taq ReadyMix (Sigma) and 200 nM of forward and reverse primers (Supplementary Table 5). RT–qPCR was then performed on the QuantStudio 6 Flex Real-Time PCR System (Applied Biosystems) at 95 °C for 10 min, 40 cycles of 95 °C for 15 s and 60 °C for 1 min, followed by a melt curve stage. Mean threshold cycles were determined from 2–3 technical replicates. Relative expression levels were calculated using the comparative Ct method, by normalization to *GAPDH* and relative to CS12 human PGCs or soma (Supplementary Figs. 1 and 2).

Statistics and reproducibility. Statistical analyses were performed using parametric methods as described in the text and figure legends with exact P values reported. The number of biological replicates for each experiment is stated in the figure legend.

Life Sciences Reporting Summary. Further information on experimental design is available in the Life Sciences Reporting Summary.

Data availability. mtDNA-seq data that support the findings of this study are available in Supplementary Table 5 and are deposited in the BioSample database under accession codes SAMN08022267, SAMN08022310, SAMN08022311, SAMN08022312, SAMN08022313, SAMN08022314, SAMN08022315, SAMN08022316, SAMN08022317, SAMN08022318, SAMN08022319 and SAMN08022320. RNA-seq data generated by this study have been deposited in the Gene Expression Omnibus (GEO) under the accession codes GSM2060944 (for hPGC female week 4) and GSM2060945 (for somatic cells female week 4). Previously published RNA-seq data that were reanalysed here are available under accession codes SRX857044, SRX857046, SRX901022, SRX901024, SRX901025, SRX901026, SRX901027, SRX901028, SRX901029, SRX901030 and SRX901031. Statistics source data for Figs. 2f–h and 5a,c are provided in Supplementary Table 6. All other data supporting the findings of this study are available from the corresponding author on reasonable request.

References

33. Villesen, P. & Fredsted, T. Fast and non-invasive PCR sexing of primates: apes, Old World monkeys, New World monkeys and Strepsirrhines. *BMC Ecol.* **6**, 8 (2006).
34. Noli, L., Capalbo, A., Ogilvie, C., Khalaf, Y. & Ilic, D. Discordant growth of monozygotic twins starts at the blastocyst stage: a case study. *Stem Cell. Rep.* **5**, 946–953 (2015).
35. Sterio, D. C. The unbiased estimation of number and sizes of arbitrary particles using the disector. *J. Microsc.* **134**, 127–136 (1984).
36. Li, H. & Durbin, R. Fast and accurate short read alignment with Burrows-Wheeler transform. *Bioinformatics* **25**, 1754–1760 (2009).
37. Li, H. et al. The Sequence Alignment/Map format and SAMtools. *Bioinformatics* **25**, 2078–2079 (2009).
38. Koboldt, D. C. et al. VarScan: variant detection in massively parallel sequencing of individual and pooled samples. *Bioinformatics* **25**, 2283–2285 (2009).
39. Wang, K., Li, M. & Hakonarson, H. ANNOVAR: functional annotation of genetic variants from high-throughput sequencing data. *Nucleic Acids Res.* **38**, e164 (2010).

nature cell biology

SUPPLEMENTARY INFORMATION

https://doi.org/10.1038/s41556-017-0017-8

In the format provided by the authors and unedited.

Segregation of mitochondrial DNA heteroplasmy through a developmental genetic bottleneck in human embryos

Vasileios I. Floros[1,2], Angela Pyle[3], Sabine Dietmann[4], Wei Wei[1,2], Walfred W. C. Tang[5], Naoko Irie[5], Brendan Payne[4], Antonio Capalbo[6,7], Laila Noli[8,9], Jonathan Coxhead[4], Gavin Hudson[4], Moira Crosier[10], Henrik Strahl[11], Yacoub Khalaf[8,9], Mitinori Saitou[12,13], Dusko Ilic[8,9], M. Azim Surani[5] and Patrick F. Chinnery[1,2*]

[1]MRC-Mitochondrial Biology Unit, University of Cambridge, Cambridge, UK. [2]Department of Clinical Neurosciences, Cambridge Biomedical Campus, University of Cambridge, Cambridge, UK. [3]Wellcome Trust Centre for Mitochondrial Research, Institute of Genetic Medicine, Newcastle University, Newcastle upon Tyne, UK. [4]Wellcome Trust-Medical Research Council Stem Cell Institute, University of Cambridge, Cambridge, UK. [5]Wellcome Trust Cancer Research UK Gurdon Institute, University of Cambridge, Cambridge, UK. [6]GENERA, Centre for Reproductive Medicine, Clinica Valle Giulia, Rome, Italy. [7]GENETYX, Reproductive Genetics Laboratory, Marostica, Italy. [8]Division of Women's Health, Faculty of Life Sciences and Medicine, King's College London, London, UK. [9]Assisted Conception Unit, Guy's Hospital, London, UK. [10]Human Developmental Biology Resource, Institute of Genetic Medicine, Newcastle University, Newcastle upon Tyne, UK. [11]Centre for Bacterial Cell Biology, Institute for Cell and Molecular Biosciences, Newcastle University, Newcastle upon Tyne, UK. [12]Department of Anatomy and Cell Biology, Graduate School of Medicine, Kyoto University, Kyoto, Japan. [13]JST, ERATO, Kyoto, Japan. Vasileios I. Floros and Angela Pyle contributed equally to this work. *e-mail: pfc25@cam.ac.uk

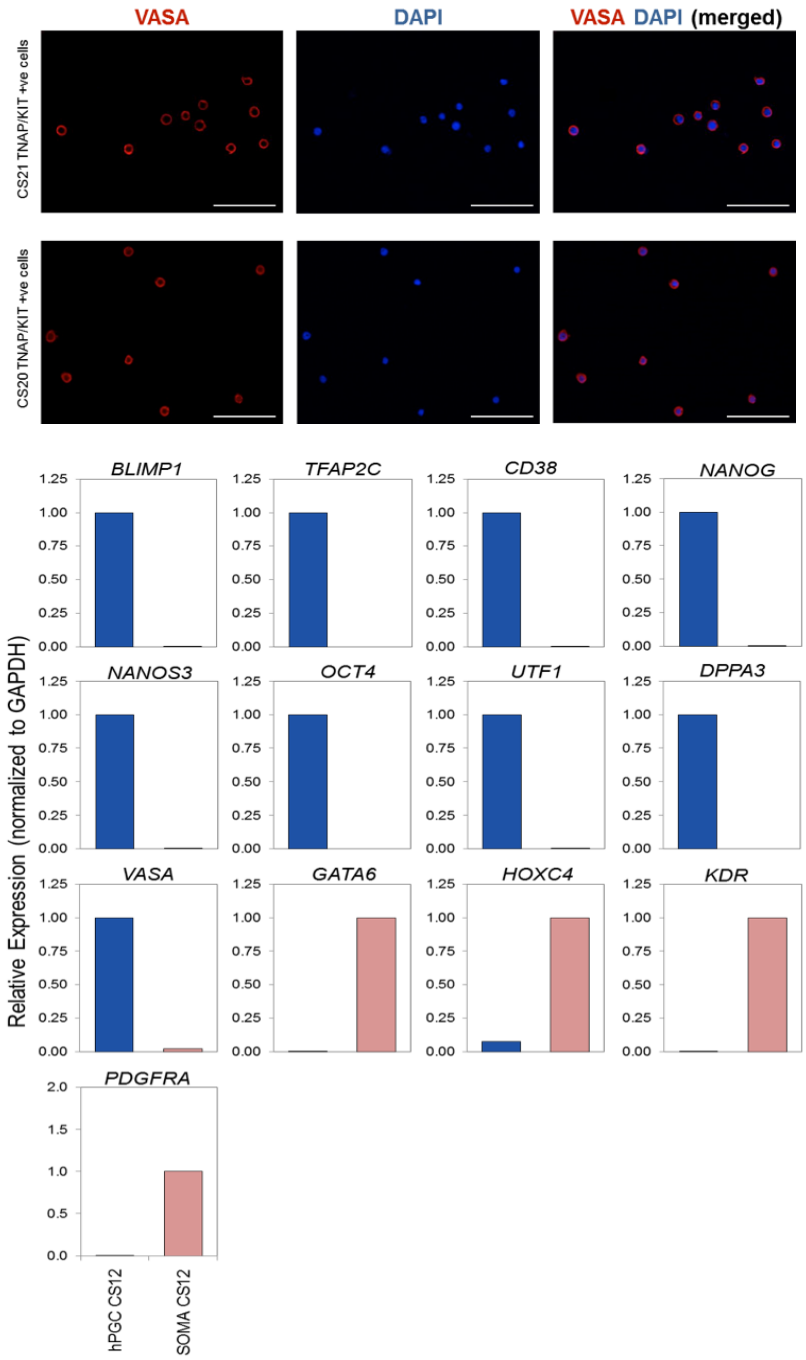

Supplementary Figure 1. Flow cytometry and RT-qPCR analysis of germ cells and somatic cells. Upper = Immuno-staining of FACS human PGCs positive for TNAP and c-KIT stained with anti-VASA antibody. Scale Bar = 100 µm. Lower = expression analysis of TNAP/SSEA4/CD38 triple positive (hPGCs CS12) and TNAP/SSEA4/CD38 triple negative (SOMA CS12) sorted cells. Relative expression levels are shown with normalization to *GAPDH*. Data shown represent two independent biological replicates with similar results.

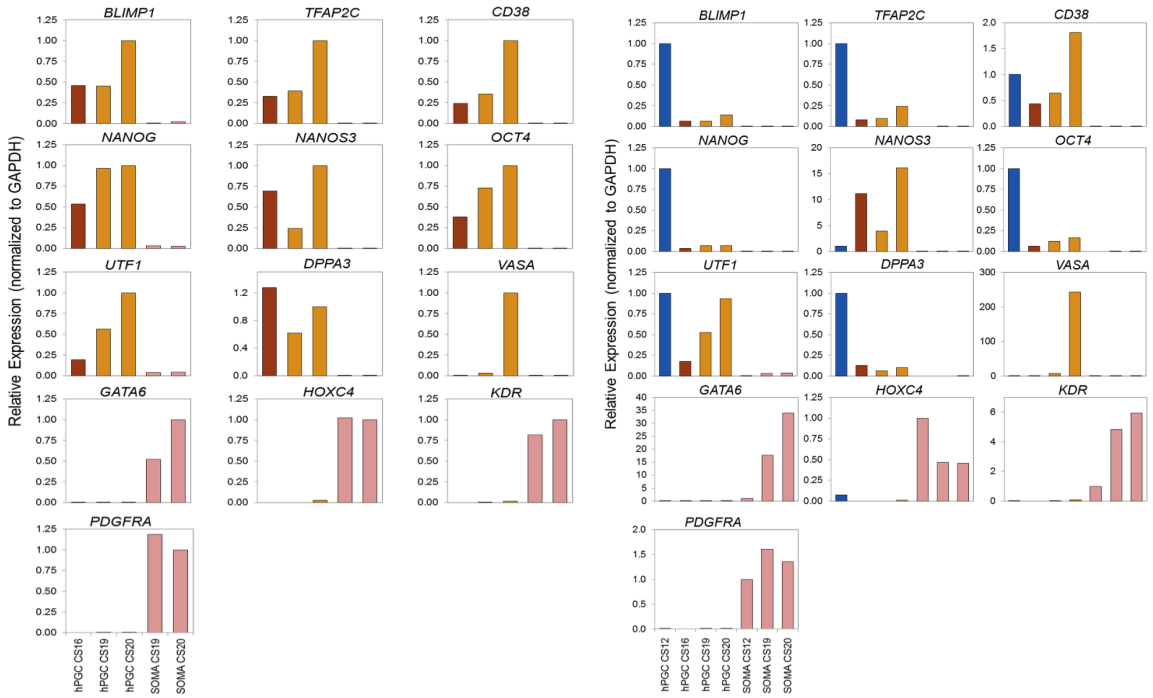

Supplementary Figure 2. RT-qPCR analysis for germ cell specific and soma transcripts. Left = Expression analysis of TNAP/AP double positive (hPGCs CS16-20) and TNAP/AP double negative (SOMA CS19-20) sorted cells. Relative expression levels are shown with normalization to *GAPDH*. Right = Comparison of expression level across all stages CS12- CS20. Relative expression levels are shown with normalization to *GAPDH*. Data shown represent two independent biological replicates with similar results.

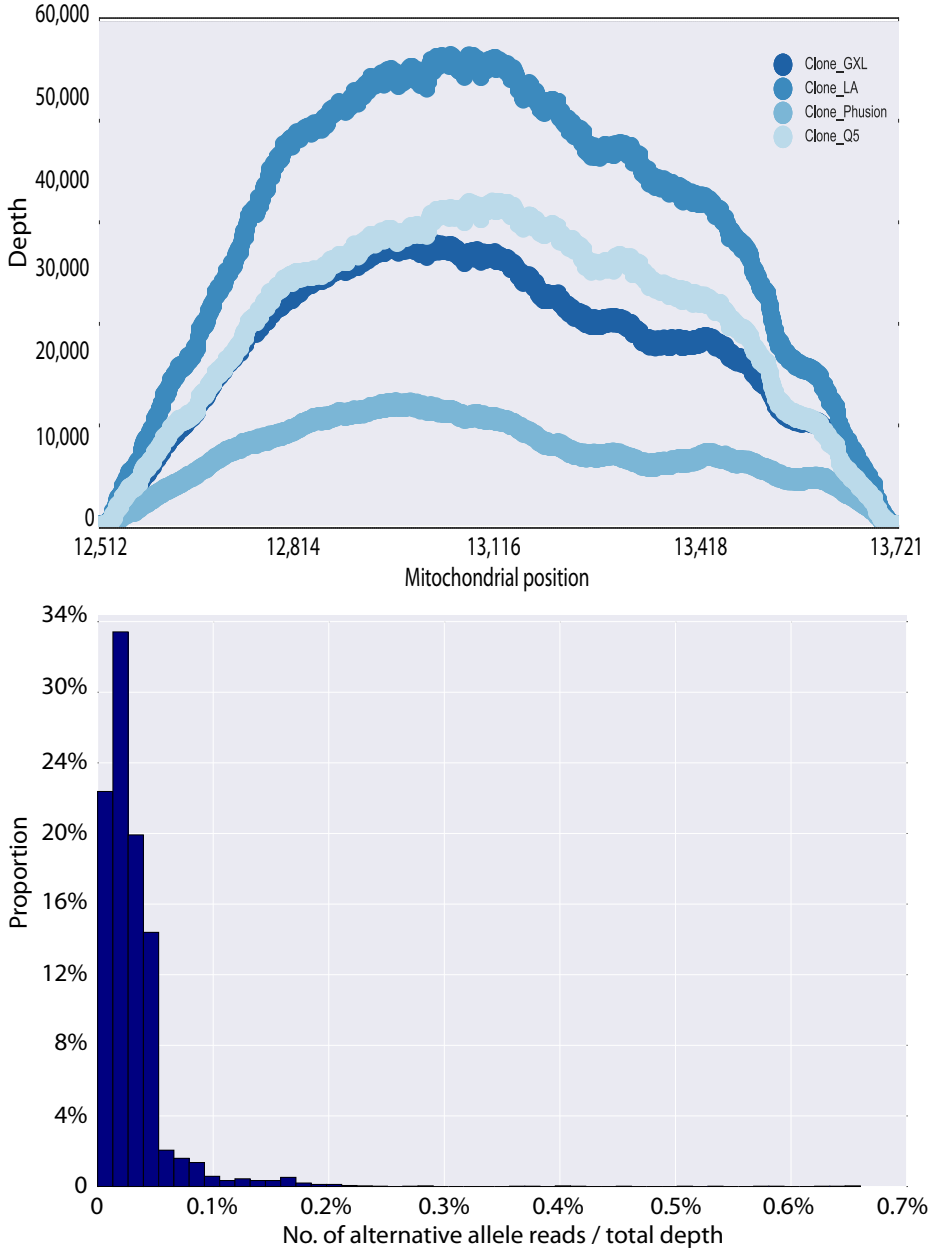

Supplementary Figure 3. Ultra-deep sequencing quality. Amplification of a mtDNA template comparing PrimeSTAR GXL DNA polymerase (used to sequence mtDNA in the cell lysates) and LA, Phusion and Q5 DNA polymerases. The sequencing and bioinformatic analysis used the same protocol described in the Methods. (A) Sequencing depth of the cloned mtDNA fragment. (B) Variant allele frequency (VAF) distribution. No sequence variants present at VAF ≥1%. Variants detected at VAF>1% in the cell lysates are therefore highly likely to have been present in the original mtDNA molecules and are not artefacts introduced during the sequencing. MtDNA sequencing was performed once using each different polymerase.

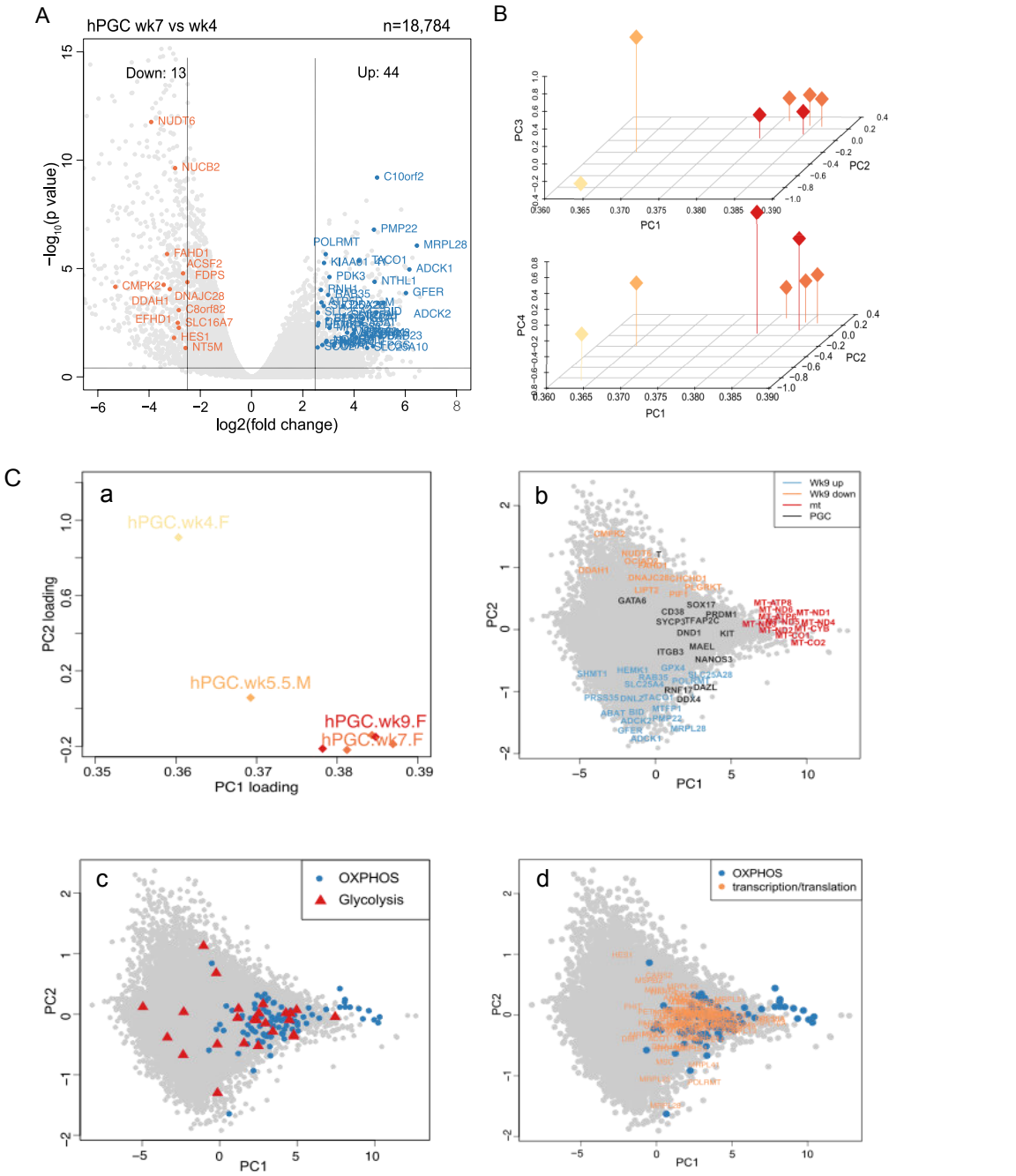

Supplementary Figure 4. RNAseq of human primordial germ cells (PGCs). (A) Differentially expressed genes of Wk 7 (n = 3 independent replicates) and Wk 4 hPGCs (the experiment was performed once). Volcano plot showing differentially expressed genes (from MitoCarta2.0 list) between week 7 and week 4 hPGCs [log2(fold change)>2.5, p < 0.05, *DEseq*, two-sided]. A list of these genes is shown in Supplementary Table 4. (B) Principal component analysis (PCA) in hPGC samples. PCA of RNA-seq expression for MitoCarta2.0 genes in hPGC samples (n = 7 embryos). **a**, PC1,2 and 3 and **b**, PC1,2 and 4. A two-dimensional principal components analysis (PC2 against PC1) is shown in Fig. 5e. (C) Two-dimensional principal components analyses of RNA-seq gene expression. (PC2 against PC1) of all transcripts for the different stages of hPGCs (inner panel **a**). Corresponding plots of PC scores indicates the weight of various genes on PC2 and PC1 (inner panels **b**, **c** and **d**). MitoCarta2.0 transcripts up or down regulated from 4 (n = 1 embryo) to 9 Wk (n = 2 cell embryos, see also Fig. 4e) are shown in inner panel **b** together with mtDNA-encoded transcripts and PGC-associated transcripts. Respiratory electron chain genes and genes involved in glycolysis are indicated in inner panel **c**. Transcripts for mitochondrial transcription and translation and respiratory chain are shown in inner panel **d**.

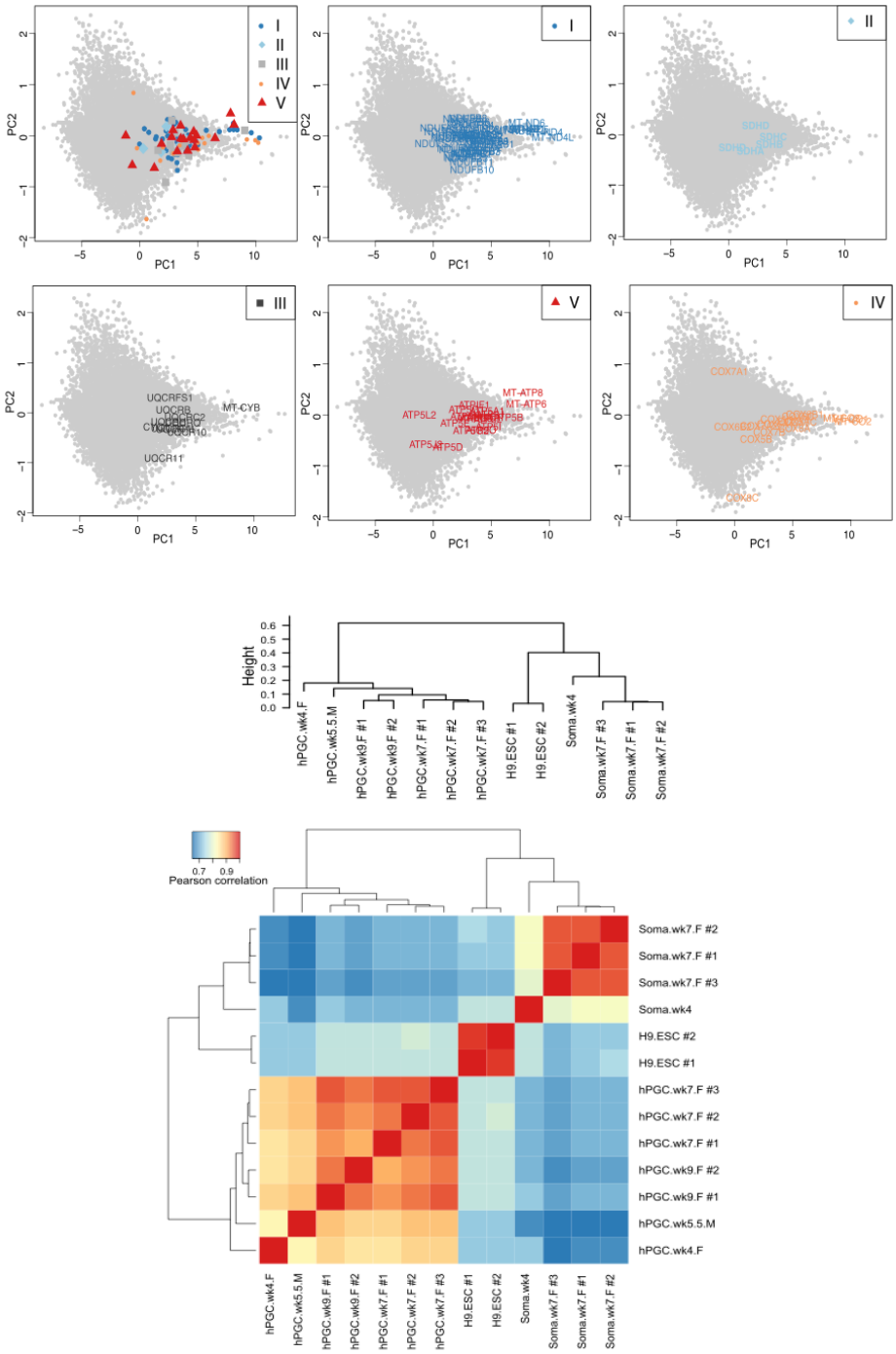

Supplementary Figure 5. 2-D PCA of the respiratory electron transport chain complexes & gene expression correlation of hPGCs, soma and hESCs samples. Upper = PC2 against PC1 of all transcripts for the different complexes of the respiratory electron transport chain genes (total n = 13 transcriptomes, the figure shows the number of independent replicates in each group). Corresponding plots of PC scores indicates the weight of each complex on PC2 and PC1. Top left panel shows all five complexes together, rest of the panels show each complex individually. Lower = Gene expression correlation of hPGCs, soma and hESCs samples. Pearson correlation heat map (two-sided) of gene expression (log_2(normalized read counts)) in various samples with unsupervised hierarchical clustering shown in the upper panel. The color key indicates the correlation coefficient. See also Fig. 5a&b.

Supplementary Tables Legends

Supplementary Table 1. Oligonucleotide primer sequences.
qPCR primer sequences for human mtDNA (revised Cambridge Reference Sequence (rCRS); GenBank accession number NC_012920.1).
qPCR primer sequences for mouse mtDNA (Mus musculus mitochondrion, NC_005089.1).
PCR primer sequences for human mtDNA, 9 primer pairs. (revised Cambridge Reference Sequence (rCRS); GenBank accession number NC_012920.1).
PCR primer sequences for human mtDNA, 2 primer pairs. (revised Cambridge Reference Sequence (rCRS); GenBank accession number NC_012920.1).
RT-qPCR primer sequences

Supplementary Table 2. Number of embryos studied. The number of embryos studied, the gender, and number of cells studies from each embryo. (CS = Carnegie stage = CS, F = Female, sequenced = number of cells sequenced)

Supplementary Table 3. PGC number and mtDNA molecules. The number of primordial germ cells and the corresponding number of mtDNA molecules at each embryonic stage in mouse and human embryos.

Supplementary Table 4. Genes up or down regulated. log2(fold change)>2.5, $p < 0.05$ in wk9 and wk7 hPGCs compared to wk4 hPGCs. The genes listed for hPGC wk9 vs wk4 are also shown in Fig. 4F and coloured in Fig. 4E.

Supplementary Table 5. MtDNA deep sequencing data. MtDNA variants detected in the sequenced PGCs showing the sequence read quality and variant allele frequency.

Supplementary Table 6. Statistics Source Data. Data values plotted in the figures

Supplementary Video Legends

Supplementary Movie 1. Human primordial germ cell. Nikon Structured Illumination Microscope (N-SIM) image of a human PGC labelled with anti-TOM20 isolated from a Carnegie Stage 12 embryo.

Supplementary Movie 2. Human primordial germ cell. Nikon Structured Illumination Microscope (N-SIM) image of a human PGC labelled with anti-TOM20 isolated from a Carnegie Stage 12 embryo. with mitochondria identified and counted by IMARIS software.